

CONFIDENTIAL

**Oil Sands Bitumen Emulsion Upgrading by Using *In Situ*
Hydrogen Generated through the Water Gas Shift Reaction**

by

Lei Jia

A thesis

presented to University of Waterloo

in fulfillment of

the thesis requirement for the degree of

Doctor of Philosophy

in

Chemical Engineering

Waterloo, Ontario, Canada 2014

© Lei Jia 2014

Author's Declaration

I hereby declare that I am the sole author of this thesis. This is a true copy of the thesis, including any required final revisions, as accepted by my examiners.

I understand that my thesis may be made electronically available to the public.

A handwritten signature in black ink, appearing to read 'Luthi', is positioned on the left side of the page.

Acknowledgements

My Waterloo journey started with a \$5,000 budget, and that was my grandma's saving for 20 years. Born and raised from an ordinary Chinese family in a decadent city, I would have never dreamed of studying abroad. I would first thank my grandma, Xiangzhi Huang, for her love and initial financial support. I wish her rest in peace in heaven.

Then I would like to express my sincere gratitude to my supervisors, Dr. Flora T.T. Ng and Dr. Garry L. Rempel, for their excellent guidance, caring and patience throughout my PhD study. Their attitudes, behaviors and enthusiasm set the bar for my future career and life.

I am also going to give special recognitions to Dr. Yuxiang Rao, who initiated the bitumen upgrading study presented in this thesis. Thanks to his enduring guidance in experimental design, result analysis and trouble shooting, I became more eligible to handle a complicated research project independently. I would also extend my appreciation to other members from Dr. Ng's research group: Kun Liu, Aziz Alghamdi, Yuanqing Liu, Lu Dong, Sunyoung Gong, Chris Choy, Jennifer Moll, Arman Hassan, Nagaraju Pasupulety, Donghua Zuo, Kamalakar Gunda, Amir Irvani, Yinmei Ye, Behnam Goortani, Zhiwei Qi, Bill O'Keefe, Aijaz Baig, Chau Mai, Aashishi Gaurav, Saurabh Patankar and Manish Tiwari for their support, encouragement and enlightening discussion throughout this long journey. I also need to mention several members from Dr. Rempel's research group, and they are Jialong Wu, Yin Liu, Yan Liu, Lijuan Yang, Suwadee Kongparakul, Hui Wang, Minghui Liu, Ting Li and Ray Zou for their kindly help and support and/or the access to their equipment and characterization facilities in Dr. Rempel's laboratory.

I would like to thank Fred Pearson, Andreas Korinek and Carmen Andrei in the Canadian Centre for Electron Microscopy (CCEM) for their technical support in HRTEM, EDX and STEM; Megan Fair from McMaster University for the asphaltenes CHN analysis; Nina Heinig from Department of Chemistry for her patience instruction in SEM and EDX. A special thanks also to

Mr. Ralph Dickhout, Mr. Bert Habicher, Ravindra Singh and Mr. Rick Hecktus for their technical expertise, patience and humor. I would also acknowledge the staff of the Department of Chemical Engineering at the University of Waterloo, Elizabeth Bevan, Judy Caron, Rose Guderian and Ingrid Sherrer, for their supports in my graduate study, life and CEGSA events.

Financial support from the Natural Sciences and Engineering Research Council (NSERC) of Canada, Strategic Project Program, Waterloo Institute for Nanotechnology (WIN) Fellowship, Ontario Graduate Scholarship (OGS), and TD Bank Graduate Scholarships in the Environment are gratefully appreciated.

I would also extend my acknowledgement to several fine gentlemen in Husky Energy, and they are Rodger Bernar, Ian Buchannan, Edward Choy and Sherwin Chase. Their mentorship, discussion and industrial engineering education through my daily work helped me refine the quality of this thesis.

Thank my parents, Genxin Jia and Bingxia Mu, who'd tried their best to raise me and encourage me to be independent and have the ambition to change my life. A special thanks to my brother and sister in law, Yi Jia and Yan Yan, without whom I may have to worry so much about my parents. I am also grateful to my parents in law, Xuyan Zhu and Xiaohong Lu, for treating me like their own son. Thank you for your efforts and accompanying for my root in China.

Finally and most importantly, I would like to thank my wife Wei Zhu. Her support, quiet patience and unwavering love were undeniably the bedrock upon which the past 3 years of my life have been built. Her tolerance of my occasional vulgar moods is a testament in itself of her unyielding devotion and love.

For Una, and her little brother on the way...

Abstract

Canada has a large reserve of oil sands bitumen which is highly viscous and contains high percentages of asphaltenes and heteroatoms. Currently hot water extraction or steam injection is used in recovering the bitumen as emulsions, which then requires extensive demulsification and water/oil separations. The separated water cannot be reused or disposed of without further purification; while the dewatered bitumen needs to be blended with diluent to meet pipeline transportation specifications. Due to this burdensome production process, production of bitumen from Canadian oil sands is extremely vulnerable to the extremely high capital costs, increased diluent transportation costs, constrained pipeline capacity and stricter environmental regulations. A single-stage emulsion upgrading process was developed by Flora T.T. Ng and her research group, where the emulsified water was directly activated using the water gas shift reaction (WGSR) to provide *in situ* H₂. Successful implementation of this novel process could reduce the water separation footprint, produce pipeline transportable oil without diluent and purify the emulsified water without massive water treatment before it could be used for hot water extraction or steam generation to recover the bitumen. Moreover, higher oil quality (like heteroatom removal, total acid number reduction, improved stability, etc.) would be obtained without building an expensive H₂ plant. The key to the process is the use of *in situ* H₂ and a nano unsupported MoS₂ based catalyst, which has been proven during the early-stage studies. In order to further improve the technology readiness for this novel emulsion upgrading process, a series of studies have been performed on three aspects of this process: *oil*, *water* and *catalysts*.

Previous research on this single stage bitumen upgrading process has focused on (a) the production and reactivity of *in situ* H₂; (b) the hydrotreating performance and mechanisms, such as hydrodesulfurization (HDS), hydrodenitrogenation (HDN), hydrodearomatization (HDA), etc. The main focus of this thesis is on the conversion of asphaltene in Cold Lake bitumen emulsion upgrading and the water purification feasibility validation during Athabasca bitumen upgrading. In addition, the reaction conditions were also studied to pursue improved liquid yield and less

hydrocarbon loss in order to maximize potential technology value with less capital and operational cost in future applications. During the investigation of this complex reaction system, process chemistry is discussed: like how the asphaltenes are converted, the effect of water, impact of catalysts.

Water purification was first proven feasible via the emulsion upgrading process, where the majority of metals deposited in the solid residue, and more than 90% of the organic acids were found removed from the actual oil sands process affected water (OSPW). Although we have reported in early emulsion upgrading studies that metal ions were removed from the water associated with the bitumen emulsion, there has been so far no report on the removal of naphthenic acids. This organic acid removal from OSPW observed in this present study indicated the potential removal capability of the most unwanted toxicity source, naphthenic acids, through emulsion upgrading from both oil and water phases. This thesis provides a detailed study on the removal of model compounds for naphthenic acids, such as 2-naphthoic acid and substituted benzoic acid, etc. A preliminary naphthenic acids removal reaction mechanism is proposed, where hydrodeoxygenation (HDO) was found to be the main reaction pathway. Effects of reaction conditions, promoter addition and co-existing hydrotreating reactions are also discussed. The results show that the naphthenic acids removal occurred during the emulsion upgrading process conditions, and added considerable synergy to emulsion upgrading technology with water treatment and corrosion prevention.

Nano unsupported catalysts involved in emulsion upgrading were also studied using advanced characterization methods. Effects of temperature, time, H₂ source and promoter are discussed. Some morphology-activity correlations were observed, and the *in situ* H₂ generated through the WGSR was found to produce shorter and less stacked MoS₂ (002) crystalline structures than externally supplied molecular H₂. It was also observed that the synergistic promotional behaviours of Co and Ni were not mainly dependent on the morphology changes; but instead, intrinsic activity changes probably played a more important role in Co and Ni promoted catalysts.

Table of Contents

List of Figures	xv
List of Tables	xxviii
Chapter 1 Challenge, Opportunity and Technology	1
1.1 Background.....	1
1.1.1 Canadian oil sands industry overview	1
1.1.2 Oil sands extraction methods.....	4
1.1.3 Pipeline transportation	8
1.2 Upgrading and partial upgrading	10
1.2.1 Upgrading	10
1.2.2 Partial Upgrading.....	20
1.2.3 Summary of existing/emerging full upgrading and partial upgrading processes	31
1.3 Novel emulsion upgrading technology	33
1.4 Objectives	34
Chapter 2 Experimental and Methodology	37
2.1 Feedstocks, catalyst precursors and reaction gases.....	37
2.1.1 Feedstocks.....	37
2.1.2 Catalyst precursor	38
2.1.3 Reaction gases.....	38
2.2 Autoclave reactor operation.....	38
2.2.1 Reactors.....	39
2.2.2 Run preparation.....	42
2.2.3 Sampling during reaction.....	44
2.2.4 Completion of the run	45

2.3 Product separation and collection after reaction.....	46
2.3.1 General product separation and collection.....	46
2.3.2 Asphaltenes separation.....	47
2.4 Basic analytical equations.....	49
2.4.1 Mass balance.....	49
2.4.2 Yield, WGSR conversion and water consumption.....	49
2.5 Product characterization.....	50
2.5.1 Oil analysis.....	50
2.5.2 Asphaltenes analysis.....	51
2.5.3 Coke and metal residue analysis.....	53
2.5.4 Gas analysis.....	54
2.5.5 Water analysis.....	54
2.6 Catalysts synthesis, collection and characterization.....	56
2.6.1 Synthesis of <i>in situ</i> catalyst and <i>ex situ</i> catalyst.....	56
2.6.2 Catalysts collection.....	56
2.6.3 Catalysts characterization.....	58
Chapter 3 Upgrading of Cold Lake Bitumen Emulsion through a Novel Emulsion Upgrading Process.....	60
3.1 Literature review.....	60
3.1.1 Cold Lake and Athabasca bitumen.....	60
3.1.2 Asphaltenes.....	61
3.1.3 Major processes in bitumen upgrading.....	64
3.1.4 WGSR during emulsion upgrading with model compounds.....	68
3.1.5 Feasibility study of Cold Lake bitumen emulsion upgrading.....	69
3.2 WGSR during Cold Lake bitumen emulsion upgrading.....	70

3.3 Evaluation of upgrading results	71
3.3.1 Effect of temperature	73
3.3.2 Effect of reaction time	77
3.3.3 Effect of reaction atmosphere	82
3.3.4 Effect of catalyst concentration	89
3.3.5 Effect of Ni as a promoter.....	92
3.4 Conclusions.....	96
Chapter 4 Upgrading of Athabasca Bitumen through a Novel Emulsion Upgrading Process	98
4.1 Introduction.....	98
4.2 Upgrading results and discussion.....	99
4.2.1 Significance of MoS ₂ catalyst and <i>in situ</i> H ₂	99
4.2.2 Effect of reaction time	102
4.2.3 Effect of water and the MoS ₂ catalyst.....	104
4.2.4 Effect of Ni as a promoter.....	108
4.2.5 Effect of reaction atmosphere by using Ni/MoS ₂ catalyst.....	110
4.2.6 Effect of V as an inhibitor.....	112
4.2.7 Deactivation investigation by using “soft solids” instead of fresh catalysts	114
4.3 Metal deposits and spent catalyst characterization	116
4.3.1 XRD analysis of deposited metals sulfides from Athabasca bitumen	116
4.3.2 SEM and elemental analysis of the spent catalysts from Athabasca bitumen upgrading	117
4.4 OSPW purification through novel process	119
4.4.1 Determination of anion and cation contents in OSPW	120
4.4.2 The OSPW purification performance	122
4.5 Conclusions.....	125

Chapter 5 Naphthenic Acids Removal in both Oil and Water Phases through a Novel Emulsion Upgrading Process	127
5.1 Literature review	127
5.2 Preliminary investigation	133
5.2.1 Model compound study for naphthenic acid removal.....	133
5.2.2 Elimination of carboxyl group in 2-NA through novel process	134
5.2.3 Characterization of 2-NA with HPLC	135
5.2.4 Characterization of 2-NA removal reaction products with GC-FID and GC-MS	136
5.2.5 Kinetic study for 2-NA removal	141
5.2.6 Proposed reaction mechanism for 2-NA removal.....	145
5.3 Results and discussion	147
5.3.1 Simultaneous WGS and 2-NA removal	147
5.3.2 Effect of reaction temperature	150
5.3.3 Effect of gas feed	154
5.3.4 Effect of catalysts.....	156
5.3.5 Effect of water.....	164
5.3.6 Simultaneous 2-NA removal and HDS of DBT with <i>in situ</i> H ₂	171
5.3.7 Simultaneous 2-NA removal and HDA of naphthalene (NAPH) with <i>in situ</i> H ₂	176
5.3.8 Effect of metal additives	181
5.3.9 C7-BA removal	188
5.3.10 Electron microscope characterization of spent MoS ₂ catalysts	190
5.4 Conclusions.....	192
Chapter 6 Characterization of the Catalysts used in LGO upgrading	195
6.1 Introduction.....	195
6.2 Literature review	195

6.2.1 Catalysts for HDS	195
6.2.2 Catalysts for HDA.....	199
6.2.3 Design of nano unsupported catalyst for bitumen upgrading	202
6.2.4 Regeneration and recycle of spent unsupported hydrotreating catalysts.....	205
6.3 Preliminary study of the catalyst morphology in LGO upgrading	208
6.4 XRD analysis of spent MoS ₂ catalysts from the LGO experiments	210
6.5 BET analysis of spent catalyst from LGO and C16 experiments	211
6.6 HRTEM analysis of spent Ni-MoS ₂ catalysts from LGO experiments	213
6.6.1 Crystalline structure and component of the spent Ni-MoS ₂ catalysts from LGO experiments.....	213
6.6.2 Reaction temperature effect on crystalline structure formation.....	216
6.6.3 Reaction time effect on crystalline structure formation.....	217
6.7 SEM analysis of C16 <i>ex situ</i> Ni-MoS ₂ catalysts and spent MoS ₂ based catalysts from the LGO experiments.....	219
6.7.1 C16 <i>ex situ</i> Ni-MoS ₂ vs. spent Ni-MoS ₂ from LGO experiments	219
6.7.2 Other unpromoted and promoted spent MoS ₂ catalysts from LGO experiments	228
6.8 Conclusions.....	232
Chapter 7 Effect of Preparation Conditions on the Morphology of Fresh Unsupported <i>Ex Situ</i> MoS₂ based Catalyst Synthesized in a Toluene/Water Emulsion	234
7.1 Introduction.....	234
7.2 Fresh <i>ex situ</i> MoS ₂ catalysts – proxy for <i>in situ</i> MoS ₂ catalysts.....	234
7.3 Statistical analysis of MoS ₂ catalysts slab structures by using HRTEM	236
7.4 Results and discussion	239
7.4.1 Effect of temperature	239
7.4.2 Effects of <i>In situ</i> H ₂ vs. molecular H ₂ on catalyst morphology	249
7.4.3 Effect of Co.....	254

7.4.4 Effect of Ni	258
7.5 Conclusions.....	273
Chapter 8 Conclusions and Recommendations.....	276
8.1 Conclusions.....	276
8.2 Process review and recommendations	278
Reference	281

List of Figures

Figure 1-1	US crude imports by country (compiled from US Energy Information Administration data)	1
Figure 1-2	Map of Western Canada oil sands reserves	3
Figure 1-3	Schematic of a mining process (Imperial-Oil).....	5
Figure 1-4	Schematic of a CSS process (Imperial-Oil).....	6
Figure 1-5	Scematic of SAGD process (Peacock 2010).....	7
Figure 1-6	Map of Canadian and US pipelines and refineries (CAPP 2013).....	8
Figure 1-7	Diagram of slurry reactor used in hydroconversion	15
Figure 1-8	Husky Lloydminster upgrader flow diagram (Husky-Energy 2011).....	17
Figure 1-9	Nexen Long Lake integrated SAGD and upgrading process flow diagram with OrCrude [®] technology (Birdgeneau 2008).....	18
Figure 1-10	Boiling point distribution of typical full upgrading process products (courtesy: CrudeMonitor.ca).....	19
Figure 1-11	Concept of partial upgrading integration with oil sands bitumen <i>in situ</i> production (Colyar 2010).....	21
Figure 1-12	Process flow diagram of I ^Y Q [®] process and the mechanism of the core fluidiazed coker (Brown and Monaghan 2011).....	24
Figure 1-13	Flow diagram of the HTL [®] process (Cabrera, Hillerman et al. 2012).....	26
Figure 1-14	Process flow diagram of the SCWC [®] process (JGC 2013).....	28
Figure 1-15	Process flow diagram of Hi-Q [®] process with material balance at operation of 1,500 bbl/day (MEG-Energy 2012, 2013)	30
Figure 1-16	Comparison of novel upgrading process and the current extracting and diluting process	34
Figure 2-1	Schematic of 300mL AISI SS-316 Autoclave batch reactor (Moll 1999).....	40
Figure 2-2	Experimental setup of Autoclave Engineers 300 ml HC-276 bolted closure Autoclave and sampling system (Choy 2009)	41
Figure 2-3	Schematic diagram of the 1L reactor's sampling system	42
Figure 2-4	General product separation and collection flow chart for bitumen upgrading experiments	47

Figure 2-5	Asphaltene separation and collection procedure following ASTM D2007-80.....	48
Figure 2-6	(a) n-pentane mixture stirring with a condensing system in a fume hood; (b) asphaltene solids collected after filtration	49
Figure 2-7	TGA example for calculating coke content in solid residue.....	54
Figure 2-8	Vacuum drying system for separating and collecting catalysts (Liu 2010).....	57
Figure 3-1	Proposed molecular structure of asphaltenes (Gray, Tykwinski <i>et al.</i> 2011).....	62
Figure 3-2	Scheme of HDS of DBT pathways using <i>in situ</i> H ₂ over unsupported Mo sulfide catalysts. Abbreviations: DBT - dibenzothiophene, BP - biphenyl, TH-DBT - tetrahydrodibenzothiophene, CHB - cyclohexylbenzene, DCH - dicyclohexyl) (Liu 2010)	65
Figure 3-3	Scheme of naphthalene hydrogenation (Broderick, Sapre <i>et al.</i> 1982)	67
Figure 3-4	Gas changes in WGSR with and without the HDS of DBT presence (Lee and Ng 2006)	69
Figure 3-5	Viscosity and API Gravity changes under different upgrading conditions (Moll 1999)	70
Figure 3-6	Gas changes in WGSR with simultaneous bitumen emulsion upgrading (415°C, 80g bitumen, 10g H ₂ O, 585psi CO, 15psi H ₂ S, 1408 ppmw Mo, 2 hours).....	71
Figure 3-7	Cold Lake bitumen emulsion before and after reaction. Highlight: upgraded oil formed stable meniscus over water for months. (405°C, 80g Cold Lake bitumen emulsion, 585psi CO, 15psi H ₂ S, 1408 ppmw Mo, 2 hours).....	72
Figure 3-8	Yield distribution of Cold Lake bitumen emulsion upgrading products at different reaction temperatures (80g Cold Lake bitumen emulsion, 585psi CO, 15psi H ₂ S, 1408 ppmw Mo, 2 hours)	74
Figure 3-9	S content (left), N:C and H:C ratios (right) of asphaltenes collected from Cold Lake bitumen emulsion upgrading experiments at different reaction temperatures (80g Cold Lake bitumen emulsion, 585psi CO, 15psi H ₂ S, 1408 ppmw Mo, 2 hours).....	76
Figure 3-10	GPC chromatographs of asphaltenes collected from Cold Lake bitumen emulsion upgrading experiments at different reaction temperatures (80g Cold Lake bitumen emulsion, 585psi CO, 15psi H ₂ S, 1408 ppmw Mo, 2 hours)	77
Figure 3-11	Yield distribution of Cold Lake bitumen emulsion upgrading products at different reaction times (405°C, 80g Cold Lake bitumen emulsion, 585psi CO, 15psi H ₂ S, 1408 ppmw Mo, 1-3 hours)	78

Figure 3-12	S content (left), N:C and H:C ratios (right) of asphaltenes collected from Cold Lake bitumen emulsion upgrading experiments at different reaction times (405°C, 80g Cold Lake bitumen emulsion, 585psi CO, 15psi H ₂ S, 1408 ppmw Mo, 1-3 hours)	80
Figure 3-13	FT-IR spectrums (with zoom-in region from 1500cm ⁻¹ to 1800 cm ⁻¹) of asphaltenes collected from Cold Lake bitumen emulsion upgrading experiments at different reaction times (405°C, 80g Cold Lake bitumen emulsion, 585psi CO, 15psi H ₂ S, 1408 ppmw Mo, 1-3 hours)	81
Figure 3-14	GPC chromatographs of asphaltenes collected from Cold Lake bitumen emulsion upgrading experiments at different reaction times (405°C, 80g Cold Lake bitumen emulsion, 585psi CO, 15psi H ₂ S, 1408 ppmw Mo, 1-3 hours)	82
Figure 3-15	Yield distribution of Cold Lake bitumen emulsion upgrading products at different reaction atmospheres (405°C, 80g Cold Lake bitumen emulsion, 585psi feed gas, 15psi H ₂ S, 1408 ppmw Mo, 2 hours)	83
Figure 3-16	S content (left), N:C and H:C ratios (right) of asphaltenes collected from Cold Lake bitumen emulsion upgrading experiments at different reaction atmospheres (405°C, 80g Cold Lake bitumen emulsion, 585psi feed gas, 15psi H ₂ S, 1408 ppmw Mo, 2 hours)	85
Figure 3-17	GPC chromatographs of asphaltenes collected from Cold Lake bitumen emulsion upgrading experiments at different reaction atmospheres (405°C, 80g Cold Lake bitumen emulsion, 585psi feed gas, 15psi H ₂ S, 1408 ppmw Mo, 2 hours)	86
Figure 3-18	Weight loss curves (dashed) and heat flow curve (solid) during the oxidation of asphaltenes collected from Cold Lake bitumen emulsion upgrading experiments at different reaction atmospheres (405°C, 80g Cold Lake bitumen emulsion, 585psi feed gas, 15psi H ₂ S, 1408 ppmw Mo, 2 hours).....	87
Figure 3-19	Metal contents in asphaltenes collected from Cold Lake bitumen emulsion upgrading experiments at different reaction atmospheres (405°C, 80g Cold Lake bitumen emulsion, 585psi feed gas, 15psi H ₂ S, 1408 ppmw Mo, 2 hours)	88
Figure 3-20	Metal balance during the upgrading under different reaction atmospheres (405°C, 80g Cold Lake bitumen emulsion, 585psi feed gas, 15psi H ₂ S, 1408 ppmw Mo, 2 hours)	89
Figure 3-21	Yield distribution of Cold Lake bitumen emulsion upgrading products at different Mo concentrations (405°C, 80g Cold Lake bitumen emulsion, 585psi CO, 15psi H ₂ S, 2 hours)	90

Figure 3-22	S content (left), N:C and H:C ratios (right) of asphaltenes collected from Cold Lake bitumen emulsion upgrading experiments at different Mo concentrations (405°C, 80g Cold Lake bitumen emulsion, 585psi CO, 15psi H ₂ S, 2 hours)	91
Figure 3-23	GPC chromatographs of asphaltenes collected from Cold Lake bitumen emulsion upgrading experiments at different Mo concentrations (405°C, 80g Cold Lake bitumen emulsion, 585psi CO, 15psi H ₂ S, 2 hours)	92
Figure 3-24	Yield distribution of Cold Lake bitumen emulsion upgrading products with and without Ni as a promoter (405°C, 80g Cold Lake bitumen emulsion, 585psi CO, 15psi H ₂ S, 1408ppmw Mo, Ni:Mo=0.6, 2 hours).....	93
Figure 3-25	S content (left), N:C and H:C ratios (right) of asphaltenes collected from Cold Lake bitumen emulsion upgrading experiments with and without Ni as a promoter (405°C, 80g Cold Lake bitumen emulsion, 585psi CO, 15psi H ₂ S, 1408ppmw Mo, Ni:Mo=0.6, 2 hours).....	95
Figure 3-26	GPC chromatographs of asphaltenes collected from Cold Lake bitumen emulsion upgrading experiments with and without Ni as a promoter (405°C, 80g Cold Lake bitumen emulsion, 585psi CO, 15psi H ₂ S, 1408ppmw Mo, Ni:Mo=0.6, 2 hours).....	95
Figure 4-1	Dirty water (OSPW or PAW) and the purified water after emulsion upgrading (415°C, 80g Athabasca bitumen, 10mL OSPW, 585psi CO, 15psi H ₂ S, 1408ppmw Mo, 2 hours)	99
Figure 4-2	Yield distribution of Athabasca bitumen upgrading products with N ₂ only, MoS ₂ +molecular H ₂ and MoS ₂ + <i>in situ</i> H ₂ (415°C, 80g Athabasca bitumen, no OSPW, 585psi feed gas, 15psi H ₂ S, 0 or 1408ppmw Mo, 2 hours)	100
Figure 4-3	Pressure changes during reaction with N ₂ only, MoS ₂ +molecular H ₂ and MoS ₂ + <i>in situ</i> H ₂ (415°C, 80g Athabasca bitumen, no OSPW, 585psi feed gas, 15psi H ₂ S, 0 or 1408ppmw Mo, 2 hours)	102
Figure 4-4	Yield distribution of Athabasca bitumen upgrading products at different reaction times (415°C, 80g Athabasca bitumen, 5mL OSPW, 585psi CO, 15psi H ₂ S, 1408ppmw Mo, 1-2 hours)	103
Figure 4-5	Yield distribution of Athabasca bitumen upgrading products at different OSPW loadings with and without MoS ₂ (415°C, 80g Athabasca bitumen, 0 or 10mL OSPW, 585psi CO, 15psi H ₂ S, 0 or 1408ppmw Mo, 2 hours)	105

Figure 4-6	Yield distribution of Athabasca bitumen upgrading products with and without Ni as promoter (415°C, 80g Athabasca bitumen, 5 or 10 mL OSPW, 585psi CO, 15psi H ₂ S, 1408ppmw Mo, Ni:Mo=0.6, 2 hours).....	108
Figure 4-7	Yield distribution of Athabasca bitumen upgrading products under different reaction atmospheres by using Ni/MoS ₂ catalyst (415°C, 80g Athabasca bitumen, 5mL OSPW, 585psi feed gas, 15psi H ₂ S, 1408ppmw Mo, Ni:Mo=0.6, 2 hours).....	110
Figure 4-8	Yield distribution of Athabasca bitumen upgrading products with and without V for Ni/MoS ₂ catalyst (415°C, 80g Athabasca bitumen, 10mL OSPW, 585psi CO, 15psi H ₂ S, 1408ppmw Mo, Ni:Mo=0.6, V:Mo=0.6, 2 hours).....	112
Figure 4-9	Yield distribution of Athabasca bitumen upgrading products by using fresh catalyst and “soft solid” (415°C, 80g Athabasca bitumen, 5mL OSPW, 585psi CO, 15psi H ₂ S, 1408ppmw Mo, 2 hours).....	114
Figure 4-10	XRD pattern for metal sulfides deposits product in reaction without catalyst precursor loading	117
Figure 4-11	SEM images of the same area of the spent MoS ₂ catalysts from bitumen experiments under 10000 times magnification from SE2 detector (left) and BSD detector (right)	118
Figure 4-12	SEM images of the spent MoS ₂ catalysts from bitumen experiments under 139470 times (left) and 348220 times (right) magnification from SE2 detector.....	118
Figure 4-13	SEM image of the spent MoS ₂ catalysts from bitumen experiments under 1000 times magnification from BSD detector and atomic ratio calculated from EDX data in red square.	119
Figure 4-14	Calibration curve examples of sulfate in IC (left) and V in ICP (right).....	120
Figure 4-15	IC chromatograph of feedstock water at 500 dilution times	121
Figure 5-1	Publications trends on naphthenic acids (generated by Sci-Finder).....	128
Figure 5-2	Corrosion caused by naphthenic acid in downstream refineries.....	131
Figure 5-3	Common model compounds in naphthenic acid research.....	133
Figure 5-4	FT-IR spectrums of 2-NA feed and product in toluene solution (415°C, 80ml toluene, 10ml water, 15psi H ₂ S, 585psi CO, ~1641ppmw 2-NA in toluene, 673ppmw Mo, 2hours)	135
Figure 5-5	HPLC chromatograph and calibration curve for 2-NA.....	136

Figure 5-6	Example of GC-MS library identification of unknown chemicals	137
Figure 5-7	Example of GC-MS library identification of unknown chemicals	138
Figure 5-8	Identification of 2-NA removal products with GC-FID	139
Figure 5-9	Calibration curves for 2-NA, benzoic acid and C7-BA test in GC-FID.....	140
Figure 5-10	Mole percentage changes during the 2-NA removal reaction (300°C, 80ml toluene, 10ml water, 15psi H ₂ S, 585psi CO, ~1641ppmw 2-NA in toluene, 673ppmw Mo, 2hours)	141
Figure 5-11	Plot of ln([2-NA] ₀ /[2-NA] _t) values with time (300°C, 80ml toluene, 10ml water, 15psi H ₂ S, 585psi CO, ~1641ppmw 2-NA in toluene, 673ppmw Mo, 2hours)	143
Figure 5-12	Plot of sum of [product]/[2-NA] ₀ *(-k _{2-NA removal}) values with time (300°C, 80ml toluene, 10ml water, 15psi H ₂ S, 585psi CO, ~1641ppmw 2-NA in toluene, 673ppmw Mo, 2hours)	144
Figure 5-13	Proposed reaction mechanism for 2-NA removal: (a) decarboxylation and consecutive chain hydrogenation reactions; (b) hydrodeoxygenation and consecutive chain hydrogenation reactions; (c) cracking.....	146
Figure 5-14	(a) Mole percentage of each gas component during simultaneous WGSR and 2-NA removal; (b) Plots of ln([CO] ₀ /[CO] _t) values with time with and without 2-NA (340°C, 80ml toluene, 10ml water, 15psi H ₂ S, 585psi CO, ~1641ppmw 2-NA in toluene, 673ppmw Mo, 2hours)	148
Figure 5-15	(a) WGSR conversion during WGSR with and without 2-NA; (b) H ₂ partial pressure with time (340°C, 80ml toluene, 10ml water, 15psi H ₂ S, 585psi CO, ~1641ppmw 2-NA in toluene, 673ppmw Mo, 2hours).....	149
Figure 5-16	Reaction oil phase evaluation at different reaction temperatures: (a) 2-NA conversion with time; (b) Product distribution at 120 min. (80ml toluene, 10ml water, 15psi H ₂ S, 585psi CO, ~1641ppmw 2-NA in toluene, 673ppmw Mo, 2hours)	151
Figure 5-17	Reaction oil phase evaluation with different gas feeds: (a) 2-NA conversion with time; (b) Benzoic acid mole percentage with time (300°C, 80ml toluene, 10ml water, 15psi H ₂ S, 585psi gas feed, ~1641ppmw 2-NA in toluene, 673ppmw Mo, 2hours).....	154
Figure 5-18	Reaction oil and gas phases evaluation with different catalysts: (a) 2-NA conversion with time; (b) WGSR conversion with time (300°C, 80ml toluene, 10ml water, 15psi	

H₂S if added, 600psi total pressure, CO as gas feed, ~1641ppmw 2-NA in toluene, 337ppmw Mo, 2hours) 157

Figure 5-19 Reaction oil and gas phases evaluation at different MoS₂ loadings: (a) 2-NA conversion with time; (b) WGS conversion with time. (300°C, 80ml toluene, 10ml water, 15psi H₂S, 585psi CO, ~1641ppmw 2-NA in toluene, 0~673ppmw Mo, 2hours)..... 159

Figure 5-20 2-NA conversion with time by using different catalysts under H₂ (300°C, 80ml toluene, 10ml water, 15psi H₂S if added, 600psi total pressure, H₂ as gas feed, ~1641ppmw 2-NA in toluene, 337ppmw Mo, 2hours) 161

Figure 5-21 2-NA conversion with and without MoS₂ addition under N₂ (300°C, 80ml toluene, 10ml water, 15psi H₂S, 585psi N₂, ~1641ppmw 2-NA in toluene, 337ppmw Mo, 2hours) 163

Figure 5-22 Reaction oil and gas phases evaluation at different water loadings under CO: (a) 2-NA conversion with time; (b) WGS conversion with time (300°C, 80ml toluene, 10~20ml water, 15psi H₂S, 585psi CO, ~1641ppmw 2-NA in toluene, 673ppmw Mo, 2hours) 165

Figure 5-23 Reaction oil evaluation at different water loadings under N₂: (a) 2-NA conversion with time; (b) Benzoic acid mol percentage with time (300°C, 80ml toluene, 10~20ml water, 15psi H₂S, 585psi N₂, ~1641ppmw 2-NA in toluene, 673ppmw Mo, 2hours)..... 168

Figure 5-24 Effect of water under CO and N₂: (a) yield of HDO products; (b) reaction rate constants; (c) final product distribution (300°C, 80ml toluene, 10~20ml water, 15psi H₂S, 585psi CO or N₂, ~1641ppmw 2-NA in toluene, 673ppmw Mo, 2hours) 169

Figure 5-25 Reaction oil evaluation with and without DBT addition: (a) 2-NA conversion with time at 300°C; (b) 2-NA conversion with time at 340°C; (c) DBT conversion with time at 300°C; (d) DBT conversion with time at 340°C (300~340°C, 80ml toluene, 10ml water, 15psi H₂S, 585psi CO, ~1641ppmw 2-NA, ~5000ppmw DBT, 337ppmw Mo, 2~3hours) 172

Figure 5-26 Kinetic analysis of HDS of DBT with and without 2-NA addition at 340°C: (a) HDS of DBT with simultaneous 2-NA removal; (b) HDS of only DBT (340°C, 80ml toluene, 10ml water, 15psi H₂S, 585psi CO, ~1641ppmw 2-NA, ~5000ppmw DBT, 337ppmw Mo, 2hours) 174

Figure 5-27 Reaction oil evaluation with and without NAPH addition: (a) 2-NA conversion with time at 300°C; (b) NAPH conversion with time at 300°C; (c) NAPH conversion with time at

320°C (300~320°C, 80ml toluene, 10ml water, 15psi H ₂ S, 585psi CO, ~1641ppmw 2-NA, ~5000ppmw NAPH, 337ppmw Mo, 2hours).....	177
Figure 5-28 Kinetic analysis of HDA of NAPH with and without 2-NA addition at 320°C: (a) HDA of NAPH with simultaneous 2-NA removal; (b) HDA of only NAPH (320°C, 80ml toluene, 10ml water, 15psi H ₂ S, 585psi CO, ~1641ppmw 2-NA, ~5000ppmw NAPH, 337ppmw Mo, 2hours)	178
Figure 5-29 Reaction oil and gas phases evaluation with different metal additives under CO: (a) 2-NA conversion with time; (b) WGS conversion with time; (c) rate constants for different pathways of 2-NA removal and WGS (300°C, 80ml toluene, 10ml water, 15psi H ₂ S, 585psi CO, ~1641ppmw 2-NA in toluene, 673ppmw Mo, metal:Mo ratio=0.2, 2hours)	182
Figure 5-30 Plots of $\ln([2\text{-NA}]_0/[2\text{-NA}]_t)$ or $\ln([2\text{-NA}]_0/[2\text{-NA}]_t)/[\text{H}_2]$ values with time: (a) Mo pseudo-first order rate plotting; (b) Mo pseudo-first order rate plotting with [H ₂] adjustment; (c) Co-Mo pseudo-first order rate plotting; (d) Co-Mo pseudo-first order rate plotting with [H ₂] adjustment; (e) Ni-Mo pseudo-first order rate plotting; (f) Ni-Mo pseudo-first order rate plotting with [H ₂] adjustment;.....	185
Figure 5-31 C7-BA conversion change with time with different gas feeds compared to the reaction without catalyst under CO (300°C, 80ml toluene, 10ml water, 15psi H ₂ S, 585psi gas feed, 5224ppmw C7-BA in toluene, 377ppmw Mo, 2hours)	188
Figure 5-32 GC-MS chromatographs of C7-BA removal product collected at 120min (300°C, 80ml toluene, 10ml water, 15psi H ₂ S, 585psi gas feed, 5224ppmw C7-BA in toluene, 377ppmw Mo, 2hours)	189
Figure 5-33 Electron microscope images of spent MoS ₂ catalysts: (a) TEM image at low magnification, (b) HRTEM image with high magnification, and (c) STEM image at high magnification (340°C, 80ml toluene, 10ml water, 15psi H ₂ S, 585psi CO, ~1641ppmw 2-NA, 673ppmw Mo, 2hours).....	191
Figure 6-1 Intrinsic activities (A _i in ordinate) of transition metal sulfides for the hydrodesulphurization of dibenzothiophene (HDS of DBT) at 530 K. (Lacroix, Boutarfa <i>et al.</i> 1989)	196
Figure 6-2 MoS ₂ structures involved in the HDS of thiophene and the schematic overview of the reactions (Besenbacher, Brorson <i>et al.</i> 2008)	197

Figure 6-3	Electron orbits and occupation of different transition promoters. (Harris and Chianelli 1986).....	198
Figure 6-4	High-angle annular dark-field scanning transmission electron microscopy (HAADF-STEM) images and DFT simulation of unpromoted, Co-promoted and Ni-promoted MoS ₂ catalysts (Besenbacher, Brorson <i>et al.</i> 2008).....	199
Figure 6-5	The proposed new concept “LT-HAD” for catalyst design based on shape-selective exclusion, H ₂ spillover, and two types of sulfur resistance. The black dots indicate metal particles on internal surface (Song 2003).....	200
Figure 6-6	Intrinsic activities (A _i in ordinate) of transition metal sulfides for the hydrogenation of biphenyl (HDA of BP) at 530 K. (Lacroix, Boutarfa <i>et al.</i> 1989).....	201
Figure 6-7	Simplified process scheme of the Eurecat regeneration process (Marafi and Stanislaus 2002).....	208
Figure 6-8	XRD patterns of unpromoted MoS ₂ catalysts and MoS ₂ catalysts with different metal additives derived from LGO experiments (391°C, 100ml LGO, 10ml water, 10psi H ₂ S, 590psi CO, 1408ppmw Mo, Metal:Mo=0.6, 2hours).....	210
Figure 6-9	Langmuir adsorption and desorption isotherm curve and BET surface area plot examples (for NiMoS ₂ catalyst prepared in C16: 390°C, 300ml C16, 30ml water, 30psi H ₂ S, 570psi CO, 1408ppmw Mo, Ni:Mo=0.6, 2hours).....	211
Figure 6-10	TEM images of the spent Ni-MoS ₂ catalysts from LGO experiments at low resolution (390°C, 300ml LGO, 30ml water, 30psi H ₂ S, 570psi CO, 1408ppmw Mo, Ni:Mo=0.6, 2hours)	213
Figure 6-11	HRTEM images and EDX spectrum of the spent Ni-MoS ₂ catalysts from LGO experiments at high resolution (390°C, 300ml LGO, 30ml water, 30psi H ₂ S, 570psi CO, 1408ppmw Mo, Ni:Mo=0.6, 2hours).....	215
Figure 6-12	TEM (left) and HRTEM (right) images of the spent Ni-MoS ₂ catalysts from LGO experiments at different reaction temperatures (100°C and 200°C, 300ml LGO, 30ml water, 30psi H ₂ S, 570psi CO, 1408ppmw Mo, Ni:Mo=0.6).....	216
Figure 6-13	TEM (left) and HRTEM (right) images of the spent Ni-MoS ₂ catalysts from LGO experiments at different reaction temperatures (300°C and 390°C, 300ml LGO, 30ml water, 30psi H ₂ S, 570psi CO, 1408ppmw Mo, Ni:Mo=0.6).....	217

Figure 6-14	HRTEM images of the spent Ni-MoS ₂ catalysts from LGO experiments at 0min (top) and 120min (bottom) (390°C, 300ml LGO, 30ml water, 30psi H ₂ S, 570psi CO, 1408ppmw Mo, Ni:Mo=0.6, 0min and 120min)	218
Figure 6-15	SEM images of <i>ex situ</i> Ni-MoS ₂ catalysts in C16 under 10000 times magnification from SE2 detector (left) and BSD detector (right) (390°C, 300ml C16, 30ml water, 30psi H ₂ S, 570psi CO, 1408ppmw Mo, Ni:Mo=0.6, 2hours)	219
Figure 6-16	SEM images of <i>ex situ</i> Ni-MoS ₂ catalysts in C16 under 20000 times magnification from SE2 detector (left) and BSD detector (right) (390°C, 300ml C16, 30ml water, 30psi H ₂ S, 570psi CO, 1408ppmw Mo, Ni:Mo=0.6, 2hours)	220
Figure 6-17	SEM images of <i>ex situ</i> Ni-MoS ₂ catalysts in C16 under 50000 times magnification from SE2 detector (left) and BSD detector (right) (390°C, 300ml C16, 30ml water, 30psi H ₂ S, 570psi CO, 1408ppmw Mo, Ni:Mo=0.6, 2hours)	221
Figure 6-18	EDX analysis images of <i>ex situ</i> Ni-MoS ₂ catalysts in C16: (a) and (b) top two- from left to right; (c) bottom (390°C, 300ml C16, 30ml water, 30psi H ₂ S, 570psi CO, 1408ppmw Mo, Ni:Mo=0.6, 2hours).....	222
Figure 6-19	SEM images of the spent Ni-MoS ₂ catalyst from LGO experiments under 200 times magnification from SE2 detector (left) and BSD detector (right) (390°C, 300ml LGO, 30ml water, 30psi H ₂ S, 570psi CO, 1408ppmw Mo, Ni:Mo=0.6, 2hours).....	223
Figure 6-20	SEM image of the spent Ni-MoS ₂ catalyst from LGO experiments under 100000 (left) and 50000 times (right) magnification from SE2 detector (390°C, 300ml LGO, 30ml water, 30psi H ₂ S, 570psi CO, 1408ppmw Mo, Ni:Mo=0.6, 2hours)	224
Figure 6-21	SEM image of the cokes existing in the spent Ni-MoS ₂ catalyst from LGO experiments under 10000 (top left) and 139000 (top right) times magnification from SE2 detector, 80000 times magnification from BSD detector (bottom) (390°C, 300ml LGO, 30ml water, 30psi H ₂ S, 570psi CO, 1408ppmw Mo, Ni:Mo=0.6, 2hours).....	225
Figure 6-22	SEM image of cokes and the spent Ni-MoS ₂ catalyst from LGO experiments under 10000 times magnification from BSD detector (390°C, 300ml LGO, 30ml water, 30psi H ₂ S, 570psi CO, 1408ppmw Mo, Ni:Mo=0.6, 2hours)	226
Figure 6-23	EDX analysis image of the cokes and the spent Ni-MoS ₂ catalyst from LGO experiments (390°C, 300ml LGO, 30ml water, 30psi H ₂ S, 570psi CO, 1408ppmw Mo, Ni:Mo=0.6, 2hours)	227

Figure 6-24	SEM images of the spent MoS ₂ catalysts from LGO experiments under 100000 times magnification from SE2 detector (391°C, 100ml LGO, 10ml water, 10psi H ₂ S, 590psi CO, 1408ppmw Mo, 2hours).....	228
Figure 6-25	SEM images of the spent Co-MoS ₂ catalysts from LGO experiments under 100000 times magnification from SE2 detector (left) and BSD detector (right) (391°C, 100ml LGO, 10ml water, 10psi H ₂ S, 590psi CO, 1408ppmw Mo, Co:Mo=0.6, 2hours)	229
Figure 6-26	EDX analysis images of the spent Co-MoS ₂ catalysts from LGO experiments in different areas (391°C, 100ml LGO, 10ml water, 10psi H ₂ S, 590psi CO, 1408ppmw Mo, Co:Mo=0.6, 2hours).....	230
Figure 6-27	SEM images of the spent Fe-MoS ₂ catalysts from LGO experiments under 200000 times magnification from BSD detector (391°C, 100ml LGO, 10ml water, 10psi H ₂ S, 590psi CO, 1408ppmw Mo, Fe:Mo=0.6, 2hours).....	231
Figure 6-28	SEM images of the spent V-MoS ₂ catalysts from LGO experiments under 50000 times magnification from SE2 detector (top left) and BSD detector (top right); SEM images of LGO-tested V-MoS ₂ catalysts under 100000 times magnification from SE2 detector (bottom) (391°C, 100ml LGO, 10ml water, 10psi H ₂ S, 590psi CO, 1408ppmw Mo, V:Mo=0.6, 2hours).....	232
Figure 7-1	Analysis of HRTEM image by using <i>Digital Micrograph</i> software	238
Figure 7-2	TEM (left) and HRTEM (right) images of the fresh <i>ex situ</i> MoS ₂ catalysts collected at different temperatures under H ₂	241
Figure 7-3	Slab length distributions (0.2nm incremented in big chart; 1nm incremented in small chart) of fresh <i>ex situ</i> MoS ₂ catalysts prepared with under H ₂ collected at different temperatures	242
Figure 7-4	Stacking number distributions (distribution curve in small chart) of fresh <i>ex situ</i> MoS ₂ catalysts prepared with under H ₂ collected at different temperatures	243
Figure 7-5	TEM (left) and HRTEM (right) images of the fresh <i>ex situ</i> MoS ₂ catalysts collected at different temperatures under CO.....	246
Figure 7-6	Slab length distributions (0.2nm incremented in big chart; 1nm incremented in small chart) of fresh <i>ex situ</i> MoS ₂ catalysts prepared with under CO collected at different temperatures	247
Figure 7-7	Stacking number distributions (distribution curve in small chart) of fresh <i>ex situ</i> MoS ₂ catalysts prepared with under CO collected at different temperatures	248

Figure 7-8	Slab length distributions (0.2nm incremented) of fresh <i>ex situ</i> MoS ₂ catalysts prepared with <i>in situ</i> H ₂ and molecular H ₂ collected at different temperatures.....	251
Figure 7-9	Stacking number distributions of fresh <i>ex situ</i> MoS ₂ catalysts prepared with <i>in situ</i> H ₂ and molecular H ₂ collected at different temperatures.....	252
Figure 7-10	TEM (left) and HRTEM (right) images of the fresh <i>ex situ</i> Co-MoS ₂ catalysts with different Co:Mo ratios collected at 390°C under CO	255
Figure 7-11	Slab length distributions (0.2nm incremented in big chart; 1nm incremented in small chart) of fresh <i>ex situ</i> Co-MoS ₂ catalysts with different Co:Mo ratios collected at 390°C under CO	256
Figure 7-12	Stacking number distributions (distribution curve in small chart) of fresh <i>ex situ</i> Co-MoS ₂ catalysts with different Co:Mo ratios collected at 390°C under CO	257
Figure 7-13	TEM (left) and HRTEM (right) images of the fresh <i>ex situ</i> Ni-MoS ₂ catalysts with different Ni:Mo ratios collected at 390°C under CO	259
Figure 7-14	Slab length distributions (0.2nm incremented in big chart; 1nm incremented in small chart) of fresh <i>ex situ</i> Ni-MoS ₂ catalysts with different Ni:Mo ratios collected at 390°C under CO	261
Figure 7-15	Stacking number distributions (distribution curve in small chart) of fresh <i>ex situ</i> Ni-MoS ₂ catalysts with different Ni:Mo ratios collected at 390°C under CO.....	262
Figure 7-16	TEM (left) and HRTEM (right) images of the fresh <i>ex situ</i> Ni-MoS ₂ catalysts with different Ni:Mo ratios collected at 340°C under CO	266
Figure 7-17	Slab length distributions (0.2nm incremented in big chart; 1nm incremented in small chart) of fresh <i>ex situ</i> Ni-MoS ₂ catalysts with different Ni:Mo ratios collected at 340°C under CO	267
Figure 7-18	Stacking number distributions (distribution curve in small chart) of fresh <i>ex situ</i> Ni-MoS ₂ catalysts with different Ni:Mo ratios collected at 340°C under CO.....	268
Figure 7-19	TEM (left) and HRTEM (right) images of the fresh <i>ex situ</i> Ni-MoS ₂ catalysts with different Ni:Mo ratios collected at 300°C under CO	269
Figure 7-20	Slab length distributions (0.2nm incremented in big chart; 1nm incremented in small chart) of fresh <i>ex situ</i> Ni-MoS ₂ catalysts with different Ni:Mo ratios collected at 300°C under CO	270

Figure 7-21 Stacking number distributions (distribution curve in small chart) of fresh *ex situ* Ni-MoS₂ catalysts with different Ni:Mo ratios collected at 300°C under CO..... 271

List of Tables

Table 1-1	Oil sands reserves as of Dec 31, 2011 in units of billion barrels (BMO-Capital-Market 2013) ²	
Table 1-2	Typical Canadian oil sands bitumen crude properties (Selucky, Ruo <i>et al.</i> 1977, Selucky, Chu <i>et al.</i> 1977, 1978).....	4
Table 1-3	Example of Alberta oil sands bitumen valuation methodology (CAPP 2013).....	9
Table 1-4	Current residue upgrading processes (Rana, Sámano <i>et al.</i> 2007)	12
Table 1-5	Qualities of typical full upgrading process products (courtesy: Crude Monitor.ca)	19
Table 1-6	Comparison of selected partial upgrading and full upgrading technologies.....	31
Table 2-1	Grades and purities of major reaction gases.....	38
Table 2-2	Reactors used in this thesis for different purposes.....	39
Table 2-3	Summary of reaction conditions in different reactors.....	44
Table 3-1	Blending inspections of oil sands bitumen dilbit products (data compiled from Crude Monitor)	60
Table 3-2	Ni and V in asphaltene derived from a Canadian heavy crude (Semple, Phillip <i>et al.</i> 1990)	61
Table 3-3	Aromatics distribution in various distillates (Cooper and Donnis 1996)	66
Table 3-4	Cold Lake bitumen emulsion upgrading performance at different reaction temperatures (80g Cold Lake bitumen emulsion, 585psi CO, 15psi H ₂ S, 1408 ppmw Mo, 2 hours)	75
Table 3-5	Cold Lake bitumen emulsion upgrading performance at different reaction times (405°C, 80g Cold Lake bitumen emulsion, 585psi CO, 15psi H ₂ S, 1408 ppmw Mo, 1-3 hours)	79
Table 3-6	Cold Lake bitumen emulsion upgrading performance at different reaction atmospheres (405°C, 80g Cold Lake bitumen emulsion, 585psi feed gas, 15psi H ₂ S, 1408 ppmw Mo, 2 hours)	84
Table 3-7	Cold Lake bitumen emulsion upgrading performance at different Mo concentrations (405°C, 80g Cold Lake bitumen emulsion, 585psi CO, 15psi H ₂ S, 2 hours)	91
Table 3-8	Cold Lake bitumen emulsion upgrading performance with and without Ni as a promoter (405°C, 80g Cold Lake bitumen emulsion, 585psi CO, 15psi H ₂ S, 1408ppmw Mo, Ni:Mo=0.6, 2 hours)	94

Table 4-1 Athabasca bitumen upgrading performance with N ₂ only, MoS ₂ +molecular H ₂ and MoS ₂ + <i>in situ</i> H ₂ (415°C, 80g Athabasca bitumen, no OSPW, 585psi feed gas, 15psi H ₂ S, 0 or 1408ppmw Mo, 2 hours).....	101
Table 4-2 Athabasca bitumen upgrading performance at different reaction times (415°C, 80g Athabasca bitumen, 5mL OSPW, 585psi CO, 15psi H ₂ S, 1408ppmw Mo, 1-2 hours).....	104
Table 4-3 Athabasca bitumen upgrading performance at different OSPW loadings with and without MoS ₂ (415°C, 80g Athabasca bitumen, 0 or 10mL OSPW, 585psi CO, 15psi H ₂ S, 0 or 1408ppmw Mo, 2 hours).....	106
Table 4-4 Athabasca bitumen upgrading performance with and without Ni as promoter (415°C, 80g Athabasca bitumen, 5 or 10 mL OSPW, 585psi CO, 15psi H ₂ S, 1408ppmw Mo, Ni:Mo=0.6, 2 hours)	109
Table 4-5 Athabasca bitumen upgrading performance under different reaction atmospheres by using Ni/MoS ₂ catalyst (415°C, 80g Athabasca bitumen, 5mL OSPW, 585psi feed gas, 15psi H ₂ S, 1408ppmw Mo, Ni:Mo=0.6, 2 hours)	111
Table 4-6 Athabasca bitumen upgrading performance with and without V for Ni/MoS ₂ catalyst (415°C, 80g Athabasca bitumen, 10mL OSPW, 585psi CO, 15psi H ₂ S, 1408ppmw Mo, Ni:Mo=0.6, V:Mo=0.6, 2 hours).....	113
Table 4-7 Athabasca bitumen upgrading performance by using fresh catalyst and “soft solid” (415°C, 80g Athabasca bitumen, 5mL OSPW, 585psi CO, 15psi H ₂ S, 1408ppmw Mo, 2 hours)	115
Table 4-8 Concentrations of metal cations and some inorganic anions in the OSPW before and after emulsion upgrading (415°C, 80g Athabasca bitumen, 10mL OSPW, 585psi N ₂ or CO, 15psi H ₂ S, 0 or 1408ppmw Mo, Ni:Mo=0.6, 2 hours)	123
Table 4-9 Removal of cations and anions in the OSPW after emulsion upgrading (415°C, 80g Athabasca bitumen, 10mL OSPW, 585psi N ₂ or CO, 15psi H ₂ S, 0 or 1408ppmw Mo, Ni:Mo=0.6, 2 hours)	124
Table 5-1 List of Naphthenic acid concentration in different water samples by FT-IR and GC-MS (Grewer, Young <i>et al.</i> 2010)	129
Table 5-2 WGSR, HDS of DBT, 2-NA removal in both oil and water phases (415°C, 80ml toluene, 10ml water, 15psi H ₂ S, 585psi CO, ~1641ppmw 2-NA in toluene, 5000ppmw DBT, 673ppmw Mo, 2hours).....	147

Table 5-3 Comparison of WGSR with simultaneous WGSR and 2-NA removal (340°C, 80ml toluene, 10ml water, 15psi H ₂ S, 585psi CO, ~1641ppmw 2-NA in toluene, 673ppmw Mo, 2hours)	150
Table 5-4 Summary of effect of temperature on 2-NA removal (80ml toluene, 10ml water, 15psi H ₂ S, 585psi CO, ~1641ppmw 2-NA in toluene, 673ppmw Mo, 2hours)	153
Table 5-5 Summary of effect of gas feed on 2-NA removal (300°C, 80ml toluene, 10ml water, 15psi H ₂ S, 585psi gas feed, ~1641ppmw 2-NA in toluene, 673ppmw Mo, 2hours)	156
Table 5-6 Summary of effect of catalyst under CO on 2-NA removal (300°C, 80ml toluene, 10ml water, 15psi H ₂ S if added, 600psi total pressure, CO as gas feed, ~1641ppmw 2-NA in toluene, 337ppmw Mo, 2hours)	158
Table 5-7 Summary of effect of MoS ₂ loading under CO on 2-NA removal (300°C, 80ml toluene, 10ml water, 15psi H ₂ S, 585psi CO, ~1641ppmw 2-NA in toluene, 0~673ppmw Mo, 2hours)	160
Table 5-8 Summary of effect of catalyst under H ₂ on 2-NA removal (300°C, 80ml toluene, 10ml water, 15psi H ₂ S if added, 600psi total pressure, H ₂ as gas feed, ~1641ppmw 2-NA in toluene, 337ppmw Mo, 2hours)	162
Table 5-9 Summary of MoS ₂ catalyst addition on 2-NA removal under N ₂ (300°C, 80ml toluene, 10ml water, 15psi H ₂ S, 585psi N ₂ , ~1641ppmw 2-NA in toluene, 337ppmw Mo, 2hours)	164
Table 5-10 Summary of effect of water on 2-NA removal under CO and N ₂ (300°C, 80ml toluene, 10-20ml water, 15psi H ₂ S, 585psi CO or N ₂ , ~1641ppmw 2-NA in toluene, 673ppmw Mo, 2hours)	170
Table 5-11 Summary of simultaneous 2-NA removal and HDS of DBT (300~340°C, 80ml toluene, 10ml water, 15psi H ₂ S, 585psi CO, ~1641ppmw 2-NA, ~5000ppmw DBT, 337ppmw Mo, 2~3hours)	175
Table 5-12 Summary of simultaneous 2-NA removal and HDA of NAPH (300~320°C, 80ml toluene, 10ml water, 15psi H ₂ S, 585psi CO, ~1641ppmw 2-NA, ~5000ppmw NAPH, 337ppmw Mo, 2hours)	180
Table 5-13 Summary of 2-NA removal with different metal additives (300°C, 80ml toluene, 10ml water, 15psi H ₂ S, 585psi CO, ~1641ppmw 2-NA in toluene, 673ppmw Mo, metal:Mo ratio=0.2, 2hours)	187

Table 5-14	Reaction rate constants obtained under H ₂ and CO (300°C, 80ml toluene, 10ml water, 15psi H ₂ S, 585psi gas feed, ~5000ppmw C7-BA in toluene, 377ppmw Mo, 2hours)	190
Table 6-1	Main causes of catalyst deactivation in different oil refining and petrochemical processes (Dufresne 2007).....	206
Table 6-2	BET results of spent catalysts from LGO experiments and fresh Ni-MoS ₂ catalyst made in hexadecane (C16) (Spent catalysts: 391°C, 100ml LGO, 10ml water, 10psi H ₂ S, 590psi CO, 1408ppmw Mo, Metal:Mo=0.6, 2hours; <i>Ex situ</i> NiMo catalyst: 0-390°C, 300ml C16, 30ml water, 30psi H ₂ S, 570psi CO, 1408ppmw Mo, Metal:Mo=0.6, 0-2hours).....	212
Table 6-3	Atom number percentages in each spots in Figure 6-18 obtained by EDX.....	222
Table 6-4	Atom number percentages in each spots in Figure 6-26.....	230
Table 7-1	Atomic ratio results collected from EDX analysis for fresh <i>ex situ</i> MoS ₂ catalysts prepared with <i>in situ</i> H ₂ and molecular H ₂ collected at different temperatures.....	249
Table 7-2	Average slab length, stacking number and layer distance results of fresh <i>ex situ</i> MoS ₂ catalysts prepared with <i>in situ</i> H ₂ and molecular H ₂ collected at different temperatures.	253
Table 7-3	Atomic ratio results collected from EDX analysis for fresh <i>ex situ</i> Co-MoS ₂ catalysts with different Co:Mo ratios collected at 390°C under CO	258
Table 7-4	Average slab length, stacking number, layer distance results of fresh <i>ex situ</i> MoS ₂ , Co-MoS ₂ and Ni-MoS ₂ catalysts with different Co or Ni:Mo ratios collected at 390°C under CO together with conversion results for HDN of quinolone referred from Lee's thesis (Lee 2004)	263
Table 7-5	Average slab length, stacking number and layer distance results of fresh <i>ex situ</i> Ni-MoS ₂ catalysts with different Ni:Mo ratios collected at 300°C, 340°C and 390°C under CO...	272
Table 7-6	Atomic ratio results collected from EDX analysis for fresh <i>ex situ</i> Ni-MoS ₂ catalysts with different Ni:Mo ratios collected at 300°C, 340°C and 390°C under CO.....	273
Table 8-1	Comparison of emulsion upgrading process (with and without catalyst) with selected partial upgrading and full upgrading technologies	279

Chapter 1 Challenge, Opportunity and Technology

1.1 Background

1.1.1 Canadian oil sands industry overview

The oil sands are loose sand or partially consolidated sandstone containing naturally occurring mixtures of sand, clay, and water, saturated with a dense and extremely viscous form of petroleum technically referred to as bitumen. Due to complexity and high cost of extracting oil from oil sands from reservoirs, very limited efforts have been made on this precious natural resource until the 1960s. With the depletion of conventional petroleum sources, the economic value of oil sand bitumen has been unlocked by increased crude oil prices and implementation of new extracting and processing technologies. Meanwhile, recent substantial investments in US coking capacity, has allowed refiners to process heavier, sour crude like Canadian oil sands bitumen. Consequently oil sands bitumen has been pushed to the forefront of the petroleum industry.

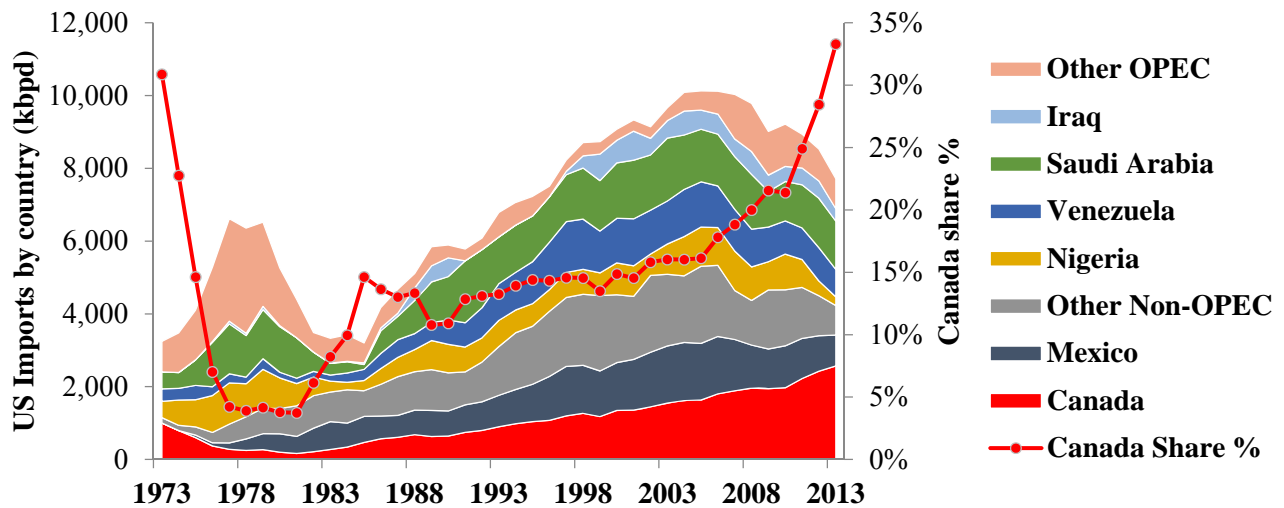


Figure 1-1 US crude imports by country (compiled from US Energy Information Administration data)

As shown in Figure 1-1, the volume of Canadian crude exports to US reached 2,551 million barrel per day in 2013, occupying 1 third of US crude import market. Canada is by far the United States' top crude supplier, with Saudi Arabia a distant second.

Table 1-1 Oil sands reserves as of Dec 31, 2011 in units of billion barrels (BMO-Capital-Market 2013)

	Ultimate Potential	Initial Volume in Place	Ultimate Recoverable	Initial Established	Cumulative Production	Remaining Established	Active Development
Mineable							
Athabasca	138.4	130.9	69.2	38.8	5.2	33.6	22.6
In Situ							
Athabasca	na	1,395.0	na	71.2	0.3	71.0	0.9
Cold Lake	na	183.1	na	35.2	2.6	32.6	2.0
Peace River	na	135.7	na	31.7	0.1	31.5	0.1
In Situ	2,378.7	1,713.5	245.4	138.1	3.0	135.1	3.0
Total	2,517.1	1,844.4	314.6	177.0	8.1	168.9	25.6

Source: Energy Resources Conservation Board, BMO Capital Markets

Geologically oil sands resources are located in Western Canada, especially in Alberta. As shown in Figure 1-2, three major oil sands reserves are labelled in Athabasca, Peace River and Cold Lake, among which Athabasca has the largest volume as shown in Table 1-1. According to a 2013 Energy Source Conservation Board (ERCB) report, Canada holds proven reserves of 1.84 trillion barrels of original oil in place, ranking No.1 in the world. About 10% of the reserves, 177 billion barrels have been proven to be recoverable at current prices by using current technology (BMO-Capital-Market 2013). These reserves are second in size compared to Saudi Arabia. With the continuous improvement of exploration and production technologies, Canadian oil sands have the potential to provide nearly 2.5 trillion barrels of reserve and 314 billion barrels could be potentially recovered.

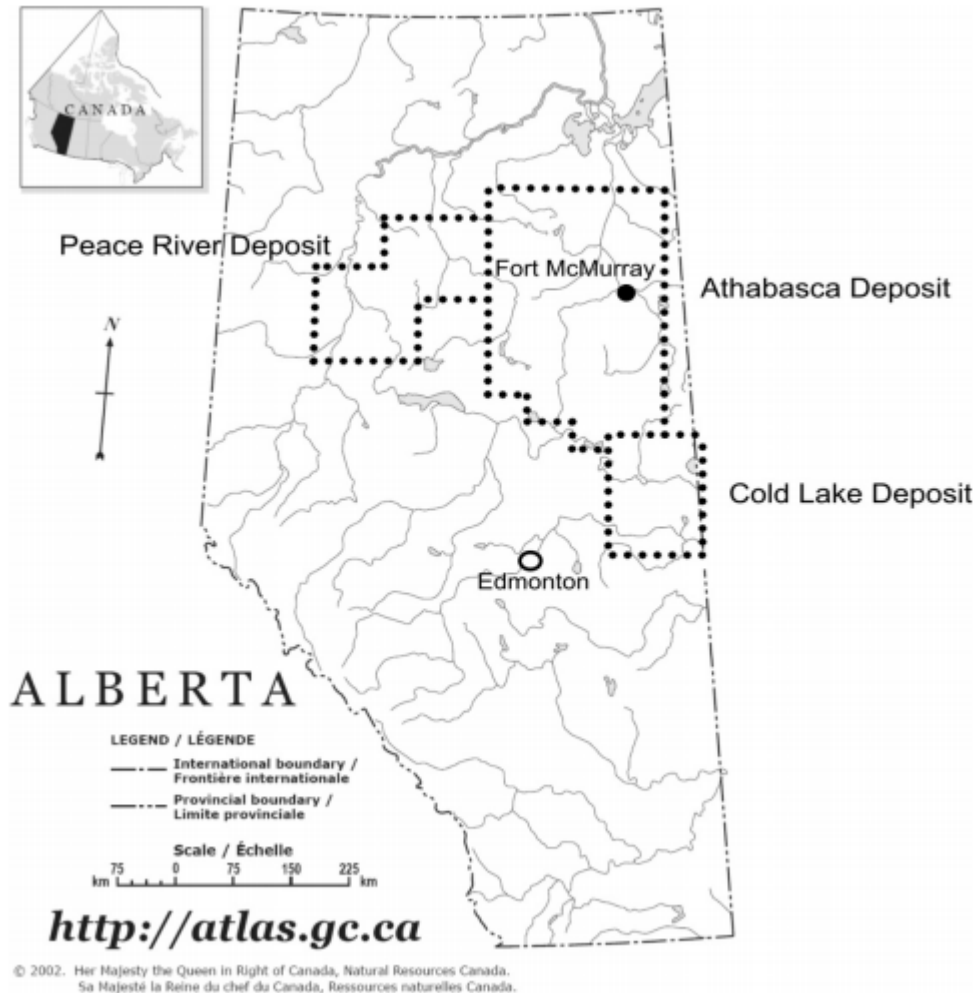


Figure 1-2 Map of Western Canada oil sands reserves

However, oil sands bitumen is known for its high asphaltene content, high viscosity, high coke deposits and high sulfur content as shown in Table 1-2. For instance, Athabasca bitumen has the highest asphaltene content, leading to the lowest API gravity and highest viscosity. The viscosity of Athabasca bitumen is as high as 19000 cSt even at 40 °C, making it impossible to flow under normal conditions. Due to these poor properties, the upgrading of Canadian oil sands bitumen is extremely difficult compared with other feedstocks. Besides this decline of oil feedstock quality, stricter environment regulation and growing petroleum market demand also pose a lot of challenges to bitumen upgrading. The upgrading of bitumen still needs more investigation and efforts from worldwide experts, especially our Canadian scientists and engineers.

Table 1-2 Typical Canadian oil sands bitumen crude properties (Selucky, Ruo *et al.* 1977, Selucky, Chu *et al.* 1977, 1978)

	Cold Lake	Lloydminster	Athabasca
Crude Inspections			
Gravity, °API	11-13	13	8-9
Viscosity @40 °C, cSt	1100	1000	19000
Asphaltenes, wt%	15.3	16.9	19.8
Sulfur, wt%	5.1	4.7	5.1
Nitrogen, wt%	0.45	0.53	0.56
Nickel, ppm	200	140	150
Vanadium, ppm	490	190	290

1.1.2 Oil sands extraction methods

Usually, conventional crude oil is extracted by drilling oil wells into a petroleum reservoir directly, which allows oil to flow into the wells under natural reservoir pressures. Sometimes (especially at the end of a field's life) artificial lift and techniques such as gas injection or water flooding are usually used to maintain the production rate due to the depleted reservoir pressure. Because of the extremely high viscosity, oil sands bitumen barely flows toward the producing wells under normal reservoir conditions. As a result, the oil sands bitumen can only be extracted by surface strip mining or *in situ* techniques which reduce the viscosity by injecting steam, solvents, and/or hot air into the sands. These processes use more water and require larger amounts of energy than conventional oil extraction.

1.1.2.1 Mining process

Kearl Process Overview

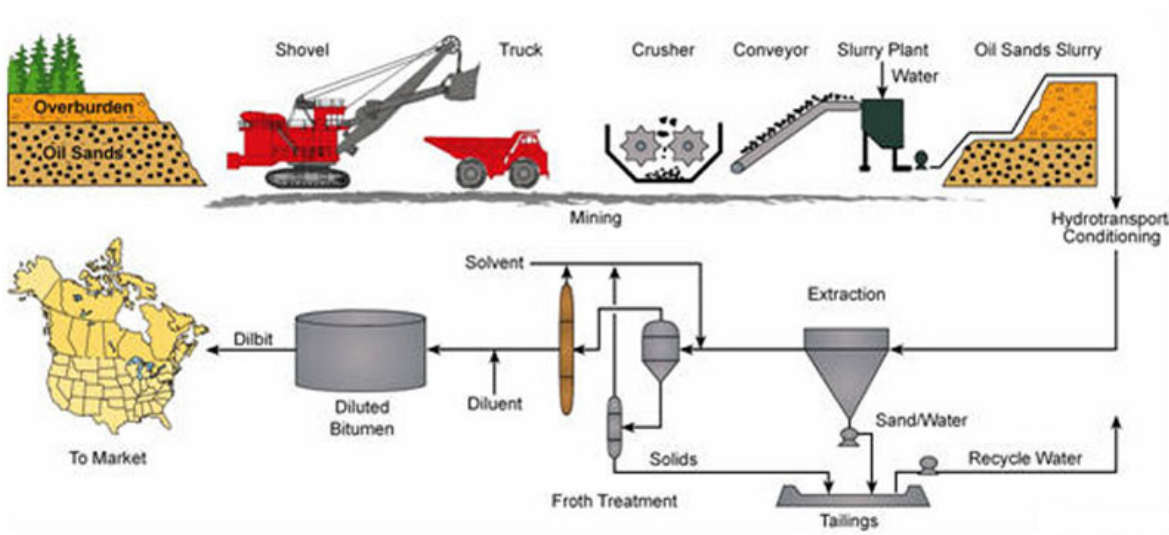


Figure 1-3 Schematic of a mining process (Imperial-Oil)

If the oil sands are near the surface, they are collected via surface mining, a process that begins with large trucks and shovels. However, only 20% of all oil sands are close enough to the surface to be mined. After excavation, hot water and caustic soda (NaOH) are added to the sands, and the resultant slurry is piped to the extraction plant where it is agitated and the oil skimmed off from the top. Provided that the water chemistry is appropriate to allow bitumen to separate from sand and clay, the combination of hot water and agitation releases bitumen from the oil sand, and allows small air bubbles to attach to the bitumen droplets. The bitumen froth floats to the top of separation vessels, and is further treated to remove residual water and fine solids. Diluent is used in the extraction step for enhanced extraction performance. As shown in Figure 1-3, Imperial Oil Kearl mining project implements the diluent enhanced extraction method in their froth treatment step, whereas, paraffinic solvents are chosen as diluent for rejecting asphaltenes from bitumen. Consequently, the product's viscosity is significantly reduced, allowing less diluent usage for pipeline transportation. However, all current mining projects create tailings ponds, which allow disposal water to segregate for 20 years or more to remove clays, asphaltenes, etc. Although a lot

of efforts have been focused on reducing the tailings ponds, they still have a large environmental impact.

1.1.2.2 *In situ* production processes

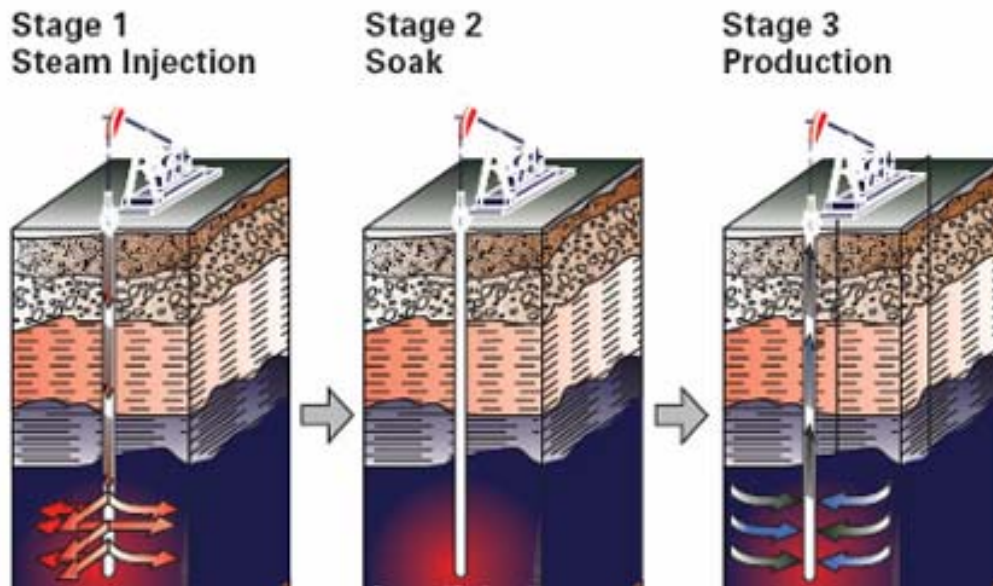


Figure 1-4 Schematic of a CSS process (Imperial-Oil)

The Cyclic Steam Stimulation (CSS) method has been used by Imperial Oil at Cold Lake since 1985, and by Canadian Natural Resources at Primrose and Wolf Lake and by Shell Canada at Peace River. If the oil sands are deeper underground, they're recovered using "*in situ*" techniques which remove oil from oil sands while leaving the sand in place. High pressure steam is injected to soften and dilute the bitumen underground so that the bitumen can flow to the well during the production phase as shown in Figure 1-4. Usually CSS can achieve around 20-25% recovery.

Steam-assisted gravity drainage (SAGD) technology was invented by Dr. Roger Butler in the 1970's at Imperial Oil, and was successfully commercialized by Cenovus in the late 1990's. SAGD has provided a major breakthrough in production technology; since it is cheaper than CSS,

allows higher oil production rates, and recovers up to 60% of the oil in place. Steam injection techniques have been widely used to recover the viscous heavy oil buried deep underground. As shown in Figure 1-5, a pair of horizontal wells are drilled underground into the oil sands bearing stratum. Steam is then injected into the formation through the upper well, which heats up the bitumen. Heated bitumen becomes a less viscous emulsion and flows under the influence of gravity into the lower well. The liquefied hot bitumen is pumped out of this lower well along with the condensed water. The process involves use of saturated steam at around 550 psi pressure. (Speight 2007)

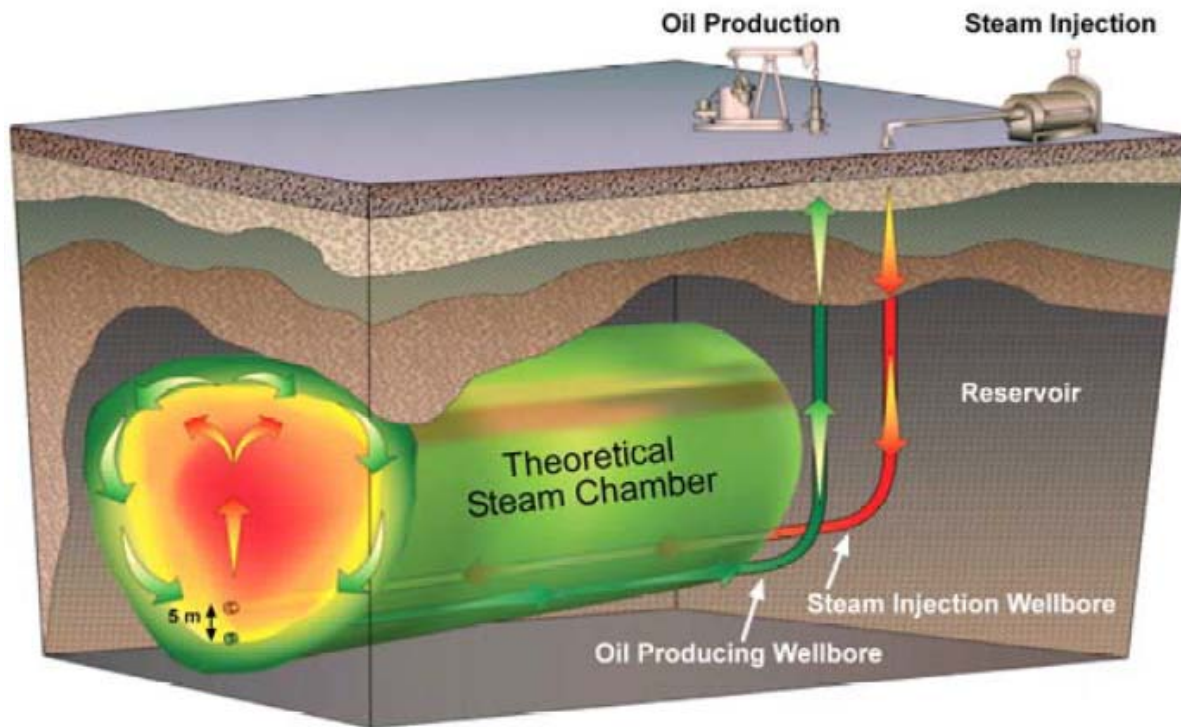


Figure 1-5 Schematic of SAGD process (Peacock 2010)

Inorganic components in SAGD produced water such as Na, Ca, Mg, Si, will affect the oil removal performance in the produced water before it is recycled to a steam generator; while the organic acids will also cause corrosion issues for surface facilities. Considerable expenses have

arisen in treating the produced water that is extracted along with the bitumen to produce sufficiently clean feed water for the steam generator. As a result, SAGD plants are often considered as water treatment plants with bitumen as a “by-product”.

1.1.3 Pipeline transportation

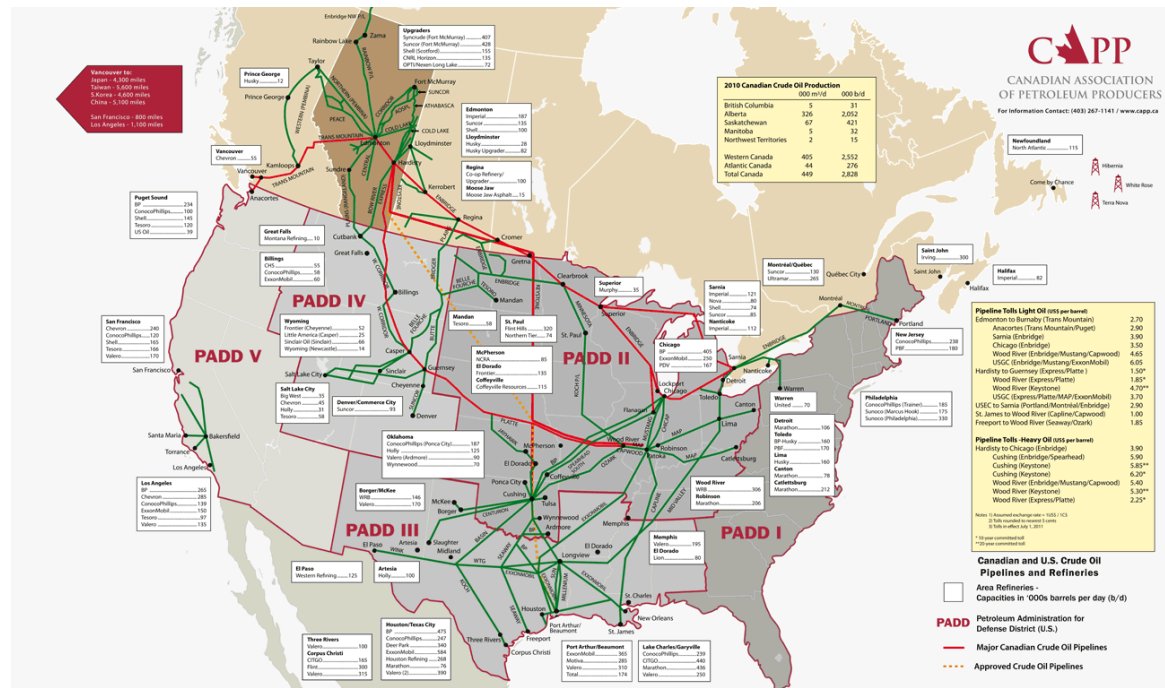


Figure 1-6 Map of Canadian and US pipelines and refineries (CAPP 2013)

As a commodity, crude oil needs to be transported to market to realize its value. As shown in Figure 1-6 the existing pipelines and refineries in the US have provided ideal markets for Canadian oil sand crudes. However, the high viscosity of raw bitumen and cold weather limit the piping capability of oil sand bitumen. As shown in Table 1-2, the API gravities of Canadian oil sands bitumen are in the range of around 8 to 13; while the piping standard for Cold Lake blend requires a API gravity of more than 19 and a viscosity of no more than 350 cSt@7°C (Enbridge 2013). In order to reduce the viscosity and improve the API gravity to meet the piping standard, diluent has been widely used as an additive. The mixture, “dilbit”, contains around a 3:1 ratio of

bitumen and diluent. To meet transport viscosity specifications, many oil producers use a diluent fraction that could be even as high as 29% to 35% of the transported heavy oil. Diluent comes from naphtha - the light end of crude, which is also spiked with volatile gas components such as propane, butane, etc. After the dilbit is shipped to upgrader/refinery, another returning pipe is required to return separated diluent back to the field, since diluent cannot be produced on site. This increases the costs for building and operating pipes; it also restrains the pipeline capacity.

Due to the limited production of diluent in Canada, some oil producers without an upgrader/refinery option, need to import diluent from the US at a high price, and sell dilbit to the US where the diluent is extremely underestimated in value. It has been reported that the extra operating cost/discount caused by diluent shipping is as high as around \$20 per barrel (CAPP 2013). As shown in Table 1-3, the price difference between West Canadian Select (WCS, designed price for Canadian crude) settlement price and bitumen royalty value at Hardisty (an actual Canadian crude sold price) in early 2013 could be as high as \$17 to \$26 per barrel, which was mainly caused by the total acid number (TAN) discount and diluent shipping cost. Although an increased global crude price could reimburse part of this cost, the current diluent piping is the major limitation for the future of Canadian oil sands business.

Table 1-3 Example of Alberta oil sands bitumen valuation methodology (CAPP 2013)

2013	Foreign exchange rate	WCS Settlement Price \$US/bbl	WCS Dilbit Volume Fraction	WCS Bitumen Synbit Premium \$US/bbl	WCS Blend Density kg/m ³ @15°C	Condensate "CRW" (diluent) Allowance Price \$Cdn/m ³	Condensate "CRW" (diluent) Density kg/m ³ @15°C	Royalty Value of bitumen @Hardisty \$US/bbl
Jan	0.9921	62.11	0.98	3.71	921.2	685.45	714.2	38.12
Feb	1.0098	58.40	0.99	3.96	921.0	691.10	720.6	32.46
Mar	1.0247	66.72	0.98	3.88	921.2	665.40	719.0	47.82
Apr	1.0187	68.87	0.98	3.61	921.2	653.01	712.1	52.17

To make things worse, the large expansion in bitumen production and potential increasing diluent prices, drive oil companies to seek out optional ways of piping bitumen. It has been reported that oil sands output is projected to double to 3.8 million barrels by 2022, according to Alberta's energy regulator. While Alberta diluent prices spiked \$11 from the fourth-quarter of 2012 to average \$108 a barrel in the first three months of 2013, and will undoubtedly increase in the next few years with the large increase in demand. In order to turn around the current distressful bitumen piping business, oil producers have put huge expectations on emerging upgrading or partial upgrading technologies.

1.2 Upgrading and partial upgrading

1.2.1 Upgrading

Upgrading (or full upgrading) is a process using fractional distillation and/or chemical treatment to convert bitumen before the oil is processed by oil refineries. Full upgrading produces either finished, saleable products, such as gasoline or diesel, or a high-quality synthetic crude oil (SCO) that contains no vacuum residue. This process can:

- a) Lower bitumen's viscosity to be pumped through pipelines;
- b) Separate heavy fractions (like asphaltenes, vacuum residues, cokes);
- c) Reduce TAN for less corrosion discount in pipelines and downstream vessels;
- d) Remove sulfur, nitrogen and metals (nickel and vanadium) in order to increase product value and protect downstream refinery catalysts.

Based on the characteristics of upgrading technology, there are two major categories of upgrading: thermal cracking/coking process and hydrogen (H₂) addition process.

1.2.1.1 Thermal cracking/coking process

Coking units convert heavy feedstocks into a solid coke and lower boiling hydrocarbon products through thermal C-C bond cleavage. Once saturated by adding H₂, the light product is suitable as a feedstock to other refinery units to be converted into higher value products. From a chemical

reaction viewpoint, coking can be considered as a severe thermal cracking process in which the reactions are allowed to proceed to completion. Coke is the by-product of this process, and the sulfur and metal contents of the coke can be very high (~8% by weight). There are two major coking processes: (a) delayed coking and (b) fluid coking.

Although the thermal cracking/coking process is cheap, safe and reliable, it suffers from extremely high hydrocarbon loss (nearly 40%). The rejected hydrocarbons in coke form have zero or even negative values (due to shipping and disposal costs). Light end (C3-C5) product could be blended into the synthetic crude product to increase the production volume. However, this product is not favoured by downstream refineries, and certain penalties could be charged for processing these unfavoured products. With low oil yield, more zero-or-negative value product generation, the thermal cracking/coking process is not the most economical process for Canadian oil producers. As a result, many companies have started to implement a H₂ addition process for upgrading their bitumen.

1.2.1.2 H₂ addition process

1.2.1.2.1 Hydroconversion, hydrocracking and hydrotreating

There are three types of H₂ addition processes widely used in Canada: (a) hydroconversion, (b) hydrocracking and (c) hydrotreating. Hydroconversion involves combining catalytic activity with thermal cracking with a reaction temperature in cracking regime. The catalyst used in hydroconversion is usually a supported-metal sulfide catalyst (Mo+Ni/Al₂O₃). Hydrocracking is aimed at converting heavy distillates into feeds for gasoline by using catalysts having both cracking and hydrogenation activity, like zeolites. Hydrocracking is mainly used for refineries, and the H₂ pressure is higher than that used for hydroconversion. Hydrotreating processes, similar to a hydroconversion process, uses a Mo based catalyst for removing sulfur, nitrogen and metals from the oil. The temperature used in hydrotreating is lower than that used for hydroconversion, which is insufficient for cracking the oil.

Hydroconversion is widely used for Canadian bitumen primary upgrading purposes, such as the Husky, Shell, and Syncrude upgraders. The number of hydrocracking processes in Canada is limited due to market reasons. However, there are still certain refineries which use the hydrocracking process, like Shell’s Scotford upgrader and Suncor’s Edmonton upgrader. In most of the thermal cracking/coking and H₂ addition processes, hydrotreating is used for saturating unstable cracked products and to remove heteroatoms. The presence of H₂ and Mo based catalysts suppresses coke formation, and also helps remove heteroatoms, add value and stabilize the oil.

1.2.1.2.2 Fixed bed, ebullated bed and slurry reactors for residue upgrading

Fix bed, ebullated bed and slurry reactors are the three major technologies used for residue upgrading. Extensive investment and research has been carried out for developing these 3 reactor designs as shown in Table 1-4.

Table 1-4 Current residue upgrading processes (Rana, Sámano *et al.* 2007)

Reactor type	Process	Licenser
Fixed bed	Continuous catalyst replacement (OCR)	Chevron
	Hycon, Bunker type reactor	Shell
	Hyvahl, swing reactor concept	Axen
Ebullated bed	H-Oil	Axen (HRI/IFP)
	T-Star	Chevron
	LC-Fining	ABB Lummus, Amoco oil (BP)
Slurry reactor	Microcat RC	Exxon Mobil
	Veba combi cracking	KBR, BP
	Hydrocracking distillation hydrotreating (HDH)	Intevep
	Cash, Chevron activated slurry hydroprocessing	Chevron
	Eni slurry technology (EST)	Eni S.p.A.,
	CANMET	UOP

Fixed bed hydroprocessing is targeted at the hydrotreatment of heavy fractions with simultaneous hydrodesulfurization (HDS), hydrodenitrogenation (HDN), hydrodemetallization (HDM), hydrodearomatization (HDA) and asphaltene conversion. The hydrocracking activity remains moderate. This process reduces impurity levels and provides additional quantities of high quality oil feedstocks for Fluid Catalytic Cracking (FCC) and Resid Fluid Catalytic Cracking (RFCC) processes. The fixed bed process technology is applied extensively and has the highest usage in industrial applications due to its technical maturity, lower cost, and reliable performance. However, fixed bed reactors have problems in treating particularly heavy feeds with heteroatoms, and especially metal and asphaltenes. The current solution is to use a series of fixed bed reactors for obtaining a relatively high conversion of such heavy feedstocks. Such designs come with high cost, making it commercially impractical for certain feedstocks.

Compared to the problematic fix bed process, moving bed and especially ebullated bed technologies have been developed with numerous advantages in both performance and efficiency. In an ebullated bed process, H₂ and oil feed enter the bottom of reactor and flow upward through a catalyst bed. This allows expanding and back-mixing in the bed, and minimizes bed plugging. Instead of being fixed, the catalysts are maintained in an ebullient condition with an upflowing feed. This process is able to convert most of the refractory heavy feedstock into either distillate or low sulfur fuel oils (Morel, Kressmann *et al.* 1997). An ebullated bed reactor allows periodic withdrawal and addition of the catalyst without interrupting the operation. This allows for continuous operation when treating feedstocks with high asphaltenes and metal content. The bed design also provides ample free space between the particles, which allows entrained solids to pass through the bed without accumulation, plugging or increased pressure drop. As a result, fine catalyst particles (diameter <1 mm) can be utilized for increasing the reaction rate significantly. The catalysts used in an ebullated bed are similar to those used in a fixed bed and both involve a supported type of catalyst containing small amounts of one or more active promoter metals such as Mo with Co or Ni deposited on a support material such as alumina or silica. Compared to fixed bed catalysts, the ebullated bed catalysts are smaller which facilitates suspension by the liquid phase in the reactor; the ebullated bed catalysts are also mechanically stronger. (Sherwood 2000, Reynolds 2002). Currently, there are two major ebullated bed processes in commercial

service: the H-Oil[®] process and the LC-Fining[®] process. The Husky Lloydminster upgrader is uses the H-Oil[®] process, while the Shell Scotford upgrader utilizes the LC-Fining[®] technology.

The slurry bed process is a hydrocracking process which involves the presence of catalysts and H₂ at high pressure and temperature. The reaction involves mainly thermal cracking, and the goal is to convert residue into high value lighter distillates. The presence of catalyst and H₂ restrains coke formation and leads to more stable products (Zhang, Liu *et al.* 2007). As shown in Figure 1-7, catalyst pellets (unsupported catalyst is preferred) are suspended into liquid in the slurry reactor. H₂ is bubbled into the reactor from the bottom. The H₂ is then absorbed into the liquid from the bubble surface. The absorbed gas diffuses through the liquid onto the catalyst surface, where it starts to diffuse into the catalyst pellet and initiate the reaction. The reactants are well mixed and kept in suspension and flow upward in the reactor. The product and catalyst are separated at the top of the reactor (high pressure high temperature separator). Coke formed during the reaction will deposit on the surface of the catalyst and discharge from the reactor, eliminating bed plugging problems. Solid particles are recovered with the unconverted organic fraction at the bottom of the separation section by distillation or by solvent deasphalting (SDA). The slurry bed process shows its special superiority in treating heavy oils containing large amount of metals, carbon residue and asphaltenes. This process is also featured with its flexibility on product selectivity and yield. Generally speaking, the slurry bed process is a residue processing technology which has several advantages such as a simple process flow scheme, flexible operation and process reliability, high space velocity and good conversion rates, with no bed plugging problem and a wider adaptability to different sources of raw materials. The main disadvantage is that the operability is more difficult than for the other processes.

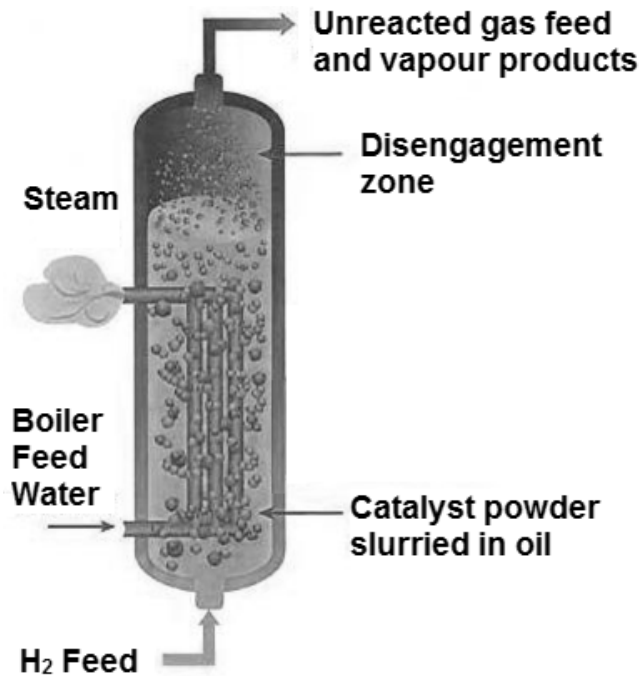


Figure 1-7 Diagram of slurry reactor used in hydroconversion

In a slurry bed reactor process, product yields are dependent on the extent of the conversion, and further processing is needed to obtain high-quality products. Typical operating conditions in the reactor are temperatures of 420-460°C, a pressure of 10- 20MPa, LHSV 0.5-2.0 h⁻¹ and a single pass conversion of 70-85%. The slurry bed process was first used in Germany as early as 1929 for hydrogenation of coal to produce oil. Later, the process was used to handle crude oil when oil supplies were limited. Recently, this process was adapted to convert vacuum residue feeds. Typical slurry based bitumen upgrading processes are: Eni Slurry Technology (EST[®]) by Eni S.p.A., Vacuum Resid Slurry Hydrocracking (VRSH[®]) process by Chevron, Veba Combi Cracking (VCC[®]) by KBR, Heavy Residue Hydroconversion (HRH[®]) process by Mobis Energy and Uniflex[®] process (previously known as the CANMET[®] process) by UOP. Although there are still further steps required before the slurry bed process can be commercialized, it would be more competitive after optimizing the design, decreasing the cost and adding high-activity catalysts to the process.

1.2.1.2.3 Typical full upgrading processes for oil sands bitumen

In Western Canada, all but one of the currently operating upgraders or those under construction have utilized well-established coking (delayed and fluid) and ebullated bed processes for conversion of the vacuum residue in the heavy oil or bitumen. For two of the currently operating upgraders (Syncrude Canada and Husky Energy), both ebullated-bed hydrocracking and coking are utilized with the unconverted vacuum residue from the ebullated-bed process being routed to the coker. For example, the Husky Lloydminster upgrader plant block flow diagram is shown in Figure 1-8. Besides the core ebullated bed for hydroconversion, the process contains fractionators, which are the atmosphere/vacuum towers to separate light fractions (like naphtha, jet oil and gas oil) from bitumen in order to reduce the working load of the hydroconversion reactor. A H_2 plant is also used to provide sufficient H_2 for hydroconversion and hydrotreating. A delayed coker is used to convert vacuum residue into light oil and coke. Due to extensive thermal cracking, olefins and di-olefins are formed causing poor upgraded oil stability. As a result, secondary hydrotreating steps are implemented to eliminate olefins and di-olefins. As a bonus, the secondary hydrotreating reduces heteroatoms like sulfur, nitrogen and metal, improving the product quality for higher price. By blending butane, naphtha and upgraded/hydrotreated distillates, the plant produces a Husky Synthetic Blend of premium quality for downstream refineries as shown in Table 1-5 and Figure 1-10.

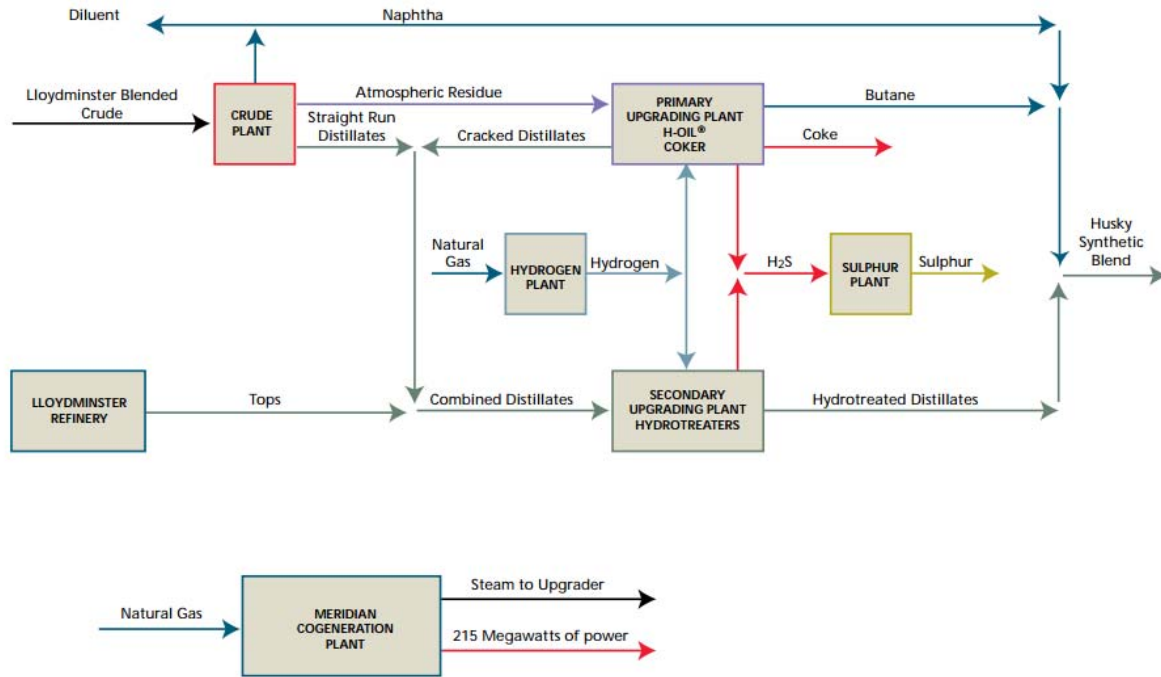


Figure 1-8 Husky Lloydminster upgrader flow diagram (Husky-Energy 2011)

The only currently operating upgrader in Canada not using well-established technologies is the Nexen Long Lake upgrader. The core technology for this upgrader is called the OrCrude[®] process. Unlike many of the new upgrading processes investigated, the OrCrude[®] process is not a new unique reactor and/or catalyst technology developed for the heavy oil industry. As shown in Figure 1-9, it is an integration of three well-known process steps, atmospheric and vacuum distillation, solvent deasphalting and thermal cracking. The products from the OrCrude[®] Process are: (a) a very heavy asphaltene stream which is sent to a gasifier to produce hydrogen, steam, syngas and power and (b) a low API gravity sour synthetic crude oil (SCO) which is sent to a high-pressure hydrocracker to produce the final SCO (Hood 1998, Hood, Rettger *et al.* 2001, Rettger, Goldstein *et al.* 2004). The SCO does not contain any vacuum residue and the process is thus considered as full upgrading. The gasifier and hydrocracker are not part of the OrCrude[®] process but would be included in a typical upgrader. An OrCrude based heavy oil upgrader will not require any natural gas. The upgrader hydrocracker is a licensed technology and produces 34-40° API gravity SCO with a high associated H₂ consumption. Typical oil product qualities have been summarized in Table 1-5 and Figure 1-10.

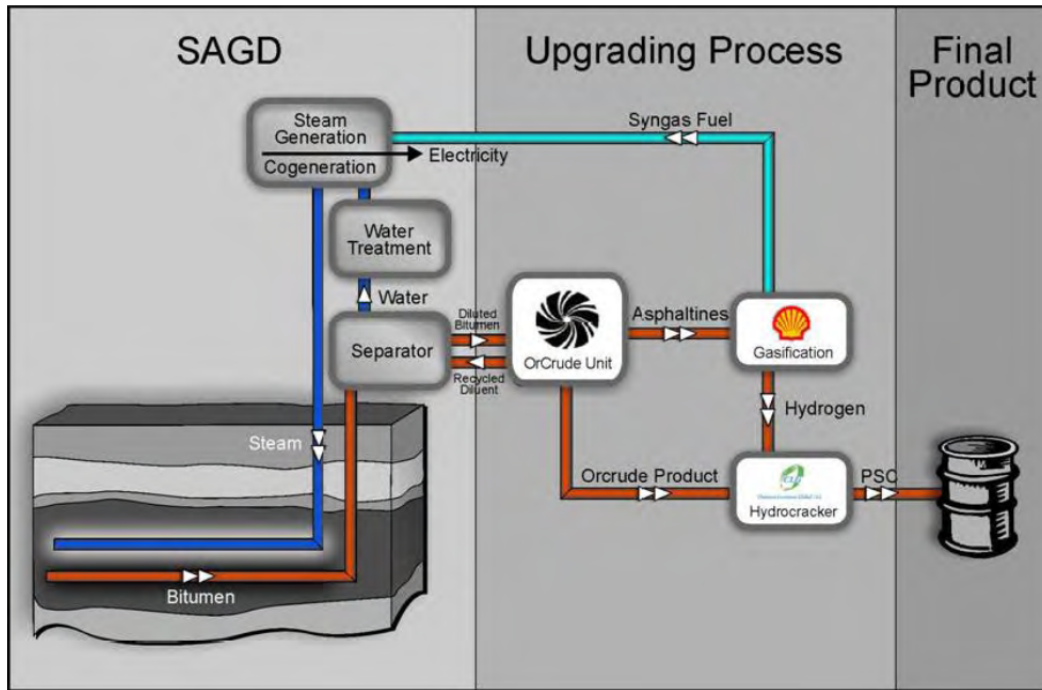


Figure 1-9 Nexen Long Lake integrated SAGD and upgrading process flow diagram with OrCrude[®] technology (Birdgeneau 2008)

The OrCrude[®] Process is a technically feasible approach which produces a relatively low SCO yield, around 80-83% vol., (Bronicki 2007, Rettger, Goldstein *et al.* 2008) and a high quantity of excess energy (steam, power, and raw syngas) and fits well with a SAGD process (NEXEN 2011). The strongest weaknesses are the low SCO yield, high investment (primarily the gasification step) and the applicability to SAGD feeds only. With current and expected long-term low natural gas prices, the OrCrude[®] Process is not economically feasible. Given the current low natural gas price (\$4/MMBTU), it is not expected that additional OrCrude[®] projects will be implemented.

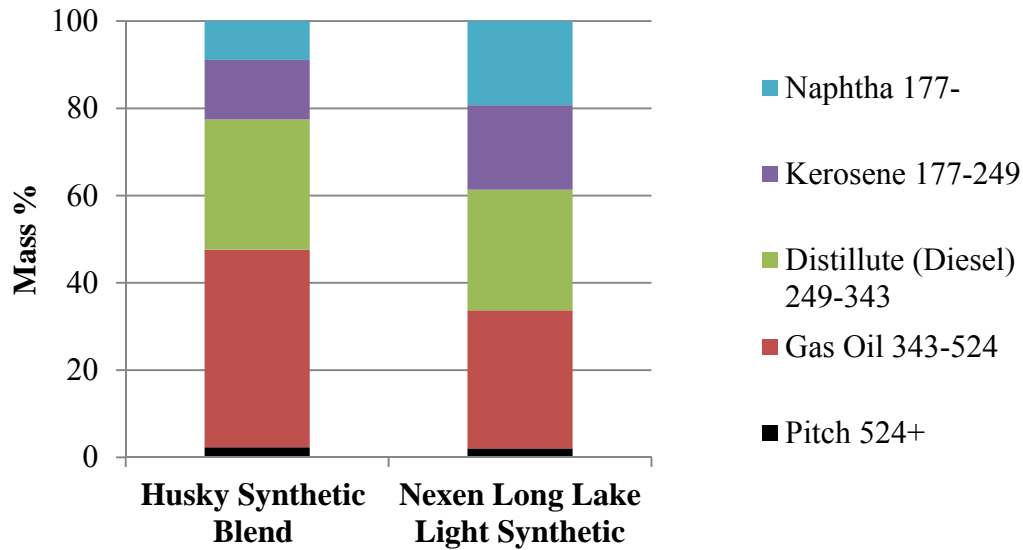


Figure 1-10 Boiling point distribution of typical full upgrading process products (courtesy: CrudeMonitor.ca)

In summary, full upgrading appears to be the solution for avoiding the use of diluent for long distance pipe transportation, especially for transporting bitumen to US refineries. However, full upgrading process produce over-qualified oil for a refinery. Diluent supplies and, established refinery markets have created a large discount on the SCO product price, making full upgrading process much less profitable. Considering the additional high capital/operating costs for a full upgrading plant, most oil producers have to stick with diluent blending assisted transportation.

Table 1-5 Qualities of typical full upgrading process products (courtesy: Crude Monitor.ca)

	Husky Synthetic Blend	Long Lake Light Synthetic
Density (kg/m^3)	866.5	831.2
Gravity ($^{\circ}API$)	31.7	38.6
Sulphur (wt%)	0.1	0.07
Vanadium (mg/L)	0.2	1.5
Olefins (wt%)	0.6	-

1.2.2 Partial Upgrading

In order to reduce cost and avoid over-upgrading of oil sands bitumen, investors and engineers have expended large efforts on emerging partial upgrading technologies. As the name implies, partial upgrading is aimed at partially upgrading the crude just to produce transportable SCO meeting pipeline specifications for gravity and viscosity (i.e., is pumpable). Typically this requires a minimum API gravity of 19° and a maximum 7°C viscosity of 350cSt. Acceptable partially upgraded SCO will not require dilution with natural gas condensate or other lighter oils to be transported via a pipeline. It is typically implemented onsite in remote areas. Compared to a full upgrading process, partial upgrading requires a relatively low investment due to no major H₂ plant, no catalyst usage, etc. In addition, partial upgrading has a much simpler process configuration and less complexity than full upgrading. Partial upgrading produces an SCO that typically contains 5-30% vacuum residue and distillation products that require additional hydrotreating. Many new partial upgrading technologies include two primary steps, a low-investment thermal cracking of the vacuum residue followed by combustion of the heavy unconverted product, which is typically coke. The combustion of the coke or heavy unconverted product (residue, asphaltenes) can produce the steam needed for the process and all or a portion of that required for SAGD. This makes partial upgrading ideal when integrated with SAGD. This integrated concept is shown in Figure 1-11. The thermal cracking of the residue is accomplished by various techniques including the use of heat, sound energy, kinetic energy and irradiation. In some of the new partial upgrading processes, catalytic cracking is utilized. Since the catalyst cost for partial upgrading can be prohibitive, development efforts have included the use of inexpensive and recyclable catalytic materials.

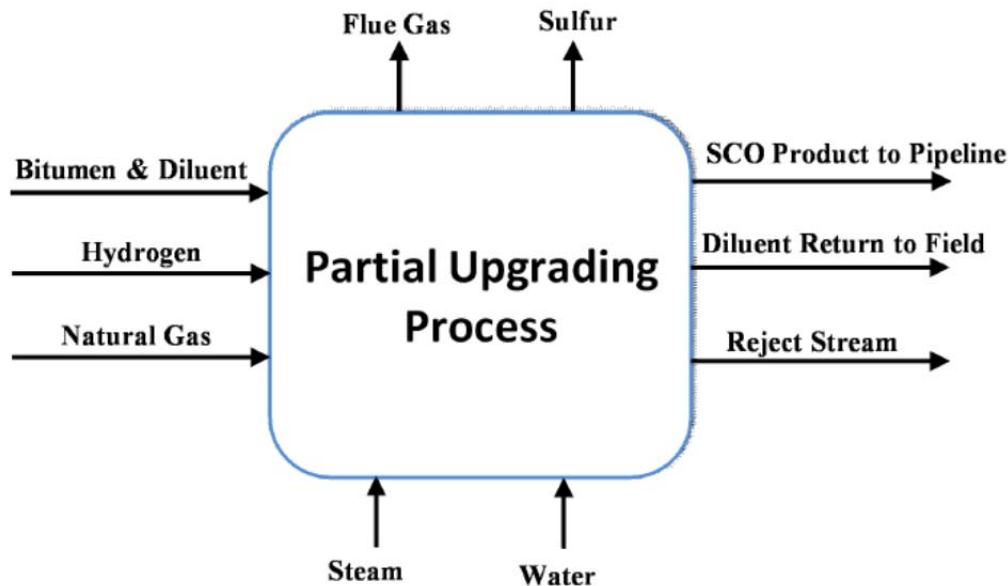


Figure 1-11 Concept of partial upgrading integration with oil sands bitumen *in situ* production
(Colyar 2010)

Technically speaking, partial upgrading can be also divided into two categories: *physical separations* and *chemical reactions*. *Physical separation* usually utilizes specific paraffinic solvents (propane to hexane; C₃-C₆) for removing asphaltenes from bitumen. For example, the ROSE[®] process licensed by KBR uses a SDA unit to remove the asphaltenes and produce high-quality deasphalted oil (DAO) for lube oil blending, or for further processed hydrocrackers, hydrotreaters and/or FCC units. Similar technology is also implemented in Imperial Oil's Kearl mining project, called paraffinic froth treatment (PFT[®]) technology. Paraffinic solvents are added in the froth treatment step to reject significant amount of asphaltenes, creating pipeline transportable oil. These physical separation technologies require minimum energy, and save on relevant greenhouse gas emissions. The major cost is the cost of the solvent recovery units. On the other hand, more traditional partial upgrading technologies belong to the *chemical reaction* category as they change product quality through reactions like coking, thermal cracking, hydrocracking, hydrotreating, bio-upgrading, etc. Low temperature bio-upgrading by bacteria requires the least energy and cost, but its technology readiness is still extremely low. In contrary,

high temperature (>470°C) partial upgrading technologies have been investigated extensively. The level of additional developments for partial upgrading technologies required is a subjective estimate of the extent of further process definition, R&D, product evaluations and economic valuations required to bring the technology to commercial readiness.

Besides the lack of commercial experience, the largest issues concerning the implementation of the partial upgrading of heavy oil are:

- a) The stability and compatibility of the SCO Product – As discussed above, many of the new processes utilize thermal cracking to convert all or a portion of the vacuum residue in the feedstock. Thermally cracked materials tend to be unstable and can form solids on storage or when combined with other pipeline or refinery streams. Many of the new partial upgrading processes include technology features that claim to minimize the instability of the product relative to delayed coking. These include lower operating temperatures, short reactor residence times, near complete conversion, and separation of the feedstock asphaltenes. Stability and compatibility testing of the final SCO is required to confirm these claims.
- b) The value of SCO products – Typical partially upgraded SCO has a low API gravity (~20°), fairly high sulfur and relatively low vacuum residue content. There is no current commercially sold SCO with similar specifications; the closest analog is dilbit based on Cold Lake and Lloydminster heavy oils. These dilbits, however, have much higher vacuum residue contents than partially upgraded SCO. Dilbit historically sells at approximately 25% discount to WTI. Licensors of the new partial upgrading processes have sometimes aggressively estimated discounts (below WTI) for their SCO in the range of 0 to 20% based in part on the benefit of low vacuum residue content. The economic viability of a partial upgrading route is highly dependent on the price received for the SCO product and discounts of 10-15% (below WTI) and above is typically required.

Many new licensors have constructed, or are planning to build large-scale demonstration plants that will lengthen the commercialisation schedule but provide considerable confidence in the technology. There have already been several partial upgrading technologies proven with high

technical readiness, such as: I^YQ[®] Process by ETX Systems Inc., HTL[®] Process by Ivanhoe Energy, SCWC[®] Process by JGC, HI-Q[®] Process by MEG Energy, etc.

1.2.2.1 I^YQ[®] process by ETX Systems

As an example of the high temperature partial upgrading technology, the I^YQ[®] process was invented by the ETX system. It combines two commercially proven technologies; plug-flow dryer and fluid bed coking, using revolutionarily designed short-contact coking techniques. As shown in the detailed coker structure in Figure 1-12, the bed of inert solids or coke is vertically fluidized by recycled product gas and moves via gravity, in a horizontal direction. The feed oil (vacuum residue) is sprayed on the hot solids as they enter the reactor. The oil reacts to form vapor (eventually liquids and non-condensable gas) and coke which deposits on the solid particles. The resident time is very short, and this prevents the over-coking of hydrocarbons. Solid fines are removed from the reactor vapor via cyclones and the condensable vapor is recovered as the product oil. The solids formed in the reactor are now “coked” and are routed to a partial oxidation (POX) burner and a circulated fluidized-bed boiler to burn off the coke (for steam generation) and also to reheat the solids before recycling to the reactor (ETX-Systems 2009).

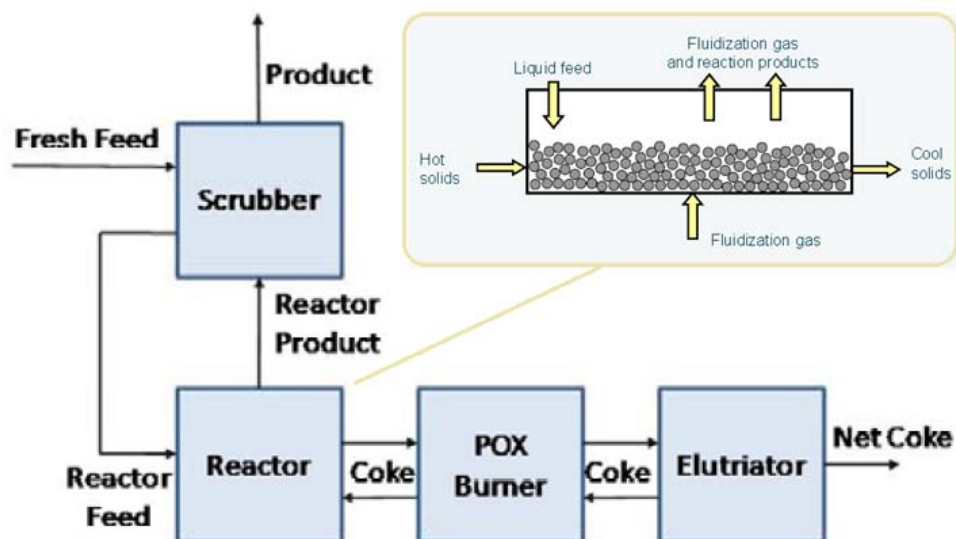


Figure 1-12 Process flow diagram of I^YQ[®] process and the mechanism of the core fluidized coker (Brown and Monaghan 2011)

The I^YQ[®] cross flow fluidized bed has a horizontal flow of sand (or coke) and a vertical flow of gas. This separates the residence times of the solids and gas. The rates of solid and gas can be optimized to maximize liquids production, minimize hydrocarbon loss and allow lower operating temperatures (Brown 2012). Recycle of the I^YQ[®] unconverted residue increases the level of vacuum residue conversion and the API gravity of the net SCO product. The recycle will also decrease the viscosity of the net SCO liquid product (Monaghan, Porter *et al.* 2012). It was reported that the I^YQ[®] process produced 82% wt. liquid oil products, like heavy sour crude and light naphtha products through its 1 barrel per day pilot operation. Without blending the total volume yield reached nearly 90% (LeSage 2009, Brown and Monaghan 2011). By separating and recycling the light end cracked gas product as fuel gas, the total energy balance of the I^YQ[®] technology could almost sustain its own natural gas requirement (Monaghan, Brown *et al.* 2012). The I^YQ[®] process adds calcium hydroxide (lime) with the crude feedstock, in order to: (a) neutralize the acids in the crude distillates (reduces TAN value) and (b) provide a sorbent for sulfur removal. It has been reported that there is no H₂ requirement for the I^YQ[®] process; however, a minimal amount of H₂ is required to hydrotreat light naphtha products for removing olefins/di-olefins generated through coking. In addition to this stability issue, another big

drawback is the large coke yield which is around 12%. The disposal of this considerable amount of coke will result in significant cost in transportation and landfill.

1.2.2.2 Heavy to Light Oil (HTL[®]) process by Ivanhoe Energy

Similar to the I^YQ[®] process, the HTL[®] process is also a high temperature fast coking process. The design originates from a fluid catalytic cracking (FCC) process. Instead of using catalyst, the HTL[®] process uses hot sand circulating in the reactor, and acyclone and burner to realize thermal pyrolysis, partial coking and coke combustion under low pressure. This technology produces a moderate yield of heavy SCO and a considerable amount of excess energy usually in the form of steam. The process was invented by the Ensyn Group in the 1980's for the conversion of wood and other biomass fuels. Six relatively small biomass commercial plants have been constructed and operated. These biomass facilities produce a "bio-oil" or "bio-fuel" and carbon from wood and other organic wastes (Freel and Graham 1998, 1999). The critical aspects of the HTL[®] process chemistry are rapid feedstock heat-up rate via mixing with the hot carrier and a short reaction residence time of less than a few seconds with minimal back-mixing. The above aspects result in fast pyrolysis which stops the thermal chemical reactions before the intermediates can degrade to non-reactive products, such as coke. A significant advantage of the HTL[®] process is reduced coke yield relative to traditional delayed or fluid coking processes (Freel and Graham 2012). Key design aspects are the initial mixing of the hot carrier and feedstock and the transport type reactor (Pavel, Silverman *et al.* 2012). The latter feature must include a relatively high velocity with minimal back mixing to avoid any particle or vapor residence time distribution (Pavel, Silverman *et al.* 2012).

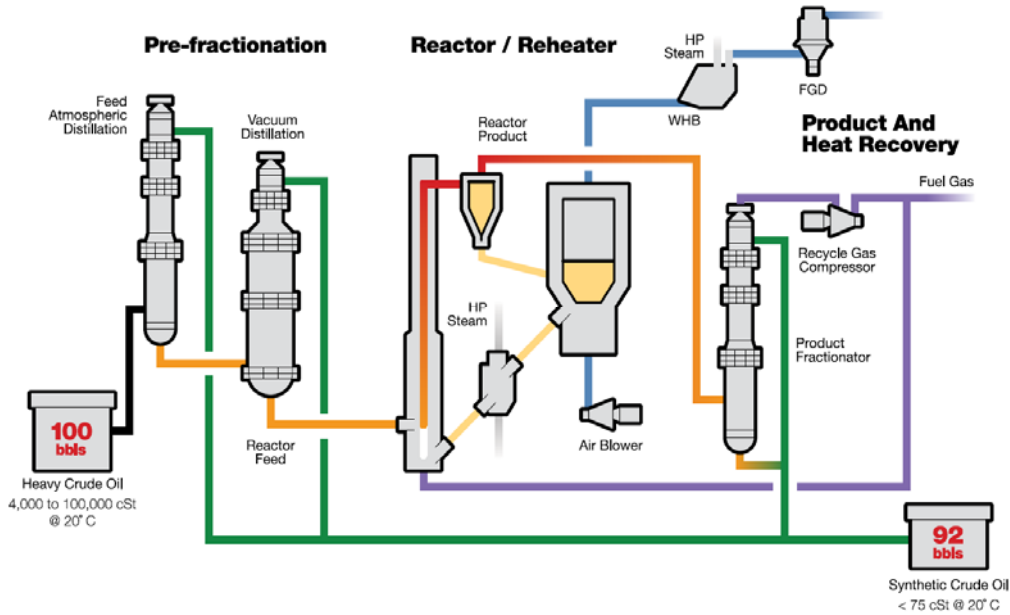


Figure 1-13 Flow diagram of the HTL[®] process (Cabrera, Hillerman et al. 2012)

A process flow diagram for the HTL[®] process is shown in Figure 1-13. Feed oil is initially fractionated to produce vacuum residue and distillate products. The vacuum residue is mixed with a hot inert carrier (sand), and then very quickly raised to high temperature where pyrolysis and thermal cracking occurs. The coked sand and conversion vapors are quickly transported in a riser-type reactor. The residence time in the reactor and cyclone separators is very short and the heavy liquid products are quickly quenched using distillate HTL[®] product. The rapid heating and short residence time are the critical aspects of the technology and insure that the reactions can be stopped prior to the production of unstable thermally cracked or coking-type products. The hot carrier (sand), captured in the cyclones, contains coke and other heavy material deposited on its surface. The regeneration occurs in the sand reheater to burn-off the coke and to provide a reheated carrier for the HTL[®] Reactor. Similar to the I^YQ[®] process, flue gas from the regenerator must be treated with lime before being vented to the atmosphere. The liquid products are blended together along with the straight run distillates to form the final SCO product. It has been reported that the HTL[®] process could produce 92% vol. SCO product after blending. The HTL[®] process could potentially export 0.8 million BTU per barrel energy after sustaining its own operation. Compared to the I^YQ[®] process, the HTL[®] process involves an integrated coke burner in its core

design, which utilizes all cracked gases and especially coke for generating energy. Consequently, there is no coke disposal issue. As a thermal process, product stability is questionable. It is highly possible that certain hydrotreating will be required to remove olefins/di-olefins. The H₂ consumption should be very close to the H₂ consumption number in the I^YQ[®] process.

1.2.2.3 Supercritical Water Cracking (SCWC[®]) process by JGC

Unlike most of other high temperature partial upgrading processes, the SCWC[®] process utilizes supercritical water (SCW). Once water is heated and pressurized over its critical point (374.15°C and 3206.2 psi), it has unique physical properties, such as density, viscosity and diffusivity, etc. It has been heavily investigated for its role in upgrading and partial upgrading. It was reported that the supercritical water could potentially donate H₂ (Daud, Pinilla *et al.* 2012). However, recent research published by Morimoto proved that the major role of the supercritical water was only phase separation (Morimoto, Sugimoto *et al.* 2014). In this way, the SCWC[®] process could be a combination of physical separation and chemical reaction. Physically, asphaltenes are extracted by SCWC[®] process from bitumen; chemically, the high temperature and pressure is favoured by thermocracking, during which the supercritical water also forms layers in the asphaltene micelles providing less probability for asphaltenes to condense. In this way, premium oil products can be produced containing very small amounts of heavy bottoms; and minimum coke is formed with the presence of supercritical water under coking/cracking conditions.

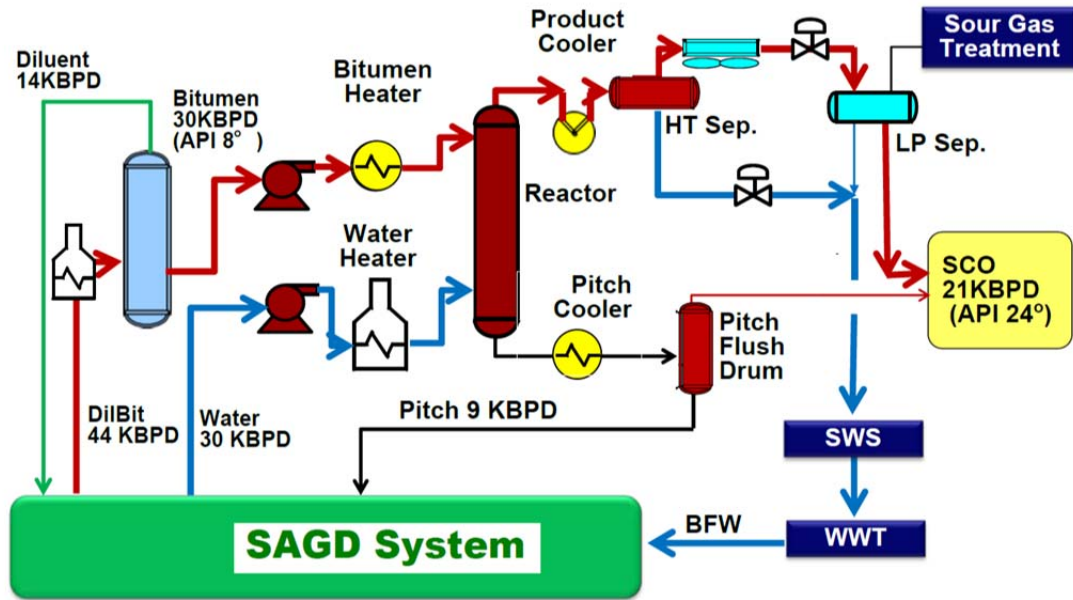


Figure 1-14 Process flow diagram of the SCWC[®] process (JGC 2013)

As shown in Figure 1-14, the process flow diagram for the SCWC[®] process is designed for upgrading bitumen with separated water instead of the emulsion coming from wellhead. The process involves a diluent recovery unit (DRU) for returning diluent, and heaters for both oil and water. To reach supercritical condition, a large amount of energy will be consumed here, especially for water heating. It will be much easier and economical if the emulsion could be fed directly. The reason is that the temperature of wellhead emulsion is nearly 300°C, which is very close to 374°C, the critical temperature of water. Due to the extreme corrosive property of supercritical water (Zhang, Tang *et al.* 2009), the core reactor is built of hastelloy material, an expensive anticorrosion reactor material. Consequently, the capital cost for the SCWC[®] process is very high. Furthermore, the reliability of this process will be highly affected due to more frequent reactor turnover for corrosion inspection. It was claimed by JGC that around 75% vol. pipeline transportable oil production in 2009 was obtained from bench top batch reactor tests (Kayukawa 2009). However, the indicated yield was only around 70% vol. based on pilot results (JGC 2013). This low oil yield would cut nearly 1/3 of product sale revenue. Around 30% vol. hydrocarbons were converted into pitch products, which were rich in asphaltenes, extremely viscous and much less valuable. Pitch was proposed by JGC for returning to the SAGD site as a

boiler fuel. However, the existing boiler on the SAGD site, is a once through steam generator (OTSG), which is only designed for natural gas instead of pitch. Hence, a specific boiler would have to be built for burning this pitch fuel. Considering the expensive rail freight cost vs. piping, burning SCWC[®] pitch products for the SAGD process is not economically favourable. Despite economic and engineering concerns, this technology is still technically interesting. It has received funding support from both the Canadian and Alberta government for designing, constructing and operating a 5-barrel per day pilot plant in Edmonton (Dettman, Liu *et al.* 2012).

1.2.2.4 Hi-Q[®] process by MEG Energy

There are also many other technologies using both physical separation and chemical reaction. One example is the Hi-Q[®] process licensed by MEG Energy, which is a combination of thermocracking and SDA. As shown in Figure 1-14, the Hi-Q process contains a DRU to separate the diluent from the SAGD feedstock. Then a thermocracker is designed after the DRU to mildly crack the oil. After this mild thermocracking the asphaltenes become easier to be precipitated and separated in the supercritical C5 SDA unit (Corcadden, Bruce *et al.* 2013). Hydrotreating of the naphtha product is included in the flow diagram but not discussed in the patent application. After combining the DAO with hydrotreated light fractions separated by a atmosphere tower, pipeline transportable oil is produced (MEG-Energy 2012, Corcadden, Bruce *et al.* 2013). This technology has been successfully tested in a 5 barrel per day pilot plant and is pending for commercial demo plant construction.

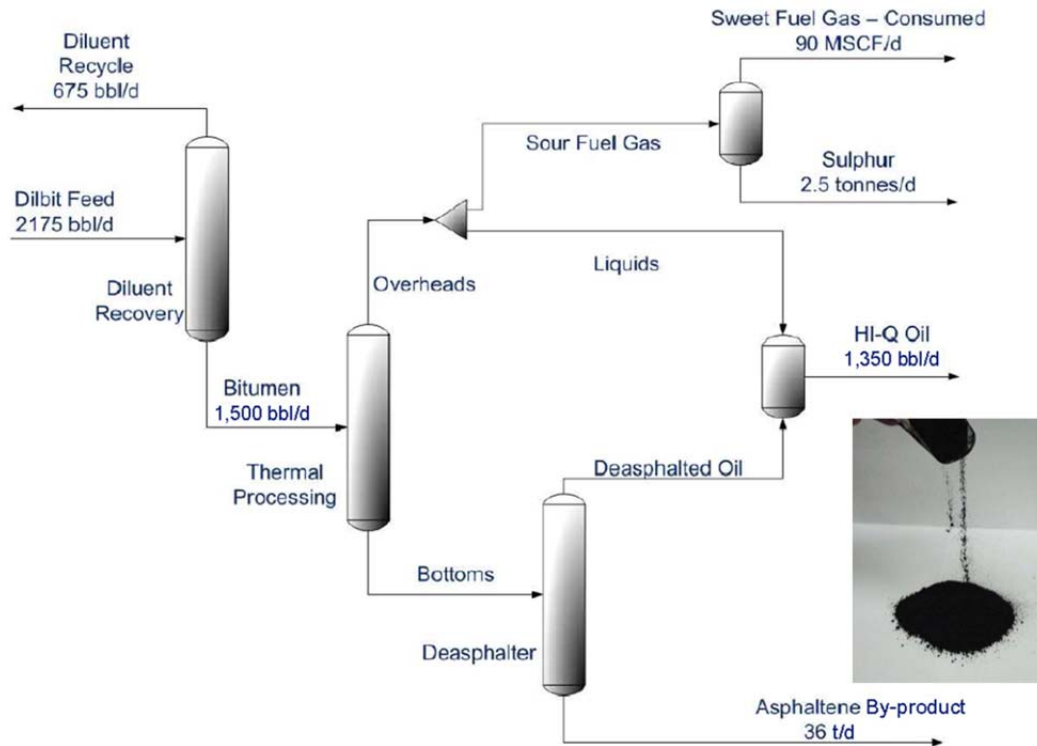


Figure 1-15 Process flow diagram of Hi-Q[®] process with material balance at operation of 1,500 bbl/day (MEG-Energy 2012, 2013)

The reported SCO yield can reach as high as 90% vol. It benefits from a mild thermocracking step, where only a few hydrocarbons suffer condensation and coking (MEG-Energy 2012, Corscadden, Bruce *et al.* 2013). Minimal H₂ is needed in the hydrotreating step to stabilize the SCO product. Based on the olefin yield in final products, the Hi-Q SCO product requires less H₂ compared to the I^YQ[®], HTL[®] and SCWC[®] processes as shown in Table 1-7. Compared to the SCWC[®] process by JGC, the rejected hydrocarbon level is much less. An asphaltene sample picture is shown in Figure 1-15. These asphaltene powders are ultra-fine and troublesome for product storage and transportation. However, the small powder size provides asphaltene a large interphase for heat transfer, if they are burnt in a gasifier. Further economic, business and engineering design is under-going for this emerging technology.

1.2.3 Summary of existing/emerging full upgrading and partial upgrading processes

As discussed above, partial upgrading is promising for producing pipeline transportable product compared to expensive full upgrading processes. Table 1-6 summarizes the performances of several selected partial upgrading technologies with OrCrude[®] as a reference of full upgrading technology.

Table 1-6 Comparison of selected partial upgrading and full upgrading technologies

	I ^Y Q [®]	HTL [®]	SCWC [®]	Hi-Q [®]	OrCrude [®]
Yield, wt.	82%	86%	65%	70%	82%
Yield, vol.	90%	92%	70%	83%	90%
SCO Quality	Medium	Poor	Medium	Medium	Very High
SCO Stability	Poor	Poor	Poor	Medium	High
Additional Capital for Improved Stability	High	High	High	Medium	-
Rejected Carbon Stream	Coke	Coke	Pitch	Asphaltenes	Asphaltenes
Rejected carbon yield, wt.	12%	-	35%	15%	-
Catalyst Usage	No	No	No	No	Yes
Initial Capital Cost	Low	Low	High	Low	Very High
Operating Cost	Low	Low	Medium	Very Low	Very High
Energy Production	Medium	High	-	Low	High
Additional Capital for Improved Energy Production	Medium	-	Very High	High	-

Among these 5 technologies it is clear that the HTL[®] process provides the highest SCO yield with around 86% wt. yield and 92% vol. yield. On the contrary, the SCWC[®] process suffers from the lowest SCO yield, since most of the heavy fractions have been converted into low-value pitch product. The OrCrude[®] process provides a similar yield with the HTL[®] process; however, this yield is lower than most of the other full upgrading technologies (usually >100% due to H₂ addition). The reason for this is that large portion of hydrocarbons were rejected in the form of asphaltenes, and the asphaltenes were then fed into a gasifier for energy production. Due to the hastelloy material requirement, the SCWC[®] process has the highest initial capital cost. The large energy consumption for heating and pressuring water to supercritical conditions also involves high operating costs for this technology. In thermocracking olefins and di-olefins are generated; this affects the product stability for the I^YQ[®], HTL[®], SCWC[®] and Hi-Q[®] processes.

Hydrotreatment is then required for all of these partial upgrading products. The required hydrotreatment is less severe than the hydrotreatment in a full upgrading process according to the limited olefin/di-olefin content, since there are no HDS, HDN or HDM requirements. If H₂ is needed, building a H₂ plant on site is expensive due to the high total installation factor (actual cost/equipment cost) in the Northern Alberta area ~10 (only around 4 in Edmonton). Much higher additional capital and operating costs should be expected for hydrotreating the partially upgraded SCO.

From an energy perspective, the HTL[®] process exceeds the rest of the partial upgrading technologies since an integrated coke burner is required in its design. Cracked gases and coke can be both consumed for energy production. The I^YQ[®], SCWC[®] and Hi-Q[®] processes all reject carbons, which require specific burners. Considering the amount of rejected carbon/hydrocarbon, different sizes of burner would need to be designed. In this way, the most expensive burner will be required for burning nearly 35% wt. pitch as fuel; the I^YQ[®] extra burner will be less costly as there is only around 12% wt. coke produced.

Based on the above discussion, it is concluded that none of the existing partial upgrading technologies is satisfactory. The concerns are:

- a) No catalyst usage - high energy intensity to maintain kinetics to minimize reactor size;
- b) No H₂ usage - leading to poor SCO product stability;
- c) Typical thermal processes cannot reduce enough TAN, unless H₂ is added;
- d) If hydrotreatment is required, the cost for building and operating a H₂ plant is very high;
- e) Thermal process yielded ~15% coke or fuel gases - production loss;
- f) Asphaltenes separated by SDA or SCW have very low value (nearly charcoal price ~\$4/bbl).

As a result, it would be ideal to have a technology which can produce pipeline transportable oil with none or less of the concerns listed above.

1.3 Novel emulsion upgrading technology

A novel one step partial upgrading process wherein emulsion breaking and upgrading occur in the same reactor using *in situ* H₂ generated from water present in the emulsion via the water gas shift reaction (WGSR) was developed by Prof. Flora T.T Ng and her research group (Ng and Tsakiri 1988, Ng and Tsakiri 1992). As shown in Figure 1-16 this process could produce pipeline transportable oil at a moderate temperature and pressure. No diluent is needed for blending. Excellent hydrotreating performance was achieved without any required H₂ supply during the upgrading. With the assistance of *in situ* H₂, product quality (like stability, TAN and S%) will be theoretically better than the SCOs produced by thermal partial upgrading processes like I^YQ[®], HTL[®], SCWC[®] and Hi-Q[®]. Since water is used as a feedstock in this novel emulsion upgrading process, it does not require extensive emulsion breaking steps (for oil/water separation) leading to synergy with existing oil sands mining and SAGD facilities for future expansion. In addition, this process demonstrated operational flexibility. The upgrading can be controlled to produce high quality SCO with rejection of highly viscous oil residue (HVOR). Similar to the rejected hydrocarbons in partial upgrading processes, this by-product could be fed into a gasifier (or a POX) for producing energy and syngas, which can be recycled for sustaining the emulsion upgrading. One key for this process is a new nano unsupported catalyst (unsupported) derived from a Mo precursor. As synthesized a highly active nano unsupported Mo sulfide catalyst can interact more efficiently with the large molecules present in the bitumen, and achieve better quality and yield of oil products under moderate reaction conditions. This helps emulsion upgrading technology stand out among most of the partial upgrading technologies.

As a summary, this novel emulsion upgrading process has the following advantages:

- a. Produce pipeline transportable SCO product without diluent blending
- b. Excel most of other existing thermal partially upgraded products in stability, TAN and sulfur content

- c. Requires no H₂ plant
- d. Reduce emulsion breaking or froth treatment steps
- e. Potentially self-sustainable in energy and syngas supply with the help of a gasifier

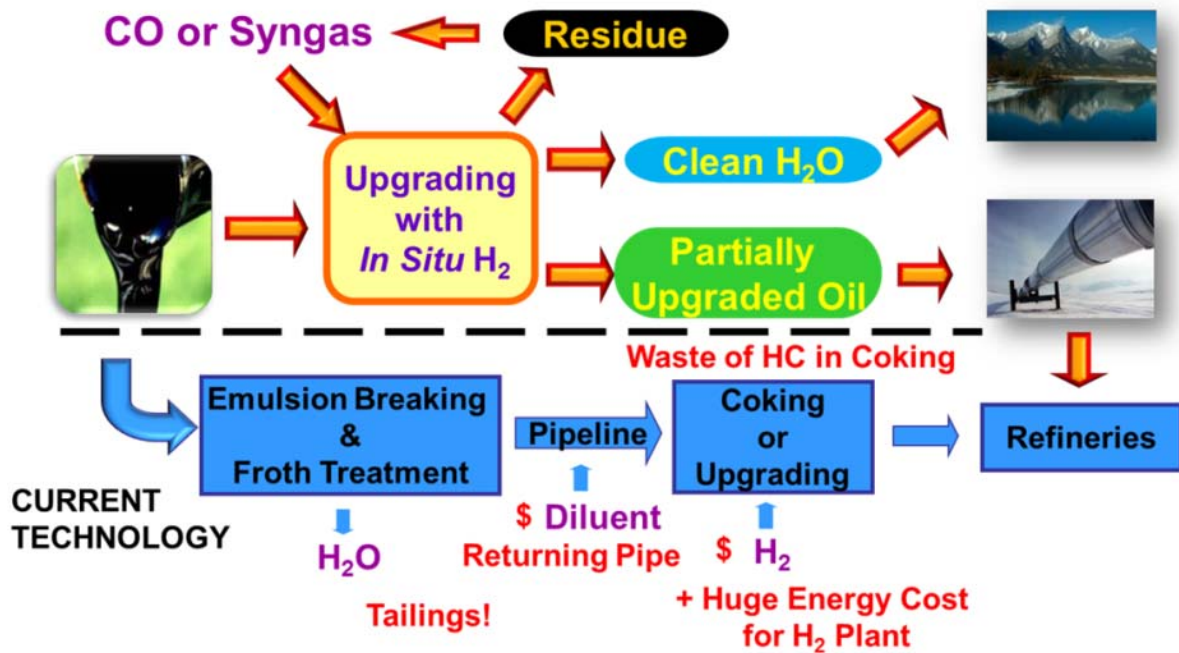


Figure 1-16 Comparison of novel upgrading process and the current extracting and diluting process

1.4 Objectives

Previous work done at a bench scale level has demonstrated that *in situ* H₂ is feasible and even more effective than molecular H₂ for upgrading and hydrotreating Cold Lake bitumen emulsions (22wt% H₂O, 4.4 wt% S dry, 8780 cP@40°C), which meant that *in situ* H₂ is a promising and economical alternative source of molecular H₂ for industrial upgrading processes (Moll, Li *et al.* 2000). The role of water has been discussed in fundamental studies. For example, hydrotreating research on different model compounds such as HDS of dibenzothiophene (DBT) (Lee and Ng 2006), 4,6-dimethyldibenzothiophene (4,6-DMDBT) (Liu and Ng 2010), HDN of quinolone

(Zhang 2005, Lee and Ng 2006) and carbazole (Liu and Ng 2010), HDA of naphthalene (Zhang 2005, Choy 2009) has been accomplished to demonstrate different processes occurring inside this complex bitumen upgrading reaction system. Different cross-interaction between HDS and HDN has also been discussed, and competitive adsorption on the catalyst surface exists in this upgrading system (Liu and Ng 2010). Besides the fundamental research, some practical studies on upgrading actual oil samples such as a straight-run diesel fraction (161-343°C) and oil sands derived light gas oil (LGO) with this novel technology have been completed and its feasibility confirmed (Siewe and Ng 1998, Jia, Alghamdi *et al.* 2012).

At this stage, the concept of this novel emulsion upgrading technology has been validated. However, more development is required to move it from a bench top scale to a pilot plant. In order to provide information to gain a further understanding of the potential of this process for commercialization, it is important to explore other unknowns in this complex process, such as:

- a) **To understand how asphaltenes are converted during this emulsion upgrading process;**
- b) **To assess water purification performance especially the removal of the most unwanted toxicity sources -- naphthenic acids;**
- c) **To carry out a more thorough understanding of the *in situ* catalysts.**

In order to solve these questions, experiments on actual bitumen samples have been completed and will be discussed in Chapter 3 and Chapter 4. Chapter 3 involves Cold Lake bitumen emulsion upgrading, with emphasis on the upgrading of asphaltenes. Chapter 4 is concerned with Athabasca bitumen upgrading, where dry bitumen was fed with dirty water as representative for oil sand process affected water (OSPW). This made it possible to investigate the effect of water and water purification performance. Chapter 5 provides a detailed mechanistic study of how the emulsion was treated, especially for removing the most unwanted toxicity source – naphthenic acids in both the oil and water phases. Chapter 6 reports on a characterization study of the catalyst involved in light gas oil (LGO) upgrading. The effect of temperature, time, LGO and promoters on catalyst morphologies will be discussed. Chapter 7 provides a deeper level of

characterization and statistical study on the fresh *ex situ* catalysts synthesized under various conditions. Some correlations between particle morphology and activity were observed and analyzed.

Chapter 2 Experimental and Methodology

2.1 Feedstocks, catalyst precursors and reaction gases

2.1.1 Feedstocks

A Cold Lake bitumen emulsion was used as a feedstock for emulsion upgrading. This bitumen emulsion feedstock came from an Alberta *in situ* steam injection plant and contained 9.8% asphaltenes, 3.5%wt S, 30.0% pitch (524°C+) and 15.6% H₂O. There was no free water observed in the sample, and all the water was well emulsified. This emulsified water was used as the feed for the WGSR, and there was no additional water fed. The Athabasca bitumen feed came from an Alberta mining plant, and the sampling point was after froth treatment as described in Chapter 1. As a result, most of water was demulsified and separated from the oil phase. There was free water observed at the bottom of the sample barrel, and the water was dirty water extracted through froth treatment. It contained emulsified oil, metal cations, inorganic and organic anions (like naphthenic acids). This dirty water was fed as a representative of OSPW. Due to geological differences in deposits, Athabasca bitumen has poorer quality. The sample used in this study contained 4.1%wt S and 54.5%wt pitch and around 1.2% H₂O. The light gas oil (LGO) sample was derived from Alberta oil sands, and it contained 2.4%wt S and 12.5%wt pitch. In the *ex situ* catalyst synthesis, hexadecane (C₁₆H₃₄) or C16 in short, purchased from Fisher Scientific with 99.9% purity, was also used to replace LGO as the oil solvent in order to form less coke on the catalyst surface.

In the naphthenic acid removal study, various model compounds were selected for representing naphthenic acids, including: 2-naphthoic acid (2-NA, C₁₀H₇COOH, purity: 98%) and 4-heptylbenzoic acid (C7-BA, C₁₄H₂₀O₂ purity: 97%) purchased from Aldrich Chemical. Toluene (C₇H₈, purity: 99%), purchased from Fisher Scientific was used to dissolve model compounds to represent the oil phase. Various volumes of deionized water were added to provide a representative emulsion. For a feedstock of 2-NA in toluene with 10mL water, for example: the

2-NA concentrations in oil and water phases were 1641ppmw in oil and 84.1 ppmw in water phases, respectively. In order to improve miscibility, the oil/water mixer was sonicated for 20min before the oil and water phases were examined.

2.1.2 Catalyst precursor

Phosphomolybdic acid (PMA, $12\text{MoO}_3 \cdot \text{H}_3\text{PO}_4 \cdot x\text{H}_2\text{O}$, purity: 99.9%) purchased from Aldrich Chemical was used as a catalyst precursor. The Mo concentration in the PMA solution was monitored by ICP to adjust the loading volume for accurate total Mo loading. A typical Mo concentration was around 45000~50000 ppmw. For evaluating the effects of different metals, NiSO_4 , CoSO_4 , FeSO_4 , $\text{C}_{10}\text{H}_{14}\text{O}_5\text{V}$, and K_2CO_3 were chosen as the precursors for Ni, Co, V, Fe and K. Among the metal precursors, nickel sulfate ($\text{NiSO}_4 \cdot x\text{H}_2\text{O}$, purity: 99.8%) was purchased from Fisher Scientific; cobalt (II) sulfate ($\text{CoSO}_4 \cdot x\text{H}_2\text{O}$, purity: 99.9%) was purchased from Aldrich Chemical.

2.1.3 Reaction gases

Reaction gases, CO, H_2 , H_2S , and N_2 were purchased from Paraxair. CO was used to produce *in situ* H_2 through the WGSR. Molecular H_2 was used as the *ex situ* reaction medium. Catalyst sulfiding was operated under a H_2S environment. N_2 was mainly used for thermal cracking and leak detection. The product grades and purities of the above gases are shown in Table 2-1.

Table 2-1 Grades and purities of major reaction gases

Gas	Product grade	Purity
H_2	5.0	99.999%
CO	2.5	99.5%
N_2	5.0 UH	99.999%
H_2S	2.6	99.6%

2.2 Autoclave reactor operation

2.2.1 Reactors

The upgrading reaction was carried out in three different autoclave batch reactors as shown in Table 2-2.

Table 2-2 Reactors used in this thesis for different purposes

300mL AISI SS-316 batch Autoclave reactor	300mL HC-276 batch Autoclave reactor	1L SS-316 batch Autoclave reactor
Bitumen upgrading; LGO upgrading	<i>Ex situ</i> catalyst synthesis; Model compounds reaction	Catalyst synthesis in LGO and hexadecane

2.2.1.1 300mL AISI SS-316 batch Autoclave reactor

A 300mL AISI SS-316 batch Autoclave reactor was used in the upgrading experiments for the Cold Lake bitumen emulsion, Athabasca bitumen and LGO. The reactor was made of stainless steel 316L, and equipped with a Magnedrive II assembly stirrer. The working volume is 249mL. The system was heated by a wall heater controlled by a Honeywell Universal Digital Controller (UDC-200Mini Pro). The system pressure was measured with an Omega PX-300 pressure transducer. As shown in Figure 2-1, a stainless steel liner was used in the bitumen upgrading experiments, due to the high viscosity of bitumen and upgraded product. There was a gas outlet tube installed to collect gas phase samples during the reaction. Due to the poor mass balance caused by this valve opening during the bitumen experiments, only a few experiments were carried out in this way for the purpose of determining changes in the gas phase composition during the reaction. Cooling water is used to cool the reactor head and sampling tube.

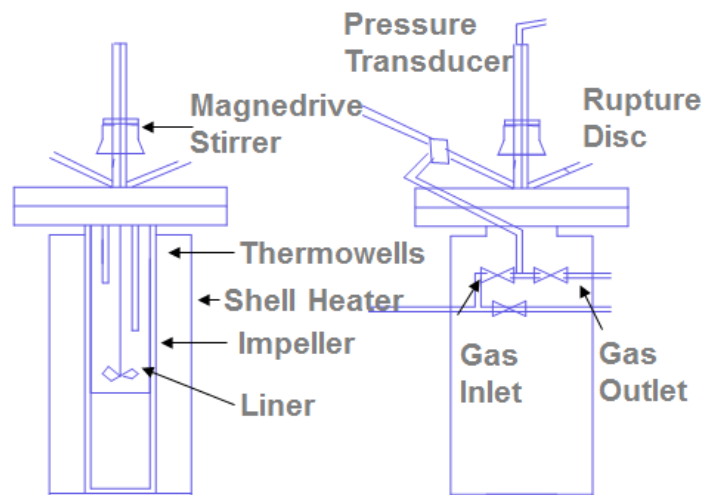


Figure 2-1 Schematic of 300mL AISI SS-316 Autoclave batch reactor (Moll 1999)

2.2.1.2 300mL HC-276 batch Autoclave reactor

A 300mL HC-276 batch Autoclave reactor was used in the *ex situ* catalyst synthesis and model compound studies, such as HDS of DBT, naphthenic acid removal, etc. The reactor was made of Hastelloy C-276 which has a high resistance to corrosion, which usually occurs under supercritical water conditions. The autoclave is equipped with a Magnedrive stirrer, which was periodically disassembled and cleaned to ensure no deposit was on the Magnedrive bearings. The reactor working volume was 257mL. Two Omega PX209-30V85GI pressure transducers and two Omega K-type thermocouples were installed to measure pressure and temperature separately. This reactor was installed by members of the Ng laboratory with a comprehensive sampling system. This allowed independent measurements of temperature in both the liquid and gas phases for upper and lower reactor region samples. As shown in Figure 2-2, all valves and lines from the reactor to valve 1 and valve 12 are made of Hastelloy C-276 material. Except for the fittings downstream of valve 5 and valve 16 which are Swagelok SS-316 compression fittings, the rest of the fittings and valves are all made by Hastelloy C-276. Both liquid and gas sampling systems are installed with pressure indicators and proportional relief valves designed to open when the pressure reaches 85 psig to ensure safety. A thermocouple installed inside the 150 ml liquid sample expansion vessel was used to measure the temperature of the sample.

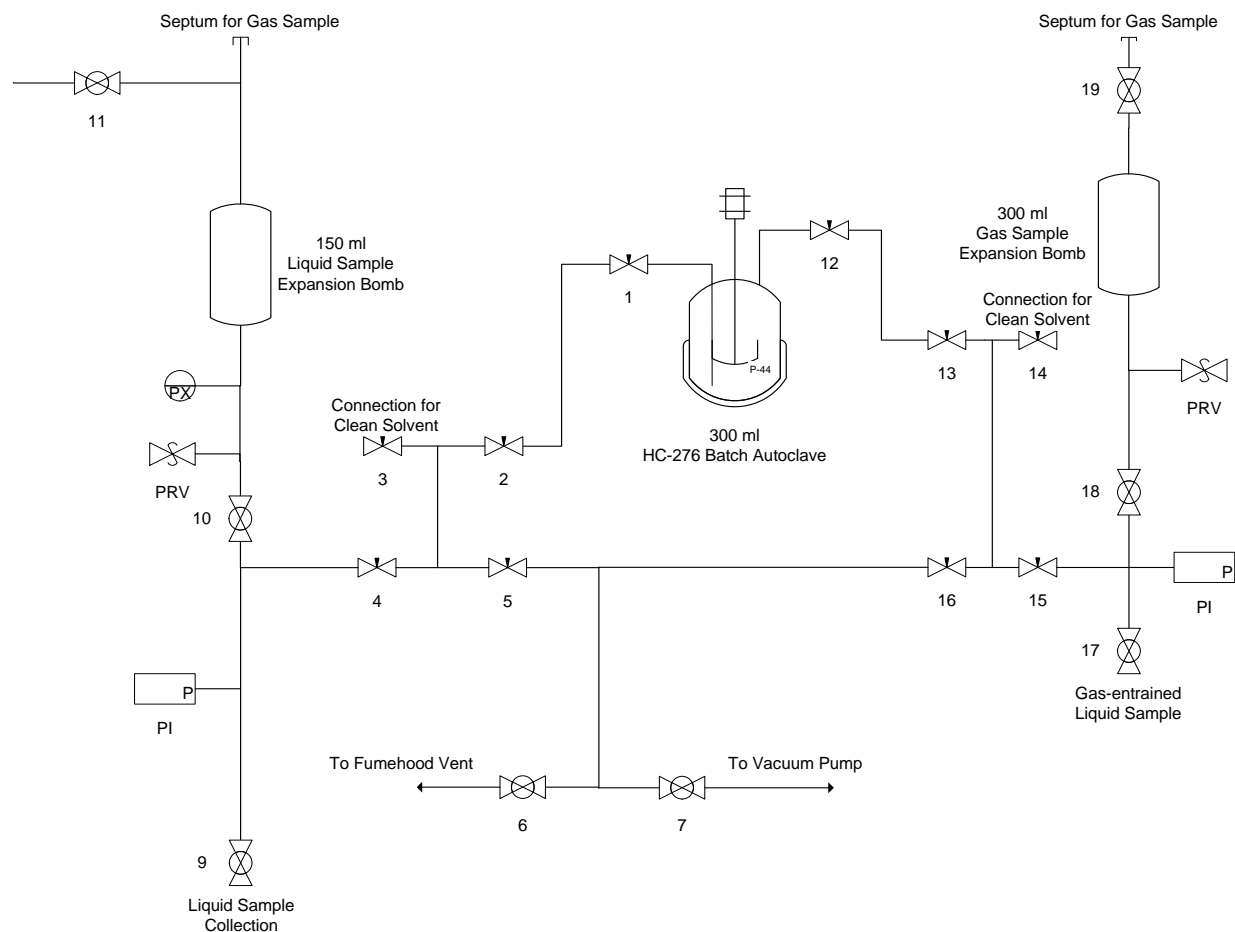


Figure 2-2 Experimental setup of Autoclave Engineers 300 ml HC-276 bolted closure Autoclave and sampling system (Choy 2009)

2.2.1.3 1L SS-316 batch Autoclave reactor

Some LGO upgrading experiments were carried out in a 1L SS-316 batch Autoclave reactor. The majority of experiments carried out in this reactor were related with *ex situ* catalyst synthesis, since it has a larger volume, and is capable of providing sampling during the reaction. A schematic diagram of the reactor with its sampling system is shown in Figure 2-3. The reactor vessel and all the fittings were made of stainless steel 316. The working volume of the reactor is 995mL. The reactor was also equipped with a magnetic drive impeller. An insulated electric furnace sleeve was installed for heating, and the furnace was controlled by an Omega model 2011 temperature controller. An Omega pressure transducer was also installed with a 0-10000 psi pressure gauge.

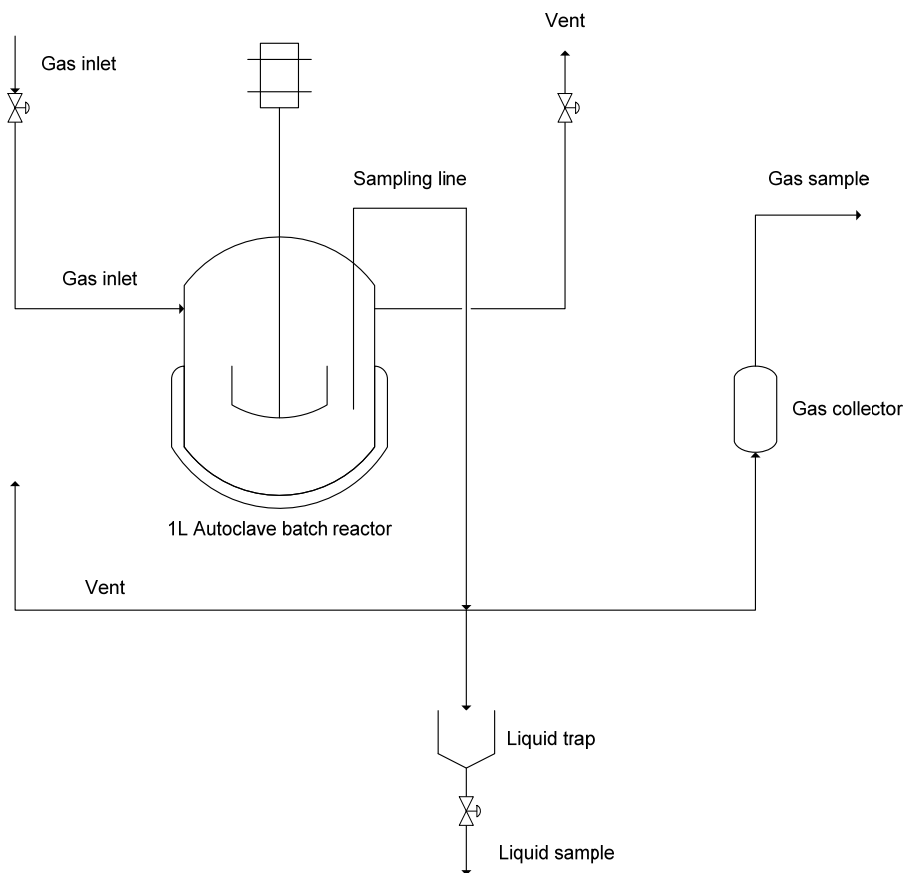


Figure 2-3 Schematic diagram of the 1L reactor's sampling system

2.2.2 Run preparation

2.2.2.1 Charging, sealing and leak test

Oil feeds were measured and transferred into the clean batch reactor vessel using a glass pipette when the oil feed was not bitumen. Aqueous feeds, including water and/or the liquid catalyst precursor solution, were charged via an Eppendorf pipette by controlling the total water volume. If solid samples, like *ex situ* catalyst, metal salts, were added, they were measured by an electronic balance and then transferred by weighing papers into the vessel followed by rinsing the weighing papers with oil or the aqueous phase. In a typical bitumen upgrading experiment, the bitumen emulsion or dry bitumen was put into the reactor liner, and then the liner was transferred into a 300mL SS-316 Autoclave batch reactor. Then the reactor was sealed with a metal sealing gasket, sprayed with a dry thin layer of Dow Molycoat lubricant. A cooling water line and a thermocouple were attached when the 300mL SS-316 Autoclave batch reactor was

used. After the installation, the reactor was flushed 3 times with 300psi N₂. Then 1800 psi N₂ was purged into the autoclave for a leak test. The system pressure was monitored for an hour to ensure that there was no/minimal gas leakage. A slight pressure drop (~30psi) was expected due to the dissolution of the gas in the liquid. Then the main reaction gas (CO, H₂, syngas or N₂) was flushed into the reactor to a pressure of 300psi for 3 times to get rid of the remaining N₂. After that, a certain amount of H₂S (typically 15psi) was charged into the system. The presence of H₂S was mainly used for catalysts *in situ* pre-sulfidation during the reaction and maintaining catalytic activity. It should be noted that the loading of H₂S should be carried out as quickly as possible due to the high H₂S solubility in the oil and water phases. After flushing the remaining H₂S with the reaction gas from the gas tube into a sulfur adsorption tower containing EDTA-Fe and NaHCO₃ solution, the reactor vessel was pressurized with reaction gas up to 600 psi. After insulating the reactor vessel outside of the heating jacket, the heating program and stirring were initiated and the reaction was carried out under a specified temperature and pressure.

The experiments were carried out with an initial total pressure of 600 psi at room temperature. The heating ramp was set at 4°C/min. Various reaction temperatures, reaction times, atmospheres, catalyst loading and metal addition were examined as summarized in Table 2-3.

Table 2-3 Summary of reaction conditions in different reactors

		300mL SS-316 reactor			300mL HC-276 reactor		1L SS-316 reactor
Experiments		Cold Lake bitumen emulsion upgrading	Athabasca bitumen upgrading	LGO upgrading	Naphthenic acids removal	Fresh <i>ex situ</i> catalysts synthesis	Catalyst synthesis in LGO and C16
Liquid feeds		Bitumen emulsion	Bitumen + dirty water	LGO + water	Toluene solution + water	Toluene solution + water	LGO or C16 + water
	Oil	80g	80g	100 mL	80 mL	100 mL	300 mL
	Additional water	-	0, 5 or 10 mL	5, 10 or 15 mL	10, 15 or 20 mL	10	30 mL
	Catalyst type, <i>if used</i>	MoSx	MoSx or soft solids	MoSx	MoSx or MoO	MoSx	MoSx
	Catalyst precursor	PMA	PMA	PMA	PMA	PMA	PMA
	Mo loading (<i>ppmw</i>), <i>if used</i>	704 or 1408	1408	1408	0, 168, 337 or 673	28160	1408
	Type of metal additives, <i>if used</i>	Ni	Ni, V or Ni+V	Ni, Co, Fe, V or K	Ni or Co	Ni or Co	Ni
	Metal:Mo ratio	0.6:1	0.6:1	0.6:1	0.2:1	0.3, 0.5 or 0.7:1	0.6:1
	Major reaction gases	N ₂ , CO, H ₂ or CO+ H ₂	N ₂ , CO, H ₂ or CO+ H ₂	CO, H ₂ or CO+ H ₂	N ₂ , CO, H ₂ or CO+ H ₂	CO or H ₂	CO
Pressure	P _{Total} (psi)	600	600	600	600	600	600
	P _{H₂S} (psi)	15	15	10	15	30	30
	Temperature (°C)	395, 405 or 415	415	390 or 410	300, 340 or 415	300, 340, 390	0 - 390
	Ramp (°C/min)	4	4	4	4	4	4
	Stirring speed (rpm)	900	900	900	900	900	900
	Reaction time (h)	1, 2 or 3	1 or 2	2	2	0	0 - 2

2.2.3 Sampling during reaction

During the reaction, gas and liquid samples were collected by opening sampling valves. Before the actual sampling, the sampling tube was usually evacuated using an oil pump, and then flushed by opening the sampling valves for sampling accuracy. Typically 2 to 3 flushes were carried out before the reaction reached sampling temperature/time. Every time when sampling

valve was opened for sampling (~30sec), the system pressure dropped 20-40 psi. A Hamilton sampling syringe was then used to store the gas from the expansion vessel for GC analysis. After releasing the leftover pressure in the expansion vessel through a vent line, the rest of the liquid sample was collected in glass sample bottles for further liquid characterization. Sampling time, temperature, pressure and other reaction conditions were recorded. The sample bottles were also weighted before and after collection in order to calculate sample weight for a mass balance. It should be noted that when the Hastelloy C-276 reactor was used for sampling, it was necessary to clean the sampling tube after each use. As shown in Figure 2-2, wash toluene was added through a funnel from valve #3 to rinse the sampling tube. By repeating this rinse 3 times, most of the oil phase was removed. This was then followed by 3 ethanol rinses, which removed the aqueous phase and especially catalyst due to ethanol's high polarity. The whole cleaning procedure was completed by flushing the sampling tube with high pressure air, which finally evaporated the leftover ethanol and left a clean tube for the next sampling operation. A sampling procedure summary is shown in Appendix C.

2.2.4 Completion of the run

At the end of the reaction period, the reaction was stopped by turning off the heater and the heating jacket (furnace) was also removed with insulated gloves for safety considerations. Stirring was reduced to 100-200 rpm to prevent overheating near the reactor wall from coke formation. The Hastelloy C-276 reactor was equipped with cooling air line near the stirrer; however, the cooling air should not be opened until the reaction temperature dropped below 200 °C. This was because the sudden low temperature introduced by cooling air might crack and damage the reactor. When the reactor reached room temperature, the final temperature and pressure were recorded, followed by pressure release and gas sample collection. After a N₂ purge for removing the leftover H₂S dissolved in liquid, the reactor was opened. Toluene, ethanol and acetone were used to clean the reactor and stirrer after the product collection.

2.3 Product separation and collection after reaction

2.3.1 General product separation and collection

In the experiments involving bitumen, gases were collected in a 3-litre Sensidyne TEDLAR gas sampling bag after the reaction. There was only oil and solid residues and H₂O inside the reactor. During the pressure release, some light oil was trapped in a flask placed in ice-salt bath. Some other light oil was gathered from outside the liner via a glass pipette. The rest of the oil was poured out from the liner. Some highly viscous oil residue (HVOR) stuck to the liner inner-wall, and could not be poured out. The HVOR could be heavy oil, however, it was expected to be an asphaltene-rich fraction like pitch (the precursor for coke formation). Since asphaltenes can be dissolved in toluene, the HVOR was rinsed with toluene to collect the asphaltenes. Detailed asphaltene separation and collection will be discussed in Section 2.3.2. After filtering the remnants from the HVOR toluene rinse and the rest of the oil product, some solids residues were collected, which were mainly coke and spent catalyst. Figure 2-4 describes the whole procedure for sample collection, where the final upgraded oil and water were separated and collected in a graduated separatory funnel.

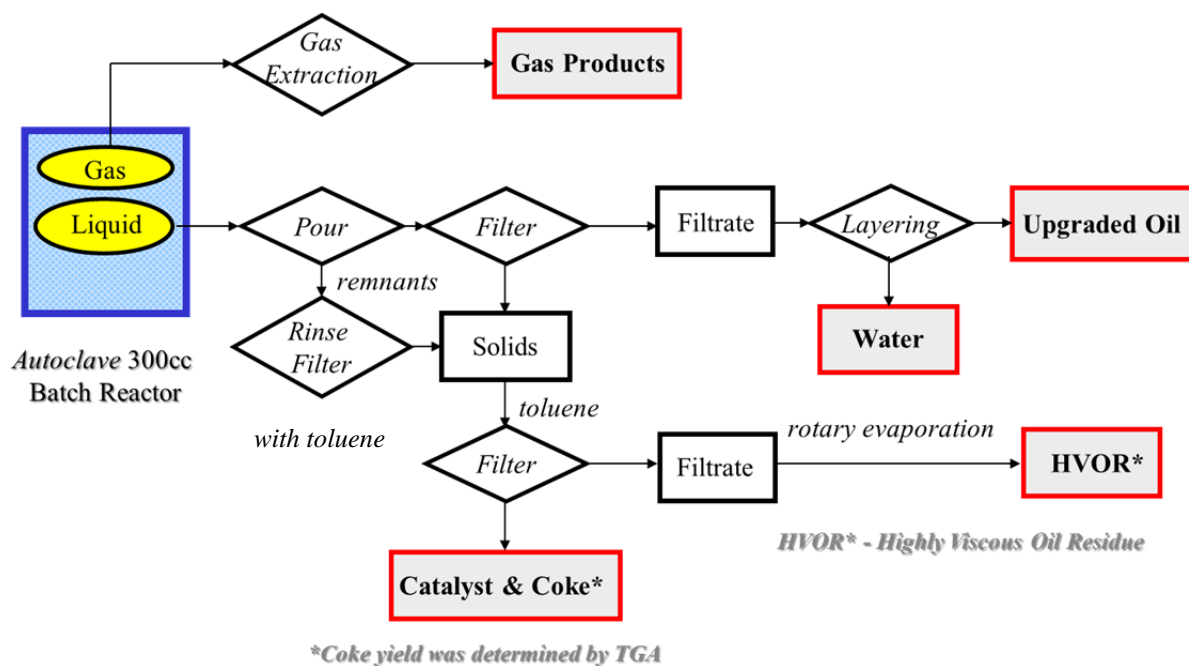


Figure 2-4 General product separation and collection flow chart for bitumen upgrading experiments

2.3.2 Asphaltenes separation

In the experiments involving bitumen, asphaltenes were separated and collected following ASTM D2007-80 standard procedure, whereby toluene and n-pentane were used as the solvents. As shown in Figure 2-4, the HVOR was rinsed with a large amount of toluene, where the filtrate contained asphaltenes. According to ASTM D2007-80, the feed needs to be dissolved using a 1:1 ratio of toluene. As a result, the toluene diluted HVOR was evaporated in a rotary evaporator to remove all the toluene. Then the weight collected in the round evaporation flask was considered as the weight for HVOR asphaltene collection. The upgraded oil also contains asphaltenes, so part of upgraded oil product was measured for asphaltene collection after obtaining a yield calculation and mass balance. As shown in Figure 2-5, a 1:1 ratio toluene was added based on the weight of HVOR or oil product. After removing the toluene insoluble solids by filtration with a #42 filter paper, a 40:1 ratio of n-pentane was mixed with the filtrate.

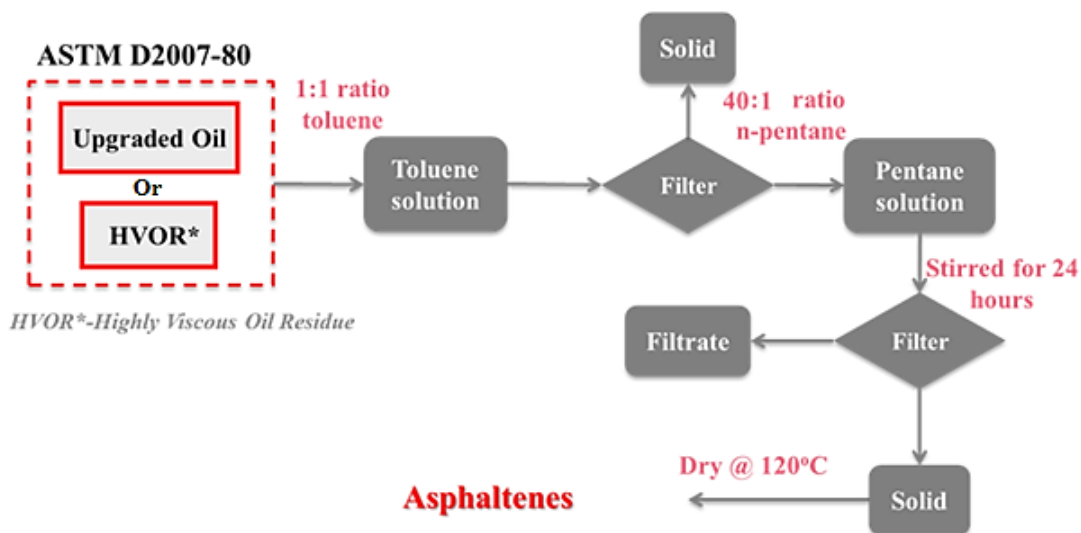


Figure 2-5 Asphaltene separation and collection procedure following ASTM D2007-80

In order to prevent the loss of volatile n-pentane, a cooling water condenser was installed as shown in Figure 2-6(a). After stirring for 24 hours, the 40:1 ratio n-pentane solution was filtered with a #42 filter paper and the insoluble solids were collected as shown in Figure 2-6(b). After drying at 120 °C in an oven overnight and weighing, the mass of asphaltenes in the HVOR or the oil product was determined. With additional information like the HVOR yield, upgraded oil yield and the weight of oil product used for asphaltene collection, the total asphaltene contents were calculated.



Figure 2-6 (a) n-pentane mixture stirring with a condensing system in a fume hood; (b) asphalenes solids collected after filtration

2.4 Basic analytical equations

2.4.1 Mass balance

Based on the products collected, the mass balance was defined as below. Inlet: oil feed, H₂O feed, catalyst precursor, gas charged (H₂S and reaction gases); Outlet: Oil products, leftover H₂O, gas products. As a result, the mass balance was calculated based on Eq. 2-1:

$$\text{Mass balance \%} = \frac{m(\text{oil products}) + m(\text{H}_2\text{O left}) + m(\text{solids}) + m(\text{gas products})}{m(\text{oil feed}) + m(\text{H}_2\text{O feed}) + m(\text{catalyst precursor}) + m(\text{gas charged})} \times 100\% \quad (\text{Eq. 2-1})$$

2.4.2 Yield, WGS conversion and water consumption

For the oil samples the product yield is another important value, and the calculation was carried out using Eq. 2-2:

$$\text{Product yield\%} = \frac{m(\text{oil products})}{m(\text{oil feedstock}) - m(\text{H}_2\text{O})} \times 100\% \quad (\text{Eq. 2-2})$$

By combining ideal gas law and the normalized gas component percentages, the mole numbers of CO and CO₂ could be obtained. Accordingly the WGSR was evaluated through calculating CO conversion based on these mole numbers. Hence the WGSR conversion can be calculated based on Eq. 2-3.

$$\text{WGSR Conversion\%} = \frac{n(\text{CO}_2)}{n(\text{CO})+n(\text{CO}_2)} \times 100\% \quad (\text{Eq. 2-3})$$

Water consumption was also considered as the role of H₂O in reaction is uncertain. Besides being a reagent in the WGSR, and a high partial pressure provider, water itself could also possibly be a hydrogen donor. The consumption of water was calculated based on Eq. 2-4.

$$\text{H}_2\text{O Consumption\%} = \frac{m(\text{total H}_2\text{O})-m(\text{H}_2\text{O left})}{m(\text{total H}_2\text{O})} \times 100\% \quad (\text{Eq. 2-4})$$

2.5 Product characterization

2.5.1 Oil analysis

2.5.1.1 Gas Chromatography -Simulated Distillation (GC-SIMDIS)

Agilent 6890N GC-SIMDIS was used to analyze the boiling point distribution of the products. The GC was equipped with a 10m×530μm×2.65μm DB-1 capillary column and a flame ionization detector (FID). ASTM D2887x method was used, which covered boiling points from 100°C to 615°C. Before each injection, oil samples were diluted 50 times using carbon disulfide. Characterization and calibration details are shown in Appendix A.1.

2.5.1.2 X-Ray Fluorescence (XRF)

The total sulfur content in the liquid or solid samples was analyzed via an Oxford Lab-X 3000s X-Ray Fluorescence spectrometer (XRF). The detection limit was 10 ppmw S. Characterization and calibration details are shown in Appendix A.2. Besides excess H₂S and MoS₂ catalyst, the upgraded oil and HVOR were the major S containing components among all of the products. So the final S content was defined according to Eq. 2-5.

$$m(\text{S in product}) = c(\text{S in upgraded oil}) \times m(\text{upgraded oil}) + c(\text{S in HVOR}) \times m(\text{HVOR})$$

(Eq. 2-5)

Accordingly, the total S removal was calculated using Eq. 2-6:

$$\text{S removal\%} = \frac{m(\text{S in bitumen feedstock}) - m(\text{S in product})}{m(\text{S in bitumen feedstock})} \times 100\%$$

(Eq. 2-6)

2.5.1.3 GC-FID/TSD/PFPD

A Varian CP-3800 GC was equipped with a VF-05MS capillary column; three detectors: FID, thermionic specific detector (TSD) and pulsed flame photometric detector (PFPD). These three detectors could simultaneously carry out identification and quantitative analysis. TSD and PFPD specific for N and S species were used to detect some of the complex refractory compounds. A Varian CP-3800 gas chromatograph equipped with a 30m× 0.32mm VF-05MS capillary column. FID was mainly used to analyze the components in organic phase (such as 2-NA, DBT, 2-methyl-naphthalene, naphthalene, tetralin, benzoic acid, etc.). Characterization details are shown in Appendix A.3

2.5.1.4 GC-Mass Spectrometry (GC-MS)

A Varian CP-3800 equipped with Varian Saturn 2000 mass spectrometer was used for identifying unknown products in the oil phase. The column in GC-MS was an Agilent 30m× 0.25mm DB-5MS capillary column. Characterization details are shown in Appendix A.4.

2.5.2 Asphaltenes analysis

2.5.2.1 Gel Permeation Chromatography (GPC)

Asphaltene molecular sizes were analyzed using a Viscotek 2100 GPC. The column set was a linear combination of PolyAnalytik organic mixed bed column PAS-103-L, PAS-104-L and PAS-105-L with exclusion limit at 70×10^3 Da, 4×10^3 Da and 4×10^6 Da respectively. The asphaltene samples were dissolved in HPLC level tetrahydrofuran (THF), and the concentration

was controlled at ~1%. The injection volume was 100uL, and the flow rate of the THF mobile phase was 1mL/min. Three detectors were used in the GPC: ultra violet (UV) detector, right angle light scattering (RALS) detector and low angle light scattering (LALS) detector.

2.5.2.2 Fourier Transform Infrared Spectroscopy (FT-IR)

Asphaltene structural analysis was carried out via a Thermal Nicolet 6700 Fourier transform infrared spectroscopy (FT-IR). Asphaltene powders were ground with KBr before pressurized sample pallet preparation.

2.5.2.3 Simultaneous Differential Scanning Calorimetry and Thermogravimetric Analysis (DSC-TGA)

A TA SDT Q600 DSC-TGA was used to analyze the effect of oxidation on the asphaltenes. After extracting the asphaltenes, the samples were carefully transferred into an alumina pan. The test experiments were operated under an air atmosphere with a flow rate of 100mL/min, to a final temperature of 1000°C with ramp of 20°C/min. The temperature, weight, heat flow and temperature difference signals were recorded using a dynamic method.

2.5.2.4 Inductively Coupled Plasma Emission Spectrometer (ICP)

In order to analyze the metal content in the asphaltenes, a Teledyne Prodigy ICP was used. Since asphaltenes are solids and insoluble in water, the samples require high temperature/pressure digestion by inorganic acids. As a result, the extracted asphaltenes were measured and dissolved using a 1:1 ratio of nitric acid (HNO₃, HPLC grade) and hydrochloric acid (HCl, HPLC grade) in an Anton Paar HPA-S high pressure asher. Then the solutions were collected and diluted before ICP characterization. ICP standard solutions were purchased from Thermo Fisher Scientific.

2.5.2.5 Other elemental analysis (CHN)

A Therm FlashEA 1112 elemental analyzer at McMaster University was used for analyzing C, H and N contents in asphaltenes. The elemental analyzer is equipped with two combustion columns,

one for the analysis of C, H, N and S under high oxygen conditions, while the other column is set up for O analysis in an O-free environment. Before the analysis, asphaltenes were first weighed into aluminium cups for CHNS analysis or into silver cups for O analysis. This was done using a Mettler Toledo balance capable of weighing down into the microgram range. However, the oxygen column and S detector were both not functioning. Consequently, only the CHN components were analyzed for evaluating the N removal and hydrogenation performances based on the N:C and H:C ratios.

2.5.3 Coke and metal residue analysis

2.5.3.1 TGA

Coke yield was also determined by using the same SDT Q600 TGA used for asphaltene oxidation studies (see Section 2.5.2.3). The toluene insoluble solid residues collected after filtration were ground before the analysis. The same operating condition was used here: (a) air atmosphere, (b) flow rate of 100mL/min, (c) final temperature of 1000°C (d) ramp at 20°C/min. As shown in Figure 2-7, there were three stages of weight loss in the coke oxidation from room temperature to 1000°C: the first loss around 100°C was caused by moisture loss; the second loss typically occurred at around 400°C and the final weight loss was caused by the metal sulfides oxidation. Usually all carbon residues (coke) were burnt out around 400°C, so the coke mass could be calculated based on the weight loss occurring around 400°C.

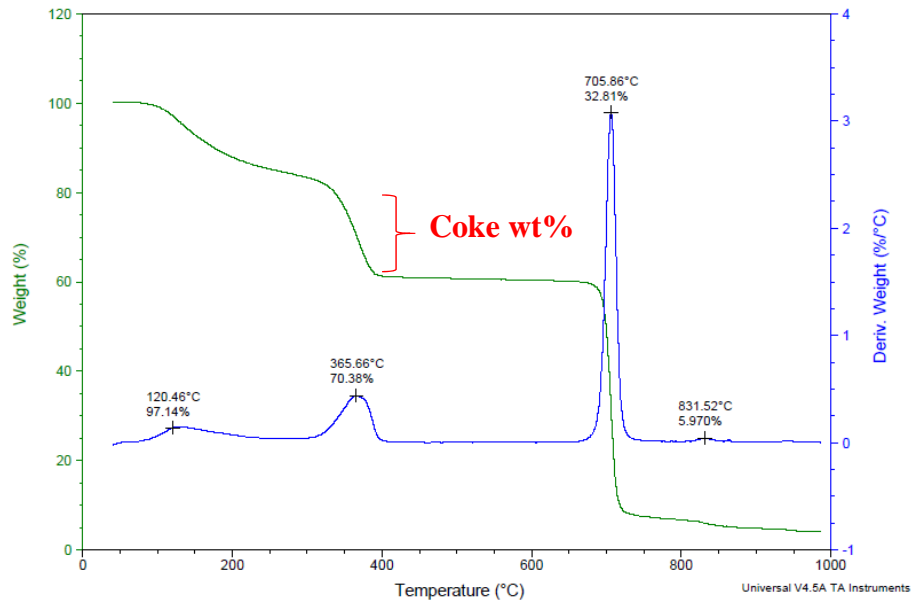


Figure 2-7 TGA example for calculating coke content in solid residue

2.5.4 Gas analysis

2.5.4.1 Refinery gas analyzer (RGA)

An Agilent 3000A micro GC RGA was used to analyze the gas components. This information was used to track the progress of the WGSR and cracking during the upgrading. The micro GC was equipped with four thermal conductivity detectors (TCD) and with four columns: 5A molecular sieve, Plot U, Alumina and OV-1 columns. Characterization and calibration details are shown in Appendix A.5.

2.5.5 Water analysis

2.5.5.1 Ion exchanged chromatography (IC)

A Dionex DX-500 ion exchange chromatograph equipped with an auto sampler was used for the qualitative and quantitative analysis of anions and organic acids in the water samples before and after the upgrading. Since the water amount in the final product was very limited, some extra water was weighed out and added. There were two advantages of adding water:

- a) to reduce the error caused by the hard-to-collect water near the emulsion interphase;

b) to adjust the ion concentration within the IC detecting upper-limit (main reason).

After centrifugation, most of the oil was located at the top of the water, which made it easy for collecting most of the water by a glass pipette. Then the rest of the oil residue in water was further removed by filtration with a #42 filter paper. The OSPW feedstock water in Athabasca bitumen study was directly collected, centrifuged, filtered and diluted 500 times before the IC injection. The Dionex IC control panel and calibration details are shown in Appendix A.6. Combined with the water volume results measured by using a graduated separatory funnel and the dilution times before the injection, the final water dilution times could be calculated based on Eq. 2-7. The dilution times were carefully recorded for the water treatment performance calculation.

$$\text{Dilution times} = \frac{V(\text{H}_2\text{O})_0 + V(\text{H}_2\text{O})_{\text{extra}}}{V(\text{H}_2\text{O})_0} \times \text{dilution times before IC injection} \quad (\text{Eq. 2-7})$$

2.5.5.2 ICP

A Teledyne Prodigy ICP was used for analyzing the metal ion components in the OSPW samples before and after treatment. Dilution with 2% nitric acid (or 2% hydrofluoric acid for Nb, V, Mo and W analysis) was carried out based on each element's standard solution requirement.

2.5.5.3 High pressure liquid chromatography (HPLC)

A Waters Alliance 2690 HPLC equipped with an Agilent C18 reverse-phase column and a Waters 996 photodiode array detector was utilized to identify and quantify the model compound contents in the water phase. The column temperature was 50°C and the highest pressure limit was 2500 psi. The eluting phases were 2mol/L H₂SO₄, acetonitrile and degassed ultra-pure water (filtered). Their flow rates contributed 10%, 80% and 10% to the total flow rate at 1ml/min. Chromatograph and calibration curve examples can be found in Figure 5-5.

2.6 Catalysts synthesis, collection and characterization

2.6.1 Synthesis of *in situ* catalyst and *ex situ* catalyst

The *in situ* catalyst is defined as the catalyst prepared and used for catalysis in one step; while the *ex situ* catalyst is the catalyst prepared and used in two separated steps. For instance, the *in situ* catalysts in bitumen, LGO or model compound experiments were the catalysts generated freshly for *in situ* catalysis in a one step process. On the contrary, *ex situ* catalysts were prepared in organic solvents (like toluene or hexadecane) without only hydroprocessing targeted compounds (like asphaltenes, sulfur species, nitrogen species, organic acids or poly-aromatics, etc.), and then collected and dried as solids. These dry solids were then loaded in a separate reaction and used as catalysts. Detailed experimental condition can be found in Table 2-3.

2.6.2 Catalysts collection

After the reaction was finished and reactor was cooled down, the reaction pressure was recorded and then released to a gas sampling bag. Then N₂ was used to flush out the leftover H₂S for 3 times before reactor was opened. As described for the actual oil or model compound upgrading experiments, the spent catalysts were usually collected through filtration and rinsed with organic solvents (first toluene, followed by ethanol before drying). In order to prevent oxidation of MoS₂, the filtration was usually carried out in glove bag filled with N₂. Due to the complexity of the bitumen upgrading reactions, the spent catalysts were filtered in air.

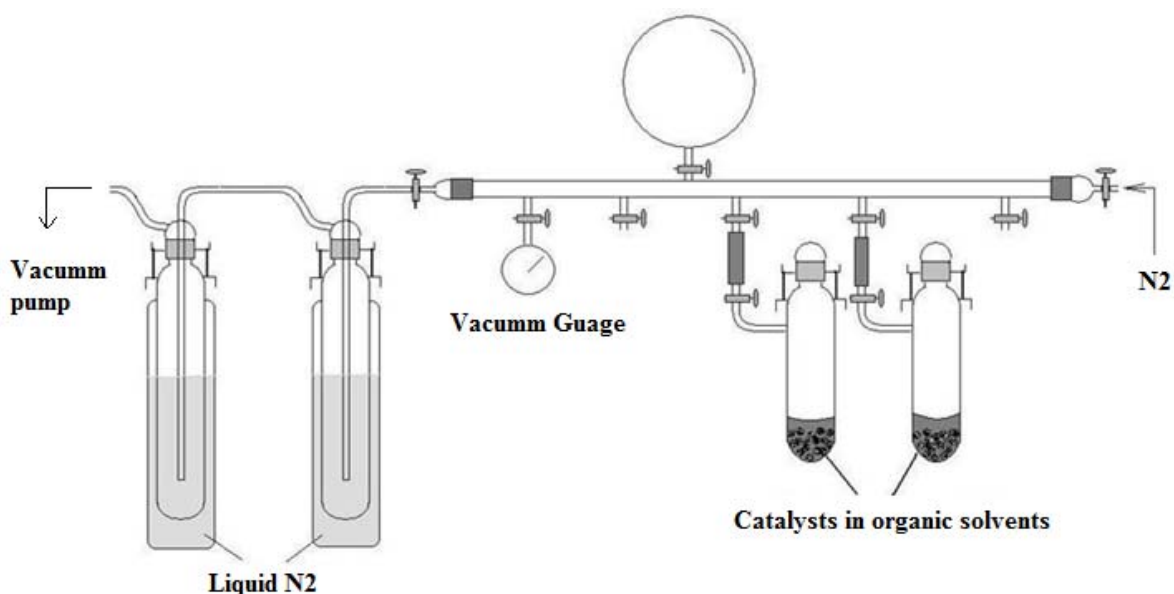


Figure 2-8 Vacuum drying system for separating and collecting catalysts (Liu 2010)

When *ex situ* catalysts were prepared in toluene, the catalyst collection was different from that for the spent catalysts. The procedure was similar to the *in situ* catalyst collection until after flushing H₂S. Instead of opening the reactor, 100psi N₂ was charged and used to pressurize the *ex situ* catalyst out of reactor through the liquid phase sampling line. Ethanol was used to rinse the sampling tube quickly after releasing. As discussed before, ethanol was an ideal solvent for collecting catalysts because of its polarity. In addition, its low boiling point made it much easier to be separated from the catalysts through evaporation. All catalyst powders were sealed in a glass vacuum drying bottle as shown in Figure 2-8, and then connected to the vacuum drying system by using a freeze-thaw technique. Liquid N₂ was used for condensing vaporized organic solvents and preventing them from damaging the pump. After separation, the drying bottles were filled with N₂, and stored in glove bags for future characterization and reaction. It should be noted that *ex situ* catalysts prepared in hexadecane were not separated through the freeze-thaw method due to their much higher boiling point than toluene. Much higher vacuum would be required for their separation. So filtration in a glove bag was used for collecting this type of *ex situ* catalyst.

2.6.3 Catalysts characterization

2.6.3.1 X-Ray Diffraction (XRD)

XRD measurements were performed on a Bruker UXS D8 Focus X-ray diffractometer using Cu K α ($\lambda=1.54056$ Å). The step size was 0.05°/min over a 2 θ range of 10-70°. Before carrying out the measurement, the catalysts were ground in a glove bag to prevent oxidation by air.

2.6.3.2 Brunauer–Emmett–Teller (BET)

Some fresh and spent catalysts from LGO upgrading were characterized by a Micromeritics Gemini 3243 BET. The surface area and pore volume changes were observed. The catalysts were outgassed with a N₂ flow at 120°C overnight before the measurement.

2.6.3.1 Scanning Electron Microscope (SEM) and Energy-Dispersive X-Ray Spectroscopy (EDX)

An LEO 1530 Field Emission SEM equipped with secondary electron detector (SE2) and backscattered detector (BSD) was used. One layer of gold should be coated before the measurement as MoS₂ was not conductive. After coating gold in a Desk II Gold Sputter/Etch Unit (Denton Vacuum, LLC), catalyst solids which were attached on sample holders were characterized under 5kV electron beams in high vacuum conditions (lower than 1.5×10⁻⁵ mBar). Sometimes 25kV electron beam was also used to meet the requirement of EDX analysis of Mo, whose identification peaks appear in the range of 16-21kV.

2.6.3.2 Transmission Electron Microscopy (TEM) and EDX

Spent catalyst powders collected after filtration were washed with ethanol, acetone and then sonicated in acetone to disperse the particles. One drop of the solution was deposited on a holey-carbon film supported on Cu grids. The sample on the grid was examined using a JEOL 2010 TEM operated at an accelerating voltage of 200keV. Valuable regions were chosen for Bruker D8 FOCUS energy dispersive X-ray spectrometer (EDX) analysis. This EDX used 1.54184 Å as K α and was equipped with a 2.5 mm primary siller slit, 0.6 mm divergence slit, 0.1 mm detector slit and 0.6 mm anti-scattering slit. A FEI Titan 80-300 Cubed high-angle annular dark-field

scanning transmission electron microscopy (HAADF-STEM) was also used in testing some samples for collecting a few electron microscopy images and EDX information.

Chapter 3 Upgrading of Cold Lake Bitumen Emulsion through a Novel Emulsion Upgrading Process

3.1 Literature review

3.1.1 Cold Lake and Athabasca bitumen

Cold Lake and Athabasca bitumen are produced from adjacent areas shown in Figure 1-2, with the Athabasca region located north of Cold Lake. However, the oil sands bitumen produced in these two areas have distinctive properties as a result of different geophysical reservoir formations. It is known that Athabasca bitumen is “heavier” than Cold Lake bitumen. As shown in Table 3-1, ~33% diluent is needed to dilute Athabasca bitumen to meet pipeline transportation specification; while only ~23% diluent is able to make Cold Lake bitumen flow in pipelines. The vacuum residue contents are also significantly different for these two crudes. As shown in Table 3-1, Athabasca dilbit product contains ~47% vacuum resid after blending with 33% diluent; while Cold Lake dilbit product contains only 39% vacuum resid after blending with even ~33% less diluent (23% diluent vol.%). As discussed in Table 1-2, Athabasca bitumen contains higher asphaltene content than Cold Lake bitumen. The variance could be probably attributed to the different asphaltene content and relevant chemistry.

Table 3-1 Blending inspections of oil sands bitumen dilbit products (data compiled from Crude Monitor)

	Cold Lake	Athabasca
Blend Inspections		
Diluent, vol%	23	33
Gravity, °API	19	21
Viscosity @7 °C, cSt	~350	~350
Sulfur, wt%	3.5	4.0
Vac. Residue Cont., wt%	39	47

3.1.2 Asphaltenes

Heavy oil feed exists in the form of a colloidal solution that consists of 3 major fractions: oils, resins and asphaltenes. Asphaltene is defined as the group of large molecules which can be separated from heavy oil feed by precipitating with paraffinic hydrocarbons such as pentane, hexane and heptane (Chilingarian and Yen 1978, Mullins, Sheu *et al.* 2007). Asphaltenes are dark brown chemicals containing poly-aromatic structures with long aliphatic chains, and their molecular structures have been discussed in various literatures (Suzuki, Itoh *et al.* 1982, Gray 2010, Alshareef, Scherer *et al.* 2011, Gray, Tykwinski *et al.* 2011, da Costa, Stoyanov *et al.* 2012, Gray, Bagheri *et al.* 2012, Stoyanov, da Costa *et al.* 2013). Except for C and H, some heteroatoms like S, O, N and metals were determined in asphaltenes. As shown in Table 3-2, a high concentration of Ni and V were found in asphaltenes in the form of porphyrin structures. A typical asphaltene molecule contains aromatic rings with paraffinic chains. Intermolecular forces include: acid-base interactions, H bonding, coordination complexes, van der Waals hydrophobic pockets and π - π stacking (Gray, Tykwinski *et al.* 2011) as shown in Figure 3-1,. Even the individual forces are weak; the combined forces could perform considerable impact on asphaltene structure and properties, following supramolecular chemistry (Murgich 2002).

Table 3-2 Ni and V in asphaltene derived from a Canadian heavy crude (Semple, Phillip *et al.* 1990)

Metal Concentration (ppm)		V in Porphyrin concentration (wt%)
Ni	V	12
820	320	

Asphaltenes come from the heaviest fraction in bitumen and contribute to high aromaticity and viscosity (Chilingarian and Yen 1978). As a natural surfactant, asphaltenes in bitumen would enhance the formation of the bitumen emulsion. In the upstream operation, the presence of asphaltenes was also reported as one of the possible initiatives for sedimentation, plugging, corrosion and fouling during production, storage and transportation (Pugsley, Pernitsky *et al.* 2013). Downstream, asphaltenes are known for their adsorption tendency onto refining

equipment, such as pumps, heat exchangers et al (Rana, Samano *et al.* 2007). Asphaltenes also inhibit upgrading by poisoning refinery catalysts with their high heteroatom (S, N and O) content, trace metals (V, Fe and Ni) (Bartholomew 2001, Marchal, Abdessalem *et al.* 2010), and coke formation (Artok, Su *et al.* 1999). Hence, the removal of asphaltenes before or during bitumen upgrading plays a crucial role in the oil industry.

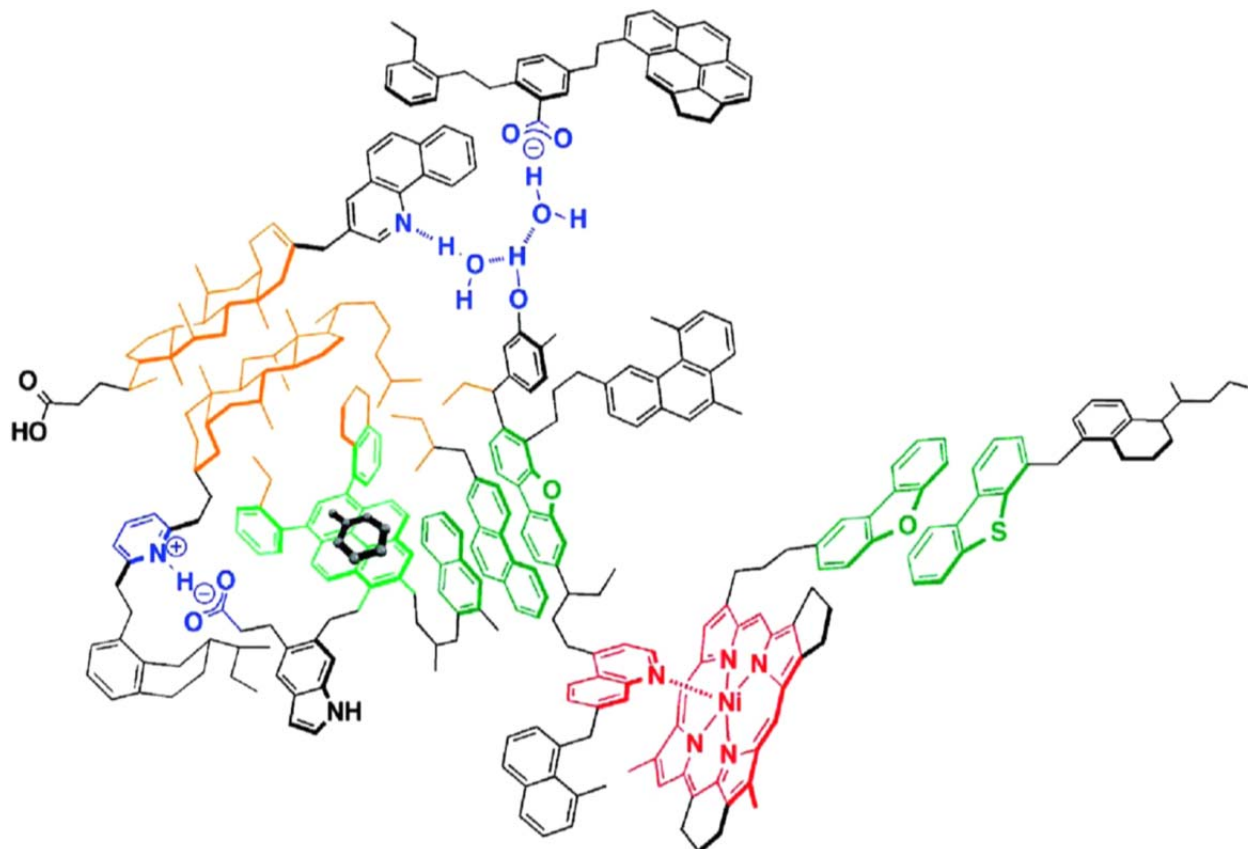


Figure 3-1 Proposed molecular structure of asphaltenes (Gray, Tykwinski *et al.* 2011)

There are three main methodologies practiced to mitigate the negative impacts of asphaltenes: stabilization, rejection and upgrading of asphaltenes. In order to stabilize asphaltenes, diluents (Akbarzadeh, Hammami *et al.* 2007), solubilizing chemicals (Gonzalez and Middea 1991, Gonzalez and Moreira 1991, Chang and Fogler 1996, Leon, Rogel *et al.* 1999, Bilden and Jones 2000, Barcenas, Orea *et al.* 2008), or stabilizing oils (Hasan, Ghannam *et al.* 2010) have been used to moderate potential asphaltene precipitation. This approach usually results in a high

operational cost due to the consumption of chemical/oils. It also requires extensive experience and knowledge to achieve reliable operation. Compared to the stabilization method, asphaltene rejection operates in exactly the opposite way. Paraffinic solvents (propane to hexane; C₃-C₆) have been used to reject asphaltenes through solvent deasphaltene (SDA) (Rana, Samano *et al.* 2007). As discussed in Section 1.2, the KBR ROSE[®] process is an industrial example of asphaltene rejection. In the paraffinic froth treatment (PFT[®]) process, the SDA process is combined with emulsion extraction to separate water, reject asphaltenes and produce pipeline transportable oil. Some physical separation methods were also developed for rejecting asphaltenes. For example, ceramic membrane ultrafiltration was reported by Prof. Keven Smith's research group by using heavy oil as feedstock (Duong and Smith 1997). Selective adsorption by using mineral based sorbents, silica/alumina, glass, metals, metal oxides, carbon and polymers were extensively studied (Woodle 1973, Johnson, Hribik *et al.* 1988, Reno 1988, Yao 1989, Ngan 1989, Kuehl 1996, Bilden and Jones 2000, Osaheni, Bablin *et al.* 2008, Osaheni, Fyvie *et al.* 2012, Osaheni, Fyvie *et al.* 2012, Ou and Strack 2009). Generally, asphaltene rejection separates asphaltenes as co-products with much less value compared to crude. If asphaltenes are not gasified or burnt for coal value by building expensive coke/pitch gasifiers or burner, these large amounts of co-products actually have only negative value because landfill is required. Technologies like enhanced pyrolysis (Hosseinpour, Mortazavi *et al.* 2014), selective oxidation (Rankin, Vreeland *et al.* 2011), supercritical water upgrading (Sato, Mori *et al.* 2010), and ultrasound cavitation (Kaushik, Kumar *et al.* 2012) were investigated to add more value into asphaltenes. Nevertheless, these technologies have quite significant operational costs. If these technologies were installed on site, they will suffer extremely high construction costs in northern Alberta; if installed off site for lower capital costs, the transportation cost through rail may double or even triple the total operational costs. Currently there is no other proven technology available which could add enough value into asphaltenes at low cost to satisfy market needs. Hence, converting asphaltenes into useful liquid fuel through hydroprocessing or upgrading becomes the key challenge for heavy oil research. Compared to the vacuum resid in refineries, asphaltenes were not fluidized enough to be fed into a resid hydrocracker or coker. Accordingly, asphaltenes need to be upgraded within bitumen or heavy oil to potentially realize their value as a hydrocarbon fuel.

Yen and Mullin suggested the “Yen-Mullin model” with stepwise aggregation of asphaltenes from a molecule (1.5 nm) into a nano aggregate (2 nm) and a cluster (5 nm) (Mullins 2011, Mullins, Sabbah *et al.* 2012). In general, in upgrading processes these aggregated asphaltene molecules tend to agglomerate as a result of various attractive forces, which are highly dependent on the asphaltene source and the physical/chemical environment. Hence, the dispersion of asphaltenes from being condensed during upgrading is crucial. It is known that the asphaltene compatibility depends on the relationship between resins and asphaltenes. As poly-aromatic compounds with less polarity, resins could form micelles with asphaltenes through weak physical bonds to stabilize the asphaltenes from precipitation and condensation (Strausz, Mojelsky *et al.* 1992). Asphaltene locates at the core of micelles with resin on the external surface for dispersion. As a result, the conversion rates for resin and asphaltenes should be controlled; otherwise the coagulation of asphaltenes will lead to more sediment formation on the catalyst surface (Ancheyta, Rana *et al.* 2005). In order to get homogeneous hydrotreated oil products, more emphasis should be put on the upgrading condition control.

3.1.3 Major processes in bitumen upgrading

Speight mentioned in his book “The chemistry and technology of petroleum” about the objectives for hydroprocessing of bitumen or heavy oil, including (Speight 2007):

- a) Reduce metals, organic sulfur and nitrogen content;
- b) Convert low value, high boiling Conradson carbon residues (CCR) to distillate and naphtha through H₂ addition;
- c) Increase API gravity and reduce viscosity.

3.1.3.1 Hydrodesulfurization (HDS)

Organic sulfur species in bitumen can cause significant environmental problems and poison downstream noble metal catalysts. HDS is a catalytic chemical process widely used to remove sulfur from natural gas and from refined petroleum products such as gasoline or petrol, jet fuel, kerosene, diesel fuel, etc.

It was concluded that HDS of DBT-type compounds occur through two parallel reactions as indicated in Fig 3-2: (a) direct desulfurization (DDS) which yields biphenyl-type compounds, and (b) desulfurization through hydrogenation (HYD) which first gives tetrahydrodibenzothiophene and then cyclohexylbenzene-type compounds when CoMo/alumina catalyst were used (Bataille, Lemberton *et al.* 2000). Liu reported in 2010 that BP cannot be converted into CHB when using *in situ* MoS₂ catalysts for an emulsion upgrading process (Liu 2010).

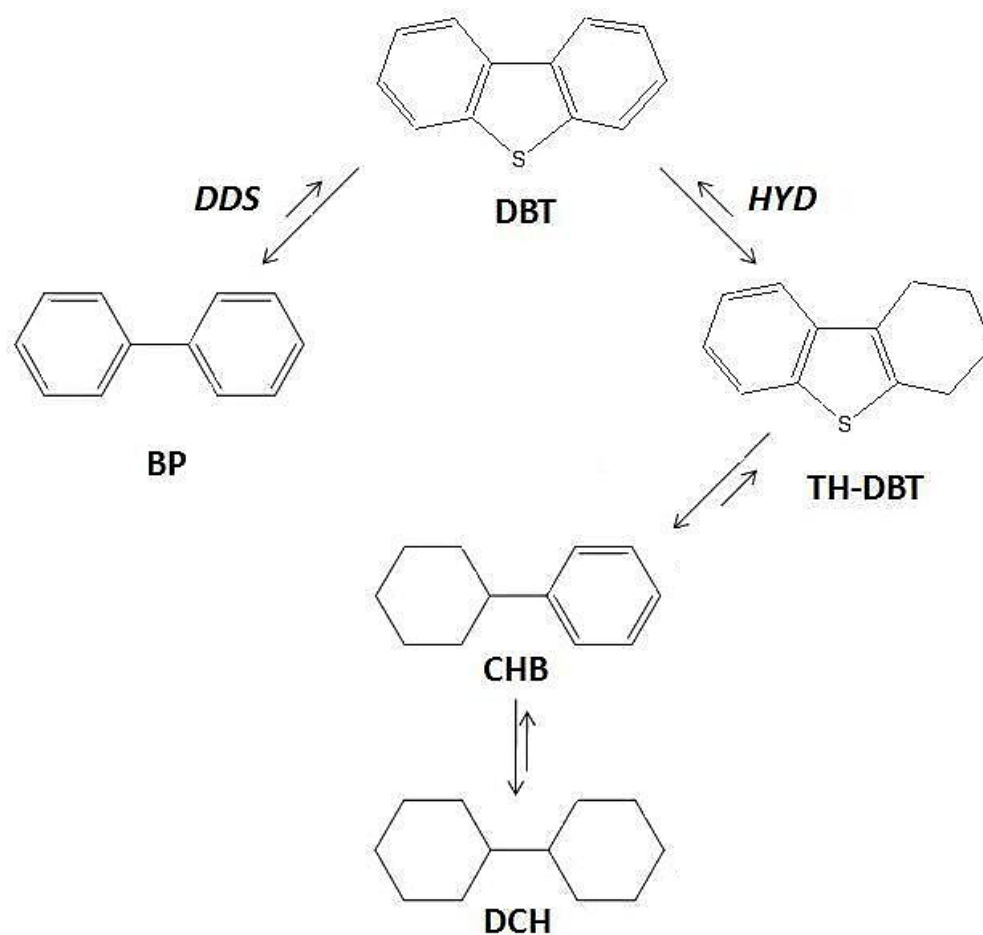


Figure 3-2 Scheme of HDS of DBT pathways using *in situ* H₂ over unsupported Mo sulfide catalysts. Abbreviations: DBT - dibenzothiophene, BP - biphenyl, TH-DBT - tetrahydrodibenzothiophene, CHB - cyclohexylbenzene, DCH - dicyclohexyl) (Liu 2010)

3.1.3.2 Hydrodearomatization (HDA)

Organic aromatic compounds in bitumen can cause significant environmental problems, as they increase emissions of particulate exhaust. In several regions such as Europe and California, the aromatic content in gasoline and diesel fuels is regulated to reduce emissions of particulates (Hochhauser 2000). Aromatics mainly exist in middle distillates and bitumen derived heavy oil is one major source for multi-aromatic compounds. Table 3-3 provides a summary of typical data for different distillates.

Table 3-3 Aromatics distribution in various distillates (Cooper and Donnis 1996)

Property	Heavy FCC gasoline	Light coker gasol	Light atoms gasol	Light cycle oil	Heavy atoms. gasol
Mean average boiling points (MeABP) /°C	195	259	289	291	322
Specific gravity @15°C	0.84	0.861	0.846	0.997	0.864
Aromatics /vol%					
Mono	38.8	16.3	16.5	8.2	22.5
Di	5.5	16.4	7.0	69.8	8.5
Tri	0.5	8.0	0.1	4.0	0.7
Total	44.8	40.7	23.6	82.0	31.7

HDA that is achieved by hydrogenating aromatic rings plays a key role in hydrotreating processes. As it has been reported that the S content of three or larger ring aromatic compounds controls heavy oil desulfurization (Choudhary, Parrott *et al.* 2008). It is also believed that deep HDS and HDN, partial HDA of aromatic rings facilitates the cleavage of C-S and C-N bonds to liberate H₂S and NH₃, respectively (Ho 2004). Moreover, aromatic hydrogenation can improve hydrocracking by facilitating saturated hydrocarbon production via the cleavage of the aromatic rings on metal and acid catalysts (McVicker, Daage *et al.* 2002). In this way the hydrogenation of polycyclic aromatic hydrocarbons to monocyclic aromatics can improve quality without increasing diesel particulate emissions.

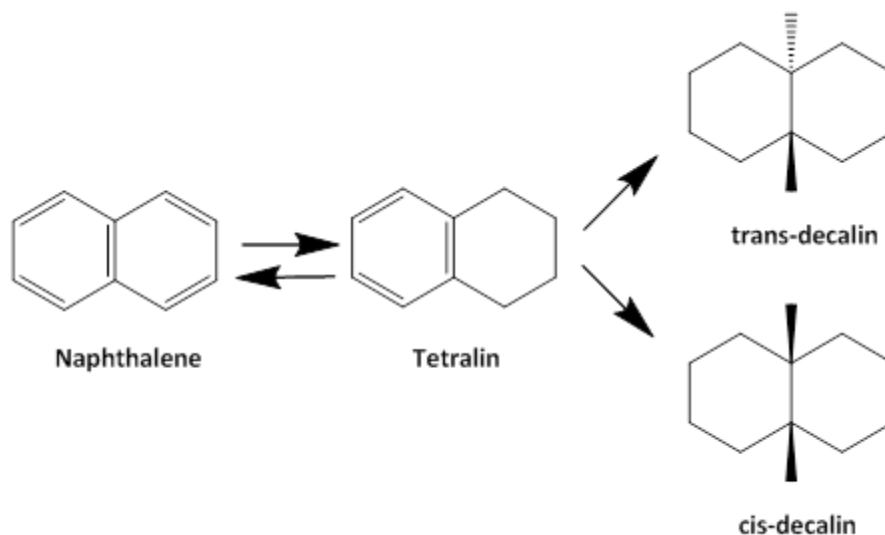


Figure 3-3 Scheme of naphthalene hydrogenation (Broderick, Sapre *et al.* 1982)

The above scheme shown in Figure 3-3 shows the mechanism of hydrogenation of naphthalene. As shown in the scheme, hydrogenation of naphthalene is a multi-step reaction, which initially forms tetralin from naphthalene. Then tetralin can be hydrogenated to cis- and trans-decalin. The hydrogenation to tetralin is the fastest as the initial step. The second hydrogenation step to decalins is also fast on noble metal catalysts. However, when MoS_2 is used as catalyst, the second hydrogenation from tetralin is much slower where trans-decalin is the main product (Broderick, Sapre *et al.* 1982). HDA has been shown to be a highly exothermic process, with a reaction heat in the range of 63-71 kJ/mol H_2 (Broderick, Sapre *et al.* 1982).

In order to explain the detailed reaction mechanism, some hypothetical reaction processes have been proposed and verified. A metal-hydride species was proposed as the intermediate for hydrogenation over heterogeneous reduced metal catalysts (Cotton 1999). Usually after the formation of metal hydrides, the aromatics will be adsorbed via π -adsorption on the active sites near the hydride. Then the hydride will be inserted into the aromatic species, followed by a final reductive elimination. Consequently, some unsaturated site or vacancies will be created for the continuous reaction. As reported by Jacobson in 1999, H_2 reacts with S and removes S from the catalyst surface, leaving a sulfur vacancy. Then heteroaromatic and aromatic substrates will

coordinate with this sulfur vacancy, which will be the key step for the catalytic activity (Jacobsen, Törnqvist *et al.* 1999).

From kinetic studies on model compounds, hydrogenation is close to being zero-order in the reactant hydrocarbon due to strong adsorption of the aromatic species on the noble metal sites (Cooper and Donnis 1996). It has been reported that mononuclear aromatics such as benzene and benzene derivatives are the species which are more difficult to hydrogenate (Broderick, Sapre *et al.* 1982). The conversion rate for the hydrogenation of naphthalene to tetralin is an order of magnitude greater than for the hydrogenation of tetralin to decalins; another similar tendency was also discovered in the hydrogenation of benzene to cyclohexane (Broderick, Sapre *et al.* 1982). Compared with tetralin, m-xylene was noted to be two times harder to hydrogenate (Ho 1994).

3.1.3.3 Hydrocracking

The formation of asphaltenes is believed to begin with a cleavage of a C-C bond forming free radical species. Then these small free radicals polymerize into large aggregates of asphaltenes. This formation can be prevalent at low pressure and high temperature conditions, which will cause a large oil loss during the process. Increasing the H₂ partial pressure or addition of dissociated H₂ will be another method to decrease polymerization of asphaltenes and cokes, as H₂ can promote the ring-opening of poly-aromatics for higher gas oil production (Vernon 1980). Compared with thermal coking, hydrocracking can achieve a higher conversion of feed into a better quality product. The introduction of catalyst can result in much less asphaltene production with less oil loss. As the free radical intermediate, H· formed on the catalyst surface can react with hydrocarbon free radicals, suppressing asphaltenes and coke formation (Liu, Kong *et al.* 2009).

3.1.4 WGS during emulsion upgrading with model compounds

Although water has been widely reported as an inhibitor for many hydrotreating processes (Laurent and Delmon 1993, Chadwick, Oen *et al.* 1996), the WGS would not restrain HDS in

emulsion upgrading (Lee and Ng 2006). It was reported by Flora Ng's research group that the major apparent change was the change of H₂ concentration in the gas phase. Shown in Figure 3-4 reaction gases were identified and measured during the WGSR with and without simultaneous HDS of DBT reaction at 340°C. It is noticed that the WGSR showed a similar trend, as CO₂ was increasing. Only the H₂ concentration decreased by 10% in WGSR+HDS compared to only WGSR due to the H₂ consumption during HDS of DBT.

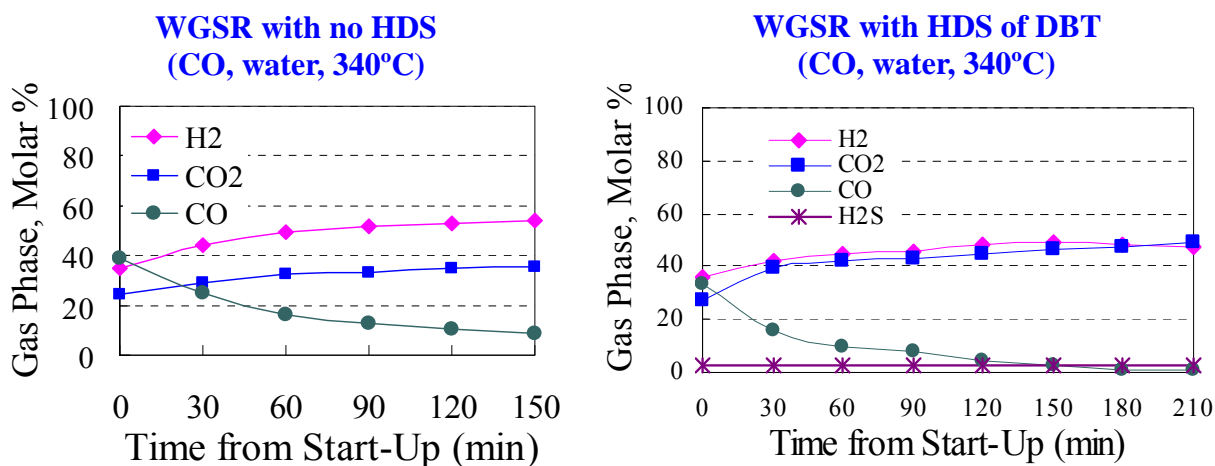


Figure 3-4 Gas changes in WGSR with and without the HDS of DBT presence (Lee and Ng 2006)

3.1.5 Feasibility study of Cold Lake bitumen emulsion upgrading

The feasibility of emulsion upgrading has been investigated by Ng's lab, especially for its partial upgrading performance for pipeline transportation (Moll 1999). It was validated that *in situ* H₂ generated through the WGSR exhibited better partial upgrading performance than molecular H₂. As shown in Figure 3-5, Canadian oil sand bitumen emulsions (50000cSt@40°C, 10° API) were upgraded by using either *in situ* H₂ or molecular H₂. The yellow columns represent viscosity and the purple columns represent API gravity respectively. This indicates that oil produced after 2 hours by using CO was suitable for pipeline transportation by producing ~23° API oil; while the oil produced by using molecular H₂ did not meet pipeline transportation spec (21° API). This exhibited excellent vis-breaking and hydrogenation performances for *in situ* H₂ over molecular

H₂ which could be attributed to the high activity of *in situ* H₂ as demonstrated in a number of publications (Liu and Ng 1999, 1999, 1999, Liu, Ng *et al.* 1999, Moll, Li *et al.* 2000, Lee, Zhang *et al.* 2006, Liu, Choy *et al.* 2007, Liu, Jia *et al.* 2013).

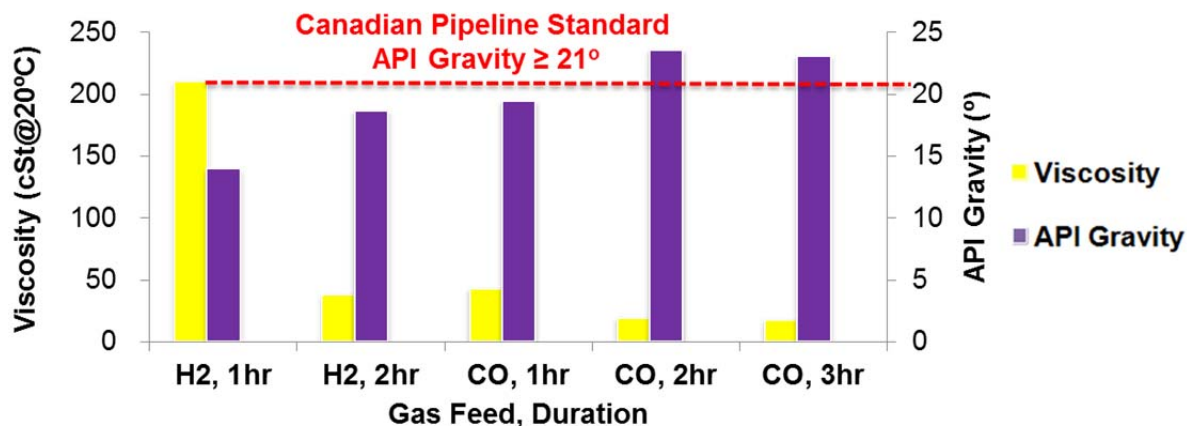


Figure 3-5 Viscosity and API Gravity changes under different upgrading conditions (Moll 1999)

3.2 WGSR during Cold Lake bitumen emulsion upgrading

Similar to the observations provided in Section 3.1.4, the H₂ consumption was also observed in bitumen upgrading. As shown in Figure 3-6, reaction gases were characterized by RGA during bitumen emulsion upgrading. Samples were taken every 30 min during the reaction once the reaction temperature reached 415 °C. It was shown that CO decreased with an increase in CO₂ production. H₂ concentration, instead of increasing and remaining steady in WGSR+HDS, increased and finally dropped to less than 20 mol%. This was because bitumen upgrading required much more H₂ than model compound hydrotreating. Nevertheless, the WGSR demonstrated similar performance as in the model compound studies.

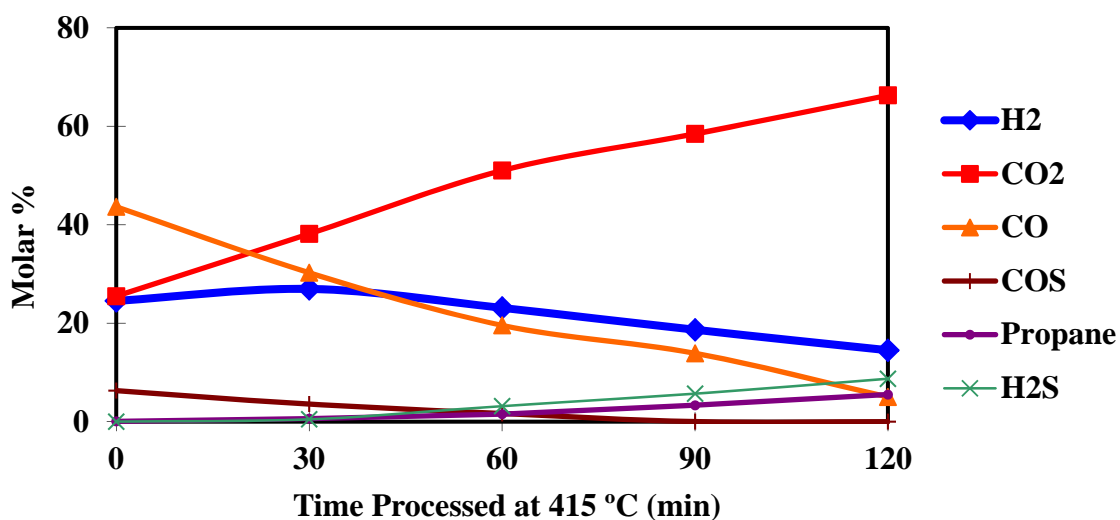


Figure 3-6 Gas changes in WGSR with simultaneous bitumen emulsion upgrading (415°C, 80g bitumen, 10g H₂O, 585psi CO, 15psi H₂S, 1408 ppmw Mo, 2 hours)

3.3 Evaluation of upgrading results

The research discussed in this chapter is an extension of a previous feasibility study, which focuses more on the effect of different conditions at a lower temperature to prevent over-upgrading. Considering less processing difficulty of the Cold Lake bitumen emulsion, a lower temperature of 405°C was used. As an important evaluation standard in bitumen upgrading research, the removal of asphaltenes could provide deasphaltene performance related with S removal and oil quality; while the asphaltenes solid can also be investigated for some structure change before and after the upgrading.

Cold Lake Bitumen Emulsion

Upgraded Oil



Figure 3-7 Cold Lake bitumen emulsion before and after reaction. Highlight: upgraded oil formed stable meniscus over water for months. (405°C, 80g Cold Lake bitumen emulsion, 585psi CO, 15psi H₂S, 1408 ppmw Mo, 2 hours)

As shown in Figure 3-7, the pictures of the Cold Lake bitumen emulsion before and after reaction were taken. It is apparent that the upgraded oil could flow easily compared to the feedstock, which was consistent with the preliminary findings. Furthermore, the stability of the upgraded oil was also evaluated by observing any precipitation at the oil water interphase during storage. Shown in the highlighted picture in Figure 3-7, the meniscus formed between the oil and water product interphase was stable and lasted months, indicating excellent stability of the partially upgraded product. This is a major advantage of this novel emulsion upgrading technology compared to most of the thermal partial upgrading technologies such as HTL[®] and I^YQ[®]. It is possible that the *in situ* H₂ derived during the WGSR hydrogenated any formed olefin or di-olefins, improving the oil stability significantly.

3.3.1 Effect of temperature

Based on the same “80g Cold Lake bitumen emulsion, 585psi CO, 15psi H₂S, 1408 ppmw Mo, 2 hours” condition, the effect of reaction temperature was examined. The mass balances for 395°C, 405°C and 415°C were 92.4%, 90.7% and 87.7% respectively.

Figure 3-8 demonstrates the yield distribution of all the products after the reaction, which contains the upgraded oil fractions like naphtha (177°C-), kerosene (177-249°C), distillate (249-343°C), heavy gas oil (343-524°C) and pitch (524°C+). These results are a combination of upgraded oil yield and boiling point distribution results obtained by using GC-SIMDIS. The lighter fraction, the higher the oil quality was the product. Pitch contributes most to the oil viscosity and API density. In addition, refineries usually give zero or negative value of pitch, because the pitch fraction would be eventually fractionated in a vacuum tower resid, which could only be treated through coking or resid upgrading. As a result, higher pitch conversion indicates better upgrading performance and higher upgraded product value. The other parts in yield distribution like HVOR, coke, metal residue and loss to the gas phase represent the yield of the products after the reaction. Among them, the HVOR contains a large portion of precipitated asphaltenes, which could initiate reactor fouling, so a lower HVOR yield would be preferred. It should be noted that the pitch shown in the product distribution was different from that of the HVOR. Pitch represented the vacuum residue fraction in the oil (524°C+); while HVOR was the asphaltene-rich product that stuck to the reactor liner walls after reaction. The pitch content was obtained through GC-SIMDIS analysis on the liquid oil product; while the HVOR amount was calculated by subtracting the mass of the clean liner from the mass of liner after reaction (and after pouring the liquid oil product) as discussed in Section 2.3.1. The loss to the gas phase was typically caused by cracked gas formation and mass balance error.

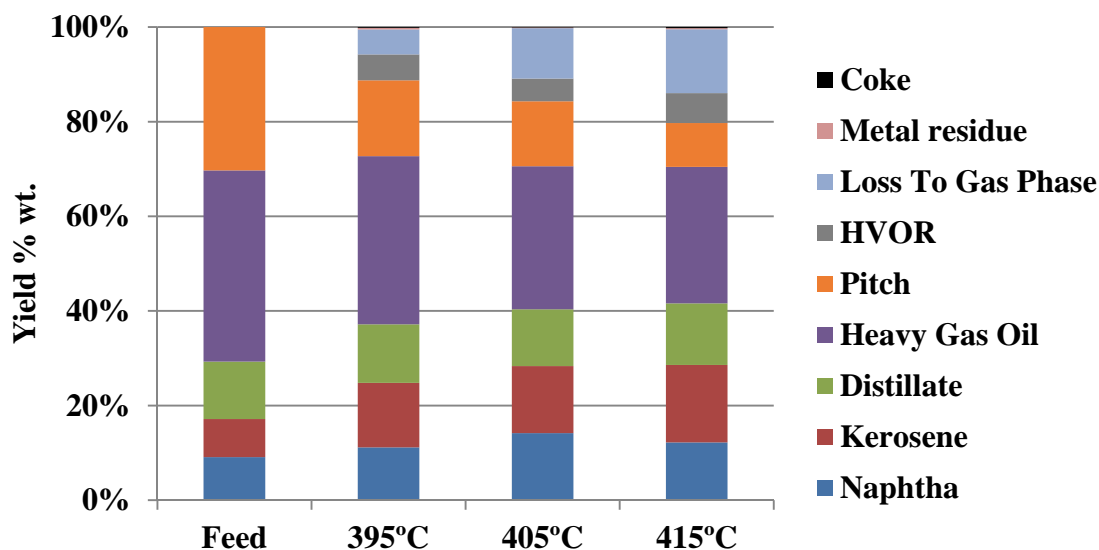


Figure 3-8 Yield distribution of Cold Lake bitumen emulsion upgrading products at different reaction temperatures (80g Cold Lake bitumen emulsion, 585psi CO, 15psi H₂S, 1408 ppmw Mo, 2 hours)

Detailed yield numbers and other upgrading performance are listed in Table 3-4. It is clearly shown that higher oil quality was achieved at higher temperature since more light fractions were formed. To increase the product value, more pitch was converted at higher temperature, as pitch conversion increased from 47% at 395°C to 69% at 415°C. However, a lower yield was obtained at 415°C with more mass lost into the gas phase. This was caused by the higher thermocracking preference at higher temperature, which provided high quality oil by sacrificing production loss. It should also be noted that less naphtha (12.2%) was produced at 415°C compared to the naphtha yield (14.2%) at 405°C. This could be caused by the cracking of naphtha fractions into light ends like C1-C4. In addition, the operating pressure was too high (3778psi) at 415°C, which was under supercritical water conditions (over 374.15°C and 3206.2 psi). As discussed in Chapter 1, supercritical conditions should be avoided in order to prevent: (a) severe reactor corrosion and (b) asphaltene rejection by supercritical water. To prevent this, a temperature of 405 °C is preferred over 415 °C for Cold Lake bitumen emulsion upgrading. Reaction under 395°C required the lowest pressure compared to 405°C and 415°. However, the pitch conversion was only 47% along with the lowest sulfur removal 44%. This lower product quality might

require longer reaction time to produce the desired products. As a result, 405°C was chosen as the main reaction temperature for Cold Lake bitumen emulsion upgrading.

It should also be noticed that the coke yield was extremely low in the emulsion upgrading. Only coke with a 0.1% yield was achieved at 405°C. The coke yield was still only 0.2% by increasing temperature to 415°C. Compared to regular 10-20% coke formation in delayed cokers, the emulsion upgrading could add a significant amount of value by preventing production loss. This excellent performance was attributed to the high activity of the *in situ* formed nano unsupported MoS₂ catalyst. This novel catalyst diffused evenly into asphaltenes, upgraded the asphaltene, and also prevented condensation for coke formation. More HVOR and coke yield were observed at 395°C, which should not be caused by thermocracking. This could be explained by systematic error, like the long waiting time required for reactor cooling. Experimental reproducibility was discussed in Appendix E.1.

Table 3-4 Cold Lake bitumen emulsion upgrading performance at different reaction temperatures (80g Cold Lake bitumen emulsion, 585psi CO, 15psi H₂S, 1408 ppmw Mo, 2 hours)

	395°C	405°C	415°C
Upgraded Oil Yield%	89	84	80
Pitch Conversion%	47	54	69
Max. Pressure (psi)	3210	3491	3778
WGSR Conversion%	80	78	88
H ₂ mole%	15	17	14
Asphaltene removal %	64	66	66
S Removal%	44	52	48
HVOR Yield%	6	5	6
Coke Yield%	0.2	0.1	0.2

XRF and CHN analysis were performed on asphaltenes in order to determine the S content, N:C ratio and H:C ratio in asphaltenes. Figure 3-9 provides evidence of the high hydrotreating activity on asphaltenes of the nano unsupported MoS₂ catalyst with *in situ* H₂. It was observed that S was removed from asphaltenes by using the *in situ* unsupported nano MoS₂ catalyst. The

asphaltene S content dropped from 6.6% into 5.2%, 4.7% and 4.5% respectively at 395°C, 405°C and 415°C. The asphaltenes' H:C ratio increased from 0.094 to 0.106 and 0.095 at 395°C and 405°C, indicating good hydrogenation capability when using the *in situ* unsupported nano MoS₂ catalyst at low temperature. With increased temperature, a lower H:C was achieved. This might be caused by thermocracking, which favors bond breaking instead of H₂ addition. However, N, one of the most difficult heteroatoms to remove, was not removed from asphaltenes, since the N:C ratio increased after reaction. The N:C ratio even increased at high temperature. This was suspected as being caused by the loss of paraffinic side chains due to thermocracking.

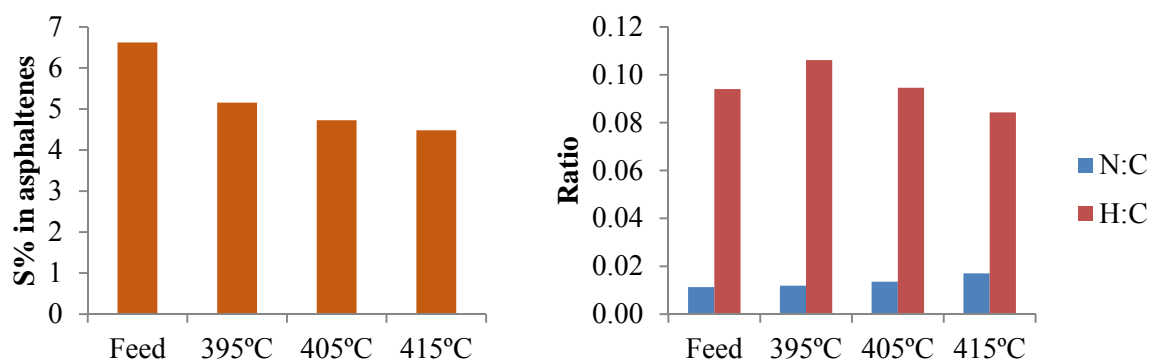


Figure 3-9 S content (left), N:C and H:C ratios (right) of asphaltenes collected from Cold Lake bitumen emulsion upgrading experiments at different reaction temperatures (80g Cold Lake bitumen emulsion, 585psi CO, 15psi H₂S, 1408 ppmw Mo, 2 hours)

GPC was used to qualitatively analyze the molecular size distribution. Since smaller molecules prefer to stay on the gel column and are eluted after the larger molecules, the retention time of the GPC chromatographs indicate the relative molecular size. From left to right, molecular size decreases. Figure 3-10 shows the GPC chromatographs of asphaltenes collected from the Cold Lake bitumen emulsion feed and upgraded oil at different reaction temperatures. At 395°C, the molecular size distribution did not shift much compared to the asphaltene feed, indicating an unchanged asphaltene molecular size. As a result, no matter how much H₂ addition was performed on asphaltenes, a certain amount of cracking occurred; otherwise, a very low pitch conversion should have been obtained. On the other hand, the distribution shifted to the right

when the reaction temperature was increased to 405°C and 415°C. This was caused by thermocracking of the asphaltenes. Interestingly, the molecular size did not become smaller at 415°C compared to 405 °C. This GPC analysis provided some insight into why 405°C was the optimal temperature for producing a high quality oil product with a satisfactory yield.

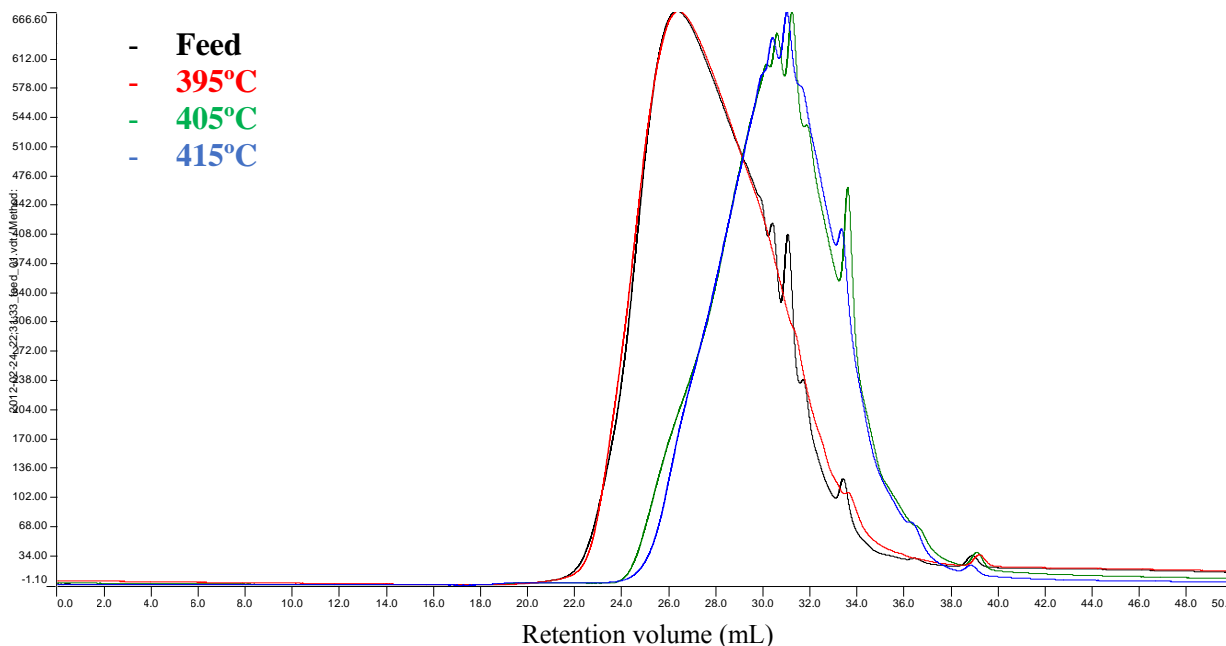


Figure 3-10 GPC chromatographs of asphaltenes collected from Cold Lake bitumen emulsion upgrading experiments at different reaction temperatures (80g Cold Lake bitumen emulsion, 585psi CO, 15psi H₂S, 1408 ppmw Mo, 2 hours)

3.3.2 Effect of reaction time

Based on the same “405°C, 80g Cold Lake bitumen emulsion, 585psi CO, 15psi H₂S, 1408 ppmw Mo, 1-3 hours” reaction condition, the various effects of changing reaction time were examined. The mass balances for 1h, 2h and 3h were 90.5%, 90.7% and 75.5% respectively. It should be noted that the low mass balance was mainly caused by poor estimation of gaseous product yields using the idea gas law. When the cracked gas yield was low, the error in the mass balance was not that significant.

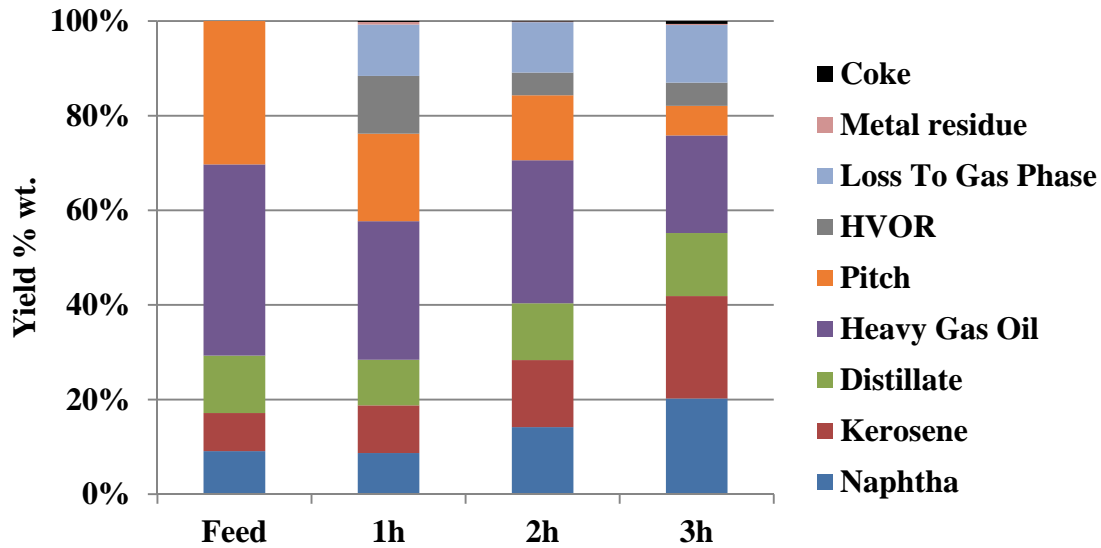


Figure 3-11 Yield distribution of Cold Lake bitumen emulsion upgrading products at different reaction times (405°C, 80g Cold Lake bitumen emulsion, 585psi CO, 15psi H₂S, 1408 ppmw Mo, 1-3 hours)

As shown in Figure 3-11 and Table 3-5, more and more light fractions were produced with longer reaction duration. From 1h to 3h, pitch conversion increased from 38% to 79%; asphaltenes removal increased from 49% to 78%. Upgraded oil yield increased from 76% to 84% from 1h to 2h. Usually there was no other reason for oil loss except coke and gas production through thermocracking. The only possibility was that the bitumen emulsion was not fully demulsified and upgraded at 1h, and the emulsified bitumen stayed in the HVOR phase due to its extremely high viscosity. This could be identified by the high HVOR yield 12.2% at 1h, which was much lower (4.8%) at 2h. As a result, more than 1h residence time should be applied for future engineering design. Upgraded oil yield was lower after 3h of reaction, and the coke yield increased from 0.1% to 0.6%. This implies that excess thermocracking occurred from 2h to 3h. This long residence-time over-upgrading produced high quality oil with sacrifice of low production and high coke formation.

Table 3-5 Cold Lake bitumen emulsion upgrading performance at different reaction times (405°C, 80g Cold Lake bitumen emulsion, 585psi CO, 15psi H₂S, 1408 ppmw Mo, 1-3 hours)

	1h	2h	3h
Upgraded Oil Yield%	76	84	82
Pitch Conversion%	38	54	79
Max. Pressure (psi)	3399	3491	3297
WGSR Conversion%	76	78	74
H ₂ mole%	19	17	17
Asphaltene removal %	49	66	78
S Removal%	42	52	52*
HVOR Yield%	12	5	5
Coke Yield%	0.2	0.1	0.6

* Data was collected following different XRF calibration performed with long interval (nearly 9 months)

Figure 3-12 clearly illustrates the S removal realized by the *in situ* nano unsupported MoS₂ catalyst on asphaltenes. The asphaltene S content was reduced from 6.6% to 4.3% after 3h. The H:C ratio remained constant after 2h, followed by a decrease at 3h, indicating that 2h should be chosen compared to 3h for preventing asphaltene condensation. No N removal in the asphaltenes was observed; instead the N:C ratio had increased due to the cleavage of paraffinic side chains through thermocracking.

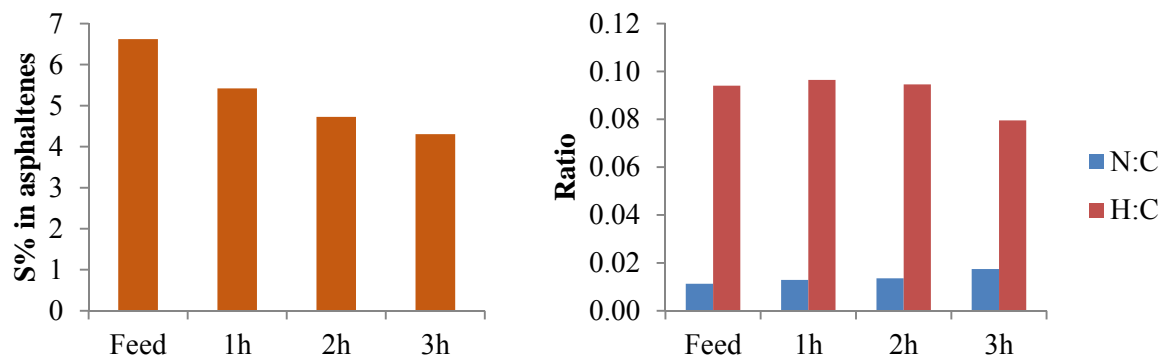


Figure 3-12 S content (left), N:C and H:C ratios (right) of asphaltene collected from Cold Lake bitumen emulsion upgrading experiments at different reaction times (405°C, 80g Cold Lake bitumen emulsion, 585psi CO, 15psi H₂S, 1408 ppmw Mo, 1-3 hours)

One interesting observation was that the carbonyl functional group (1698cm^{-1}) was almost completely removed at 3h as seen from the FT-IR spectrum shown in Figure 3-13. This removal was likely due to hydrogenation instead of cracking, since more alcohol/phenol O-H groups were formed through hydrogenating the carbonyl groups during the 2h to 3h reaction period. This can be seen from the increased alcohol/phenol O-H stretch adsorption peak (wide peak from 3000cm^{-1} to 3700cm^{-1}) shown in Figure 3-13. This increased alcohol/phenol O-H signal also indicated the presence of carboxylic functional groups with carbonyl signals at 1698cm^{-1} .

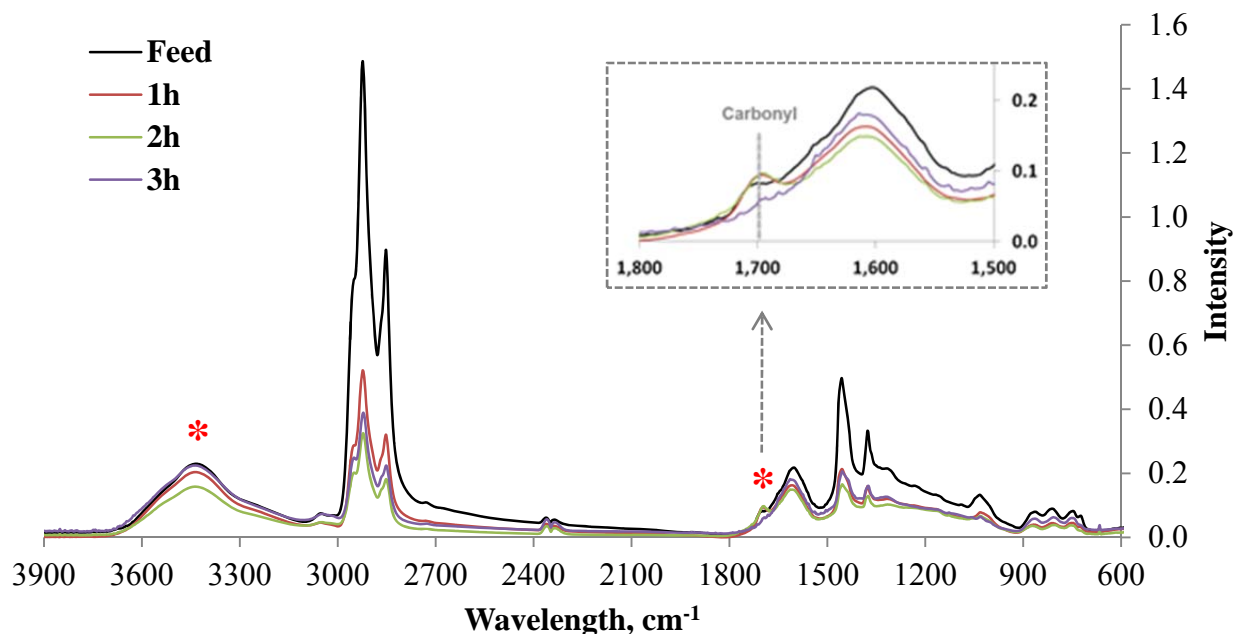


Figure 3-13 FT-IR spectrums (with zoom-in region from 1500cm^{-1} to 1800cm^{-1}) of asphaltenes collected from Cold Lake bitumen emulsion upgrading experiments at different reaction times (405°C , 80g Cold Lake bitumen emulsion, 585psi CO, 15psi H_2S , 1408 ppmw Mo, 1-3 hours)

Figure 3-14 provides a clear view as to how the asphaltene molecular size shifted during the upgrading. Within the first hour of reaction, the asphaltenes size became smaller than the feed; the size continued to decrease from 1h to 2h; and no significant change in size from 2h to 3h was observed. This finding confirmed that no obvious hydrocracking occurred for asphaltene size reduction after 2h. It was possible that more asphaltene condensation with coke formation occurred instead of hydrocracking due to the drop in H_2 partial pressure. Thermal cracking became dominant, and more light fractions were converted into gases. Considering acceptable demulsification performance and in order to prevent over-upgrading, 2h was the ideal reaction time compared to 1h or 3h.

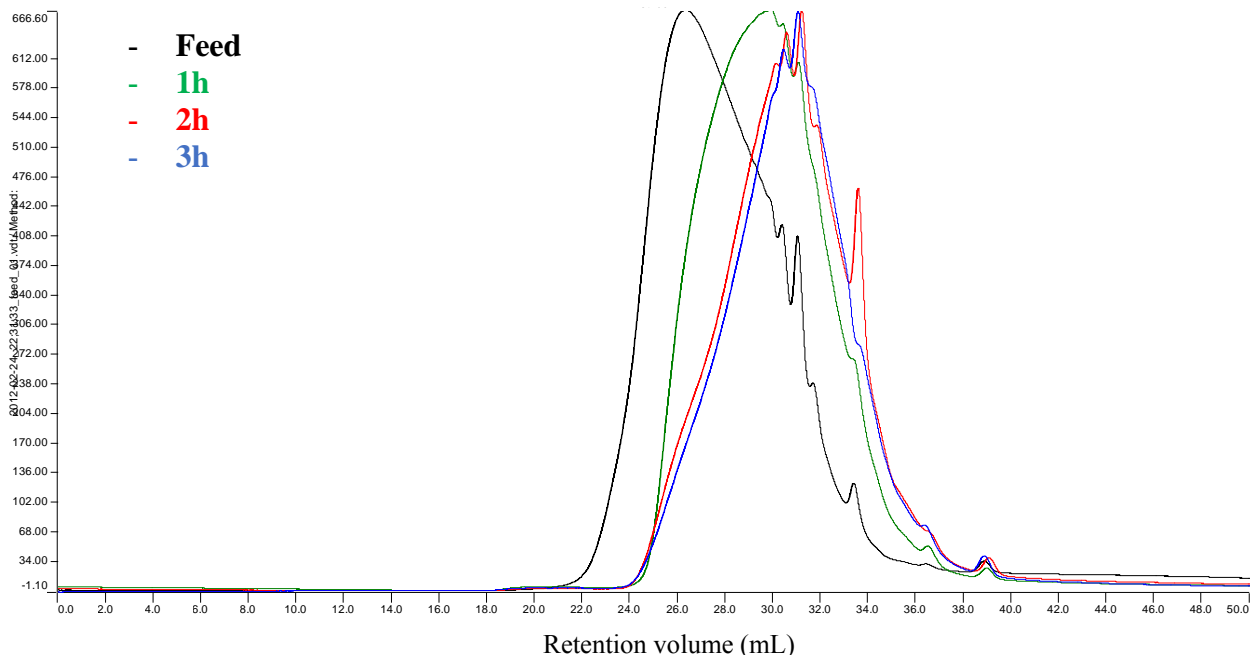


Figure 3-14 GPC chromatographs of asphaltenes collected from Cold Lake bitumen emulsion upgrading experiments at different reaction times (405°C, 80g Cold Lake bitumen emulsion, 585psi CO, 15psi H₂S, 1408 ppmw Mo, 1-3 hours)

3.3.3 Effect of reaction atmosphere

Based on the same “405°C, 80g Cold Lake bitumen emulsion, 585psi feed gas, 15psi H₂S, 1408 ppmw Mo, 2 hours” reaction condition, reaction atmosphere effects were examined. The mass balances for N₂, H₂, CO+ H₂ and CO were 95.4%, 94.1%, 95.7% and 90.7% respectively.

Under a N₂ atmosphere the best oil quality was obtained with 17.6% naphtha and only 5.8% pitch content as shown in Figure 3-15. The asphaltene removal reached as high as 72% compared to 64-66% achieved under other atmospheres. As a trade-off, the N₂ atmosphere resulted in a low S removal (23%), extremely high HVOR yield (13.6%) and a coke yield (1.0%) compared to the other atmospheres. Additionally, the maximum pressure observed was the highest under N₂. This could be explained by additional cracked gas formation under N₂, since there was no H₂ to capture free radicals formed through thermocracking. When *in situ* H₂ or molecular H₂ was introduced, the reaction pressure and coke formation were reduced significantly. As shown in

Table 3-6, the maximum pressure for the H₂ condition was only 2937psi. When CO was present, the pressure increased. This was because CO consumed H₂O and formed CO₂ and H₂; while H₂ was consumed when it was added into hydrocarbons. It can be clearly seen that *in situ* H₂ exhibited a similar upgrading performance as molecular H₂ based on the oil yield and quality. As an advantage over molecular H₂, *in situ* H₂ inhibited coke formation from 0.6% (under H₂) to 0.1% (under CO), which was a 79% reduction.

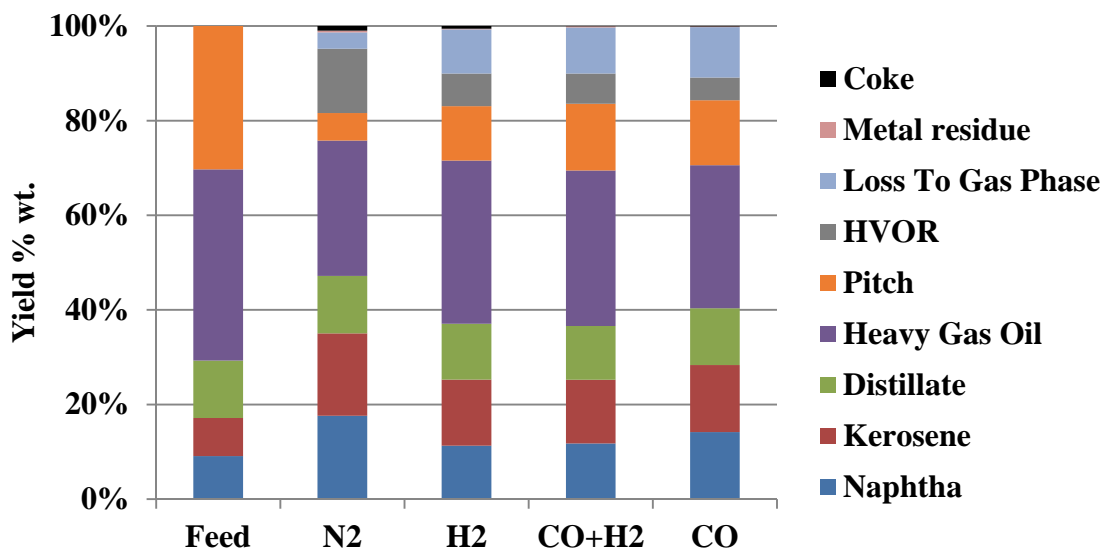


Figure 3-15 Yield distribution of Cold Lake bitumen emulsion upgrading products at different reaction atmospheres (405°C, 80g Cold Lake bitumen emulsion, 585psi feed gas, 15psi H₂S, 1408 ppmw Mo, 2 hours)

Although *in situ* H₂ or molecular H₂ provided better yield and less coke, the reaction performance under N₂ with H₂O presence at 405°C was still very attractive. Compared to existing coking processes, the reaction condition used in this research was at a lower temperature around the lower end of cracking regime, which slowed the cracking reaction for coke formation. In addition, supercritical water was generated under this reaction condition, which has been reported to affect the reaction with its special asphaltene separation and coke inhibition (Morimoto, Sugimoto *et al.* 2014). Considering this interesting upgrading performance under this

condition, some future research could be planned. However, the corrosion tendency of supercritical water will limit the application of upgrading under N₂ in the presence of H₂O.

Table 3-6 Cold Lake bitumen emulsion upgrading performance at different reaction atmospheres (405°C, 80g Cold Lake bitumen emulsion, 585psi feed gas, 15psi H₂S, 1408 ppmw Mo, 2 hours)

	N ₂	H ₂	CO+H ₂	CO
Upgraded Oil Yield%	82	83	84	84
Pitch Conversion%	81	62	53	54
Max. Pressure (psi)	3734	2937	3149	3491
WGSR Conversion%	-	-	80	78
H ₂ mole%	2	75	15	17
Asphaltene removal %	72	64	64	66
S Removal%	23	49	64	52
HVOR Yield%	14	7	6	5
Coke Yield%	1.0	0.6	0.1	0.1

In contrast to S removal in the overall product, the removal of S from asphaltenes was more difficult. As shown in Figure 3-16, S was removed to a certain level in asphaltenes even under N₂. This HDS under N₂ might be realized through the interaction between supercritical water and asphaltenes, as it has been reported that supercritical water could remove sulfur (Daud, Pinilla *et al.* 2012, Patwardhan, Kida *et al.* 2012, Patwardhan, Timko *et al.* 2013). Molecular H₂ provided slightly higher S removal from asphaltenes compared to *in situ* H₂. The N:C and H:C ratios in Figure 3-16 provide a clear view of how different atmospheres affected on the asphaltenes. For example, N:C was the highest under N₂; while H:C was the lowest under N₂. More thermocracking should occur under N₂, and asphaltenes were condensed and became more aromatic. On the contrary, molecular H₂ and/or *in situ* H₂ inhibited asphaltene condensation by saturating free radicals. This was likely the reason for the low coke yield at 405°C in emulsion upgrading. Interestingly, it was found that the H:C ratio increased slightly with higher CO fractions, indicating an improved hydrogenation ability of *in situ* H₂ compared to molecular H₂.

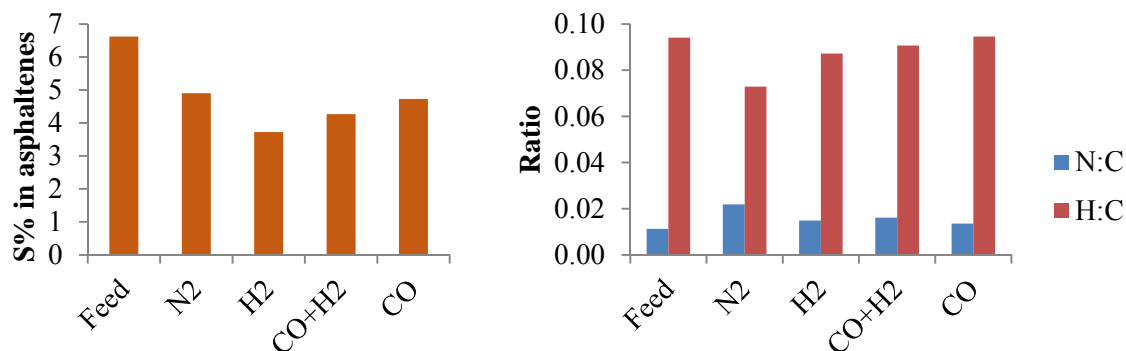


Figure 3-16 S content (left), N:C and H:C ratios (right) of asphaltenes collected from Cold Lake bitumen emulsion upgrading experiments at different reaction atmospheres (405°C, 80g Cold Lake bitumen emulsion, 585psi feed gas, 15psi H₂S, 1408 ppmw Mo, 2 hours)

GPC chromatographs in Figure 3-17 further show the thermocracking inhibition of molecular H₂ or *in situ* H₂ compared to a N₂ atmosphere. It should be noted that the level of asphaltenes became smaller under all conditions, since a certain degree of cracking occurred during the reaction due to either thermocracking or hydrocracking. The asphaltene size was the smallest under N₂, since it is likely that only thermocracking occurred which produced smaller asphaltenes and a high coke yield due to the condensation of the cracked asphaltene free radicals. However, asphaltene size was prevented from becoming small through unfavourable thermocracking under H₂, CO+H₂ and CO. The cracked free radicals from asphaltenes were captured by either *in situ* H₂ or molecular H₂. This observation is consistent with the CHN results discussed in the previous paragraph.

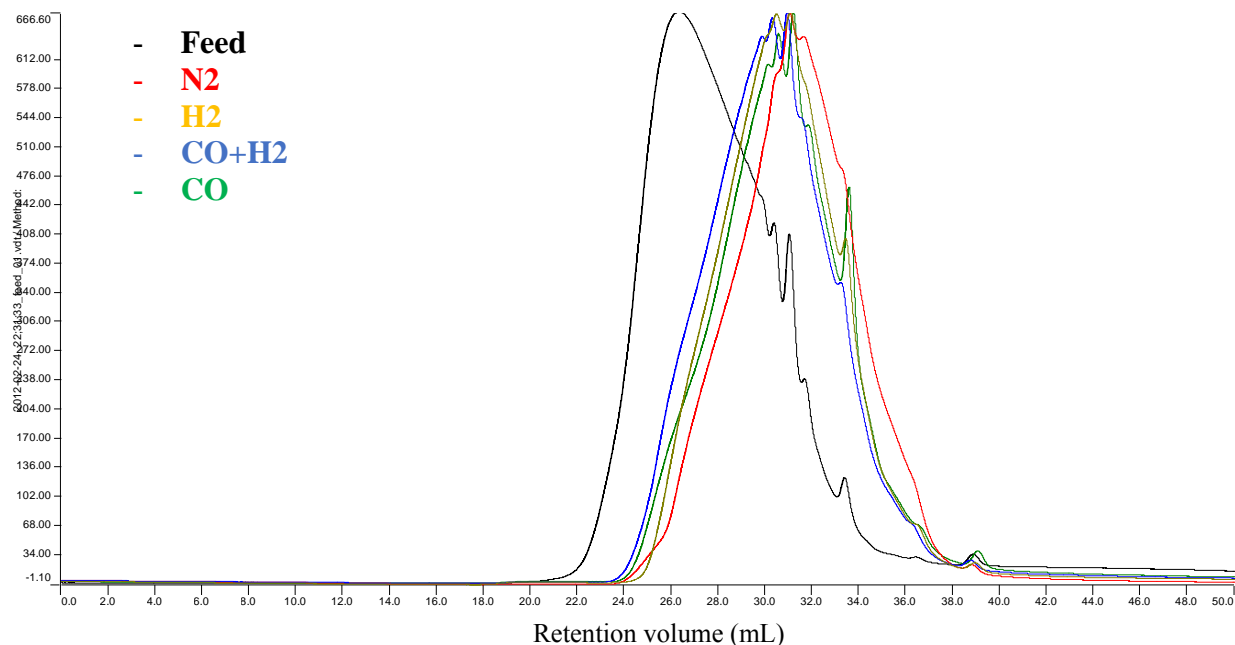


Figure 3-17 GPC chromatographs of asphaltenes collected from Cold Lake bitumen emulsion upgrading experiments at different reaction atmospheres (405°C, 80g Cold Lake bitumen emulsion, 585psi feed gas, 15psi H₂S, 1408 ppmw Mo, 2 hours)

Oxidation of asphaltene samples within a DSC-TGA revealed structural information. As shown in Figure 3-18, weight percentage and heat flow were recorded during programmed heating oxidation of asphaltenes under an air flow. The results clearly show that an early heat flow peak was obtained for asphaltenes treated under a N₂ condition. This heat flow peak at a lower boiling point indicated less paraffinic structures in the asphaltenes (Alcazar-Vara and Buenrostro-Gonzalez 2013), which could be caused by thermocracking. Under N₂, thermal cracking occurred but there was no added H₂ source to cap the cracked free radicals and hence more coke was produced. Asphaltene structures became slightly condensed under H₂, CO+ H₂ and CO conditions. Similar to the CHN and GPC results, the asphaltenes were cracked under H₂, CO+ H₂ and CO atmospheres through hydrocracking.

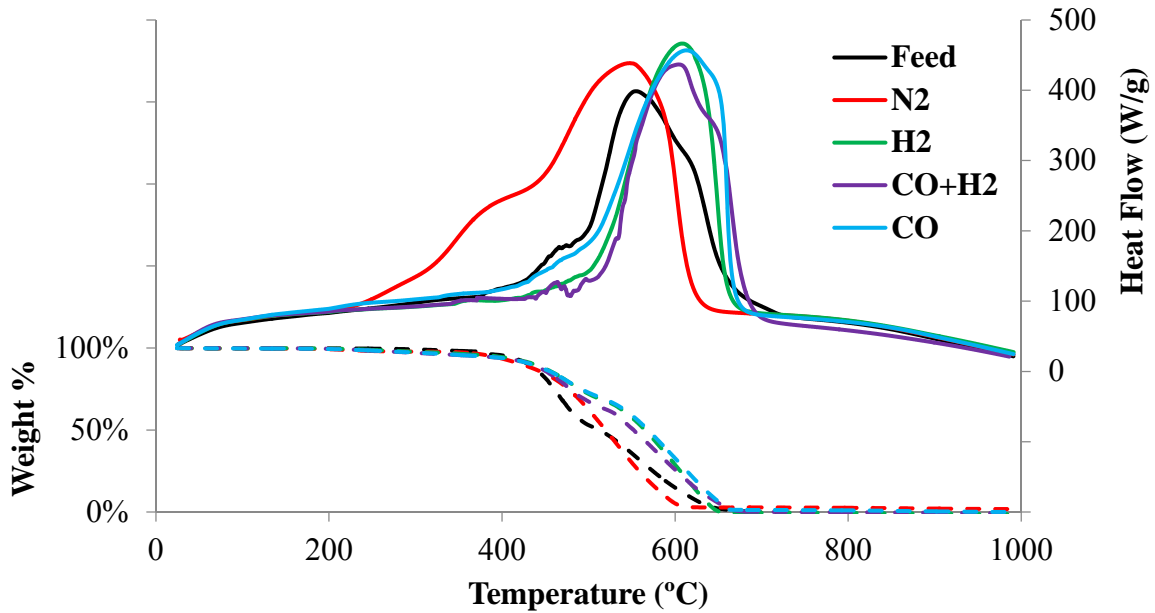


Figure 3-18 Weight loss curves (dashed) and heat flow curve (solid) during the oxidation of asphaltenes collected from Cold Lake bitumen emulsion upgrading experiments at different reaction atmospheres (405°C, 80g Cold Lake bitumen emulsion, 585psi feed gas, 15psi H₂S, 1408 ppmw Mo, 2 hours)

Elemental analysis of the asphaltenes was performed by digesting asphaltenes followed by ICP analysis. Figure 3-19 shows that Ni and V were barely removed from the asphaltenes metalloporphyrin structures by using either molecular H₂ or *in situ* H₂. The major HDM of bitumen with either molecular H₂ or *in situ* H₂ depended on the removal of asphaltenes. However, Ni and V were removed from asphaltene molecules to produce coke under N₂ atmosphere, where V was 66.6% removed and Ni was 35.3% removed.

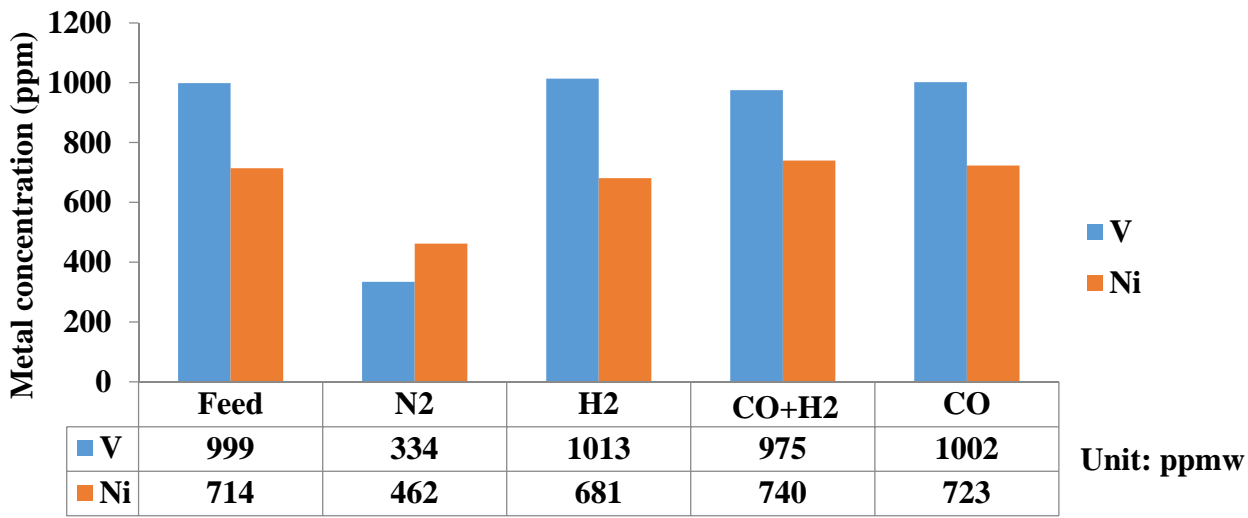


Figure 3-19 Metal contents in asphaltenes collected from Cold Lake bitumen emulsion upgrading experiments at different reaction atmospheres (405°C, 80g Cold Lake bitumen emulsion, 585psi feed gas, 15psi H₂S, 1408 ppmw Mo, 2 hours)

In order to track where the metals were removed to, the toluene insoluble residues (coke with spent catalyst) were also analyzed through digestion and ICP to provide a metal balance as shown in Figure 3-20. It can be found that the Ni and V total mass was almost the same when H₂ was added. It is interesting that the removed V and Ni from asphaltenes eventually deposited in the solid residue, as the Ni and V mass in solid residue was higher than under H₂, CO+H₂ and CO atmospheres. This was attributed to the thermocracking preference under the N₂ atmosphere, which is in agreement with previous findings.

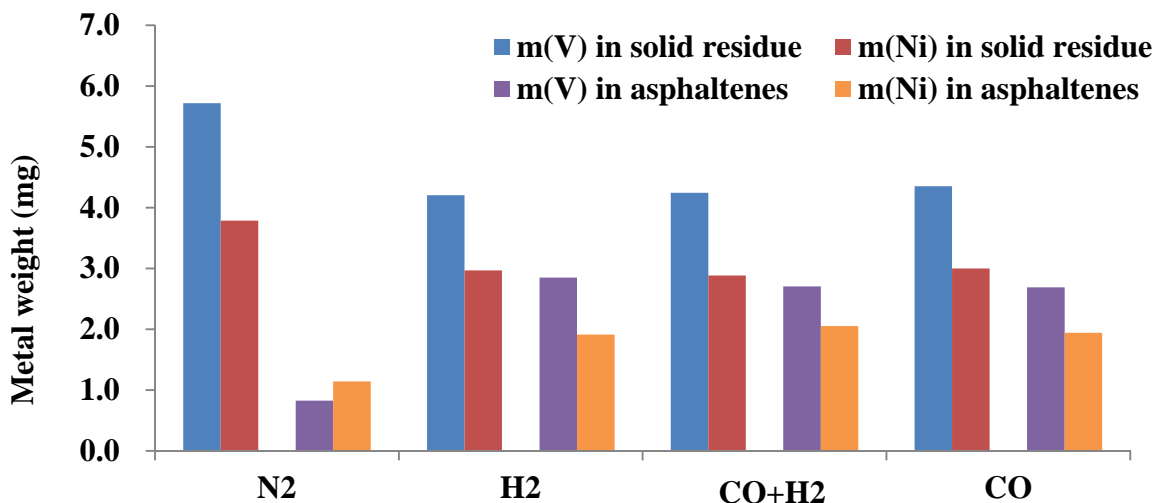


Figure 3-20 Metal balance during the upgrading under different reaction atmospheres (405°C, 80g Cold Lake bitumen emulsion, 585psi feed gas, 15psi H₂S, 1408 ppmw Mo, 2 hours)

3.3.4 Effect of catalyst concentration

Based on the same “405°C, 80g Cold Lake bitumen emulsion, 585psi CO, 15psi H₂S, 2 hours” reaction condition, the effect of catalyst amount was examined. The mass balances for 704 ppmw and 1408 ppmw Mo are 90.5% and 90.7% respectively.

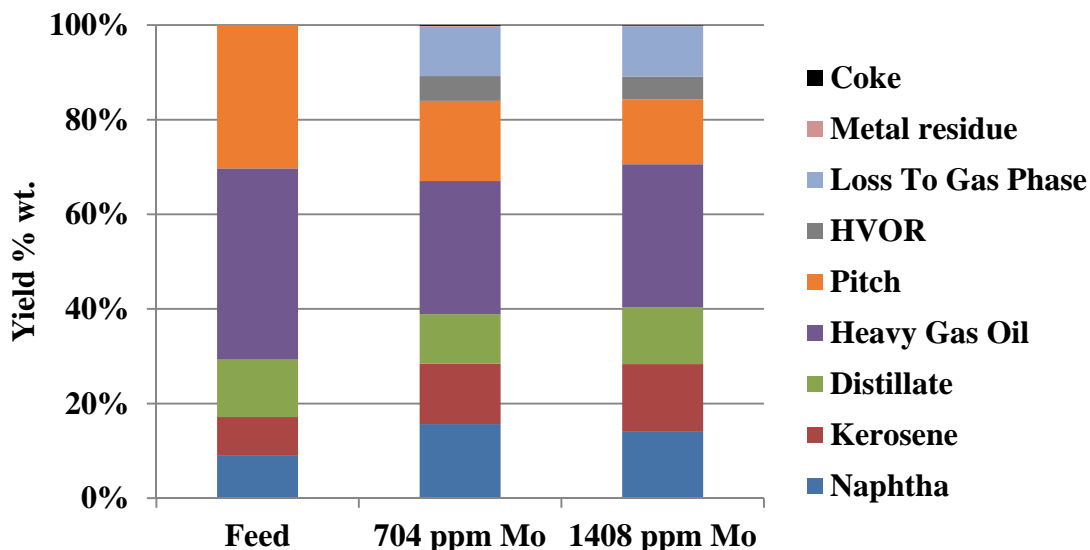


Figure 3-21 Yield distribution of Cold Lake bitumen emulsion upgrading products at different Mo concentrations (405°C, 80g Cold Lake bitumen emulsion, 585psi CO, 15psi H₂S, 2 hours)

Doubling the Mo concentration from 704 ppmw to 1408 ppmw did not improve product yield and quality significantly. As shown in Figure 3-21 and Table 3-7, yields and oil qualities were very close when using 704 ppmw and 1408 ppmw Mo. The only notable variances were the slightly higher pitch conversion (54% vs 43%) and asphaltene conversion (66% vs 53%) when using more catalyst. As discussed, the *in situ* formed nano unsupported MoS₂ was proposed to diffuse into the oil feed, and caused the upgrading, especially on the heavy fractions like asphaltenes. When more catalyst was present in the reaction, more asphaltenes were upgraded as shown in Table 3-6. However, this asphaltene/pitch removal improvement did not provide a distinguishable contribution to the overall observed upgrading performance.

Table 3-7 Cold Lake bitumen emulsion upgrading performance at different Mo concentrations (405°C, 80g Cold Lake bitumen emulsion, 585psi CO, 15psi H₂S, 2 hours)

	704 ppm Mo	1408 ppm Mo
Upgraded Oil Yield%	84	84
Pitch Conversion%	43	54
Max. Pressure (psi)	3602	3491
WGSR Conversion%	83	78
H ₂ mole%	18	17
Asphaltene removal %	53	66
S Removal%	46	52
HVOR Yield%	5	5
Coke Yield%	0.2	0.1

The S removal using 704 ppmw and 1408 ppmw Mo were also very close as shown in Figure 3-22. A similar trend was also observed in the changes of the N:C ratios. A minor improvement on H:C by using 1408 ppmw Mo was noticed, indicating possible more hydrogenation when more catalyst was present.

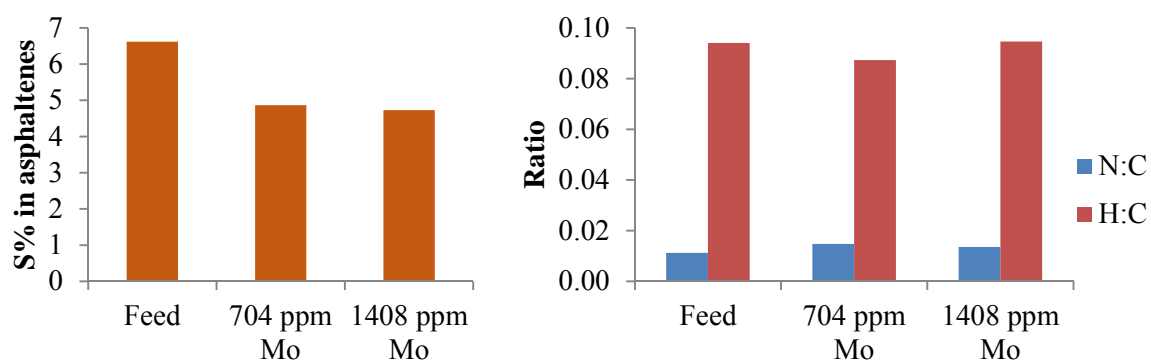


Figure 3-22 S content (left), N:C and H:C ratios (right) of asphaltenes collected from Cold Lake bitumen emulsion upgrading experiments at different Mo concentrations (405°C, 80g Cold Lake bitumen emulsion, 585psi CO, 15psi H₂S, 2 hours)

As shown in Figure 3-23, no apparent reduction in asphaltene size was observed by using different Mo loadings. The small right-shift for the 704 ppmw condition might be due experimental error. It could also be because that the asphaltenes tended to crack more when less catalyst interacted with them.

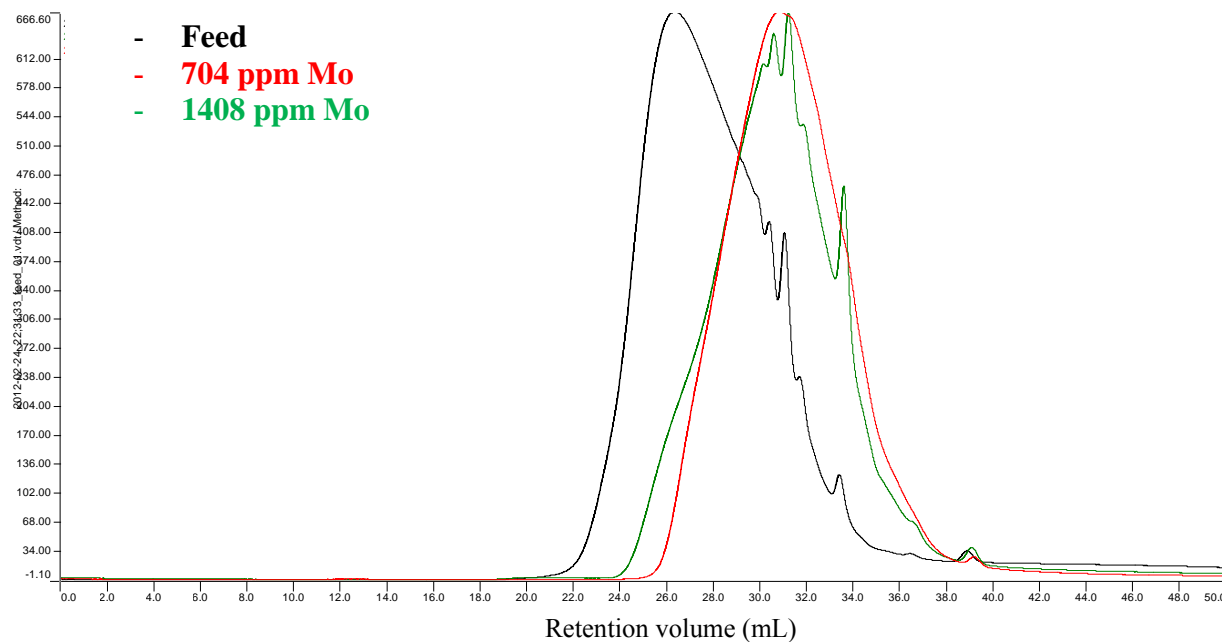


Figure 3-23 GPC chromatographs of asphaltenes collected from Cold Lake bitumen emulsion upgrading experiments at different Mo concentrations (405°C, 80g Cold Lake bitumen emulsion, 585psi CO, 15psi H₂S, 2 hours)

3.3.5 Effect of Ni as a promoter

Based on the same “405°C, 80g Cold Lake bitumen emulsion, 585psi CO, 15psi H₂S, 1408ppmw Mo, Ni:Mo=0.6, 2 hours” reaction condition, the effects of metals were examined. The mass balances for Mo and Ni-Mo were 90.7% and 88.7% respectively.

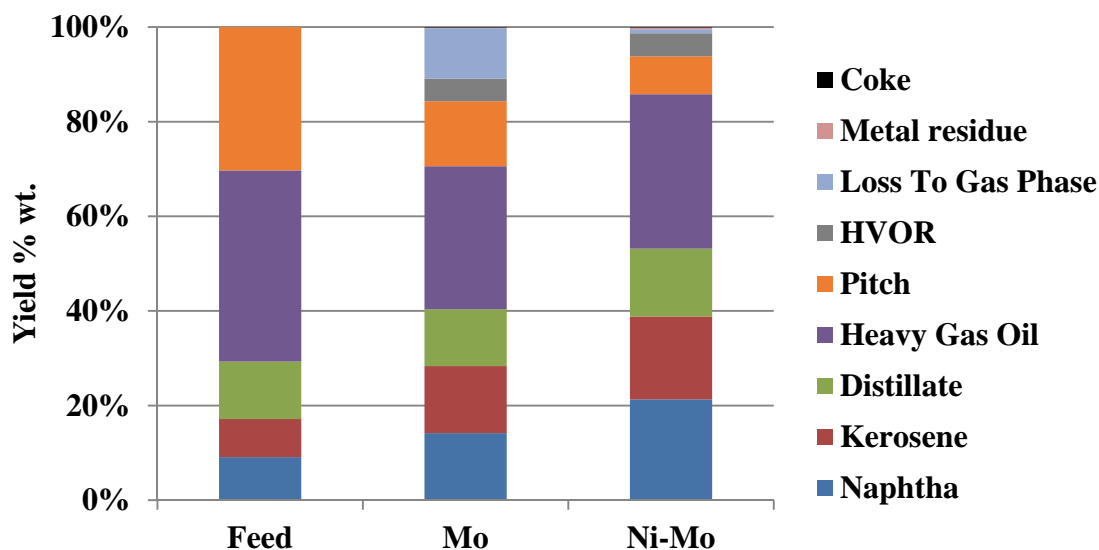


Figure 3-24 Yield distribution of Cold Lake bitumen emulsion upgrading products with and without Ni as a promoter (405°C, 80g Cold Lake bitumen emulsion, 585psi CO, 15psi H₂S, 1408ppmw Mo, Ni:Mo=0.6, 2 hours)

As shown in Figure 3-24 and Table 3-8, both oil yield and oil quality were improved dramatically when Ni was introduced. The upgraded oil yield increased from 84% to 94%! In addition, the pitch conversion reached 73% with 21.3% naphtha content in the final product. It seemed cracking was significantly promoted by adding Ni. However, there was almost no additional HVOR and coke formation when Ni-MoS₂ was used shown in Table 3-8. No obvious WGSR, asphaltene removal or HDS improvement was noticed when Ni was added. From a reaction condition perspective, the reaction pressure was reduced by nearly 450 psi when using Ni promoted MoS₂. This would considerably reduce the risk of supercritical water formation within the reactor, and benefit future engineering design with less corrosion and a cheaper reactor.

Table 3-8 Cold Lake bitumen emulsion upgrading performance with and without Ni as a promoter (405°C, 80g Cold Lake bitumen emulsion, 585psi CO, 15psi H₂S, 1408ppmw Mo, Ni:Mo=0.6, 2 hours)

	Mo	Ni-Mo
Upgraded Oil Yield%	84	94
Pitch Conversion%	54	73
Max. Pressure (psi)	3491	3052
WGSR Conversion%	78	79
H ₂ mole%	17	12
Asphaltene removal %	66	60
S Removal%	52	50*
HVOR Yield%	5	5
Coke Yield%	0.1	0.1

* Data was collected following different XRF calibration performed with long interval (nearly 9 months)

The characterization of asphaltenes might reveal the role of Ni. As shown in Figure 3-25, no distinguishable HDS improvement was found by adding Ni. The introduction of Ni, on the other hand, seemed to enhance the hydrocracking reaction, because the N:C ratio increased and the H:C ratio decreased when Ni was added. Asphaltenes became more condensed, accordingly the N content and the aromaticity increased. In the presence of highly active *in situ* H₂ to capture free radicals, there was no additional coke formation with promoted cracking by using Ni-MoS₂. As a result, Ni is confirmed to be a good promoter in emulsion upgrading when *in situ* H₂ is involved.

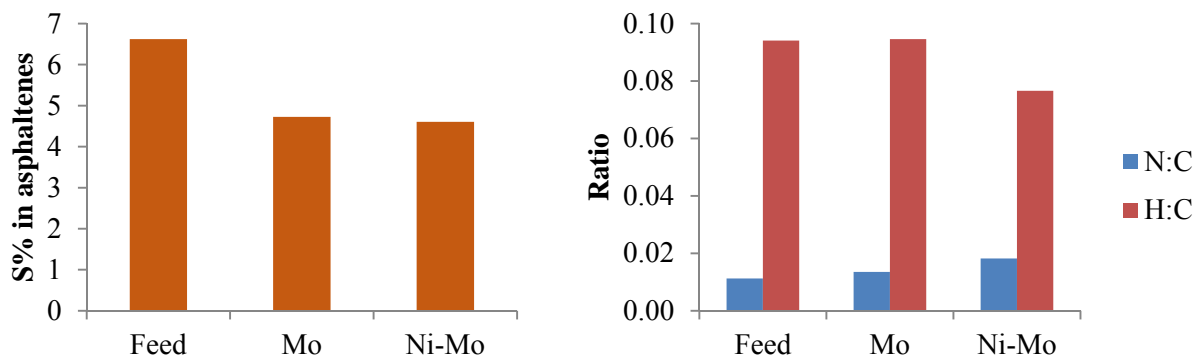


Figure 3-25 S content (left), N:C and H:C ratios (right) of asphaltenes collected from Cold Lake bitumen emulsion upgrading experiments with and without Ni as a promoter (405°C, 80g Cold Lake bitumen emulsion, 585psi CO, 15psi H₂S, 1408ppmw Mo, Ni:Mo=0.6, 2 hours)

As shown in Figure 3-26, no apparent improvement of asphaltene size was found by using Ni-MoS₂.

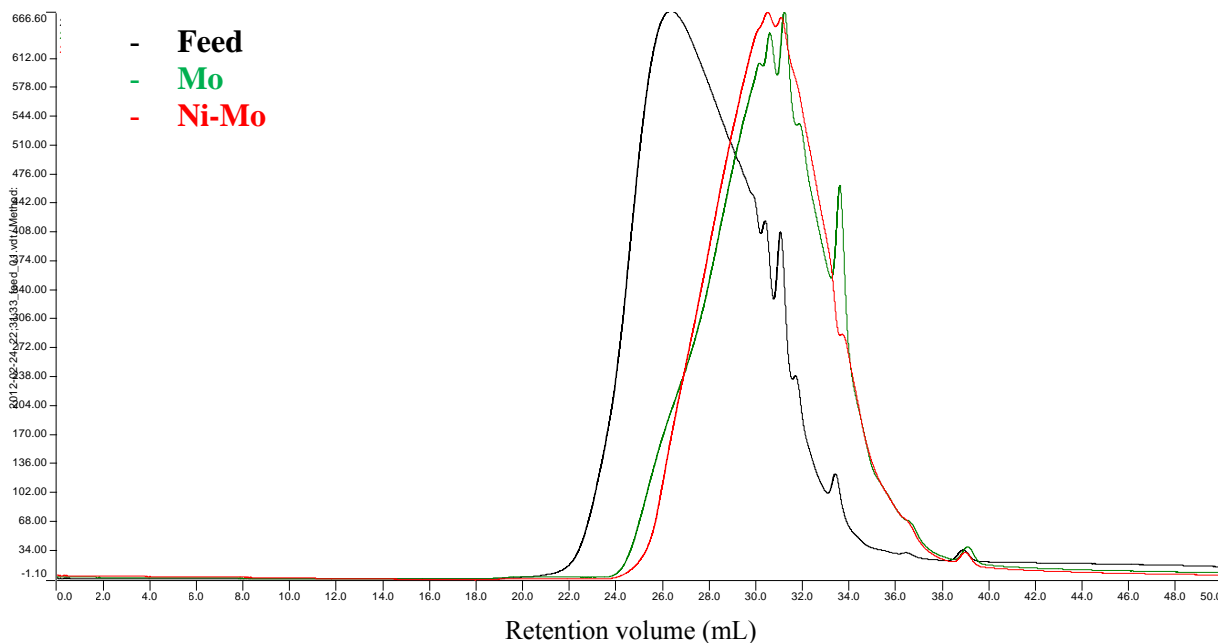


Figure 3-26 GPC chromatographs of asphaltenes collected from Cold Lake bitumen emulsion upgrading experiments with and without Ni as a promoter (405°C, 80g Cold Lake bitumen emulsion, 585psi CO, 15psi H₂S, 1408ppmw Mo, Ni:Mo=0.6, 2 hours)

3.4 Conclusions

Cold Lake bitumen emulsion was successfully upgraded by using *in situ* formed MoS₂ and *in situ* H₂ derived from the WSGR. The WSGR occurred simultaneously with the upgrading reactions with *in situ* H₂ being consumed for hydrocracking and hydrotreating. The upgraded oil product was lighter than water, stable without precipitation and could easily flow (at room temperatures), indicating ideal partial upgrading performance for pipeline transportation.

405°C was found to be the optimal temperature to produce high conversion and liquid yield with low coke and HVOR yields. 2h was the ideal reaction duration achieving “demulsification + upgrading” and preventing over-upgrading. *In situ* H₂ showed a similar upgrading performance as molecular H₂ at a lower H₂ partial pressure with even less coke formation. Good upgrading performance was also obtained under N₂ at 405°C. Under this condition, supercritical water contributed to the relatively high liquid yield and low coke yield compared to the normal coking reaction. However, the corrosion tendency of supercritical water would eventually constrain the practical application of this reaction condition. 704ppmw Mo was observed to provide similar upgrading performance as 1408ppmw Mo. Lower Mo loading should be further studied for reducing catalyst cost. As a promoter, Ni benefited the emulsion upgrading with increased oil yield and no extra coke or HVOR formation. It was noticed that the promoted hydrocracking reaction with the Ni-MoS₂ catalyst might be the main reason for this improved upgrading performance.

Asphaltenes were separated and characterized to investigate their component and structural change. It was observed that asphaltenes were also upgraded during the reaction, for example, less S, less carbonyl, smaller molecular size, etc. When there was no external H₂ source, asphaltenes preferred condensation through thermocracking, resulting in more HVOR and a higher coke yield. In the presence of molecular H₂ or *in situ* H₂, this asphaltene condensation was prevented, which eventually benefited upgrading by providing more liquid yield and less coke/HVOR yield. Additionally, asphaltenes were also hydrogenated by these external H₂

sources, where *in situ* H₂ showed slightly better HDS and HDA capabilities than molecular H₂ based on the asphaltene S content and H:C ratio results. However, N, Ni and V were not removed from asphaltene molecules during emulsion upgrading. The HDN and HDM of the bitumen emulsion depended on the removal of asphaltene only.

Chapter 4 Upgrading of Athabasca Bitumen through a Novel Emulsion Upgrading Process

4.1 Introduction

Due to geophysical reasons, Athabasca bitumen is more difficult to be upgraded compared to Cold Lake bitumen. Some typical bitumen properties are shown in Table 1-2. In order to further confirm the feasibility of emulsion upgrading technology, Athabasca bitumen was chosen as feed oil for the study presented in this chapter. This Athabasca bitumen sample was taken right after froth treatment unit from an Alberta *in situ* producer, and found containing 4.1%wt S and 54.5%wt pitch and around 1.2% H₂O. Since most of the emulsified water was removed in the froth treatment step. This low emulsified water content brought the flexibility for testing the effect of different amounts of water on the overall upgrading performance.

Part of Chapter 4 includes a discussion on the feasibility of water treatment through emulsion upgrading technology. The bitumen sample barrel came with dirty water separated after froth treatment. This water was a good representative for oil sands process affected water (OSPW) or process affected water (PAW), which have created environmental concerns. This dirty water was added as feed water for WGSR with the Athabasca bitumen for emulsion upgrading. Typical emulsion breaking process on a lab scale, like distillation, would leave the impurities in the oil phase, which usually makes it impossible for feed water quality analysis. The utilization of dirty water has overcome this dilemma. Water qualities before and after emulsion upgrading were analyzed to examine potential water treatment performance on emulsion upgrading.



Figure 4-1 Dirty water (OSPW or PAW) and the purified water after emulsion upgrading (415°C, 80g Athabasca bitumen, 10mL OSPW, 585psi CO, 15psi H₂S, 1408ppmw Mo, 2 hours)

As shown in Figure 4-1, the OSPW was purified after emulsion upgrading into a clean water phase with almost no apparent emulsified oil residues. The brownish color in the water product was caused by Fe³⁺. Detailed characterization will be discussed in this chapter. It should be noted that 415°C was used as the upgrading temperature by considering the upgrading difficulty caused by the poorer quality of Athabasca bitumen compared to Cold Lake bitumen emulsions.

4.2 Upgrading results and discussion

4.2.1 Significance of MoS₂ catalyst and *in situ* H₂

Based on the same “415°C, 80g Athabasca bitumen, no OSPW, 585psi feed gas, 15psi H₂S, 0 or 1408ppmw Mo, 2 hours” reaction condition, the significance of a nano MoS₂ catalyst and *in situ* H₂ was examined compared to coking. The mass balances for Coking with N₂, MoS₂+ H₂ and MoS₂+CO conditions were 90.8%, 83.9% and 89.4% respectively. Since there was around 1.2% emulsified water present in bitumen feed (water collected/measured through emulsion breaking by heat), the coking scenario was able to be simulated by using a N₂ atmosphere without catalyst

loading. Although the coking temperature is usually much higher than 415°C, this provided the best comparison for identifying the effect of the nano MoS₂ catalyst and *in situ* H₂ with the existing feedstock and equipment. It should be noticed that no water was added in the reactions with MoS₂, and the 1.2% emulsified water was the only water source for WGSR in generating *in situ* H₂.

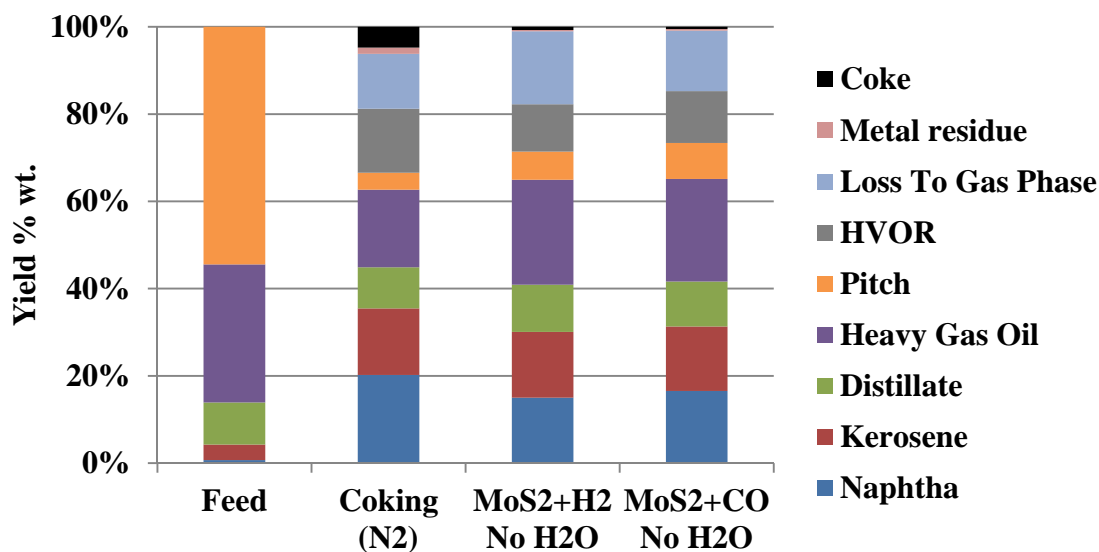


Figure 4-2 Yield distribution of Athabasca bitumen upgrading products with N₂ only, MoS₂+molecular H₂ and MoS₂+*in situ* H₂ (415°C, 80g Athabasca bitumen, no OSPW, 585psi feed gas, 15psi H₂S, 0 or 1408ppmw Mo, 2 hours)

Similar to the yield and quality analysis provided in Chapter 3, the yield and product quality are also presented in Figure 4-2. The lightest oil was produced through coking with 20.2% naphtha content and 87% pitch conversion as shown in Table 4-1. Nevertheless, this high quality came with high yield loss and coke yield. The yield was only 67% compared to the 71% and 73% by using MoS₂ and an additional H₂ source. The coke yield by coking under N₂ was 4.7%, which was 7 times and 10 times that of the coke yields when using molecular H₂ and *in situ* H₂ with MoS₂. Since the temperature was relatively low, the actual coking process will produce even less oil product with much more coke. When MoS₂ was used with an additional H₂ source, the

thermocracking was controlled providing more yield and relatively less upgraded oil, which was beneficial for partial upgrading. Besides, the system maximum pressure was significantly reduced once MoS₂ was used with an external H₂ source. Figure 4-3 provides a clear example as to how thermocracking was reduced. Pressure did not increase substantially as it did in coking, because much less cracked gases were formed. Additionally, S removal was also improved when MoS₂ and an external H₂ source were used because of the HDS reaction. As shown in Table 4-1, the S removal increased from 28% to 46% and 38%, respectively, for the MoS₂+H₂ and MoS₂+CO systems. Hence, the presence of MoS₂ and a H₂ source were crucial for the emulsion upgrading process. Detailed reaction conditions for the control experiments will be discussed in the following sections of this chapter.

Table 4-1 Athabasca bitumen upgrading performance with N₂ only, MoS₂+molecular H₂ and MoS₂+*in situ* H₂ (415°C, 80g Athabasca bitumen, no OSPW, 585psi feed gas, 15psi H₂S, 0 or 1408ppmw Mo, 2 hours)

	Coking (N ₂)	MoS ₂ +H ₂ No H ₂ O	MoS ₂ +CO No H ₂ O
Upgraded Oil Yield%	67	71	73
Pitch Conversion%	87	82	79
Max. Pressure (psi)	2442	1929	1866
WGSR Conversion%	-	-	82
H ₂ mole%	-	36	6
S Removal%	28	46	38
HVOR Yield%	15	11	12
Coke Yield%	4.7	0.7	0.5

It is interesting that in Figure 4-3 the pressure kept decreasing for the MoS₂ + *in situ* H₂ condition; while pressure stopped decreasing and went up at 60 minutes for the MoS₂ + molecular H₂ condition. This could be attributed to *in situ* H₂'s high activity for capturing thermally cracked free radicals, which prevented cracked gas formation. Or it could be explained as having a high hydrocracking preference for *in situ* H₂ over MoS₂, which typically did not produce cracked gases like thermocracking does. Considering the much lower H₂ mole percentage (6%, determined after reaction) by using CO compared to the H₂ mole percentage

(36%) by using molecular H₂, a similar upgrading performance was obtained under these two conditions which implied an extremely high activity for *in situ* H₂. As only 1.2% water was used in the WGSR for generating *in situ* H₂, a detailed H₂ activity comparison will be discussed with more additional water fed in experiments.

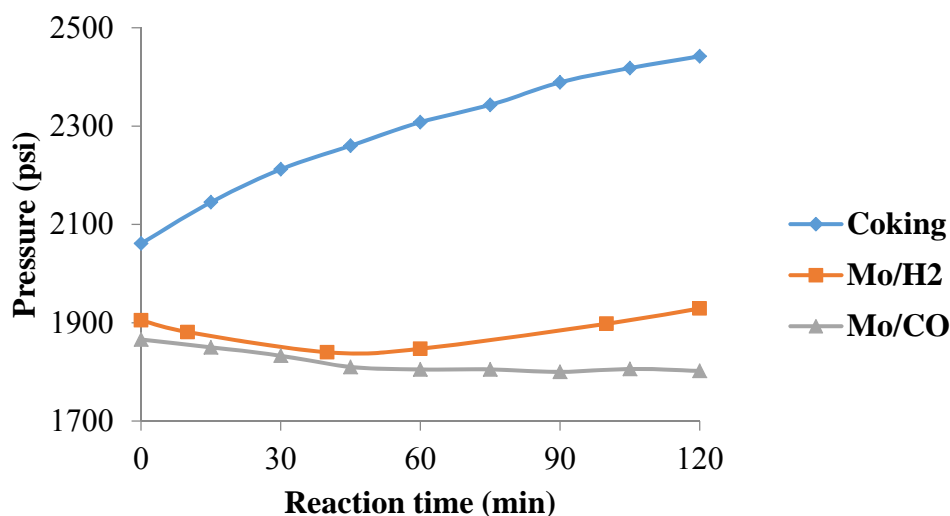


Figure 4-3 Pressure changes during reaction with N₂ only, MoS₂+molecular H₂ and MoS₂+*in situ* H₂ (415°C, 80g Athabasca bitumen, no OSPW, 585psi feed gas, 15psi H₂S, 0 or 1408ppmw Mo, 2 hours)

4.2.2 Effect of reaction time

Based on the same “415°C, 80g Athabasca bitumen, 5mL OSPW, 585psi CO, 15psi H₂S, 1408ppmw Mo, 1-2 hours” reaction condition, the effect of reaction time was examined. The mass balances for 1h, 1.5h and 2h conditions were 91.6%, 96.3% and 91.0% respectively. As discussed before, Athabasca bitumen is of a poorer quality than the Cold Lake bitumen emulsion due to its higher pitch content and lower water content. Hence the upgrading of this oil feedstock requires more severe reaction conditions. In addition, higher reaction rates are also desired, which help to reduce reaction residence time. Shorter residence time would eventually result in smaller reactor size, further diminishing the process capital cost.

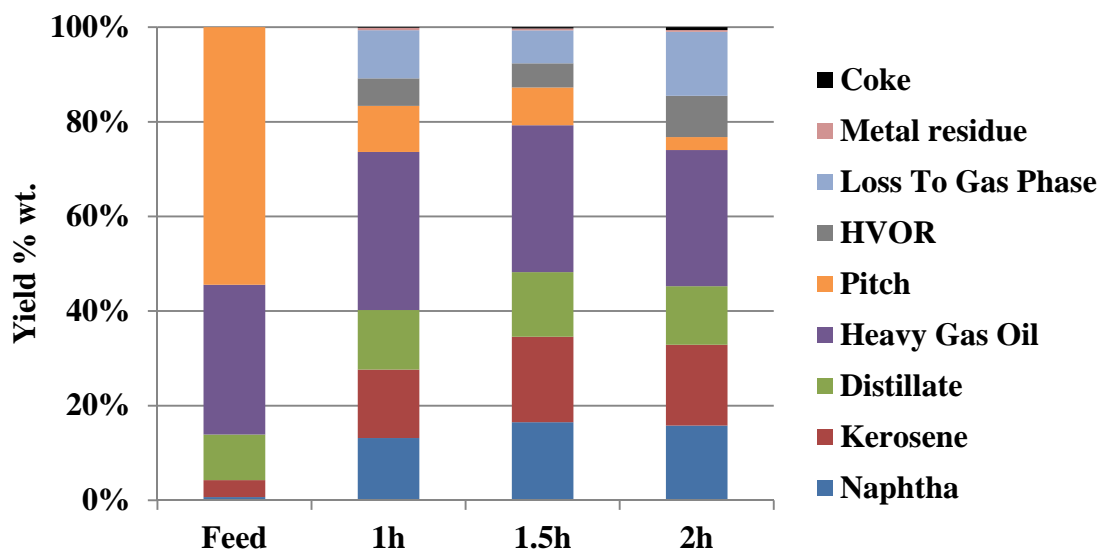


Figure 4-4 Yield distribution of Athabasca bitumen upgrading products at different reaction times (415°C, 80g Athabasca bitumen, 5mL OSPW, 585psi CO, 15psi H₂S, 1408ppmw Mo, 1-2 hours)

When 415°C was used as the reaction temperature, upgrading became faster. The yield increased by 4% (from 83% to 87%) after 1h to 1.5h, indicating on-going upgrading. However, an obvious yield reduction (from 87% to 77%) is shown from 1.5h to 2h in Figure 4-4, which was the result of increased thermal cracking preference under a depleted H₂ partial pressure. The increased HVOR (8.7%) and coke yield (0.6%) shown in Table 4-2 also confirmed the over-upgrading under the 2h condition. Furthermore, over-upgrading provided higher pitch conversion (88%), about 10% bitumen was lost into gas, coke and HVOR streams, leading to poor economics for future engineering design.

Table 4-2 Athabasca bitumen upgrading performance at different reaction times (415°C, 80g Athabasca bitumen, 5mL OSPW, 585psi CO, 15psi H₂S, 1408ppmw Mo, 1-2 hours)

	1h	1.5h	2h
Upgraded Oil Yield%	83	87	77
Pitch Conversion%	76	80	88
Max. Pressure (psi)	2855	2325	2349
WGSR Conversion%	71	80	85
H ₂ mole%	12	6	6
S Removal%	31	26	31
HVOR Yield%	6	5	9
Coke Yield%	0.1	0.3	0.6

Due to time constrain, the remaining experiments were still carried out for 2h duration. However, more research on 1.5h should be planned on this project for future commercialization.

4.2.3 Effect of water and the MoS₂ catalyst

As an important factor for emulsion upgrading technology, water was added in different amounts for investigating its role in the emulsion upgrading process. The effect of water is discussed in this section with and without the addition of catalysts. Additionally the effect of catalyst can be understood, too. Coking (under a N₂ atmosphere without catalyst or added water) was listed as a reference for comparison. Based on the same “415°C, 80g Athabasca bitumen, 0 or 10mL OSPW, 585psi CO, 15psi H₂S, 0 or 1408ppmw Mo, 2 hours” reaction condition, the effect of water and nano MoS₂ catalyst was examined. The mass balances for “Coking”, “No MoS₂/No H₂O”, “No MoS₂/5mL H₂O”, “No MoS₂/10mL H₂O”, “MoS₂/No H₂O”, “MoS₂/5mL H₂O” and “MoS₂/10 mL H₂O” conditions were 90.8%, 84.8%, 89.3%, 90.2%, 89.4%, 91.0% and 92.4% respectively.

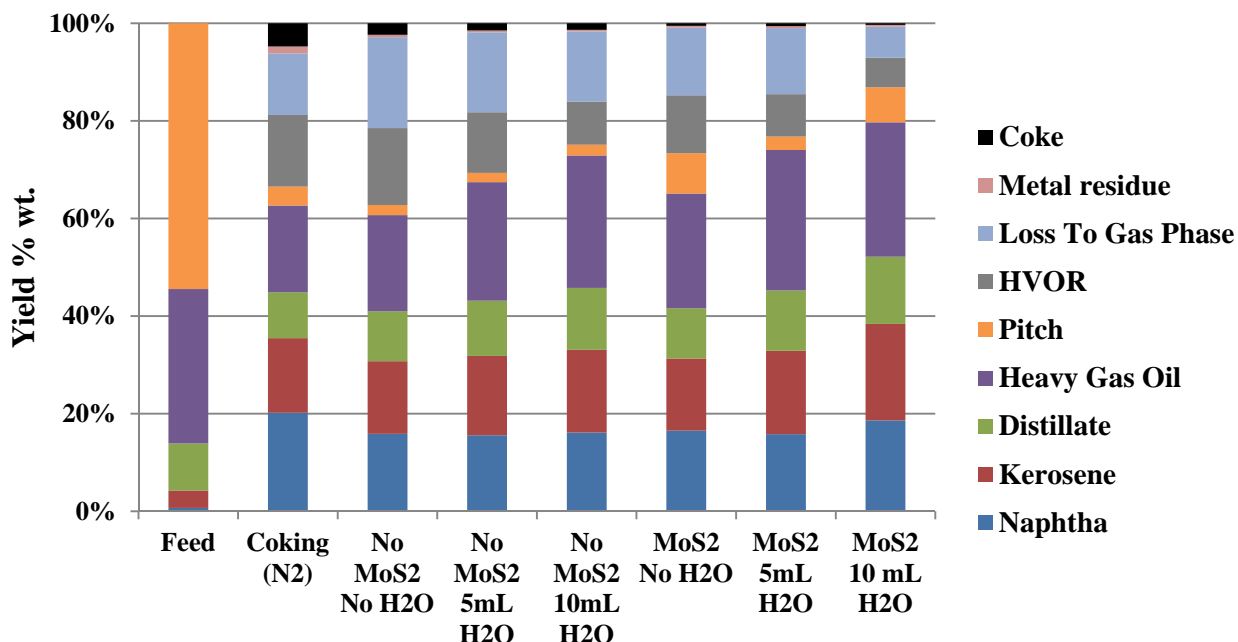


Figure 4-5 Yield distribution of Athabasca bitumen upgrading products at different OSPW loadings with and without MoS₂ (415°C, 80g Athabasca bitumen, 0 or 10mL OSPW, 585psi CO, 15psi H₂S, 0 or 1408ppmw Mo, 2 hours)

As shown in Figure 4-5, the upgrading performance under a CO atmosphere without catalyst or water was similar to coking. When no catalyst or water was added under a CO atmosphere, the system pressure (1775psi) was much lower than the coking pressure (2442psi) as shown in Table 4-3. This is understandable in that *in situ* H₂ was generated through the WGSR from only 1.2% emulsified water in bitumen. The thermocracking reaction might be inhibited by capturing free radicals with this small amount of *in situ* H₂. This inhibition can also be distinguished by comparing the coke yield, and only 2.3% coke was formed with this small amount of *in situ* H₂ compared 4.7% in a coking reaction. The high HVOR yield in “No MoS₂/No H₂O” condition was expected as a result for both poor emulsion breaking and asphaltene condensation. When 5mL and 10mL water were added, more H₂ was formed. The H₂ mole% increased from 5% to 10%. The HVOR yield was reduced from 15.8% to 12.4% and 8.8% respectively. The coke yield was also reduced from 2.3% to 1.5% and 1.3%. This further indicated the thermocracking inhibition ability of *in situ* H₂ during emulsion upgrading. In addition to that, much higher yields

were achieved with similar pitch conversion. The yield increased from 63% without water to 69% and 75% by adding 5mL and 10mL water. The 75%wt yield is much better than the 65% and 70% weight yields of SCWC[®] and HI-Q[®] processes shown in Table 1-8. Water seemed to improve emulsion upgrading by providing higher yield and inhibiting thermocracking with *in situ* H₂. As shown in Table 4-3, the pressure increased from 1775psi to 2246psi and 2750psi by adding 5mL and 10mL water respectively.

Table 4-3 Athabasca bitumen upgrading performance at different OSPW loadings with and without MoS₂ (415°C, 80g Athabasca bitumen, 0 or 10mL OSPW, 585psi CO, 15psi H₂S, 0 or 1408ppmw Mo, 2 hours)

	Coking (N ₂)	No MoS ₂ No H ₂ O	No MoS ₂ 5mL H ₂ O	No MoS ₂ 10mL H ₂ O	MoS ₂ No H ₂ O	MoS ₂ 5mL H ₂ O	MoS ₂ 10 mL H ₂ O
Upgraded Oil Yield%	67	63	69	75	73	77	87
Pitch Conversion%	87	90	90	89	79	88	81
Max. Pressure (psi)	2442	1775	2246	2750	1866	2349	2916
WGSR Conversion%	-	66	81	71	82	85	75
H ₂ mole%	-	5	7	10	6	6	8
S Removal%	28	36	39	35	38	31	30
HVOR Yield%	14.7	15.8	12.4	8.8	11.9	8.7	6.1
Coke Yield%	4.7	2.3	1.5	1.3	0.5	0.6	0.3

After the addition of the nano MoS₂ catalyst, the yield increased dramatically. After MoS₂ addition, the upgraded oil yields were increased by 8-10% at different water loading. The best yield was achieved by adding 10mL of water and catalyst. The yield was as high as 87%, higher than all the partial upgrading technologies shown in Table 1-8. The HVOR and coke yields were also further reduced by using the MoS₂ catalyst. Only 0.3% coke and 6.1% HVOR were collected for the “MoS₂/10mL H₂O” condition. These significant improvements are derived from the highly active *in situ* formed nano unsupported MoS₂ catalyst. On one hand, the MoS₂ catalyzed WGSR generates more *in situ* H₂. As shown in Table 4-3, when no water was added, the WGSR conversion increased from 66% to 82% when using MoS₂. The WGSR conversion also increased about 4% with MoS₂ when 5mL or 10mL water was added. Addition of 5mL

water seemed to be most favourable, while 10mL of water decreased the WGS conversion. This reduced WGS conversion at 10mL might be caused by the increased pressure or a deactivation effect of water on the catalyst (Laurent and Delmon 1993, Chadwick, Oen *et al.* 1996). On the other hand, nano MoS₂ catalyst could be dispersed on the asphaltenes catalyzing the hydrocracking reaction, leading to improved upgrading performance without significant coke formation like thermocracking or coking. In this way, catalyst addition was crucial to the emulsion upgrading process.

The effect of water was similar with or without catalyst. Higher yields and less coke formation were obtained with water addition. This resulted in decreased HDS performance and higher pressures. It was reported by Israelachvili that the asphaltene-asphaltene interactions could be significantly altered by the presence of water. Water was reported to increase the short range attractions across the oil by discrete charge-charge and acid-base interactions. Accordingly, water could penetrate the asphaltene aggregate layers to swell the asphaltenes, build up water layers at the asphaltene inter-surfaces and eventually displace the asphaltene aggregates (Drummond and Israelachvili 2004). The fundamental results of this study may indicate that the water involved in emulsion upgrading might inhibit the condensation of asphaltene aggregates and prevent them from being condensed for coke formation. Although the pressure generated at the “MoS₂/10mL H₂O” condition was the highest at 2916 psi, this pressure was close to a normal ebullated bed reactor operating pressure. Hence, supercritical water corrosion should not be significant under this pressure. For oil quality consideration, 5mL seemed an optimal loading as it provided enough *in situ* H₂ through the WGS for hydrocracking and not too much excess water to inhibit upgrading. However, from a partial upgrading perspective, a higher yield might be more attractive. In this way, 10mL should be considered for engineering design. The choice between quality and yield can be revealed by economic analysis and further research.

It was interesting that the HDS performance was not affected by adding MoS₂. The same results were obtained for the WGS especially with 5mL and 10mL water loading conditions. These results were not as expected, since MoS₂ has always been found to catalyze the HDS and WGS in model compound research. There could be several reasons for this observation. First, the

bitumen is extremely difficult to process compared to model compounds. The majority of S is located in the asphaltene molecules, making S harder to be removed through normal HDS. The second reason, which was most likely, is that the catalyst might be severely contaminated by either coke or metal deposits like Ni and V during the reaction. V is known to inhibit the *in situ* MoS₂ catalyst in emulsion upgrading (Jia, Alghamdi *et al.* 2012). In order to have a clear understanding of this possible deactivation, more research has been implemented and will be discussed in the following sections in this chapter.

4.2.4 Effect of Ni as a promoter

Based on the same “415°C, 80g Athabasca bitumen, 5 or 10 mL OSPW, 585psi CO, 15psi H₂S, 1408ppmw Mo, Ni:Mo=0.6, 2 hours” reaction condition, the effect of Ni as a promoter was examined. The mass balances for MoS₂/5mL H₂O, Ni/MoS₂/5mL H₂O, MoS₂/10 mL H₂O and Ni/MoS₂/10 mL H₂O conditions were 91.0%, 92.1%, 92.4% and 92.3% respectively.

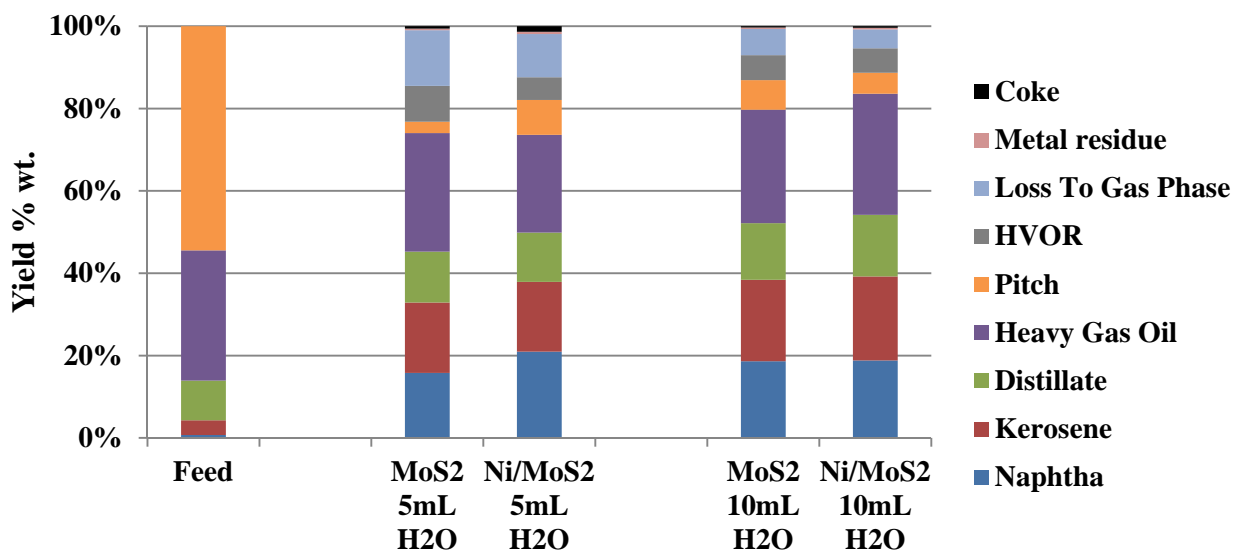


Figure 4-6 Yield distribution of Athabasca bitumen upgrading products with and without Ni as promoter (415°C, 80g Athabasca bitumen, 5 or 10 mL OSPW, 585psi CO, 15psi H₂S, 1408ppmw Mo, Ni:Mo=0.6, 2 hours)

The effect of Ni was evaluated for both 5mL water and 10mL water loadings. It can be seen that the yield was improved with Ni addition. The upgraded oil yield increased from 77% to 82% for the 5mL water case; and from 87% to 89% for the 10mL water case. This was consistent with previous model compound studies. Hence, Ni was further confirmed as a promoter for the emulsion upgrading process. The HVOR yield was also reduced from 8.7% to 5.5% for the 5mL water condition. No significant change in HVOR yield or coke yield for the 10mL water condition was observed. Hence Ni promoted the emulsion upgrading with improvement in oil yield, inhibition of HVOR and with no extra coke formation. So far, the best results obtained were for the condition “Ni/MoS₂/10 mL H₂O” with 89% wt yield, 84% pitch conversion, 5.9 HVOR yield and only 0.4% coke yield. More optimization research should be planned based on this condition.

Table 4-4 Athabasca bitumen upgrading performance with and without Ni as promoter (415°C, 80g Athabasca bitumen, 5 or 10 mL OSPW, 585psi CO, 15psi H₂S, 1408ppmw Mo, Ni:Mo=0.6, 2 hours)

	5mL H ₂ O		10mL H ₂ O	
	MoS ₂	Ni/MoS ₂	MoS ₂	Ni/MoS ₂
Upgraded Oil Yield%	77	82	87	89
Pitch Conversion%	88	79	81	84
Max. Pressure (psi)	2349	2513	2916	2862
WGSR Conversion%	85	86	75	76
H ₂ mole%	6	5	8	7
S Removal%	31	29	30	40
HVOR Yield%	9	6	6	6
Coke Yield%	0.6	1.4	0.3	0.4

Unlike model compound studies, HDS and WGSR were not apparently promoted by adding Ni. This could be attributed to active site deactivation caused by V deposition, like the same phenomena observed on a comparison with and without the MoS₂ catalyst. A detailed deactivation study will be discussed in the following sections.

4.2.5 Effect of reaction atmosphere by using Ni/MoS₂ catalyst

Based on the same “415°C, 80g Athabasca bitumen, 5mL OSPW, 585psi feed gas, 15psi H₂S, 1408ppmw Mo, Ni:Mo=0.6, 2 hours” reaction condition, the effect of reaction atmosphere was examined. The mass balances for H₂, CO+ H₂ (1:1 ratio) and CO conditions were 94.2%, 92.1% and 91.9% respectively.

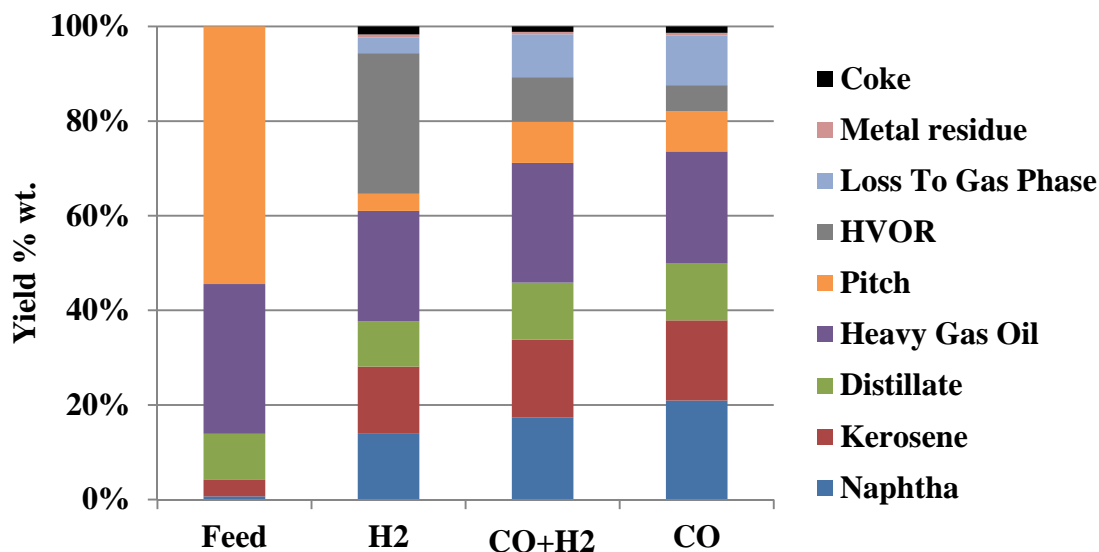


Figure 4-7 Yield distribution of Athabasca bitumen upgrading products under different reaction atmospheres by using Ni/MoS₂ catalyst (415°C, 80g Athabasca bitumen, 5mL OSPW, 585psi feed gas, 15psi H₂S, 1408ppmw Mo, Ni:Mo=0.6, 2 hours)

Similar to the high activity of *in situ* H₂ as discussed in Chapter 3, *in situ* H₂ inhibited thermocracking by providing excellent yield, moderate pitch conversion and very low coke and HVOR yields at very low H₂ mole%. Different from the experiments with Cold Lake bitumen emulsion, the Athabasca bitumen upgrading yield by using molecular H₂ was much lower than using *in situ* H₂ from CO+H₂ or CO as shown in Figure 4-7. The HVOR yield for the H₂ condition shown in Table 4-5 was 29.7%, which was much higher than reactions with *in situ* H₂. There could be two possible reasons: (a) *in situ* H₂ performed thermocracking inhibition, which

led to reduced condensation for HVOR formation; (b) bitumen feed under H₂ was not fully demulsified. The second insight seems more reasonable, as Moll reported a similar poor emulsion breaking performance of molecular H₂ than for *in situ* H₂ (Moll 1999). In addition, the coke formation by using H₂ was only 1.7%, which was not significant. Compared to the Cold Lake bitumen emulsion, Athabasca bitumen is much more difficult to be treated and upgraded. This was why there is such a high HVOR fraction obtained under the H₂ condition.

Table 4-5 Athabasca bitumen upgrading performance under different reaction atmospheres by using Ni/MoS₂ catalyst (415°C, 80g Athabasca bitumen, 5mL OSPW, 585psi feed gas, 15psi H₂S, 1408ppmw Mo, Ni:Mo=0.6, 2 hours)

	H ₂	CO+H ₂	CO
Upgraded Oil Yield%	65	80	82
Pitch Conversion%	87*	78	79
Max. Pressure (psi)	2436	2513	2513
WGS Conversion%	-	86	86
H ₂ mole%	26	3	5
S Removal%	29	30	29
HVOR Yield%	30	9	6
Coke Yield%	1.7	1.2	1.4

* This number should be lower considering the unreacted bitumen in HVOR fraction

Although the pitch conversions by using syngas and CO as shown in Table 4-5 were lower than 87% by using H₂, the actual pitch conversion by using H₂ in this study should be lower considering the unreacted bitumen in HVOR stream. So it cannot be concluded that molecular H₂ demonstrated better pitch conversion capability. Instead, the improved performance of generating upgraded oil indicated that *in situ* H₂ was much more active than molecular H₂ in upgrading the Athabasca bitumen to make it less viscous. As long as *in situ* H₂ was involved in the reaction, the emulsion-breaking was much improved compared to molecular H₂. It is seen in Table 4-5 that the HVOR yield decreased from 29.7% with H₂ to 9.4% when using CO+H₂ and

only 5.5% by using only CO. It should also be noted that *in situ* H₂ provided similar HDS ability compared to molecular H₂ at a much lower H₂ mole% as shown in Table 4-5.

4.2.6 Effect of V as an inhibitor

Based on the same “415°C, 80g Athabasca bitumen, 10mL OSPW, 585psi CO, 15psi H₂S, 1408ppmw Mo, Ni:Mo=0.6, V:Mo=0.6, 2 hours” reaction condition, the effect of Ni as a promoter was examined. The mass balances for Ni/MoS₂ and V+Ni/MoS₂ conditions were 92.3% and 84.4% respectively.

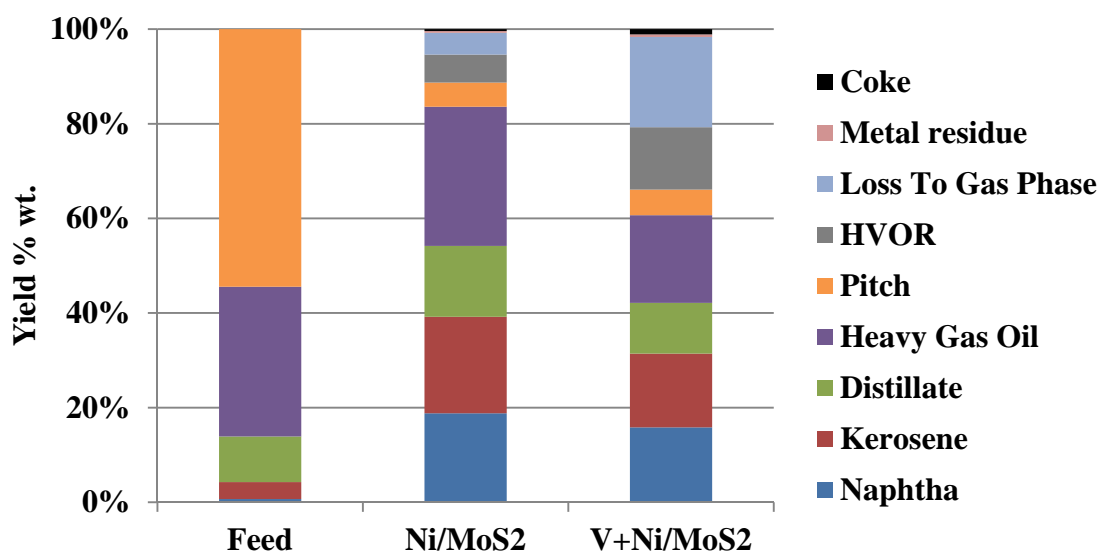


Figure 4-8 Yield distribution of Athabasca bitumen upgrading products with and without V for Ni/MoS₂ catalyst (415°C, 80g Athabasca bitumen, 10mL OSPW, 585psi CO, 15psi H₂S, 1408ppmw Mo, Ni:Mo=0.6, V:Mo=0.6, 2 hours)

As a well-known inhibitor for MoS₂ based catalyst in hydrotreating and hydrocracking processes, V could deposit on the catalyst active sites and deactivate the catalyst (Liu 2010). Some model compounds (Moll 1999) and LGO (Alghamdi 2009, Jia, Alghamdi *et al.* 2012) studies have been carried out in emulsion upgrading technology, and confirm V’s inhibition effect. As shown in Figure 4-8, the yield decreased from 89% to 66% by adding V to Ni/MoS₂. The HVOR yield was

also increased from 5.9% to 13.2% with a 1.1% coke yield. The decreased oil yield and the increased HVOR and coke yield indicated higher thermocracking preference over hydrocracking on the catalyst surface. Usually this decrease could be a result of either decreasing the H₂ pressure or loss of catalyst active sites. As shown in Table 4-6 the H₂ mole% was 9%, which was 2% more than the 7% obtained without V addition. It should be noted that the experimental error for the gas component analysis was very low at only a ppm level (determined by GC provider - INFICON). V should deactivate the Ni/MoS₂ catalyst, resulting in less active sites for the hydrocracking reaction. The underutilized *in situ* H₂ without any hydrocracking active sites eventually react with each other and form molecular H₂. This is why there are 2% more H₂ formed by adding V although the WGSR conversion was reduced slightly from 76% to 74%. It is interesting in that HDS was not significantly inhibited by adding V. This could be either due to experimental error caused by XRF analysis; or maybe the NiMoS₂ catalyst was contaminated by the V deposited from bitumen itself. Detailed solid characterization presented in the following sections provides evidence for the deposition of V on spent catalysts.

Table 4-6 Athabasca bitumen upgrading performance with and without V for Ni/MoS₂ catalyst (415°C, 80g Athabasca bitumen, 10mL OSPW, 585psi CO, 15psi H₂S, 1408ppmw Mo, Ni:Mo=0.6, V:Mo=0.6, 2 hours)

	Ni/MoS ₂	Ni+V/MoS ₂
Upgraded Oil Yield%	89	66
Pitch Conversion%	84	84
Max. Pressure (psi)	2862	2781
WGSR Conversion%	76	74
H ₂ mole%	7	9
S Removal%	40	40
HVOR Yield%	6	13
Coke Yield%	0.4	1.1

The results presented above shows that V was confirmed as an inhibitor for the emulsion upgrading process. The deposition of V from bitumen happened, and deactivated the catalysts. In order to investigate the catalyst life time, a simple reuse of “soft solids” (HVOR + spent catalyst

+ metal residue) was carried out in batch reactor. Detailed results will be discussed in the next section.

4.2.7 Deactivation investigation by using “soft solids” instead of fresh catalysts

Based on the same “415°C, 80g Athabasca bitumen, 5mL OSPW, 585psi CO, 15psi H₂S, 1408ppmw Mo, 2 hours” reaction condition, the deactivation by using “soft solids” was investigated. The mass balances for the 1st Run and 2nd Run under “soft solids” conditions were 91.0% and 91.5% respectively. The “soft solids” came from the reactor after a previous reaction, and contained mainly HVOR and a certain amount of spent catalyst containing metal deposits. These “soft solids” were then loaded in the reactor to replace the catalyst precursor to simulate a continuous reaction with a batch reactor.

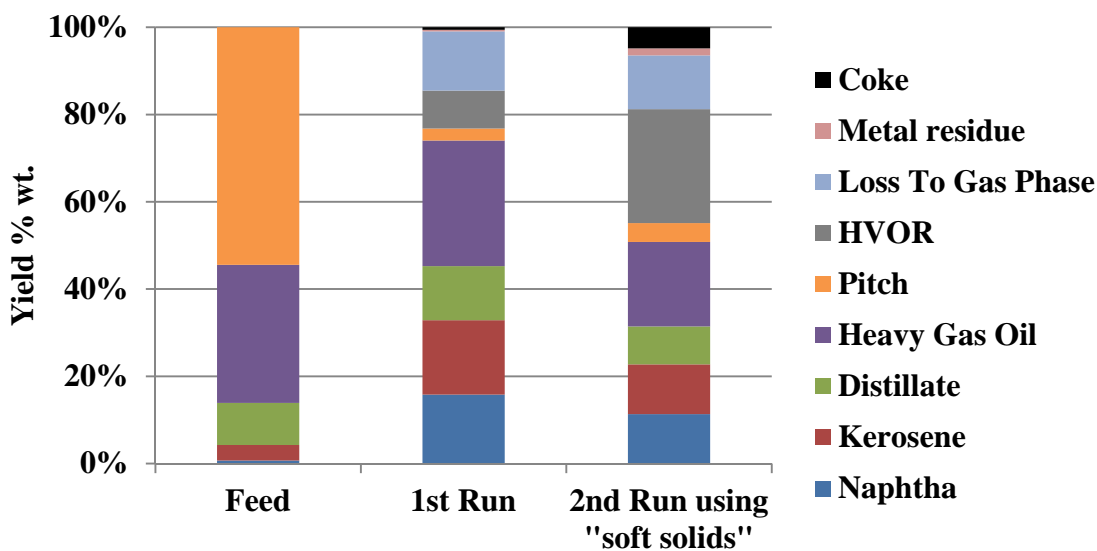


Figure 4-9 Yield distribution of Athabasca bitumen upgrading products by using fresh catalyst and “soft solid” (415°C, 80g Athabasca bitumen, 5mL OSPW, 585psi CO, 15psi H₂S, 1408ppmw Mo, 2 hours)

In Figure 4-9, it is obvious that the addition of “soft solids” somewhat reduced the upgraded oil yield and led to a much higher HVOR and coke yields. The upgraded oil yield was reduced from 77% to 55%. The HVOR yield increased from 8.7% to 26.1%; while the coke yield increased

from 0.6% to 4.8%. This poor performance by using “soft solids” indicated catalyst deactivation. As previously reported, the deposit of V significantly deactivated the MoS₂ catalyst active sites (Harris and Chianelli 1986), and resulted in a similar poor upgrading performance as shown in Figure 4-8 and Table 4-6. Hence, it is highly possible that V was one of the reasons for causing the low oil yield. The 26% HVOR contained two streams: (a) unreacted bitumen and (b) condensed asphaltenes formed through thermocracking. By comparing the HVOR and coke yields for the V added reaction, it should be noted that the thermocracking was even more preferred, as the HVOR and coke yields were even greater by using “soft solids”. In this way, V deposition contributed to only part of the poor performance. Considering the high asphaltene-rich HVOR amount present in reaction, it was proposed that more coke was formed on the catalyst blocking the active sides from being functional. Then more thermocracking occurred, generating more HVOR and coke.

Table 4-7 Athabasca bitumen upgrading performance by using fresh catalyst and “soft solid” (415°C, 80g Athabasca bitumen, 5mL OSPW, 585psi CO, 15psi H₂S, 1408ppmw Mo, 2 hours)

	1st Run	2nd Run using “soft solids”
Upgraded Oil Yield%	77	55
Pitch Conversion%	88	86
Max. Pressure (psi)	2349	2103
WGSR Conversion%	85	84
H ₂ mole%	6	5
S Removal%	31	30
HVOR Yield%	9	26
Coke Yield%	0.6	4.8

As a consequence of catalyst deactivation, less oil would be produced. To make things worse, the accumulated HVOR (mainly asphaltenes) in reactor would eventually cause fouling issues in reactors. The foulants would stick to the reactor walls, leading to much lower heat transfer efficiency. Fouling is a very common operational problem for residue hydrocracking processes. It occurs in almost all of the slurry bed residue hydro-processes. In order to solve this potential issue for emulsion upgrading technology in future engineering design, an ebullated bed reactor

should be considered first. As discussed in Chapter 1 the catalyst bed could be removed from the reactor from time by time, at which time the generated HVOR and coke could be taken out of the reactor. When new catalyst was loaded by either installation of a new bed or new liquid precursor, the reaction reliability can be maintained. More research and especially engineering design should be continued based on the results obtained from the present research.

4.3 Metal deposits and spent catalyst characterization

4.3.1 XRD analysis of deposited metals sulfides from Athabasca bitumen

Ni, Fe and V were contained in the Athabasca bitumen feedstock. During reaction these metals were finally deposited on the solid residues which contained spent catalysts and cokes. XRD was used for testing these metal deposits from the bitumen feedstock. As shown in Figure 4-10, Ni sulfide, Fe sulfide and V sulfide existed in the final coke and metal sulfides solids without loading of the Mo precursor.

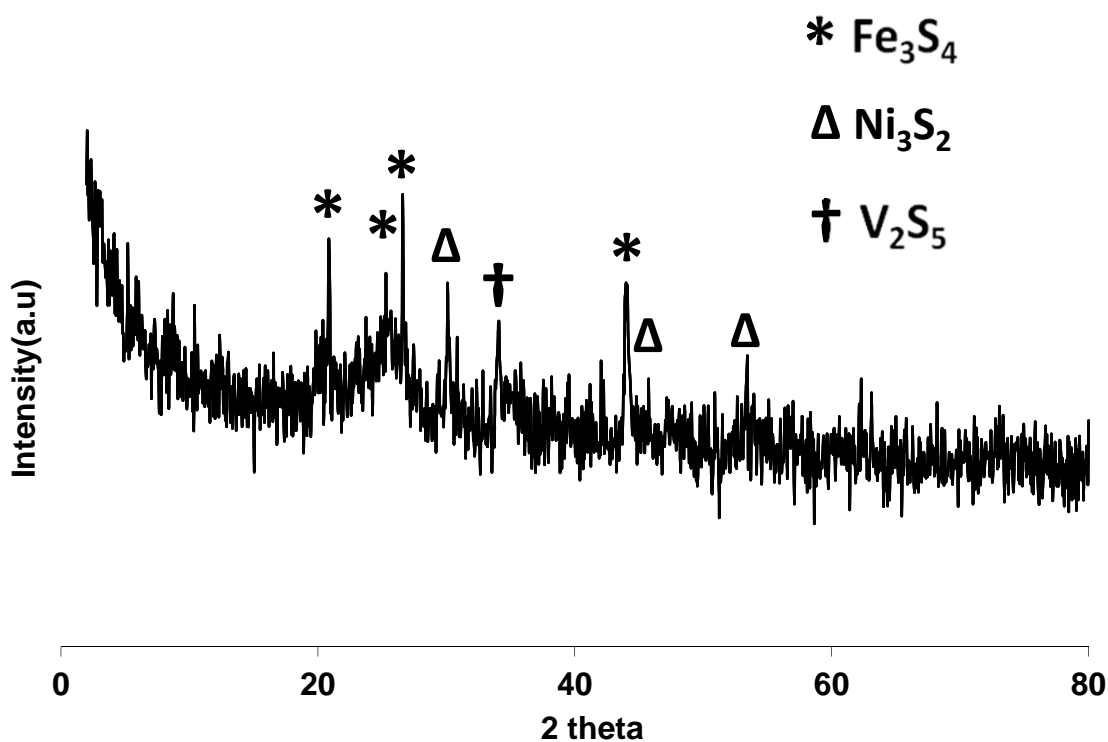


Figure 4-10 XRD pattern for metal sulfides deposits product in reaction without catalyst precursor loading

4.3.2 SEM and elemental analysis of the spent catalysts from Athabasca bitumen upgrading

The spent catalysts' surface structure was observed by using SEM with a SE2 detector. While BSD is one useful tool for distinguishing metal and inorganic elements when using SEM. Elements with higher atomic number provide stronger signals as shown as lighter areas compared to elements with lower atomic number. Comparison of SE2 and BSD images provide insight of how the metals are distributed on the final spent catalysts. However, the bitumen feedstock was full of impurity deposits and easily caused coke formation, which presented a big challenge for spent catalyst solid testing. As a comparison shown below in Figure 4-11, the BSD image showed a large amount of small lighter spots distributed in darker areas, which meant the metal sulfide catalysts located inside the surrounding coke and other lower metal rich components.

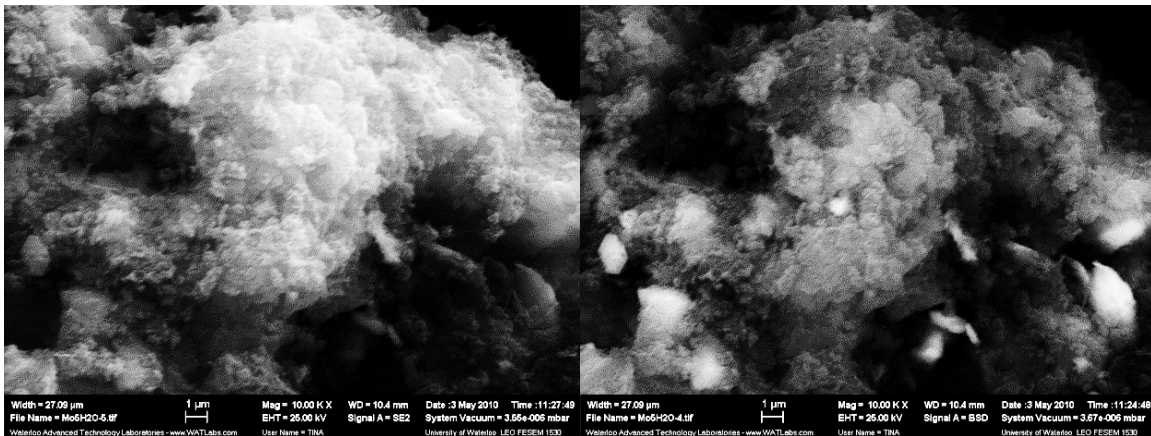


Figure 4-11 SEM images of the same area of the spent MoS₂ catalysts from bitumen experiments under 10000 times magnification from SE2 detector (left) and BSD detector (right)

Only a few merged or coke-coated particle residues could be found after the reaction in bitumen, as shown in Figure 4-12. In most cases, only irregular structures were observed. This was due to the intense reaction condition and the complex bitumen deposits.

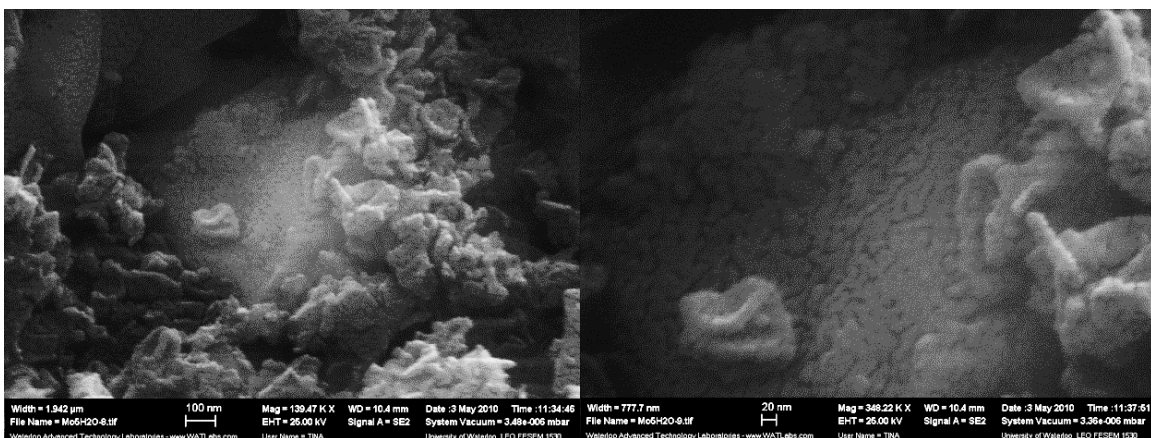


Figure 4-12 SEM images of the spent MoS₂ catalysts from bitumen experiments under 139470 times (left) and 348220 times (right) magnification from SE2 detector

The complicated atom signal list in Figure 4-13 from the EDX data showed massive deposits on the final solid products, which contained C, O, Na, Al, Si, P, K, Ca, Ti, V, Mn, Fe, Ni, W, Mo and S. Quantification of Mo, S and some important metals became extremely difficult as carbon from both coke and carbon tape contributed too many signals, causing considerable error for the other elements.

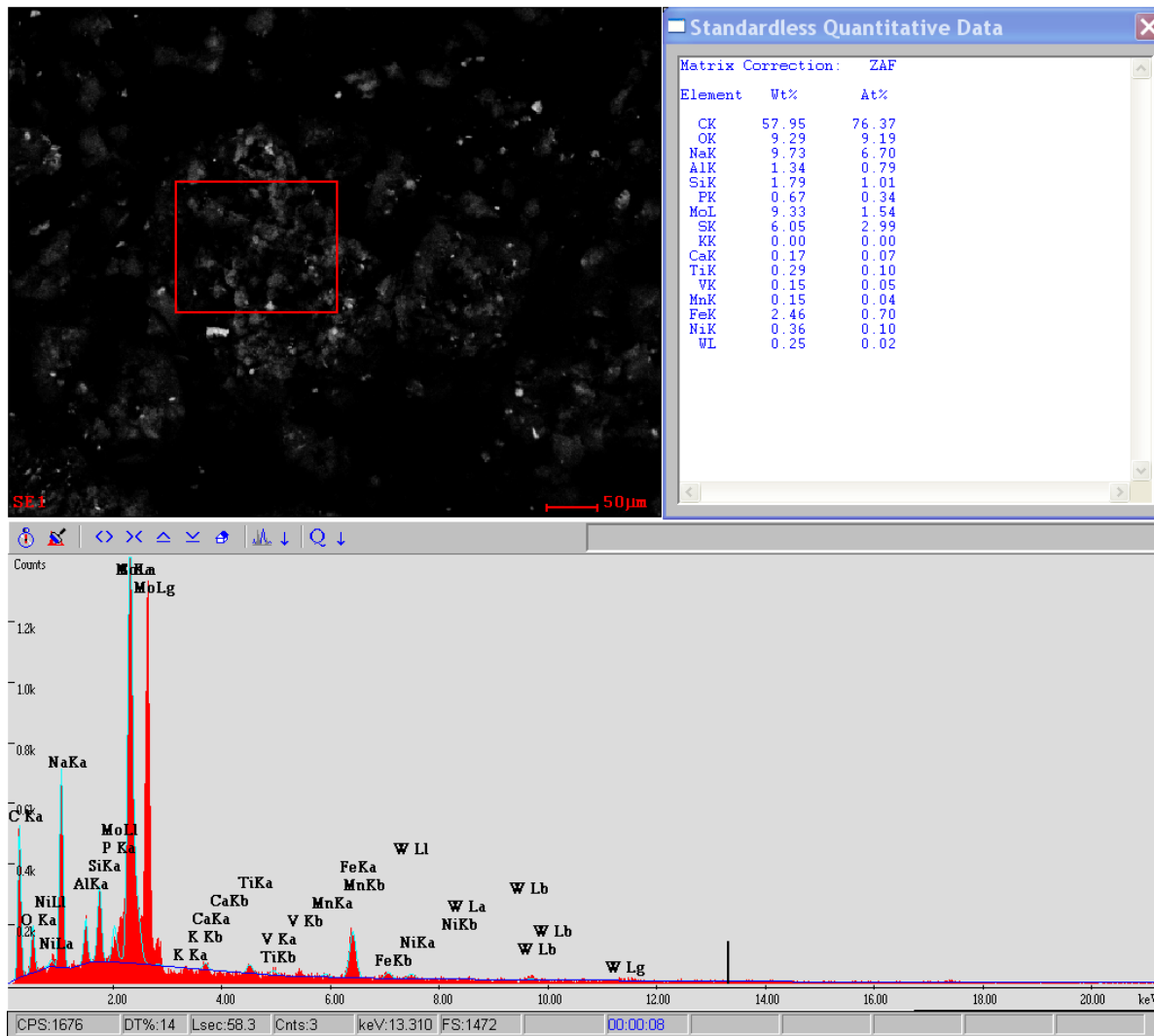


Figure 4-13 SEM image of the spent MoS₂ catalysts from bitumen experiments under 1000 times magnification from BSD detector and atomic ratio calculated from EDX data in red square.

4.4 OSPW purification through novel process

The dirty water derived from the oil sand froth treatment contained different metal ions and anions which exceeded acceptable environmental standards. Through our novel bitumen upgrading process, this dirty water might not only be used as an *in situ* H₂ donor but also could be purified. Anion and cation removals were studied to validate this hypothesis.

4.4.1 Determination of anion and cation contents in OSPW

As shown in Figure 4-1, the water after emulsion upgrading was a clear aqueous phase with a brownish color caused by the metal ions or dissolved organics. In order to quantitatively understand the water purification performance, IC and ICP were used for analyzing multiple anion and cation contents before and after the reaction. Calibration curve examples for IC and ICP are shown in Figure 4-14 for sulfate and V. The rest of the IC calibration curves are listed in Appendix A. 6.

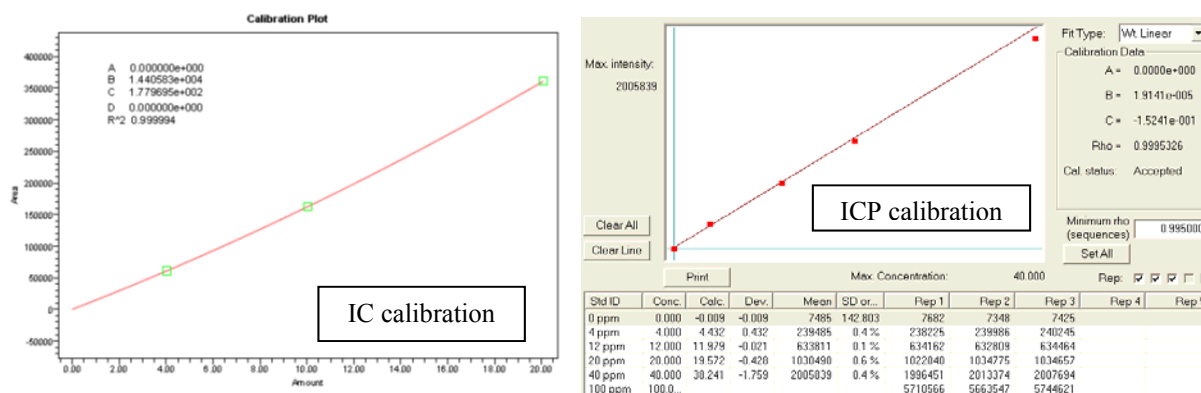


Figure 4-14 Calibration curve examples of sulfate in IC (left) and V in ICP (right)

Figure 4-15 shows the IC chromatograph of the feedstock water at 500 times dilution. Chloride, carbonate and sulfate were identified at retention times of 2.498min, 3.383min and 4.793min. There was an earlier peak shown at 2.009min, which was attributed to amphiphile organics. Considering the composition of the emulsion, especially the potential small oil drops emulsified

in the water phase, naphthenates or other organic acid anions were likely to be the components identified at 2.009min.

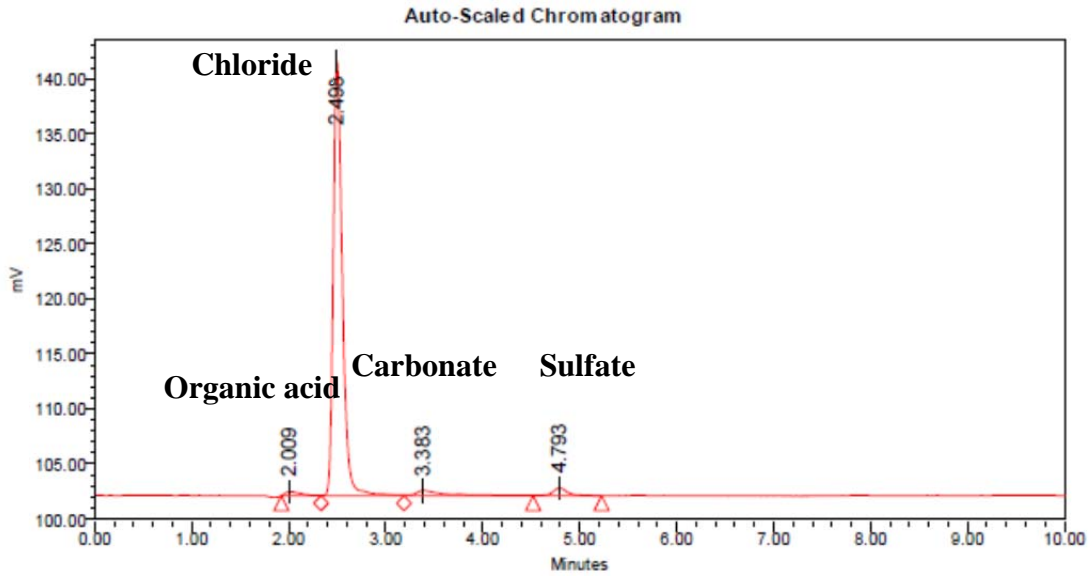


Figure 4-15 IC chromatograph of feedstock water at 500 dilution times

Since chloride and sulfate could be calibrated with standard solutions, their concentrations (before and after the reaction) were easily calculated through calibration curves. The removal was calculated based on mass by considering the feedstock water and final water volumes using Eq. 4-1 and Eq.4-2. Importantly, the addition of NiSO_4 as promoter precursor (if used) introduced sulfate in the feedstock. Therefore, the initial sulfate mass was included in the feedstock sulfate.

$$\text{Chloride removal\%} = \frac{\text{conc}(\text{chloride})_0 \times V_0 - \text{conc}(\text{chloride})_t \times V_t}{\text{conc}(\text{chloride})_0 \times V_0} \times 100\% \quad (\text{Eq. 4-1})$$

$$\text{Sulfate removal\%} = \frac{\text{conc}(\text{sulfate})_0 \times V_0 + m(\text{sulfate in NiSO}_4) - \text{conc}(\text{sulfate})_t \times V_t}{\text{conc}(\text{sulfate})_0 \times V_0 + m(\text{sulfate in NiSO}_4)} \times 100\% \quad (\text{Eq. 4-2})$$

Due to the lack of standard solutions, carbonate and organic acid anion were only identified but not calibrated. Hence peak areas through integration were the only method for estimating the carbonate and organic acid removal performance. Eq. 4-3 and Eq. 4-4 show the basic calculations.

$$\text{Carbonate removal\%} = \frac{\text{Peak area(carbonate)}_0 \times V_0 - \text{Peak area(carbonate)}_t \times V_t}{\text{Peak area(carbonate)}_0 \times V_0} \times 100\% \quad (\text{Eq. 4-3})$$

$$\text{Organic acid removal \%} = \frac{\text{Peak area(organic acid)}_0 \times V_0 - \text{Peak area(organic acid)}_t \times V_t}{\text{Peak area(organic acid)}_0 \times V_0} \times 100\% \quad (\text{Eq. 4-4})$$

Compared to IC, the ICP identification and calibration were more straightforward. Metal cation removal was also calculated based on mass by combining concentrations determined by ICP and water volumes (before and after reactions). Typical metal cation calculation was carried out using Eq. 4-5.

$$\text{Metal cation removal\%} = \frac{\text{conc(metal)}_0 \times V_0 - \text{conc(metal)}_t \times V_t}{\text{conc(metal)}_0 \times V_0} \times 100\% \quad (\text{Eq. 4-5})$$

4.4.2 The OSPW purification performance

Since all metals, chloride and sulfate can be quantitatively measured, their concentrations in the OSPW before and after upgrading are listed in Table 4-8. “N₂/H₂O”, “Mo/CO/H₂O” and “Ni-MoS₂/CO/H₂O” were chosen to represent several typical reaction conditions. The reaction temperature was 415°C. 80g of Athabasca bitumen and 10mL OSPW were fed into the reaction. Under the “N₂/H₂O” condition, there was no catalyst precursor or *in situ* H₂ generated via the WGSR but only 10mL OSPW under a N₂ atmosphere. Under the “Mo/CO/H₂O” and “Ni-MoS₂/CO/H₂O” conditions, PMA was added to form *in situ* MoS₂ based catalysts; CO was the

atmosphere for generating *in situ* H₂ by reacting with 10mL added OSPW. The only difference between the “Mo/CO/H₂O” and “Ni-MoS₂/CO/H₂O” conditions was the addition of Ni as a promoter, representing the best reaction condition as discussed in previous sections. It is interesting that the Na concentration was very high at 38302ppm, which was equivalent to ~3.8%. It should be noted that NaOH was added in the froth treatment in order to break the emulsion by forming ionic naphthenates instead of naphthenic acids, which formed a stable interphase between oil and water. In this way, the feedstock OSPW contained large amounts of Na, and this was confirmed via the ICP results shown in Table 4-8. It is obvious that the concentrations of most metals were reduced to a very small value after emulsion upgrading, no matter which catalyst or atmosphere was used. Since Ca, Mg, Na are the major water treatment targets in mining and *in situ* production plants, nearly 100% removal of them could potentially bring considerable synergy for implementing emulsion upgrading technology with existing mining or *in situ* production plants. It is also seen in Table 4-8 that chloride and sulfate were both reduced to a certain level, where the sulfate concentration increased from 166ppm to 545ppm under the “Ni-MoS₂/CO/H₂O” condition. This was because that NiSO₄ was used as a Ni precursor.

Table 4-8 Concentrations of metal cations and some inorganic anions in the OSPW before and after emulsion upgrading (415°C, 80g Athabasca bitumen, 10mL OSPW, 585psi N₂ or CO, 15psi H₂S, 0 or 1408ppmw Mo, Ni:Mo=0.6, 2 hours)

Reaction Conditions	<u>Metal Cations Conc.</u> (ppm)								<u>Anions Conc.</u> (ppm)	
	Fe	Ca	Zn	Na	K	Mg	W	V	Cl ⁻	SO ₄ ²⁻
OSPW Feed	20	250	48	38302	473	145	118	41	6215	166
N ₂ /H ₂ O	3	0	7	80	10	8	8	4	299	96
MoS ₂ /CO/H ₂ O	1	0	0	72	0	0	4	9	324	196
Ni-MoS ₂ /CO/H ₂ O	2	0	5	64	7	4	14	4	291	545

After calculating total mass removal based on Eq. 4-1 to Eq. 4-5, the cation and anion removals are shown in Table 4-9. With knowledge of the peak areas of carbonate and organic acids their removal can also be discussed. As shown in Table 4-9, there was no doubt that almost all the

metals had been removed after the reaction. When the catalyst and *in situ* H₂ were used, the metal removal improved slightly (to nearly 100%). Since the metal was almost completely removed under even the N₂/H₂O condition without catalyst or H₂ source; the metal removal should be attributed to the metal deposition on the solids residues. XRD and SEM results in the previous section have shown that different metal deposits on the final metal residues or spent catalysts. Especially the EDX result shown in Figure 4-13 confirmed that many metals' exist on the spent catalysts, like Na, Ca, V, K, Fe, Ni, W, etc. These metals were also (by ICP result) removed from the OSPW through emulsion upgrading. In this way, metal deposition was the main approach for removing these metals from OSPW.

Table 4-9 Removal of cations and anions in the OSPW after emulsion upgrading (415°C, 80g Athabasca bitumen, 10mL OSPW, 585psi N₂ or CO, 15psi H₂S, 0 or 1408ppmw Mo, Ni:Mo=0.6, 2 hours)

Reaction Conditions	<u>Metal Removal %</u>								<u>Anions Removal %</u>			
	Fe	Ca	Zn	Na	K	Mg	W	V	Cl ⁻	SO ₄ ²⁻	CO ₃ ²⁻	Org. Acids
N ₂ /H ₂ O	96	100	96	100	99	98	98	97	99	83	98	-112*
MoS ₂ /CO/H ₂ O	99	100	100	100	100	100	99	96	99	78	93	83
Ni-MoS ₂ /CO/H ₂ O	99	100	99	100	100	100	99	99	100	76	92	94

* Organic acids might be generated through reaction under N₂ atmosphere

The removal of chloride, sulfate and carbonate was also very effective, except for the added NiSO₄ effect on sulfate removal. Overall, a significant amount of anions were removed. The most interesting observation was the removal of organic acid anions by using MoS₂ (or Ni-MoS₂) with *in situ* H₂. For reactions like “N₂/H₂O”, organic acids the removal was negative, indicating more organic acid anions present (in mass) in the final water phase. This could be caused by severe thermocracking, where more small organic acids molecules might be generated from the cracking of bigger resin or asphaltene fractions from the oil phase. These small organic acids were more soluble in the water phase than large resin or asphaltene molecules. Hence more organic acids were detected in the water phase after reaction. However, when MoS₂ (or Ni-MoS₂)

and *in situ* H₂ were used, a large amount of organic acids in water phases were removed. As shown in Table 4-9, the organic acid removal was 83% and 94% for “Mo/CO/H₂O” and “Ni-MoS₂/CO/H₂O” respectively. Naphthenic acids were expected to contribute to the majority of the organic acid groups in the OSPW. This excellent organic acid removal performance suggested the possibility of removing naphthenic acid via this novel emulsion upgrading process. Some model compounds research has been carried out and will be discussed in Chapter 5 to investigate the basic mechanism.

4.5 Conclusions

Similar to the Cold Lake bitumen emulsion, the current emulsion upgrading technology has also demonstrated its feasibility in treating Athabasca bitumen, which is more difficult to upgrade. Compared to traditional coking processes, emulsion upgrading prohibited thermocracking and reduced the system pressure. The *in situ* H₂ formed via WGSR was proposed to actively capture free radicals in hydrocracking, and produced less cracked gases, much less coke and HVOR. Reaction kinetics was improved at 415°C, and 1.5h was the ideal reaction time under this condition in order to prevent undesired over-upgrading. Water benefits emulsion upgrading by providing higher yields and inhibiting thermocracking with *in situ* H₂. However, the reaction results in higher pressure by feeding more water. 5mL water loading seemed to be optimal for providing enough *in situ* H₂ and not too much excess water to inhibit hydrotreating and pitch conversion; while 10mL loading provided a much higher yield. This provided the flexibility for producing different oil products based on changing market needs. When the price of premium-quality oil escalates, less water could be fed for producing more pitch conversion; however, when crude price goes high (high pitch conversion is not appreciated), more water could be charged to increase the partially upgraded crude volume. The choice between quality and quantity should be answered by refinery economic studies, like LP models and market demands. Ni was found to promote emulsion upgrading with improvement in oil yield, inhibition of HVOR and with no extra coke formation. *In situ* H₂ demonstrated much higher activity than molecular H₂ for upgrading Athabasca bitumen without leaving considerable unreacted viscous bitumen. V was observed as an inhibitor by depositing and deactivating the catalyst active sites. Experiments

involving using “soft solids” caused catalyst deactivation. Coke formation and V deposition were considered as being the main reasons for this poor performance. XRD and SEM results also confirmed the deposition of multiple metals and coke formation on the spent catalysts. In order to solve this potential problem, an ebullated bed reactor should be considered rather than a slurry bed reactor in future engineering design.

OSPW involved in the reaction was confirmed not only used as an *in situ* H₂ donor, but also could be purified. This suggests the potential of direct cleaning of the emulsified water in the bitumen emulsion feedstock, which could bring tremendous synergy to existing mining and *in situ* production plants. Most of the metal cations are removed through metal deposition. Some anions were also removed, where possible organic acid removal was observed. This observation revealed potential naphthenic acid removal capability of the emulsion upgrading technology. Some fundamental research will be discussed in the Chapter 5 with model compounds to understand the basic mechanisms of organic acid removal.

Chapter 5 Naphthenic Acids Removal in both Oil and Water Phases through a Novel Emulsion Upgrading Process

5.1 Literature review

The rapid expansion of Alberta's oil sands industry presents several challenges with respect to the protection of local freshwater resources such as the Athabasca River basin. Most of the freshwater imported by oil sands mines is used in hot water extraction, a flotation process that separates bitumen from sand. The resulting tailing water is referred to as oil sand process-affected water (OSPW). OSPW is alkaline, slightly brackish, with heavy metal content and acutely toxic to aquatic biota due to high concentrations of organic acids leached from the bitumen during extraction. Naphthenic acids are one of the major organic acid groups in OSPW. Due to the complex chemical composition of naphthenic acids, a great variety of structures and compositions fall within the classification of naphthenic acids (Tomczyk, Winans *et al.* 2001). Generally, they are described as a mixture of naturally-occurring, aliphatic or alicyclic carboxylic acids that are recognized by the general formula of $C_nH_{2n}C_ZO_2$, where n represents the number of carbon atoms in the molecule and Z specifies hydrogen deficiency in the case of cyclic naphthenic acids (Brient 1995). It has been shown that naphthenic acids are toxic to a variety of organisms and they present harmful effects in the environment (Dokholyan and Magomedov, 1983, Kamaluddin and Zwiasek, 2002, Rogers, Wickstrom *et al.* 2002, Young, Orr *et al.* 2007). The Environmental Protection and Enhancement Act (Alberta 2000) requires the submission of an environmental impact assessment report before the development of any oil sands project. In these assessments, the background concentrations of naphthenic acids in surface and ground waters must be addressed. Currently, natural surface fresh waters in the oil sands regions are regularly monitored for naphthenic acids (RAMP 2008). The presence of naphthenic acids in petroleum also contributes to the acidity of crude oils and therefore they are one of the major sources of corrosion in oil pipelines and distillation units in oil refineries. As a result, research on naphthenic acids has been emphasized during the past decades. Figure 5-1 shows

that publications on naphthenic acids increased significantly during the past ten years (the previous peak in 1970s was due to the early application of oils sand processes).

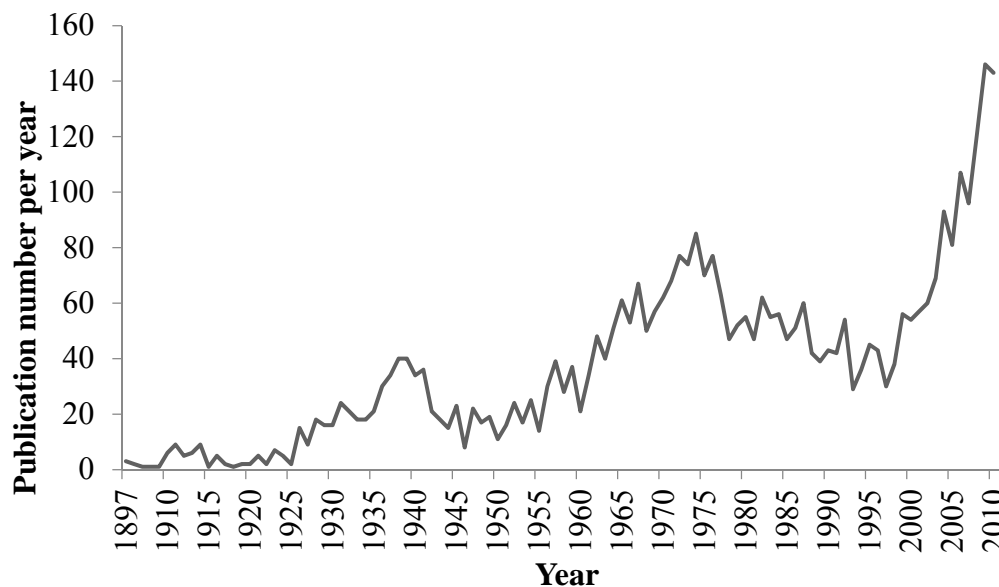


Figure 5-1 Publications trends on naphthenic acids (generated by Sci-Finder)

FT-IR and GC-MS have been applied to characterize and quantify the naphthenic acids in different OSPW samples, as shown in Table 1 (Grewer, Young *et al.* 2010). Although the differences between FT-IR and GC-MS results are still under discussion, the naphthenic acids concentration of Suncor's tailing water was determined to be 30-130 mg/L as shown in Table 5-1, which provides a concentration basis for choosing model naphthenic acids for experiments.

Table 5-1 List of Naphthenic acid concentration in different water samples by FT-IR and GC-MS (Grewer, Young *et al.* 2010)

Sample source	Sample	Naphthenic acids (mg/L)	
		by FTIR	by GC-MS
Syncrude	MLSB	44	28
	WIP	60	36
	Pond 9	20	7
	Demo Pond	14	6
Suncor	Pond 2/3	63	47
	Pond 5	38	26
	SAGD	130	38
	Tailings pond	35	18
	Athabasca River	0.08	<0.03
	Gregoire Lake	0.25	<0.03
	North Saskatchewan River	0.7	0.04
	Red Deer River	0.05	<0.03
	Bow River	0.05	<0.03
South Saskatchewan River	0.05	<0.03	

In order to treat water contaminated with naphthenic acids, many approaches have been studied and reported, including bioremediation, ozonation, adsorption, photolysis, photocatalysis *et al.* Bioremediation of OSPW has been investigated for a long time; however, the current techniques have provided limited success to date (Quagraine, Peterson *et al.* 2005, Biryukova, Fedorak *et al.* 2007, Han, Scott *et al.* 2008). The long retention time required in this process is one reason. In addition, bioremediation is affected by naphthenic acids' structures. Natural bioremediation is only suitable for naphthenic acids with a high degree of aliphatic chains and/or methyl-substituted cycloalkane rings (Han, Scott *et al.* 2008). Regarding the importance of the sample source, it been reported that the naphthenic acids in oil sands tailings water are less biodegradable than commercial naphthenic acids tested under laboratory conditions (Scott, MacKinnon *et al.* 2005). Recently, several papers have been published by Prof. Scott's research group on treating naphthenic acids via ozonation (Scott, Zubot *et al.* 2008, Gamal El-Din, Fu *et al.* 2011). Compared to bioremediation, ozonation is superior as it can treat higher molecular

weight alkyl branched naphthenic acids ($n \geq 22$, $-12 \leq z \leq -6$). However, ozonization could not completely degrade naphthenic acids, and it can produce various by-products like aldehydes, ketones, peroxides and other carboxylic components (Kannel and Gan 2012). As a result, combined bioremediation and ozonation were investigated, where ozonation was found to accelerate biodegradation and reduce total toxicity (Martin, Barri *et al.* 2010, Wang, Chelme-Ayala *et al.* 2013). Adsorption has also been studied to remove naphthenic acids from OSPW by using adsorbents like organic rich soils (Peng, Headley *et al.* 2002, Janfada, Headley *et al.* 2006), clays (Zou, Han *et al.* 1997), petroleum coke (Yuan, Tong *et al.* 2010, Gamal El-Din, Fu *et al.* 2011, Zubot, MacKinnon *et al.* 2012), cyclodextrin-based polymers (Mohamed, Wilson *et al.* 2011) and activated carbon (Azad, Abedi *et al.* 2013, Iranmanesh 2013). Among the above mentioned adsorbents, petroleum coke is promising due to its relatively low cost. Within controlled petroleum coke content, pH and temperature, structurally complex naphthenic acids ($12 \leq n \leq 18$ and $z = -10, -12$) could be effectively removed from OSPW (Kannel and Gan 2012). It has also been reported that petroleum coke adsorption combined with ozonation improved naphthenic acid removal (Gamal El-Din, Fu *et al.* 2011). Reducing the re-activation costs for reliable performance of the sorbents is the key for its future development. Photolysis has also reported to be an alternative for removing naphthenic acids from natural river water (McMartin, Headley *et al.* 2004) and OSPW (Drzewicz, Afzal *et al.* 2010). It was found that UV at 254nm was the most effective radiation source for cleaving higher molecular weight naphthenic acids into smaller fragments (McMartin, Headley *et al.* 2004). CNRL reported a combined method with UV and H_2O_2 , and achieved improved naphthenic acid removal performance (Drzewicz, Afzal *et al.* 2010). Photocatalysis is similar to photolysis except for the usage of catalysts. TiO_2 catalysts were explored and found to be effective in removing naphthenic acids under UV (Headley, Du *et al.* 2009, Mishra, Meda *et al.* 2010). However, the effectiveness of photocatalytic degradation is also limited to small molecular weight compounds ($6 \leq n \leq 12$, $-6 \leq z \leq 0$) (Kannel and Gan 2012).

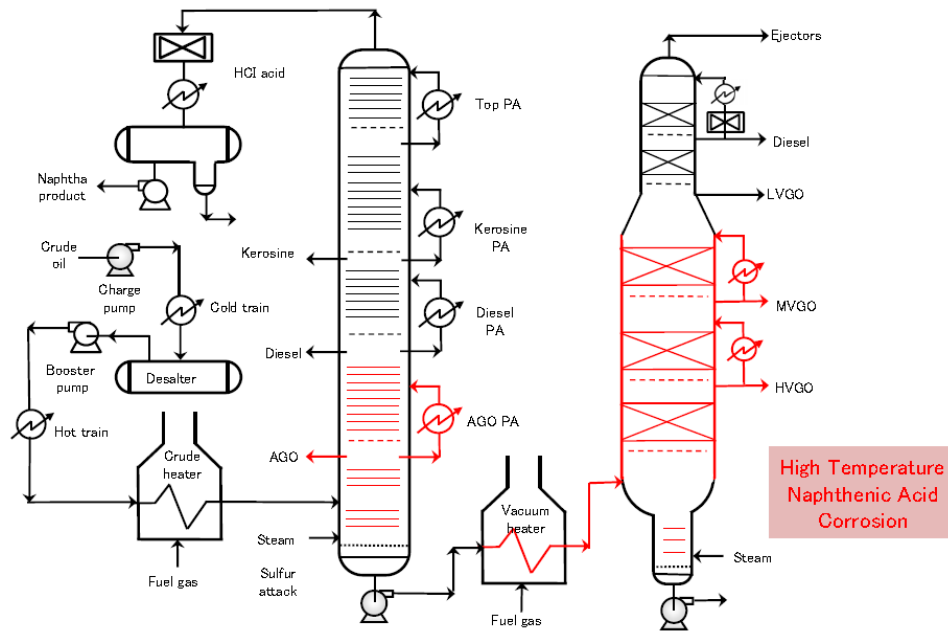


Figure 5-2 Corrosion caused by naphthenic acid in downstream refineries

Removing naphthenic acid compounds from oils is regarded as one of the most important processes in heavy oil upgrading, since naphthenic acids contribute to high temperature corrosion in atmospheric tower and vacuum tower units as shown in Figure 5-2. Existing industrial practices either depend on dilution or caustic washing methods to reduce the total acid number (TAN) from heavy crude oils. However, neither of these approaches is entirely satisfactory. For instance, blending a high TAN crude oil with a low TAN crude oil may reduce the naphthenic acid content to an acceptable level; however, the acidic compounds remain and the value of the low TAN oil is diminished. Caustic treatment can substantially remove naphthenic acids, but the process generates significant amounts of wastewater and emulsions that are problematic to treat. In particular, once an emulsion is formed, it is very difficult to remove. Besides the conventional industrial method, some novel catalytic processes have been tested at the bench scale. Catalytic neutralization can be used for removing naphthenic acid from bitumen-derived heavy-vacuum gas oil (HVGO) by using CaO and BaO (Ding, Rahimi *et al.* 2009). Esterification of naphthenic acids with methanol has also been utilized to form methyl-naphthenates. Wang et al. have studied the removal of the naphthenic acids in heavy fractions of petroleum by means of an ammonia solution of ethylene glycol (Wang, Sun *et al.* 2007). Another

approach is the catalytic decarboxylation of naphthenic acids, which is based on the adsorption of naphthenic acids on various potential solid catalysts. This method has been explored by research groups of Prof. Gray and Dr. Zhang (Zhang, Ma *et al.* 2003, 2004, 2004, Tang and Zhang 2006, Zhang, Ma *et al.* 2006, Yang and Gray 2008). Gray investigated several alkali and alkali earth metal oxides and carbonates for their performance in naphthenic acid removal through catalytic decarboxylation. Based on TAN measurements and FTIR results, the catalyst effectiveness was ranked as $\text{Li}_2\text{O} > \text{CaO} > \text{BaO} > \text{MgO} > \text{CaCO}_3$ (Yang and Gray 2008). Zhang's study suggested the possibility of low-temperature and large-scale industrial MgO for naphthenic acid removal. MgO serves as a catalyst and promotes the decarboxylation reaction. ZnO was also applied as a decarboxylation catalyst for naphthenic acid removal (Ding, Rahimi *et al.* 2009). It is known that crude the TAN could be reduced through hydroprocessing. However, there are few reports on naphthenic acid removal through hydroprocessing. One paper was published by Exxon Research and Engineering Company on removing naphthenic acid using hydrotreating catalysts. The TAN was found to decrease from 3.7 to 0.5 with Ni/Mo or Co/Mo supported catalysts used for residue hydrotreating (Kenneth L. Trachte 1997). A detailed mechanism for naphthenic acid hydrotreatment is expected to be very complicated (cracking, decarboxylation, etc.) and has not been reported yet.

In this chapter, emulsion upgrading technology was investigated for its potential naphthenic acid removal performance. Model compounds were selected and tested to represent naphthenic acids in an emulsion upgrading process. Excellent naphthenic acid removal was achieved in both oil and water phases at the bench scale. A detailed naphthenic acid removal mechanism during emulsion upgrading was proposed, where hydrodeoxygenation (HDO) was the dominant reaction pathway. Effects of reaction temperature, gas feed, catalysts, water, metal additives, sulfur species and poly aromatics were studied. The emulsified water was found to generate *in situ* H_2 for hydrotreating and upgrading as a pre-treatment of the oil sands bitumen emulsion for pipeline transport. Therefore, the water in an oil sands bitumen emulsion will be separated without an individual oil/water separation step (like froth treatment or free water knock-out unit) and prevent discharging OSPW directly into the environment. As a bonus, the TAN of the oil and the naphthenic acid amount in the OSPW will be significantly reduced. Compared to other

alternatives for naphthenic acid removal from oil and water phases, emulsion upgrading has realized integrated naphthenic acid removal in a single step partial upgrading process, which brings potential commercialization opportunities for this novel technology towards an economic and environmental friendly application.

5.2 Preliminary investigation

5.2.1 Model compound study for naphthenic acid removal

Cyclohexanecarboxylic acid, cyclohexane propionic acid, benzoic acid, 4-heptylbenzoic acid and 2-naphthoic acid have been widely used for representing naphthenic acids in fundamental studies (Breger and Burton 1946, Csuros, Makadi *et al.* 1948, Takemura, Nakamura *et al.* 1985, Artok and Schobert 2000, Zhang, Ma *et al.* 2003, Del Rio, Hadwin *et al.* 2006, Zhang, Ma *et al.* 2006). In this research, 4-heptylbenzoic acid (C7-BA) and 2-naphthoic acid (2-NA) have been chosen due to their substitution and high aromaticity as shown in Figure 5-3. C7-BA has a long substitution chain on the benzene ring; while 2-NA has higher aromaticity.

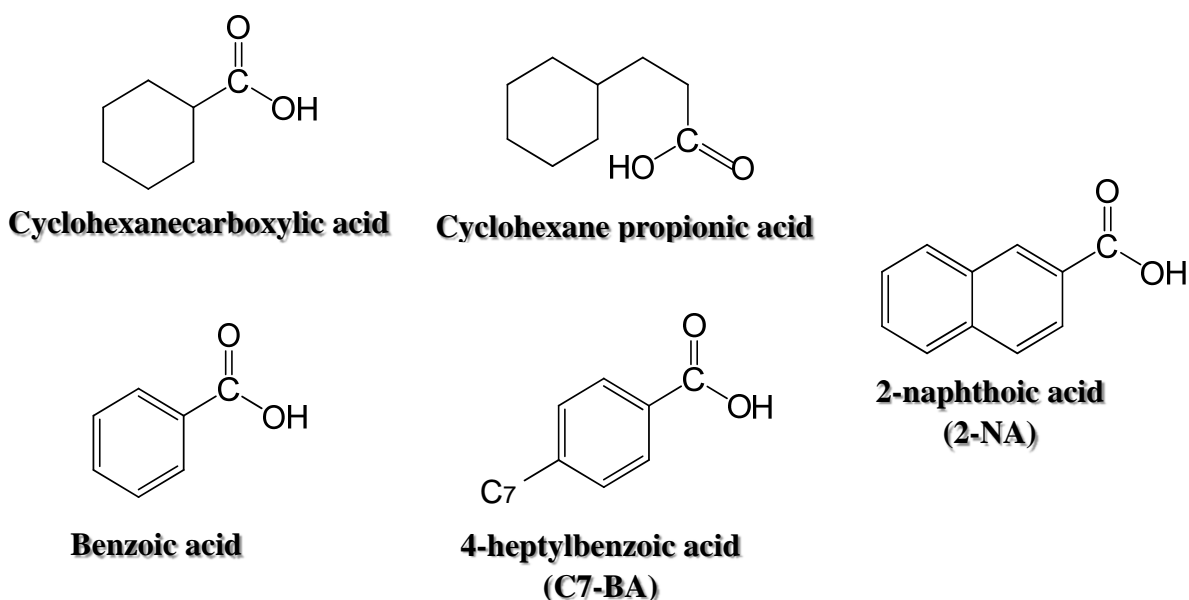


Figure 5-3 Common model compounds in naphthenic acid research

Model compounds were dissolved in toluene before being mixed with water for reaction. No special reconstitution was carried out for emulsifying the toluene solution and water. However, in order to improve mixing, sonication was implemented before analyzing different feed components in both the oil and water phases. This sonication was only performed for the characterization of the reaction feedstock.

5.2.2 Elimination of carboxyl group in 2-NA through novel process

FT-IR was used initially for evaluating the removal of carboxyl groups. The C=O stretching vibration relevant adsorption peaks were referred as: C=O stretching, internally bonded, 1670-1650 cm^{-1} ; C=O stretching, 1700-1680 cm^{-1} and a-halogen substituted C=O, 1740-1705 cm^{-1} . By comparing the spectra of a 2-NA feed in toluene and the treated NA product toluene solution shown in Figure 5-4, it is clear that almost all the relevant peaks representing C=O groups were removed in the final product. This result shows this elimination of carboxyl peaks indicated the 2-NA removal during this novel bitumen emulsion upgrading process.

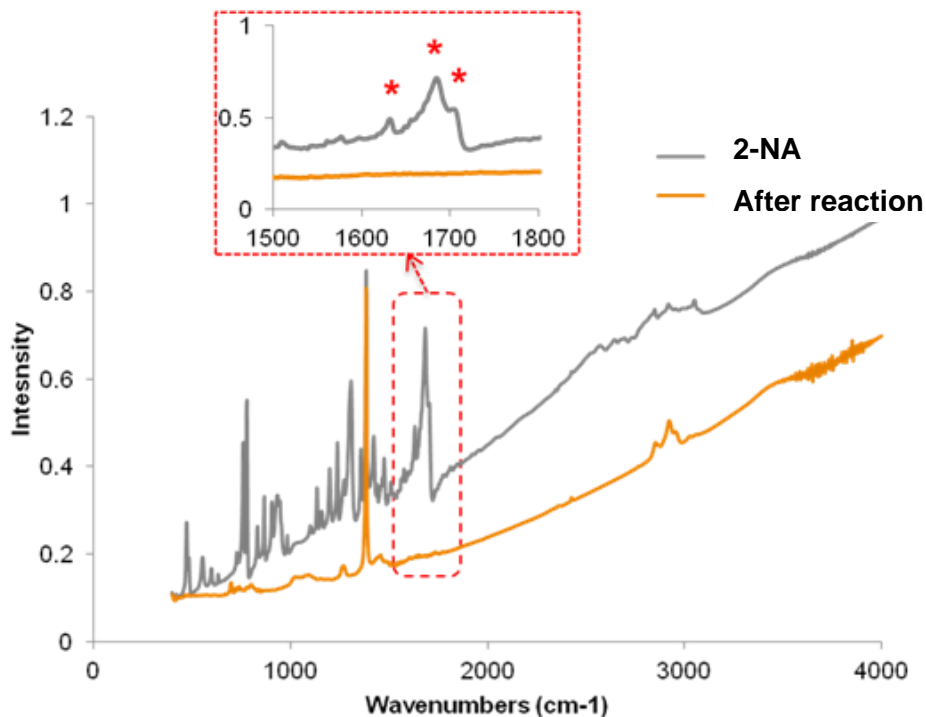


Figure 5-4 FT-IR spectrums of 2-NA feed and product in toluene solution (415°C, 80ml toluene, 10ml water, 15psi H₂S, 585psi CO, ~1641ppmw 2-NA in toluene, 673ppmw Mo, 2hours)

5.2.3 Characterization of 2-NA with HPLC

A HPLC chromatograph and calibration curve for 2-NA is shown in Figure 5-5. 2-NA was identified at a retention time of 1.607min; other peaks present in the chromatograph might be impurities from the commercial 2-NA feedstock. Due to the relatively large organic structure of the 2-NA molecule, HPLC separation suffered tails for the 2-NA peak. This created considerable difficulty for the accurate calibration. By performing a large amount of calibration tests, the best calibration curve was achieved with a R² of 0.9769.

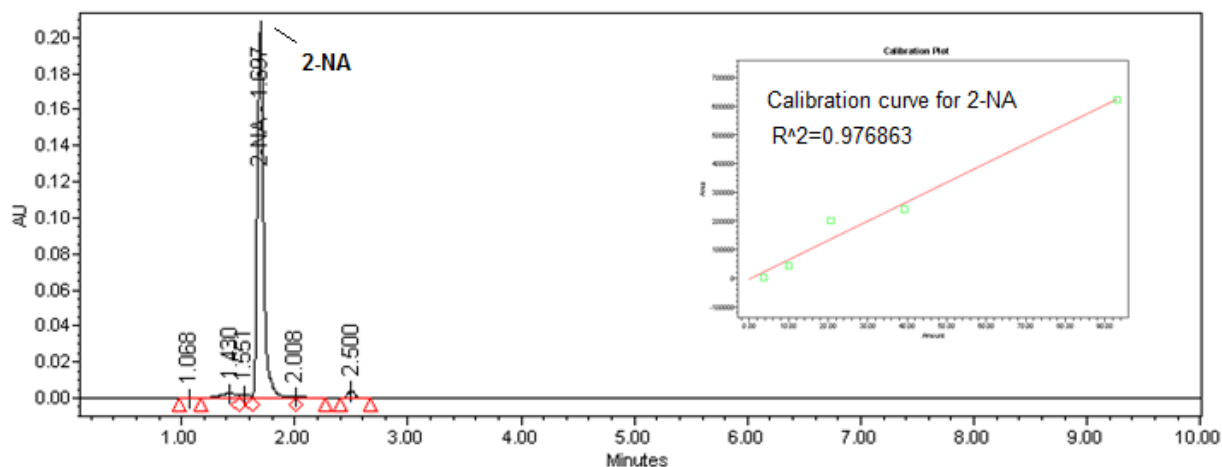


Figure 5-5 HPLC chromatograph and calibration curve for 2-NA

With the calibrated HPLC detection results, 2-NA conversion in water phase was calculated based on 2-NA concentrations and the water mass before and after reaction. The calculations were carried out using Eq. 5-1.

$$\text{Conversion (2-NA)}^w = \frac{[2\text{-NA}]_0^w \times m(\text{water})_0 - [2\text{-NA}]_f^w \times m(\text{water})_f}{[2\text{-NA}]_0^w \times m(\text{water})_0} \times 100\% \quad (\text{Eq. 5-1})$$

$[2\text{-NA}]_0^w$ was the 2-NA concentration in the water phase of the mixture of 80 ml 1.2675g/L 2-NA toluene solution with 10 ml de-ionized water and $[2\text{-NA}]_f^w$ was the 2-NA concentration in the final water product.

5.2.4 Characterization of 2-NA removal reaction products with GC-FID and GC-MS

Since GC-MS used the same type of column (30m× 0.32mm VF-05MS capillary column) as that was used in GC-FID, the chromatographs of GC-MS and GC-FID were relatively similar under a controlled heating program. This resulted in a convenience in referring the GC-MS identification for further GC-FID identification and calibrations. In order to obtain an ideal separation, a slower heating ramp was used in the GC-MS than in the GC-FID.

A typical GC-MS library panel is shown in Figure 5-6, where tetralin was selected as an example to demonstrate how the GC-MS library identifies unknown chemicals. In the presented list of chemical candidates, tetralin had the highest probability at 81.28%.

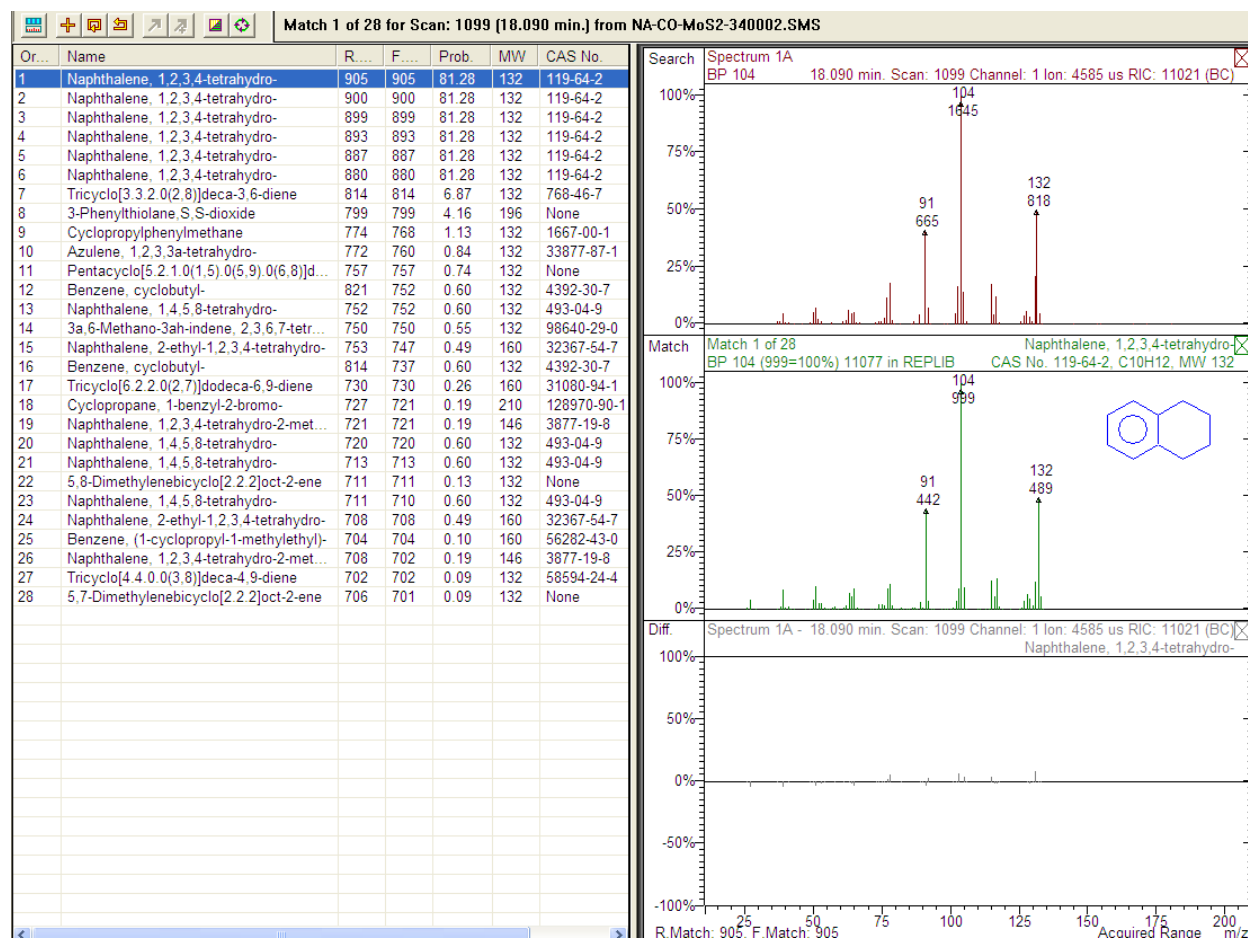


Figure 5-6 Example of GC-MS library identification of unknown chemicals

After identifying all the relevant peaks involved in the 2-NA removal, a proposed GC-MS chromatograph with chemical labels is shown in Figure 5-7. This is then used as a reference for selecting pure chemicals in the GC-FID identification and calibration.

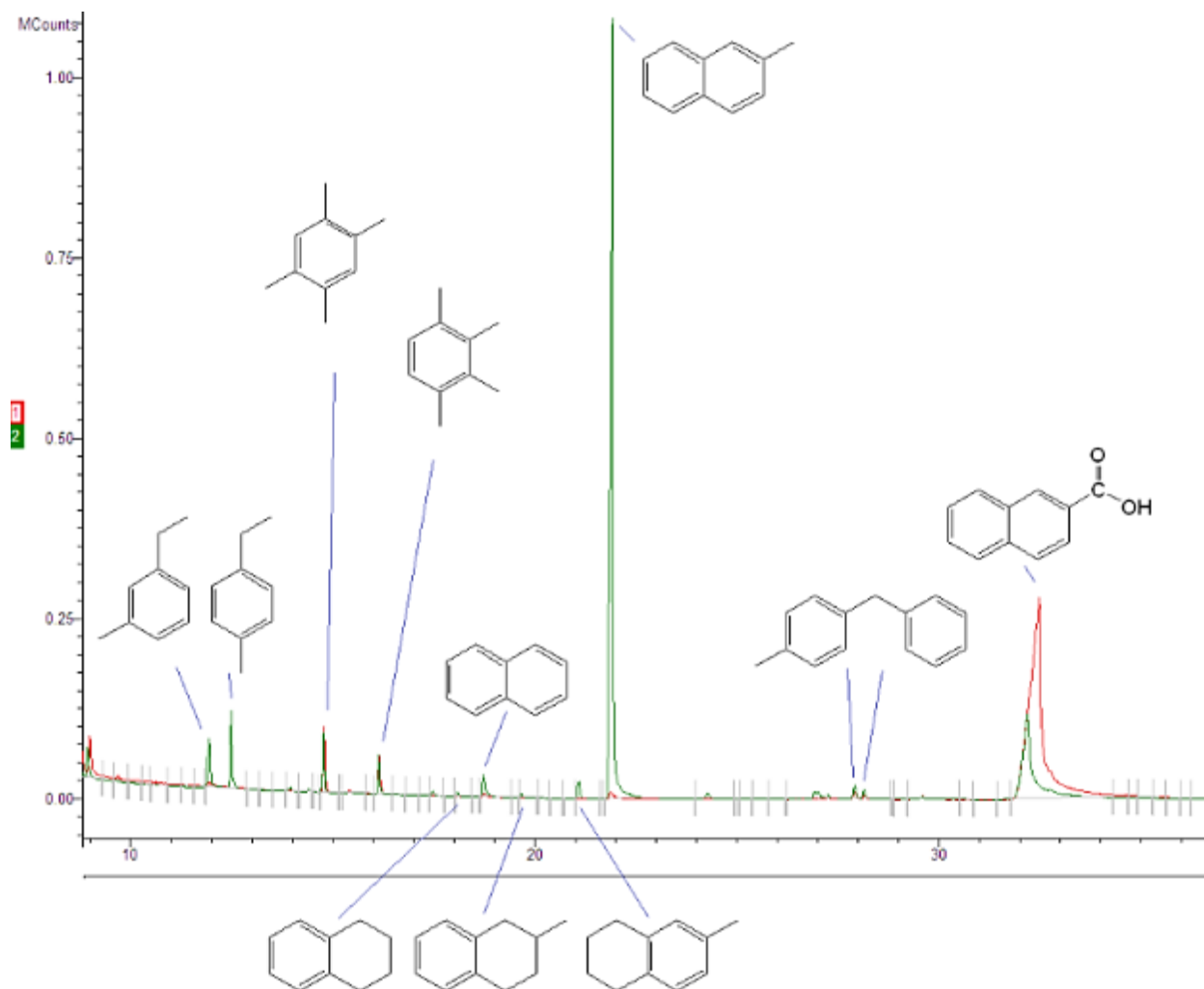


Figure 5-7 Example of GC-MS library identification of unknown chemicals

With the reference of the GC-MS results, the purchased chemicals used in the GC-FID identification were found to match the retention time of previously unknown chemicals, which confirmed the estimated GC-MS results. By combining the GC-FID and GC-MS observations, the GC-FID chromatograph is shown in Figure 5-8, where the identified peaks include benzoic acid, decalin, tetralin, naphthalene, 1,2,3,4-tetrahydro-2-methylnaphthalene, 1,2,3,4-tetrahydro-6-methylnaphthalene and 2-methylnaphthalene.

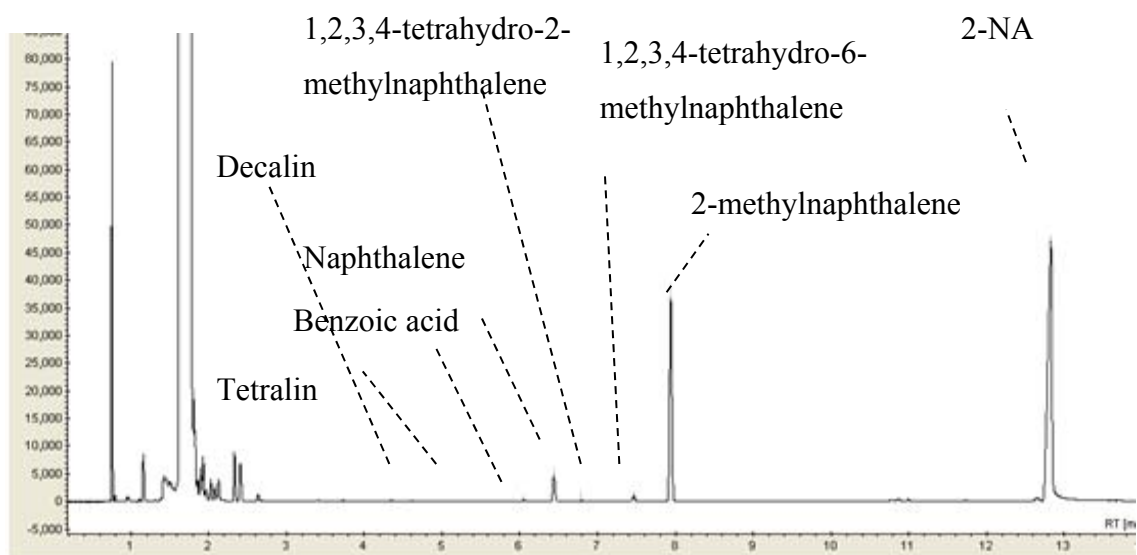
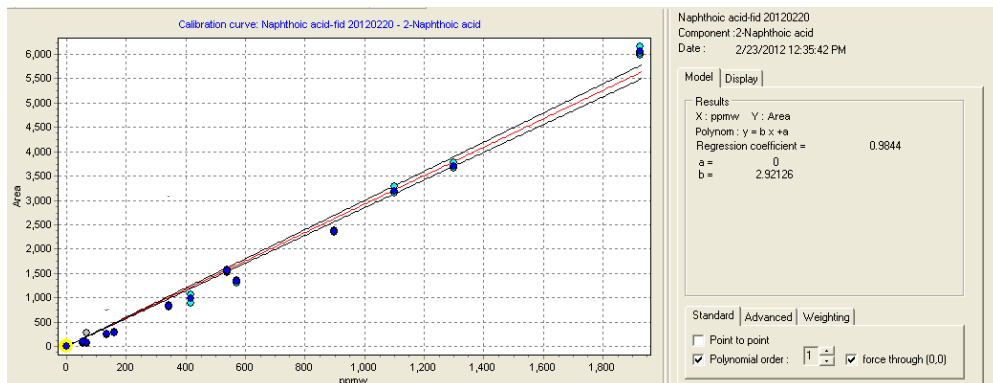


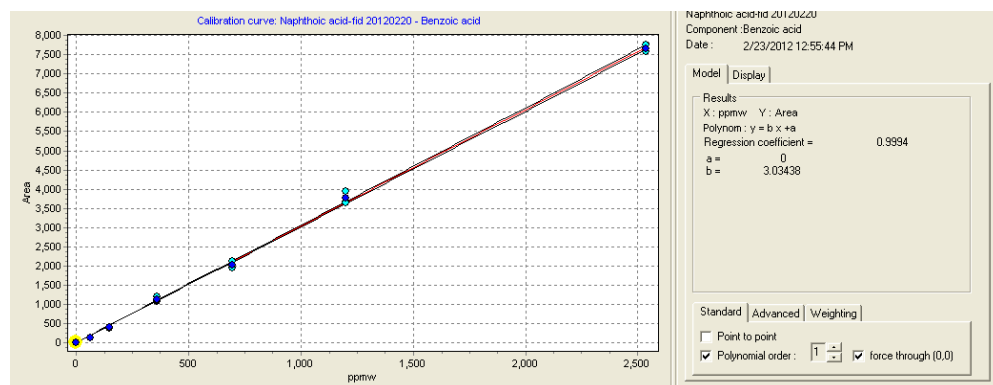
Figure 5-8 Identification of 2-NA removal products with GC-FID

The calibration of acid is difficult for the GC-FID, which gives a wide peak with a tail in the chromatographs. As a result, the calibration of 2-NA required more calibration stages. The final R^2 for 2-NA based on 12 concentration stages of calibration was 0.9844 as shown in Figure 5-9(a). Calibration for benzoic acid and C7-BA are shown in Figure 5-9(b) and Figure 5-9(c), and the R^2 for them was 0.9994 and 0.9924 respectively.

(a) 2-NA



(b) benzoic acid



(c) C7-BA

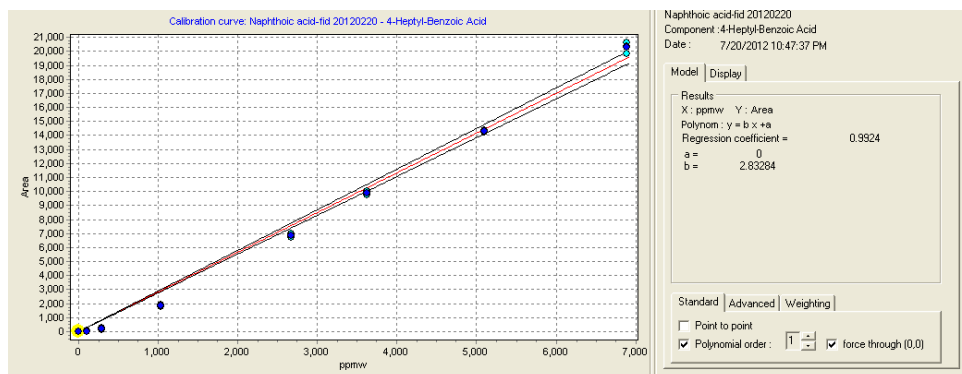


Figure 5-9 Calibration curves for 2-NA, benzoic acid and C7-BA test in GC-FID

5.2.5 Kinetic study for 2-NA removal

Figure 5-10 provides an example of the mole percentages of the reactant and products obtained during the reaction.

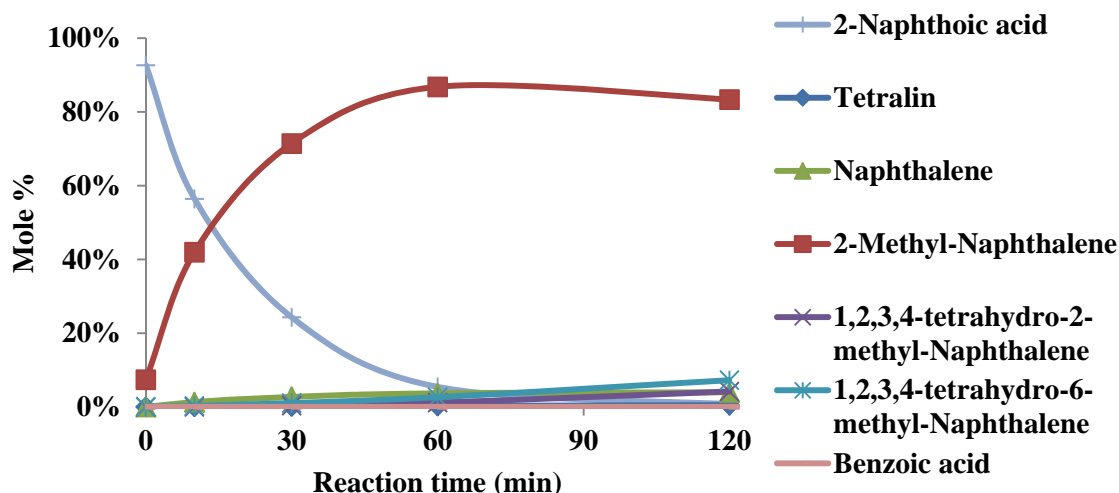


Figure 5-10 Mole percentage changes during the 2-NA removal reaction (300°C, 80ml toluene, 10ml water, 15psi H₂S, 585psi CO, ~1641ppmw 2-NA in toluene, 673ppmw Mo, 2hours)

It was found that the concentration of 2-NA decreased with an increase in 2-methylnaphthalene, which should be the hydrodeoxygenation (HDO) product of 2-NA. It was interesting that the 2-methylnaphthalene concentration stopped increasing and started to decrease after 60min. This indicated the consecutive hydrogenation reaction of this HDO product occurred to produce 2-methylnaphthalene. Hence, 2-methylnaphthalene and its relevant hydrogenated products (1,2,3,4-tetrahydro-2-methylnaphthalene, and 1,2,3,4-tetrahydro-6-methylnaphthalene, 2-methyldecahydronaphthalene) represented the final HDO products. During the reaction, the formation of 2-decahydro-methyl-naphthalene was hardly observed in either by GC-MS or GC-FID. Hence, the hydrogenation did not occur for the partially hydrogenated HDO products (1,2,3,4-tetrahydro-2-methylnaphthalene and 1,2,3,4-tetrahydro-6-methylnaphthalene), which thus saves some H₂ from being used in further hydrogenation. Moreover, this incomplete hydrogenation brings some additional benefit for hydroprocessing. Since tetralin and chemicals with similar structures (1,2,3,4-tetrahydro-2-methylnaphthalene, and 1,2,3,4-tetrahydro-6-methylnaphthalene) have a high activity for eliminating coke formation due to its ability of

donating *in situ* H₂ to hydrogenate the coke on catalyst surface (Zhao, Gray *et al.* 2008). Naphthalene, tetralin and decalin were also identified in both GC-FID and GC-MS tests. They represented the products of the decarboxylation reaction, among which tetralin and decalin were the consecutive hydrogenated products of naphthalene. Benzoic acid was also found in the 2-NA reaction product when no H₂ or catalysts were used. Detailed analysis of 2-NA removal under N₂ without catalyst is shown in Appendix D. Hence, benzoic acid was probably the product of 2-NA through a cracking reaction, where the aromatic ring was opened and cleavage of 2-NA occurred. When H₂ was used for 2-NA removal, no benzoic acid product was found in either the GC-MS or GC-FID during the reaction. This is expected to be caused by the hydrogenation of benzoic acid in toluene. Since toluene was the solvent and elution phase, it was not able to capture all the 2-NA cracking product content, thus causing difficulties for future kinetic studies. Details will be discussed in the following kinetic study and the sample kinetic calculations in Appendix D.

Since the decreasing trend for 2-NA was very close to a 1st order reaction, it was assumed that the H₂ (or hydride) concentration was relatively constant. The 2-NA removal reaction can be analyzed as a pseudo-first order reaction. Its reaction rate can be written according to Eq. 5-2.

$$-\frac{d[2-NA]}{dt} = k_{NA\ removal} \cdot [2-NA] \quad (\text{Eq. 5-2})$$

Eq. 5-2 can be integrated to obtain Eq. 5-3.

$$\ln \frac{[2-NA]_0}{[2-NA]_t} = k_{NA\ removal} \cdot t \quad (\text{Eq. 5-3})$$

Therefore, $\ln([2-NA]_0/[2-NA]_t)$ will have linear relationship with respect to time. As an example, this linear relationship is shown in Figure 5-11. The slope is the pseudo-first order reaction rate constant for 2-NA removal.

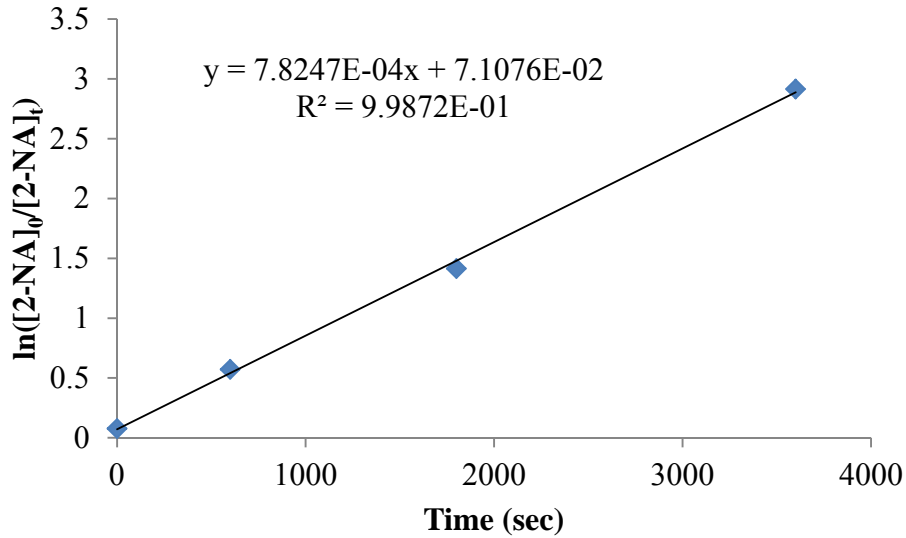


Figure 5-11 Plot of $\ln([2-NA]_0/[2-NA]_t)$ values with time (300°C, 80ml toluene, 10ml water, 15psi H₂S, 585psi CO, ~1641ppmw 2-NA in toluene, 673ppmw Mo, 2hours)

The production of each product from different reaction pathways depends on its reaction rate. For example, the generating rate for the total HDO production can be expressed according to Eq. 5-4.

$$\frac{d[HDO \text{ product}]}{dt} = k_{HDO} \cdot [2 - NA]_t \quad (\text{Eq. 5-4})$$

Based on Eq. 5-3, $[2-NA]_t$ can be substituted. After integration Eq. 5-4 will be transformed into Eq. 5-5.

$$\frac{[HDO \text{ product}] \cdot (-k_{2-NA \text{ removal}})}{[2-NA]_0} = k_{HDO} \cdot \{\exp(-k_{2-NA \text{ removal}} \cdot t) - 1\} \quad (\text{Eq. 5-5})$$

By plotting $\frac{[HDO \text{ product}] \cdot (-k_{2-NA \text{ removal}})}{[NA]_0}$ with $\{\exp(-k_{2-NA \text{ removal}} \cdot t) - 1\}$, the slope of the line will be the pseudo first order reaction rate constant for HDO. The rate constant for decarboxylation and cracking can be achieved in the same way, as shown in Eq. 5-6 and Eq. 5-7.

$$\frac{[\text{decarboxylation product}] \cdot (-k_{2\text{-NA removal}})}{[2\text{-NA}]_0} = k_{\text{decarboxylation}} \cdot \{\exp(-k_{2\text{-NA removal}} \cdot t) - 1\}$$

(Eq. 5-6)

$$\frac{[\text{cracking product}] \cdot (-k_{2\text{-NA removal}})}{[2\text{-NA}]_0} = k_{\text{cracking}} \cdot \{\exp(-k_{2\text{-NA removal}} \cdot t) - 1\}$$

(Eq. 5-7)

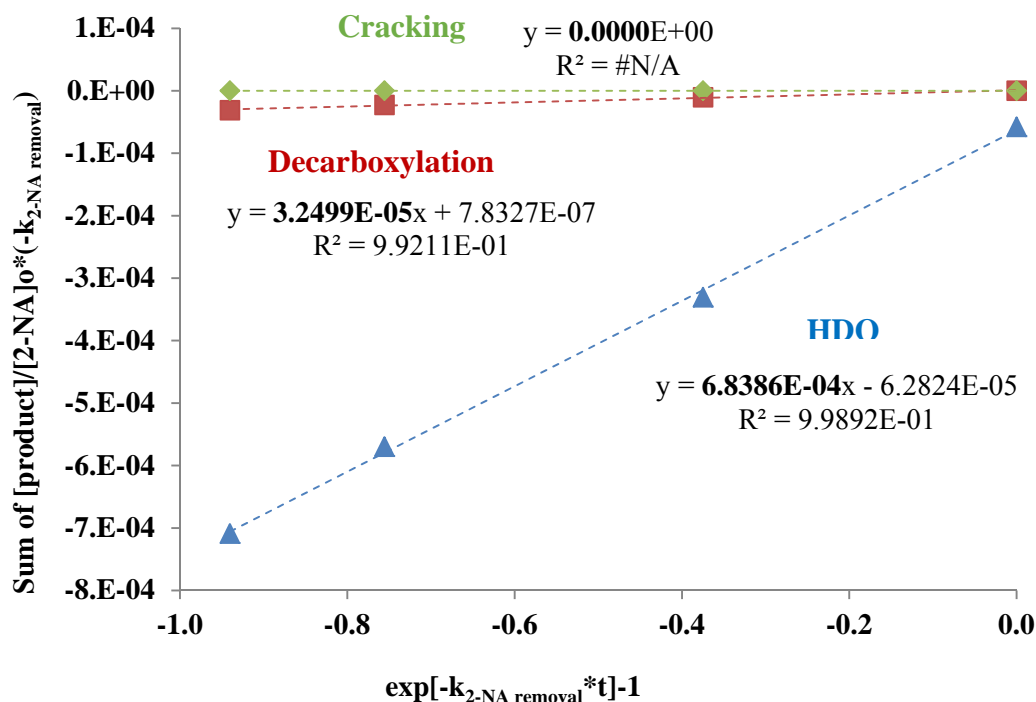


Figure 5-12 Plot of sum of $[\text{product}]/[2\text{-NA}]_0 \cdot (-k_{2\text{-NA removal}})$ values with time (300°C, 80ml toluene, 10ml water, 15psi H₂S, 585psi CO, ~1641ppmw 2-NA in toluene, 673ppmw Mo, 2hours)

In Figure 5-12, the linear relationships are shown for decarboxylation, HDO and cracking. It is noticed the cracking pathway has no slope as expected from prior discussion. This is because of the limited determination capability for the cracking product in the presence of H₂ (the cracking products benzoic acid would be hydrogenated into toluene, which was the same as the reaction solvent). When no H₂ was used for 2-NA removal, benzoic acid was identified, providing evidence for the cracking pathway. A detailed kinetic study for 2-NA removal under N₂ is shown

in Appendix D. Since no other reaction product was observed or confirmed by GC-FID and GC-MS, the cracking rate constant was calculated using Eq. 5-8.

$$k_{cracking} = k_{2-NA\ removal} - k_{decarboxylation} - k_{HDO} \quad (\text{Eq. 5-8})$$

5.2.6 Proposed reaction mechanism for 2-NA removal

In summary, the 2-NA removal reaction includes three primary reaction pathways (together with subsequent chain hydrogenation reactions) shown in Figure 5-13. The three primary reaction pathways are: decarboxylation, HDO and cracking. Decarboxylation is a common reaction for removing naphthenic acids by using basic metal oxide catalysts. The removed carboxyl group becomes CO₂, losing one carbon from the oil and finally increasing greenhouse gas emissions. In emulsion upgrading process, the decarboxylation selectivity was less than 6%. On the contrary, H₂ was added to 2-NA through HDO and saved the carbon from being wasted or released as a greenhouse gas. This environmental favorable pathway had 87% selectivity, and the HDO products were found to be over 97% in the final product distribution at the end of reaction.

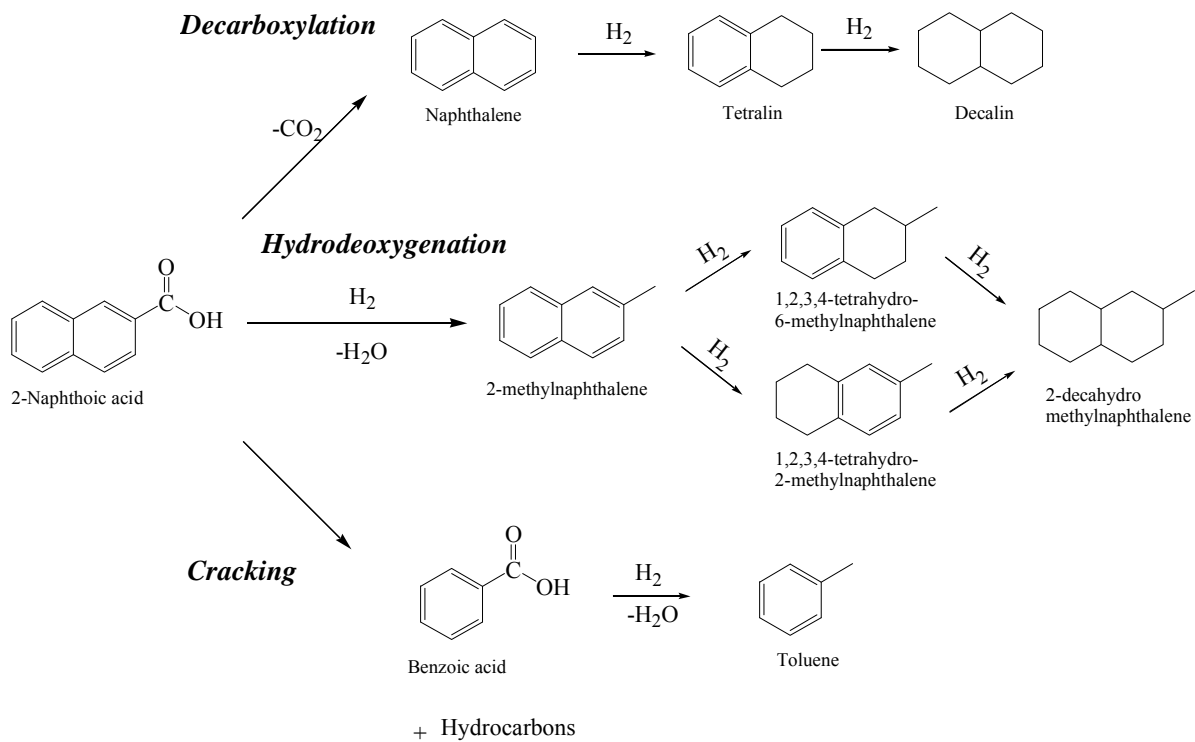


Figure 5-13 Proposed reaction mechanism for 2-NA removal: (a) decarboxylation and consecutive chain hydrogenation reactions; (b) hydrodeoxygenation and consecutive chain hydrogenation reactions; (c) cracking.

5.3 Results and discussion

5.3.1 Simultaneous WGSR and 2-NA removal

In order to verify the feasibility of the “Upgrading/WGSR/2-NA Removal” tri-process, an “HDS-WGSR-2-NA Removal” model has been established. The reaction was carried out at 415°C, and excellent WGSR, HDS and 2-NA removals were achieved as shown in Table 3. This means HDS, WGSR and 2-NA removal can be realized at 415°C, indicating the “Upgrading-WGSR-NA Removal” tri-process is feasible. However, it is not enough to demonstrate the effects among WGSR, upgrading and 2-NA removal, since most of the 2-NA had been removed at the beginning of the reaction. In order to have a more specific understanding of these three processes, some comparison experiments were implemented. The mutual effects between upgrading and 2-NA removal will be discussed in the following sections. In this section, only the mutual effects between WGSR and 2-NA removal will be discussed.

Table 5-2 WGSR, HDS of DBT, 2-NA removal in both oil and water phases (415°C, 80ml toluene, 10ml water, 15psi H₂S, 585psi CO, ~1641ppmw 2-NA in toluene, 5000ppmw DBT, 673ppmw Mo, 2hours)

Reactions involved	Conversion
WGSR	81.5%
HDS	93.2%
2-NA Removal (Oil)	99.7%
2-NA Removal (Water)	99.9%

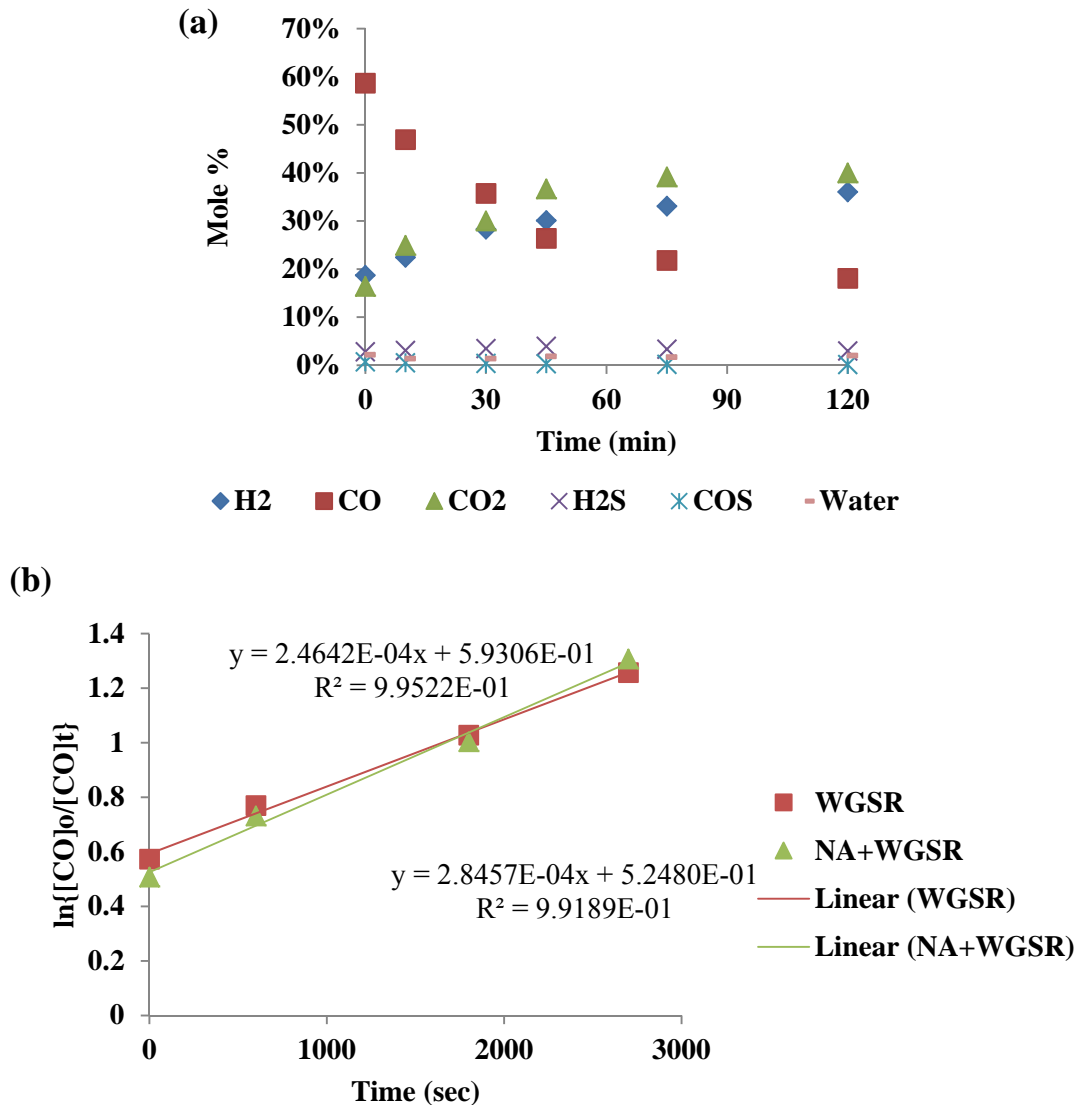


Figure 5-14 (a) Mole percentage of each gas component during simultaneous WGSR and 2-NA removal; (b) Plots of $\ln\{[CO]_0/[CO]_t\}$ values with time with and without 2-NA (340°C, 80ml toluene, 10ml water, 15psi H₂S, 585psi CO, ~1641ppmw 2-NA in toluene, 673ppmw Mo, 2hours)

The mole percentages of each gas component are determined by using RGA shown in Figure 5-14(a). It is found that the CO mole percentage decreased with increasing CO₂ and H₂. As the concentration of H₂O was large and constant during the WGSR, the WGSR reaction rate could be calculated following pseudo-first order reaction kinetics according to Eq. 5-2 and Eq. 5-3; it is easy to obtain Eq. 5-9. The plots of $\ln\{[CO]_0/[CO]_t\}$ vs. time gave linear relationships as shown

in Figure 5-14(b). The slopes were the reaction rate constants for WGSR with and without 2-NA addition.

$$\ln \frac{[CO]_0}{[CO]_t} = k_{WGSR} \cdot t \quad (\text{Eq. 5-9})$$

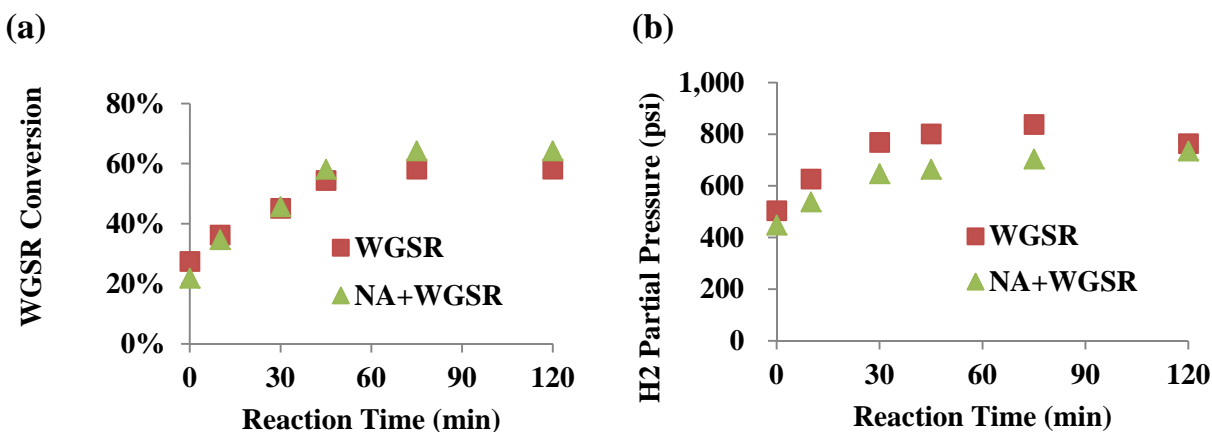


Figure 5-15 (a) WGSR conversion during WGSR with and without 2-NA; (b) H₂ partial pressure with time (340°C, 80ml toluene, 10ml water, 15psi H₂S, 585psi CO, ~1641ppmw 2-NA in toluene, 673ppmw Mo, 2hours)

The WGSR seemed to be affected by 2-NA addition at a lower reaction temperature, 340°C. The WGSR conversion was increased during the removal of 2-NA as shown in Figure 5-15(a), and it increased from 58% to 64% at 120min. This is because the 2-NA removal reaction consumed H₂ generated in the WGSR as shown in Figure 5-15(b). The H₂ partial pressure was lower for the simultaneous WGSR and 2-NA removal, and this H₂ consumption shifted the reaction towards the higher WGSR conversion side.

Table 5-3 Comparison of WGSR with simultaneous WGSR and 2-NA removal (340°C, 80ml toluene, 10ml water, 15psi H₂S, 585psi CO, ~1641ppmw 2-NA in toluene, 673ppmw Mo, 2hours)

	WGSR	2-NA+WGSR
WGSR Conversion %	58.2	64.2
k _{WGSR} (10 ⁻⁵ s ⁻¹)	24.6	28.5
H ₂ Partial Pressure (psi)	763	735
Max. Pressure (psi)	2421	2400

With the kinetic information of the WGSR with and without addition of 2-NA, the effect of 2-NA on WGSR can be precisely discussed. As listed in Table 5-3 the WGSR reaction rate constant was $2.5 \times 10^{-4} \text{ s}^{-1}$, while the k_{WGSR} with 2-NA was $2.8 \times 10^{-4} \text{ s}^{-1}$. The WGSR was not inhibited by the addition of 2-NA based on the observations in this section. This may be explained by the higher adsorption preference of CO and H₂O over MoS₂ than 2-NA. It has been reported that CO and H₂O adsorb more strongly than oxygenated compounds during the HDO of furan (Badawi, Paul *et al.* 2011).

5.3.2 Effect of reaction temperature

Experiments were carried out at 300°C, 340°C and 415°C (at an initial loading of 600psi pressure at room temperature) to evaluate the effect of reaction temperature on 2-NA. In Table 5-4 it is seen that at 300°C the maximum pressure reached 2066psi, which was around 1000psi lower than that at 415°C. The WGSR was favored at high temperature as the WGSR conversion increased from 51.6% to 77.9% when the reaction temperature was increased from 300°C to 415°C. The WGSR reaction rate constant was also doubled from $14.8 \times 10^{-5} \text{ s}^{-1}$ to $28.5 \times 10^{-5} \text{ s}^{-1}$ by increasing the temperature from 300°C to 340°C. Since the WGSR almost reached equilibrium (maximum conversion) at the beginning of the reaction at 415°C, it was not possible to calculate the pseudo-first order reaction rate constant at 415°C. Due to the relatively low WGSR conversion the H₂ partial pressure was only 651psi at 300°C, which is generally too low for hydrotreating. However, the 2-NA conversion still reached nearly 100% in both the oil and water phases at 300°C after 2 hours.

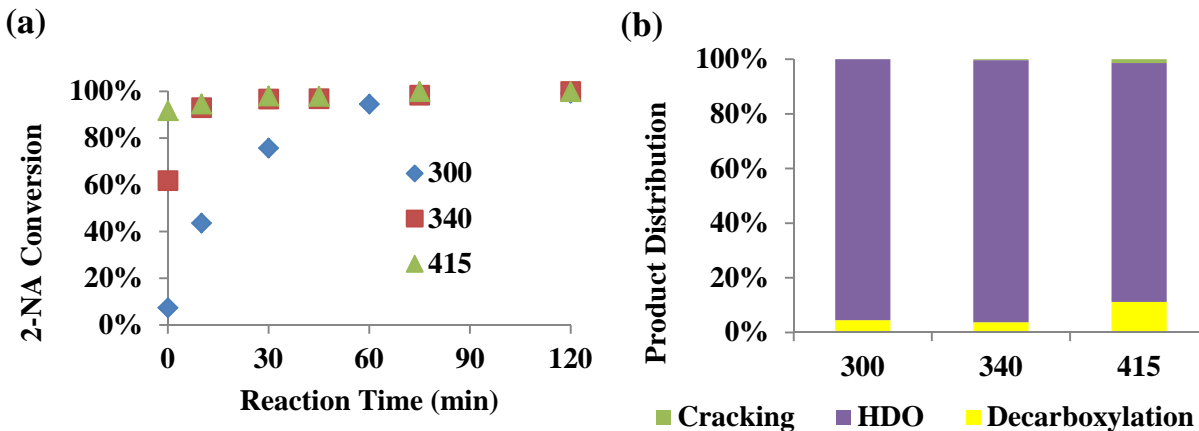


Figure 5-16 Reaction oil phase evaluation at different reaction temperatures: (a) 2-NA conversion with time; (b) Product distribution at 120 min. (80ml toluene, 10ml water, 15psi H₂S, 585psi CO, ~1641ppmw 2-NA in toluene, 673ppmw Mo, 2hours)

2-NA was almost completely removed from the water phase from 300°C to 340°C as shown in Table 5-4. Figure 5-16(a) demonstrates the 2-NA conversion changes determined by GC-FID. It is noticed that most of the 2-NA had already been removed at the beginning of the reaction at 340°C and 415°C. As a result, the kinetic data collected at higher temperatures was not accurate. As listed in Table 5-4 more cracking product (benzoic acid), decarboxylation products (naphthalene, tetralin and decalin) were produced at the higher temperature suggesting higher cracking and decarboxylation selectivity at higher temperature. While the product distribution at 300°C shown in Figure 5-16(b) demonstrated that 95.5% of the final total products were HDO products. By calculating the selectivity following Eq.5-10, Eq. 5-11 and Eq.5-12, it was found that the selectivity of HDO at 300°C was 87.5%, which was much higher than the selectivity of decarboxylation (4.1%) and cracking (8.4%). As discussed in the previous reaction mechanism, HDO is regarded as the most economic and environmental friendly pathway. It is concluded that the low system pressure requirement, relatively low initial conversion, excellent HDO selectivity and acceptable water purification performance indicates 300°C as a reasonable temperature for the following research. Experimental reproducibility was discussed in Appendix E.2.

$$Selectivity_{Decarboxylation} = \frac{k_{Decarboxylation}}{k_{2-NA\ removal}} \times 100\% \quad (\text{Eq. 5-10})$$

$$Selectivity_{HDO} = \frac{k_{HDO}}{k_{2-NA\text{ removal}}} \times 100\% \quad (\text{Eq. 5-11})$$

$$Selectivity_{Cracking} = \frac{k_{Cracking}}{k_{2-NA\text{ removal}}} \times 100\% \quad (\text{Eq. 5-12})$$

Mass balance, oil and water yields calculations are summarized in the Eq. 5-13, 5-14 and 5-15.

$$Mass\ balance\ \% = \frac{m(oil\ solution)_f + m(water)_f + m(PMA\ solution)_f + m(gas\ feeds)_f}{m(oil\ solution)_o + m(water)_o + m(PMA\ solution)_o + m(gas\ feeds)_o} \times 100\% \quad (\text{Eq. 5-13})$$

$$Oil\ Yield\ \% = \frac{m(oil\ solution)_f}{m(oil\ solution)_o} \times 100\% \quad (\text{Eq. 5-14})$$

$$Water\ Yield\ \% = \frac{m(water)_f}{m(water)_o + \rho(water) \cdot V(PMA\ solution)^*} \times 100\% \quad (\text{Eq. 5-15})$$

* *The water in PMA solution was also considered as water feed.*

Table 5-4 Summary of effect of temperature on 2-NA removal (80ml toluene, 10ml water, 15psi H₂S, 585psi CO, ~1641ppmw 2-NA in toluene, 673ppmw Mo, 2hours)

	300°C	340°C	415°C
2-NA Conversion % in Oil	99.2	98.4	100.0
2-NA Conversion % in H ₂ O	99.3	99.9	99.9
k _{2-NA Removal} (10 ⁻⁵ s ⁻¹)	78.2	-	-
k _{Decarboxylation} (10 ⁻⁵ s ⁻¹)	3.2	-	-
k _{HDO} (10 ⁻⁵ s ⁻¹)	68.4	-	-
k _{Cracking} (10 ⁻⁵ s ⁻¹)	6.6	-	-
Product Distribution % at 120min			
Decarboxylation	4.5	3.7	11.9
HDO	95.5	95.7	86.2
Cracking	0.0	0.6	2.0
WGSR Conversion %	41.7	64.2	77.9
k _{WGSR} (10 ⁻⁵ s ⁻¹)	14.8	28.5	-
H ₂ Partial Pressure (psi)	555	735	806
Max. Pressure (psi)	2066	2400	3026
Oil yield %	91.6	90.7	90.1
Water yield %	43.5	29.7	27.1
Mass balance %	83.7	82.3	81.2

5.3.3 Effect of gas feed

CO, H₂ and N₂ were chosen as the reaction gas feeds for 2-NA removal. As shown in Table 5-5 the H₂ partial pressure under molecular H₂ was about twice that of the H₂ partial pressure under the CO condition. This low H₂ partial pressure under CO might have a negative effect for removing 2-NA. Additionally CO was reported as an essential inhibitor for HDO of biomass (Badawi, Paul *et al.* 2011), making the HDO under CO more difficult compared to HDO under molecular H₂.

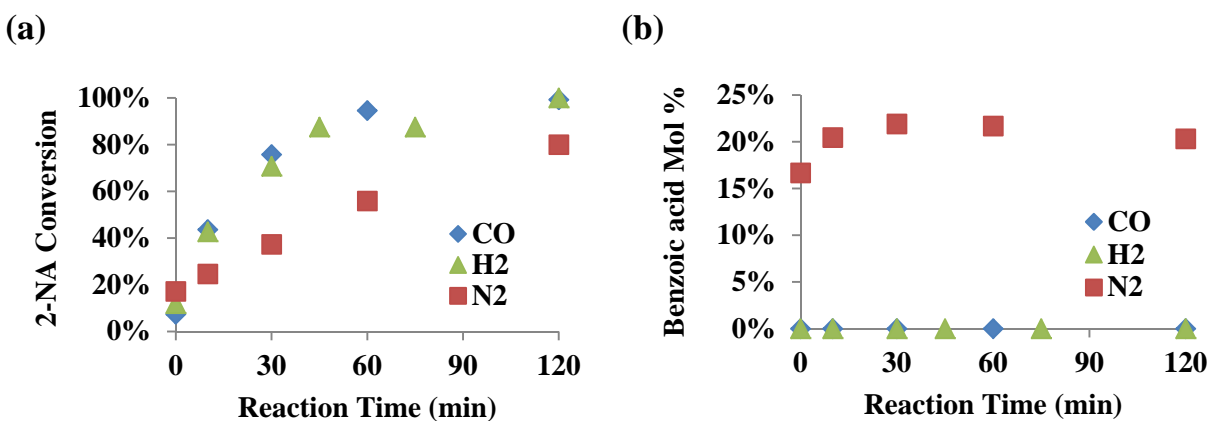


Figure 5-17 Reaction oil phase evaluation with different gas feeds: (a) 2-NA conversion with time; (b) Benzoic acid mole percentage with time (300°C, 80ml toluene, 10ml water, 15psi H₂S, 585psi gas feed, ~1641ppmw 2-NA in toluene, 673ppmw Mo, 2hours)

As shown in Figure 5-17(a) and Table 5-5, 99.2% and 99.3% 2-NA removal was achieved when CO was used as gas feed; while molecular H₂ removed 100% 2-NA in oil and 99.4% 2-NA in water after 2 hours. Kinetic analysis reveals that the 2-NA removal rate constants were $78.2 \times 10^{-5} \text{ s}^{-1}$, $70.1 \times 10^{-5} \text{ s}^{-1}$ and $17.5 \times 10^{-5} \text{ s}^{-1}$ for CO, H₂ and N₂. It is observed that both decarboxylation and especially HDO were improved by using CO, which contributed an improvement in 2-NA removal. Among all these three gas feeds, CO exhibited the highest HDO selectivity at 87.4%, compared to the 84.9% and 80.6% for H₂ and N₂. It was notable that CO had a higher 2-NA removal ability compared to molecular H₂ at such a low H₂ partial pressure in the presence of a HDO inhibitor, CO. This outstanding HDO activity in the presence of CO could be derived from (a) the high activity of *in situ* H₂ generated through the WGS; (b) the more active nano catalyst generated through PMA collapse by using CO (Liu 2010). Higher decarboxylation selectivity

was achieved by using *in situ* H₂ than molecular H₂. However, cracking selectivity decreased from 13.7% to 8.4% by switching from H₂ to CO. This anti-cracking preference of this novel process may be explained by the high activity of *in situ* H₂.

It was also noticed that 2-NA removal was realized by only using N₂ and water. The 2-NA removal reached 80% in oil and 96.1% in water as shown in Table 6. The major product in the beginning was benzoic acid, derived from cracking. However, benzoic acid also contributed to toxicity and acidity. As the reaction proceeded, more and more naphthalene and 2-methylnaphthalene were produced without any hydrogenated products. By observing the benzoic acid concentration change as shown in Figure 5-17(b), it appeared that the production of benzoic acid had started and almost finished after the reactor reached 300°C. The concentration of benzoic acid did not change significantly after the reaction started, while increasing amounts of decarboxylation and HDO products changed the final yield% distribution. The cracking product was only 15.8% in the final product distribution. There was some H₂ detected (~8psi) in the gas phase of the N₂ run as shown in Table 5-5, and water may be the H₂ source. Hence the major pathway under N₂ was expected to be HDO. The origin of such excellent HDO performance at such low H₂ partial pressure under N₂ seemed to be due to the *in situ* generated nano unsupported MoS₂ catalyst. The effect of the catalyst under a N₂ atmosphere will be discussed in Section 5.3.4. More *in situ* solid characterization (like *in situ* FT-IR) should be carried out in future for investigating the *in situ* catalyst's adsorption performance under N₂. In the HDO reaction under N₂, since water was present to be a potential H₂ source, the effect of water under N₂ will be discussed in the following Section 5.3.5.

Table 5-5 Summary of effect of gas feed on 2-NA removal (300°C, 80ml toluene, 10ml water, 15psi H₂S, 585psi gas feed, ~1641ppmw 2-NA in toluene, 673ppmw Mo, 2hours)

	CO	H ₂	N ₂
2-NA Conversion % in Oil	99.2	100.0	80.0
2-NA Conversion % in H ₂ O	99.3	99.4	96.1
k _{2-NA Removal} (10 ⁻⁵ s ⁻¹)	78.2	70.1	17.5
k _{Decarboxylation} (10 ⁻⁵ s ⁻¹)	3.2	0.9	0.6
k _{HDO} (10 ⁻⁵ s ⁻¹)	68.4	59.5	14.1
k _{Cracking} (10 ⁻⁵ s ⁻¹)	6.6	9.6	2.8
Selectivity %			
Decarboxylation	4.2	1.3	3.5
HDO	87.4	84.9	80.6
Cracking	8.4	13.7	15.8
Product Distribution % at 120min			
Decarboxylation	4.5	1.6	3.2
HDO	95.5	98.4	71.4
Cracking	0.0	0.0	25.4
WGSR Conversion %	41.7	-	-
H ₂ Partial Pressure (psi)	555	1478	8
Max. Pressure (psi)	2066	1794	1926
Oil yield %	91.6	91.9	91.2
Water yield %	43.5	67.6	68.2
Mass balance %	83.7	88.2	87.1

5.3.4 Effect of catalysts

5.3.4.1 Comparison of MoS₂ and MoO₃ catalysts under CO

Transition metal oxide catalysts have been reported as decarboxylation catalysts for naphthenic acid removal (Zhang, Ma *et al.* 2006, Ding, Rahimi *et al.* 2009). In this section, two different catalysts were examined for 2-NA removal. One was a nano unsupported MoS₂ catalyst, and the other was a nano unsupported MoO₃ catalyst. They both involved PMA as the Mo precursor; however, the difference was the use of H₂S for sulfurization in the case of preparing the nano unsupported MoS₂ catalyst. In the experiment with MoO₃, only CO and water were used and black catalyst powders were formed. 337ppm Mo was loaded for generating the Mo catalysts, and the reaction was carried out at 300°C with 600psi as the initial total pressure.

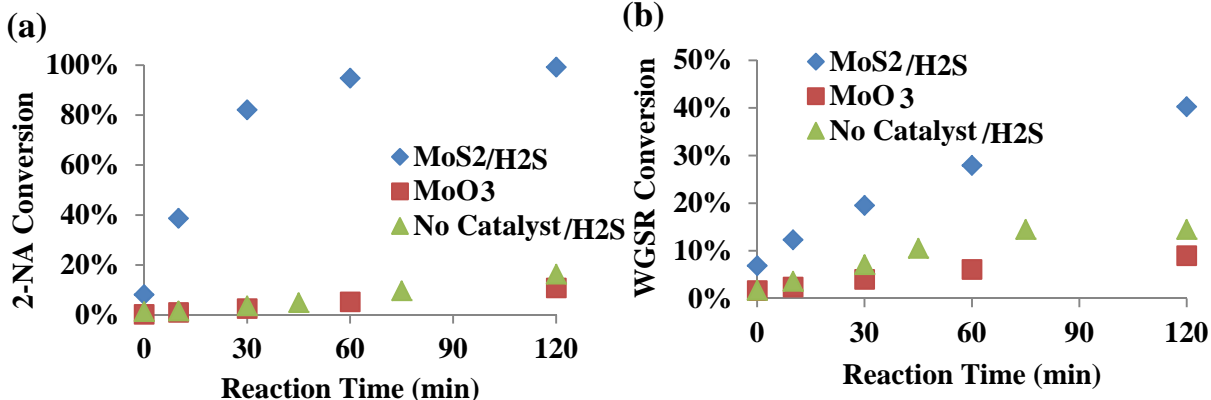


Figure 5-18 Reaction oil and gas phases evaluation with different catalysts: (a) 2-NA conversion with time; (b) WGSR conversion with time (300°C, 80ml toluene, 10ml water, 15psi H₂S if added, 600psi total pressure, CO as gas feed, ~1641ppmw 2-NA in toluene, 337ppmw Mo, 2hours)

Figure 5-18(a) and Figure 5-18(b) present the different effects of MoS₂ and MoO₃ on 2-NA removal and the WGSR, and a reaction without catalyst is also shown as a reference. It is noticed that the introduction of MoS₂ significantly improved the 2-NA removal and the WGSR. As shown in Table 5-6 the 2-NA removal conversion was increased from 16.3% to 99.2% at 2hours. The 2-NA removal rate increased almost 40 times from $2.3 \times 10^{-5} \text{ s}^{-1}$ to $81.2 \times 10^{-5} \text{ s}^{-1}$. All three reaction pathways were improved, and especially the HDO pathway was accelerated from $2.0 \times 10^{-5} \text{ s}^{-1}$ to $70.7 \times 10^{-5} \text{ s}^{-1}$. The WGSR conversion reached 40.3% when carried out in the presence of MoS₂, and the WGSR rate constant increased from $6.4 \times 10^{-5} \text{ s}^{-1}$ to $13.9 \times 10^{-5} \text{ s}^{-1}$. The H₂ partial pressure increased from 293psi to 559psi with MoS₂, and this was an additional reason why the 2-NA was removed so well with MoS₂. On the other hand, MoO₃ did not improve either 2-NA removal or the WGSR as did MoS₂. Both the conversion and the reaction rate remained the same or decreased slightly for 2-NA removal (both oil and water) and the WGSR when using MoO₃ vs. no catalyst with H₂S. It is known that MoO₃ catalyzes the WGSR. The poor WGSR catalytic performance may be due to the effect of H₂S in the no catalyst base case. MoS₂ is a better catalyst than MoO₃. By comparing the reaction rates for the different 2-NA removal pathways, it can be observed that MoO₃ enhanced the decarboxylation rate constant slightly from $0.3 \times 10^{-5} \text{ s}^{-1}$ to $0.6 \times 10^{-5} \text{ s}^{-1}$, which is consistent with pervious publications on the use of transition

metal oxides ability for decarboxylation (Zhang, Ma *et al.* 2006, Ding, Rahimi *et al.* 2009). However, MoO₃ was not a catalyst for HDO.

Table 5-6 Summary of effect of catalyst under CO on 2-NA removal (300°C, 80ml toluene, 10ml water, 15psi H₂S if added, 600psi total pressure, CO as gas feed, ~1641ppmw 2-NA in toluene, 337ppmw Mo, 2hours)

	No Catalyst w/H ₂ S	MoO ₃	MoS ₂ w/H ₂ S
2-NA Conversion % in Oil	16.3	10.8	99.2
2-NA Conversion % in H ₂ O	87.8	85.2	99.3
k _{2-NA Removal} (10 ⁻⁵ s ⁻¹)	2.3	1.6	81.2
k _{Decarboxylation} (10 ⁻⁵ s ⁻¹)	0.27	0.56	4.8
k _{HDO} (10 ⁻⁵ s ⁻¹)	2.0	1.0	70.7
k _{Cracking} (10 ⁻⁵ s ⁻¹)	0.03	0.05	5.8
Selectivity %			
Decarboxylation	11.7	35.8	5.9
HDO	87.2	61.1	87.0
Cracking	1.1	3.1	7.1
Product Distribution % at 120min			
Decarboxylation	11.3	35.9	8.2
HDO	88.7	61.6	91.8
Cracking	0.0	2.5	0.0
WGSR Conversion %	14.5	9.0	40.3
k _{WGSR} (10 ⁻⁵ s ⁻¹)	6.4	2.9	13.9
H ₂ Partial Pressure (psi)	293	136	559
Max. Pressure (psi)	1955	1649	1973
Oil yield %	91.8	96.5	92.0
Water yield %	52.1	47.3	45.3
Mass balance %	84.5	87.5	85.0

5.3.4.2 Effect of MoS₂ loading under CO

In order to determine the catalytic effect of MoS₂ for the 2-NA removal experiments, several comparison experiments were designed at 300°C with different MoS₂ loading. No catalyst, 168ppm Mo, 337ppm Mo and 673ppm Mo conditions were examined with relevant 2-NA:Mo

molecular ratios at 0, 5.4, 2.7 and 1.4 respectively. The results in Figure 5-19(a) and Table 5-7 clearly display the crucial influence of MoS₂. Figure 5-19(b) shows the WGSR conversion change with time with the loading of different Mo concentrations. The WGSR was very slow ($6.4 \times 10^{-5} \text{ s}^{-1}$) with only 14.5% conversion if no catalyst was added. If Mo was added, the WGSR was enhanced in both conversion and reaction rate. As shown in Table 5-7 the WGSR conversion increased to more than 40% and the WGSR rate constant was around $14 \times 10^{-5} \text{ s}^{-1}$. This promoted WGSR finally resulted in a higher H₂ partial pressure leading to better 2-NA removal performance. Nevertheless, a further increase of catalyst concentration from 337ppm to 673ppm Mo did not increase the conversion or the rate constants as shown in Figure 5-19(b) and Table 5-7. It is possible that the reaction was 1st or zero order with respect to Mo; while the 2-NA loading was too low to react with the overfed Mo catalysts.

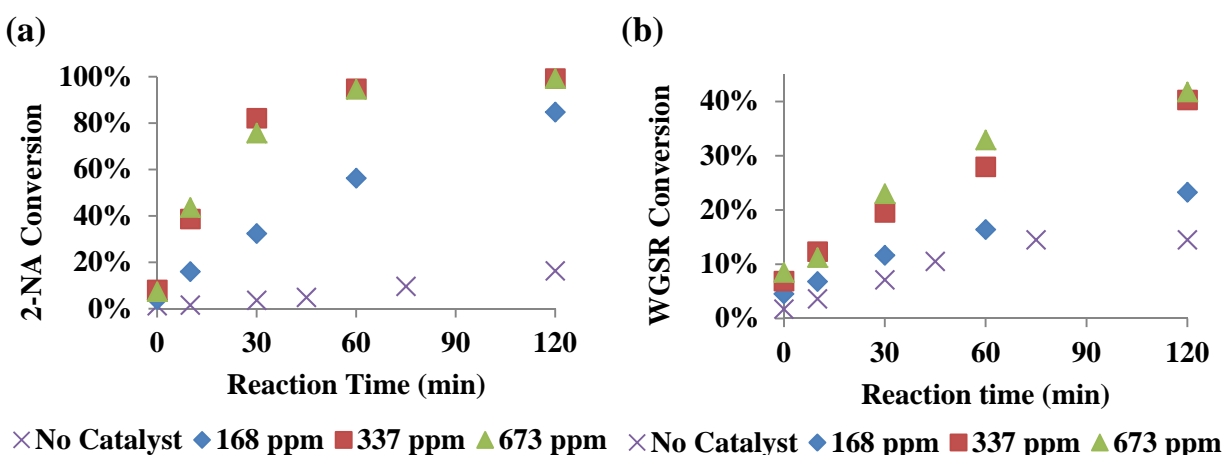


Figure 5-19 Reaction oil and gas phases evaluation at different MoS₂ loadings: (a) 2-NA conversion with time; (b) WGSR conversion with time. (300°C, 80ml toluene, 10ml water, 15psi H₂S, 585psi CO, ~1641ppmw 2-NA in toluene, 0~673ppmw Mo, 2hours)

A similar trend has been found for 2-NA removal. There was almost no 2-NA removed and only a few products were produced when there was no catalyst. However, only 168ppm Mo addition increased the oil phase 2-NA removal from 16.3% to 84.7% and the water phase 2-NA removal from 87.8% to 97.8% at 120min. The 2-NA removal rate increased more than 10 times from $2.3 \times 10^{-5} \text{ s}^{-1}$ to $25.5 \times 10^{-5} \text{ s}^{-1}$. Higher 2-NA removal was achieved by doubling the Mo loading from 168ppm Mo to 337ppm Mo. The 2-NA removal rate increased more than 3 times from

$25.5 \times 10^{-5} \text{ s}^{-1}$ to $81.2 \times 10^{-5} \text{ s}^{-1}$. The performance of 337ppm Mo and 673ppm Mo were very close with almost the same 2-NA removal performance (in oil and water phases), rate and selectivity. Since 337ppm had a similar performance as 673ppm, 337ppm Mo should be loaded for further investigation in order to reduce catalyst consumption.

Table 5-7 Summary of effect of MoS₂ loading under CO on 2-NA removal (300°C, 80ml toluene, 10ml water, 15psi H₂S, 585psi CO, ~1641ppmw 2-NA in toluene, 0~673ppmw Mo, 2hours)

	No Catalyst	168 ppm	337 ppm	673 ppm
2-NA Conversion % in Oil	16.3	84.7	99.2	99.2
2-NA Conversion % in H ₂ O	87.8	97.8	99.3	99.3
k _{2-NA Removal} (10 ⁻⁵ s ⁻¹)	2.3	25.5	81.2	78.2
k _{Decarboxylation} (10 ⁻⁵ s ⁻¹)	0.3	3.0	4.8	3.2
k _{HDO} (10 ⁻⁵ s ⁻¹)	2.0	21.2	70.7	68.4
k _{Cracking} (10 ⁻⁵ s ⁻¹)	0.0	1.3	5.8	6.6
Selectivity %				
Decarboxylation	11.7	11.8	5.9	4.2
HDO	87.2	82.9	87.0	87.4
Cracking	1.1	5.3	7.1	8.4
Product Distribution % at 120min				
Decarboxylation	11.9	13.3	8.2	4.5
HDO	88.1	86.7	91.8	95.5
Cracking	0.0	0.0	0.0	0.0
WGSR Conversion %	14.5	23.2	40.3	41.7
k _{WGSR} (10 ⁻⁵ s ⁻¹)	6.4	8.1	13.9	14.8
H ₂ Partial Pressure (psi)	293	449	559	555
Max. Pressure (psi)	1955	1900	1973	2066
Oil yield %	91.8	91.1	92.0	89.6
Water yield %	52.1	54.8	45.3	47.3
Mass balance %	84.5	85.8	85.0	84.1

5.3.4.3 Comparison of MoS₂ and MoO₃ catalysts under H₂

Since the comparison of MoS₂ and MoO₃ catalysts for 2-NA removal under CO involved the WGS, different WGS conversions should be obtained for MoS₂ and MoO₃. This resultant H₂ partial pressure difference might affect the evaluation of the catalyst for 2-NA removal. In order to eliminate the effect of the WGS, MoS₂ and MoO₃ catalysts were tested for 2-NA removal under only H₂. The preparation of MoS₂ and MoO₃ were the same as the preparation under CO. In the experiment with MoO₃, H₂S was not used for converting PMA into H₂S or for maintaining sulfides. The reaction was carried out at 300°C and 600psi as the initial total pressure.

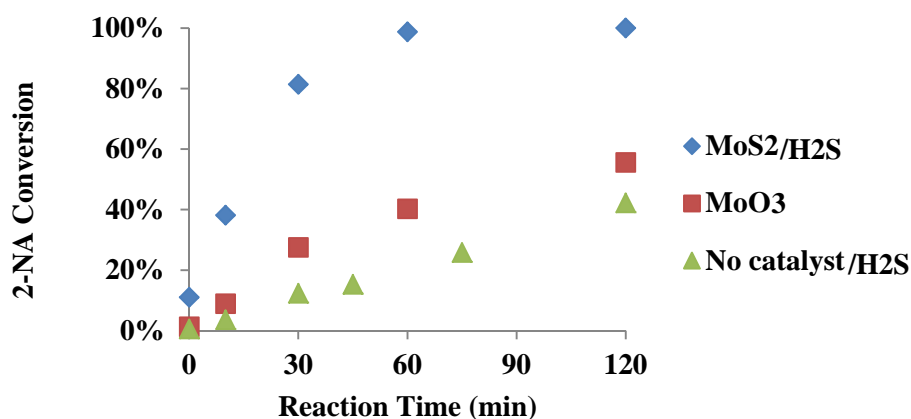


Figure 5-20 2-NA conversion with time by using different catalysts under H₂ (300°C, 80ml toluene, 10ml water, 15psi H₂S if added, 600psi total pressure, H₂ as gas feed, ~1641ppmw 2-NA in toluene, 337ppmw Mo, 2hours)

Although MoO₃ was found to be quite inactive for 2-NA removal under CO, it acted as a catalyst for 2-NA removal under H₂. As shown in Figure 5-20 and Table 5-8 Mo increased the 2-NA conversion from 42.2% to 55.6%, although the 2-NA removal in water decreased from 90.9% to 85.2%. The 2-NA removal rate increased from $6.5 \times 10^{-5} \text{ s}^{-1}$ to $14.2 \times 10^{-5} \text{ s}^{-1}$ by using MoO₃. Among all the pathways for 2-NA removal under H₂, not only was the decarboxylation improved, but the HDO was also enhanced. The HDO rate constant increased from $5.6 \times 10^{-5} \text{ s}^{-1}$ to $12.6 \times 10^{-5} \text{ s}^{-1}$. This implies that MoO₃ is capable of catalyzing HDO. MoO₃ also demonstrated a very low cracking selectivity of only 0.1%, and most of this decreased cracking selectivity finally contributed to the decarboxylation pathway. It should be noted that the water yield with MoO₃

was much lower than the water yield with MoS₂, which indicates a complicated water involved reaction mechanism when using MoO₃. Nevertheless, MoS₂ acted much better than MoO₃ with or without the effect of the WGSR. The conversion reached about 100% at 60min by using MoS₂ with H₂, and the 2-NA removal reaction constant was 88.9×10⁻⁵ s⁻¹ which was about 6 times higher than the rate constant when MoO₃ was used. High HDO enhancement in the presence of MoS₂ was considered as the main reason for this activity difference.

Table 5-8 Summary of effect of catalyst under H₂ on 2-NA removal (300°C, 80ml toluene, 10ml water, 15psi H₂S if added, 600psi total pressure, H₂ as gas feed, ~1641ppmw 2-NA in toluene, 337ppmw Mo, 2hours)

	No Catalyst w/H ₂ S	MoO ₃	MoS ₂ w/H ₂ S
2-NA Conversion % in Oil	42.2	55.6	100.0
2-NA Conversion % in H ₂ O	90.9	85.2	99.7
k _{2-NA Removal} (10 ⁻⁵ s ⁻¹)	6.5	14.2	88.9
k _{Decarboxylation} (10 ⁻⁵ s ⁻¹)	0.9	1.6	2.2
k _{HDO} (10 ⁻⁵ s ⁻¹)	5.6	12.6	80.2
k _{Cracking} (10 ⁻⁵ s ⁻¹)	0.03	0.02	6.4
Selectivity %			
Decarboxylation	13.8	11.2	2.5
HDO	85.7	88.6	90.2
Cracking	0.5	0.1	7.2
Product Distribution % at 120min			
Decarboxylation	12.6	11.5	3.4
HDO	87.4	88.5	96.6
Cracking	0.0	0.0	0.0
WGSR Conversion %	-	-	-
H ₂ Partial Pressure (psi)	1554	1346	1478
Max. Pressure (psi)	1759	1649	1788
Oil yield %	87.0	90.0	87.3
Water yield %	66.1	59.1	60.8
Mass balance %	84.3	85.8	88.2

5.3.4.4 Effect of MoS₂ catalysts under N₂

As discussed for the effect of gas feed, it was interesting to realize 2-NA removal with the help of the *in situ* nano unsupported MoS₂ catalyst in the presence of only N₂. The final high activity was proposed to derive from the high activity of the *in situ* MoS₂. In this section, two

comparison experiments are presented to demonstrate the impact of this novel *in situ* generated nano unsupported MoS₂ catalyst.

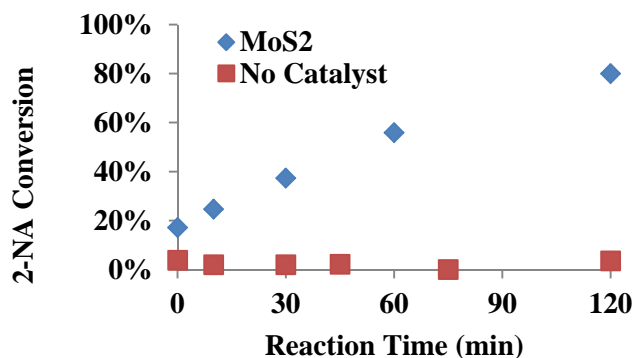


Figure 5-21 2-NA conversion with and without MoS₂ addition under N₂ (300°C, 80ml toluene, 10ml water, 15psi H₂S, 585psi N₂, ~1641ppmw 2-NA in toluene, 337ppmw Mo, 2hours)

Although the reaction under N₂ without the MoS₂ catalyst generated a slightly higher H₂ partial pressure (28 psi), there was almost no 2-NA removal observed. There was no benzoic acid formation either, and only a small amount of naphthalene and 2-methylnaphthalene were generated. As a result, the conversion changed very little as shown in Figure 5-21. The 2-NA conversion was only 0.1% without catalyst; while 80% conversion was achieved in the presence of the MoS₂ catalyst. As shown in Table 5-9 the operating pressure was much higher without the addition of catalyst. The lower water yield (49.6%) without catalyst indicates that more water was consumed during the reaction without MoS₂, producing more H₂ which increased the total reaction pressure. The low water yield might also be attributed to the loss of water during sampling. A detailed reaction mechanism under this condition was complicated, since subcritical water might be involved and affect the reaction. Further research should be implemented to understand the process under this condition in the future. It should also be noted that the introduction of catalyst influenced the selectivity of the reaction. The introduction of MoS₂ resulted in a large amount of benzoic acid formation at the beginning and finally yielded around 71.4% HDO products. Under a N₂ atmosphere, MoS₂ reduced the consumption of water, decreased the reaction pressure and also removed 2-NA from both the oil and water phases.

Table 5-9 Summary of MoS₂ catalyst addition on 2-NA removal under N₂ (300°C, 80ml toluene, 10ml water, 15psi H₂S, 585psi N₂, ~1641ppmw 2-NA in toluene, 337ppmw Mo, 2hours)

	No Catalyst	MoS ₂
2-NA Conversion % in Oil	0.1	80.0
2-NA Conversion % in H ₂ O	89.6	96.1
k _{2-NA Removal} (10 ⁻⁵ s ⁻¹)	<0.05	17.5
k _{Decarboxylation} (10 ⁻⁵ s ⁻¹)	-	0.6
k _{HDO} (10 ⁻⁵ s ⁻¹)	-	14.1
k _{Cracking} (10 ⁻⁵ s ⁻¹)	-	2.8
Product Distribution % at 120min		
Decarboxylation	15.0	3.2
HDO	85.0	71.4
Cracking	0.0	25.4
H ₂ Partial Pressure (psi)	28	8
Max. Pressure (psi)	2400	1926
Oil yield %	86.6	91.2
Water yield %	49.6	68.2
Mass balance %	81.3	87.1

5.3.5 Effect of water

5.3.5.1 Effect of water on 2-NA removal under CO

Bitumen emulsions contain about 30% water; however, the previous experiments used only 10g water (~12.6% in mass). It is necessary to treat more water in one reaction. However, there are several concerns for adding more water:

- H₂O was reported as an inhibitor for the HDO process (Badawi, Paul *et al.* 2011, Badawi, Paul *et al.* 2011);
- Additional H₂O may cause many uncertainties for the reaction system as the physical properties (supercritical or subcritical) were not clear;
- Significantly higher operation pressure would be obtained by water addition.

The 2-NA removal in the water phase is an important evaluation for this process. However, the low yield of purified water would limit the potential application of this. 10mL, 15mL and 20mL water amounts were chosen in this section to represent three different water mass percentages

(12.6%, 17.8% and 22.4%). The effects of different water amounts on 2-NA removal, operating pressure and final clean water yields have been examined and will be discussed.

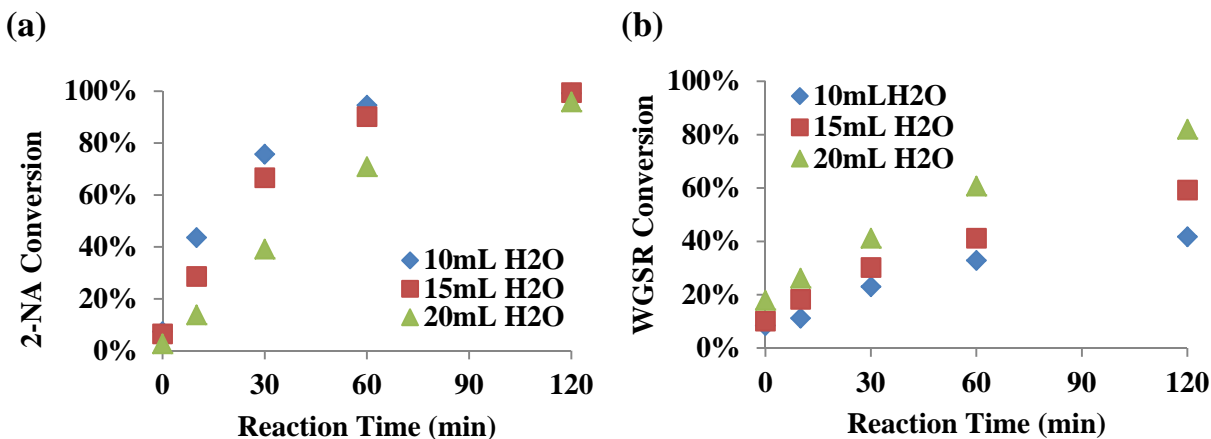


Figure 5-22 Reaction oil and gas phases evaluation at different water loadings under CO: (a) 2-NA conversion with time; (b) WGSR conversion with time (300°C, 80ml toluene, 10~20ml water, 15psi H₂S, 585psi CO, ~1641ppmw 2-NA in toluene, 673ppmw Mo, 2hours)

As shown in Figure 5-22(b), the WGSR was significantly improved when more water was added as a reagent. Consequently a higher H₂ partial pressure was obtained with higher WGSR conversion. As shown in Table 5-10 the H₂ partial pressure increased from 555psi to 1087 psi by increasing the water loading from 10mL to 20mL. However, the 2-NA removal was not improved even though higher H₂ partial pressure was attained when using more water. In fact, the reaction was inhibited slightly with the addition of more water, because the 2-NA conversion became lower as shown in Figure 5-22(a). In Table 5-10 it is found that the 2-NA removal rate decreased from the initial $78.2 \times 10^{-5} \text{ s}^{-1}$ with 10mL water to $71.8 \times 10^{-5} \text{ s}^{-1}$, and finally $34.0 \times 10^{-5} \text{ s}^{-1}$ by loading 15mL and 20mL water respectively. By analyzing the reaction rate of each reaction pathway it is noticed that the decarboxylation rate was not influenced, where $k_{\text{decarboxylation}}$ was around $3 \sim 4 \times 10^{-5} \text{ s}^{-1}$. On the other hand, both HDO and the cracking pathways were significantly inhibited. The HDO rate constant decreased from $68.4 \times 10^{-5} \text{ s}^{-1}$ to $29.8 \times 10^{-5} \text{ s}^{-1}$ by increasing the water loading from 10mL to 20mL; while the cracking rate constant decreased from $6.6 \times 10^{-5} \text{ s}^{-1}$ to $1.0 \times 10^{-5} \text{ s}^{-1}$. Among all of these three reaction pathways, the inhibition of HDO essentially influenced the total 2-NA removal. This observation is in agreement with the known water

inhibition effect on HDO of bio-fuels (Badawi, Cristol *et al.* 2009, Badawi, Paul *et al.* 2011, Badawi, Paul *et al.* 2011). Water destabilized the catalyst surface structure and reduced the catalyst activity. Based on a DFT study, water led to the exchange of an important fraction of edge sulfur atoms on the MoS₂ catalysts and changed the active sites (Badawi, Paul *et al.* 2011). In addition, there was a competitive adsorption between H₂O and oxygen containing compounds (Badawi, Paul *et al.* 2011). A further competitive adsorption study of the effect of water and HDO pathway might be able to reveal the detailed mechanism.

Due to the inhibition on both HDO and cracking, decarboxylation appeared to be of higher selectivity, although it maintained its own reaction rate. As shown in Table 5-10 the decarboxylation selectivity increased from 4.2% to 9.5%, leading to an increase in the decarboxylation product distribution from 4.5% to 10.1%. However, this selectivity and product distribution change was not favored for 2-NA removal and hydrotreating as discussed previously. Consequently the 2-NA removal under CO is more favorable under lower water loading. By comparing the operating pressures in Table 5-10, it is noticed that the maximum pressure increased significantly with additional water: the operation pressure increased more than 400 psi after adding an additional 10mL of water.

Based on the analysis in this section, it can be concluded that the additional water increased the operating pressure and inhibited the 2-NA removal in the oil phase. However, no significant inhibition in the water phase for 2-NA removal was observed. The removals were still very high at around 99.3~99.5%. In addition, more water yields were obtained with more water addition, which means this process can treat more dirty water. As shown in Table 5-10 the water yield% increased from 43% to 56%. It would be ideal to have both high 2-NA conversion and purified water yields, so a higher water amount should be examined in future under the reactor pressure limit. With respect to the data regarding “inhibition, pressure and water yields” with different amounts of water, computational simulation like ASPEN-HYSYS could be applied to predict the optimal condition.

5.3.5.2 Effect of water on 2-NA removal under N₂

Since the addition of the nano unsupported MoS₂ catalyst has been shown to be important for 2-NA removal under N₂, the effect of water should be discussed by comparing the feasibilities of 2-NA treatment with N₂ and CO. Given the positive effect of MoS₂ catalyst and the negative inhibition of water, it was possible to examine the highest water limit under such a catalyst addition amount. Accordingly 10mL, 15mL and 20mL water were added in the 2-NA removal experiments under N₂. Similar to the results reported in the previous section “effect of water under CO”, the system pressure increased significantly with the addition of water as shown in Table 5-10. However, the H₂ partial pressure did not increase (5~8psi) with more water addition, as there was almost no WGS. So the WGS should not be regarded as the H₂ source for reactions under N₂, and super- or sub-critical water could be responsible for the 2-NA removal. As shown in Figure 5-23, all the 2-NA removal under N₂ reached a certain conversion (~20%) during the beginning of the reaction. Over the duration of the reaction the 2-NA conversion slowly increased. The initial formation of benzoic acid as shown in Figure 5-23(b) indicated the cracking pathway which was responsible for this conversion at the beginning of reaction. It should also be noted that the mole percentage of benzoic acid increased during the beginning of the reaction but did not change considerably with time, no matter how much water loaded. The formation of this benzoic acid reached a constant value, which was the result of the equilibrium of the cracking pathway. It is also possible that the “cracking of 2-NA + H₂O of benzoic acid” chain reactions reached equilibrium and benzoic acid was formed as an intermediate. A detailed mechanistic study should be carried out for benzoic acid removal under N₂.

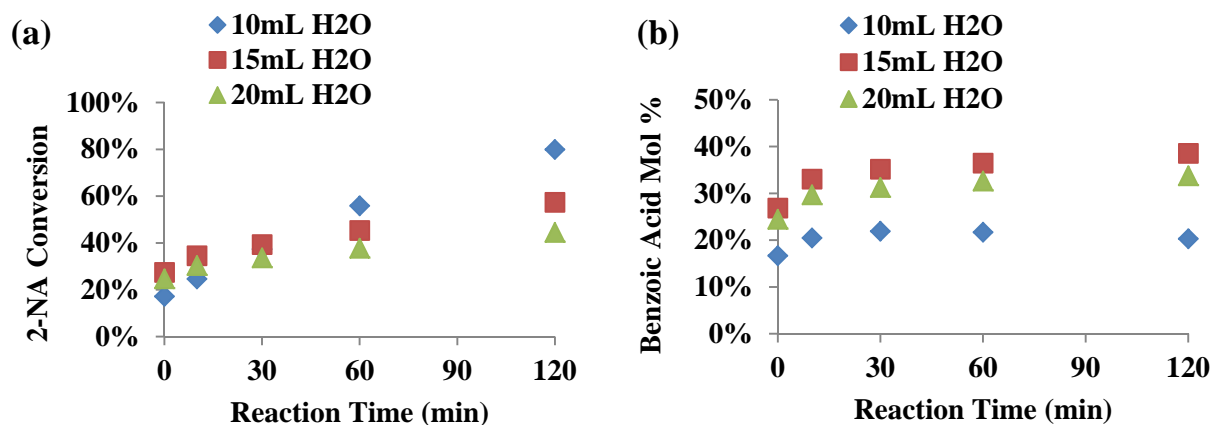


Figure 5-23 Reaction oil evaluation at different water loadings under N_2 : (a) 2-NA conversion with time; (b) Benzoic acid mol percentage with time (300°C, 80ml toluene, 10~20ml water, 15psi H_2S , 585psi N_2 , ~1641ppmw 2-NA in toluene, 673ppmw Mo, 2hours)

It is obvious that additional water inhibited the 2-NA removal as shown in Figure 5-23(a) and Table 5-10. The 2-NA conversion at 120min decreased from 80% to 44.5% on increasing water from 10mL to 20mL. 2-NA removal in water also dropped from 96.1% to 65.1% and 87.7% respectively by loading more water. The kinetic results shown in Table 5-10 clearly demonstrate this inhibition of water on 2-NA removal under N_2 . The 2-NA removal rate constant decreased from $17.5 \times 10^{-5} \text{ s}^{-1}$ to $3.9 \times 10^{-5} \text{ s}^{-1}$ by increasing water loading from 10mL to 20mL. By analyzing the reaction pathway it is observed that this inhibition was a result of the inhibition on HDO. This trend can also be observed in the Figure 5-24(a) by tracking the yield changes of the HDO products. Under CO with 10mL water the HDO reaction rate was fast and it reached equilibrium in around 30min. With the addition of water the reaction slowed down, but the reaction could still reach equilibrium. In presence of water, the catalyst under N_2 was deactivated by losing its HDO yield. Figure 5-24(b) gives a much clearer understanding of the effect of water on the reaction rate of each pathway. It appears that water inhibited the HDO reaction as discovered under both CO and N_2 , and this situation was much worse under N_2 no matter whether the H_2 partial pressure increased or decreased. The HDO removal rate constant under N_2 dropped from $14.1 \times 10^{-5} \text{ s}^{-1}$ to $1.5 \times 10^{-5} \text{ s}^{-1}$, which was a nearly 90% decline. This was due to the competitive adsorption of water compared with 2-NA, or water might destroy the catalyst active sites. On the other hand, decarboxylation and cracking pathways were not affected very much by increasing

the addition of water. So decarboxylation and cracking pathways might depend on different active sites compared to HDO. Due to this strong inhibition on HDO, cracking started to take over the reaction selectivity from 15.8% to 56.2% as shown in Figure 5-24(c), and benzoic acid occupied 75.9% of the final products which contained no benzoic acid at all when CO was used.

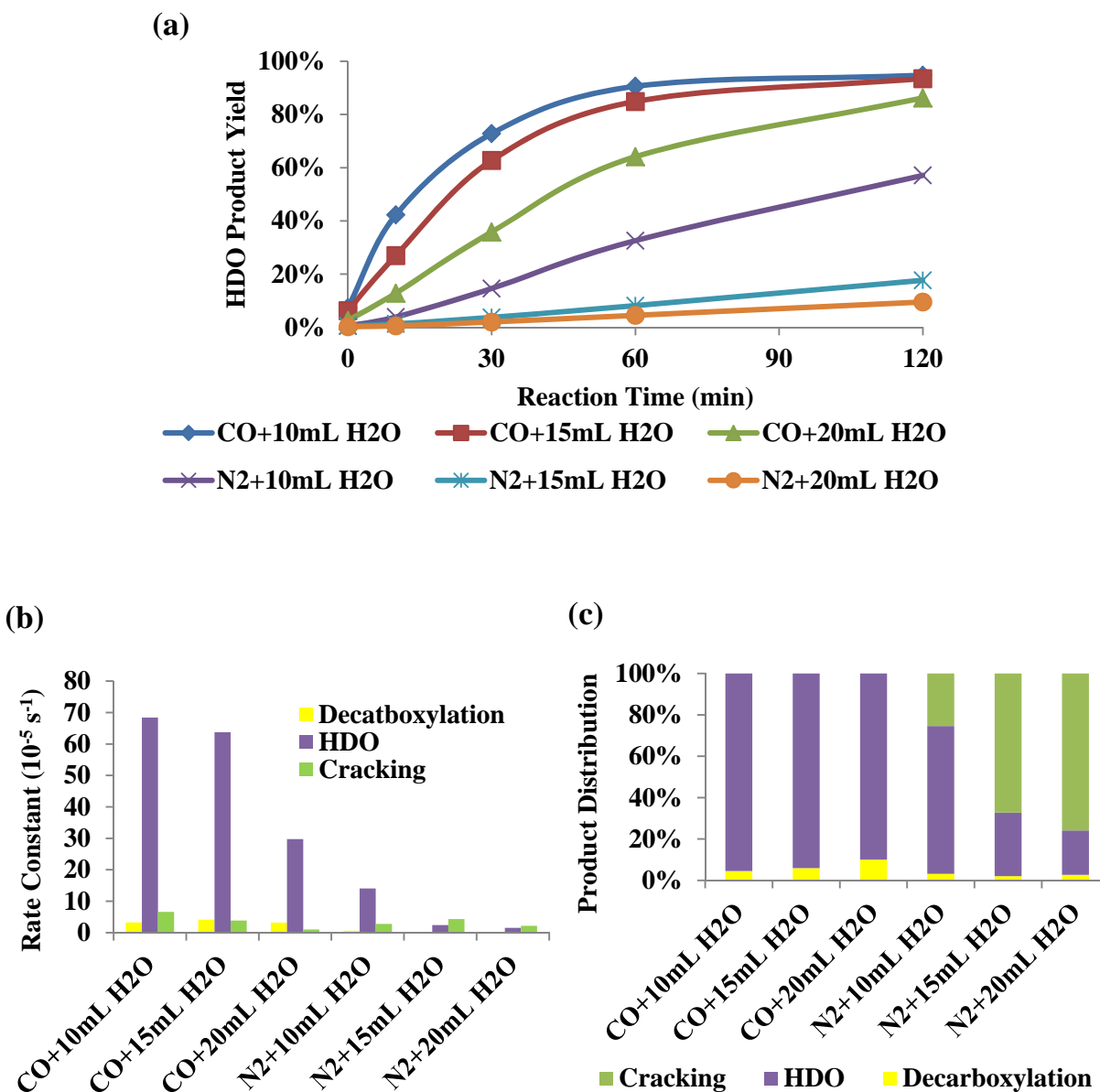


Figure 5-24 Effect of water under CO and N₂: (a) yield of HDO products; (b) reaction rate constants; (c) final product distribution (300°C, 80ml toluene, 10~20ml water, 15psi H₂S, 585psi CO or N₂, ~1641ppmw 2-NA in toluene, 673ppmw Mo, 2hours)

In conclusion, CO was a much better reaction gas feed producing high HDO activity but also maintained certain catalyst stability in the presence of water.

Table 5-10 Summary of effect of water on 2-NA removal under CO and N₂ (300°C, 80ml toluene, 10-20ml water, 15psi H₂S, 585psi CO or N₂, ~1641ppmw 2-NA in toluene, 673ppmw Mo, 2hours)

	CO			N ₂		
	10mL H ₂ O	15mL H ₂ O	20mL H ₂ O	10mL H ₂ O	15mL H ₂ O	20mL H ₂ O
2-NA Conversion % in Oil	99.2	99.4	95.9	80.0	57.4	44.5
2-NA Conversion % in H ₂ O	99.3	99.3	99.5	96.1	65.1	87.7
k _{2-NA Removal} (10 ⁻⁵ s ⁻¹)	78.2	71.8	34.0	17.5	7.0	3.9
k _{Decarboxylation} (10 ⁻⁵ s ⁻¹)	3.2	4.1	3.2	0.6	0.2	0.2
k _{HDO} (10 ⁻⁵ s ⁻¹)	68.4	63.7	29.8	14.1	2.4	1.5
k _{Cracking} (10 ⁻⁵ s ⁻¹)	6.6	3.9	1.0	2.8	4.3	2.2
Selectivity %						
Decarboxylation	4.2	5.8	9.5	3.5	3.0	4.9
HDO	87.4	88.8	87.5	80.6	34.9	38.9
Cracking	8.4	5.4	3.0	15.8	62.0	56.2
Product Distribution % at 120min						
Decarboxylation	4.5	6.0	10.1	3.2	2.0	2.7
HDO	95.5	94.0	89.9	71.4	30.8	21.4
Cracking	0.0	0.0	0.0	25.4	67.2	75.9
WGSR Conversion %	41.7	59.3	82.0	-	-	-
k _{WGSR} (10 ⁻⁵ s ⁻¹)	14.8	23.7	33.6	-	-	-
H ₂ Partial Pressure (psi)	555	1056	1087	8	5	6
Max. Pressure (psi)	2066	2262	2458	1926	2165	2331
Oil yield %	91.6	91.9	91.3	91.2	92.6	94.6
Water yield %	43.5	51.2	56.0	68.2	87.0	69.1
Mass balance %	83.7	84.2	82.6	87.1	89.8	87.3

5.3.6 Simultaneous 2-NA removal and HDS of DBT with *in situ* H₂

Organic sulfur species in bitumen are able to cause significant environmental problems and poison downstream noble metal catalysts. HDS is a catalytic chemical process widely used to remove sulfur from natural gas and from refined petroleum products such as gasoline or petrol, jet fuel, kerosene, diesel fuel, etc. As shown in Table 3, simultaneous 2-NA removal and HDS of DBT was achieved at 415°C. 93.2% conversion of DBT was obtained with almost 100% removal of 2-NA in both the oil and water phases. This means the combined HDO and HDS process is feasible during the novel bitumen emulsion upgrading process presented in this thesis. However the high reaction temperature made it difficult to analyze the mutual effect of 2-NA removal and HDS on the DBT processes. 2-NA was almost all removed in the beginning of reaction, which resulted in no effect on the HDS of DBT. As a result, the simultaneous 2-NA removal and HDS of the DBT process was investigated at lower temperatures (300 °C and 340°C) to understand the relationship between these two reactions.

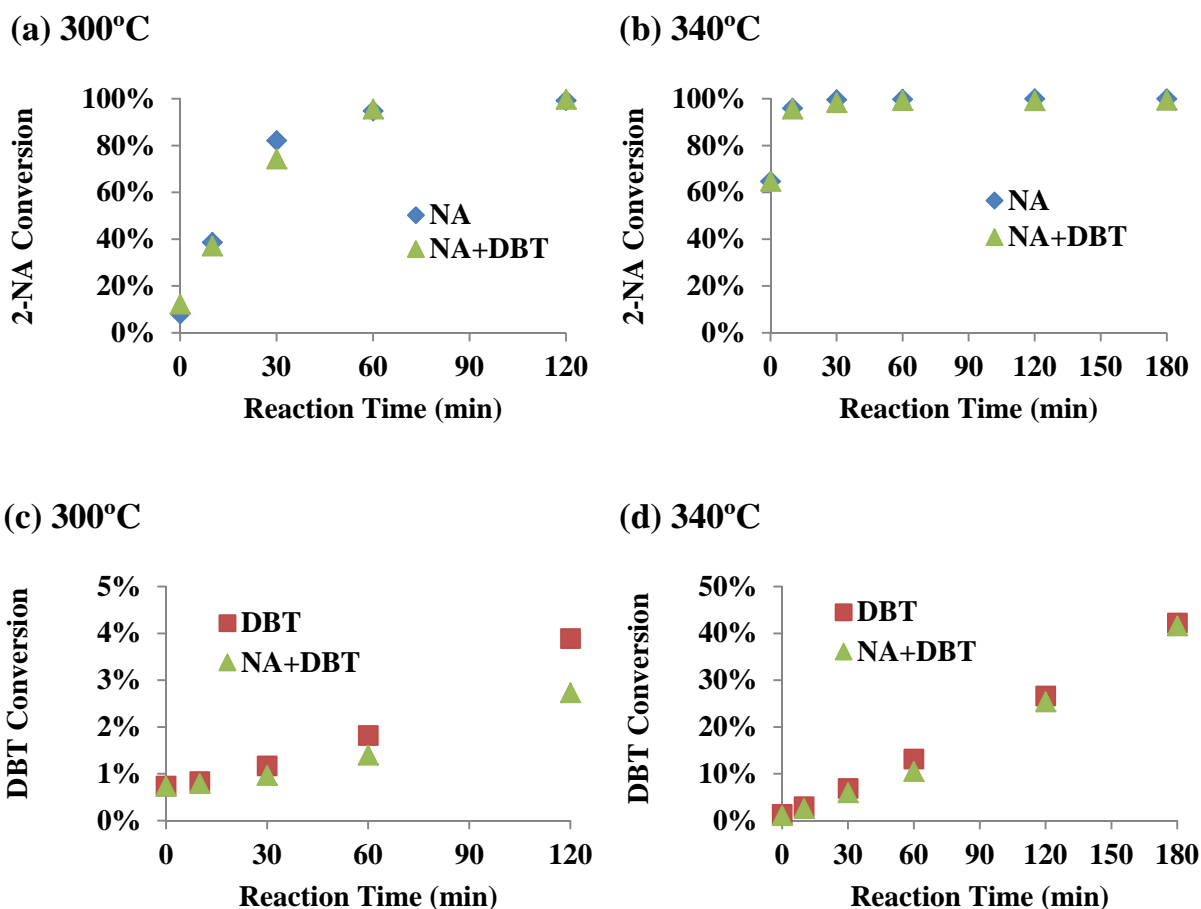


Figure 5-25 Reaction oil evaluation with and without DBT addition: (a) 2-NA conversion with time at 300°C; (b) 2-NA conversion with time at 340°C; (c) DBT conversion with time at 300°C; (d) DBT conversion with time at 340°C (300~340°C, 80ml toluene, 10ml water, 15psi H₂S, 585psi CO, ~1641ppmw 2-NA, ~5000ppmw DBT, 337ppmw Mo, 2~3hours)

As shown in Table 5-11, Figure 5-25(a) and Figure 5-25(b), the 2-NA conversions in the oil and water phases did not change significantly on the addition of DBT at either 300°C or 340°C. The 2-NA removal reaction rate was around $81\sim 85 \times 10^{-5} \text{ s}^{-1}$ with a $70\sim 73 \times 10^{-5} \text{ s}^{-1}$ HDO reaction rate at 300°C as shown in Table 5-11. The HDO selectivity was also stable at 85~87% at 300°C no matter whether DBT was added or not. Due to the high initial 2-NA conversion, it was difficult to collect kinetic results at 300°C. The WGSR rates were also very close to each other at around $36\sim 40 \times 10^{-5} \text{ s}^{-1}$ at 300°C and $46\sim 53 \times 10^{-5} \text{ s}^{-1}$ at 340°C. It appears that the addition of DBT did not

affect either 2-NA removal or the WGSR. This can be explained by the stronger adsorption of 2-NA and water than sulfur species on the catalyst active sites. On the other hand, DBT conversion was affected by 2-NA removal at 300°C as shown in Figure 5-25(c). Due to the low reaction temperature, the DBT conversion reached only 3.9% after 2 hours; however the DBT conversion in the presence of 2-NA was even lower at 2.7%. The inhibition can be clearly noticed as the pseudo-first order rate of HDS of DBT decreased from $0.3 \times 10^{-5} \text{ s}^{-1}$ to $0.2 \times 10^{-5} \text{ s}^{-1}$. The rates for the two reaction pathways: DDS (direct-desulfurization) and HYD (hydrogenation) also decreased by about 50% as shown in Table 5-11. It seems that 2-NA inhibited both pathways of HDS, so the HDS selectivity distribution did not change very much. DDS was around 26~27%, and HYD was about 73~74%. The same trend was also observed for the HDS of DBT at 340°C. Due to the quick removal of 2-NA at 340°C, 2-NA only inhibited the initial HDS rate which decreased from $4.1 \times 10^{-5} \text{ s}^{-1}$ to $2.8 \times 10^{-5} \text{ s}^{-1}$. Both HDS pathways were suppressed with decreased DDS and HYD reaction rates; the selectivity of the DDS decreased slightly more than HYD. This suggests that the 2-NA molecule preferred to adsorb on DDS active sites more than on the HYD active sites, although adsorption occurred on both sites. It has been reported that oxygen species had a higher tendency to adsorb on the MoS₂ catalyst than sulfur species (Laurent and Delmon 1993), which could be the reason for this inhibition on HDS of DBT. 2-NA was easier to adsorb on the MoS₂ catalyst surface and reacted with *in situ* H₂, while DBT had a lower likelihood to adsorb on the catalyst for HDS. This is why 2-NA removal was not affected by DBT at either 300°C or 340°C. 2-NA occupied most of the active sites on MoS₂; DBT had less catalyst active sites available for the HDS reaction (both DDS and HYD active sites), until 2-NA was eventually removed. This phenomenon is shown in Figure 5-25(d): the DBT conversion in “NA+DBT” reached almost the same level as the HDS conversion in “DBT” only after most of the 2-NA was removed. After removing 2-NA at 340°C the DBT conversion reached around 41.6%, which was also close to the 42.2% of the DBT conversion without 2-NA.

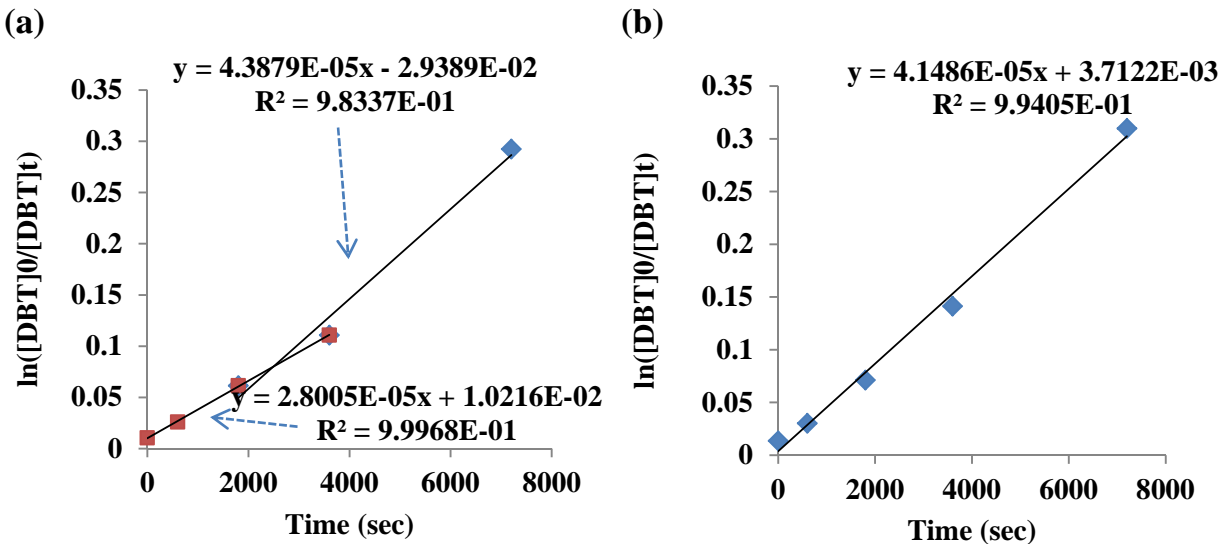


Figure 5-26 Kinetic analysis of HDS of DBT with and without 2-NA addition at 340°C: (a) HDS of DBT with simultaneous 2-NA removal; (b) HDS of only DBT (340°C, 80ml toluene, 10ml water, 15psi H₂S, 585psi CO, ~1641ppmw 2-NA, ~5000ppmw DBT, 337ppmw Mo, 2hours)

Note: color difference in (a) represents the selection of points (before and after 2-NA was consumed) for creating trend lines.

Figure 5-26 reveals this inhibition of 2-NA on the HDS rate of DBT. In Figure 5-26(a) the slopes represent the HDS rate constant which increased after 30min, when most of the 2-NA was removed. The initial rate was lower at $2.8 \times 10^{-5} \text{ s}^{-1}$, while the final rate was higher at $4.4 \times 10^{-5} \text{ s}^{-1}$. Figure 5-26(b) shows the rate ($4.1 \times 10^{-5} \text{ s}^{-1}$) in the absence of 2-NA, which was very close to the final rate in Figure 5-26(a). This indicates that the catalyst active sites retained their activities without permanent deactivation caused by 2-NA for the HDS reaction. H₂S is likely required to maintain HDS activity by providing a sulfiding condition in reactor.

Table 5-11 Summary of simultaneous 2-NA removal and HDS of DBT (300~340°C, 80ml toluene, 10ml water, 15psi H₂S, 585psi CO, ~1641ppmw 2-NA, ~5000ppmw DBT, 337ppmw Mo, 2~3hours)

	300°C			340°C		
	NA	DBT	NA+DBT	NA	DBT	NA+DBT
2-NA Conversion % in Oil	99.2	-	99.8	100.0	-	99.3
2-NA Conversion % in H ₂ O	99.3	-	99.9	99.5	-	99.9
k _{2-NA Removal} (10 ⁻⁵ s ⁻¹)	81.2	-	85.2	-	-	-
k _{Decarboxylation} (10 ⁻⁵ s ⁻¹)	4.8	-	4.3	-	-	-
k _{HDO} (10 ⁻⁵ s ⁻¹)	70.7	-	73.0	-	-	-
k _{Cracking} (10 ⁻⁵ s ⁻¹)	5.8	-	7.9	-	-	-
Selectivity %						
Decarboxylation	5.9	-	5.1	-	-	-
HDO	87.0	-	85.6	-	-	-
Cracking	7.1	-	9.3	-	-	-
Product Distribution % at the end of reaction						
Decarboxylation	8.2	-	4.0	19.4	-	15.4
HDO	91.8	-	96.0	80.6	-	84.6
Cracking	0.0	-	0.0	0.0	-	0.0
DBT Conversion %	-	3.9	2.7	-	42.2	41.6
k _{DBT Removal} (10 ⁻⁵ s ⁻¹)	-	0.31	0.19	-	4.1	2.8
k _{DDS} (10 ⁻⁵ s ⁻¹)	-	0.09	0.05	-	2.2	1.3
k _{HYD} (10 ⁻⁵ s ⁻¹)	-	0.22	0.14	-	1.9	1.4
HDS Selectivity %						
DDS	-	27.6	25.6	-	52.7	48.0
HYD	-	71.7	73.7	-	46.0	51.0
WGSR Conversion %	40.3	40.6	35.7	48.8	46.0	52.7
k _{WGSR} (10 ⁻⁵ s ⁻¹)	13.9	14.8	11.2	16.5	14.8	14.8
H ₂ Partial Pressure (psi)	559	621	544	739	720	796
Max. Pressure (psi)	1973	1986	1908	2383	2304	2329
Oil yield %	92.0	94.0	89.7	92.0	89.8	88.4
Water yield %	45.3	47.3	46.1	29.3	38.2	44.1
Mass balance %	85.0	86.9	83.1	80.7	81.0	81.3

5.3.7 Simultaneous 2-NA removal and HDA of naphthalene (NAPH) with *in situ* H₂

Hydrodearomatization (HDA) which is achieved by hydrogenating aromatic rings plays a key role in hydrotreating processes. As it has been reported that the content of three and larger ring aromatic compounds controls heavy oil desulfurization (Choudhary, Parrott *et al.* 2008). It is also believed that in deep hydrodesulfurization and hydrodenitrogenation, partial hydrogenation of aromatic rings facilitate the cleavage of C-S and C-N bonds to liberate H₂S and NH₃, respectively (Ho 2004). Moreover, HDA can improve hydrocracking by facilitating saturated hydrocarbons production via the cleavage of the aromatic rings on the metal and acid catalysts (McVicker, Daage *et al.* 2002). In this way HDA of polycyclic aromatic hydrocarbons to monocyclic aromatics can improve quality without increasing diesel particulate emissions. As a result, the simultaneous 2-NA removal and HDA of NAPH was conducted in order to evaluate the mutual effects of these two processes.

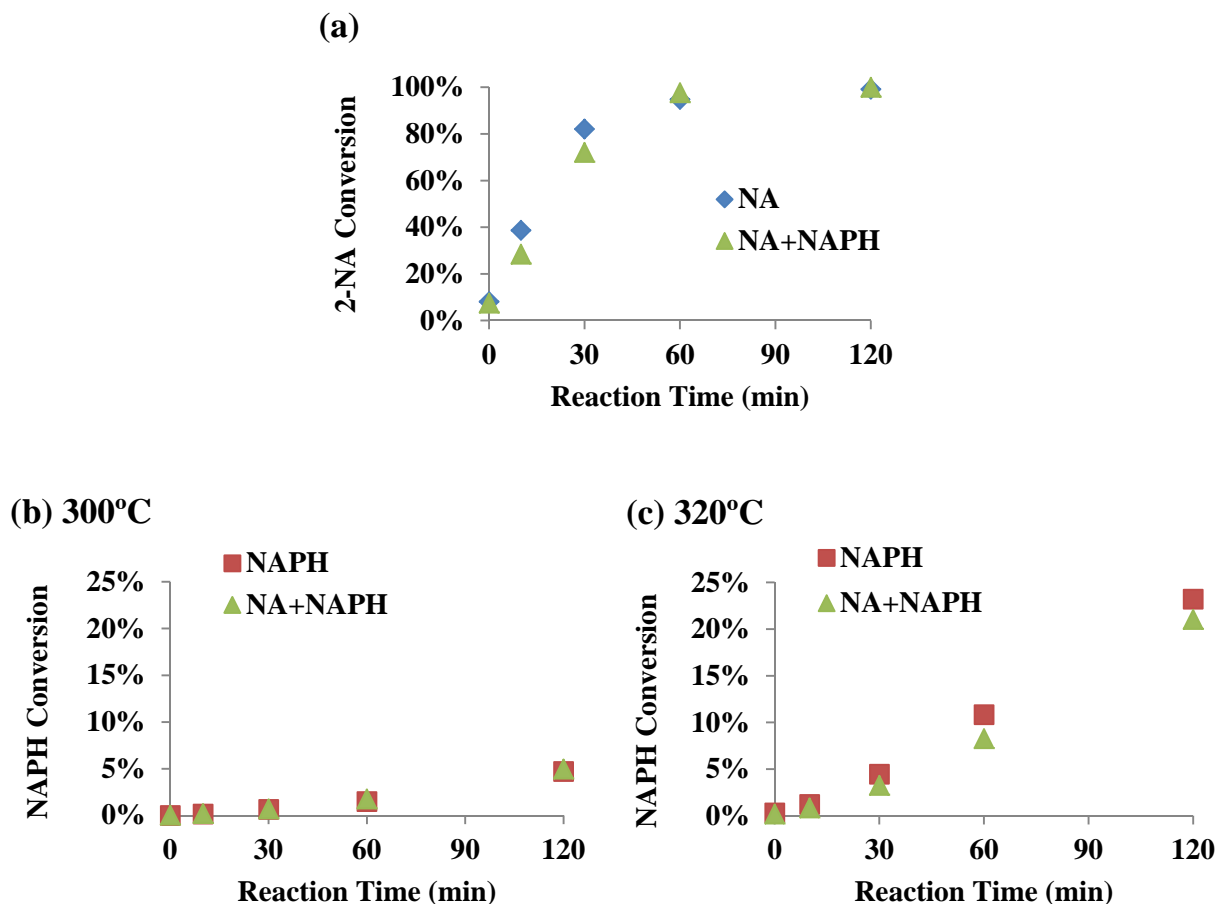


Figure 5-27 Reaction oil evaluation with and without NAPH addition: (a) 2-NA conversion with time at 300°C; (b) NAPH conversion with time at 300°C; (c) NAPH conversion with time at 320°C (300~320°C, 80ml toluene, 10ml water, 15psi H₂S, 585psi CO, ~1641ppmw 2-NA, ~5000ppmw NAPH, 337ppmw Mo, 2hours)

As shown in Table 5-12 and Figure 5-27(a), the 2-NA removal comparison was carried out with and without the addition of NAPH at 300°C. It was noticed that the 2-NA conversions in both oil and water phases were almost the same no matter whether NAPH was added or not. It should be noted that NAPH was also the product of the decarboxylation of 2-NA, so the addition of NAPH made it difficult to analyze the decarboxylation kinetics. However, the rate of 2-NA removal at 300°C was still available and deemed quite accurate. It was noticed that this 2-NA removal rate decreased from $81.2 \times 10^{-5} \text{ s}^{-1}$ to $68.3 \times 10^{-5} \text{ s}^{-1}$, which was a 16% decline. Since NAPH, a product of the decarboxylation of 2-NA, was added in this reaction, the decarboxylation rate was unable

to be calculated. However, this 2-NA removal rate decline could still be attributed to the HDO rate change. It is found that the HDO rate dropped from $70.7 \times 10^{-5} \text{ s}^{-1}$ to $62.7 \times 10^{-5} \text{ s}^{-1}$, which resulted in a decrease in the 2-NA removal rate on the addition of NAPH. NAPH and 2-NA have similar molecular structures; however, 2-NA is expected to have stronger adsorption ability due to its carboxylic acid group. The competitive adsorption between these two molecules inhibited the HDA of NAPH instead of the 2-NA removal. Hence this inhibition on 2-NA removal by NAPH addition was caused by some reason other than competitive adsorption. As shown in Table 5-12 the H_2 partial pressure dropped from 559 psi to 471 psi, thus, reduced by 16%. It should be noted that the HDA of NAPH required a large amount of H_2 for hydrogenating the aromatic rings. And the H_2 partial pressure drop was exactly same as the 2-NA rate constant drop. This phenomenon implies that the inhibition of NAPH on 2-NA removal could be a result of a drop in H_2 partial pressure instead of competitive adsorption.

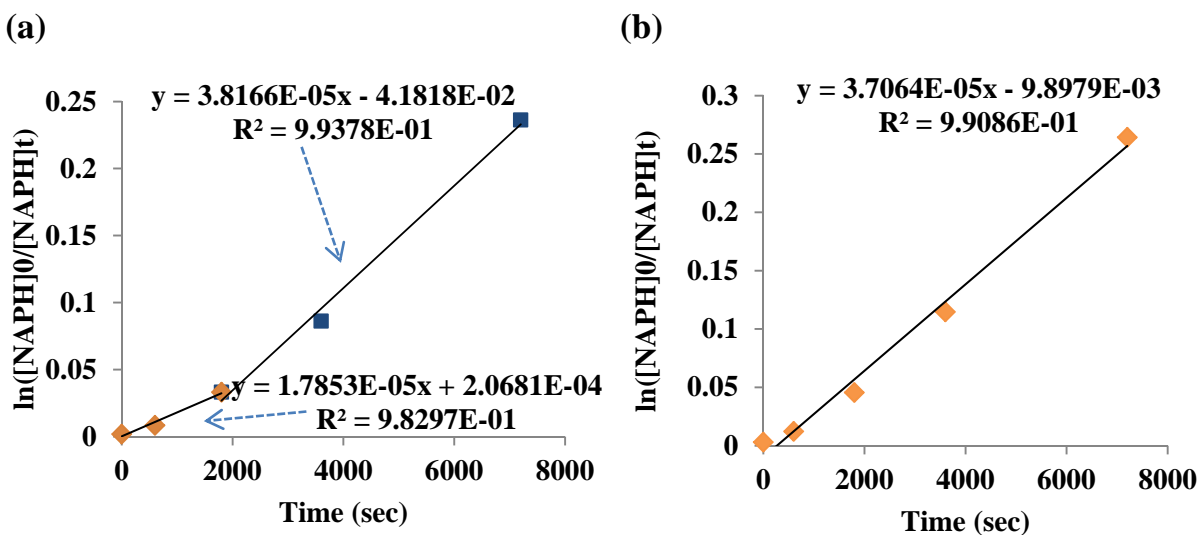


Figure 5-28 Kinetic analysis of HDA of NAPH with and without 2-NA addition at 320°C: (a) HDA of NAPH with simultaneous 2-NA removal; (b) HDA of only NAPH (320°C, 80ml toluene, 10ml water, 15psi H_2S , 585psi CO , ~1641ppmw 2-NA, ~5000ppmw NAPH, 337ppmw Mo, 2hours)

Figure 5-27(b) demonstrates the NAPH conversion change with simultaneous 2-NA removal at 300°C. It is noticed that the NAPH conversion was extremely low (~5%) at 300°C, and the final

conversion change was not significant for the addition of 2-NA. The HDA rate constants were also very close at around $0.4 \times 10^{-5} \text{ s}^{-1}$. This small difference made it difficult to analyze the effect of 2-NA on HDA of NAPH. At a higher temperature, a more significant difference for the reaction was observed. For instance, a slight change in the NAPH conversion is observed in Figure 5-27(c), where the NAPH conversion dropped from 23.2% to 21%. The HDA reaction rate decreased from $3.7 \times 10^{-5} \text{ s}^{-1}$ to $1.8 \times 10^{-5} \text{ s}^{-1}$ with the addition of 2-NA. It is also interesting that the system maximum operation pressure and H_2 partial pressure increased with the addition of 2-NA. This could be explained by the additional water produced via the HDO of 2-NA. The water increased the system pressure and also reacted with CO to generate more H_2 . Since a higher H_2 partial pressure was achieved to improve HDA, competitive adsorption would be the only possible cause for 2-NA's inhibition for the HDA of NAPH. Figure 5-28 represents how this competitive adsorption inhibited the HDA reaction. As shown in Figure 5-28(a) the HDA rate constant was only $1.78 \times 10^{-5} \text{ s}^{-1}$ before most of the 2-NA was removed; the HDA rate constant increased to $3.82 \times 10^{-5} \text{ s}^{-1}$ after 30min. This value was very close to the rate constant obtained without 2-NA addition at $3.71 \times 10^{-5} \text{ s}^{-1}$ as shown in Figure 5-28(b). Similar to the simultaneous HDS and 2-NA removal, competitive adsorption on catalyst active sites also existed in the simultaneous HDA and 2-NA removal. 2-NA had relatively higher adsorption ability to absorb on the catalyst active sites, which reduced the HDS and HDA reaction rates. Once most of the 2-NA was removed, the active sites started to react with DBT and NAPH with almost the same reaction rate as the fresh catalyst. This restoration of catalyst activity is important for the feasibility of future of a combined bitumen emulsion upgrading process. Oxygen species have been reported for exchange of the MoS_2 catalyst edge structure and deactivation of the catalysts, hence the existence of naphthenic acids were highly possible to deactivate the MoS_2 catalysts, thus leading a loss in hydrotreating activity. It would be ideal for the catalyst to restore its activity after removing all the naphthenic acids without losing activity, since most hydrotreating reactions occur at higher temperature. The activity restoration observed for both simultaneous HDS and 2-NA removal and simultaneous HDA and 2-NA removal suggests possible future application of this novel process. The existence of H_2S as a reducing atmosphere has been proposed to be responsible for maintaining this catalyst activity. Further investigations on the effect of H_2S should be carried out in order to gain a better understanding of this process.

Table 5-12 Summary of simultaneous 2-NA removal and HDA of NAPH (300~320°C, 80ml toluene, 10ml water, 15psi H₂S, 585psi CO, ~1641ppmw 2-NA, ~5000ppmw NAPH, 337ppmw Mo, 2hours)

	300°C			320°C	
	NA	NAPH	NA+NAPH	NAPH	NA+NAPH
2-NA Conversion % in Oil	99.2	-	100.0	-	100.0
2-NA Conversion % in H ₂ O	99.3	-	100.0	-	100.0
k _{2-NA Removal} (10 ⁻⁵ s ⁻¹)	81.2	-	68.3	-	-
k _{Decarboxylation} (10 ⁻⁵ s ⁻¹)	4.8	-	-	-	-
k _{HDO} (10 ⁻⁵ s ⁻¹)	70.7	-	62.7	-	-
k _{Cracking} (10 ⁻⁵ s ⁻¹)	5.8	-	-	-	-
Selectivity %					
Decarboxylation	5.9	-	-	-	-
HDO	87.0	-	-	-	-
Cracking	7.1	-	-	-	-
NAPH Conversion %	-	4.7	5.0	23.2	21.0
k _{NAPH Removal} (10 ⁻⁵ s ⁻¹)	0.0	0.43	0.38	3.7	1.8
WGSR Conversion %	40.3	35.6	33.6	33.7	41.3
k _{WGSR} (10 ⁻⁵ s ⁻¹)	13.9	11.7	11.0	12.4	18.5
H ₂ Partial Pressure (psi)	559	408	471	695	708
Max. Pressure (psi)	1973	1609	1824	2218	2147
Oil yield %	92.0	92.4	88.5	90.8	89.4
Water yield %	45.3	38.4	37.1	48.3	41.0
Mass balance %	85.0	83.0	83.4	83.9	84.6

5.3.8 Effect of metal additives

Ni and Co are known as common promoters for hydrotreating catalysts. For this novel one-step process which combines upgrading with 2-NA removal, the effect of promoters should be discussed to determine the effects of these two metals on 2-NA removal. Ni and Co have been reported to provide higher catalyst activity and stability based on publications on biomass HDO reactions by using hydrotreating catalysts; however, there have been no publications regarding the HDO of 2-NA by using Ni or Co promoted catalyst. In the biomass studies, Co promoted the HDO performance of supported catalysts in HDO of furan (Chary, Rao *et al.* 1991, Chiranjeevi, Kumar *et al.* 2002), methyl-substituted phenols (Massoth, Politzer *et al.* 2006). It was reported by Bui that the HDO of guaiacol has two reaction pathways hydrogenation (HYD) and direct (DDO), which individually are each carried out on a single catalytic site. Bui also realized that the presence of the CoMoS phase in unsupported the MoS₂ catalyst increased the direct DDO pathway involved in guaiacol conversion strongly (Bui, Laurenti *et al.* 2011). Furthermore, some DFT research has been carried out from which it was reported that Co increased not only the intrinsic activity of the catalyst (promotion effect) but also stabilized the active phase in the presence of water (passivation effect). This passivation effect was because a result in that Co atoms prevent sulfur–oxygen exchanges on the catalyst surface (Badawi, Paul *et al.* 2011). In addition, Co and Ni have also been looked at as promoters for HDO of biomass such as furan (Chary, Rao *et al.* 1991, Chiranjeevi, Kumar *et al.* 2002). Some DFT work on Ni-Mo catalysts has been carried out in France and it was reported that the activation energy was smaller for NiMoS than for MoS₂ for the HDO of methyl propanoate, propanoic acid, propanal, propanol (Dupont, Lemeur *et al.* 2011). Moreover, Ni and Co were shown to promote the WGS in a novel emulsion upgrading process (Jia, Al-Ghamdi *et al.* 2011). The increased H₂ partial pressure is expected to have some positive influence on 2-NA removal. In this section Ni and Co were chosen as metal additives for 2-NA removal experiments. The metal:Mo ratio was 0.2 :1.

Increased WGS conversions were observed by adding Co and especially Ni as shown in Figure 5-29(b). The WGS conversion increased from 41.7% to 54.3% and 70.3% by adding Co and Ni respectively. The WGS rate constant also increased from $14.8 \times 10^{-5} \text{ s}^{-1}$ with unpromoted MoS₂ to $19.7 \times 10^{-5} \text{ s}^{-1}$ (Co-Mo) and $25.4 \times 10^{-5} \text{ s}^{-1}$ (Ni-Mo). However this improvement in the WGS

finally resulted in only a slight increase in the H₂ partial pressure, due to the consumption of H₂ for 2-NA removal.

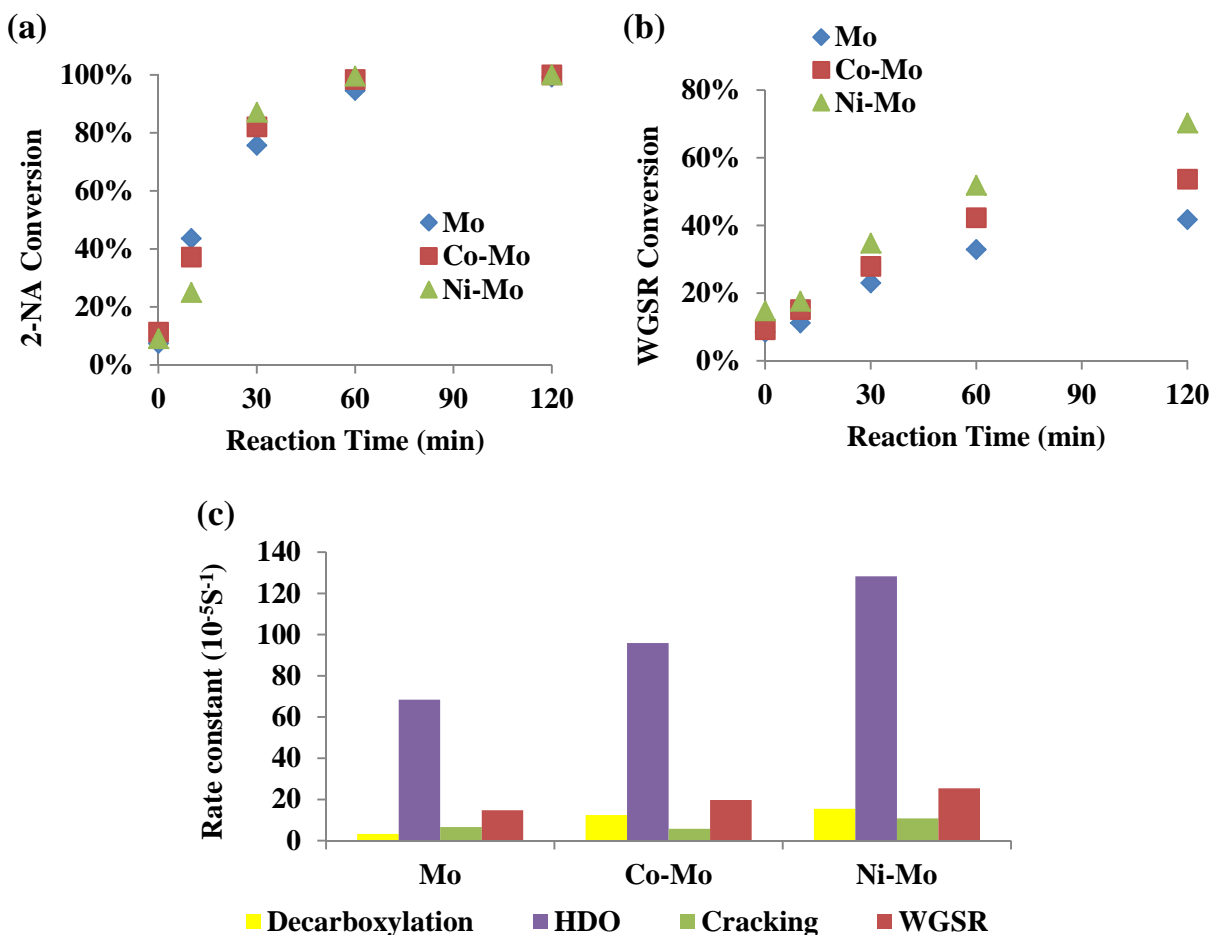


Figure 5-29 Reaction oil and gas phases evaluation with different metal additives under CO: (a) 2-NA conversion with time; (b) WGSR conversion with time; (c) rate constants for different pathways of 2-NA removal and WGSR (300°C, 80ml toluene, 10ml water, 15psi H₂S, 585psi CO, ~1641ppmw 2-NA in toluene, 673ppmw Mo, metal:Mo ratio=0.2, 2hours)

The 2-NA conversion change shown in Figure 5-29(a) does not reveal any distinguishable promotion with the addition of Co and Ni. Co and Ni addition only slightly increased 2-NA removal in both the oil and water phases as shown in Table 5-13. 2-NA was almost completely removed after a short time of around 60min, which was very similar for Mo, Co-Mo and Ni-Mo. The sampling points collected before 60 minutes would determine the reaction rates. Based on a

pseudo-first order rate analysis, promotion was observed as the 2-NA removal rate constant increased from $78.2 \times 10^{-5} \text{ s}^{-1}$ (unpromoted Mo) to $114.1 \times 10^{-5} \text{ s}^{-1}$ (Co-Mo) and $154.6 \times 10^{-5} \text{ s}^{-1}$ (Ni-Mo) shown in Table 5-13. This incremental increase in the rate constant with Co-Mo and Ni-Mo compared to unpromoted Mo was 46% and 98% respectively. Among all of the 2-NA removal reaction pathways it is noticed that the Co and Ni promoted both decarboxylation and HDO pathways. As shown in Table 5-13 the decarboxylation rate constant increased from $3.2 \times 10^{-5} \text{ s}^{-1}$ (unpromoted Mo) to $12.5 \times 10^{-5} \text{ s}^{-1}$ (Co-Mo) and $15.5 \times 10^{-5} \text{ s}^{-1}$ (Ni-Mo); while the HDO rate also increased from $68.4 \times 10^{-5} \text{ s}^{-1}$ (unpromoted Mo) to $95.9 \times 10^{-5} \text{ s}^{-1}$ (Co-Mo) and $128.3 \times 10^{-5} \text{ s}^{-1}$ (Ni-Mo). The selectivity distribution was slightly varied with the addition of Co and Ni. Decarboxylation was more favored for both Co and Ni, and the relative selectivity increased from 4% to 10~11%. This is consistent with a previous publication regarding the role of Ni on biomass decarboxylation, which claimed that the Ni present in Ni monosulfide enhanced the decarbonylation pathway (Ruinart, Dupont *et al.* 2012). However, HDO selectivity decreased slightly from 87% to 83~84%, due to the smaller promotion compared with decarboxylation as observed in the rate constant changes. The origin of this HDO promotion could be derived from two possibilities: (a) the increasing H_2 partial pressure for HDO due to the promotion of the WGS; (b) the Ni present in the NiMoS mixed phase acted as a true synergistic promoter for the HDO reaction involving an aldehyde intermediate (Ruinart, Dupont *et al.* 2012). In order to verify reason (b), different metal:Mo ratios should be tested, as the formation of CoMoS or NiMoS are strongly affected by metal:Mo ratios. Besides this point some solid characterization like HRTEM, XRD and EDX will be required for investigating these mixed phases, which means that more work still needs to be done. On the other hand, the proposed reason (a) could be evaluated by adjusting the pseudo-first order reaction rate constant, which would eliminate the impact of the increased H_2 concentration on the reaction rate.

As discussed for the kinetic analysis, 2-NA removal is a mixed process involving decarboxylation, HDO, cracking and their relative hydrogenation reactions. Among all of these reactions, the HDO pathway and the hydrogenation reaction require H_2 as a reagent. If HDO did not constitute the major pathway for 2-NA removal, H_2 would not be considered as a reagent in calculating the rate constant. The rate equation could then be expressed as shown in Eq. 5-16, which does not involve the H_2 molecular percentage for calculation. For example, the reactions

run under N₂ had a much high decarboxylation and cracking selectivity. The linear regression of $\ln([NA]_0/[NA]_t)$ with time was always found to be acceptable, with a $R^2 \approx 0.99$. It should be noticed that the actual H₂ involved in reaction should be *in situ* H₂ which may not exist in gas phase (could be the hydride on catalyst surface). So the measurement of this active intermediate was extremely difficult. This is why Eq. 5-16 was always preferred and judged to be reliable for the kinetic analysis of 2-NA removal.

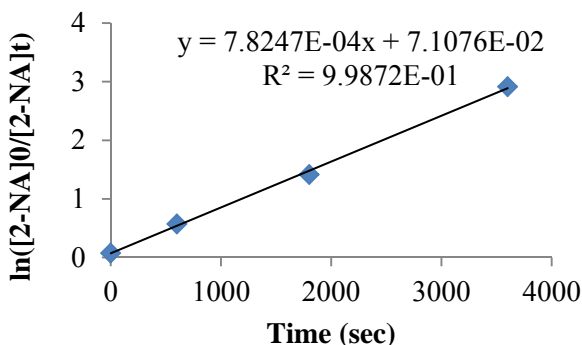
$$r_{2-NA\ removal} = k_{2-NA\ removal} \cdot [2 - NA] \quad (\text{Eq. 5-16})$$

When the HDO is the main reaction occurring, H₂ will be considered as a main reagent. If the H₂ molecular percentage did not change very much (such as for the reactions under H₂ or with low WGS conversion), the H₂ molecular percentage would be considered as a constant involved in the rate constant as a pseudo-first order reaction rate as shown in Eq. 5-17, which is what has been used for the kinetic analysis of the 2-NA removal under CO and H₂. However, the reactions with Co-Mo and Ni-Mo exhibited a large WGS conversion difference from the beginning to the end (from 10% to 70%). As a result, the H₂ molecular percentage would increase significantly. This would go against the assumption of a fairly stable H₂ molecular percentage. Hence the pseudo-first order rate would not be accurate enough, which would then require the H₂ molecular percentage to be separated out from the pseudo-first order reaction rate constant as shown in Eq. 5-17. The H₂ mole percentage, [H₂], was obtained by RGA (see Appendix B), which assumed the hydride mole percentage (if any) was proportional to the H₂ percentage in the gas phase.

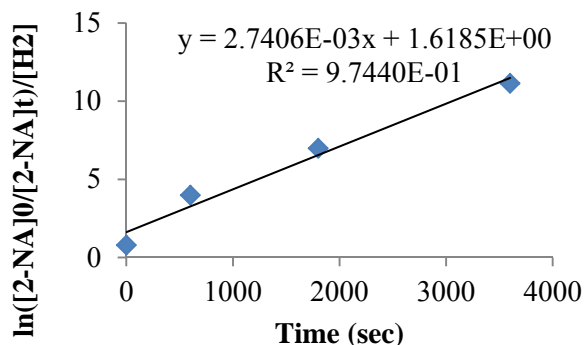
$$r_{2-NA\ removal} = k_{2-NA\ removal} \cdot [H_2] \cdot [2 - NA] = k_{2-NA\ removal}' \cdot [2 - NA] \quad (\text{Eq. 5-17})$$

In order to verify the difference of the kinetic analysis with and without this [H₂] adjustment, some comparison plots are shown in Figure 5-30.

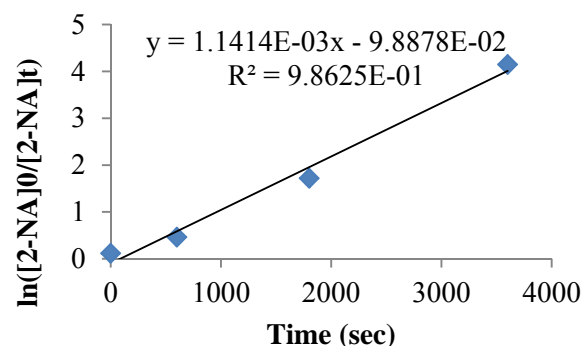
(a) Mo



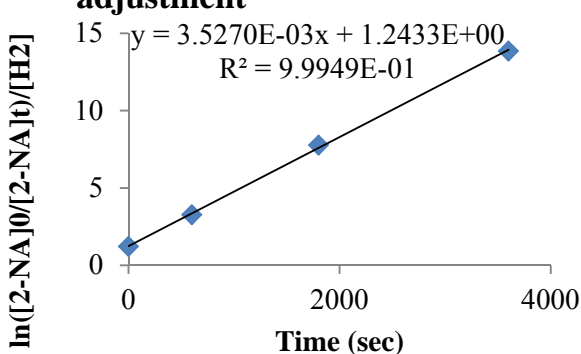
(b) Mo with [H₂] adjustment



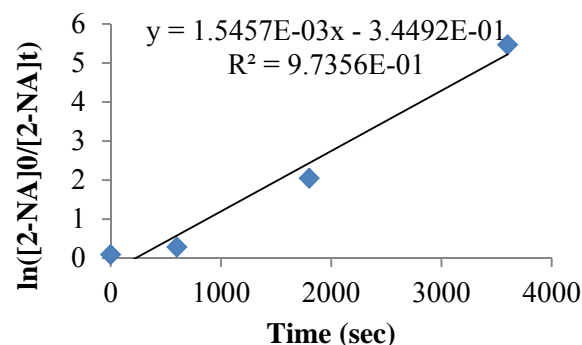
(c) Co-Mo



(d) Co-Mo with [H₂] adjustment



(e) Ni-Mo



(f) Ni-Mo with [H₂] adjustment

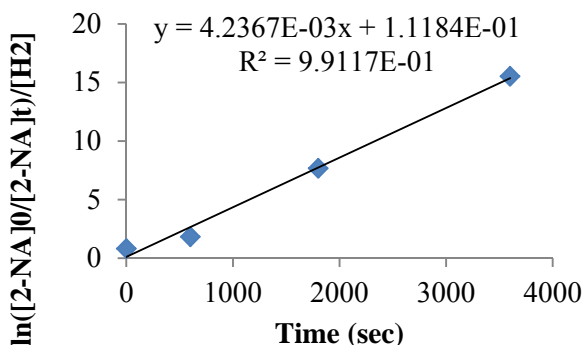


Figure 5-30 Plots of $\ln([2\text{-NA}]_0/[2\text{-NA}]_t)$ or $\ln([2\text{-NA}]_0/[2\text{-NA}]_t)/[\text{H}_2]$ values with time: (a) Mo pseudo-first order rate plotting; (b) Mo pseudo-first order rate plotting with $[\text{H}_2]$ adjustment; (c) Co-Mo pseudo-first order rate plotting; (d) Co-Mo pseudo-first order rate plotting with $[\text{H}_2]$ adjustment; (e) Ni-Mo pseudo-first order rate plotting; (f) Ni-Mo pseudo-first order rate plotting with $[\text{H}_2]$ adjustment;

It is found that a plot for Mo with the pseudo-first order rate assumption provides a very good linear regression with $R^2=0.9987$ as shown in Figure 5-30(a). When $[H_2]$ adjustment was considered for unpromoted Mo, the linear regression shown in Figure 5-30(b) had a poorer fit with $R^2=0.9744$. This is similar to the kinetic analysis for most of the results shown in previous sections of this thesis, where the linear fits were all very good. This implies that the linear regression with a fairly constant H_2 mole% assumption works well when the WGS conversion change was as small as a change from 10% to 40%. However, the additionally generated H_2 when using Co-Mo and Ni-Mo made this assumption less valid. As shown in Figure 5-30(c) and Figure 5-30(e) the fits when using Co-Mo and Ni-Mo with a constant H_2 mole% assumption show relatively poor linear fits, where the R^2 values were 0.9862 and 0.9736 respectively for Co-Mo and Ni-Mo. When the $[H_2]$ adjustment was utilized, the R^2 values increased significantly to 0.9995 and 0.9912 for Co-Mo and Ni-Mo as shown in Figure 5-30(d) and Figure 5-30(f). This means that the pseudo-first order rate calculation with a H_2 mole% adjustment is more suitable for the reactions with a larger WGS conversion change. By involving this H_2 mole% adjustment in the kinetic calculation, the effect of the WGS improvement could be eliminated from the 2-NA removal rate, which would reflect more about the activity of the catalyst itself. With this H_2 mole% adjustment, the 2-NA removal rate constants for unpromoted Mo, Co-Mo and Ni-Mo were $274.1 \times 10^{-5} \text{ s}^{-1}$, $352.7 \times 10^{-5} \text{ s}^{-1}$ and $423.7 \times 10^{-5} \text{ s}^{-1}$ respectively. This group of data represents the promotion effects of Co and Ni on MoS_2 catalyst activity without the influence of increased H_2 partial pressure. This promotion was proposed to result from a synergic effect of the CoMoS and NiMoS crystal phases. More metal:Mo ratio should be tested and some catalyst characterization should be carried out for the determination of CoMoS and NiMoS.

It should be noted that for various reasons such as the difficulty in measuring *in situ* H_2 , mixed processes with H_2 involved and H_2 non-involved reactions, the linear fitting might not be accurate unless the HDO has high selectivity and the H_2 mole% has a considerable change during the reaction. In addition, the promotion of Co and Ni should not only reflect intrinsic activity improvement, but also the catalyst stability (passivation effect) as reported previously (Badawi, Paul *et al.* 2011). Since H_2O is one major inhibitor for 2-NA removal and especially Co has been reported to fully reverse this additional catalyst deactivation, more metal additive

experiments should also be carried out with a higher water ratio. In this way, the metal's passivation effect could be fully presented for these batch reactor experiments.

Table 5-13 Summary of 2-NA removal with different metal additives (300°C, 80ml toluene, 10ml water, 15psi H₂S, 585psi CO, ~1641ppmw 2-NA in toluene, 673ppmw Mo, metal:Mo ratio=0.2, 2hours)

	Mo	Co-Mo	Ni-Mo
2-NA Conversion % in Oil	99.2	100.0	100.0
2-NA Conversion % in H ₂ O	99.3	100.0	100.0
k _{2-NA Removal} (10 ⁻⁵ s ⁻¹)	78.2	114.1	154.6
k _{Decarboxylation} (10 ⁻⁵ s ⁻¹)	3.2	12.5	15.5
k _{HDO} (10 ⁻⁵ s ⁻¹)	68.4	95.9	128.3
k _{Cracking} (10 ⁻⁵ s ⁻¹)	6.6	5.8	10.8
*k_{2-NA Removal} (10⁻⁵ s⁻¹) after [H₂] adjustment	274.1	352.7	423.7
Selectivity %			
Decarboxylation	4.2	10.9	10.0
HDO	87.4	84.0	83.0
Cracking	8.4	5.1	7.0
Product Distribution % at 120min			
Decarboxylation	4.5	7.7	11.0
HDO	95.5	92.3	89.0
Cracking	0.0	0.0	0.0
WGSR Conversion %	41.7	54.3	70.3
k _{WGSR} (10 ⁻⁵ s ⁻¹)	14.8	19.7	25.4
H ₂ Partial Pressure (psi)	555	591	697
Max. Pressure (psi)	2066	2033	1997
Oil yield %	91.6	88.9	91.2
Water yield %	43.5	39.6	36.9
Mass balance %	83.7	85.4	85.0

* If the [H₂] adjustment was made, the reaction rates for 2-NA removal would be 274.1×10⁻⁵ s⁻¹, 352.7×10⁻⁵ s⁻¹ and 423.7×10⁻⁵ s⁻¹ for Mo, Co-Mo and Ni-Mo respectively.

5.3.9 C7-BA removal

Similar experiments were also implemented with C7-BA as the target compound. C7-BA is another model compound representing naphthenic acids. It has lower aromaticity than 2-NA but longer substitution chains on the aromatic rings. The solubility of C7-BA in toluene is higher than 2-NA, and the initial concentration used for C7-BA removal was around 5224 ppmw.

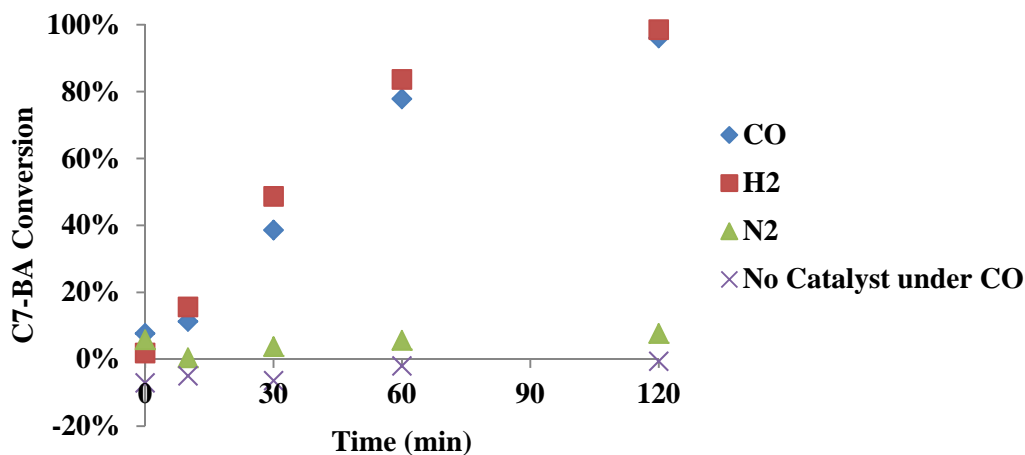


Figure 5-31 C7-BA conversion change with time with different gas feeds compared to the reaction without catalyst under CO (300°C, 80ml toluene, 10ml water, 15psi H₂S, 585psi gas feed, 5224ppmw C7-BA in toluene, 377ppmw Mo, 2hours)

As shown in Figure 5-31, both CO and H₂ converted most of the C7-BA in the oil phase (96.0% under CO and 98.6% under H₂). There was only 7.7% conversion under N₂, and no reaction occurred without catalyst under CO. The negative conversion could be the result of the loss of solvent during sampling of the batch reaction. This observation was very similar to that of the 2-NA removal experiments. The GC-MS result demonstrates that there were three reaction pathways, which were similar to the three pathways for 2-NA removal. Under CO or H₂, heptylbenzene and 1-heptyl-4-methylbenzene were generated as the products of decarboxylation and HDO; while under a N₂ atmosphere, benzoic acid was detected indicating a cracking pathway. As shown in the GC-MS chromatographs in Figure 5-32 the peak for 1-heptyl-4-methylbenzene was much larger than the other products, indicating a very high selectivity for the HDO pathway under both CO and H₂, which was also observed for 2-NA removal.

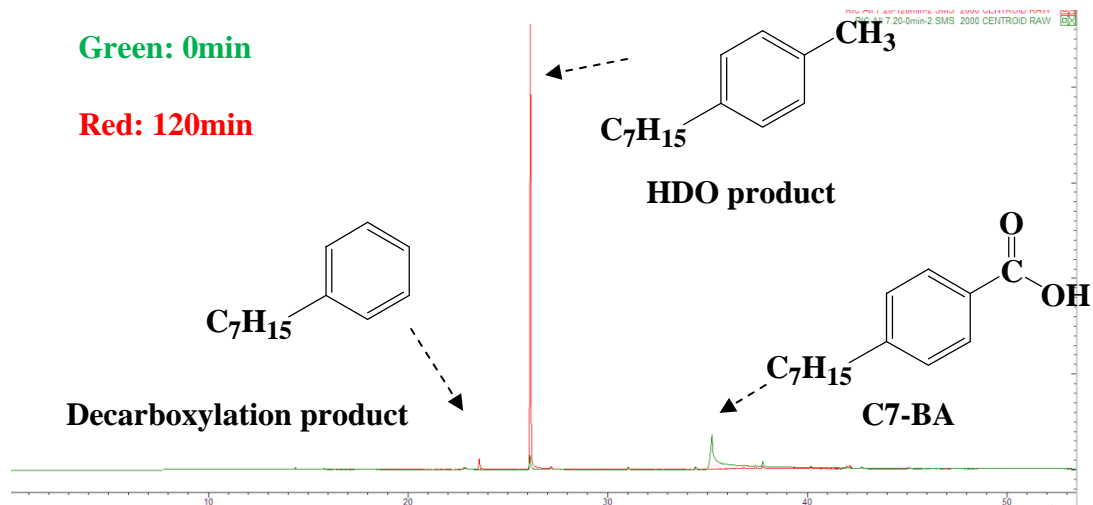


Figure 5-32 GC-MS chromatographs of C7-BA removal product collected at 120min (300°C, 80ml toluene, 10ml water, 15psi H₂S, 585psi gas feed, 5224ppmw C7-BA in toluene, 377ppmw Mo, 2hours)

However, the kinetic analysis results shown in Table 5-14 represent the difference between H₂ and CO on C7-BA removal. The C7-BA removal reaction rate constants were $62.8 \times 10^{-5} \text{ s}^{-1}$ and $48.2 \times 10^{-5} \text{ s}^{-1}$ when using H₂ and CO respectively. Unlike the 2-NA removal, higher activity was achieved under molecular H₂ instead of *in situ* H₂. This could be due to the aromaticity and substitution difference between these two feedstocks. *In situ* H₂ might be more suitable for reacting with higher aromatic chemicals than molecular H₂. A detailed reaction mechanistic study should be carried out to investigate the main reason for this. However, naphthenic acid removal by using this novel process should be much improved if the reaction temperature was increased. As a result the H₂ partial pressure would increase resulting in a better hydrotreating performance, which would certainly facilitate the 2-NA removal with *in situ* H₂.

Table 5-14 Reaction rate constants obtained under H₂ and CO (300°C, 80ml toluene, 10ml water, 15psi H₂S, 585psi gas feed, ~5000ppmw C7-BA in toluene, 377ppmw Mo, 2hours)

	H ₂	CO
k C7-BA Removal (10⁻⁵ s⁻¹)	62.8	48.2

5.3.10 Electron microscope characterization of spent MoS₂ catalysts

TEM and STEM were used for analyzing the structure of the spent MoS₂ catalysts after the 2-NA removal experiments. Similar to typical MoS₂ images obtained for other model compound reactions, the *in situ* formed MoS₂ catalysts was dispersed with a spherical structure as shown in Figure 5-33(a) at low magnification. It is clear that the catalyst particles had uniform size, with diameters around 10~20nm. When observing the catalyst edge at higher resolution, slab structures were found, as shown in Figure 5-33(b). These slabs represented the MoS₂ crystalline phase (002), which was consistent with the known MoS₂ slab structures observed under TEM characterization published (Gochi, Ornelas *et al.* 2005, Skrabalak and Suslick 2005, Albiter, Huirache-Acuna *et al.* 2006, Elizondo-Villarreal, Velázquez-Castillo *et al.* 2007, Alonso-Núñez, Huirache-Acuña *et al.* 2009, An, Lu *et al.* 2009, Gulková, Yoshimura *et al.* 2009, Nava, Pawelec *et al.* 2009, Afanasiev 2010, Lumbreras, Huirache-Acuña *et al.* 2010, Yoosuk, Song *et al.* 2010). Hence, the presence of 2-NA did not interfere with the MoS₂ catalyst formation. The slab length varied from 3-10nm, and 5-8nm was the most representative size range. It was believed that shorter slabs could result in higher active site density regions, as the hydrotreating active sites locate at the edges. Considering the similarity between HDO and other hydrotreating reactions, it could be assumed that HDO might share the same active sites with other hydrotreating reactions. If this hypothesis is true, the *in situ* unsupported MoS₂ with such a short slab length could play a crucial role in the 2-NA reaction through the HDO reaction pathway. It has been reported by Liu that *in situ* H₂ was the key for synthesizing such short slab length catalysts. The Keggin structure of PMA collapsed more easily in the presence of active *in situ* H₂ compared to molecular H₂. This might be why the MoS₂ catalysts synthesized *in situ* in emulsion upgrading technology demonstrated such high HDO activity and selectivity compared to other catalysts.

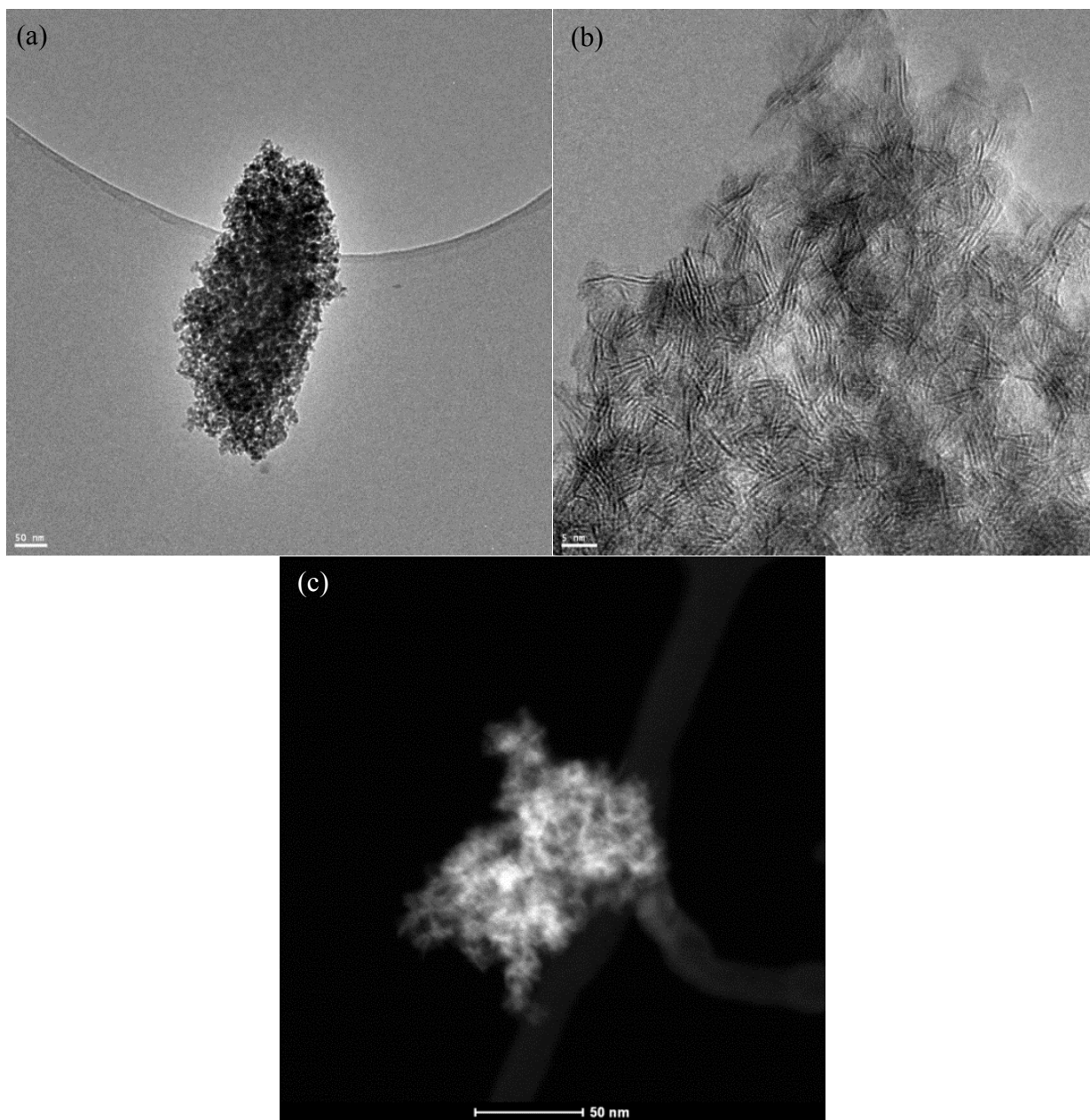


Figure 5-33 Electron microscope images of spent MoS₂ catalysts: (a) TEM image at low magnification, (b) HRTEM image with high magnification, and (c) STEM image at high magnification (340°C, 80ml toluene, 10ml water, 15psi H₂S, 585psi CO, ~1641ppmw 2-NA, 673ppmw Mo, 2hours)

STEM was also used to provide insight on how the metals distributed in catalysts. Similar to BSD in functionality, heavier metal elements with high atomic number would give stronger

signals than elements with lower atomic number. In this way, bright areas indicate the location of the metals. Shown in Figure 5-33, metals were well dispersed in the catalysts, and a similar slab structures were found to be full of metal. This further confirmed the presence of MoS₂ with a uniform metal distribution in slab structures.

5.4 Conclusions

Naphthenic acids were removed in both the oil and water phases through a novel bitumen upgrading process. 2-NA and C7-BA were selected as model compounds for studying the reaction condition and catalyst development. *In situ* H₂ and *in situ* generated nano unsupported MoS₂ catalyst accelerated this removal with their high activities. The removal of 2-NA and C7-BA both reached around 99~100% in the oil and water phases when the reaction temperature was as low as 300°C. With the help of FT-IR, HPLC, RGA, GC-MS and GC-FID, the removal of naphthenic acid model compound (2-NA or C7-BA) and the relative products were qualitatively and quantitatively analyzed. A reaction mechanism was suggested as being composed of a three-pathway reaction network involving decarboxylation, HDO, cracking and consecutive chain hydrogenation for both 2-NA and C7-BA. Pseudo-first order reaction rate constants were analyzed for 2-NA removal, and the rate constant for each pathway (decarboxylation, HDO and cracking) in 2-NA removal and the WGS. MoS₂ catalyst with outstanding activity and selectivity was the first-time reported for removing the naphthenic acid model compound 2-NA through a HDO pathway.

In this novel bitumen upgrading process, 300°C was chosen as the designed reaction temperature for a relatively low system operating pressure, low initial conversion, excellent HDO selectivity and adequate water purification. The catalysts and reaction condition could be improved at this starting point. It is also interesting that CO was more effective for 2-NA removal compared to molecular H₂, even though the H₂ partial pressure was low and CO was also known as an inhibitor for HDO. This outstanding HDO performance in the presence of CO was attributed to (a) the high activity of *in situ* H₂ generated through the WGS; (b) the active nano catalyst generated through PMA collapsed under CO. The *in situ* generated nano unsupported MoS₂

catalyst was found to facilitate the 2-NA removal rate by more than 40 times. It catalyzed both 2-NA removal and the WGSR, especially in enhancing the HDO reaction rate. Compared to MoS₂, MoO₃ only improved the decarboxylation pathway slightly, but it was not a suitable catalyst for HDO or the WGSR. 337ppm Mo was found to have similar performance as 673ppm Mo in 2-NA removal.

Another interesting result was the 2-NA removal under N₂. Although there was a certain amount of benzoic acid generated which was not detected under CO or H₂ (benzoic acid may be formed in these conditions, but was quickly hydrogenated in toluene), the major selectivity under N₂ was still toward the HDO reaction. The origin of such an appropriate HDO performance with such a low H₂ partial pressure under N₂ (~8psi) seemingly derived from the *in situ* generated nano unsupported MoS₂ catalyst. Although the introduction of MoS₂ brought some unfavorable cracking selectivity compared to the N₂ reaction without catalyst, MoS₂ still played an important role in reducing the water consumption for an acceptable clean water yield, maintaining the reaction pressure and provided a high 2-NA removal.

Decarboxylation selectivity was favored with more water under CO while HDO was hindered by adding more water. Since HDO selectivity was over 80% of the total reaction yield, the water inhibition on the HDO pathway would eventually result in inhibition of the overall 2-NA removal. However, higher water yields were obtained with more water addition, which means this process was capable of treating more dirty water. From the data regarding “inhibition, pressure and water yields” with different amounts of water, computational methods could be applied to determine the optimal ratio through experimental design. Reactor conditions were fairly similar on changing water amounts under CO and N₂. However, the HDO pathway was more easily inhibited with increasing water amounts under N₂ for 2-NA removal. CO was a much better reaction gas feed for not only achieving high HDO activity but also maintaining a certain level of catalyst stability in the presence of water. Reactions carried out under N₂ still seemed to be of interest if there could be some method for maintaining the catalyst stability, such as using different catalyst precursors or different metals (like tungsten) or adding metal promoters.

Based on kinetic analysis, it is observed that 2-NA had no inhibition effect on the WGSR, although CO and H₂O were stronger adsorbates than oxygenated compounds like furan in biomass upgrading (Badawi, Paul *et al.* 2011). In addition, 2-NA could adsorb on the active sites of the catalyst more easily than DBT and NAPH due to its oxygen containing group. As a result, the existence of 2-NA inhibited the HDS of DBT and the HDA of NAPH. However, the catalyst activity was restored when 2-NA was almost completely removed, which was consistent with a competitive adsorption mechanism. This activity restoration observed in both simultaneous “HDS + 2-NA removal” and “HDA + 2-NA removal” suggests possible future applications for this novel process. The existence of H₂S as sulfiding agent was proposed to be responsible for maintaining this catalyst activity. Due to its weak adsorbing ability, DBT did not inhibit any pathway in 2-NA removal. NAPH also had a weaker adsorption than 2-NA, but the 2-NA removal was inhibited with the introduction of NAPH. This inhibition was attributed to the H₂ consumption caused by the HDA of NAPH instead of competitive adsorption.

As common hydrotreating promoters, Co and Ni were found to improve the 2-NA removal with *in situ* H₂. Both decarboxylation and HDO pathways were promoted with increased rate constants, and Ni showed a higher promotion effect. This promotion was derived from: (a) higher H₂ partial pressure from increased WGSR conversion by using a promoter; (b) synergistic activity improvement due to the CoMoS and NiMoS formation. The pseudo-first order kinetic analysis with [H₂] adjustment revealed this rate constant improvement without H₂ mole% influence, which suggested the synergistic activity promotion by Co and Ni. Further solid characterization should be carried out to identify the CoMoS and NiMoS phases on the catalyst surface. Since H₂O was one major inhibitor for 2-NA removal, and since Co was reported to fully reverse this catalyst deactivation, more metal additive experiments should be carried out with higher amounts of water to these metals potential as promoters for the catalyst’s stability in the presence of H₂O. Some more catalyst structure research will be discussed in Chapter 6 and Chapter 7.

Chapter 6 Characterization of the Catalysts used in LGO upgrading

6.1 Introduction

Preliminary experimental results on hydrotreating of model compounds, upgrading of diesel, LGO and bitumen emulsions have shown potential applications of *in situ* nano unsupported MoS₂ catalysts. In order to understand and improve the synergistic performance of promoters on the catalysts for the WGS and upgrading, it is of importance to analyze novel nano unsupported catalysts through advanced catalyst characterization. In this chapter the characterization of catalysts involved in LGO upgrading were studied, including the effects of temperature, time, LGO and promoters.

6.2 Literature review

6.2.1 Catalysts for HDS

Mo and W sulfide catalysts are usually chosen as HDS catalysts for due to their high activity and low price. Figure 6-1 shows the HDS abilities of different transition metal sulfides. The points above horizontal line were found to have higher intrinsic activities than Mo. However, Mo and W still seem to be the optimal choices based on the price of each transition metal sulfide (Lacroix, Boutarfa *et al.* 1989).

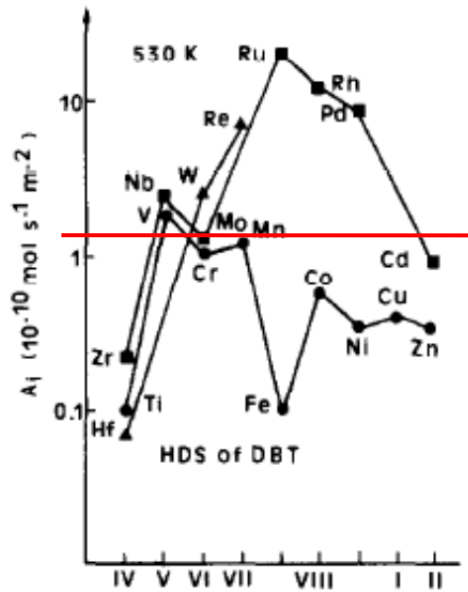


Figure 6-1 Intrinsic activities (A_i in ordinate) of transition metal sulfides for the hydrodesulfurization of dibenzothiophene (HDS of DBT) at 530 K. (Lacroix, Boutarfa *et al.* 1989)

6.2.1.1 Active sites

It is generally accepted that a S vacancy is the only active site for HDS. (Bataille, Lemberton *et al.* 2000) With the help of HAADF-STEM and density function theory (DFT), discussion of active sites for HDS has resulted in some common conclusions. By exploring the HDS of thiophene, it has been found that the active site at the S edge is a sulfur vacancy site, while the active site at the Mo edge is a brim site (located adjacent to the edge of MoS₂ slabs) and not a coordinatively unsaturated site. A thermodynamic study shows that the hydrogenation reactions take place on the brim sites, whereas the sulfur removal can take place at both S and Mo edges (Besenbacher, Brorson *et al.* 2008). As shown in Figure 6-2, the top part of the figure shows a side view of MoS₂ perpendicular to the S (1010) edge, with the S and H coverage present under HDS conditions; the lower part of the Figure shows a side view of MoS₂ perpendicular to the Mo(1010) edge, with the S and H coverage present under HDS conditions. The dotted arrows denote reactions found to be slow.

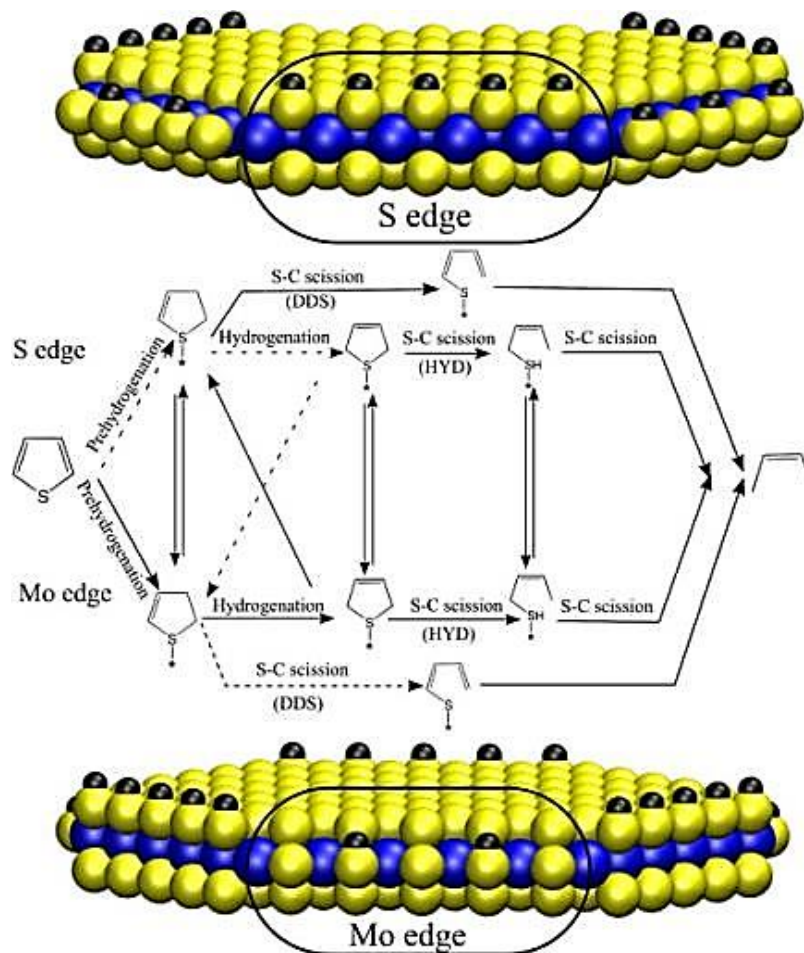


Figure 6-2 MoS₂ structures involved in the HDS of thiophene and the schematic overview of the reactions (Besenbacher, Brorson *et al.* 2008)

6.2.1.2 Promoter effects

A synergistic effect is the dominant effect of the promoter that increases the number of “d” electrons formally associated with Mo. The synergistic effect is a result of a covalent contribution to the metal-sulfur bond strength and the metal d orbital occupation. From a quantum chemistry point of view, the formal transfer of an electron from Co to Mo involves an electron transfer from the Co-S anti-bonding orbital to the Mo-S anti-bonding orbital. This results in a weakening of the Mo-S bonds. The number of 3d electrons that Co, Ni contributes to the cluster and the energies of their 3d orbitals relative to the Mo 4d orbital, make these metals unique when combined with Mo.

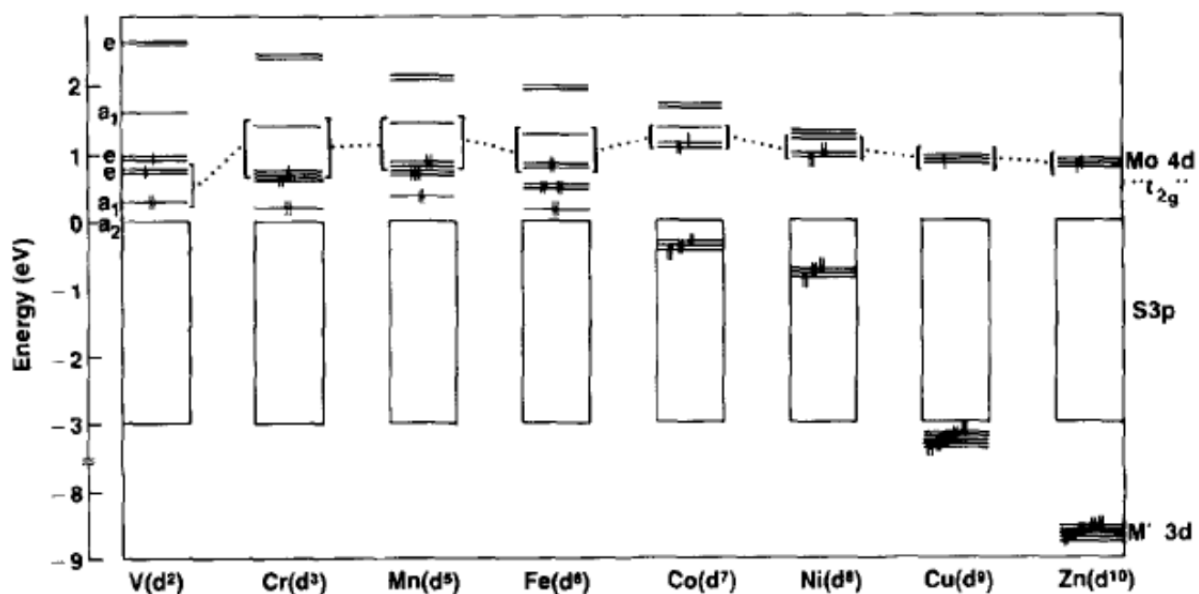


Figure 6-3 Electron orbits and occupation of different transition promoters. (Harris and Chianelli 1986)

Figure 6-3 shows the calculated valence energy levels for the MoM'S₉⁻ clusters, where M is the 3d metal shown below each level diagram. The sulfur 3s levels and the Mo 4d “e_g” levels have been omitted. The block labeled sulfur 3p represents 20 levels. The energies of all the levels are shown relative to the energy of the nonbonding a₂ level lying at the top of the sulfur 3p group of the orbital for comparison. The three Mo 4d “t_{2g}” levels are bracketed in order to distinguish them from the M's 3d levels.

Besides quantum chemistry, HAADF-STEM and DFT studies have presented observations suggesting that the promoting role of Co and Ni should be two-fold. First of all, by modifying the brim and the lower sulfur coordination condition, the electronic structure changes of (1010) Ni-Mo-S edges can attract adsorption of S-species. On the other hand, the presence of Ni-Mo-S type B clusters as shown below in Figure 6-4 clearly demonstrate that the different Co-Mo-S and Ni-Mo-S catalyst morphologies may be the keys in explaining the different selectivities of the two systems in hydrotreating processes.

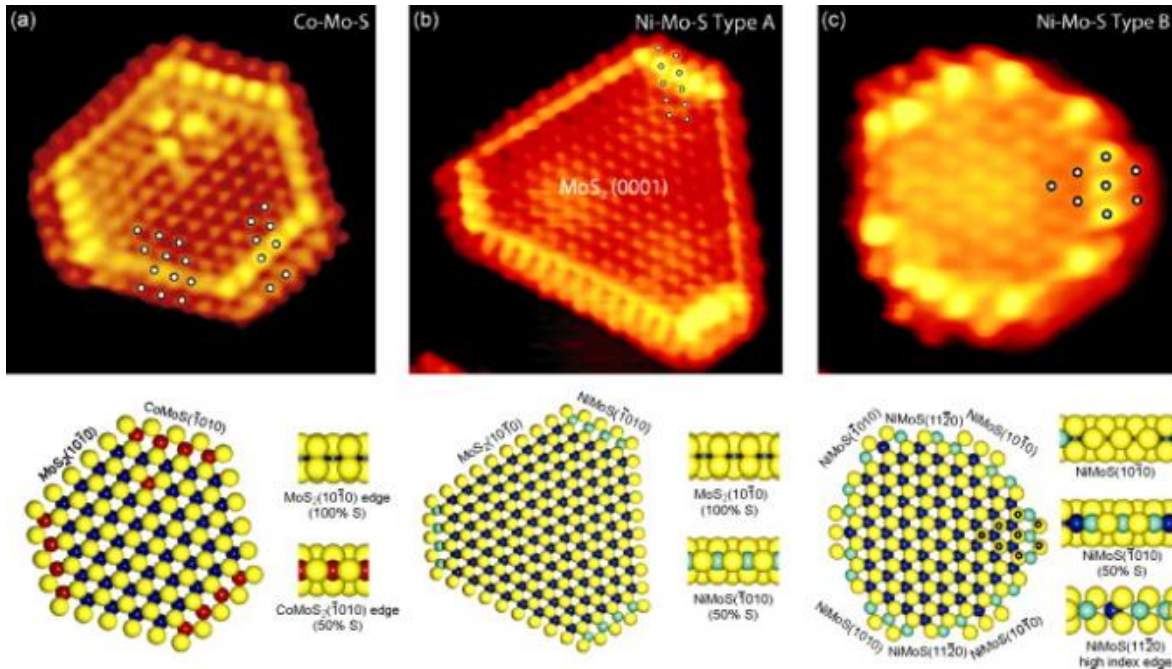


Figure 6-4 High-angle annular dark-field scanning transmission electron microscopy (HAADF-STEM) images and DFT simulation of unpromoted, Co-promoted and Ni-promoted MoS_2 catalysts (Besenbacher, Brorson *et al.* 2008)

6.2.2 Catalysts for HDA

Nowadays the best catalysts for hydrodearomatization (HDA) are noble metal catalysts such as Pt, Pd, Rh and Ru. These noble metals provide active hydrogenation even at low temperatures, and the reaction is close to zero order with respect to the hydrocarbon due to the strong adsorption of aromatic species on the noble metal sites (Cooper and Donnis 1996). However, noble metal hydrogenation catalysts can be easily poisoned by adsorption of S and N species, which are present in oil feedstocks. Therefore, the feedstock for noble metal catalysts is limited to S and N free oils. Recently some developments in supported noble metal catalysts have been made to improve catalytic performance and S and N tolerance. Pt, Pd or Pt-Pd bimetallic catalysts (Navarro, Pawelec *et al.* 2000, Jongpatiwut, Li *et al.* 2004) have been loaded on acidic oxides including TiO_2 (Lu, Lin *et al.* 2000), $\text{SiO}_2\text{-Al}_2\text{O}_3$ (Navarro, Pawelec *et al.* 2000), zeolites (Corma, Martínez *et al.* 1997, Park, Yim *et al.* 2002). Among them the LT-HAD technique,

which applies unique zeolite supports to prepare bimodal distributions of noble metal particles, is tolerant of high S content. The LT-HAD utilizes the large pores (larger than 6 Å) for hydrogenation and small pores (less than about 5 Å) for H₂ spill over to recover poisoned large holes (Song 2003), as shown in Figure 6-5.

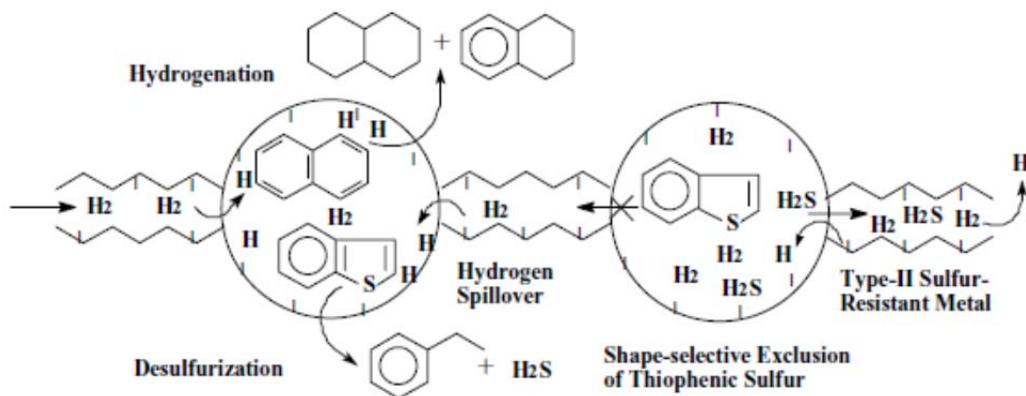


Figure 6-5 The proposed new concept “LT-HAD” for catalyst design based on shape-selective exclusion, H₂ spillover, and two types of sulfur resistance. The black dots indicate metal particles on internal surface (Song 2003)

Besides noble metal catalysts, conventional hydrotreating catalysts are also active for HDA (Babich and Moulijn 2003). Mo and W sulfides have been reported to display lower activity than Ru and Os but are the most active among non-noble metals (Pecoraro and Chianelli 1981). Similar research has been carried by Lacroix, where Mo and W were found to be less active than Nb, V, Re, Ru and Rh transition metal sulfides in the hydrogenation of biphenyl (Lacroix, Boutarfa *et al.* 1989) as shown in Figure 6-6. From an economic point of view, Mo and W are still considered to be favourable for commercial metal sulfides catalysts for HDA.

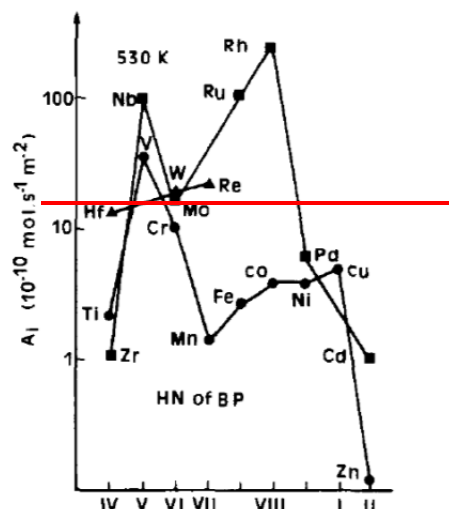


Figure 6-6 Intrinsic activities (A_i in ordinate) of transition metal sulfides for the hydrogenation of biphenyl (HDA of BP) at 530 K. (Lacroix, Boutarfa *et al.* 1989)

Nevertheless, some studies have shown that complete hydrogenation of aromatic substances on the Co-Mo and Ni-Mo sulfides supported on alumina is not possible due to equilibrium constraints under typical hydrotreating conditions (Du, Fairbridge *et al.* 2005). The kinetics is approximately first-order with respect to both H_2 and hydrocarbons (Cooper and Donnis 1996). Nowadays, $NiMoS_2/Al_2O_3$ is utilized for processes requiring high hydrogenation activity at reasonable cost. As summarized by Song (Song 2003), MoS_2 catalyst shows higher HYD selectivity than DDS in β -DBTs, which represents the high hydrogenation ability of MoS_2 . In 2000, a series of unsupported Group II- transition metal sulfide catalysts have been tested for HDS of 4,6-DMDBT. The results showed that a large amount of hydrogenated products were obtained instead of HDS products, which also showed the prospect of using hydrotreating catalysts in heavy oil HDA (Bataille, Lemberton *et al.* 2000). Recently, ExxonMobil and Albemarle have jointly commercialized a new type of unsupported catalysts called NEBULA (Eijsbouts, Mayo *et al.* 2007), which has shown significant improvements over earlier catalysts in deep HDS for distillate and 21 diesel fuels. The enhanced HDA ability is thought to partially contribute to the excellent activity of NEBULA in deep hydrodesulfurization and hydrodenitrogenation.

6.2.3 Design of nano unsupported catalyst for bitumen upgrading

6.2.3.1 Application of nano unsupported catalyst

Hydrotreating catalysts can be divided based on the employment of support: supported catalysts and unsupported catalysts (also called dispersed catalysts). Due to their high dispersion of active sites and mechanical strength, supported catalysts have been commercially used for hydrotreating especially for light gas oil or petroleum. However, the supported catalysts suffer from coke deposition on support materials resulting in a fast deactivation and short life time (Eijsbouts, Mayo *et al.* 2007). To solve this problem, unsupported catalysts have already attracted world-wide attention. Among them nano unsupported catalysts have shown good tolerance of coke deposition, highest metal utilization with no diffusion limitation and extremely high surface area for maximum interaction (Siewe and Ng 1998). Until now, there have already been five catalytic processes tested at the bench or pilot plant scale using unsupported catalysts. They are VEBA Combi Cracking (VEBA Oel), Aurabon Process (UOP), CANMET Process (Petro Canada and Canadian DOE), HFC-Process and M-Coke Process (Exxon-Mobile).

6.2.3.2 Active sites and morphology control

Active sites and catalyst morphologies play key roles in a catalysts performance. By adjusting DDS and HYD selectivity, different requirements can be met for different feed oils. For example, a bitumen emulsion contains considerable amounts of poly-aromatics that can inhibit hydrotreating reactions significantly (Choudhary, Parrott *et al.* 2008), so higher HYD is more preferable although high DDS is also desired. Morphology control is one way to influence active site distribution and dispersion. The changes on length, stacking numbers, curvatures of MoS₂ slabs will reflect the morphology-control effect and change the reaction accordingly.

Ex situ catalyst preparations are believed to be an effective way to control catalyst morphology. Ho discovered that operating at high temperatures was more effective in moderating the poisoning inhibition through weakening the adsorption of nitrogen compounds (Ho 2003). But temperature should not be too high since more fine crystalline phases will be generated causing low catalytic activity (Afanasiev 2010). Although Alonso reported that by increasing pressure

higher surface area can be achieved for better performance (Alonso, Del *et al.* 1996); higher pressure will result in a higher stacking degree, which is favored for high HYD selectivity (Yoosuk, Song *et al.* 2010). As a result, both temperature and pressure should be controlled carefully. Recently in *ex situ* preparation, adding organic solvents has been reported as an effective way for increasing the dispersion of the precursor-containing water droplet during preparation under vigorous agitation. With the help of stirring, a fine molecular dispersion of precursor molecules in the aqueous solution was obtained, which was isolated by organic solvent (Yoneyama and Song 1999, Yoosuk, Song *et al.* 2010).

Surfactants can generate uniform particle structure and dispersed sulfide active sites through preventing MoS₂ slabs from sintering. Some nonionic surfactants such as Tergitol, Imbentin and Triton have been tested in MoS₂ catalyst synthesis for HDS and the tuning of pore size was realized (Genuit, Afanasiev *et al.* 2005). The design for splitting MoS₂ slabs was also achieved with the help of surfactant. Afanasiev reported single layer, short fringes of MoS₂ were observed with in the presence of cetyltrimethylammonium chloride surfactant (Afanasiev, Xia *et al.* 1999). However, the application of surfactants is restricted to *ex situ* preparation. As normal surfactants cannot withstand severe reaction conditions in *in situ* synthesis and lose their function. Hence the design or selection of high temperature-tolerant surfactants is one challenging topic in this field.

From the perspective of active site decoration, the over-stoichiometric sulfur, which locates at the edges of MoS₂ in the form of S₂²⁻, also opens another perspective for designing active sites and deserves further investigation. It is reported that over-stoichiometric sulfur plays a key role for HDS activity and especially HYD selectivity, as well as for higher promotion of unsupported MoS₂ catalysts by Ni and Co (Afanasiev 2010). “-SH” groups can be produced from the S₂²⁻ groups by interaction with H₂, which is well-known for getting involved in the HYD pathway in HDS (Elizondo-Villarreal, Velázquez-Castillo *et al.* 2007). It has also been discovered that the edge located “-SH” groups obtained after treatment with H₂ can exchange ions with the Ni or Co metal, providing reinforced promotion (Afanasiev 2010).

6.2.3.3 Nano catalysts with higher promotion effect

Traditionally, precursor choice is believed to play an important role for better promotion (Lumbreras, Huirache-Acuña *et al.* 2010). Furthermore, synthesis conditions such as sulfiding, reducing and drying conditions are also very important especially when promoters are applied (Pashigreva, Bukhtiyarova *et al.* 2010).

Precursor choice for unsupported MoS₂ and a promoter metal such as Ni and Co has been discussed for many years. Recently there has been some new progress published, such as introducing promoter metals in heteropolyacid (HPA) precursors or using C-containing precursors. HPA that contains Co or Ni with Mo in the Keggin or Anderson structure was thought to be a promising catalyst precursor as the sulfiding can happen in the organized Co or Ni and Mo complex, resulting in a better Co-Mo or Ni-Mo interaction (Cabello, Cabrerizo *et al.* 2002, Palcheva, Spojakina *et al.* 2007, Lizama and Klimova 2008, Palcheva, Spojakina *et al.* 2009, Palcheva, Spojakina *et al.* 2010). However, the low Co/Mo or Ni/Mo ratio that is always under an optimal metal/Mo ratio of around 0.3-0.6 was the major limitation. C-containing precursors have been confirmed in 2005 for stabilizing catalyst morphology and catalytic activity (Genuit, Afanasiev *et al.* 2005). Huirache-Acuña's research group synthesized a C-containing Mo precursor which led to a significant nickel promotion of MoS₂ and WS₂ catalysts (Alonso-Núñez, Huirache-Acuña *et al.* 2009, Lumbreras, Huirache-Acuña *et al.* 2010). This precursor was called "nickel hexamethylenediammonium thiometallate", Ni/NH₃(CH₂)₆NH₃MoS₄, in short as Ni/HeDaT), which was synthesized through simple reaction of ammonium thiometallates (ATM) with hexamethylenediamine and Ni(NO₃)₂ in aqueous solution. The enhanced HDS activity derived from the high mesoporosity arose from the high precursor carbon content (Lumbreras, Huirache-Acuña *et al.* 2010). Zhou used (CH₃)₄NBr in preparing a Ni promoted tetramethylammonium tetrathiomolybdate precursor and discovered the same trend. It was reported that the introduction of a methyl chain improved the dispersion of the Ni phases, leading to lower slab stacking number and shorter slab length for higher DDS selectivity (Zhou, Yin *et al.* 2010).

The controlling of sulfiding, reducing and drying conditions have been long discussed and concluded for higher promotion level. Recently, the combination of chelating agent has gradually become noticeable for permitting a simultaneous sulfidation of both promoter and Mo. Frizi impregnated an oxidic Mo precursor with thioglycolic acid (Frizi, Blanchard *et al.* 2008). In this way, a higher sulfidation degree could be achieved, resulting in some morphology changes such as shorter slab length and more Co in the edge position. Citric acid has also been investigated for higher sulfidation degree with Mo and a promoter (Rinaldi, Kubota *et al.* 2009, Rinaldi, Usman *et al.* 2009, Rinaldi, Kubota *et al.* 2010). Sulfiding and drying procedures in synthesis need to be optimized to ensure saturation of sulfur on the catalyst. Through the introduction of the chelating agent in the *ex situ* catalyst preparation, better promotion level may be possible in our catalyst design.

6.2.4 Regeneration and recycle of spent unsupported hydrotreating catalysts

Due to the growing hydrotreating industry, hydrotreating catalysts usage is also increasing. However, coking, sintering and contamination deactivate hydrotreating catalysts to the extent of around 150,000 tons every year (Dufresne 2007). The current landfill disposal for spent catalyst has already caused both economic and environmental problems. Regeneration and recycle techniques will have a positive impact and have attracted more and more investigations. In addition, the high dispersion of unsupported MoS₂ based catalysts also suggests the possibility of catalyst recycling. Accordingly, a study on the regeneration and recycle of spent unsupported hydrotreating catalysts will be both practical and promising.

6.2.4.1 Coking, sintering and catalysts contamination

Coking is the most common process in hydrotreating. The deposit of this carbonaceous material from asphaltenes can cause initial deactivation rapidly and needs to be burnt off. Sintering is always caused at high temperatures without a suitable chemical environment, where the catalysts will be allowed to rearrange and form lower surface area agglomerates (Trimm 2001).

Catalyst contamination is another important cause for deactivation. Some of them can originate from feedstocks, containing impurities such as sodium, arsenic, nickel and vanadium; some come from additives applied during the processes, such as silicon and lead; some even derive from corrosion like iron. Table 6-1 shows some examples for the main causes of coking, sintering and catalysts contamination.

Table 6-1 Main causes of catalyst deactivation in different oil refining and petrochemical processes (Dufresne 2007)

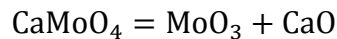
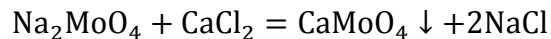
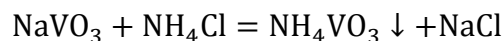
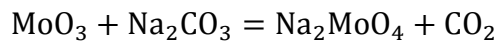
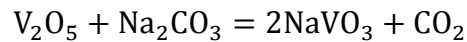
Process	Catalyst	Cause of deactivation		
		Coke	Sintering	Contamination
Diesel hydrodesulfurization	CoMo–NiMo/Al ₂ O ₃	+++	++	+
Resid hydrotreatment	NiMo–CoMo/Al ₂ O ₃	+++	+	+++
VGO hydrocracking	NiMo–NiW/SA	+++	+	+
Naphtha reforming	Pt Re Cl/Al ₂ O ₃	+++	++	+
Olefinic cuts select. hydro.	Pd–Ni/Al ₂ O ₃	++	+	++
Alkylation aromatics/olefins	Zeolite + binder	+++	–	+

6.2.4.2 Regeneration and recovery techniques

Among the three major causes of catalyst deactivation, coking, sintering and catalyst contamination, the first two can be solved through regeneration while contamination will be eliminated via recovery of different elements. Regeneration is defined as controlling the oxidation to remove coke and converting the sulfides back to oxides. This process can restore the activity of the catalyst to some extent. In addition to coke removal and re-dispersion, regeneration can sometimes also remove N-species contamination (Zeuthen, Blom *et al.* 1991). Recovery is carried out to remove different contamination after the first-step of regeneration. In general, the recovery of metals from spent catalysts could provide some economic benefit, but in most cases, environmental concerns are more important. There are two major types of metal reclaim processes for recycling: hydrometallurgy and pyrometallurgy. Hydrometallurgy is leaching the decoked residuum with the help of either sulfuric acid (Ziyadanoğulları and Aydın 2004) or caustic soda (Tsuen-Ni, Jing-Chie *et al.* 1983); while the key for the pyrometallurgy

route is melting dry catalysts in a furnace at around 1200-1500°C, leaving heavy metals to sink at the bottom as alloys. In these two different routes, most of the unfavored elements will be extracted in different steps, leaving the highly active metal for recovery. However, the pyrometallurgy route can cause extreme high energy loss; therefore hydrometallurgy is the recommended method.

Research on acid-aid recovery techniques is very limited; however, the literature on the extraction of Mo from ores can be instructive. For example, with the help of H₂SO₄, Ziyadanoğulları and coworkers had recovered uranium, nickel, molybdenum, iron and vanadium from floated asphaltite ash through combining roasting, acid leaching and organic/aqueous extraction method. The extraction yields of all elements were over 99% (Ziyadanoğulları and Aydın 2004). Besides acid-leaching, alkali-leaching is another easier way to remove inhibitors like vanadium. For example, soda was used after the roasting to react with V₂O₅, followed by treatment with water, ammonium chloride and calcium chloride. All the V will be precipitated in the form of NH₄VO₃ by reacting with NH₄Cl; while Mo will be recycled in the form of CaMoO₄ which could be decomposed into MoO₃ and CaO (Trimm 2001).



6.2.4.3 Current processes

In 2000, Gulf Chemical and Metallurgical implemented a new recycling technique which combined hydrometallurgy and pyrometallurgy. In this process, after roasting with caustic soda and leaching for removing V and Mo, the solid residue containing Co, Ni and Al would be fused

in an electric furnace to recover useful metals (Llanos and Deering 2000). In 2002, the Eurecat recycling process was presented at the 17th World Petroleum Congress, Rio de Janeiro (Marafi and Stanislaus 2002). As shown in Figure 6-7, it was mainly based on a hydrometallurgy technique.

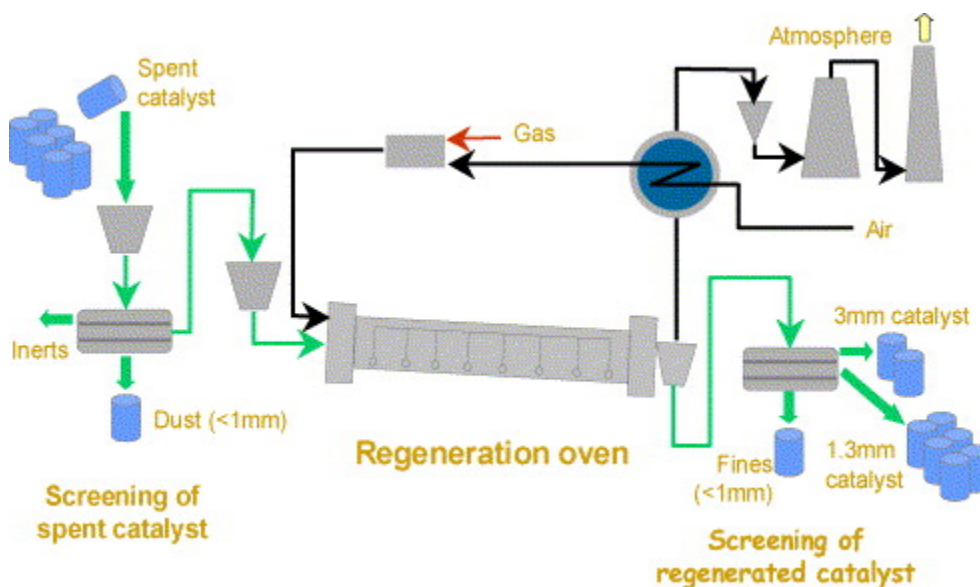


Figure 6-7 Simplified process scheme of the Eurecat regeneration process (Marafi and Stanislaus 2002)

6.3 Preliminary study of the catalyst morphology in LGO upgrading

As many experiments had been conducted dealing with sulfur-containing and nitrogen-containing model compounds in our group, some work on upgrading a real oil feedstock was carried out (Alghamdi 2009). This study has been done using real bitumen-derived light gas oil (LGO) as a good model for the bitumen-upgrading process. Abdulaziz Alghamdi had reported the effect of promoter, effect of H₂O amount, effect of syngas ratio and effect of reaction temperature on the upgrading of LGO derived from a bitumen emulsion in his thesis. At 391°C, it was found that the water gas shift reaction provided hydrogen for the HDS of LGO in the presence of the nano unsupported Mo catalysts. Total sulfur analysis obtained from XRF showed

that sulfur removal is about 32% in the presence of the unsupported Mo catalyst. In the presence of added Ni, the S removal increased to 56%. GC-TCD/PFPD identified benzothiophene (BT), dibenzothiophene (DBT), 4,6-dimethyldibenzothiophene (4,6-DMDBT) and 4,6-diethyldibenzothiophene (4,6-DEDDBT) in the complex mixture of sulfur compounds in LGO by using the standard sulfur containing compounds. It was interesting that the concentration of 4,6-DMDBT, one of the most refractory sulfur containing compounds, was found to decrease most significantly in the presence of Ni added to the Mo catalyst. Analysis of the gaseous products indicated that Ni also promoted the WGS. Fe showed no significant promoting effect for both the WGS and HDS. V and K promoted the WGS but apparently they inhibited the HDS reaction. K was found to be the strongest inhibitor for the HDS reaction since no sulfur was removed during the reaction. Water was found to have an inhibiting effect on the HDS reaction. At a high temperature, more HDS and lighter products were produced as seen in the GC-SIMDIS results (Alghamdi 2009).

This chapter is focusing on the effects of different metal ion promoters and the major factors that affected the HDS, WGS and the catalyst morphologies. Research emphasizes was placed on the characterization of the catalysts prepared. During the reactions coke formation on the catalyst was detected, blocking the real catalyst surface and bulk structure of the *in situ* catalysts. Therefore hexadecane was applied in the *ex situ* catalyst preparation for simulating the *in situ* MoS₂ catalysts chemical environment without large-scale coke deposits. Characterization of these solid catalysts can provide a clearer view of the morphologies of the *in situ* catalyst.

6.4 XRD analysis of spent MoS₂ catalysts from the LGO experiments

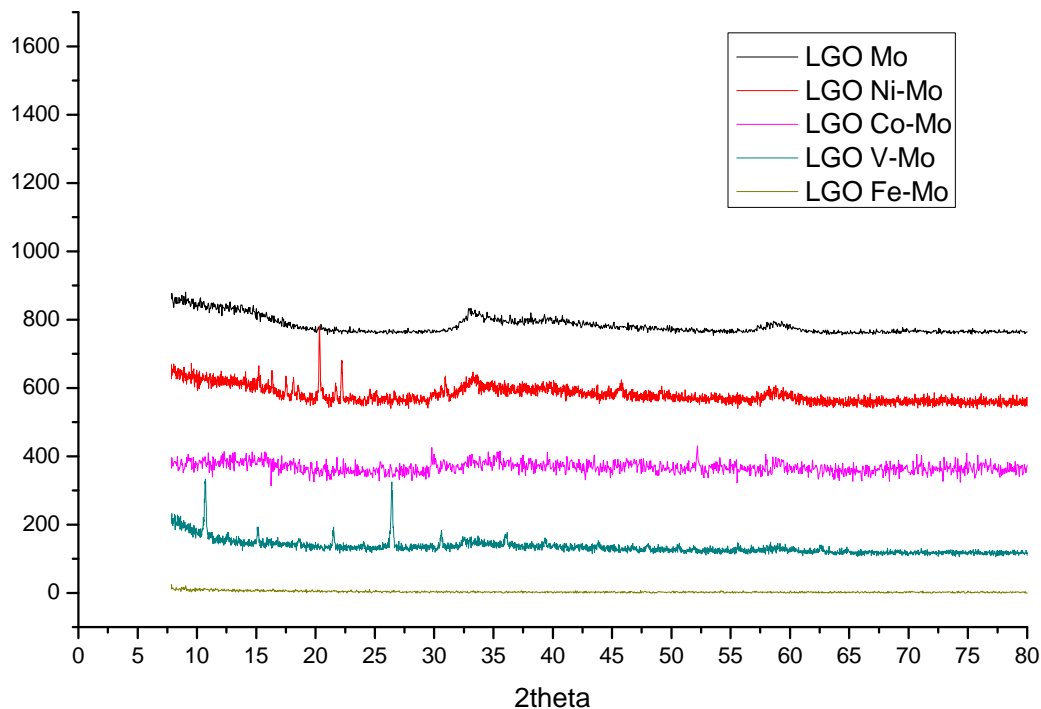


Figure 6-8 XRD patterns of unpromoted MoS₂ catalysts and MoS₂ catalysts with different metal additives derived from LGO experiments (391°C, 100ml LGO, 10ml water, 10psi H₂S, 590psi CO, 1408ppmw Mo, Metal:Mo=0.6, 2hours)

The XRD patterns of unpromoted MoS₂ catalysts and MoS₂ catalysts with different metal additives are shown in Figure 6-8. Low intensities were obtained from 10-80 degrees, reflecting a highly dispersed poly-crystalline structure of the catalyst. In samples containing MoS₂, Ni-MoS₂, Co-MoS₂ and V-MoS₂, only small molybdenum sulfide characteristic peaks were identified at $2\theta=14^\circ$, 34° and 59° , which represented the MoS₂ crystalline phase (002), (100) and (110); while no obvious MoS₂ can be found in Fe-MoS₂. Severe segregation was observed since strong Ni₃S₂ and Co₉S₈ characteristic peaks were identified. For Ni₃S₂, their peaks were located at $2\theta=22^\circ$, 32° and 45° , while for Co₉S₈ the peaks were located at 30° and 52° . The high intensity

of the V-Mo peak could be explained as being due to V sulfides, which also show interesting morphology during SEM analysis.

6.5 BET analysis of spent catalyst from LGO and C16 experiments

BET tests were performed to investigate the catalysts' surface structures. One example of isotherm curves of the MoS₂ based catalyst is shown in Figure 6-9(a). The isotherm looks like a type IV of Langmuir sorption, representing a meso-porous structure with capillary condensation. By plotting $1/[V_A \times (P_0/P - 1)]$ vs P/P_0 , a straight linear regression was achieved with the BET area calculated, as shown in Figure 6-9(b).

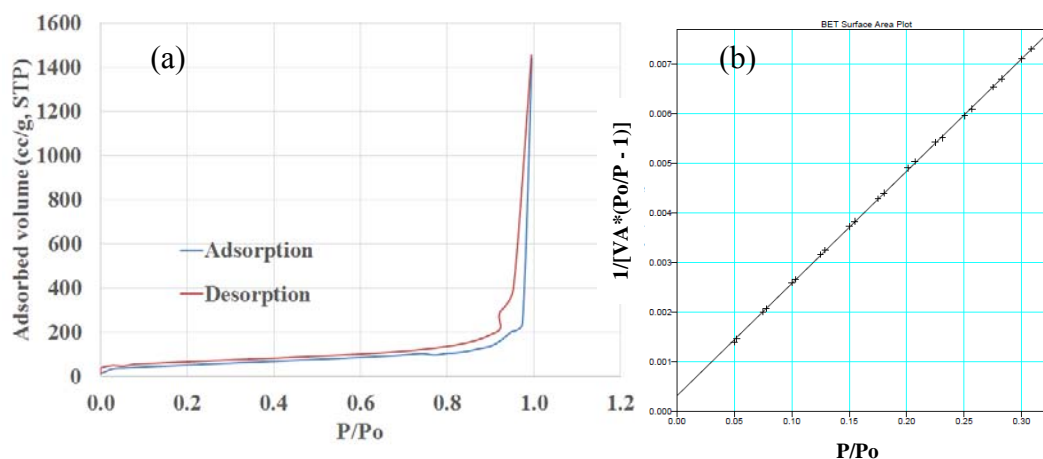


Figure 6-9 Langmuir adsorption and desorption isotherm curve and BET surface area plot examples (for NiMoS₂ catalyst prepared in C16: 390°C, 300ml C16, 30ml water, 30psi H₂S, 570psi CO, 1408ppmw Mo, Ni:Mo=0.6, 2hours)

Several spent catalysts were selected and characterized by using BET. As shown in Table 6-2, all the spent catalysts had a fairly low surface area, especially unpromoted MoS₂. The surface areas varied from 20-100 m²/g. It was reported by Lee and Liu that a typical fresh made MoS₂ catalyst from PMA had about 200-300 m²/g surface area (Lee 2004, Liu 2010). This surface area depletion could be caused by coke formation and blockage on of the catalyst's surface pores. In

order to minimize coking and simulate LGO, hexadecane (C16) was used as the solvent for preparing the *ex situ* Ni-MoS₂ catalyst, which was found to be most active during a LGO upgrading study. BET analysis on this *ex situ* catalyst revealed higher surface area at 189.6 m²/g, which was close to that reported for the *in situ* MoS₂ surface area. Although C16 had no sulfur to enhance coking on the catalyst surface, some coking might still have occurred during synthesis; while the reported surface areas were measured by using *ex situ* MoS₂ catalysts synthesized in toluene. This difference might be why this *ex situ* Ni-MoS₂ had slightly a lower surface area than the reported surface areas. However, *ex situ* Ni-MoS₂ catalyst synthesized in C16 was the most practical representative for the *in situ* formed Ni-MoS₂ catalysts. The pore volume of *ex situ* Ni-MoS₂ was 2.19 mL/g. Its adsorption average pore diameter was calculated (through 4V/A) at 470Å. This was in the meso-porous range and was in agreement with the type IV isotherm shown in Figure 6-9(a). Some more characterization was implemented on this *ex situ* Ni-MoS₂ catalyst and will be discussed in the following sections.

Table 6-2 BET results of spent catalysts from LGO experiments and fresh Ni-MoS₂ catalyst made in hexadecane (C16) (Spent catalysts: 391°C, 100ml LGO, 10ml water, 10psi H₂S, 590psi CO, 1408ppmw Mo, Metal:Mo=0.6, 2hours; *Ex situ* NiMo catalyst: 0-390°C, 300ml C16, 30ml water, 30psi H₂S, 570psi CO, 1408ppmw Mo, Metal:Mo=0.6, 0-2hours)

	Spent catalysts				<i>Ex situ</i> NiMo synthesized in C16
	Mo	NiMo	CoMo	FeMo	
Surface Area (m ² /g)	20.7	89.1	71.9	96.8	189.6
Pore Volume (mL/g)	0.0097	0.0432	0.0349	0.0469	2.1926
Adsorption Average Pore Diameter (Å)					470

6.6 HRTEM analysis of spent Ni-MoS₂ catalysts from LGO experiments

6.6.1 Crystalline structure and component of the spent Ni-MoS₂ catalysts from LGO experiments

As shown in Figure 6-10, the spent Ni-MoS₂ catalysts from the LGO experiments, were the best performing catalysts and were using TEM. At lower magnification, the agglomerated catalyst particles could be observed, with a characteristic slab structures.

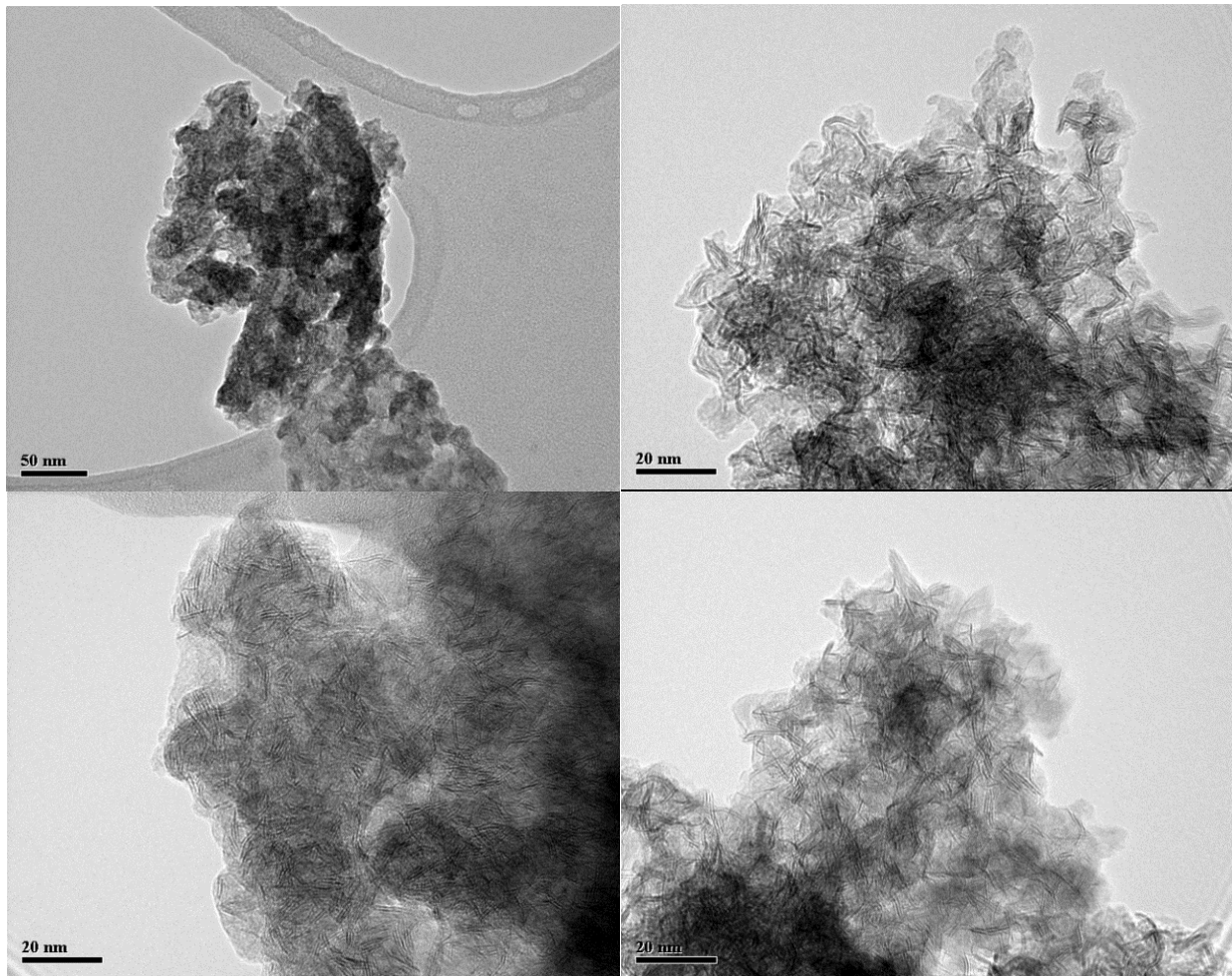


Figure 6-10 TEM images of the spent Ni-MoS₂ catalysts from LGO experiments at low resolution (390°C, 300ml LGO, 30ml water, 30psi H₂S, 570psi CO, 1408ppmw Mo, Ni:Mo=0.6, 2hours)

The MoS₂ based crystalline phases were identified by their layer structures. As shown in Figure 6-11 the high resolution TEM provided a clearer view of these slab structures, which was consistent with the MoS₂ peak results from XRD. The EDX spectrum at the bottom of Figure 6-11 demonstrated Ni existence in these slabs. However as there was no large amount of other obvious crystalline phase identified in these areas, the Ni should form a Ni-Mo-S crystalline phase instead of individual Ni sulfides phases. Nevertheless the average Ni/Mo ratio from EDX in this area was around 0.19 which was smaller than the 0.6 ratio as loaded, which meant 2/3 of the loaded Ni did not form a functional synergistic Ni-Mo-S structure. By observing the slab lengths and stacking numbers, it can be concluded that this Ni-MoS₂ catalyst had short slab lengths (around 8-10nm) and fairly low stacking numbers (usually 2-3 layers), which could be attributed to the addition of Ni (Yoosuk, Song *et al.* 2010). The short length and low stacking number observed from the HR-TEM images shown in Figure 6-11 could result in highly active catalysts.

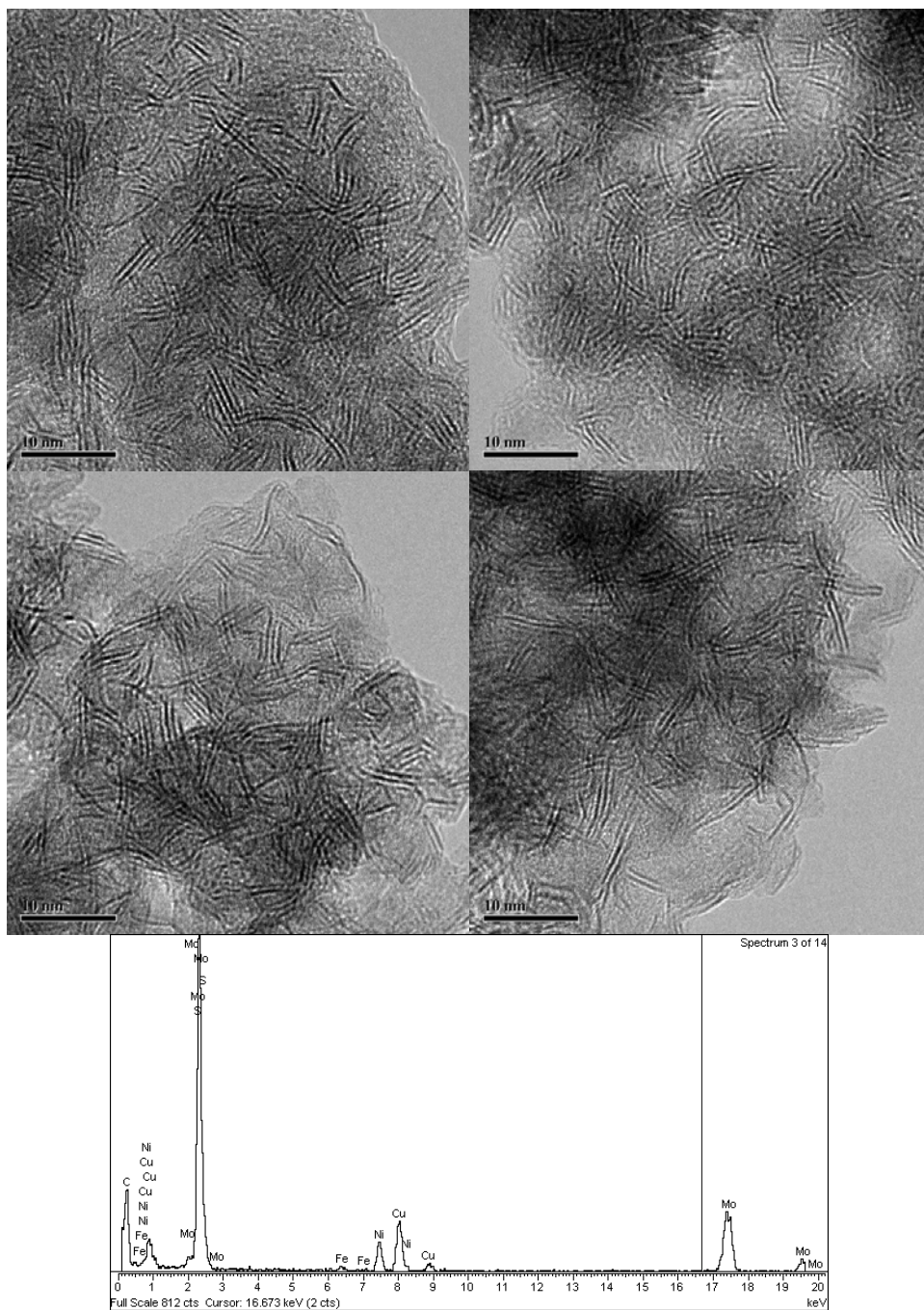


Figure 6-11 HRTEM images and EDX spectrum of the spent Ni-MoS₂ catalysts from LGO experiments at high resolution (390°C, 300ml LGO, 30ml water, 30psi H₂S, 570psi CO, 1408ppmw Mo, Ni:Mo=0.6, 2hours)

6.6.2 Reaction temperature effect on crystalline structure formation

Catalyst samples were taken at 100°C, 200°C, 300°C and 390°C, as shown in Figure 6-12 and Figure 6-13. Before 300°C there were some agglomerated particle structures formed as seen at lower magnification, but no distinguished layer crystalline phase formed until 300°C. The slab structures between 300°C and 390°C were not obviously different.

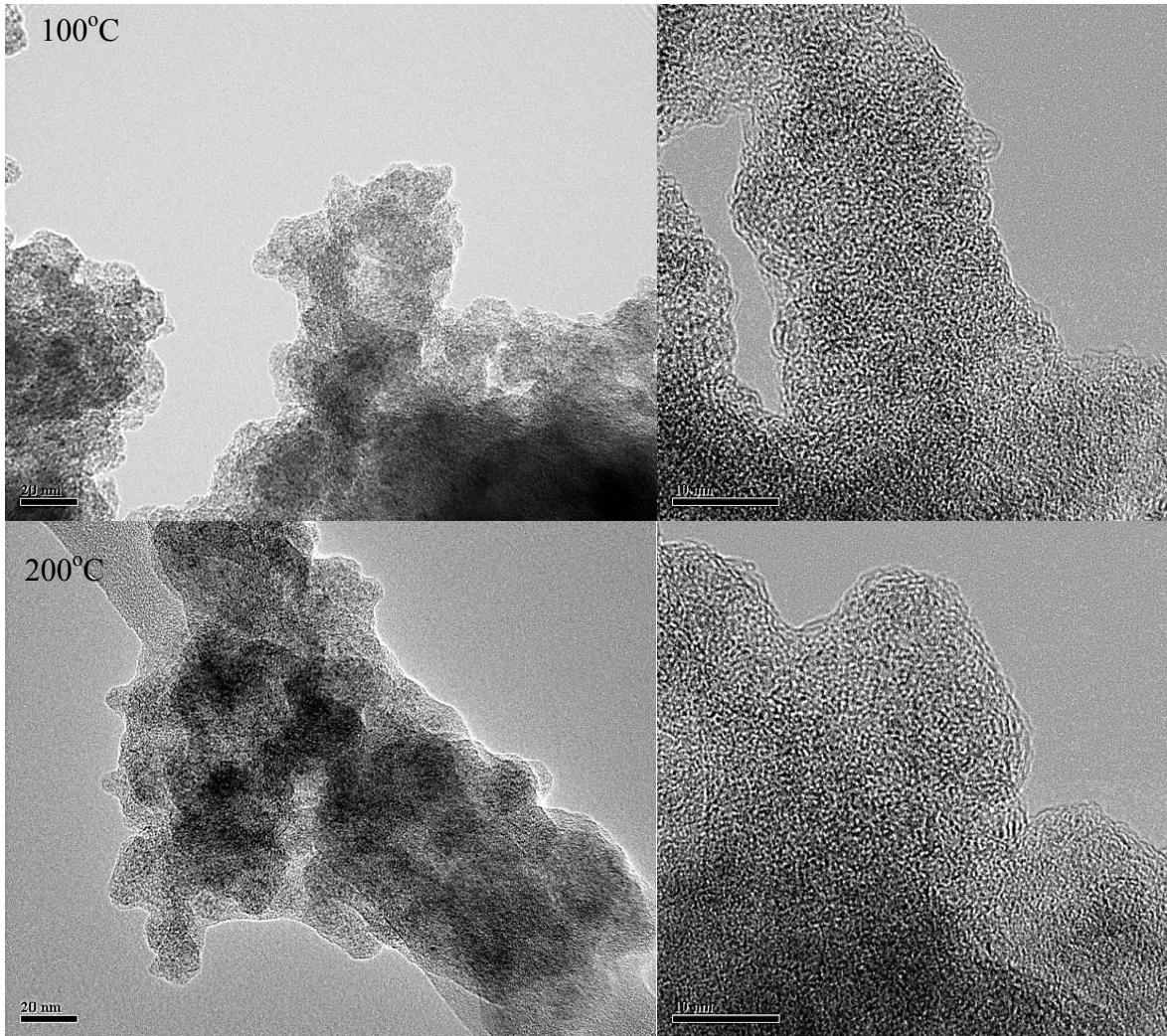


Figure 6-12 TEM (left) and HRTEM (right) images of the spent Ni-MoS₂ catalysts from LGO experiments at different reaction temperatures (100°C and 200°C, 300ml LGO, 30ml water, 30psi H₂S, 570psi CO, 1408ppmw Mo, Ni:Mo=0.6)

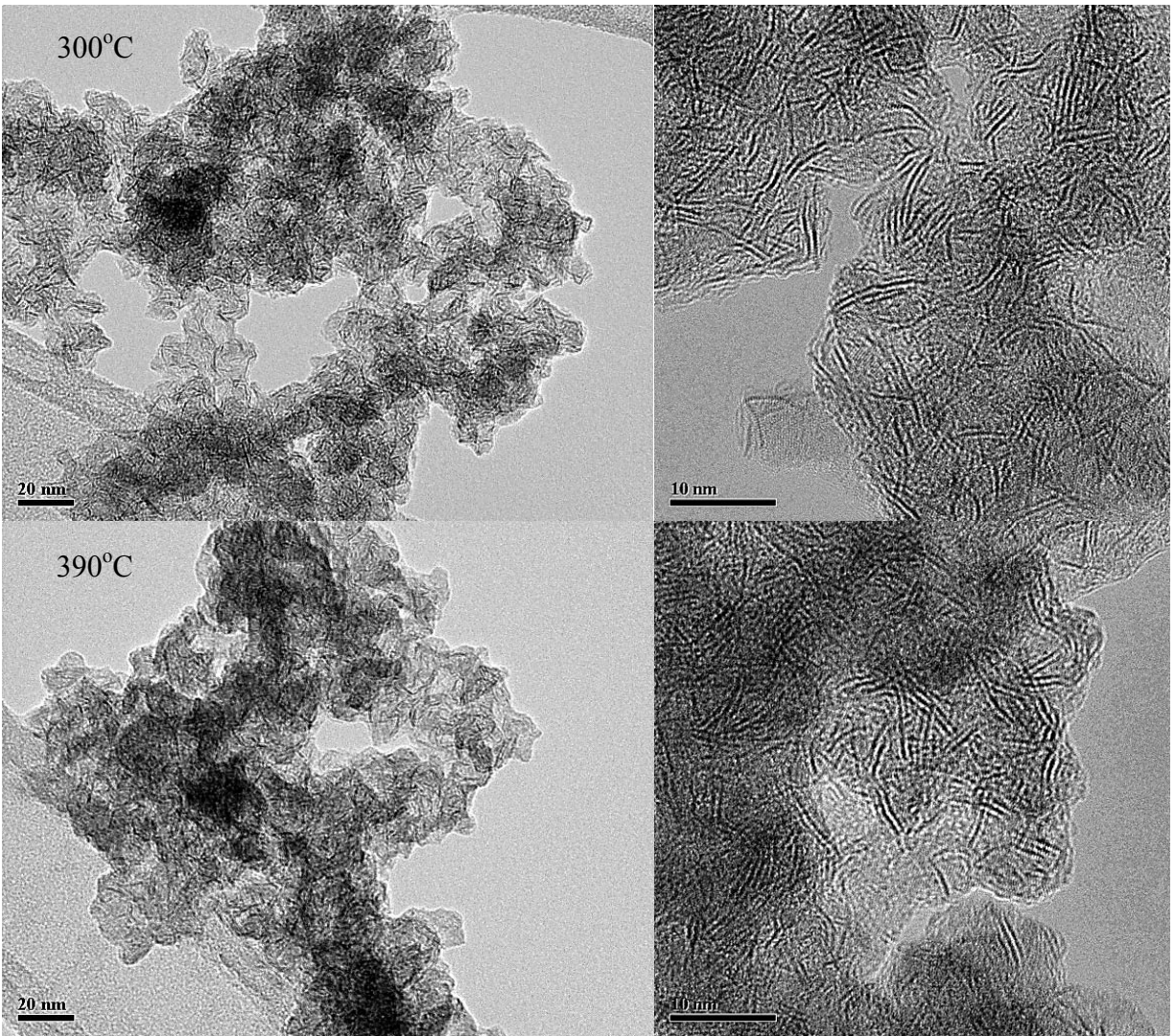


Figure 6-13 TEM (left) and HRTEM (right) images of the spent Ni-MoS₂ catalysts from LGO experiments at different reaction temperatures (300°C and 390°C, 300ml LGO, 30ml water, 30psi H₂S, 570psi CO, 1408ppmw Mo, Ni:Mo=0.6)

6.6.3 Reaction time effect on crystalline structure formation

As severe reaction could cause the same metal phase to merge together, the catalyst structure changes at different reaction times were also discussed. Reaction was operated at the optimal reaction temperature 390°C, and as shown in Figure 6-14, the slab grew longer and condensed with a higher stacking degree. These changes would result in a loss in high activity and some

variation in selectivity, which finally leads to a relatively lower life time and performance (Afanasiev 2010, Yoosuk, Song *et al.* 2010). How to prevent or minimize this drawback of unsupported catalysts will be a challenging task.

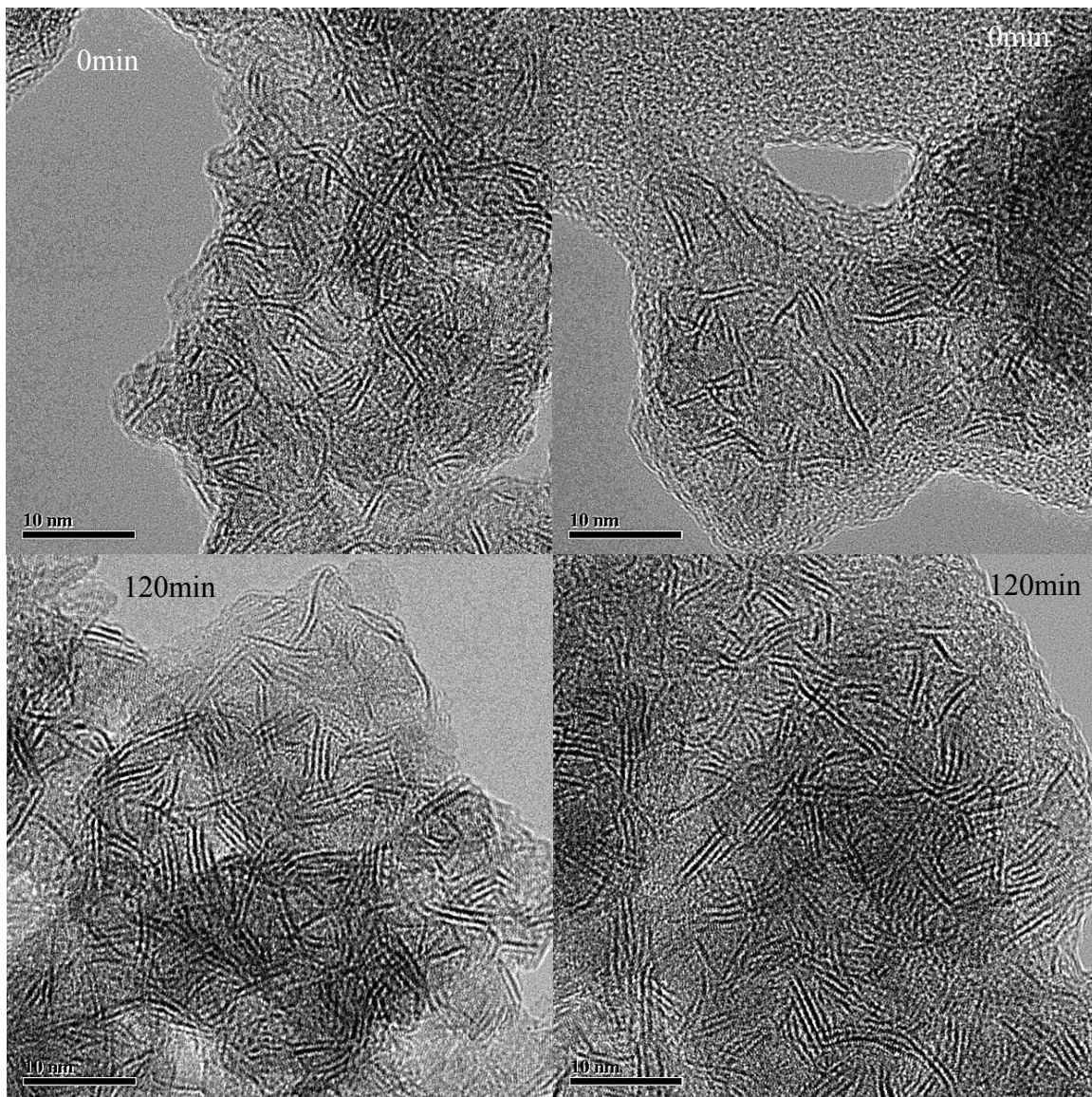


Figure 6-14 HRTEM images of the spent Ni-MoS₂ catalysts from LGO experiments at 0min (top) and 120min (bottom) (390°C, 300ml LGO, 30ml water, 30psi H₂S, 570psi CO, 1408ppmw Mo, Ni:Mo=0.6, 0min and 120min)

6.7 SEM analysis of C16 *ex situ* Ni-MoS₂ catalysts and spent MoS₂ based catalysts from the LGO experiments

6.7.1 C16 *ex situ* Ni-MoS₂ vs. spent Ni-MoS₂ from LGO experiments

6.7.1.1 C16 *ex situ* Ni-MoS₂ catalyst

Due to the formation of coke structures on the catalyst particles for the LGO experiments, the preparation of Ni-MoS₂ catalyst was carried out in C16 as a model compound to form catalyst particles with less coke formation on the surface. The SEM images of these catalysts can provide a better view of the *in situ* catalysts morphology, compared with the spent catalyst in LGO.

On comparing the detection from SE2 and BSD, the lighter parts under BSD which represented the heavier metal Mo was distributed well on all the bulky particles. In the two images below, there was no significant light or dark change in the same location as shown in Figure 6-15. Therefore no individual micrometer-scale Ni sulfide or MoS₂ was observed.

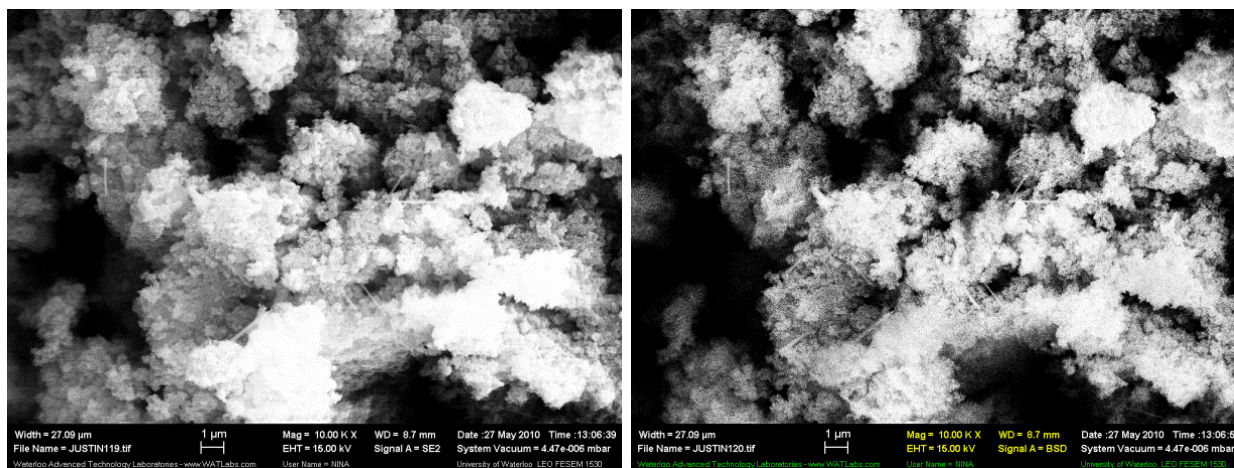


Figure 6-15 SEM images of *ex situ* Ni-MoS₂ catalysts in C16 under 10000 times magnification from SE2 detector (left) and BSD detector (right) (390°C, 300ml C16, 30ml water, 30psi H₂S, 570psi CO, 1408ppmw Mo, Ni:Mo=0.6, 2hours)

Under higher magnification the agglomerated bulky particles could be seen. In addition, some other structures were also determined. For example in Figure 6-16, the 3 small circles showed a darker area which could be Ni or a carbon rich area, the dotted bulk could be Mo rich area and the dash circle at the top-right showed some irregular wires which could be derived from Mo.

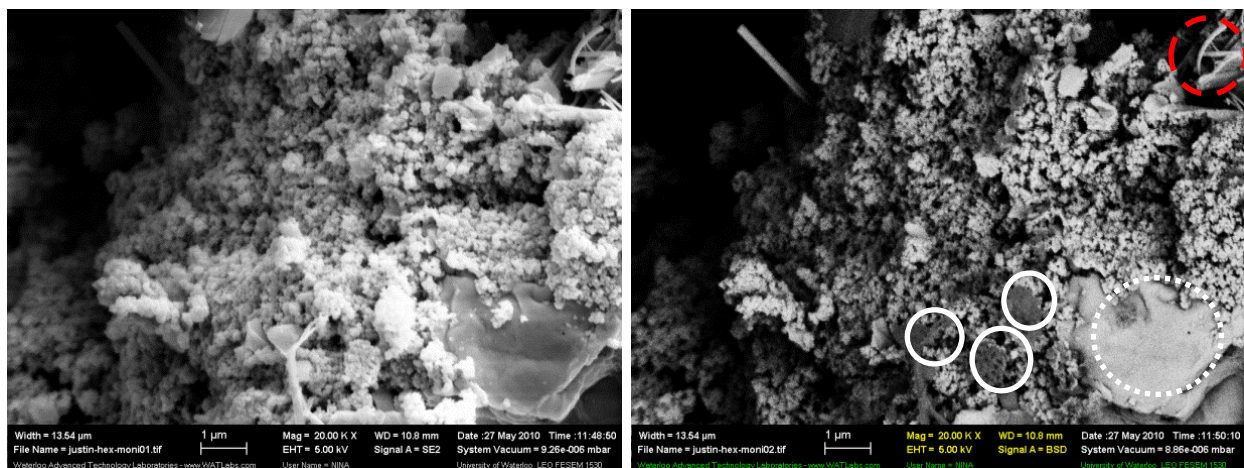


Figure 6-16 SEM images of *ex situ* Ni-MoS₂ catalysts in C16 under 20000 times magnification from SE2 detector (left) and BSD detector (right) (390°C, 300ml C16, 30ml water, 30psi H₂S, 570psi CO, 1408ppmw Mo, Ni:Mo=0.6, 2hours)

At the nanometer-scale in Figure 6-17, lots of small spheres could be seen. Their sizes were very similar, around 35-40 nm. Under BSD, everything was dispersed in a very uniform way.

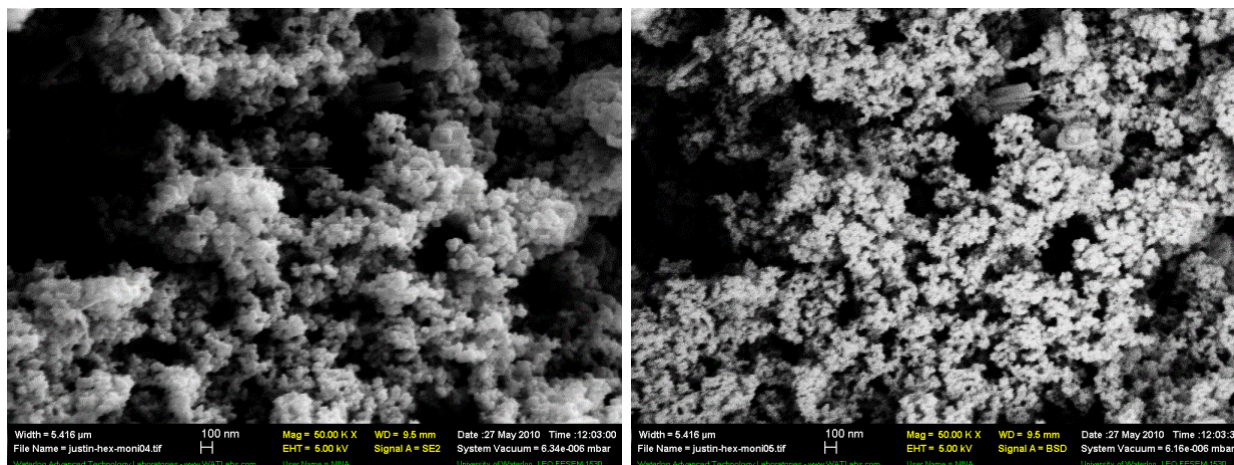


Figure 6-17 SEM images of *ex situ* Ni-MoS₂ catalysts in C16 under 50000 times magnification from SE2 detector (left) and BSD detector (right) (390°C, 300ml C16, 30ml water, 30psi H₂S, 570psi CO, 1408ppmw Mo, Ni:Mo=0.6, 2hours)

Figure 6-18 shows the EDX data for different regions of the *ex situ* Ni-MoS₂ catalysts. The atom number percentages are listed in Table 6-3. Mo/Ni varied in the different areas, which showed a slight uneven distribution of Mo and Ni in different locations on the Ni-Mo-S phase.

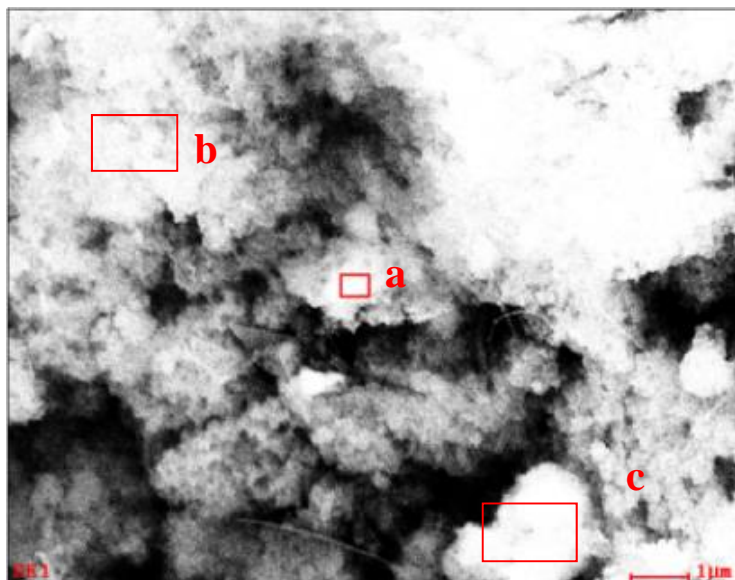


Figure 6-18 EDX analysis images of *ex situ* Ni-MoS₂ catalysts in C16: (a) and (b) top two- from left to right; (c) bottom (390°C, 300ml C16, 30ml water, 30psi H₂S, 570psi CO, 1408ppmw Mo, Ni:Mo=0.6, 2hours)

Table 6-3 Atom number percentages in each spots in Figure 6-18 obtained by EDX

Atomic %	Zone-a	Zone-b	Zone-c
Mo	28	31	35
S	53	54	51
Ni	17	13	11
Au	2	2	2

6.7.1.2 Spent Ni-MoS₂ catalyst from LGO experiments

As observed for the *ex situ* Ni-MoS₂ catalyst prepared in C16, no obvious light-dark difference was detected in each bulk particle as shown in in Figure 6-19. This means that the Ni and Mo were both dispersed very well on each particle, and no large amount of separate Mo or Ni accumulation happened. This could represent the synergistic effect from Ni on Mo as they formed a multi-metal crystalline phase instead of separate crystalline phases.

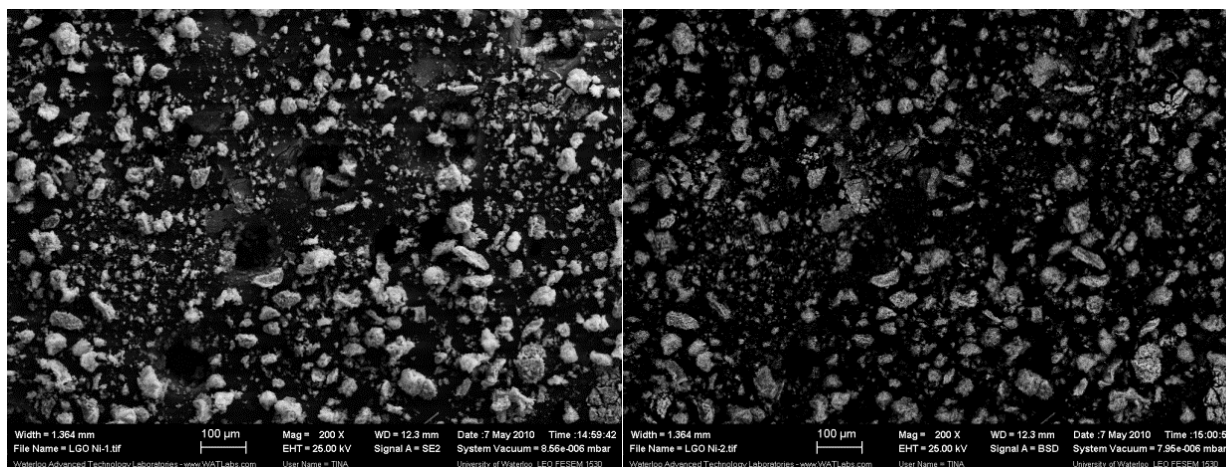


Figure 6-19 SEM images of the spent Ni-MoS₂ catalyst from LGO experiments under 200 times magnification from SE2 detector (left) and BSD detector (right) (390°C, 300ml LGO, 30ml water, 30psi H₂S, 570psi CO, 1408ppmw Mo, Ni:Mo=0.6, 2hours)

Under higher magnification, the nano-scale Ni-MoS₂ catalysts could be observed in Figure 6-20. They agglomerated with each other and were surrounded with coke deposits. The particle sizes were distributed well around 35-40 nm. Plenty of bulky irregular shapes (dash circles) were also found in the BSD image, with almost the same brightness as the particles. These bulky irregular shapes could derive from the covering and surface merging of coke; or they may arise from the poor catalyst morphology distribution after a long term hydrothermal reaction. There was only a few bulky irregular structures found in the *ex situ* Ni-MoS₂ in C16, based on the observation during analysis as shown in Figure 6-15, 6-16 and 6-17. Thus it can be concluded that the coke covering and surface merging should be the main reason.

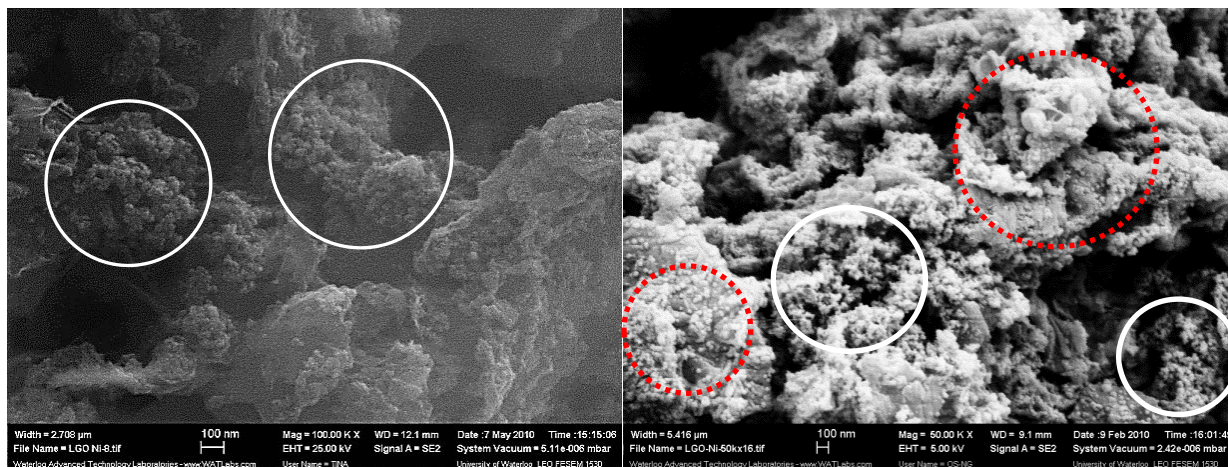


Figure 6-20 SEM image of the spent Ni-MoS₂ catalyst from LGO experiments under 100000 (left) and 50000 times (right) magnification from SE2 detector (390°C, 300ml LGO, 30ml water, 30psi H₂S, 570psi CO, 1408ppmw Mo, Ni:Mo=0.6, 2hours)

Besides nano catalysts, the coke morphology is also discussed. As shown in Figure 6-21: no specific structure was observed. Even under higher magnification there is still no regular morphology, with only a porous structure just like active carbon fibers. Under BSD, under a higher magnification no significant lighter part could be found as there was not much metal in this region.

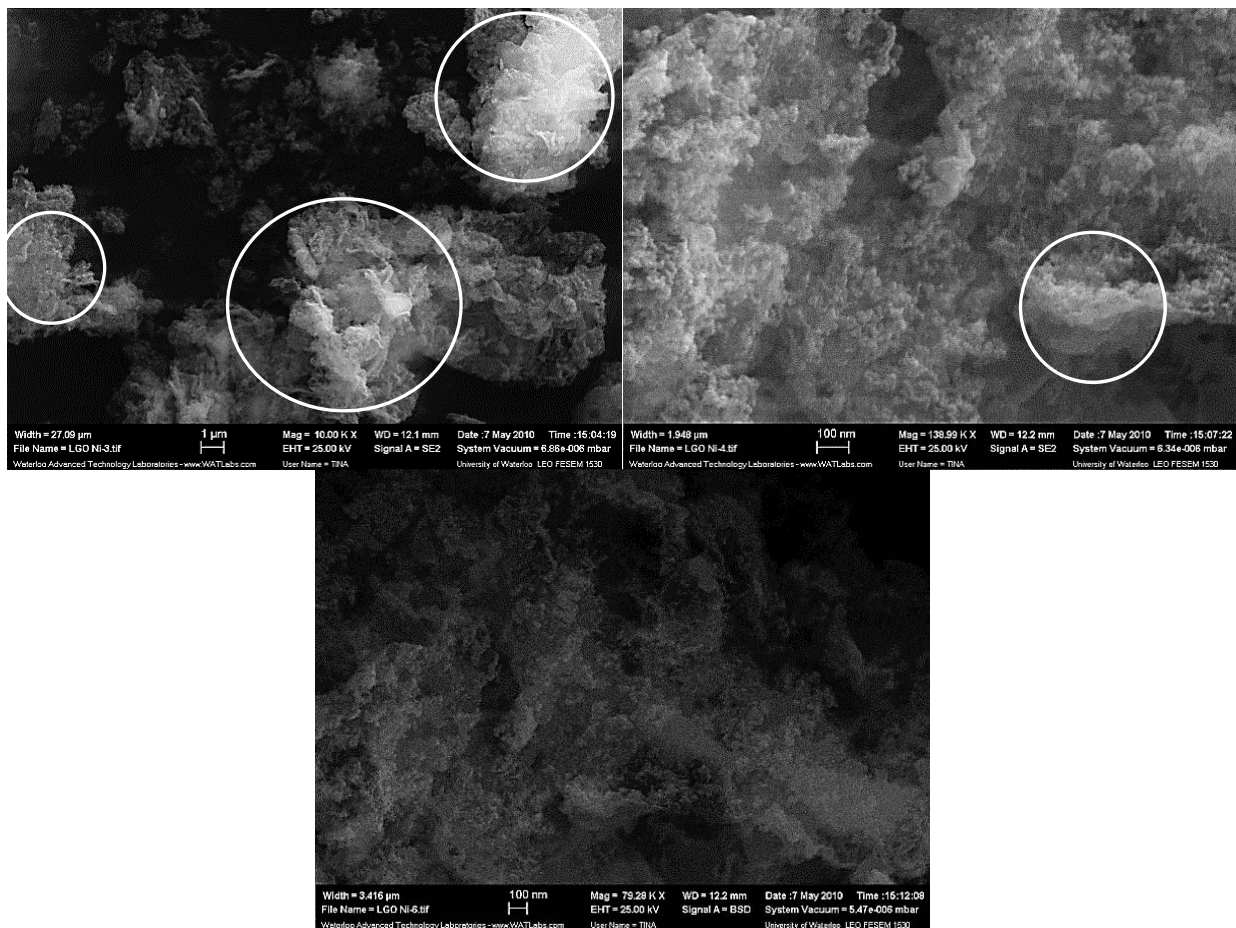


Figure 6-21 SEM image of the cokes existing in the spent Ni-MoS₂ catalyst from LGO experiments under 10000 (top left) and 139000 (top right) times magnification from SE2 detector, 80000 times magnification from BSD detector (bottom) (390°C, 300ml LGO, 30ml water, 30psi H₂S, 570psi CO, 1408ppmw Mo, Ni:Mo=0.6, 2hours)

In order to have a clearer view of metal mixtures and coke, lower magnification pictures could be helpful. As shown in Figure 6-22, the lighter parts (metal catalysts) were mixed with the darker parts (coke and metal with lower atom number).

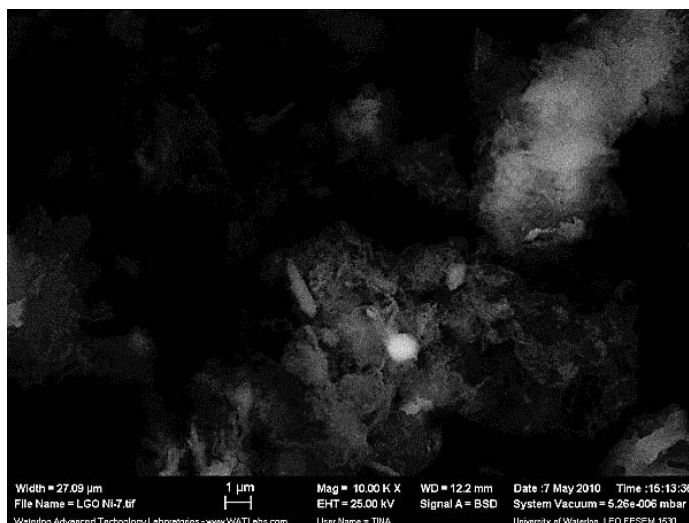


Figure 6-22 SEM image of cokes and the spent Ni-MoS₂ catalyst from LGO experiments under 10000 times magnification from BSD detector (390°C, 300ml LGO, 30ml water, 30psi H₂S, 570psi CO, 1408ppmw Mo, Ni:Mo=0.6, 2hours)

The EDX analysis in Figure 6-23 showed that the atomic ratio of each element in this lighter area (Au derived from the gold coating, and Fe came from stainless steel reactor). Ni/Mo ratio was nearly 0.27:1, which was lower than the loaded 0.6:1 but close to the EDX result obtained during TEM analysis (0.19:1).

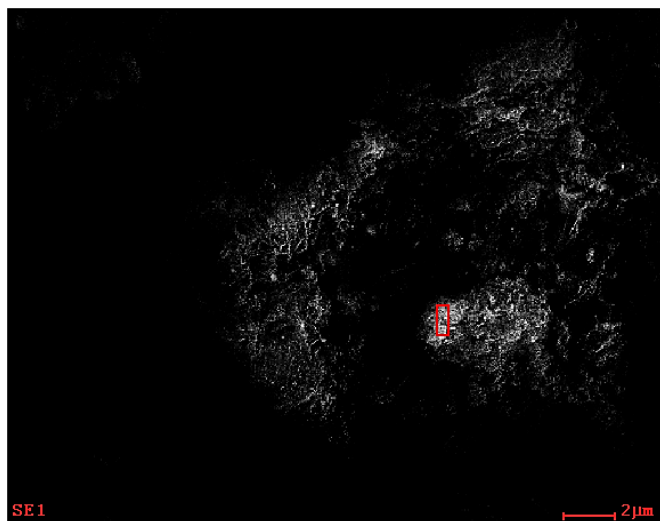


Figure 6-23 EDX analysis image of the cokes and the spent Ni-MoS₂ catalyst from LGO experiments (390°C, 300ml LGO, 30ml water, 30psi H₂S, 570psi CO, 1408ppmw Mo, Ni:Mo=0.6, 2hours)

6.7.1.3 Conclusion on hexadecane *ex situ* and spent Ni-MoS₂ catalyst in LGO

Based on all these SEM images, the formation of catalyst could be proposed. It can be concluded that after reduction and sulfiding, PMA which located at the gas and water interface began to collapse and formed MoS₂. Sometimes these MoS₂ was co-formed with other metal precursors. High speed mechanical stirring could generate a small amount of water in the oil drop resulting in nano-sized MoS₂ particles. However, the nano-size catalysts accumulated during the reaction and formed bulky particles. This was because of the similar compatibility principle, which resulted in highly polar catalysts stacked on each other instead of dispersed into the oil with a lower polarity. For the next set of experiments, some highly polar additives could be considered. Some patents have been published on this topic (Wang, Guan *et al.* 2002). These additives can be surfactant and dispersant which contain C, H, O and some ppb level of N, which may be used at high temperature around 300°C.

In all of these SEM and EDX images, no obvious Ni sulfide was observed at the micro-scale; instead Ni formed co-sulfides with Mo and provided the best performance. However, the Mo/Ni

ratio varied in different areas, not only in the spent Ni-MoS₂ catalyst in the LGO experiments but also in the *ex situ* Ni-MoS₂ catalyst prepared in hexadecane. This implies that the dispersion of Ni and Mo was uneven, and partial segregation began to happen at the nano-scale. In future more catalyst *ex situ* designing techniques should be applied in the synthesis of highly uniform Ni-Mo unsupported catalysts.

6.7.2 Other unpromoted and promoted spent MoS₂ catalysts from LGO experiments

6.7.2.1 Spent MoS₂ catalysts from LGO experiments

Nano catalysts could be examined at higher magnification, as circled in Figure 6-24, and the particle sizes were around 35-40 nm.

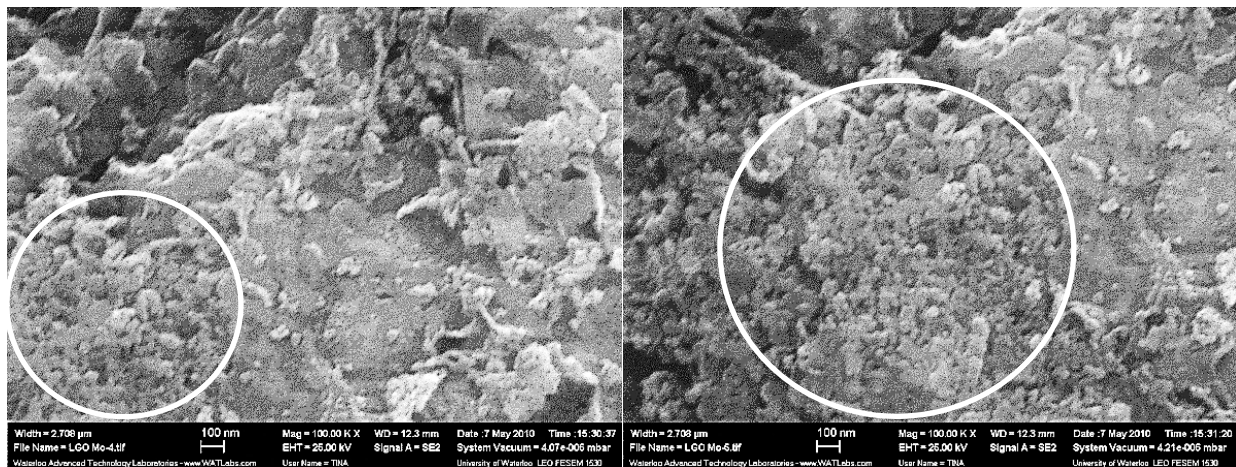


Figure 6-24 SEM images of the spent MoS₂ catalysts from LGO experiments under 100000 times magnification from SE2 detector (391°C, 100ml LGO, 10ml water, 10psi H₂S, 590psi CO, 1408ppmw Mo, 2hours)

6.7.2.2 Spent Co-MoS₂ catalysts from LGO experiments

In Figure 6-25, Co-MoS₂ particles could be distinguished easily in the nano range, and their particle sizes were similar to Mo and Ni-Mo as shown. Under BSD no light and dark occurred in the particle zone, which demonstrated that the Co-Mo catalysts were dispersed well without

individual metal sulfide on a large scale. This was consistent with the high performance of Co as a promoter.

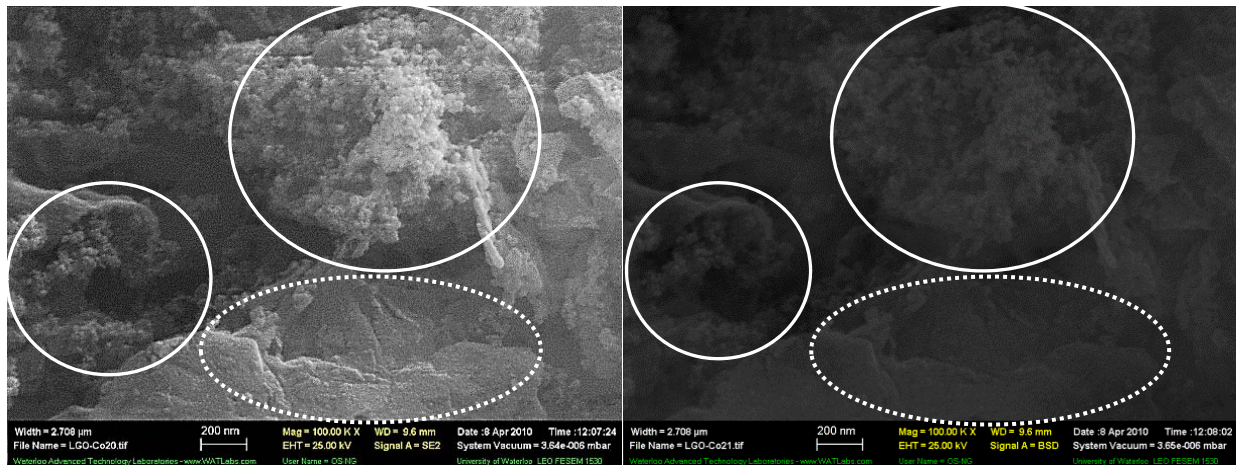


Figure 6-25 SEM images of the spent Co-MoS₂ catalysts from LGO experiments under 100000 times magnification from SE2 detector (left) and BSD detector (right) (391°C, 100ml LGO, 10ml water, 10psi H₂S, 590psi CO, 1408ppmw Mo, Co:Mo=0.6, 2hours)

The comparison of different brightness areas in Figure 6-26 could explain how the coke and crystalline phase changes affected the EDX data. Element percentage data from EDX are provided below in Table 6-4. In zone-b, carbon content was higher than in zone-a, resulting in a darker area under BSD observation with less metal present.

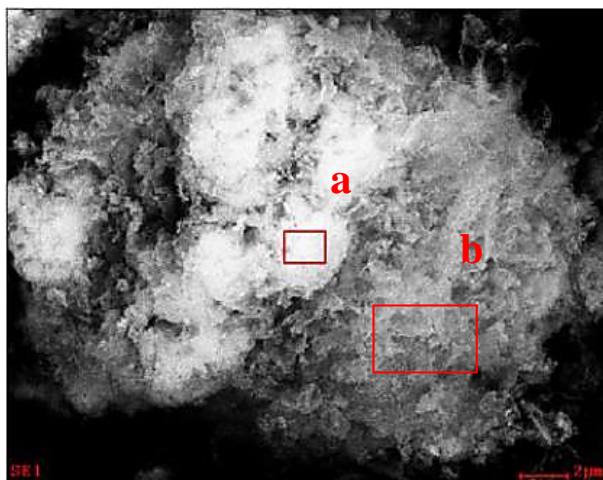


Figure 6-26 EDX analysis images of the spent Co-MoS₂ catalysts from LGO experiments in different areas (391°C, 100ml LGO, 10ml water, 10psi H₂S, 590psi CO, 1408ppmw Mo, Co:Mo=0.6, 2hours)

Table 6-4 Atom number percentages in each spots in Figure 6-26

Element	Atomic % in “a”	Atomic % in “b”
C	76	88
Mo	12	7
S	8	3
Fe	0.4	0.2
Co	4	1
Au	0.4	0.2

6.7.2.3 Spent Fe-MoS₂ catalysts from LGO experiments

Under a higher magnification in Figure 6-27, some sphere-like structures were found. But some of them seemed to combine with each other or become covered with coke. This could explain the low intensity of the Fe-MoS₂ spectrum in the XRD. Furthermore, the undistinguishable sphere and other structure were observed again, and in a large amount.

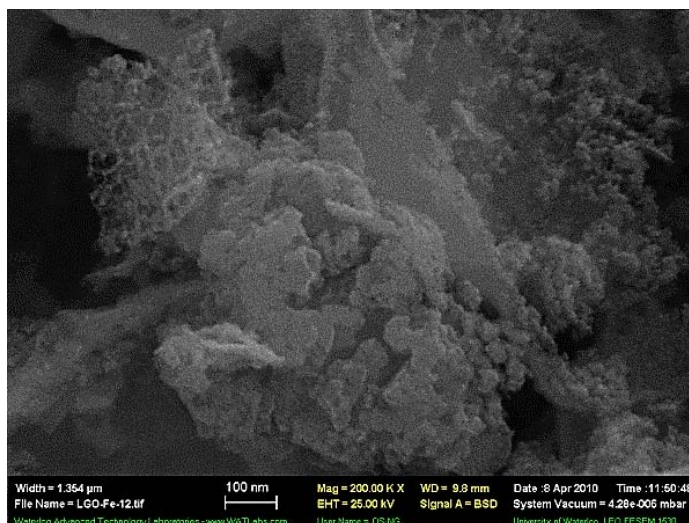


Figure 6-27 SEM images of the spent Fe-MoS₂ catalysts from LGO experiments under 200000 times magnification from BSD detector (391°C, 100ml LGO, 10ml water, 10psi H₂S, 590psi CO, 1408ppmw Mo, Fe:Mo=0.6, 2hours)

6.7.2.4 Spent V-MoS₂ catalysts from the LGO experiments

In Figure 6-28 no typical MoS₂-like particle was observed at all, even when the magnification was as high as in the nano range.

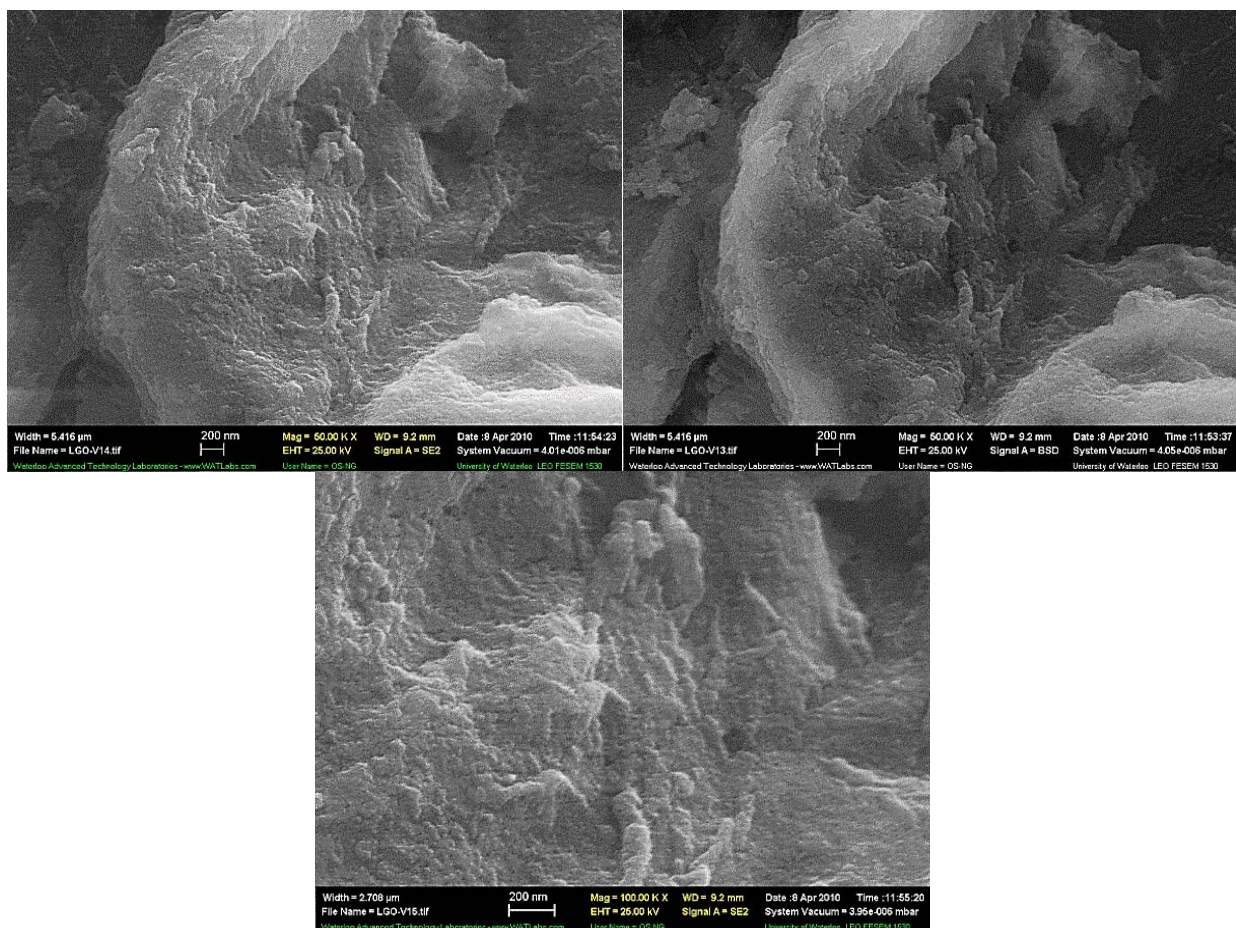


Figure 6-28 SEM images of the spent V-MoS₂ catalysts from LGO experiments under 50000 times magnification from SE2 detector (top left) and BSD detector (top right); SEM images of LGO-tested V-MoS₂ catalysts under 100000 times magnification from SE2 detector (bottom) (391°C, 100ml LGO, 10ml water, 10psi H₂S, 590psi CO, 1408ppmw Mo, V:Mo=0.6, 2hours)

6.8 Conclusions

Mo sulfide characteristic peaks were identified at $2\theta=14^\circ$, 34° and 59° , which indicated the MoS₂ crystalline phase (002), (100) and (110) in the XRD. Ni₃S₂ and Co₉S₈ crystalline phases were also observed in the Ni-MoS₂ and Co-MoS₂ spent catalysts. *Ex situ* synthesized Ni-MoS₂ in C16 exhibited a high surface area at 189.6m²/g; while other spent catalysts suffered severe coke blockage and had much smaller surface area. This coke formation was also confirmed by the EDX results.

A characteristic slab structure was observed in the TEM results. Spent Ni-MoS₂ catalyst had a slab length of around 8-10nm and low stacking numbers of 2-3 layers. This structure represented a higher catalytic activity which could be attributed to the addition of Ni. The Ni:Mo atomic ratio was around 0.19, lower than the 0.6 loading Ni:Mo ratio, indicating part of the Ni did not form the Ni-Mo-S structure. This result was further confirmed from the SEM-EDX data. Regarding the temperature effect on crystalline structure formation, it was found that no distinguished layer crystalline structure was observed until a temperature of 300°C. This layer structure became longer and more stacked with a longer reaction time, which could potentially cause activity reduction.

Spherical catalyst particles were synthesized with a size distribution of around 35~40nm as observed by SEM. Small amount of other structures could also be found. Catalyst particles agglomerated into bulky particles. Some highly stable surfactant or dispersant should be considered for preventing this agglomeration. Coke was found in irregular shapes and covered or was surrounded by bulky MoS₂ catalysts. No separate Ni₃S₂ or MoS₂ crystalline was observed at a large scale, but a light uneven Ni, Mo distribution still existed at the nano-scale on the catalyst surface due to a lack of nano-scale dispersing techniques, which was consistent with the XRD data. Regarding the spent catalysts, it was noticed that their particle sizes did not change significantly with the addition of other metals. Agglomeration was unpreventable even by adding another metal ion. Some metals, Ni or Co for instance, dispersed well with Mo and formed even distribution morphologies on a micrometer scale. These two metals provided considerable promotional synergistic effects. On the nanometer scale the uneven metal/Mo distribution was discovered on all catalyst surfaces (with and without metal additives, no matter whether a promoter was present or not). Partial segregation led to individual metal sulfide rich phases observed under EDX. Plenty of irregular coke deposits covered the MoS₂ particles in Fe-MoS₂ and V-MoS₂, and no obvious sphere structure was observed under high magnification. The XRD data of the V-MoS₂ catalysts showed the existence of MoS₂; however, Fe-MoS₂ did not show the existence of MoS₂ probably due to the large amount of coke coverage.

Chapter 7 Effect of Preparation Conditions on the Morphology of Fresh Unsupported *Ex Situ* MoS₂ based Catalyst Synthesized in a Toluene/Water Emulsion

7.1 Introduction

Chapter 7 is a deeper level characterization and statistical study on the fresh *ex situ* MoS₂ catalysts synthesized under various conditions. The correlations between morphology (slab length, stacking numbers, and elemental ratio) observed under HRTEM and EDX will be discussed with the activity results obtained from previous studies or the literature.

7.2 Fresh *ex situ* MoS₂ catalysts – proxy for *in situ* MoS₂ catalysts

As discussed in the previous chapters, unsupported *in situ* MoS₂ based catalysts play a key role in facilitating the emulsion upgrading process. This has been confirmed through both model compound and actual oil feedstock experiments. Since the catalysts are formed *in situ* during the reaction, it creates certain difficulty in characterizing the actual *in situ* catalysts, like the inaccessibility of *in situ* catalysts and the interference of targeted organic compounds or oil. Some publications reported several advanced *in situ* analytical methods for characterizing *in situ* catalysts, like *in situ* FT-IR, *in situ* temperature programmed desorption/reduction (*in situ* TPD/TPR), etc. However, these analytical studies are usually limited to the capabilities of their vessels. For example, typical *in situ* solid characterization sample vessel does not allow for the presence of oil or water; while *in situ* catalysts are formed in the oil/water emulsion. Some sample vessels might withstand certain high temperature and/or high pressure, but the price of building such vessels to meet 400°C+ and 3000psi+ conditions would be prohibitively high.

Furthermore, only limited types of characterization could be carried out under such high temperature/ high pressure conditions, such as adsorption/desorption, spectroscopy, etc. As one of the most important characterization methods for analyzing MoS₂ catalysts, electron microscopy could not be theoretically used for the *in situ* characterization of the MoS₂ catalysts. This is because a high degree vacuum is required for electron microscopy to avoid interference from other impurities, like oil, water, etc. Due to the above theoretical, practical and economic limitations, the actual characterization of *in situ* MoS₂ catalysts synthesized through high temperature and high pressure conditions are still almost impossible to be characterized under such process conditions. As a result, it is necessary to find a representative proxy for *in situ* catalysts, and analyze this proxy with conventional characterization methods like TEM, EDX, etc.

Fresh *ex situ* MoS₂ catalysts can be used as representative proxies for *in situ* MoS₂ catalysts. “Fresh” means that the catalyst was synthesized in an organic solvent free from S or N, and collected right at the target preparation temperature. This allows the collected *ex situ* catalysts to represent the *in situ* catalysts at the 0min in the actual upgrading. For example, the previously discussed C16 *ex situ* catalysts were prepared in hexadecane as the organic solvent to simulate a LGO fluid condition; the introduction of S-free C16 also minimized S initiated coke formation, providing clearer morphology for the interpretation of the spectra.

Fresh unsupported *ex situ* MoS₂ based catalysts were synthesized under various conditions using an Autoclave300mL Hastelloy C-276 batch reactor. High purity toluene was chosen as the organic phase due to its relatively low boiling point. It was also used consistently in previous model compound studies. With the help of the high pressure sampling system shown in Figure 2-2, MoS₂ catalysts were collected at the targeted reaction temperatures within a toluene/water emulsion. Then the catalysts were first filtered using a #42 filter paper, washed three times with acetone, and finally re-dispersed in deaerated ethanol for HRTEM and SEM analysis. The above separation steps were performed in a glove bag filled with N₂ for preventing oxidation of the catalysts. Due to time constraints and equipment availability, SEM analysis was not carried out.

HRTEM and EDX experiments were completed, and the detailed HRTEM/EDX experimental steps can be found in Section 2.6.3.2 of Chapter 2.

7.3 Statistical analysis of MoS₂ catalysts slab structures by using HRTEM

It is widely acknowledged that shorter slabs and/or smaller stacking numbers represent improved HYD selectivity in the HDS reaction. This was first concluded and published by Topsøe and his coworkers in a series of papers (Topsøe 2003, Lauritsen, Nyberg *et al.* 2004, Lauritsen, Kibsgaard *et al.* 2007, Moses, Hinnemann *et al.* 2007, Topsøe 2007, Besenbacher, Brorson *et al.* 2008, Kibsgaard, Tuxen *et al.* 2010). As discussed in Chapter 6, combined STEM and DFT studies revealed that the metallic-like brim sites located adjacent to the edge of MoS₂ slabs were the active sites for the HYD pathway (Moses, Hinnemann *et al.* 2007). As a result, short slabs will provide more edge active sites. It should also be noted that only the top layers of the stacked slabs could expose brims as the active sites for HYD, so lower stacking numbers would create more active sites for HYD. Compared to the DDS pathway, HYD is more difficult and usually limits the total HDS performance. In this way, MoS₂ catalysts with short slab lengths and lower stacking numbers are preferred. HRTEM analysis, which allows direct observation of the MoS₂ catalyst slab crystalline structure, has been extensively used and reported over the past decade. However, most of the early reported conclusions were based only on several selected HRTEM images. No evidence of statistical analysis was provided, like statistical sample volume, standard deviation, etc. Hence, results from these publications seem weak or lack support. Recently some statistical analysis of the slab lengths and stacking numbers has been published, and the morphology and an activity correlation has been discovered. For example, Liu analyzed 480~650 slabs per sample in her thesis, and found the slab structure difference of MoS₂ catalysts in oil and water phases (Liu 2010). Li reported that the DDS selectivity could be linearly correlated with the slab length of CoMoS₂ catalysts based on a statistical analysis for at least 150 slabs per sample (Li, Li *et al.* 2010). Recently there was another similar publication discussing the correlation between DDS selectivity with CoMoS₂/γ-Al₂O₃ catalysts with a Mo proportion at the edge sites over corner sites (Liu, Chai *et al.* 2014). The Mo location proportion was calculated by

assuming perfect hexagonal CoMoS structure and was based on 250~300 slabs in at least 10 images in a different area.

The objective of the statistical analysis to be discussed in this chapter was to discover the relationship between morphology and synthesis conditions. In order to improve the accuracy, large statistical sample volumes were chosen. For most of the samples, 400~600 slabs were measured based on 15~30 HRTEM images per sample. Moreover, at least 3 different clusters were observed per sample to collect more representative information. Professional imaging software, *Digital Micrograph*, was used for the HRTEM image analysis. As shown in Figure 7-1, slab length was measured by applying the ROI tool “curve measurement” manually. The “L” shown at bottom left of Figure 7-1 was the measured slab length. Length calibrations were performed before measurements.

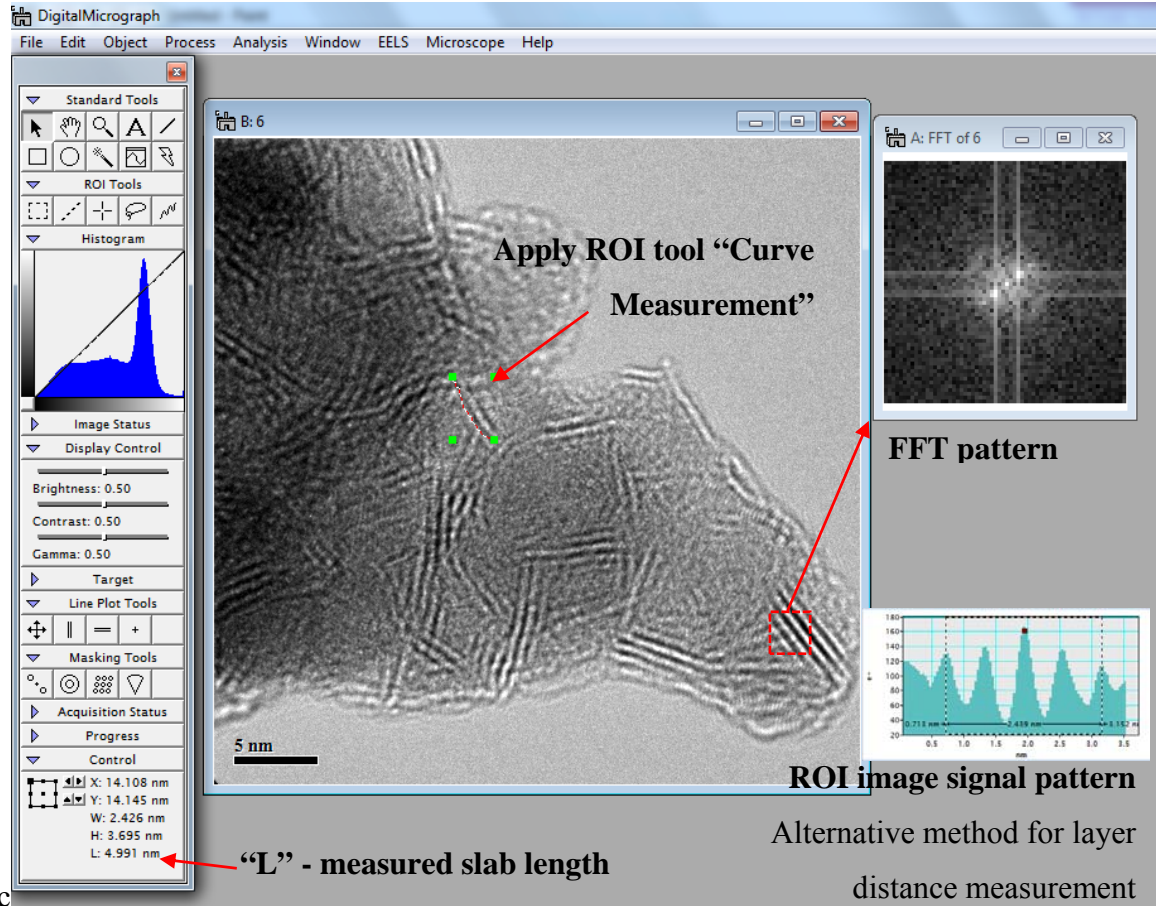


Figure 7-1 Analysis of HRTEM image by using *Digital Micrograph* software

This software also allowed fast Fourier transform (FFT) analysis of the slab patterns. As shown in the top right of Figure 7-1, the FFT pattern was collected. The distance between the two light spots could be used for measuring the layer distance. For example, in the same FFT image, the spot distance was measured at 3.271 (1/nm). By following Eq. 7-1 the layer distance was found to be equal to $2/3.271$ nm, which was 0.611 nm or 6.11 Å.

$$\text{Layer Distance} = \frac{2}{\text{Spots Distance shown in FFT}} \quad (\text{Eq. 7-1})$$

Another alternative layer distance measurement method is also listed in Figure 7-1 by using ROI image signal pattern analysis. This measurement only required perpendicular drawing across the layers, and the results in Figure 7-1 showed 0.609 nm for the layer distance, which was very close to the FFT result. Compared to the FFT method, the second method was much easier. However, it was sometimes less accurate by using FFT in MoS₂ slab analysis, because: (a) the curved slab provided a potential large noise effect in the FFT pattern; and (b) the light spot distance measurement had substantial error due to the difficulty in locating the spots. As a result, the ROI image signal pattern method was mainly used for the layer distance measurements. The layer signal pattern for each sample was shown in its selected HRTEM image. It should be noted that even the chosen second method still had considerable error due to non-perfect perpendicular cross-line drawing and poor peak selection. Due to time constraints and potential significant error, no statistical analysis was completed on the layer distance measurement. The presented layer distances are only discussed as a reference.

7.4 Results and discussion

7.4.1 Effect of temperature

7.4.1.1 Effect of temperature under H₂

Fresh *ex situ* MoS₂ catalysts were synthesized under a molecular H₂ atmosphere and collected at 300°C, 340°C and 390°C respectively. As shown in Table 2-3, the experiments were carried out under the following condition “100ml toluene, 10ml water, 30psi H₂S, 570psi H₂, 0min”.

As shown in Figure 7-2, TEM (left) and HRTEM (right) images were presented for fresh *ex situ* MoS₂ catalysts collected at 300°C, 340°C and 390°C (from top to bottom). Similar to the previously discussed TEM and HRTEM images, nano spherical particles were observed with characteristic slab-like crystalline structures representing a MoS₂ (002) phase. It is also observed that the spherical particle morphology was obtained at temperatures as low as 300°C; this was consistent with the previous findings discussed in Chapter 6. Some agglomeration was found, indicating a somewhat potential loss of activity due to the overlap of active sites. The spherical

particle structure was more distinguishable at 340°C and 390°C compared to the packed particles obtained at 300°C. This could be explained by better crystal formation of catalysts achieved with increased temperature. Nevertheless, particle sizes remained almost the same at various temperatures. This could be attributed to the good oil/water dispersion maintained by high speed stirring, where most of the Mo precursor stayed in the tiny water droplets during sulfiding.

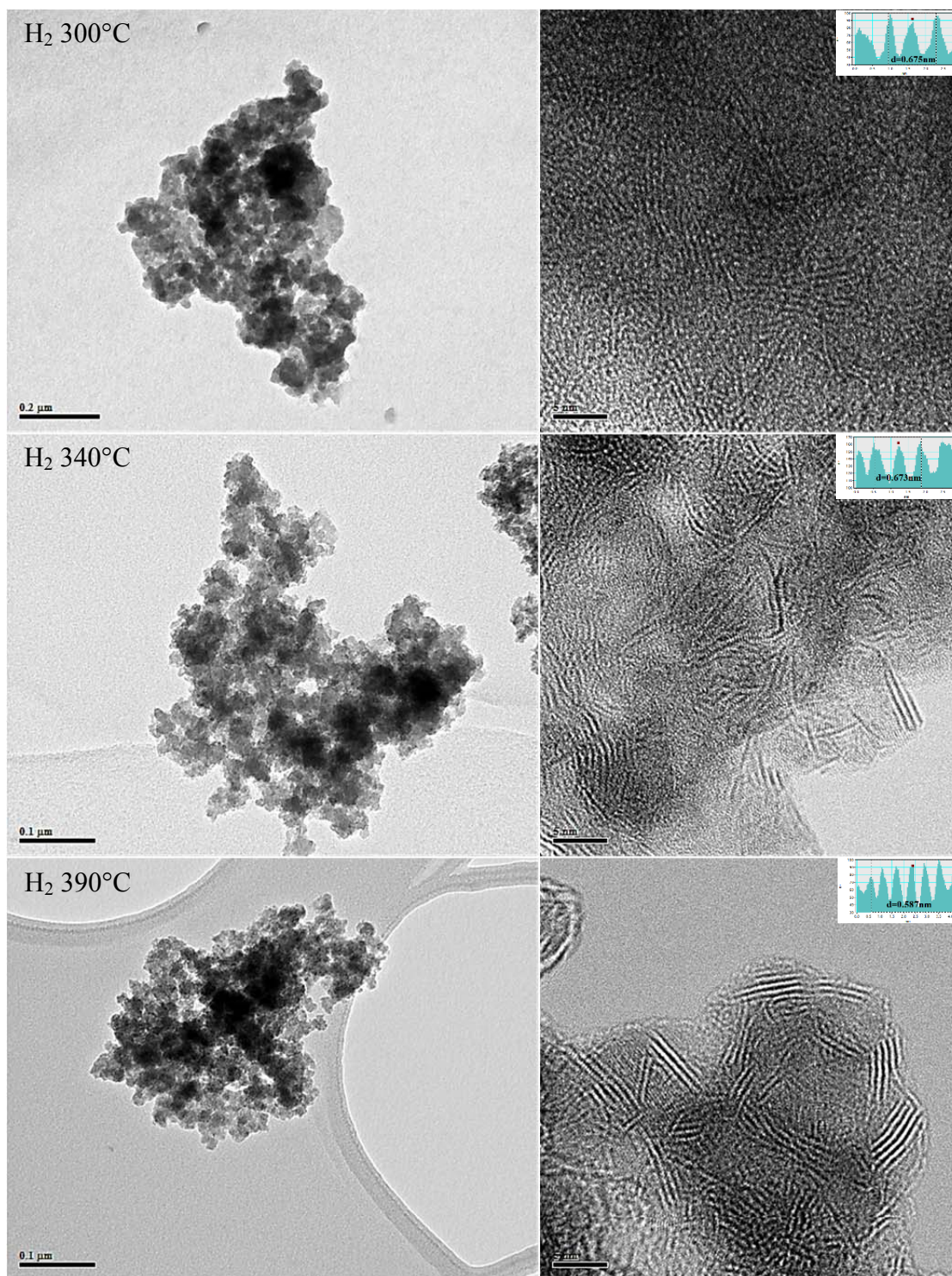


Figure 7-2 TEM (left) and HRTEM (right) images of the fresh *ex situ* MoS₂ catalysts collected at different temperatures under H₂

Another interesting observation is the gradual formation of a slab-like crystalline (002) phase with increasing temperature. As shown in Figure 7-2, only a blurred slab structure was present in catalyst collected at 300°C, which created certain difficulty in measurement and statistical analysis. As shown in Table 7-2, only 55 slabs were found available for statistical measurement in the catalyst collected at 300°C, which made the statistical result here of poor confidence for the statistical analysis. These indistinct slabs could be attributed to the poorly formed crystalline structures at low temperature. With increased temperature, the (002) phase was gradually formed with more distinguishable slab-like structures.

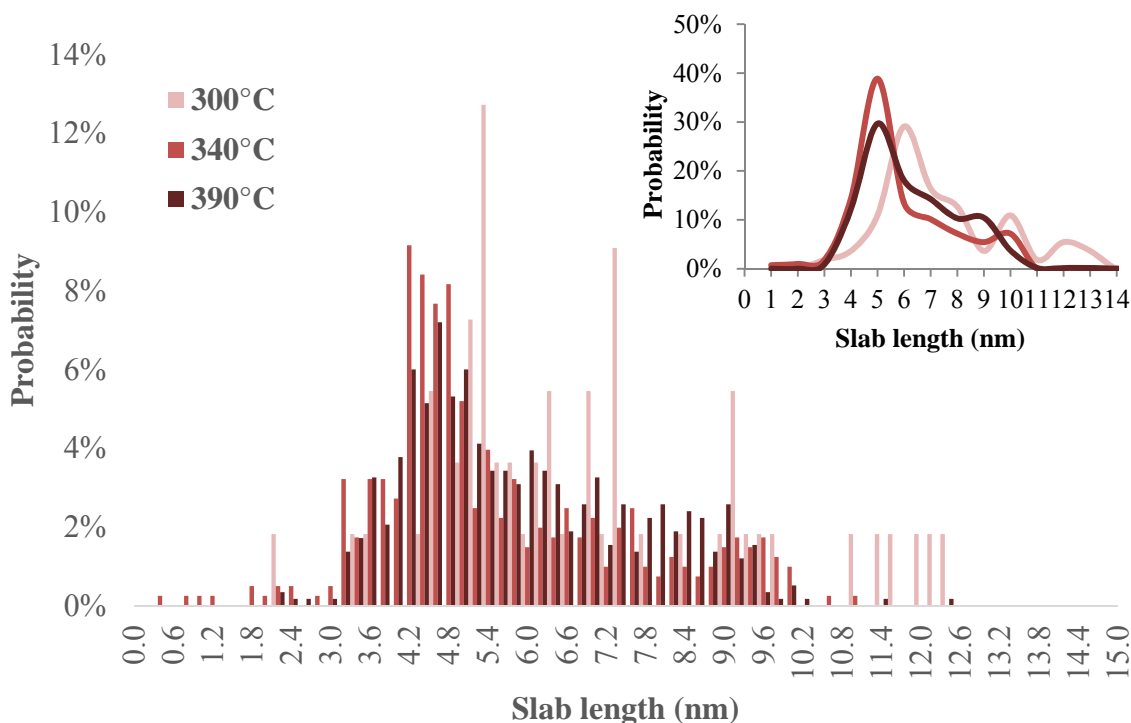


Figure 7-3 Slab length distributions (0.2nm incremented in big chart; 1nm incremented in small chart) of fresh *ex situ* MoS₂ catalysts prepared with under H₂ collected at different temperatures

Statistical analysis was performed for the slab length distribution and stacking number distribution. As shown in Figure 7-3, slab length distributions were presented for both 0.2nm

increments (big chart) and 1nm increments (small chart) styles. This allowed for a demonstration of both a detailed distribution pattern with narrow increments and a general trend with wide increments. The statistical sample volumes and results are summarized in Table 7-2. As discussed above, the blurred slabs in the catalyst collected at 300°C resulted into a much smaller statistical sample volume (only 55 slabs measured), which hence reduced the confidence of the relevant results. This was why the relatively longer slab length collected at 300°C could not contribute to the conclusion that “increased temperature reduced slab length”. Conversely, it was noticed that the higher probability for longer slabs (especially for 6~10nm range) increased from 340°C to 390°C, which indicated that higher temperature resulted in longer slabs. This was consistent with the previous discussion in Chapter 6, where more distinct and longer crystalline structures were favoured at higher temperature. The average slab lengths shown in Table 7-2 further confirmed this observation, where the average slab lengths at 340°C and at 390°C were $5.40\pm 1.91\text{nm}$ and $5.78\pm 1.75\text{nm}$ respectively.

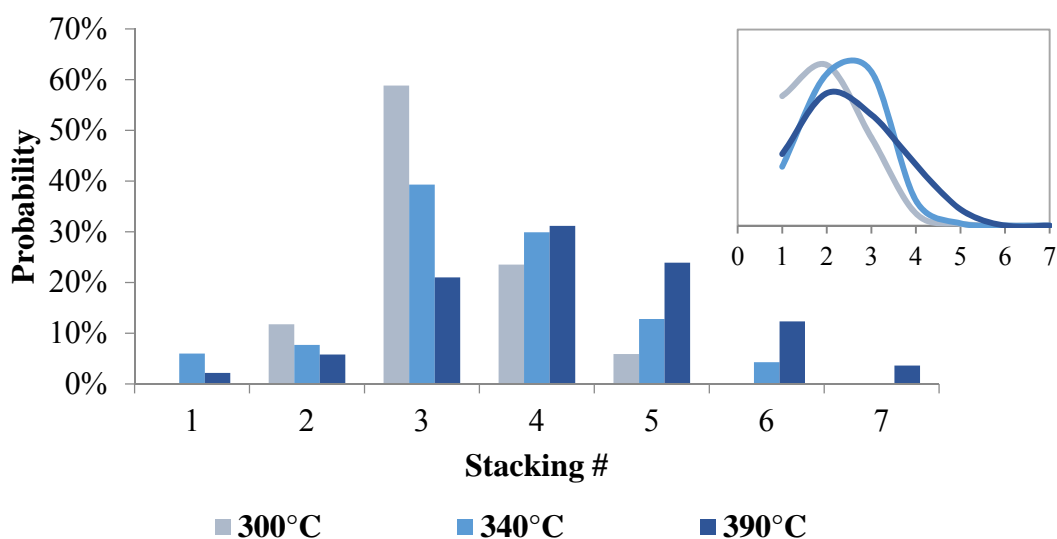


Figure 7-4 Stacking number distributions (distribution curve in small chart) of fresh *ex situ* MoS₂ catalysts prepared with under H₂ collected at different temperatures

The stacking number distributions are shown in Figure 7-4, where an increasing trend could be found - stacking numbers increased with the increasing temperature. As shown in Table 7-2, the average stacking numbers for catalysts collected at 300°C, 340°C and 390°C were 3.24 ± 0.73 , 3.49 ± 1.13 and 4.20 ± 1.29 respectively. Layer distances shown in Table 7-2 were 6.75 \AA , 6.73 \AA and 5.87 \AA for catalysts collected at 300°C, 340°C and 390°C respectively. It should be noticed that there was a certain level of error for the layer distance measurement as discussed previously. However, this observed shortening of layer distance with increased time might be correlated with the increasing of the stacking number. In this way, increasing temperature under molecular H_2 eventually resulted in a longer slab length and an increase in stacking numbers, neither of which was favoured for higher HYD performance.

Atomic ratios were also determined by using EDX during TEM analysis. At least 3 different clusters were chosen for the measurement in order to obtain the general elemental distribution. As shown in Table 7-1, the S:Mo ratios varied from 3.83 ± 0.02 at 300°C to 1.74 ± 0.05 at 340°C and to 0.62 ± 0.13 at 390°C. Lee reported detailed X-ray photoelectron spectroscopy (XPS) results for the *ex situ* unsupported nano MoS_2 catalysts, where the existence of S^{2-} and S_2^{2-} was observed (Lee 2004). This co-existence of S^{2-} and S_2^{2-} could explain why various S:Mo ratios were obtained here. It was also reported by Lee that almost all Mo^{6+} in PMA was reduced to Mo^{4+} once the reaction reached 340°C (Lee 2004); while some S^0 , S^{4+} and S^{6+} were observed up until 340°C. Hence, the catalyst obtained at 300°C in this section could have multiple anions and cations for S, which contributed to a fairly high S:Mo ratio at 3.83 ± 0.02 . When the reaction reached 340°C, the S:Mo ratio should have been more than 2:1, if there were only Mo^{4+} , S^{2-} and S_2^{2-} present. However, the S:Mo ratio was less than 2. If the experimental error was neglected, the only potential possibility was that Mo^{4+} was further reduced to a lower atomic valence state. The same thing happened to the S:Mo ratio of 0.62 ± 0.13 at 390°C. However, the EDX analytical error was larger compared to the XPS characterization. As a result, the atomic ratio results discussed here need further confirmation from other elemental analysis such as SEM/EDX or XPS.

7.4.1.2 Effect of temperature under CO

Fresh *ex situ* MoS₂ catalysts were synthesized under a CO atmosphere and collected at 300°C, 340°C and 390°C respectively. Shown in Table 2-3, the experiments were carried out following the condition “100ml toluene, 10ml water, 30psi H₂S, 570psi CO, 0min”.

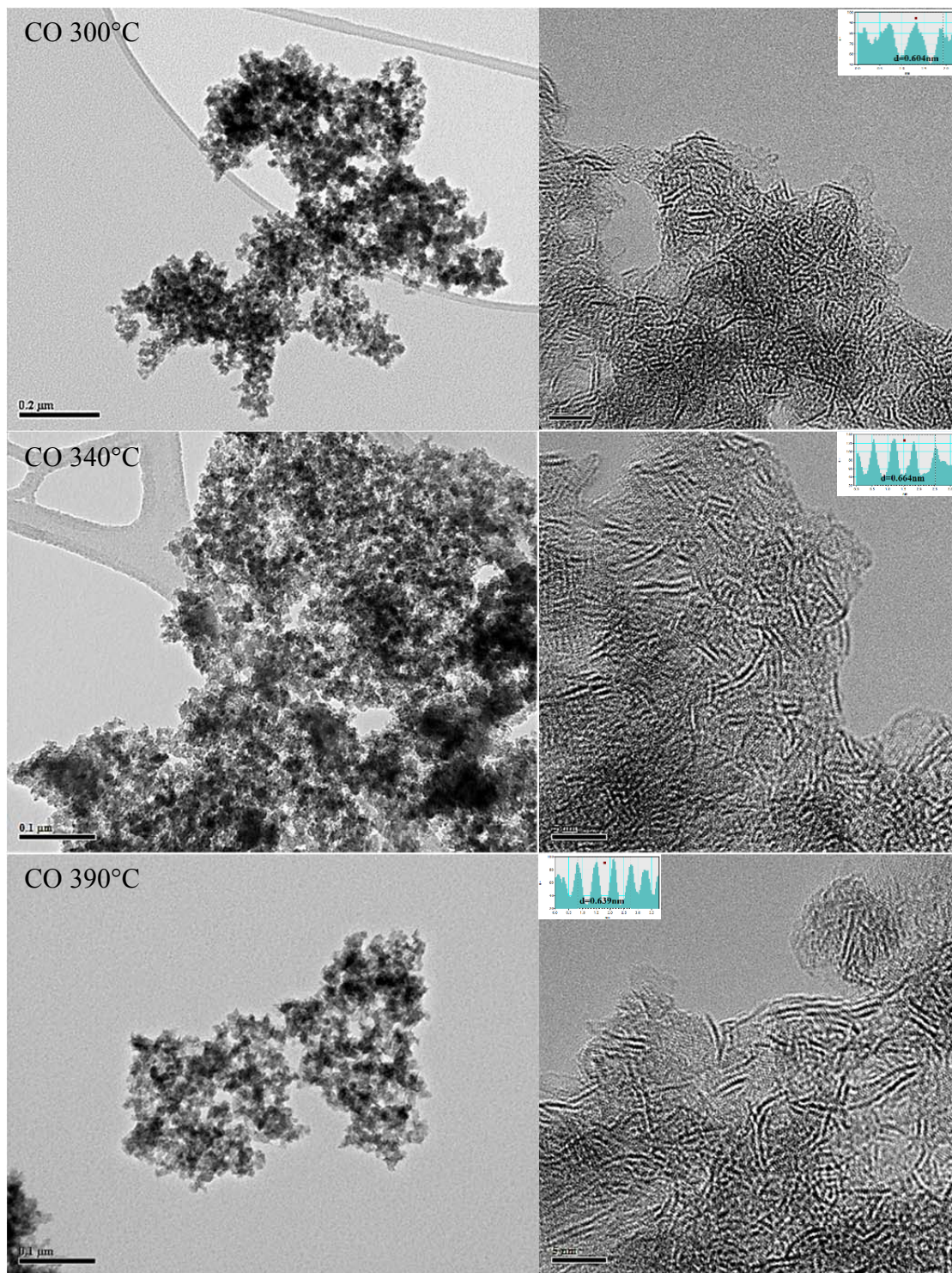


Figure 7-5 TEM (left) and HRTEM (right) images of the fresh *ex situ* MoS₂ catalysts collected at different temperatures under CO

No significant agglomeration or size change was found by increasing the temperature from 300°C to 390°C under CO, as shown in the TEM images shown in Figure 7-5. Catalyst particles still demonstrated fine dispersion at 390°C. Clear particle outlines were observed with a uniform catalyst particle size distribution (~20nm).

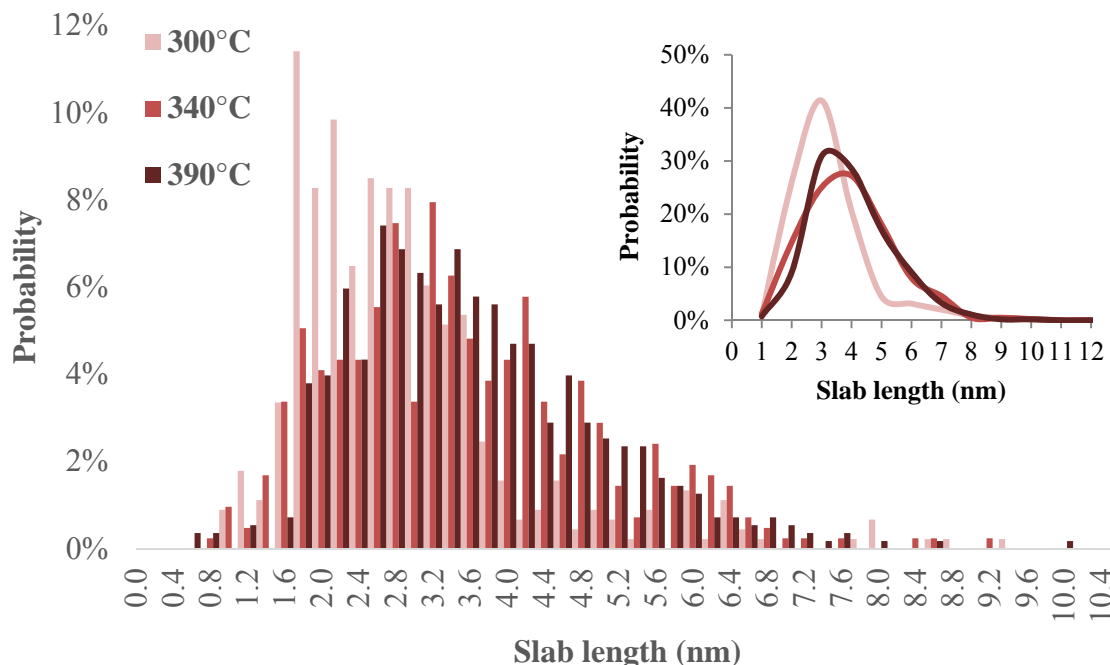


Figure 7-6 Slab length distributions (0.2nm incremented in big chart; 1nm incremented in small chart) of fresh *ex situ* MoS₂ catalysts prepared with under CO collected at different temperatures

Regarding the effect of temperature on slab length under CO, a similar trend was found as under molecular H₂. This is shown in the HRTEM images shown in Figure 7-5, where slabs became longer from 300°C to 390°C. Statistical distribution of slab lengths clearly demonstrated this finding in Figure 7-6. At 300°C, a higher probability of forming short slabs in the 1.6~3.0nm range; with increasing temperature, longer slabs, especially slabs in the 3.8~6.0nm range were preferred. The small chart with a 1nm incremented distribution also indicated a clear shift of slab lengths from left to right for the longer slabs. However, no significant slab length shift was

observed from 340°C to 390°C. The average slab lengths for the catalyst collected at 300°C, 340°C and 390°C were 2.81 ± 1.27 nm, 3.44 ± 1.42 nm and 3.51 ± 1.33 nm respectively as shown in Table 7-2. This was consistent with the previous LGO spent catalyst characterization results.

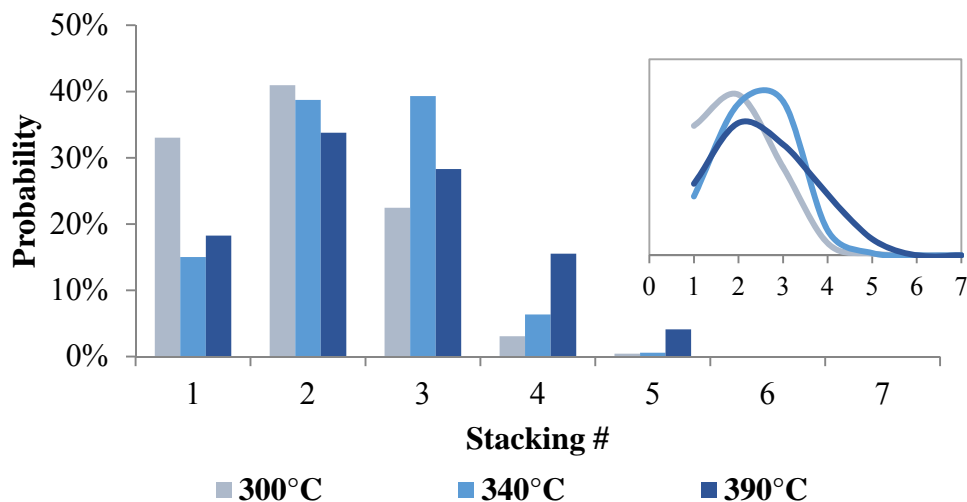


Figure 7-7 Stacking number distributions (distribution curve in small chart) of fresh *ex situ* MoS₂ catalysts prepared with under CO collected at different temperatures

Based on the HRTEM images in Figure 7-5 and the statistical slab length distributions shown in Figure 7-6, it was found that the MoS₂ slabs were more stacked with increased temperature. The average stacking numbers shown in Table 7-2 for catalysts collected at 300°C, 340°C and 390°C were 1.97 ± 0.85 , 2.39 ± 0.84 and 2.53 ± 1.08 respectively. This phenomenon was similar to the stacking behaviour under molecular H₂. It is proposed that a higher temperature allows crystalline structure to grow in both longitudinal and axial directions. One interesting thing was that the layer distance was not compressed with increasing temperature by using CO, unlike what was observed under H₂. The layer distances were 6.04Å at 300°C, 6.64Å at 340°C and 6.39Å at 390°C correspondingly. This could also be due to error in the layer distance measurement, and the stacking number and the inter-layer distance might not be correlated with each other.

7.4.2 Effects of *In situ* H₂ vs. molecular H₂ on catalyst morphology

From the results in the previous section, it is noted that *in situ* H₂ had a different impact on catalyst morphology compared to molecular H₂. When CO was used in the catalyst preparation, a spherical structure was obviously observed at temperatures as low as 300°C as shown in Figure 7-5. Interestingly, the particle outlines were much clearer compared to the catalysts prepared under molecular H₂. Moreover, the agglomeration was less severe when the catalyst was prepared under CO compared to molecular H₂.

Table 7-1 Atomic ratio results collected from EDX analysis for fresh *ex situ* MoS₂ catalysts prepared with *in situ* H₂ and molecular H₂ collected at different temperatures

	Molecular H ₂			<i>In situ</i> H ₂		
	300°C	340°C	390°C	300°C	340°C	390°C
S:Mo	3.83	1.74	0.62	1.59	1.86	1.80
<i>Std. Dev.</i>	<i>0.02</i>	<i>0.05</i>	<i>0.13</i>	<i>0.06</i>	<i>0.23</i>	<i>0.30</i>

Regarding to the slab crystalline formation, it was found that clear slabs were formed at temperatures as low as 300°C compared to the catalyst prepared under molecular H₂. This early formed slabs would potentially lead to a higher activity at low temperature or at the beginning of the reaction. Liu and Lee reported similar results based on HDS catalytic experiments and XPS studies. It was assumed by them that *in situ* H₂ generated via the WGSR provided a higher activity for reducing the Mo precursor PMA's Keggin structure, making it easier to collapse compared to molecular H₂ (Liu 2010). The observation of early slab structures under CO from this HRTEM analysis further proved their hypothesis, where *in situ* H₂ was attributed to the earlier collapse of PMA for the formation of MoS₂ catalysts. The EDX results revealed that the S:Mo ratio was lower than 2 at only 300°C as shown in Table 7-1. This was much lower than the S:Mo ratio of the catalyst collected at 300°C under molecular H₂. As discussed previously, in order to achieve such a low S:Mo ratio, no S⁰, S⁴⁺ or S⁶⁺ was expected to exist at 300°C under *in situ* H₂; the atomic valence of Mo⁶⁺ in PMA must be further reduced to less than 4 by using *in situ* H₂. This again confirmed the higher reducing ability of *in situ* H₂ over that of molecular H₂.

Another interesting observation was that the relatively shorter slabs obtained by using *in situ* H₂. As shown in Figure 7-8, the comparison of slab length distributions by using *in situ* H₂ and molecular H₂ was clearly demonstrated. Excluding the catalyst collected at 300°C under molecular H₂ involved with potential high error due to limited measured slab numbers (which had surprisingly long slabs), catalysts prepared by using *in situ* H₂ had a shorter slab length distributions compared to the catalysts prepared under molecular H₂. The statistical analysis results in Table 7-2 show that the average slab length when using *in situ* H₂ were 36% and 39% shorter than the slab lengths under molecular H₂ at 340°C and 390°C respectively. As discussed and concluded by various researchers (Moses, Hinnemann *et al.* 2007, Li, Li *et al.* 2010, Yoosuk, Song *et al.* 2010, Liu, Chai *et al.* 2014), these short slabs would result in more brim exposure for higher HYD reactivity, which could eventually lead to higher HDS catalytic activity.

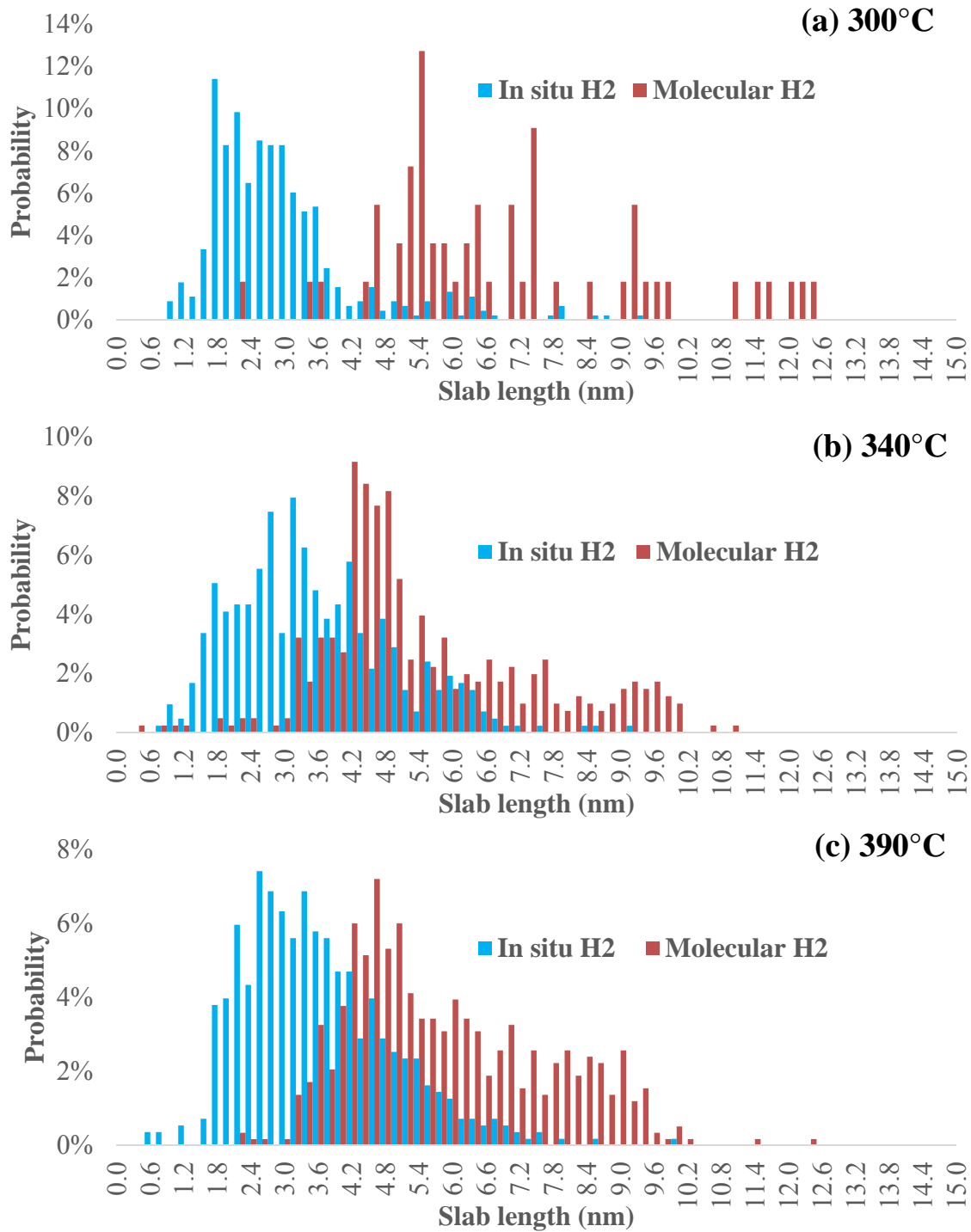


Figure 7-8 Slab length distributions (0.2nm incremented) of fresh *ex situ* MoS₂ catalysts prepared with *in situ* H₂ and molecular H₂ collected at different temperatures

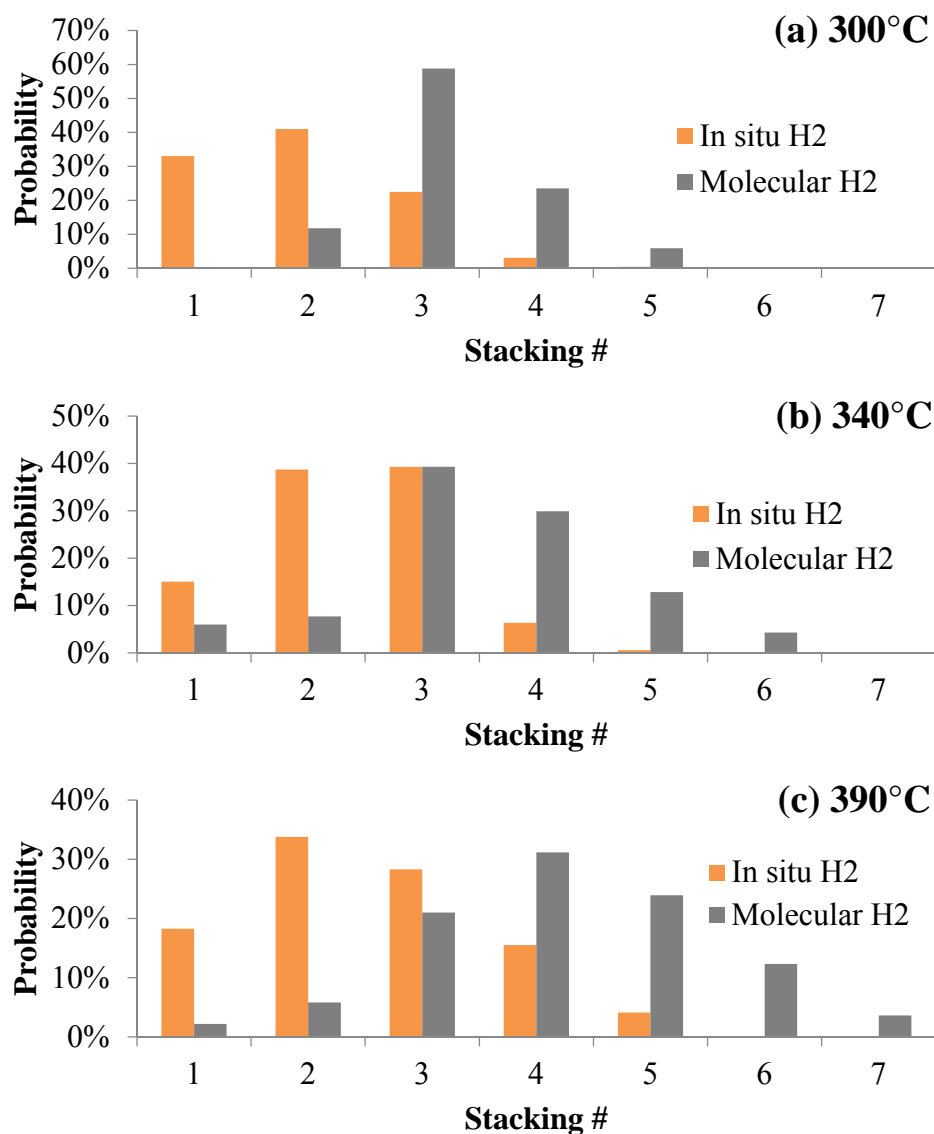


Figure 7-9 Stacking number distributions of fresh *ex situ* MoS₂ catalysts prepared with *in situ* H₂ and molecular H₂ collected at different temperatures

In addition for the shorter slab obtained, a lower stacking degree was also achieved by using *in situ* H₂. The slabs shown in Figure 7-5 were more isolated or dispersed by using *in situ* H₂ compared to the slabs obtained under molecular H₂ as shown in Figure 7-2. By comparing the stacking number distributions in Figure 7-9, it is seen that they exhibited smaller stacking number distributions when using *in situ* H₂. When molecular H₂ was used, the stacking number shifted to the right with an increased level of stacked catalysts. The average stacking numbers

shown in Table 7-2 numerically confirmed this observation. Since only the top layers of the stacked slabs could provide brim sites to catalyze the HYD pathway, a lower stacking number was preferred for higher catalytic activity. As a result, *in situ* H₂ also improved catalyst activity through “isolating” the slab layer structures, even though the detailed mechanism was unknown.

Table 7-2 Average slab length, stacking number and layer distance results of fresh *ex situ* MoS₂ catalysts prepared with *in situ* H₂ and molecular H₂ collected at different temperatures

	Avg. Slab Length (nm)	<i>Std. Dev.</i>	Avg. Stacking #	<i>Std. Dev.</i>	<i>Slab Measured</i>	Layer Distance (Å)*
Molecular H ₂						
300°C	6.81	2.34	3.24	0.73	55	6.75
340°C	5.40	1.91	3.49	1.13	404	6.73
390°C	5.78	1.75	4.20	1.29	583	5.87
<i>In situ</i> H ₂						
300°C	2.81	1.27	1.97	0.85	447	6.04
340°C	3.44	1.42	2.39	0.84	415	6.64
390°C	3.51	1.33	2.53	1.08	553	6.39

* No statistical analysis was performed in layer distance measurement.

It was also interesting to note that the layer distances were not significantly compressed with an increase in temperature when using *in situ* H₂. As shown in Table 7-2, the layer distances of the catalysts prepared under molecular H₂ were 6.75Å, 6.73Å and 5.87Å by heating from 300°C to 390°C. The layer distance reduced nearly 13% from 340°C to 390°C. While the layer distance of the catalysts prepared under CO did not exhibit such a behavior. Instead, the layer distance even increased slightly. Although the layer distance measurement had relatively a high systematic error without statistical analysis, it was observed that at least there was no obvious layer distance shortening. The (002) layer distance should be a fixed number due to the unchanged crystal structures, but sometimes the doping of Mo or S with different electron configurations might interfere with the actual crystalline structure. For example, the relatively shorter layer distance at 390°C under molecular H₂ (5.87Å) might be caused by the doping of Mo cations with less than

IV valence because of the surprisingly low S:Mo ratio (0.62:1) shown in Table 7-1. The resultant layer distance change might affect the exposure of the brim site in the stacked layer, which might be the possible as active sites for the HYD pathways. In this way, *in situ* H₂ might also contribute to a higher catalyst activity by inhibiting the slab compression caused by higher temperature. However, due to the relatively high systematic error present in layer distance measurement, discriminative discussion needs further investigation.

7.4.3 Effect of Co

Fresh *ex situ* Co-MoS₂ catalysts were synthesized under CO atmosphere and collected at 390°C with a Co:Mo atomic ratio of 0.3, 0.5 and 0.7:1 respectively. As shown in Table 2-3, the experiments were carried out following the condition “100ml toluene, 10ml water, 30psi H₂S, 570psi CO, 0min”.

As found for the unpromoted MoS₂ catalysts, spherical particles were formed with the addition of Co at various ratios as shown in Figure 7-10. No obvious particle size change was observed at different ratios. However, compared to the finely dispersed particles obtained without Co addition, the agglomeration was slightly more notable after adding Co. This could be initiated by doping the Co atoms on the existing MoS₂ crystals. This doping might modify the catalysts' surface charge, leading to the potential adhesion of particles. It was also interesting that there was almost no other obvious crystalline structure found except slabs in the HRTEM images after Co addition. This is in agreement with many previously reported results (Nava, Pawelec *et al.* 2009, Li, Li *et al.* 2010, Liu, Chai *et al.* 2014), where the majority of Co was found to exist in the Co-Mo-S crystalline phase. The rest of the Co could form Co sulfides (like Co₉S₈) which were observed through XRD analysis of the spent catalyst from the LGO upgrading.

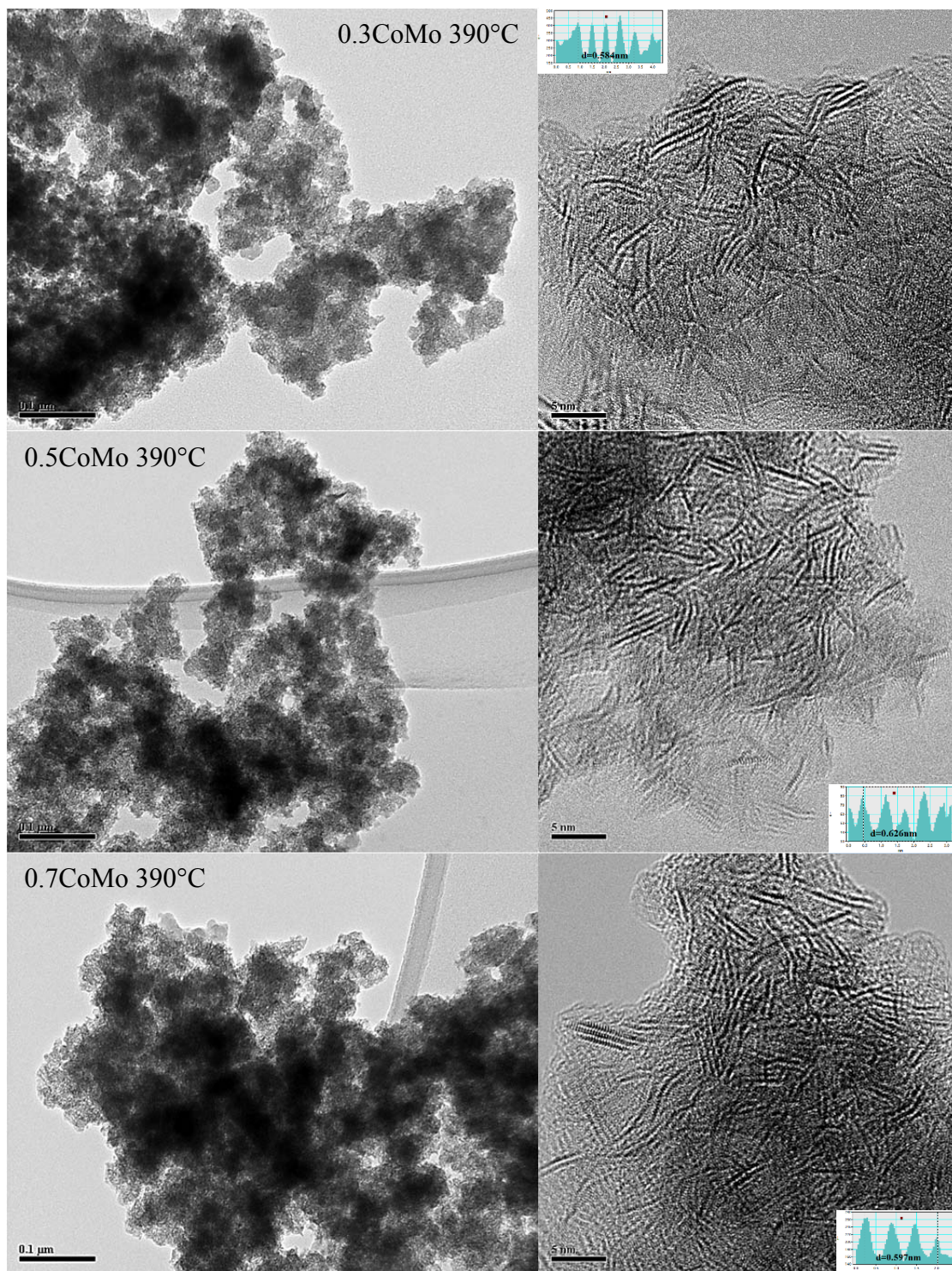


Figure 7-10 TEM (left) and HRTEM (right) images of the fresh *ex situ* Co-MoS₂ catalysts with different Co:Mo ratios collected at 390°C under CO

By observing the HRTEM as images shown in Figure 7-10, it was noticed that no apparent change of slab length occurred at different Co:Mo ratios. A statistical analysis was also performed, and the distributions for unpromoted MoS₂ and Co-MoS₂ at different Co:Mo ratios were demonstrated in Figure 7-11. The distributions shown in the 1nm incremental chart had almost the same most probable slab lengths at around 3~4nm. As shown in the 0.2nm incremental column chart in Figure 7-11, unpromoted MoS₂ did have a higher probability for having slabs in the 2.2~2.6nm range; while 0.3CoMo and 0.5CoMo had more slabs in the 1.0~2.0nm range. As shown in Table 7-4, the average slab lengths for Mo, 0.3CoMo, 0.5CoMo and 0.7CoMo were 3.51±1.33nm, 3.46±1.35nm, 3.30±1.33nm and 3.93±1.73nm respectively. Among these four samples, 0.7CoMo had the longest average slab length, which could be attributed to its slightly higher probability of slabs in the 5~8nm range as shown in Figure 7-11.

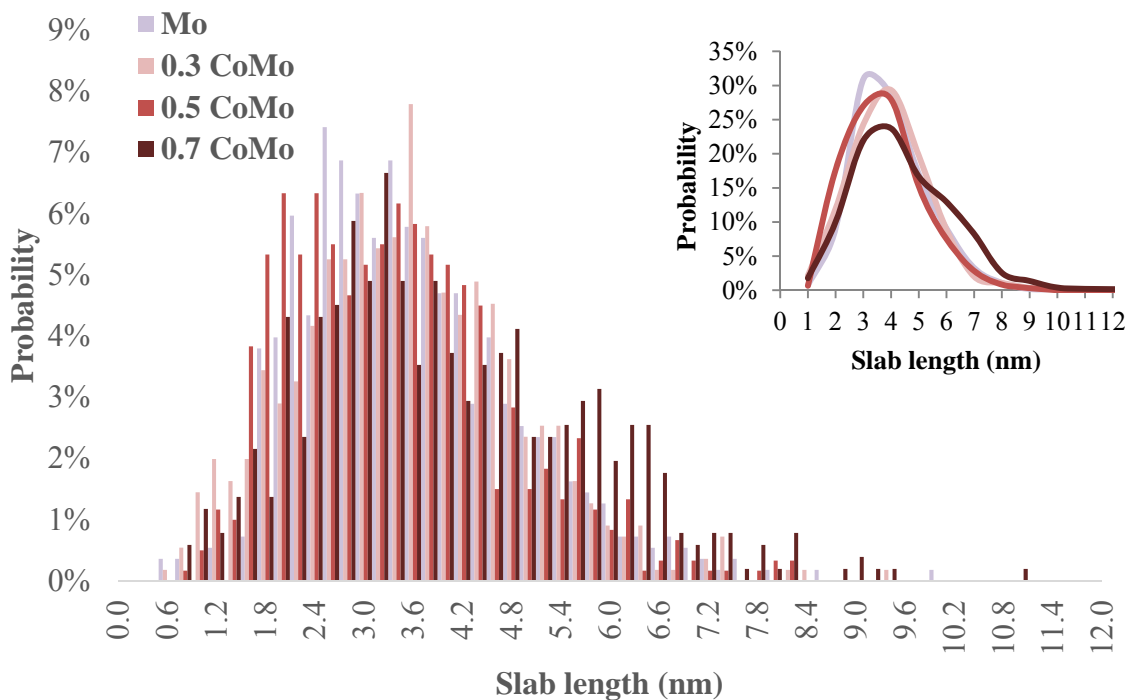


Figure 7-11 Slab length distributions (0.2nm incremented in big chart; 1nm incremented in small chart) of fresh *ex situ* Co-MoS₂ catalysts with different Co:Mo ratios collected at 390°C under CO

Unlike the negligible impact on slab length, the addition of Co resulted in a higher stacking degree. As shown in Figure 7-12, the most probable stacking number shifted from 2 to 3 after adding Co. With more Co introduced, more stacking occurred. This trend was very clear for 5-layer and 6-layer counts. The statistical average stacking numbers for Mo, 0.3CoMo, 0.5CoMo and 0.7CoMo were 2.53 ± 1.08 , 3.03 ± 1.08 , 3.51 ± 1.12 and 3.56 ± 1.36 as shown in Table 7-4, which numerically confirmed this observation. Moreover, the layer distances of 0.3CoMo, 0.5CoMo and 0.7CoMo were also smaller than the layer distance of unpromoted catalysts as shown in Table 7-4. This might be caused by the crystalline structure change with the introduction of Co.

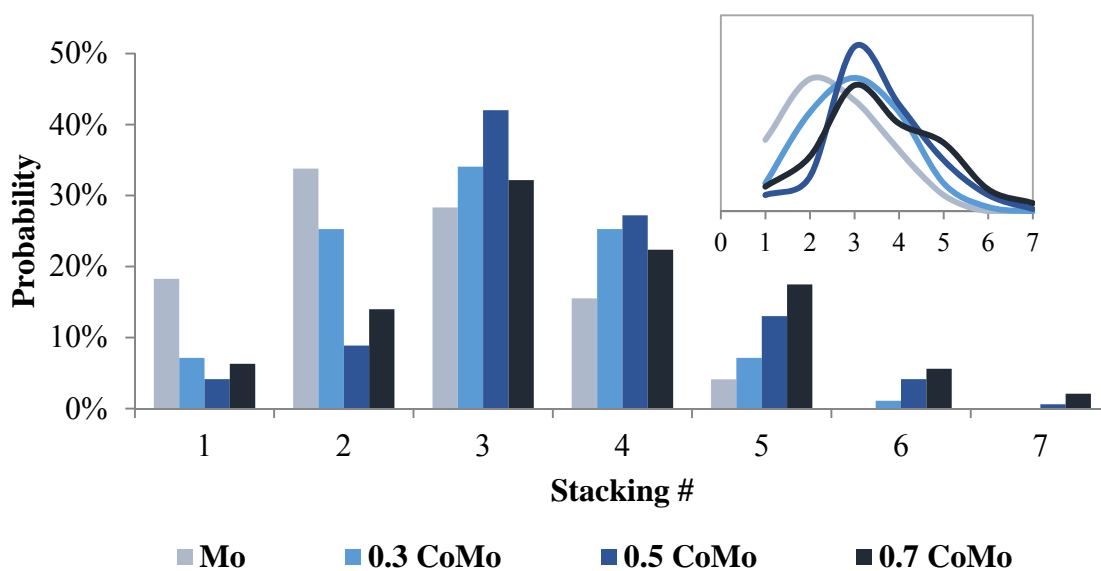


Figure 7-12 Stacking number distributions (distribution curve in small chart) of fresh *ex situ* Co-MoS₂ catalysts with different Co:Mo ratios collected at 390°C under CO

Another interesting observation was that that actual Co:Mo ratio in the catalysts did change with different loading Co:Mo ratios. However, the obtained ratios were always lower than the added ratios. As shown in Table 7-3, the obtained Co:Mo ratios were 0.20 ± 0.05 , 0.25 ± 0.01 and 0.33 ± 0.08 when the loaded Co:Mo ratios were 0.3, 0.5 and 0.7. This was similar to the findings in the EDX results of spent Co-MoS₂ catalysts in LGO upgrading, where the Co:Mo was around

0.3:1 when the loaded Co:Mo ratio was 0.6:1. It was assumed that the excess Co formed separate Co_8S_9 phases, which were identified in the XRD spectrum shown in Figure 6-8.

Table 7-3 Atomic ratio results collected from EDX analysis for fresh *ex situ* Co-MoS₂ catalysts with different Co:Mo ratios collected at 390°C under CO

	Mo	0.3CoMo	0.5CoMo	0.7CoMo
Co:Mo	-	0.20	0.25	0.33
<i>Std. Dev.</i>	-	0.05	0.01	0.08
S:(Co+Mo)	1.80	2.48	2.29	2.79
<i>Std. Dev.</i>	0.30	0.06	0.08	0.00

7.4.4 Effect of Ni

7.4.4.1 Effect of Ni at 390°C

Fresh *ex situ* Ni-MoS₂ catalysts were synthesized under CO atmosphere and collected at 390°C with Ni:Mo atomic ratio at 0.3, 0.5 and 0.7:1 respectively. As shown in Table 2-3, the experiments were carried out following the condition “100ml toluene, 10ml water, 30psi H₂S, 570psi CO, 0min”.

The Ni promoted catalysts also had spherical structures like unpromoted and Co promoted catalysts as shown from the TEM images shown in Figure 7-13. Compared to Co-MoS₂, the agglomeration was less severe when using Ni; however, the Ni-MoS₂ catalysts were still more agglomerated compared to unpromoted catalysts synthesized under CO shown in Figure 7-5. This could also be caused by the modified particle surface charge due to Ni doping. As shown in the HRTEM images in Figure 7-13, slabs were formed with Ni addition. Besides slab-like structures, no other obvious crystalline phase was found.

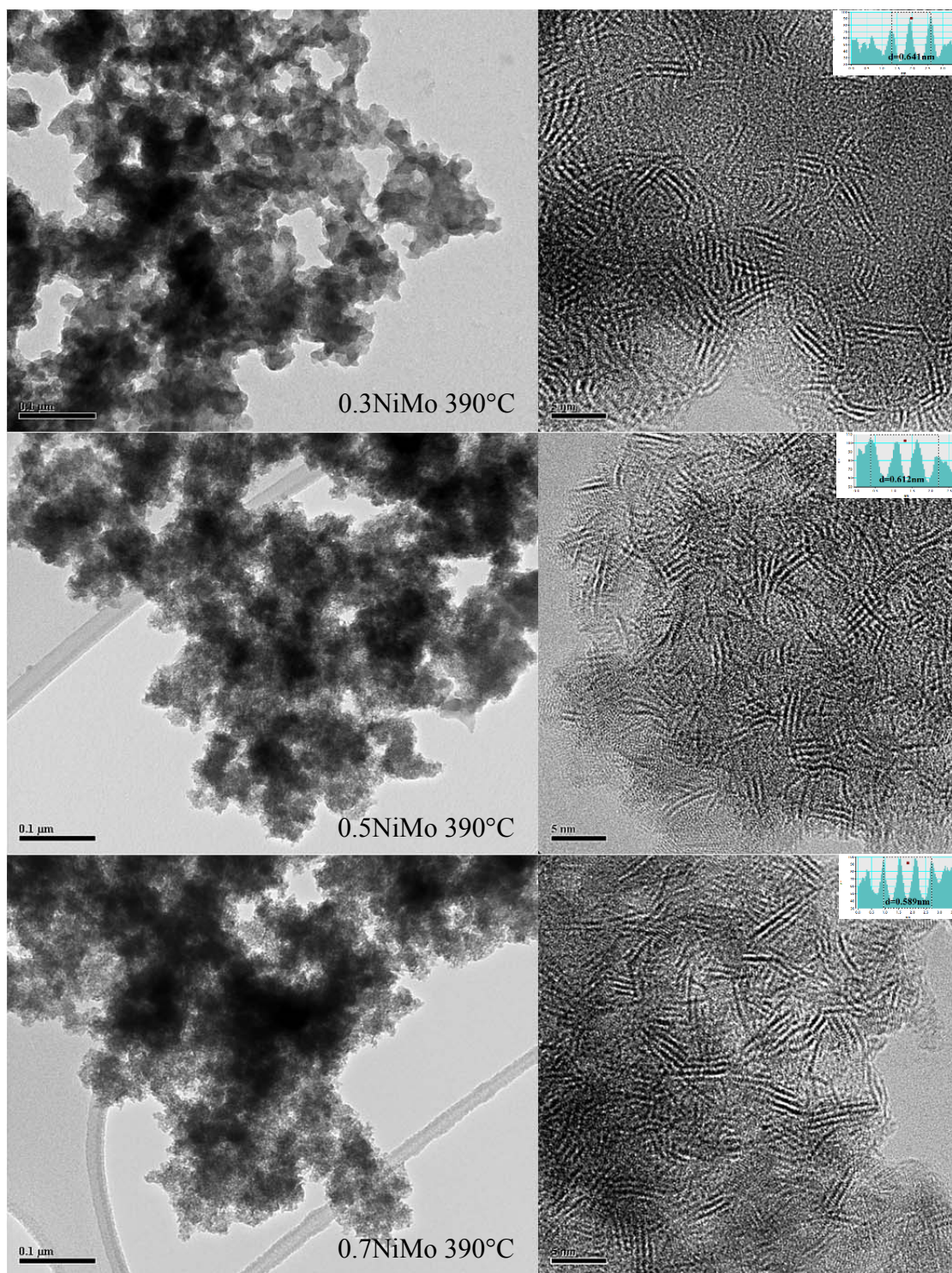


Figure 7-13 TEM (left) and HRTEM (right) images of the fresh *ex situ* Ni-MoS₂ catalysts with different Ni:Mo ratios collected at 390°C under CO

No obvious change in slab length was observed in the slabs in the HRTEM images, except some of the slabs for 0.3NiMo and 0.5NiMo were very short as shown in Figure 7-13. After statistical analysis, it was confirmed that there was indeed higher probabilities for 0.3NiMo and 0.5NiMo to have short slabs in the 1~2nm range compared to the unpromoted catalysts. This could be found in the column chart and curve distributions shown in Figure 7-14. The average slab lengths for 0.3NiMo and 0.5NiMo were $3.07\pm 1.38\text{nm}$ and $3.00\pm 1.43\text{nm}$ compared to $3.51\pm 1.33\text{nm}$ for the unpromoted catalysts. This ~14% length reduction could potentially improve the catalyst's activity. However, when Ni was added to provide a 0.7 Ni:Mo ratio, the short slabs in 1~2nm range almost disappeared as shown in Figure 7-14. This slab length change could be the result of the formation of different Ni-Mo-S crystalline (Lauritsen, Kibsgaard *et al.* 2007). For example, two types Ni-Mo-S hexagonal phases (Type A and Type B) were found in the Ni promoted MoS₂ catalysts as shown in Figure 6-4. It could be possible that a certain smaller Ni-Mo-S plates were formed with an optimal Ni:Mo ratio. If this assumption was true, 0.3NiMo and 0.5NiMo should have higher catalytic activity due to this additional morphology change.

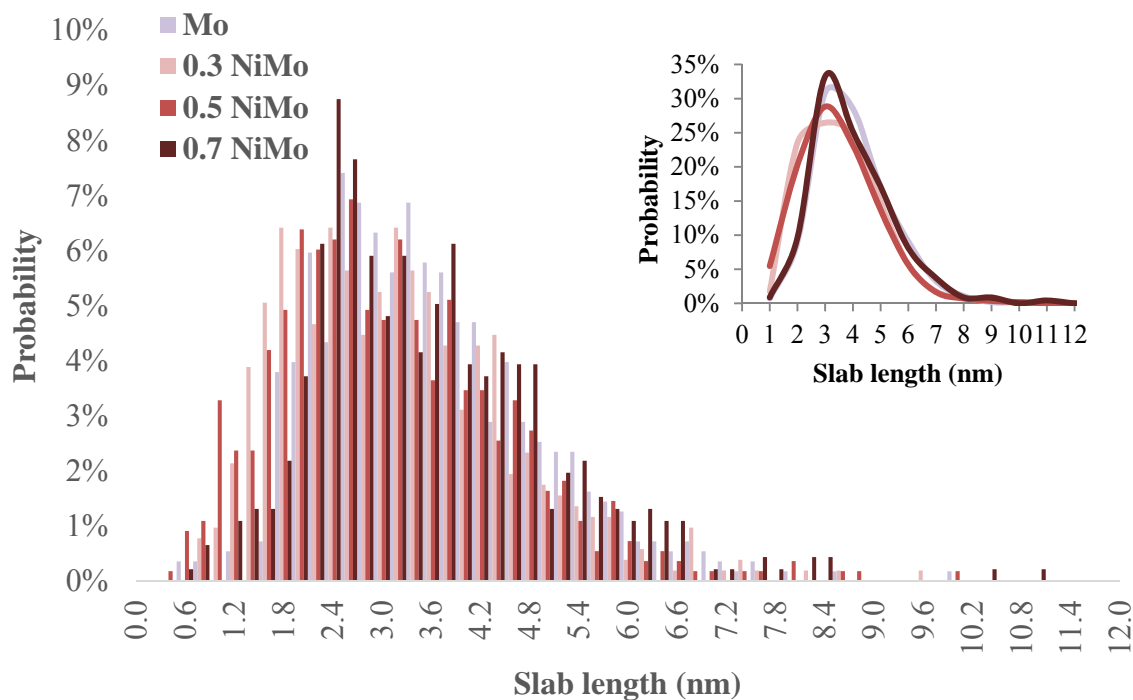


Figure 7-14 Slab length distributions (0.2nm incremented in big chart; 1nm incremented in small chart) of fresh *ex situ* Ni-MoS₂ catalysts with different Ni:Mo ratios collected at 390°C under CO

Similar to Co, the introduction of Ni also intensified the slab stacking. As shown in Figure 7-15, higher stacked structures were more probable, especially for the 5-layer and 6-layer stacked structures. The statistical average stacking numbers for Mo, 0.3NiMo, 0.5NiMo and 0.7NiMo were 2.53 ± 1.08 , 3.12 ± 1.26 , 3.10 ± 1.52 and 3.55 ± 1.23 respectively as shown in Table 7-4. Additionally, the layer distances of 0.3NiMo, 0.5NiMo and 0.7NiMo were also smaller than the layer distance of unpromoted catalysts as shown in Table 7-4. This trend was similar to those found for Co addition, which might also be caused by the crystalline structure changes. Compared to CoMo catalysts, the 0.3NiMo and 0.5NiMo had more 1-layer and 2-layer structures, which could structurally provide more brim active site exposure.

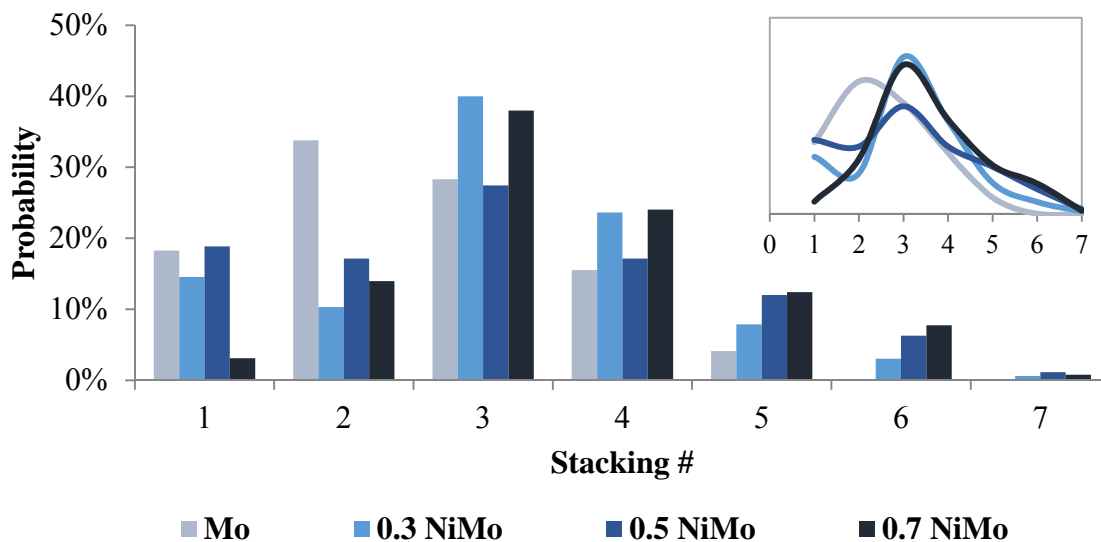


Figure 7-15 Stacking number distributions (distribution curve in small chart) of fresh *ex situ* Ni-MoS₂ catalysts with different Ni:Mo ratios collected at 390°C under CO

The Ni:Mo ratios obtained in the catalysts were also smaller than the loaded Ni:Mo ratios, which are similar to the Co results. As shown in Table 7-6, the obtained Ni:Mo ratios were 0.17 ± 0.02 , 0.33 ± 0.06 and 0.33 ± 0.10 for 0.3NiMo, 0.5NiMo and 0.7NiMo respectively. The Ni:Mo ratio have been previously studied for the spent Ni-MoS₂ catalysts in LGO upgrading, where a 0.19:1 Ni:Mo ratio was achieved when 0.6:1 Ni:Mo was added. XRD results confirmed that the Ni also existed in the formation of Ni₃S₂. This is also expected to happen in the *ex situ* Ni-MoS₂ catalysts prepared and reported in this section.

Table 7-4 Average slab length, stacking number, layer distance results of fresh *ex situ* MoS₂, Co-MoS₂ and Ni-MoS₂ catalysts with different Co or Ni:Mo ratios collected at 390°C under CO together with conversion results for HDN of quinolone referred from Lee's thesis (Lee 2004)

	Avg. Slab Length (nm)	<i>Std. Dev.</i>	Avg. Stacking Number	<i>Std. Dev.</i>	<i>Slab Measured</i>	Layer Distance (Å) *	Conv. For HDN of Quinolone (%) §
Mo	3.51	<i>1.33</i>	2.53	<i>1.08</i>	<i>553</i>	6.39	15.4
0.3 CoMo	3.46	<i>1.35</i>	3.03	<i>1.08</i>	<i>552</i>	5.84	15.5
0.5 CoMo	3.30	<i>1.33</i>	3.51	<i>1.12</i>	<i>600</i>	6.26	16.1
0.7 CoMo	3.93	<i>1.73</i>	3.56	<i>1.36</i>	<i>510</i>	5.97	14.1
0.3 NiMo	3.07	<i>1.38</i>	3.12	<i>1.26</i>	<i>514</i>	6.41	20.4
0.5 NiMo	3.00	<i>1.43</i>	3.10	<i>1.52</i>	<i>548</i>	6.12	23.3
0.7 NiMo	3.48	<i>1.46</i>	3.55	<i>1.23</i>	<i>457</i>	5.89	15.7

* No statistical analysis was performed in layer distance measurement.

§ Conversion data for HDN of quinolone were attained from Dr Roy Lee's PhD thesis, where the reaction condition was very close to the catalyst synthesis condition in this chapter (390°C, 100ml toluene, 5ml quinolone, 10ml water, 17.5psi H₂S, 700psi initial pressure with CO, 2.12×10⁻³mol total metal, 2hours)

Based on the morphology investigation, it was found that Co had an insignificant effect on slab length. Under the 0.7NiMo condition, Ni also had an inconsequential impact on slab length. Although more 1~2nm range short slabs were formed in 0.3NiMo and 0.5NiMo, the morphology change was still minor. Moreover, the addition of Co or Ni both caused higher slab stacking, and the stacking increased with a higher loaded Co:Mo or Ni:Mo ratio. In general almost all the morphology changes on adding Co and Ni did not provide "short slab and less stacking" as the preferred structures for improved catalyst activity. In spite of that, the increased stacking could inhibit catalyst activity by hindering the exposure of the top-layer brim sites. It is known that Co and Ni were the most selective promoters for Mo based hydrotreating catalysts. It was also reported by Liu, Lee, Choy and Alghamdi that Co and Ni showed promotional effects for HDS, HDA, HDN and LGO upgrading reactions through the same process (Lee 2004, Alghamdi 2009, Choy 2009, Liu 2010). Thus, there should be some other reasons which trigger off the promotional behaviour besides morphology. Morphology played an important role in controlling catalyst activity. However, when Ni or Co was added, the crystalline structure changed leading to different catalytic intrinsic activities. These intrinsic activities were determined via synergistic

quantum electron orbital conditions of the mixed metal sulfides. This was discussed in the literature review provided in Chapter 6. By analyzing the relationship between the atomic level morphology change and HDS catalytic activity by loading different metals, Kibsgaard and Topsøe reported a similar observation in 2010. It was found that when the promoter was added, the atomic level morphology changes and has no relationship with catalyst performance; instead the intrinsic activity for the mixed metal sulfides was the main reason for the promotional behaviours (Kibsgaard, Tuxen *et al.* 2010). In this section of the study, there was no significant morphology improvement observed in the promoted Co-MoS₂ and Ni-MoS₂ catalysts (except shorter slabs in 0.3NiMo and 0.5NiMo). Hence, the results here are consistent with Kibsgaard and Topsøe's work, where the morphology was not the major reason for the improved activity when a promoter was used.

It should be noted that the morphology change by using different H₂ sources was different, and the morphology-property relationship was the key. Because the morphology changes by using different H₂ sources might be the only change. When Co or Ni were involved, different crystalline structures were formed, and then the morphology played a less important role. It was also interesting that the shorter slabs in 0.3NiMo and 0.5NiMo might contribute to additional promotional performance in addition to the intrinsic activity. As referred from Lee's thesis results as shown in Table 7-4, it was found that 0.3NiMo and 0.5NiMo provided higher activity for the HDN of quinolone. The total hydrocarbon yields (representing HDN conversions) when using 0.3NiMo and 0.5NiMo were 20.4% and 23.3% compared to the unpromoted reaction at 15.4%; while 0.7NiMo could only cause a slight promotion with a 15.7% total hydrocarbon yield (Lee 2004). Although there are still many ongoing research studies on the active sites for HDS and HDN, it could be possible that the 1~2nm range slabs contributed to the promotion. More research should be carried out to understand the morphology-property correlations for 0.3NiMo and 0.5NiMo with their actual catalytic performance.

7.4.4.2 Effect of Ni at 340°C

Fresh *ex situ* Ni-MoS₂ catalysts were synthesized under a CO atmosphere and collected at 340°C with a Ni:Mo ratio of 0.3, 0.5 and 0.7:1 respectively. As shown in Table 2-3, the experiments

were carried out under the following condition “100ml toluene, 10ml water, 30psi H₂S, 570psi CO, 0min”. Similar to the *ex situ* Ni-MoS₂ catalysts collected at 390°C, spherical particles and the slab structures were formed as shown in the TEM and HRTEM images in Figure 7-16. Compared to the catalyst collected at 390°C, the catalyst collected at 340°C had relatively less agglomeration and relatively shorter slabs.

In addition to the naked eye observation, statistical analysis was also performed on the slab length and stacking number measurements. As shown in Figure 7-17, more 1~3nm range short slabs were formed with the addition of Ni (for all ratios) compared to the unpromoted catalysts. This was somewhat different to the results at 390°C, where only 0.3NiMo and 0.5NiMo provided a few more 1~2nm range short slabs. The average slab lengths for Mo, 0.3NiMo, 0.5NiMo and 0.7NiMo at 340°C were 3.44±1.42, 2.99±1.38, 3.00±1.37 and 3.19±1.56 respectively as shown in Table 7-5. Considering the effect of temperature on the crystal growth discussed in previous sections, it was understandable that more short-range slabs were formed at 340°C. These short slabs could provide limited promotion for the overall catalytic activity.

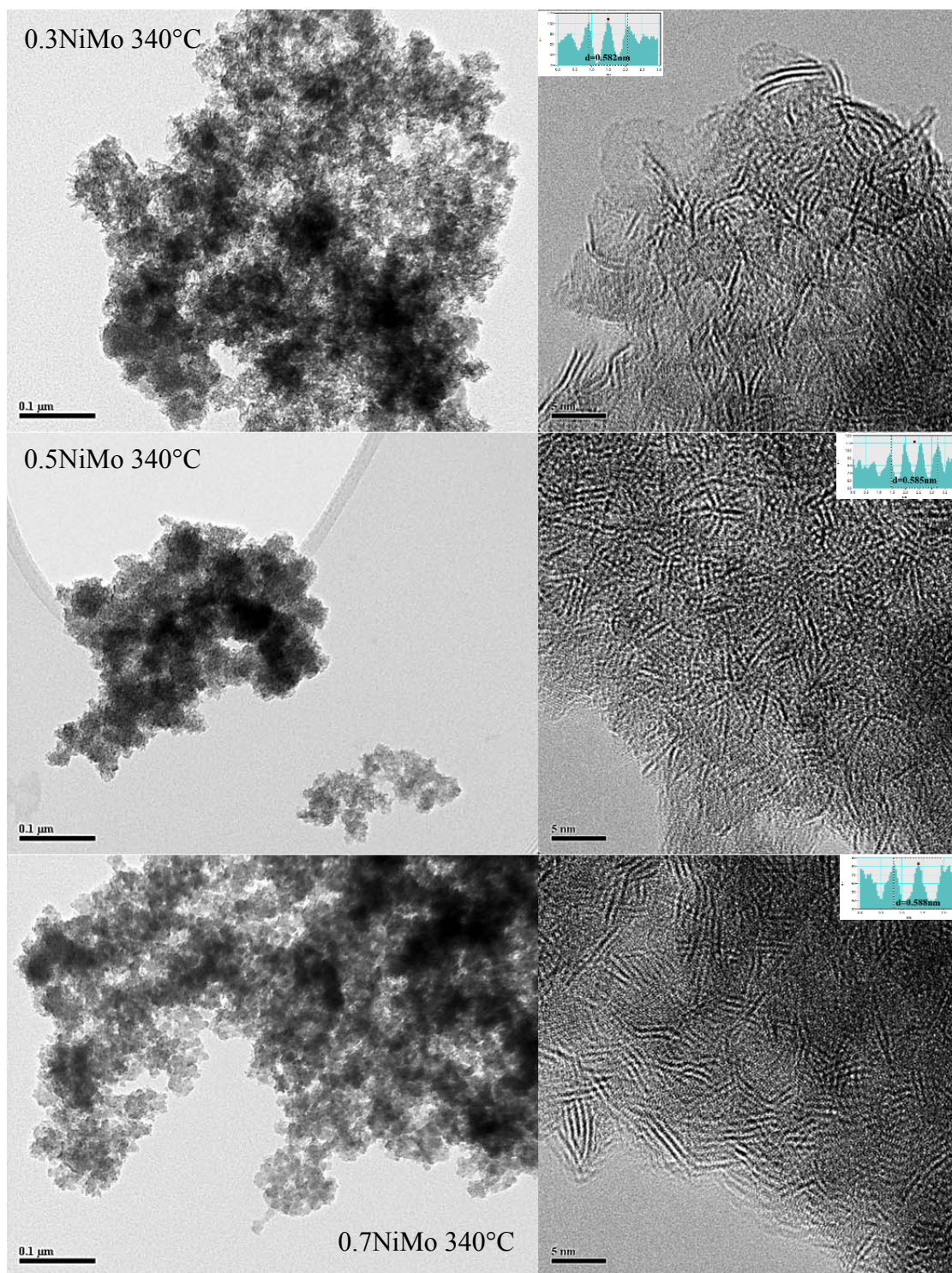


Figure 7-16 TEM (left) and HRTEM (right) images of the fresh *ex situ* Ni-MoS₂ catalysts with different Ni:Mo ratios collected at 340°C under CO

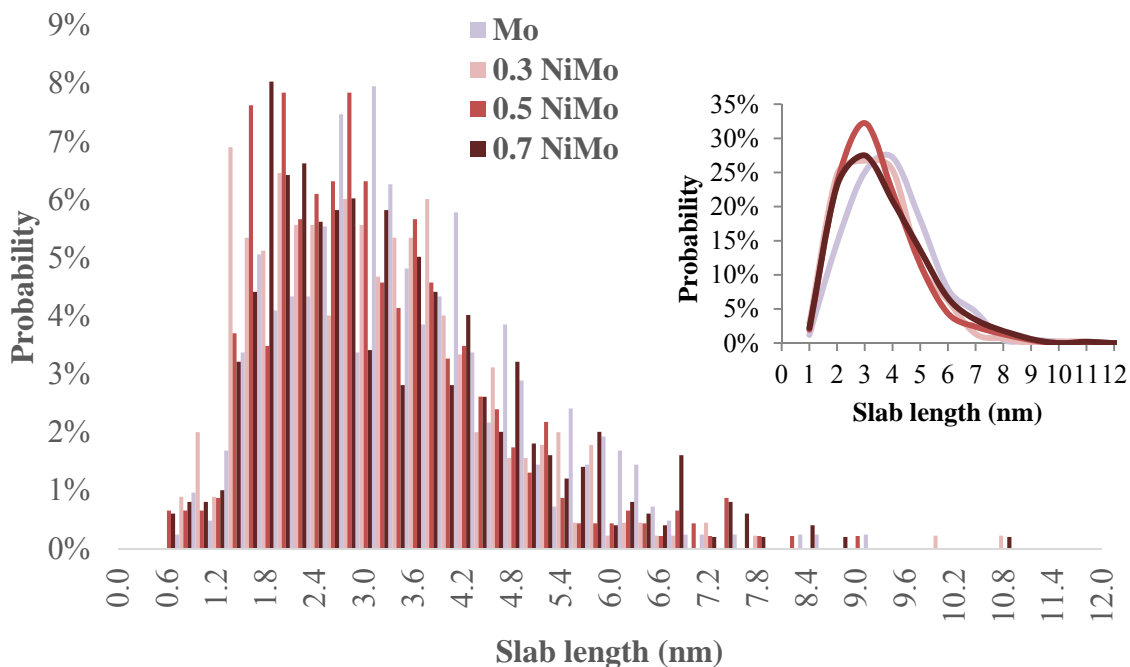


Figure 7-17 Slab length distributions (0.2nm incremented in big chart; 1nm incremented in small chart) of fresh *ex situ* Ni-MoS₂ catalysts with different Ni:Mo ratios collected at 340°C under CO

Nonetheless, no change in stacking number occurred, similar to the trend observed for in *ex situ* Ni-MoS₂ catalysts collected at 390°C. A higher stacking degree was caused with more Ni loading. The average stacking numbers were 2.39 ± 0.84 , 2.85 ± 1.12 , 3.14 ± 1.30 and 3.77 ± 1.33 for Mo, 0.3NiMo, 0.5NiMo and 0.7NiMo respectively at 340°C as shown in Table 7-5. The reduced layer distances shown in Table 7-5 also demonstrated a possible compression introduced by Ni addition. This could be caused by the crystalline structure change.

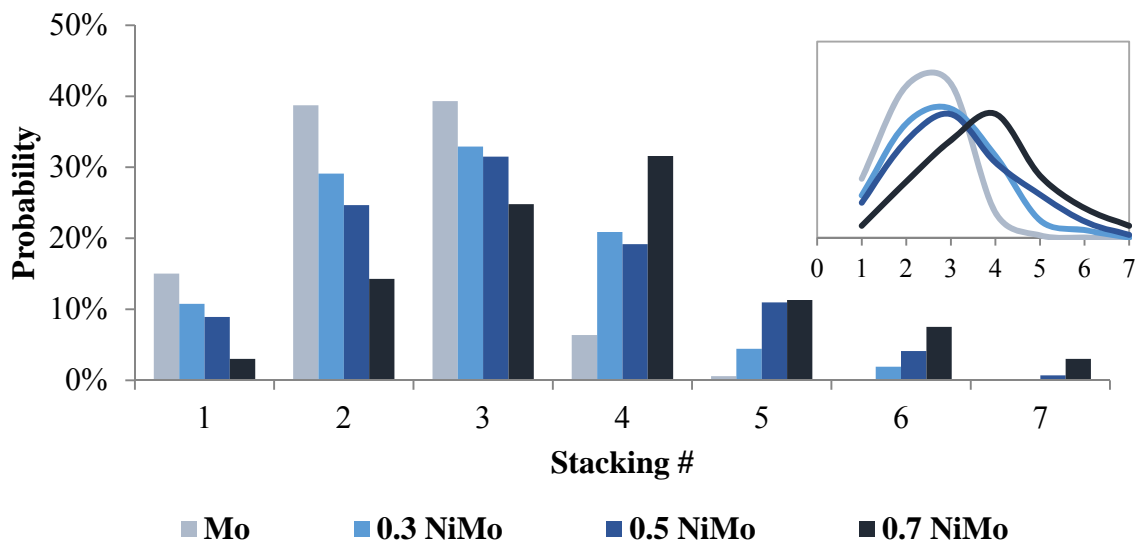


Figure 7-18 Stacking number distributions (distribution curve in small chart) of fresh *ex situ* Ni-MoS₂ catalysts with different Ni:Mo ratios collected at 340°C under CO

It was also found that a lower Ni:Mo ratio was obtained than the loaded ratio at 340°C. As shown in Table 7-6, the obtained Ni:Mo ratios were 0.21±0.07, 0.36±0.04 and 0.27±0.09 for 0.3NiMo, 0.5NiMo and 0.7NiMo respectively.

7.4.4.3 Effect of Ni at 300°C

Fresh *ex situ* Ni-MoS₂ catalysts were synthesized under a CO atmosphere and collected at 300°C with a Ni:Mo ratio of 0.3, 0.5 and 0.7:1 respectively. As shown in Table 2-3, the experiments were carried out following the condition “100ml toluene, 10ml water, 30psi H₂S, 570psi CO, 0min”.

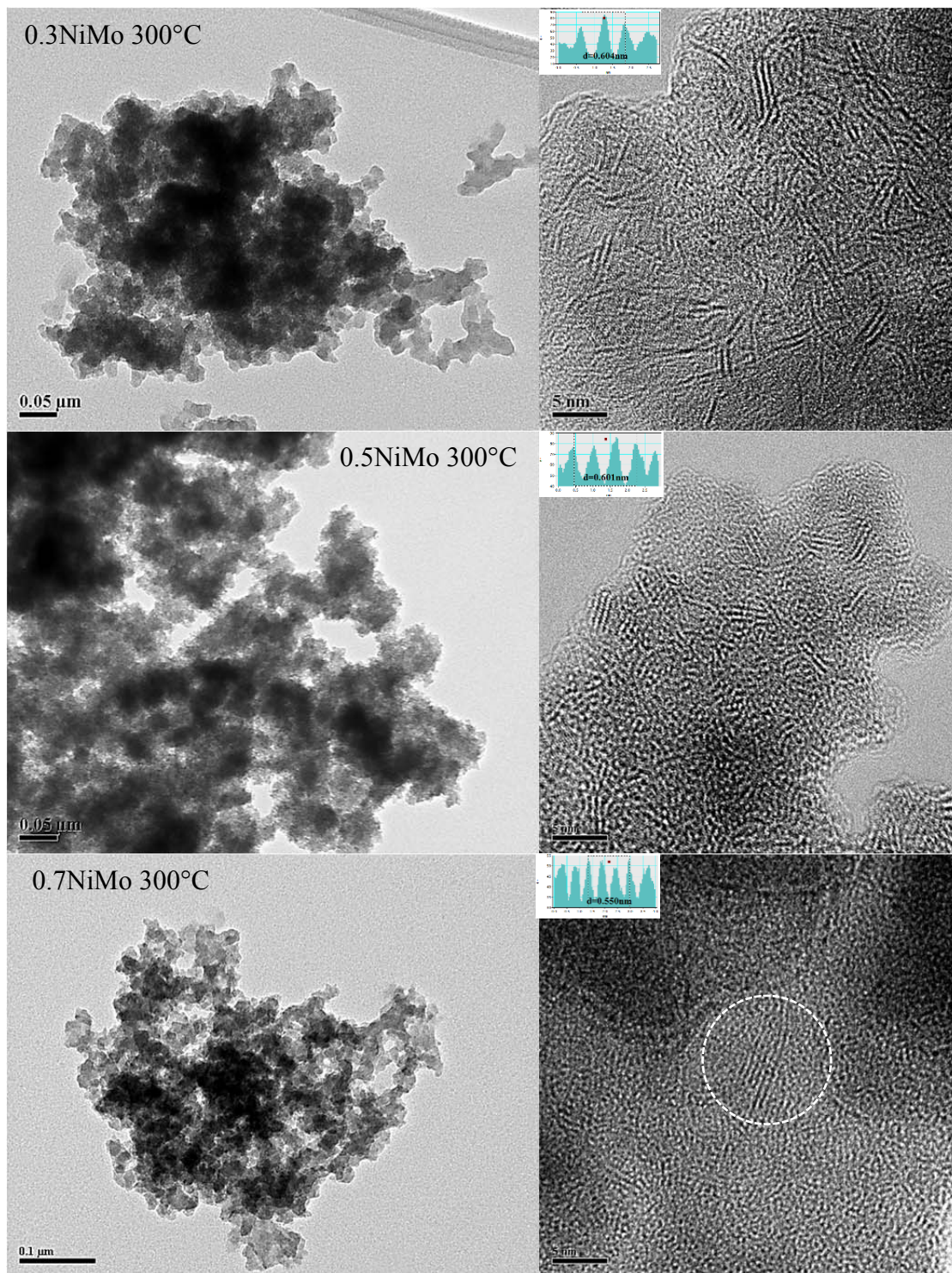


Figure 7-19 TEM (left) and HRTEM (right) images of the fresh *ex situ* Ni-MoS₂ catalysts with different Ni:Mo ratios collected at 300°C under CO

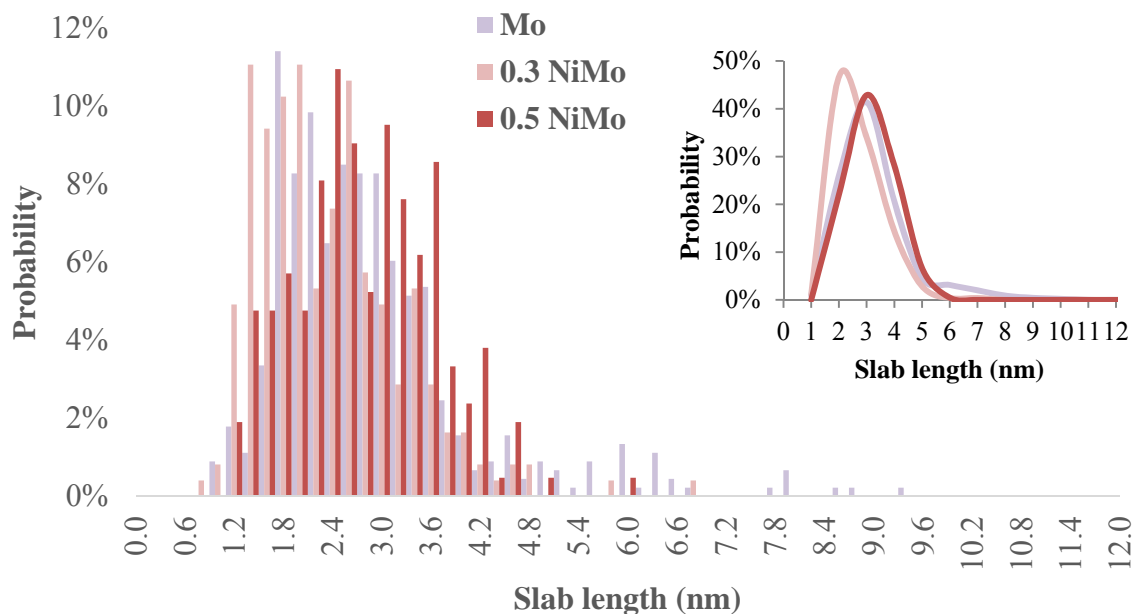


Figure 7-20 Slab length distributions (0.2nm incremented in big chart; 1nm incremented in small chart) of fresh *ex situ* Ni-MoS₂ catalysts with different Ni:Mo ratios collected at 300°C under CO

As shown in Figure 7-19, when the collection temperature was as low as 300°C, spherical structures were still obtained with fine dispersion. On the contrary, some interesting behaviour was noticed in the slab structure shown in the HRTEM images in Figure 7-19. The slab structures in 0.5NiMo were not as clear as the slabs in 0.3NiMo (although slabs in 0.3NiMo were fuzzy, too); while the slabs in 0.7NiMo were even further indistinguishable. This might be a result of poor crystallization at low temperature. Only 45 slabs could be identified and measured for statistical analysis of 0.7NiMo. As a result, the column charts in Figure 7-20 do not involve 0.7NiMo. In addition, it was found that the layer distance of 0.7NiMo was abnormally low at only 5.50Å as shown in Table 7-5. These long and stacked slabs (circled in Figure 7-19) might not even be typical of the Ni-Mo-S crystalline phase as observed in other samples.

The statistical slab length distributions in Figure 7-20 discloses an interesting left-shift of slab lengths at 300°C. The 1~3nm range short slabs were much higher in 0.3NiMo than the unpromoted Mo and 0.5NiMo at 300°C. As shown in Table 7-5, the average slab lengths for Mo, 0.3NiMo and 0.5NiMo at 300°C were $2.81\pm 1.27\text{nm}$, $2.25\pm 0.89\text{nm}$ and $2.67\pm 0.85\text{nm}$ respectively. Although the statistical sample volume was not as large as in previous measurements (only 244 slabs found due to fuzzy slab structures), these observed short slabs might improve the catalyst's activity.

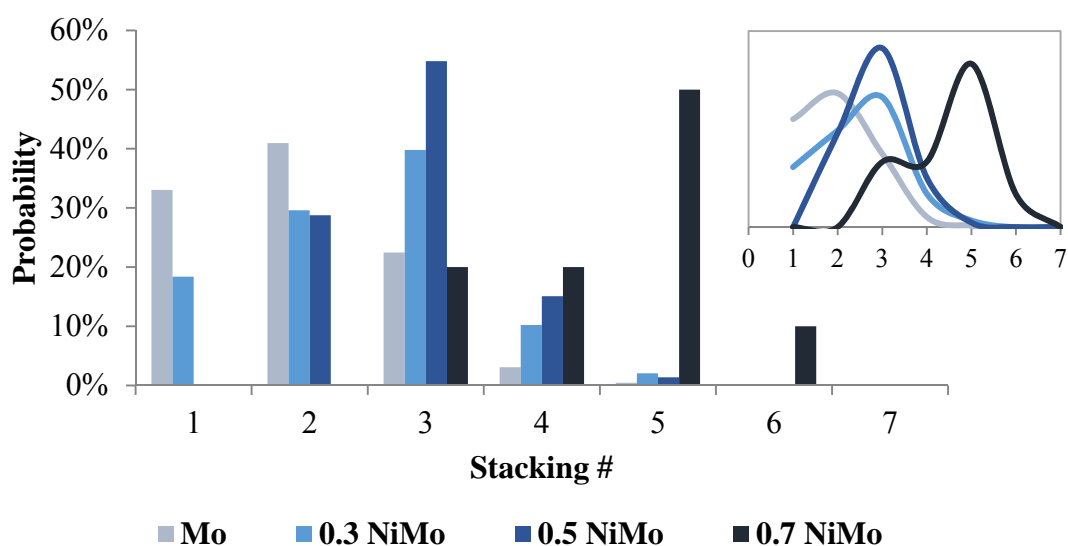


Figure 7-21 Stacking number distributions (distribution curve in small chart) of fresh *ex situ* Ni-MoS₂ catalysts with different Ni:Mo ratios collected at 300°C under CO

As shown in Figure 7-21, the stacking number increased with the addition of Ni at 300°C. The average stacking numbers for Mo, 0.3NiMo, 0.5NiMo and 0.7NiMo at 300°C were 1.97 ± 0.85 , 2.48 ± 0.97 , 2.89 ± 0.69 and 4.50 ± 0.92 respectively. However, a relatively higher probability of low stacked phases was obtained in 0.3NiMo at 300°C compared to the 0.3NiMo at higher temperatures.

Table 7-5 Average slab length, stacking number and layer distance results of fresh *ex situ* Ni-MoS₂ catalysts with different Ni:Mo ratios collected at 300°C, 340°C and 390°C under CO

	Avg. Slab Length (nm)	<i>Std. Dev.</i>	Avg. Stacking #	<i>Std. Dev.</i>	<i>Slab Measured</i>	Layer Distance (Å)*
390°C						
Mo	3.51	1.33	2.53	1.08	553	6.39
0.3 NiMo	3.07	1.38	3.12	1.26	514	6.41
0.5 NiMo	3.00	1.43	3.10	1.52	548	6.12
0.7 NiMo	3.48	1.46	3.55	1.23	457	5.89
340°C						
Mo	3.44	1.42	2.39	0.84	415	6.64
0.3 NiMo	2.99	1.38	2.85	1.12	449	5.82
0.5 NiMo	3.00	1.37	3.14	1.30	459	5.85
0.7 NiMo	3.19	1.56	3.77	1.33	498	5.88
300°C						
Mo	2.81	1.27	1.97	0.85	447	6.04
0.3 NiMo	2.25	0.89	2.48	0.97	244	6.04
0.5 NiMo	2.67	0.85	2.89	0.69	210	6.01
0.7 NiMo	6.42	2.29	4.50	0.92	45	5.50

* No statistical analysis was performed in layer distance measurement.

Besides the intrinsic activities of the Ni-MoS₂ catalysts, the high portion of short slabs and low stacked phases obtained with 0.3NiMo at 300°C could be ideal for improving catalytic activity. This is probably why the Ni-MoS₂ catalysts with a 0.2 Ni:Mo ratio demonstrated such a high promotional behaviour at 300°C in the NA removal experiments. Unfortunately, there were no additional catalytic experiments performed with the present *ex situ* Ni-MoS₂ catalysts for verification.

Table 7-6 Atomic ratio results collected from EDX analysis for fresh *ex situ* Ni-MoS₂ catalysts with different Ni:Mo ratios collected at 300°C, 340°C and 390°C under CO

	Mo	0.3NiMo	0.5NiMo	0.7NiMo
390°C				
Ni:Mo	-	0.17	0.33	0.33
Std. Dev.	-	0.02	0.06	0.10
S:(Ni+Mo)	1.80	0.56	2.53	1.53
Std. Dev.	0.30	0.02	0.09	0.31
340°C				
Ni:Mo	-	0.21	0.36	0.27
Std. Dev.	-	0.07	0.04	0.09
S:(Ni+Mo)	1.86	2.52	2.20	1.25
Std. Dev.	0.23	0.06	0.11	0.14
300°C				
Ni:Mo	-	0.35	0.36	0.13
Std. Dev.	-	0.03	0.08	0.03
S:(Ni+Mo)	1.59	2.72	1.16	1.99
Std. Dev.	0.06	0.11	0.25	0.51

7.5 Conclusions

In summary, fresh *ex situ* nano unsupported MoS₂ based catalysts were successfully synthesized and collected under various conditions. The effects of temperature, atmosphere, promoter and metal:Mo ratio were discussed through HRTEM and EDX characterization. Statistical analysis was performed on slab length and stacking number to demonstrate the general view of the catalysts crystalline structures. It is generally acknowledged that shorter and less stacked slab structures were ideal for HDS reactions. Most of the evaluation presented in this chapter was

carried out following those criteria, although some previous experiments were referred to in evaluating catalysts' activities.

Regarding the effect of temperature, it was found that longer slabs and higher stacking numbers were obtained at higher temperature. This could be the result of thermal crystal growth with less directional preference at higher temperature.

In situ H₂ exhibited excellent performance as the atmosphere for synthesizing more active *ex situ* nano unsupported MoS₂ catalyst compared to molecular H₂. Based on the discussed impacts of different H₂ sources on catalyst morphologies, the major impact of *in situ* H₂ were:

- a) Earlier formation of spherical structures with less agglomeration by using *in situ* H₂
- b) Further reduced Mo cations from Mo⁶⁺ in PMA for earlier formed slab structures
- c) Relatively shorter slabs obtained by using *in situ* H₂
- d) Lower stacking degrees by using *in situ* H₂
- e) No apparent layer structure compression by using *in situ* H₂ at higher temperature

No significant morphology improvement was observed in the promoted Co-MoS₂ and Ni-MoS₂ catalysts. Considering the substantial promotional behaviours of Co and Ni in the HDS and HDN of model compounds previously reported in our research group, the intrinsic activities of the synergistic Co-Mo-S and Ni-Mo-S phases should be the major reason for improved activity instead of morphology improvement. This is consistent with Kibsgaard and Topsøe's work. Morphology impact was proposed to be only dominant when no mixed metal sulfide was present, like the morphology changes resulting from using different H₂ sources.

Slightly different Ni effects on morphology were also observed at lower temperatures. A higher portion of short slabs were obtained in all the Ni-MoS₂ catalysts at 340°C and 0.3NiMo at 300°C. This increased probability of short slabs could potentially improve the catalyst activity, even though the morphology impact was less significant compared to the intrinsic activity when

Ni was used. Other than that, similar Ni effects were found, like higher stacking degree, lower Ni:Mo ratio than loaded, etc.

Chapter 8 Conclusions and Recommendations

8.1 Conclusions

An emulsion upgrading process has been successfully evaluated for the upgrading of Cold Lake bitumen and Athabasca bitumen emulsions using *in situ* formed MoS₂ and *in situ* H₂ derived from the WSGR. The WSGR occurs simultaneously with upgrading reactions with *in situ* H₂ consumed for hydrocracking and hydrotreating. The upgraded oil product was lighter than water, stable without precipitation and could easily flow (at room temperatures), indicating effective partial upgrading performance for pipeline transportation. During the upgrading experiments, *in situ* H₂ was found to have similar or even higher upgrading activity than molecular H₂ at a much lower H₂ partial pressure. Ni promoted emulsion upgrading provided improvement in oil yield, inhibition of HVOR formation and no extra coke yield. The promotion in the hydrocracking reaction with the Ni-MoS₂ catalyst was proposed to be the key reason for the improved upgrading performance. Water was found to be beneficial for emulsion upgrading by improving the oil yield and inhibiting thermocracking with *in situ* H₂. As a trade-off, the reaction resulted in a higher pressure with the feeding of more water. Further engineering economic studies should be implemented on the balance between increased yields vs. incremental capital and operational costs (required for higher pressure) caused by water. Asphaltenes were separated and characterized to investigate their component and structural change. It was observed that asphaltenes were also upgraded during the reaction with less sulfur, less carbonyl, and smaller molecular size. In the presence of molecular H₂ or *in situ* H₂, this asphaltene condensation was prohibited, which eventually benefited upgrading by providing more liquid yield and lower coke/HVOR yields. At the molecular level, HDS and HDA were realized for the asphaltenes, but there was no HDN or HDM occurring. OSPW involved in the reaction was found to be purified, suggesting the potential of direct cleaning of the emulsified water in the bitumen emulsion feedstock. Most of the metal cations were removed through metal deposition. Possible organic acid removal was observed, which resulted in a naphthenic acid removal study through the emulsion upgrading process.

Through a model compound study with 2-NA and C7-BA, naphthenic acids were found capable of being removed from both the oil and water phase in a novel bitumen upgrading process. *In situ* H₂ performed similarly and even exhibited a better activity for 2-NA removal compared to molecular H₂ at a much lower H₂ partial pressure in the presence of the strong HDO inhibitor CO. The *in situ* generated nano unsupported MoS₂ catalyst was found to facilitate 2-NA removal at a very fast rate. It catalyzed both 2-NA removal and the WGSR, especially in enhancing the HDO reaction rate. The reaction mechanism suggested involved a three-pathway reaction network involving decarboxylation, HDO, cracking and a consecutive chain hydrogenation for both 2-NA and C7-BA. Pseudo-first order reaction rate constants were obtained and analyzed for the 2-NA removal; each pathway in the 2-NA removal and WGSR. It was found that the HDO pathway was more easily inhibited with an increasing amount of water under N₂, resulting in poorer 2-NA removal. CO was a much better reaction gas feed for not only achieving high HDO activity but also maintaining catalyst stability in the presence of water. Co and Ni were found to improve the 2-NA removal with improved decarboxylation and HDO activities. This promotion was derived from: (a) a higher H₂ partial pressure from the increased WGSR conversion by using a promoter; and (b) the synergistic activity improvement due to the CoMoS and NiMoS formation. The mutual impacts between 2-NA removal with WGSR, HDS of DBT, and HDA of NAPH were also discussed. 2-NA exhibited no inhibition effect on the WGSR based on the kinetic analysis, since CO and H₂O were stronger adsorbates than 2-NA. 2-NA inhibited the HDS of DBT and the HDA of NAPH, since the oxygen containing functional group in 2-NA provided a stronger adsorption on the catalyst than DBT and NAPH. The 2-NA removal was inhibited by the introduction of NAPH, due to the large H₂ consumption caused by the HDA of NAPH instead of competitive adsorption.

Advanced characterization was implemented on the catalysts in LGO upgrading; the *ex situ* catalyst synthesized in the C16/water emulsion, and the *ex situ* catalysts synthesized in the toluene/water emulsion. Characterization included XRD, BET, SEM, HRTEM, and EDX. The effects of various synthesis conditions were discussed, including temperature, atmosphere, promoter and metal:Mo ratio through HRTEM and EDX. Statistical analysis was also performed

on slab length and stacking number to provide information on the catalysts' crystalline structures. *In situ* H₂ exhibited excellent performance as the atmosphere for synthesizing more active *ex situ* nano unsupported MoS₂ catalyst compared to molecular H₂. *In situ* H₂ was proposed to (a) form spherical structures earlier with less agglomeration; (b) further reduce Mo cations from Mo⁶⁺ in PMA for earlier formation of slab structures; (c) produce shorter slabs; (d) reduce stacking degrees and (e) prevent layer structure from compression at higher temperature. It was concluded that no significant morphology improvement was achieved in the promoted Co-MoS₂ and Ni-MoS₂ catalysts. The intrinsic activities of the synergistic Co-Mo-S and Ni-Mo-S phases could be the major reason for improved activity instead of morphology improvement. Morphology impact was proposed to be only dominant when no mixed metal sulfide was present, like the morphology changes occurring when different H₂ sources were used.

8.2 Process review and recommendations

As shown in Table 8-1, the emulsion upgrading process is compared with selected partial upgrading and full upgrading technologies. It should be noted that only the emulsion upgrading process has demonstrated the synergy with water treatment in mining operations, CSS or SAGD plants. The best mass yields obtained in emulsion upgrading were as high as 87% and 75% with and without catalysts. By assuming that the emulsion upgrading products meet pipeline specification (19°API, 350 cSt@7°C), the vol. yields were 95% and 82% with and without catalysts. If catalyst is not used, this yield is then higher than for SCWC[®] (65%wt.) and similar to Hi-Q[®] (70%wt.) and OrCrude[®] (82%wt.). Compared to the emulsion upgrading process, the Hi-Q[®] process has lower operational cost due to less heat required; while the OrCrude[®] plant generates its own H₂ and energy through gasification. As a result, emulsion upgrading might not be very competitive without using catalysts, although operational costs should be also low in this scenario. However, attractive mass and volume yields were achieved though the present catalytic emulsion upgrading process, higher than all other selected processes. This presents a promising future for this novel emulsion upgrading technology.

Table 8-1 Comparison of emulsion upgrading process (with and without catalyst) with selected partial upgrading and full upgrading technologies

	I ^Y Q [®]	HTL [®]	SCWC [®]	Hi-Q [®]	OrCrude [®]	Emulsion Upgrading With Cat.	Emulsion Upgrading No Cat.
Yield, wt.	82%	86%	65%	70%	82%	87%	75%
Yield, vol.	90%	92%	70%	83%	90%	95%*	82%*
SCO Quality	Medium	Poor	Medium	Medium	Very High	High	High
SCO Stability	Poor	Poor	Poor	Medium	High	High	High
<i>Additional Capital for Improved Stability</i>	High	High	High	Medium	-	-	-
Rejected Carbon Stream	Coke	Coke	Pitch	Asph.	Asph.	Coke +Pitch	Coke +Pitch
<i>Rejected carbon yield, wt.</i>	12%	-	35%	15%	-	6%	10%
Catalyst Usage	No	No	No	No	Yes	Yes	No
Initial Capital Cost	Low	Low	High	Low	Very High	High	Medium
Operating Cost	Low	Low	Medium	Very Low	Very High	Medium	Low
Energy Production	Medium	High	-	Low	High	Low	Low
<i>Additional Capital for Improved Energy Production</i>	Medium	-	Very High	High	-	High	High
Synergy with water treatment	No	No	N/A	No	No	Yes	Yes

* Volume yields were calculated by assuming API reached 19°

Considering the technology readiness with some existing and potential technical difficulties, recommendations are summarized as following to move forward this technology towards commercialization:

- 1) Initiate bench-top tests with a continuous reactor for collecting suitable results for process modelling;

- 2) Understand the product distribution by gathering complete oil and water assays;
- 3) Start corrosion and erosion investigation due to the existence of asphaltene, catalysts and sub-critical water;
- 4) Consider fouling prevention methods;
- 5) Improve the pitch separation by using cheap and reliable technology;
- 6) Design a syngas generation process, like gasification or partial oxidation;
- 7) Reduce catalyst costs by evaluating inexpensive metals, such as Fe.

References

- Afanasiev, P. (2010). "The influence of reducing and sulfiding conditions on the properties of unsupported MoS₂-based catalysts." Journal of Catalysis **269**(2): 269-280.
- Afanasiev, P., G.-F. Xia, G. Berhault, B. Jouguet and M. Lacroix (1999). "Surfactant-Assisted Synthesis of Highly Dispersed Molybdenum Sulfide." Chemistry of Materials **11**(11): 3216-3219.
- Akbarzadeh, K., A. Hammami, A. Kharat, D. Zhang, S. Allenson, J. Creek, S. Kabir, A. Jamaluddin, A. G. Marshall, R. P. Rodgers, O. C. Mullins and T. Solbakken (2007). "Asphaltenes - problematic but rich in potential." Oilfield Review **19**(2): 22-43.
- Alberta, P. o. (2000). Environmental Protection and Enhancement Act. Alberta, P. o. Province of Alberta.
- Albiter, M. A., R. Huirache-Acuna, F. Paraguay-Delgado, J. L. Rico and G. Alonso-Nunez (2006). "Synthesis of MoS₂ nanorods and their catalytic test in the HDS of dibenzothiophene." Nanotechnology **17**(14): 3473-3481.
- Alcazar-Vara, L. A. and E. Buenrostro-Gonzalez (2013). "Liquid-Solid Phase Equilibria of Paraffinic Systems by DSC Measurements", book chapter of Applications of Calorimetry in a Wide Context - Differential Scanning Calorimetry, Isothermal Titration Calorimetry and Microcalorimetry, InTech.
- Alghamdi, A. (2009). Hydrodesulphurization of Light Gas Oil using Hydrogen from the Water Gas Shift Reaction. Master of Applied Science, University of Waterloo.
- Alonso-Núñez, G., R. Huirache-Acuña, F. Paraguay-Delgado, J. Lumbreras, R. García-Alamilla, A. Castillo-Mares, R. Romero, R. Somanathan and R. Chianelli (2009). "Synthesis and Characterization of Hexamethylenediammonium Thiometallates as Precursors of MoS₂ and WS₂ Catalysts: In situ Activation During HDS of DBT." Catalysis Letters **130**(3): 318-326.
- Alonso, G., V. M. Del, J. Cruz and S. Fuentes (1996). "Study of a MoS₂ catalyst prepared in-situ for hydrodesulfurization reaction." AIP Conference Proceedings **378**: 552-555.
- Alshareef, A. H., A. Scherer, X. Tan, K. Azyat, J. M. Stryker, R. R. Tykwinski and M. R. Gray (2011). "Formation of Archipelago Structures during Thermal Cracking Implicates a Chemical Mechanism for the Formation of Petroleum Asphaltenes." Energy & Fuels **25**(5): 2130-2136.

An, G., C. Lu and C. Xiong (2009). "Study of the unsupported Ni-Mo sulfide catalyst with ultrahigh hydrogenation performance." Abstract of Papers, 238th ACS National Meeting, Washington, DC, United States, August 16-20, 2009: PETR-025.

Ancheyta, J., M. S. Rana and E. Furimsky (2005). "Hydroprocessing of heavy petroleum feeds: Tutorial." Catalysis Today **109**(1-4): 3-15.

Artok, L. and H. H. Schobert (2000). "Reaction of carboxylic acids under coal liquefaction conditions: 1. Under nitrogen atmosphere." Journal of Analytical and Applied Pyrolysis **54**(1-2): 215-233.

Artok, L., Y. Su, Y. Hirose, M. Hosokawa, S. Murata and M. Nomura (1999). "Structure and Reactivity of Petroleum-Derived Asphaltene." Energy & Fuels **13**(2): 287-296.

Azad, F. S., J. Abedi and S. Iranmanesh (2013). "Removal of naphthenic acids using adsorption process and the effect of the addition of salt." Journal of Environmental Science and Health. Part A, Toxic/Hazardous Substances & Environmental Engineering **48**(13): 1649-1654.

Babich, I. V. and J. A. Moulijn (2003). "Science and technology of novel processes for deep desulfurization of oil refinery streams: a review." Fuel **82**(6): 607-631.

Badawi, M., S. Cristol, J.-F. Paul and E. Payen (2009). "DFT study of furan adsorption over stable molybdenum sulfide catalyst under HDO conditions." Comptes Rendus Chimie **12**: 754-761.

Badawi, M., J.-F. Paul, S. Cristol and E. Payen (2011). "Guaiacol derivatives and inhibiting species adsorption over MoS₂ and CoMoS catalysts under HDO conditions: A DFT study." Catalysis Communications **12**(10): 901-905.

Badawi, M., J. F. Paul, S. Cristol, E. Payen, Y. Romero, F. Richard, S. Brunet, D. Lambert, X. Portier, A. Popov, E. Kondratieva, J. M. Goupil, J. El Fallah, J. P. Gilson, L. Mariey, A. Travert and F. Maugé (2011). "Effect of water on the stability of Mo and CoMo hydrodeoxygenation catalysts: A combined experimental and DFT study." Journal of Catalysis **282**(1): 155-164.

Barcenas, M., P. Orea, E. Buenrostro-Gonzalez, L. S. Zamudio-Rivera and Y. Duda (2008). "Study of Medium Effect on Asphaltene Agglomeration Inhibitor Efficiency." Energy & Fuels **22**(3): 1917-1922.

Bartholomew, C. H. (2001). "Mechanisms of catalyst deactivation." Applied Catalysis A: General **212**(1-2): 17-60.

Bataille, F., J.-L. Lemberon, P. Michaud, G. Pérot, M. Vrinat, M. Lemaire, E. Schulz, M. Breysse and S. Kasztelan (2000). "Alkyldibenzothiophenes Hydrodesulfurization-Promoter Effect, Reactivity, and Reaction Mechanism." Journal of Catalysis **191**(2): 409-422.

Besenbacher, F., M. Brorson, B. S. Clausen, S. Helveg, B. Hinnemann, J. Kibsgaard, J. V. Lauritsen, P. G. Moses, J. K. Nørskov and H. Topsøe (2008). "Recent STM, DFT and HAADF-STEM studies of sulfide-based hydrotreating catalysts: Insight into mechanistic, structural and particle size effects." Catalysis Today **130**(1): 86-96.

Bilden, D. M. and V. E. Jones (2000). Subterranean formation, US 6051535.

Birdgeneau, J. (2008). The Canadian Long lake Project Integrating Cogeneration and Upgrading Technologies to Athabasca Bitumen. 19th World Petroleum Congress, Spain.

Biryukova, O. V., P. M. Fedorak and A. Q. Sylvie (2007). "Bio-degradation of Naphthenic Acids by Rhizosphere Micro-organisms." Chemosphere **67**(10): 2058-2064.

BMO-Capital-Market (2013). Energy source conservation board.

Breger, I. A. and V. L. Burton (1946). "The effects of radioactivity on a naphthenic acid." Journal of the American Chemical Society **68**: 1639-1642.

Brient, J. A., Wessner, P. J., and Doyle, M. N. (1995). Naphthenic acids. Encyclopedia of Chemical Technology (4th Edition). Kroschwitz, J. I. New York, John Wiley & Sons, Ltd.: 1017-1029.

Broderick, D. H., A. V. Sapre, B. C. Gates, H. Kwart and G. C. A. Schuit (1982). "Hydrogenation of aromatic compounds catalyzed by sulfided CoO---MoO₃/γ-Al₂O₃." Journal of Catalysis **73**(1): 45-49.

Bronicki, Y. (2007). Method of and apparatus for processing heavy hydrocarbon feeds, US7297250.

Brown, W. (2012). Method for feeding a fluidized bed coking reactor, CA2822507A1.

Brown, W. and G. Monaghan (2011). Commercialization of the IYQ Upgrading Technology. World Energy Congress, Edmonton, AB, Canada.

Bui, V. N., D. Laurenti, P. Afanasiev and C. Geantet (2011). "Hydrodeoxygenation of guaiacol with CoMo catalysts. Part I: Promoting effect of cobalt on HDO selectivity and activity." Applied Catalysis B: Environmental **101**(3-4): 239-245.

Cabello, C. I., F. M. Cabrerizo, A. Alvarez and H. J. Thomas (2002). "Decamolybdodicobaltate(III) heteropolyanion: structural, spectroscopical, thermal and hydrotreating catalytic properties." Journal of Molecular Catalysis A: Chemical **186**(1-2): 89-100.

Cabrera, C. A., M. D. Hillerman and M. A. Silverman (2012). Monetizing stranded heavy oil assets in remote locations. World Heavy Oil Congress 2012.

CAPP (2013). Alberta Oil Sands Bitumen Valuation Methodology For 2013.

CAPP (2013). Crude Oil Forecast, Market & Transportation.

Chadwick, D., A. Oen and C. Siewe (1996). "Influence of water and ammonia on hydrotreating catalysts and activity for tetralin hydrogenation." Catalysis Today **29**(1-4): 229-233.

Chang, C.-L. and H. S. Fogler (1996). "Peptization and coagulation of asphaltenes in apolar media using oil-soluble polymers." Fuel Science and Technology International **14**(1 & 2): 75-100.

Chary, K. V. R., K. S. R. Rao, G. Muralidhar and P. K. Rao (1991). "Hydrodeoxygenation of furan by carbon supported molybdenum sulfide catalysts." Carbon **29**: 478-479.

Chilingarian, G. V. and T. F. Yen (1978). Developments in Petroleum Science. Chilingarian, G. V. and T. F. Yen. **7**: 1-331.

Chiranjeevi, T., P. Kumar, M. S. Rana, G. Murali Dhar and T. S. R. Prasada Rao (2002). "Physico-chemical characterization and catalysis on mesoporous Al-HMS supported molybdenum hydrotreating catalysts." Journal of Molecular Catalysis A: Chemical **181**(1-2): 109-117.

Choudhary, T. V., S. Parrott and B. Johnson (2008). "Unraveling Heavy Oil Desulfurization Chemistry: Targeting Clean Fuels." Environmental Science & Technology **42**(6): 1944-1947.

Choy, C. (2009). Naphthalene Hydrogenation with Water-Gas Shift in model Oil/Water Emulsion Slurry over MoS₂. M.A.Sc, University of Waterloo.

Colyar, J. (2010). Feasibility of Partial Upgrading of Athabasca Bitumen, Colyar Consultants.

Cooper, B. H. and B. B. L. Donnis (1996). "Aromatic saturation of distillates: an overview." Applied Catalysis A: General **137**(2): 203-223.

Corma, A., A. Martínez and V. Martínez-Soria (1997). "Hydrogenation of Aromatics in Diesel Fuels on Pt/MCM-41 Catalysts." Journal of Catalysis **169**(2): 480-489.

Corscadden, T. (2012). MEG HI-Q: Cost-effective bitumen conversion. AI-EES Technology Talk.

Link: www.ai-ees.ca/media/8025/14_corscadden_tom_energy_technologies.pdf

Corscadden, T., G. Bruce, G. Diduch, D. Hocking and D. Remesat (2013). Low complexity, high yield conversion of heavy hydrocarbons, US20130180888.

Corscadden, T., G. Bruce, G. Diduch, D. Hocking and D. Remesat (2013). Solvent de-asphalting with cyclonic separation, US20130081325.

Cotton, F. A., Wilkinson, Geoffrey, Murillo, Carlos A., Bochmann, Manfred (1999). Advanced Inorganic Chemistry, Wiley-VCH.

Csuros, Z., J. Makadi and T. Csok (1948). "Catalytic decarboxylation of organic acids." Magy. Chem. Foly. **54**: 9-19.

da Costa, L. M., S. R. Stoyanov, S. Gusarov, X. Tan, M. R. Gray, J. M. Stryker, R. Tykwinski, J. W. d. M. Carneiro, P. R. Seidl and A. Kovalenko (2012). "Density Functional Theory Investigation of the Contributions of π - π Stacking and Hydrogen-Bonding Interactions to the Aggregation of Model Asphaltene Compounds." Energy & Fuels **26**(5): 2727-2735.

Daud, M., J. L. Pinilla, P. Arcelus-Arrillaga, K. Hellgardt, R. Kandiyoti and M. Millan (2012). Heavy oil upgrading in subcritical and supercritical water: Studies on model compounds, American Chemical Society.

Del Rio, L. F., A. K. M. Hadwin, L. J. Pinto, M. D. MacKinnon and M. M. Moore (2006). "Degradation of naphthenic acids by sediment micro-organisms." Journal of Applied Microbiology **101**(5): 1049-1061.

Dettman, H. D., S. Liu and D. Duplessis (2012). Technologies for Oil Sands Crude Quality Improvement, . CCQTA/COQA Joint Meeting, Kananaskis, Alberta, Canada.

Ding, L., P. Rahimi, R. Hawkins, S. Bhatt and Y. Shi (2009). "Naphthenic acid removal from heavy oils on alkaline earth-metal oxides and ZnO catalysts." Applied Catalysis A: General **371**: 121-130.

Dokholyan, V. K., and A. K. Magomedov (1983). "Effects of sodium naphthenate on survival and some physiological-biochemical parameters of some fishes." Journal of Ichthyology **23**: 125-132.

Drummond, C. and J. Israelachvili (2004). "Fundamental studies of crude oil-surface water interactions and its relationship to reservoir wettability." Journal of Petroleum Science and Engineering **45**(1-2): 61-81.

Drzewicz, P., A. Afzal, M. G. El-Din and J. W. Martin (2010). "Degradation of a Model Naphthenic Acid, Cyclohexanoic Acid, by Vacuum UV (172 nm) and UV (254 nm)/H₂O₂." The Journal of Physical Chemistry A **114**(45): 12067-12074.

Du, H., C. Fairbridge, H. Yang and Z. Ring (2005). "The chemistry of selective ring-opening catalysts." Applied Catalysis A: General **294**(1): 1-21.

Dufresne, P. (2007). "Hydroprocessing catalysts regeneration and recycling." Applied Catalysis A: General **322**: 67-75.

Duong, A. and K. J. Smith (1997). "A model of ceramic membrane fouling during heavy oil ultrafiltration." Canadian Journal of Chemical Engineering **75**(6): 1122-1129.

Dupont, C., R. Lemeur, A. Daudin and P. Raybaud (2011). "Hydrodeoxygenation pathways catalyzed by MoS₂ and NiMoS active phases: A DFT study." Journal of Catalysis **279**(2): 276-286.

Eijsbouts, S., S. W. Mayo and K. Fujita (2007). "Unsupported transition metal sulfide catalysts: From fundamentals to industrial application." Applied Catalysis A: General **322**: 58-66.

Elizondo-Villarreal, N., R. Velázquez-Castillo, D. H. Galván, A. Camacho and M. José Yacamán (2007). "Structure and catalytic properties of molybdenum sulfide nanoplatelets." Applied Catalysis A: General **328**(1): 88-97.

Enbridge (2013). "Standards and specifications" - Enbridge Technology Inc.
Link: www.enbridgetechnology.com/products/pdf/engineering-standards.pdf

ETX-Systems (2009). IYQ Upgrading –An Industry Altering Technology for Primary Upgrading of Heavy Oil, . World Heavy Oil Congress, Puerto La Cruz, Venezuela.

Freel, B. and R. G. Graham (2012). Rapid thermal processing of heavy hydrocarbon feedstocks, US20120279825.

Freel, B. A. and R. G. Graham (1998). Method and apparatus for a circulating bed transport fast pyrolysis reactor system, US5792340.

Freel, B. A. and R. G. Graham (1999). Apparatus for a circulating bed transport fast pyrolysis reactor system, US5961786.

Frizi, N., P. Blanchard, E. Payen, P. Baranek, M. Rebeilleau, C. Dupuy and J. P. Dath (2008). "Genesis of new HDS catalysts through a careful control of the sulfidation of both Co and Mo atoms: Study of their activation under gas phase." Catalysis Today **130**(2-4): 272-282.

Gamal El-Din, M., H. Fu, N. Wang, P. Chelme-Ayala, L. Perez-Estrada, P. Drzewicz, J. W. Martin, W. Zubot and D. W. Smith (2011). "Naphthenic acids speciation and removal during petroleum-coke adsorption and ozonation of oil sands process-affected water." Science of the Total Environment **409**(23): 5119-5125.

Genuit, D., P. Afanasiev and M. Vrinat (2005). "Solution syntheses of unsupported Co(Ni)-Mo-S hydrotreating catalysts." Journal of Catalysis **235**(2): 302-317.

Gochi, Y., C. Ornelas, F. Paraguay, S. Fuentes, L. Alvarez, J. L. Rico and G. Alonso-Núñez (2005). "Effect of sulfidation on Mo-W-Ni trimetallic catalysts in the HDS of DBT." Catalysis Today **107-108**: 531-536.

Gonzalez, G. and A. Middea (1991). "Peptization of asphaltene by various oil soluble amphiphiles." Colloids and Surfaces **52**(3-4): 207-217.

Gonzalez, G. and M. B. C. Moreira (1991). "The wettability of mineral surfaces containing adsorbed asphaltenes." Colloids and Surfaces **58**(3): 293-302.

Gray, M. R. (2010). "Asphaltene reactions and aggregation: insights at the molecular level." Prepr. Symp. - Am. Chem. Soc., Div. Fuel Chem. **55**(2): 209-211.

Gray, M. R., S. R. Bagheri and W. C. McCaffrey (2012). "In Situ study of phase behavior during heavy oil conversion." Prepr. - Am. Chem. Soc., Div. Energy & Fuels **57**(2): 57-58.

Gray, M. R., R. R. Tykwinski and J. M. Stryker (2011). "Structure and aggregation of petroleum asphaltenes." Prepr. - Am. Chem. Soc., Div. Pet. Chem. **56**(2): 47.

Gray, M. R., R. R. Tykwinski, J. M. Stryker and X.-L. Tan (2011). "Supramolecular Assembly Model for Aggregation of Petroleum Asphaltenes." Energy & Fuels **25**(7): 3125-3134.

Grewer, D. M., R. F. Young, R. M. Whittal and P. M. Fedorak (2010). "Naphthenic acids and other acid-extractables in water samples from Alberta: What is being measured?" Science of The Total Environment **408**(23): 5997-6010.

Gulková, D., Y. Yoshimura and Z. Vít (2009). "Mesoporous silica-alumina as support for Pt and Pt-Mo sulfide catalysts: Effect of Pt loading on activity and selectivity in HDS and HDN of model compounds." Applied Catalysis B: Environmental **87**(3-4): 171-180.

Han, X., A. C. Scott, P. M. Fedorak, M. Bataineh and J. W. Martin (2008). "Influence of Molecular Structure on the Biodegradability of Naphthenic Acids." Environmental Science and Technology **42**(4): 1290-1295.

Harris, S. and R. R. Chianelli (1986). "Catalysis by transition metal sulfides: A theoretical and experimental study of the relation between the synergic systems and the binary transition metal sulfides." Journal of Catalysis **98**(1): 17-31.

Hasan, S. W., M. T. Ghannam and N. Esmail (2010). "Heavy crude oil viscosity reduction and rheology for pipeline transportation." Fuel **89**(5): 1095-1100.

Headley, J. V., J. Du, K. M. Peru and D. W. McMartin (2009). "Electrospray Ionization Mass Spectrometry of the Photo-degradation of Naphthenic Acids Mixtures Irradiated with Titanium Dioxide." Journal of Environmental Science and Health, Part A **44**(6): 591-597.

Ho, T. C. (1994). "Hydrogenation of Mononuclear Aromatics over a Sulfided Ni-Mo/Al₂O₃ Catalyst." Energy & Fuels **8**(5): 1149-1151.

Ho, T. C. (2003). "Inhibiting effects in hydrodesulfurization of 4,6-diethyldibenzothiophene." Journal of Catalysis **219**(2): 442-451.

Ho, T. C. (2004). "Deep HDS of diesel fuel: chemistry and catalysis." Catalysis Today **98**(1-2): 3-18.

Hochhauser, A. M. (2000). Gasoline and Other Motor Fuels, John Wiley & Sons, Inc.

Hood, R. L. (1998). Solvent deasphalting unit capable of generating power, US5843302.

Hood, R. L., P. B. Rettger, R. S. Goldstein and L. Y. Bronicki (2001). Method of and means for upgrading hydrocarbons containing metals and asphaltenes, US6274032.

Hosseinpour, N., Y. Mortazavi, A. Bahramian, L. Khodatars and A. A. Khodadadi (2014). "Enhanced pyrolysis and oxidation of asphaltenes adsorbed onto transition metal oxides nanoparticles towards advanced in-situ combustion EOR processes by nanotechnology." Applied Catalysis A: General **477**(0): 159-171.

Husky-Energy (2011). Husky Lloydminster Upgrader.

Imperial-Oil.

from http://www.imperialoil.ca/Canada-English/operations_sands_glance_101.aspx.

Iranmanesh, S. (2013). Removal of Naphthenic Acid from Water Using Biomass-based Activated Carbon. MSc, University of Calgary.

Jacobsen, C. J. H., E. Törnqvist and H. Topsøe (1999). "HDS, HDN and HYD activities and temperature-programmed reduction of unsupported transition metal sulfides." Catalysis Letters **63**: 179-183.

Janfada, A., J. V. Headley, K. M. Peru and S. L. Barbour (2006). "A laboratory evaluation of the sorption of oil sands naphthenic acids on organic rich soils." Journal of Environmental Science and Health. Part A, Toxic/Hazardous Substances & Environmental Engineering **41**(6): 985-997.

JGC (2013). "Supercritical Water Cracking Technology".

Jia, L., A. E. Al-Ghamdi and F. T. Ng (2011). Light gas oil upgrading over nano-dispersed molybdenum sulfide based catalysts through water gas shift reaction, American Chemical Society.

Jia, L., A. Alghamdi and F. T. T. Ng (2012). "Effect of metal ions on light gas oil upgrading over nano dispersed MoS_x catalysts using in situ H₂." ACS Symp. Ser. **1092**(Nanocatalysis for Fuels and Chemicals): 37-49, 33 plates.

Johnson, R. W., W. F. Hribik and L. Hilfman (1988). Process for hydrotreating a hydrocarbonaceous charge stock, US 4719007.

Jongpatiwut, S., Z. Li, D. E. Resasco, W. E. Alvarez, E. L. Sughrue and G. W. Dodwell (2004). "Competitive hydrogenation of poly-aromatic hydrocarbons on sulfur-resistant bimetallic Pt-Pd catalysts." Applied Catalysis A: General **262**(2): 241-253.

Kamaluddin, M. and J. J. Zwiazek (2002). "Naphthenic acids inhibit root water transport, gas exchange and leaf growth in aspen (*Populus tremuloides*) seedlings." Tree Physiology **22**: 1265–1270

Kannel, P. R. and T. Y. Gan (2012). "Naphthenic acids degradation and toxicity mitigation in tailings wastewater systems and aquatic environments: a review." Journal of Environmental Science and Health. Part A, Toxic/Hazardous Substances & Environmental Engineering **47**(1): 1-21.

Kaushik, P., A. Kumar, T. Bhaskar, Y. K. Sharma, D. Tandon and H. B. Goyal (2012). "Ultrasound cavitation technique for up-gradation of vacuum residue." Fuel Processing Technology **93**(1): 73-77.

Kayukawa, T. (2009). Upgrading of bitumen by using supercritical water. 5th NCUT Upgrading and Refining conference, Edmonton, Alberta, Canada.

Kenneth L. Trachte, J. B. A., Keith K. Aldous (1997). Catalytic reduction of acidity of crude oils in the absence of hydrogen Company, E. R. a. E. USA, Exxon Research and Engineering Company.

Kibsgaard, J., A. Tuxen, K. G. Knudsen, M. Brorson, H. Topsøe, E. Lægsgaard, J. V. Lauritsen and F. Besenbacher (2010). "Comparative atomic-scale analysis of promotional effects by late 3d-transition metals in MoS₂ hydrotreating catalysts." Journal of Catalysis **272**(2): 195-203.

Kuehl, Q. H. G. (1996). Removal of large molecules from a fluid, WO 1996010537.

Lacroix, M., N. Boutarfa, C. Guillard, M. Vrinat and M. Breysse (1989). "Hydrogenating properties of unsupported transition metal sulphides." Journal of Catalysis **120**(2): 473-477.

Laurent, E. and B. Delmon (1993). "Influence of oxygen-, nitrogen-, and sulfur-containing compounds on the hydrodeoxygenation of phenols over sulfided cobalt-molybdenum/gamma-alumina and nickel-molybdenum/gamma-alumina catalysts." Industrial & Engineering Chemistry Research **32**(11): 2516-2524.

Lauritsen, J. V., J. Kibsgaard, G. H. Olesen, P. G. Moses, B. Hinnemann, S. Helveg, J. K. Nørskov, B. S. Clausen, H. Topsøe, E. Lægsgaard and F. Besenbacher (2007). "Location and

coordination of promoter atoms in Co- and Ni-promoted MoS₂-based hydrotreating catalysts." Journal of Catalysis **249**(2): 220-233.

Lauritsen, J. V., M. Nyberg, J. K. Nørskov, B. S. Clausen, H. Topsøe, E. Lægsgaard and F. Besenbacher (2004). "Hydrodesulfurization reaction pathways on MoS₂ nanoclusters revealed by scanning tunneling microscopy." Journal of Catalysis **224**(1): 94-106.

Lee, R. (2004). Investigation of hydrodesulfurization of dibenzothiophene and hydrodenitrogenation of quinoline using in situ H₂ generated via water gas shift reaction over dispersed Mo-based catalysts. Ph.D., University of Waterloo.

Lee, R. Z. and F. T. T. Ng (2006). "Effect of water on HDS of DBT over a dispersed Mo catalyst using in situ generated hydrogen." Catalysis Today **116**(4): 505-511.

Lee, R. Z., M. Zhang and F. T. T. Ng (2006). "Hydrodenitrogenation of Quinoline Over a Dispersed Molybdenum Catalyst Using in situ Hydrogen." Topics in Catalysis **37**(2-4): 121-127.

Leon, O., E. Rogel, A. Urbina, A. Andujar and A. Lucas (1999). "Study of the Adsorption of Alkyl Benzene-Derived Amphiphiles on Asphaltene Particles." Langmuir **15**(22): 7653-7657.

LeSage, B. (2009). Pilot Results for a Revolutionary Cross - Flow, Fluid Bed Upgrading Process. World Heavy Oil Congress, Puerto La Cruz, Mexico.

Li, M., H. Li, F. Jiang, Y. Chu and H. Nie (2010). "The relation between morphology of (Co)MoS₂ phases and selective hydrodesulfurization for CoMo catalysts." Catalysis Today **149**(1-2): 35-39.

Liu, B., Y. Chai, Y. Li, A. Wang, Y. Liu and C. Liu (2014). "Effect of sulfidation atmosphere on the performance of the CoMo/ γ -Al₂O₃ catalysts in hydrodesulfurization of FCC gasoline." Applied Catalysis A: General **471**(0): 70-79.

Liu, C. and F. T. T. Ng (1999). "HDS of DBT using in situ generated hydrogen in the presence of dispersed Mo catalysts. I. Product distribution and reaction network." Cuihua Xuebao **20**(5): 499-504.

Liu, C. and F. T. T. Ng (1999). "HDS of DBT using in situ generated hydrogen in the presence of dispersed Mo catalysts. II. Comparison between in situ hydrogen and molecular H₂." Cuihua Xuebao **20**(5): 505-509.

Liu, C. and F. T. T. Ng (1999). "The hydrodesulfurization of dibenzothiophene by using in situ generated hydrogen in the presence of dispersed Mo catalysts. III. Effects of catalyst precursors, H₂S, CO and H₂O." Cuihua Xuebao **20**(6): 591-596.

Liu, C., F. T. T. Ng and C. Huang (1999). "Hydrodesulfurization of dibenzothiophene by using in situ generated hydrogen in the presence of dispersed Mo catalysts. IV. Lumped kinetics." Cuihua Xuebao **20**(6): 597-602.

Liu, D., X. Kong, M. Li and G. Que (2009). "Study on a Water-Soluble Catalyst for Slurry-Phase Hydrocracking of an Atmospheric Residue." Energy & Fuels **23**(2): 958-961.

Liu, K. (2010). Hydrodesulfurization and Hydrodenitrogenation of Model Compounds Using in situ Hydrogen over Nano-Dispersed Mo Sulfide Based Catalysts. Ph.D., University of Waterloo.

Liu, K., C. Choy and F. T. T. Ng (2007). "Hydrotreating synthetic crude with in situ hydrogen and nano-dispersed Mo catalyst." Prepr. - Am. Chem. Soc., Div. Pet. Chem. **52**(2): 138-140.

Liu, K., L. Jia and F. T. Ng (2013). Hydrodenitrogenation of carbazole over dispersed Mo sulfide catalyst using in situ H₂, American Chemical Society.

Liu, K. and F. T. T. Ng (2010). "Effect of the nitrogen heterocyclic compounds on hydrodesulfurization using in situ hydrogen and a dispersed Mo catalyst." Catalysis Today **149**(1-2): 28-34.

Lizama, L. and T. Klimova (2008). "Highly active deep HDS catalysts prepared using Mo and W heteropolyacids supported on SBA-15." Applied Catalysis B: Environmental **82**(3-4): 139-150.

Llanos, Z. R. and W. G. Deering (2000). Evolution of GCMC's spent catalyst operations. Proceedings of the TMS Fall Extraction and Processing Conference.

Lu, C.-M., Y.-M. Lin and I. Wang (2000). "Naphthalene hydrogenation over Pt/TiO₂-ZrO₂ and the behavior of strong metal-support interaction (SMSI)." Applied Catalysis A: General **198**(1-2): 223-234.

Lumbreras, J., R. Huirache-Acuña, E. Rivera-Muñoz, G. Berhault and G. Alonso-Núñez (2010). "Unsupported Ni/Mo(W)S₂ Catalysts from Hexamethylenediammonium Thiometallates Precursors: In Situ Activation During the HDS of DBT." Catalysis Letters **134**(1): 138-146.

Marafí, M. and A. Stanislaus (2002). Spent catalyst handling and utilization. The 17th World Petroleum Congress, Rio de Janeiro.

Marchal, C., E. Abdessalem, M. Tayakout-Fayolle and D. Uzio (2010). "Asphaltene Diffusion and Adsorption in Modified NiMo Alumina Catalysts Followed by Ultraviolet (UV) Spectroscopy." Energy & Fuels **24**(8): 4290-4300.

Martin, J. W., T. Barri, X. Han, P. M. Fedorak, M. G. El-Din, L. Perez, A. C. Scott and J. T. Jiang (2010). "Ozonation of oil sands process-affected water accelerates microbial bioremediation." Environmental Science & Technology **44**(21): 8350-8356.

Massoth, F. E., P. Politzer, M. C. Concha, J. S. Murray, J. Jakowski and J. Simons (2006). "Catalytic Hydrodeoxygenation of Methyl-Substituted Phenols: Correlations of Kinetic Parameters with Molecular Properties." The Journal of Physical Chemistry B **110**(29): 14283-14291.

McMartin, D. W., J. V. Headley, D. A. Friesen, K. M. Peru and J. A. Gillies (2004). "Photolysis of Naphthenic Acids in Natural Surface Water." Journal of Environmental Science and Health, Part A **39**(6): 1361-1383.

McVicker, G. B., M. Daage, M. S. Touvelle, C. W. Hudson, D. P. Klein, W. C. Baird, B. R. Cook, J. G. Chen, S. Hantzer, D. E. W. Vaughan, E. S. Ellis and O. C. Feeley (2002). "Selective Ring Opening of Naphthenic Molecules." Journal of Catalysis **210**(1): 137-148.

MEG-Energy (2012). MEG HI-Q: Cost-effective bitumen conversion.

MEG-Energy (2013). Energy Resources Conservation Board Application.

Mishra, S., V. Meda, A. K. Dalai, D. W. McMartin, J. V. Headley and K. M. Peru (2010). "Photocatalysis of Naphthenic Acids in Water." Journal of Water Resource and Protection **2**: 644-650.

Mohamed, M. H., L. D. Wilson, J. V. Headley and K. M. Peru (2011). "Sequestration of naphthenic acids from aqueous solution using beta-cyclodextrin-based polyurethanes." Physical Chemistry Chemical Physics **13**(3): 1112-1122.

Moll, J. (1999). Feasibility study on desulphurization of bitumen emulsion using hydrogen from the water gas shift reaction. M.A.Sc, University of Waterloo.

Moll, J. K., Z. Li and F. T. T. Ng (2000). Activity of alternating hydrogen sources for the hydrodesulphurization of diesel and bitumen in the presence of water using dispersed Mo-based catalyst, American Chemical Society.

Moll, J. K., Z. Li and F. T. T. Ng (2000). "Activity of alternative hydrogen sources for the hydrodesulfurization of diesel and bitumen in the presence of water using dispersed Mo-based catalyst." Preprints, Division of Petroleum Chemistry, Inc. **45**(4): 599-602.

Monaghan, G., S. Porter, R. Holuk, R. Sugiyama and W. Brown (2012). Process for upgrading heavy oil and bitumen products, US20120000830.

Monaghan, G. V., W. A. Brown and R. J. Pinchuk (2012). Process for converting a liquid feed material into a vapor phase product, US20120211402.

Morel, F., S. Kressmann, V. Harle and S. Kasztelan (1997). "Processes and catalysts for hydrocracking of heavy oil and residues." Studies in Surface Science and Catalysis **106**(Hydrotreatment and Hydrocracking of Oil Fractions): 1-16.

Morimoto, M., Y. Sugimoto, S. Sato and T. Takanohashi (2014). "Solvent effect of water on supercritical water treatment of heavy oil." Journal of The Japan Petroleum Institute **57**(1): 11-17.

Moses, P. G., B. Hinnemann, H. Topsøe and J. K. Nørskov (2007). "The hydrogenation and direct desulfurization reaction pathway in thiophene hydrodesulfurization over MoS₂ catalysts at realistic conditions: A density functional study." Journal of Catalysis **248**(2): 188-203.

Mullins, O. C. (2011). "The asphaltenes." Annual Review of Analytical Chemistry **4**: 393-418.

Mullins, O. C., H. Sabbah, J. Eyssautier, A. E. Pomerantz, L. Barre, A. B. Andrews, Y. Ruiz-Morales, F. Mostowfi, R. McFarlane, L. Goual, R. Lepkowitz, T. Cooper, J. Orbulescu, R. M. Leblanc, J. Edwards and R. N. Zare (2012). "Advances in Asphaltene Science and the Yen-Mullins Model." Energy & Fuels **26**(7): 3986-4003.

Mullins, O. C., E. Y. Sheu, A. Hammami and A. G. Marshall (2007). Asphaltenes, Heavy Oils, and Petroleomics.

Murgich, J. (2002). "Intermolecular forces in aggregates of asphaltenes and resins." Pet. Sci. Technol. **20**(9 & 10): 983-997.

Nava, R., B. Pawelec, J. Morales, R. A. Ortega and J. L. G. Fierro (2009). "Comparison of the morphology and reactivity in HDS of CoMo/HMS, CoMo/P/HMS and CoMo/SBA-15 catalysts." Microporous and Mesoporous Materials **118**(1-3): 189-201.

Navarro, R. M., B. Pawelec, J. M. Trejo, R. Mariscal and J. L. G. Fierro (2000). "Hydrogenation of Aromatics on Sulfur-Resistant PtPd Bimetallic Catalysts." Journal of Catalysis **189**(1): 184-194.

NEXEN (2011). Long Lake 2010 - Surface performance presentation.

Ng, F. T. T. and S. K. Tsakiri (1988). Upgrading crude oil emulsions, US 5055175, CA 1317250.

Ng, F. T. T. and S. K. Tsakiri (1992). "Activation of water in emulsion for catalytic desulphurization of benzothiophene." Fuel **71**(11): 1309-1314.

Ngan, D. Y. (1989). Process for removal of polynuclear aromatics from a hydrocarbon in an endothermic reformer reaction system, US 4804457.

Osaheni, J. A., J. M. Bablin, D. A. Haitko and G. L. Soloveichik (2008). Methods and systems for removing metals from low grade fuel, US 20080308465.

Osaheni, J. A., T. J. Fyvie, D. A. Haitko, G. A. O'Neil and P. B. Glaser (2012). Methods for regeneration of adsorbent material, US 8187991.

Osaheni, J. A., T. J. Fyvie, G. A. O'Neil and H. Matis (2012). Methods and system for removing impurities from heavy fuel, US 8088277.

Ou, J. D. Y. and R. D. Strack (2009). Apparatus and process for cracking hydrocarbonaceous feed treated to adsorb paraffin-insoluble compounds. US 20090156876.

Palcheva, R., A. Spojakina, L. Dimitrov and K. Jiratova (2009). "12-Tungstophosphoric heteropolyacid supported on modified SBA-15 as catalyst in HDS of thiophene." Microporous and Mesoporous Materials **122**(1-3): 128-134.

Palcheva, R., A. Spojakina, K. Jiratova and L. Kaluza (2010). "Effect of Co on HDS Activity of Alumina-supported Heteropolymolybdate." Catalysis Letters **137**: 216-223.

Palcheva, R., A. Spojakina, G. Tyuliev, K. Jiratova and L. Petrov (2007). "The effect of nickel on the component state and HDS activity of alumina-supported heteropolytungstates." Kinetics and Catalysis **48**(6): 847-852.

Park, K.-C., D.-J. Yim and S.-K. Ihm (2002). "Characteristics of Al-MCM-41 supported Pt catalysts: effect of Al distribution in Al-MCM-41 on its catalytic activity in naphthalene hydrogenation." Catalysis Today **74**(3-4): 281-290.

Pashigreva, A. V., G. A. Bukhtiyarova, O. V. Klimov, Y. A. Chesalov, G. S. Litvak and A. S. Noskov (2010). "Activity and sulfidation behavior of the CoMo/Al₂O₃ hydrotreating catalyst: The effect of drying conditions." Catalysis Today **149**(1-2): 19-27.

Patwardhan, P. R., Y. Kida, A. Ates, H. Hernandez, M. Timko and W. H. Green (2012). "Supercritical water desulfurization of model sulfur compounds." Prepr. - Am. Chem. Soc., Div. Pet. Chem. **57**(1): 26-27.

Patwardhan, P. R., M. T. Timko, C. A. Class, R. E. Bonomi, Y. Kida, H. H. Hernandez, J. W. Tester and W. H. Green (2013). "Supercritical Water Desulfurization of Organic Sulfides Is Consistent with Free-Radical Kinetics." Energy & Fuels **27**(10): 6108-6117.

Pavel, S. K., M. A. Silverman and S. A. Kalota (2012). Method, system, and apparatus for lift gas distribution, US20120167989.

Pavel, S. K., M. A. Silverman and S. A. Kalota (2012). Reactor feed nozzles, US20120168537.

Peacock, M. J. (2010). "Athabasca oil sands: reservoir characterization and its impact on thermal and mining opportunities" Geological Society, Petroleum Geology Conference Series, London, vol. 7: 1141-1150.

Pecoraro, T. A. and R. R. Chianelli (1981). "Hydrodesulfurization catalysis by transition metal sulfides." Journal of Catalysis **67**(2): 430-445.

Peng, J., J. V. Headley and S. L. Barbour (2002). "Adsorption of single-ring model naphthenic acids on soils." Canadian Geotechnical Journal **39**(6): 1419-1426.

Pugsley, T., D. Pernitsky, J. Grundler and E. E. Johnsen (2013). Fouling of heat transfer surface in a stream assisted gravity drainage (SAGD) in situ Facility for the recovery of oil sands bitumen. International Conference on Heat Exchanger Fouling and Cleaning, Budapest, Hungary.

Quagraine, E. K., H. G. Peterson and J. V. Headley (2005). "In Situ Bioremediation of Naphthenic Acids Contaminated Tailing Pond Waters in the Athabasca Oil Sands Region— Demonstrated Field Studies and Plausible Options: A Review." Journal of Environmental Science and Health, Part A **40**(3): 685-722.

RAMP (2008). Regional Aquatics Monitoring Program 2008 Technical Report. Province of Alberta.

Rana, M. S., V. Samano, J. Ancheyta and J. A. I. Diaz (2007). "A review of recent advances on process technologies for upgrading of heavy oils and residua." Fuel **86**(9): 1216-1231.

Rana, M. S., V. Sámano, J. Ancheyta and J. A. I. Diaz (2007). "A review of recent advances on process technologies for upgrading of heavy oils and residua." Fuel **86**(9): 1216-1231.

Rankin, J. P., J. L. Vreeland, K. E. Litz, T. M. Jordan, M. N. Rossetti and E. H. Burnett (2011). Methods for upgrading of contaminated hydrocarbon streams, US 20110108464.

Reno, M. E. (1988). Pretreatment to produce polycyclic compounds, which are removed, US 4775460.

Rettger, P., R. Goldstein and J. Arnold (2004). Method of and apparatus for upgrading and gasifying heavy hydrocarbon feeds, US6702936.

Rettger, P., R. Goldstein, J. Arnold, Y. Bronicki and J. R. Friday (2008). Method of and apparatus for upgrading and gasifying heavy hydrocarbon feeds, US7407571.

Reynolds, B. (2002). Third generation LC Fining in petrobras international seminar of heavy crude oil processing, Cenpes, Brzail

Rinaldi, N., T. Kubota and Y. Okamoto (2009). "Effect of Citric Acid Addition on Co-Mo/B₂O₃/Al₂O₃ Catalysts Prepared by a Post-Treatment Method." Industrial & Engineering Chemistry Research **48**(23): 10414-10424.

Rinaldi, N., T. Kubota and Y. Okamoto (2010). "Effect of citric acid addition on the hydrodesulfurization activity of MoO₃/Al₂O₃ catalysts." Applied Catalysis A: General **374**(1-2): 228-236.

Rinaldi, N., Usman, K. Al-Dalama, T. Kubota and Y. Okamoto (2009). "Preparation of Co-Mo/B₂O₃/Al₂O₃ catalysts for hydrodesulfurization: Effect of citric acid addition." Applied Catalysis A: General **360**(2): 130-136.

Rogers, V. V., M. Wickstrom, K. Liber and M. D. MacKinnon (2002). "Acute and subchronic mammalian toxicity of naphthenic acids from oil sands tailings." Toxicological Sciences **66**:347-55.

Ruinart, d. B. M., C. Dupont, A. Daudin, C. Geantet and P. Raybaud (2012). "Deoxygenation mechanisms on Ni-promoted MoS₂ bulk catalysts: A combined experimental and theoretical study." Journal of Catalysis **286**: 153-164.

Sato, T., S. Mori, M. Watanabe, M. Sasaki and N. Itoh (2010). "Upgrading of bitumen with formic acid in supercritical water." The Journal of Supercritical Fluids **55**(1): 232-240.

Scott, A. C., M. D. MacKinnon and P. M. Fedorak (2005). "Naphthenic Acids in Athabasca Oil Sands Tailings Waters are Less Biodegradable Than Commercial Naphthenic Acids." Environmental Science and Technology **39**: 8388-8394.

Scott, A. C., W. Zubot, M. D. MacKinnon, D. W. Smith and P. M. Fedorak (2008). "Ozonation of oil sands process water removes naphthenic acids and toxicity." Chemosphere **71**(1): 156-160.

Selucky, M., T. Ruo, Y. Chu and O. Strausz (1977). "Chromatographic studies on oil sand bitumens." Analytical Chemistry of Liquid Fuel Sources, Amer. Chem. Society: 117-127.

Selucky, M. L., Y. Chu, T. Ruo and O. P. Strausz (1977). "Chemical composition of Athabasca bitumen." Fuel **56**(4): 369-381.

Selucky, M. L., Y. Chu, T. Ruo and O. P. Strausz (1978). "Chemical composition of Cold Lake bitumen." Fuel **57**(1): 9-16.

Semple, K. M., N. C., Phillip, M. Fedorak, and D. W. S. Westlake (1990). "Characterization of asphaltenes from Cold Lake heavy oil: variations in chemical structure and composition with molecular size." Canadian Journal of Chemistry **68**: 1092-1099.

Sherwood, D. E. J. (2000). Barriers to high conversion in an ebullated bed unit-relationship between sedimentation and operability. NCUT workgroup, Edmonton, Canada

Siewe, C. N. and F. T. T. Ng (1998). "Hydrodesulfurization of Cold Lake Diesel Fraction Using Dispersed Catalysts: Influence of Hydroprocessing Medium and Sources of H₂." Energy & Fuels **12**(3): 598-606.

Skrabalak, S. E. and K. S. Suslick (2005). "Porous MoS₂ Synthesized by Ultrasonic Spray Pyrolysis." Journal of the American Chemical Society **127**(28): 9990-9991.

Song, C. (2003). "An overview of new approaches to deep desulfurization for ultra-clean gasoline, diesel fuel and jet fuel." Catalysis Today **86**(1-4): 211-263.

Speight, J. G., Ed. (2007). The Chemistry and Technology of Petroleum CRC Press.

Stoyanov, S. R., L. M. da Costa, S. Gusarov, M. R. Gray, J. M. Stryker, R. R. Tykwinski, X. Tan, J. W. d. M. Carneiro, P. R. Seidl and A. Kovalenko (2013). "Spectroscopic characterization of the supramolecular aggregation interactions of petroleum asphaltenes in solution: a multiscale modeling investigation." Prepr. - Am. Chem. Soc., Div. Energy & Fuels **58**(1): 939-940.

Strausz, O. P., T. W. Mojelsky and E. M. Lown (1992). "The molecular structure of asphaltene: an unfolding study." Fuel **71**(12): 1355-1363.

Suzuki, T., M. Itoh, Y. Takegami and Y. Watanabe (1982). "Chemical structure of tar-sand bitumens by ¹³C and ¹H n.m.r. spectroscopic methods." Fuel **61**(5): 402-410.

Takemura, Y., A. Nakamura, H. Taguchi and K. Ouchi (1985). "Catalytic decarboxylation of benzoic acid." Industrial & Engineering Chemistry Product Research and Development **24**(2): 213-215.

Tang, Y. and A. Zhang (2006). Removal of organic acids from crude petroleum and fat-based oils over metal oxide catalysts, California Institute of Technology, USA . 29 pp.

Tomeczyk, N. A., R. E. Winans, J. H. Shinn and R. C. Robinson (2001). "On the Nature and Origin of Acidic Species in Petroleum. 1. Detailed Acid Type Distribution in a California Crude Oil." Energy & Fuels **15**(6): 1498-1504.

Topsøe, H. (2003). "Developments in operando studies and in situ characterization of heterogeneous catalysts." Journal of Catalysis **216**(1-2): 155-164.

Topsøe, H. (2007). "The role of Co-Mo-S type structures in hydrotreating catalysts." Applied Catalysis A: General **322**: 3-8.

Trimm, D. L. (2001). "The regeneration or disposal of deactivated heterogeneous catalysts." Applied Catalysis A: General **212**(1-2): 153-160.

Tsuen-Ni, L., L. Jing-Chie and H. Teh-Chung (1983). "Chemical reclaiming of nickel sulfate from nickel-bearing wastes." Conservation & Recycling **6**(1-2): 55-62.

Vernon, L. W. (1980). "Free radical chemistry of coal liquefaction: role of molecular hydrogen." Fuel **59**(2): 102-106.

Wang, J., J. Guan, H. Dai, L. Zhou, M. Tang, Y. Zhang, P. Ouyang, C. Li, C. Dai and J. Wang (2002). A catalytic activity promoter used in petroleum hydrogenation. Application: WO

WO, (Nanjing University of Chemical Technology, Peop. Rep. China; Yang Zi Petrochemical Corporation Ltd.). 13 pp.

Wang, N., P. Chelme-Ayala, L. Perez-Estrada, E. Garcia-Garcia, J. Pun, J. W. Martin, M. Belosevic and M. Gamal El-Din (2013). "Impact of ozonation on naphthenic acids speciation and toxicity of oil sands process-affected water to *Vibrio fischeri* and mammalian immune system." Environmental Science & Technology **47**(12): 6518-6526.

Wang, Y. Z., X. Y. Sun, Y. P. Liu and C. G. Liu (2007). "Removal of Naphthenic Acids from a Diesel Fuel by Esterification." Energy & Fuels **21**(2): 941-943.

Woodle, R. A. (1973). Adsorption-desorption process for removing an unwanted component from a reaction charge mixture. US 3767563.

Yang, L. and M. R. Gray (2008). Liquid-phase decarboxylation of naphthenate acids in oil, American Chemical Society.

Yao, K. C. (1989). Method for removing basic nitrogen compounds from extracted oils by use of acidic polar adsorbents and the regeneration of said adsorbents, EP 0278694.

Yoneyama, Y. and C. Song (1999). "A new method for preparing highly active unsupported Mo sulfide. Catalytic activity for hydrogenolysis of 4-(1-naphthylmethyl)biphenyl." Catalysis Today **50**(1): 19-27.

Yoosuk, B., C. Song, J. H. Kim, C. Ngamcharussrivichai and P. Prasassarakich (2010). "Effects of preparation conditions in hydrothermal synthesis of highly active unsupported NiMo sulfide catalysts for simultaneous hydrodesulfurization of dibenzothiophene and 4,6-dimethyldibenzothiophene." Catalysis Today **149**(1-2): 52-61.

Young, R.F., E. A. Orr, G. G. Goss and P. M. Fedorak (2007). "Detection of naphthenic acids in fish exposed to commercial naphthenic acids or oil sands process-affected water." Chemosphere **68**:518-27.

Yuan, M., S. Tong, S. Zhao and C. Q. Jia (2010). "Adsorption of polycyclic aromatic hydrocarbons from water using petroleum coke-derived porous carbon." Journal of Hazardous Materials **181**(1-3): 1115-1120.

Zeuthen, P., P. Blom and F. E. Massoth (1991). "Characterization of nitrogen on aged hydroprocessing catalysts by temperature-programmed oxidation." Applied Catalysis **78**(2): 265-276.

Zhang, A. (2005). Aromatics hydrogenation via water gas shift reaction over unsupported catalysts. Master of applied science, University of Waterloo.

Zhang, A., Q. Ma and Y. Tang (2003). Decarboxylation of naphthenic acid model compounds, American Chemical Society.

Zhang, A., Q. Ma and Y. Tang (2004). Catalytic decarboxylation for naphthenic acid removal from crude oil: A theoretical and experimental study, American Chemical Society.

Zhang, A., Q. Ma and Y. Tang (2004). "Catalytic decarboxylation for naphthenic acid removal from crude oils - a theoretical and experimental study." Prepr. - Am. Chem. Soc., Div. Pet. Chem. **49**: 218-221.

Zhang, A., Q. Ma, K. Wang, X. Liu, P. Shuler and Y. Tang (2006). "Naphthenic acid removal from crude oil through catalytic decarboxylation on magnesium oxide." Applied Catalysis A: General **303**: 103-109.

Zhang, Q., R. Tang, K. Yin, X. Luo and L. Zhang (2009). "Corrosion behavior of Hastelloy C-276 in supercritical water." Corrosion Science **51**(9): 2092-2097.

Zhang, S., D. Liu, W. Deng and G. Que (2007). "A Review of Slurry-Phase Hydrocracking Heavy Oil Technology." Energy & Fuels **21**(6): 3057-3062.

Zhao, Y., M. R. Gray and F. Wei (2008). "Rejuvenation of Residue Hydroconversion Catalysts by H-donor Solvents." Catalysis Letters **125**(Copyright (C) 2011 American Chemical Society (ACS). All Rights Reserved.): 69-75.

Zhou, T., H. Yin, Y. Liu, Y. Chai, J. Zhang and C. Liu (2010). "Synthesis, Characterization and HDS Activity of Carbon-Containing Ni-Mo Sulfide Nano-Spheres." Catalysis Letters **134**(3): 343-350.

Ziyadanoğulları, R. and I. Aydın (2004). "Recovery of Uranium, Nickel, Molybdenum, and Vanadium from Floated Asphaltite Ash." Separation Science and Technology **39**(13): 3113 - 3125.

Zou, L., B. Han, H. Yan, K. L. Kasperski, Y. Xu and L. G. Hepler (1997). "Enthalpy of Adsorption and Isotherms for Adsorption of Naphthenic Acid onto Clays." Journal of Colloid and Interface Science **190**(2): 472-475.

Zubot, W., M. D. MacKinnon, P. Chelme-Ayala, D. W. Smith and M. Gamal El-Din (2012). "Petroleum coke adsorption as a water management option for oil sands process-affected water." Sci Total Environ **427-428**: 364-372.

Appendix A. Characterization Details

A.1 GC-SimDis

A.1.1 6890 GC Method

GC Injector:	Back Injector:
Sample Washes	5
Sample Pumps	3
Injection Volume	0.20 microliters
Syringe Size	10.0 microliters
PreInj Solvent A Washes	5
PreInj Solvent B Washes	5
PostInj Solvent A Washes	4
PostInj Solvent B Washes	4
Viscosity Delay	0 seconds
Plunger Speed	Fast
PreInjection Dwell	0.00 minutes
PostInjection Dwell	0.00 minutes

OVEN

Initial temp: 40 °C (On)	Maximum temp: 350 °C
Initial time: 0.00 min	Equilibration time: 3.00 min

Ramps:

#	Rate	Final temp	Final time
---	------	------------	------------

1	20.00	350	4.00
---	-------	-----	------

2	0.0(Off)		
---	----------	--	--

Post temp: 50 °C

Post time: 0.00 min

Run time: 19.50 min

FRONT INLET (SPLIT/SPLITLESS)

BACK INLET (HT PTV)

Mode: Split

Mode: Split

Initial temp: 50 °C (Off)

Initial temp: 350 °C (On)

Pressure: 0.00 psi (Off)

Initial time: 0.00 min

Total flow: 45.0 mL/min

Ramps:

Gas saver: Off

#	Rate	Final temp	Final time
---	------	------------	------------

Gas type: Helium

1	0.0(Off)		
---	----------	--	--

Pressure: 1.66 psi (On)

Split ratio: 2.01:1

Split flow: 26.7 mL/min

Total flow: 42.8 mL/min

Gas saver: Off

Gas type: Helium

COLUMN 1

COLUMN 2

(not installed)

Capillary Column

Model Number: J&W 145-1001

DB-HT SimDis

Max temperature: 400 °C

Nominal length: 5.0 m

Nominal diameter: 530.00 um

Nominal film thickness: 0.15um

Mode: constant pressure

Pressure: 1.66 psi

Nominal initial flow: 13.3mL/min

Average velocity: 100 cm/sec

Inlet: Back Inlet

Outlet: Front Detector

Outlet pressure: ambient

FRONT DETECTOR (FID)

BACK DETECTOR (NO DET)

Temperature: 375 °C (On)

Hydrogen flow: 40.0 mL/min (On)

Air flow: 400.0 mL/min (On)

Mode: Constant makeup flow

Makeup flow: 2.0 mL/min (On)

Makeup Gas Type: Helium

Flame: On

Electrometer: On

Lit offset: 2.0

SIGNAL 1

Data rate: 5 Hz

Type: front detector

Save Data: On

Zero: 0.0 (Off)

Range: 0

Fast Peaks: Off

Attenuation: 0

SIGNAL 2

Data rate: 50 Hz

Type: front detector

Save Data: Off

Zero: 0.0 (Off)

Range: 0

Fast Peaks: Off

Attenuation: 0

COLUMN COMP 1

Derive from front detector

COLUMN COMP 2

Derive from front detector

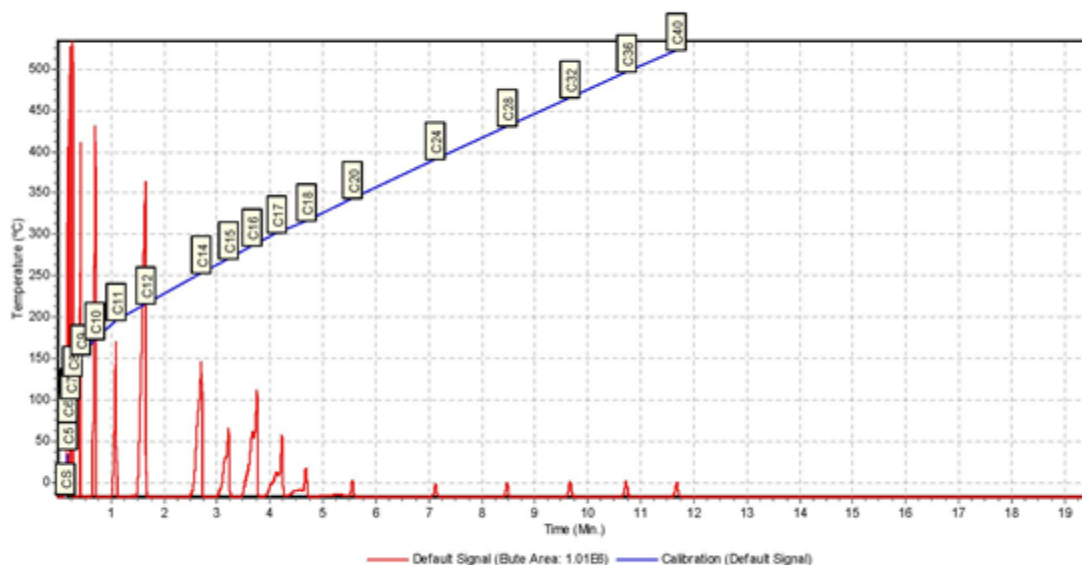
POST RUN

Post Time: 0.00 min

A.1.2 Calibration curve

Simulated Distillation Calibration Report
BP Calibration

4/14/2009 10:51:09 AM -- D2887_CAL.M
C:\HPCHEM\2\DATA\ 2009-04-14 10-16-20\202B0201.D (GC DATA FILE)



Agilent SimDis Report
4/14/2009 3:32:23 PM
Agilent Technologies

Figure A-1 Calibration curve of ASTM 2887 for GC-SimDis

A.1.3 Blank chromatograph and sample chromatograph

Blank chromatograph:

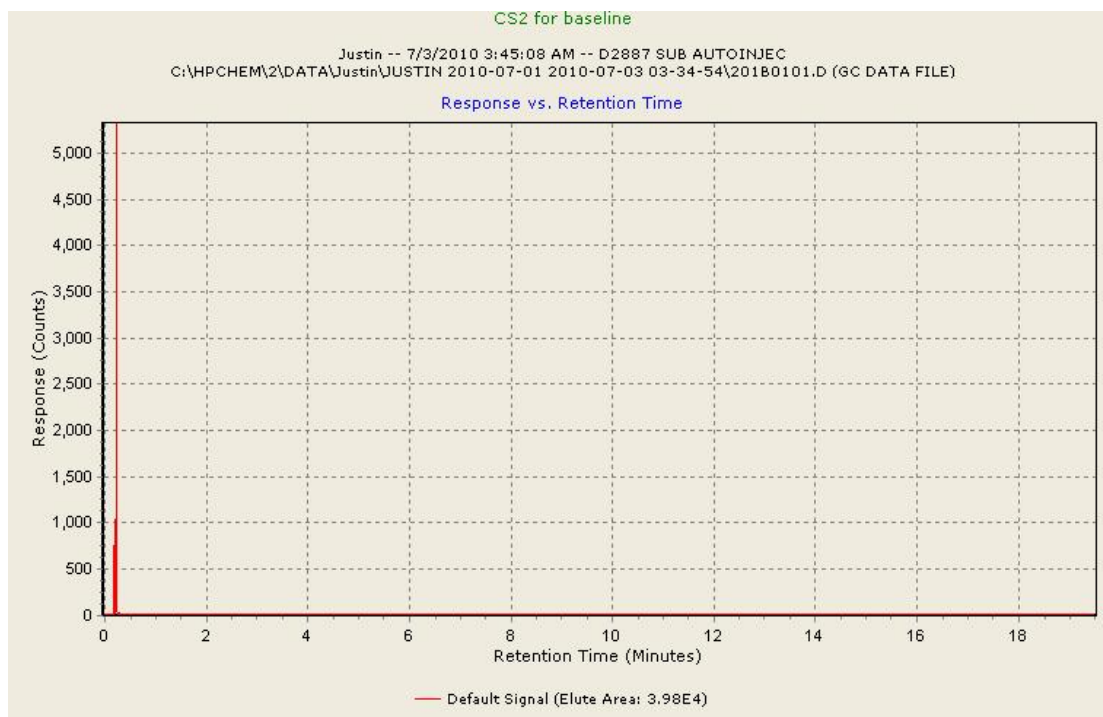


Figure A-2 Blank chromatograph from CS₂ for GC-SimDis analysis

Sample chromatograph after subtracting blank is shown below in Figure A-3. The green and purple lines represent start time and end time for integration.

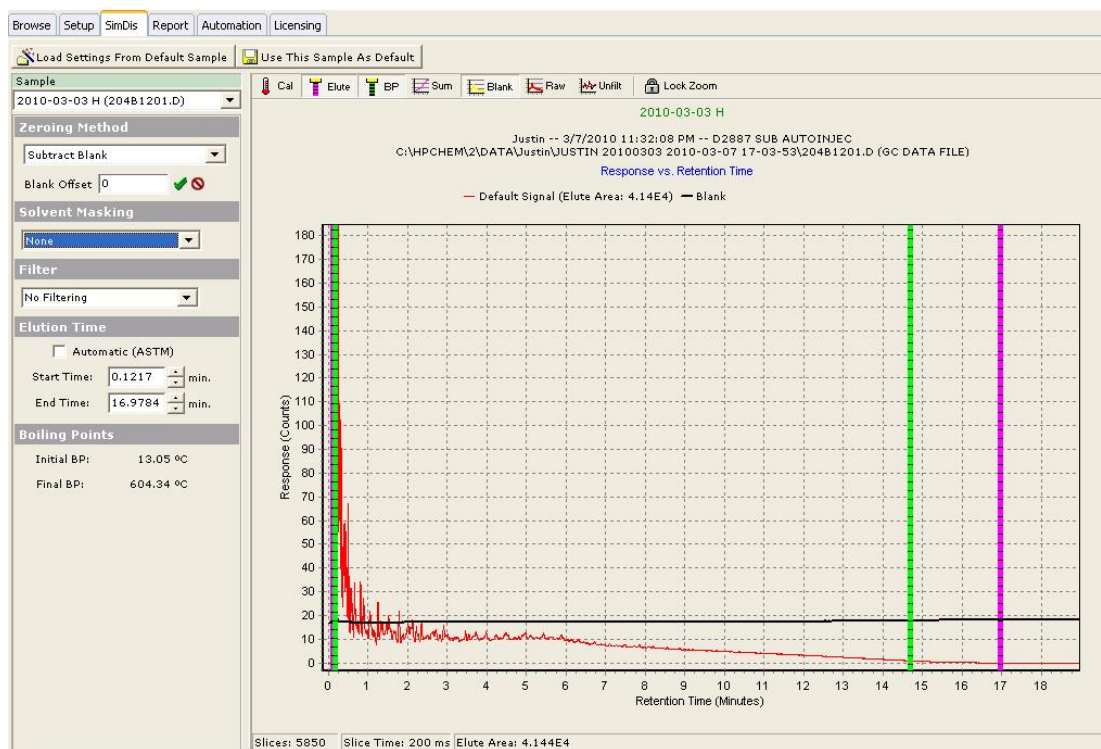


Figure A-3 Sample chromatograph after subtracting blank for GC-SimDis analysis

A.2 XRF calibration

Y was the S concentration (ppm) shown on XRF and x was the weight % of S in sample. Three points on X axis had been chosen: 0.5%, 2%, and 5%, and their concentration signal were taken and shown on Y axis. The calibration curve was shown below in Figure A-4.

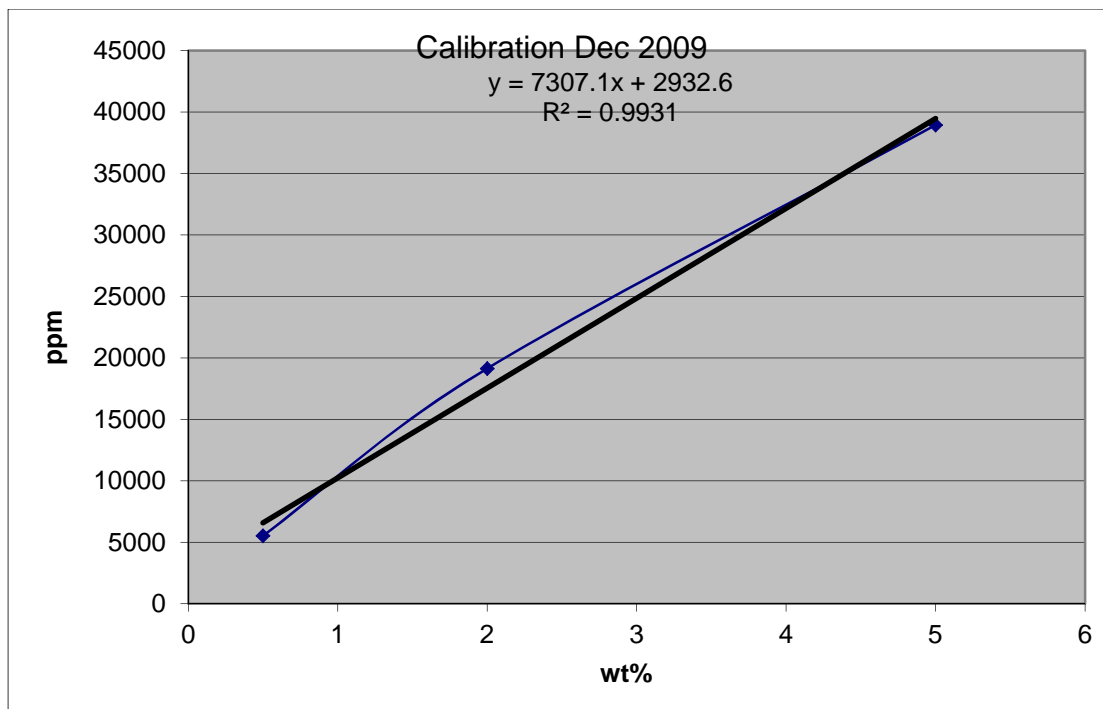


Figure A-4 XRF calibration curve for S amount analysis

A.3 GC-FID/TSD/PFPD

GC-FID method for naphthenic acid removal was shown in in the following tables. TSD and PFPD were not used in naphthenic acid removal study.

Varian CP-3800 Gas Chromatograph #1

Autosampler (8400)			
First injector used	Position 2		
Advance tray	NO		
Clean between injections	YES		
Use injection delay	NO		
Delay between injections	1.0 min		
Syringe volume	10 uL		
Injection mode	Std (Split/Splitless)		
Sample penetration depth	99 %		
Solvent penetration depth	90 %		
Default wash			
Vial	1		
Volume	5.0 uL		
Strokes	1		
Draw up speed	5.0 uL/s		
Clean mode			
Pre-injection solvent flushes	3		
Pre-injection sample flushes	3		
Post-injection solvent flushes	3		
Clean solvent source	1		
Injectors			
Front (1177 Split/Splitless)			
Split event table	Time (min)	Split state	Split ratio
	Initial	OFF	100
Type 1 EPC - Pressure program	Rate (Psi/min)	Step (Psi)	Time (min)
	Initial	0.1	0.00
	Total time		0.00
Coolable zone 1			

Heater	OFF		
Setpoint	250 °C		
Middle (1177 Split/Splitless)			
Split event table	Time (min)	Split state	Split ratio
	Initial	ON	10
Coolable zone 2			
Heater	ON		
Setpoint	250 °C		
Column oven			
Stabilization time	0.50 min		
Column oven zone			
Temperature program	Rate (°C/min)	Step (°C)	Time (min)
	Initial	80	0.00
	10.0	250	8.00
	Total time		25.00
Columns			
Front			
Carrier gas	He		
Length	15.00 m		
Inside diameter	250 µm		
Constant flow	DISABLED		
Middle			
Carrier gas	He		
Length	30.00 m		
Inside diameter	320 µm		
Constant flow	ENABLED		
Column flow	6.0 mL/min		
Pressure pulse	DISABLED		
Detectors			
Front (FID)			
Electronics	ON		
Time constant	Fast		
Type II EFC			

N2 makeup flow		28 mL/min		
H2 flow		30 mL/min		
Air flow		300 mL/min		
FID event table	Time (min)	Range	Autozero	
	Initial	12	YES	
Heat-only zone 1				
Heater		ON		
Setpoint		300 °C		
Middle (TSD)				
Time constant		Fast		
Type 12 EFC				
N2 makeup flow		28 mL/min		
H2 flow		4.5 mL/min		
Air flow		175 mL/min		
Bead current		2.400 A		
TSD event table	Time (min)	Range	Autozero	Bead power
	Initial	12	YES	ON
Heat-only zone 2				
Heater		OFF		
Setpoint		300 °C		
Rear (PFPD)				
Electronics		ON		
Type 15 EFC				
Air 1 flow		17.0 mL/min		
H2 flow		13.0 mL/min		
Air 2 flow		10.0 mL/min		
Square root mode		OFF		
Trigger level		200 mV		
Tube voltage		510 V		
Sampling delay		40 ms		
Sampling width		100 ms		
Use gain factor		YES		
Gain factor		2		

PFPD event table	Time (min)	Range	Autozero
	Initial	10	YES
Heat-only zone 3			
Heater		ON	
Setpoint		200 °C	
Output ports			
Front			
Output port program	Time (min)	Detector source	Attenuation
	Initial	Front	1
Middle			
Output port program	Time (min)	Detector source	Attenuation
	Initial	Front	1
Rear			
Output port program	Time (min)	Detector source	Attenuation
	Initial	Front	1
Miscellaneous			
Reset programs at the end of acquisition		YES	
Data rate		10 Hz	
Start automatically when ready		NO	
Wait for signal stability		NO	
Time window		0 sec	
Drift threshold		10.0 $\mu\text{V}/\text{sec}$	
Noise threshold		10.0 μV	

A.4 GC-MS

GC-MS method used in naphthenic acid removal study is shown below:

```
*****
MS Workstation - Method Listing   Fri Aug 08 11:00:47 2014
Method: justin
*****
*****
*****
3800 GC
*****
Module Address: 44

8410 Autosampler
-----
                Syringe Size: 10 uL
                Injection Mode: Std Split/Splitless
Solvent Penetration Depth: 90 %
Sample Penetration Depth: 90 %

                Default Clean Vial: III
                Default Clean Volume: 5.0 uL
                Default Clean Strokes: 1
                Default Clean Drawup Speed: 5.0 uL/sec

Clean Mode Pre-Inj Solvent Flushes: 3
Clean Mode Post-Inj Solvent Flushes: 3
Clean Mode Pre-Inj Sample Flushes: 3
Clean Mode Solvent Source: I & II

Use Prepahead: yes
Delay Time: 0.00 min

Front Valve Oven
-----
Oven Power: Off
Temperature: 50 C

Valve Table
-----
Valve 1: Sample Preconcentration Trap Valve
        Initial: SPT Trap

Valve 2: Sample Valve
        Initial: Off

Front Injector Type 1177
-----
Oven Power: On
Temperature: 250 C

Time      Split      Split
(min)     State      Ratio
-----
Initial   Off        Off
0.00     Off        Off
0.33     Off        Off

Middle Injector Type 1079
```

0.33 Off Off

Middle Injector Type 1079

Oven Power: Off
Coolant: Off
Enable Coolant at: 250 C
Coolant Timeout: 20.00 min

Temp (C)	Rate (C/min)	Hold (min)	Total (min)
60	0	20.00	20.00

Time (min)	Split State	Split Ratio
Initial	Off	Off

Rear Injector Type SPT

Oven Power: Off
Coolant: On

Enable Coolant at: 250 C
Coolant Timeout: 20.00 min

Temp (C)	Hold (min)	Total (min)
60	30.00	30.00

Front Injector EFC Type 1

Constant Column Flow: 0.7 ml/min
Pressure Pulse: none

Middle Injector EFC Type 1

Pressure (psi)	Rate (psi/min)	Hold (min)	Total (min)
0.1	0.00	0.00	0.00

Column Oven

Coolant: Off
Enable Coolant at: 40 C
Coolant Timeout: 20.00 min
Stabilization Time: 0.50 min

Temp (C)	Rate (C/min)	Hold (min)	Total (min)
35	0.0	5.00	5.00
250	10.0	3.50	30.00

Output Port A

Time (min)	Signal Source	Attenuation
---------------	------------------	-------------

Column Oven

Coolant: Off
Enable Coolant at: 40 C
Coolant Timeout: 20.00 min
Stabilization Time: 0.50 min

Temp (C)	Rate (C/min)	Hold (min)	Total (min)
35	0.0	5.00	5.00
250	10.0	3.50	30.00

Output Port A

Time (min)	Signal Source	Attenuation
Initial	Front	1

Output Port B

Time (min)	Signal Source	Attenuation
Initial	Front	1

Output Port C

Time (min)	Signal Source	Attenuation
Initial	Front	1

Data Acquisition

Detector Bunch Rate : 4 points (10.0 Hz)
Monitor Length : 64 bunched points (6.4 sec)
Front FID/TSD Scale: 1 Volts
Middle FID/TSD Scale: 1 Volts
Rear FID/TSD Scale: 1 Volts

A.5 RGA analysis

A.5.1 RGA analytic method:

A.5.1.1 Configuration of the RGA:

3000 GC Configuration	A	B	C	D
Injector Type	Backflush	Backflush	Backflush	Backflush
Carrier Gas	Argon	Helium	Helium	Helium
Column Type	Molecular Sieve	Plot U	Alumina	OV-1
Detector Type	TCD	TCD	TCD	TCD
Inlet Type	Heated	Heated	Heated	Heated

A.5.1.2 RGA set points:

3000 GC Configuration	A	B	C	D
Sample Inlet Temp., °C	100 [ON]	100 [ON]	100 [ON]	100 [ON]
Inlet Temp., °C	100 [ON]	100 [ON]	100 [ON]	100 [ON]
Column Temp., °C	110 [ON]	100 [ON]	140 [ON]	90 [ON]
Sampling Time, S	30 [ON]	30 [ON]	30 [ON]	30 [ON]
Inject Time, ms	20	20	20	20
Run Time, s	240	240	240	240
Post Run Time, s	10	10	10	10
Pressure Equilibration Time, s	10	10	10	10
Column Pressure, psi	40.00 [ON]	36.00 [ON]	40.00 [ON]	36.00 [ON]
Post Run Pressure, psi	40.00 [ON]	36.00 [ON]	40.00 [ON]	36.00 [ON]
Detector Filament	Enabled	Enabled	Enabled	Enabled
Detector Sensitivity	Standard	Standard	Standard	Standard
Detector Data Rate, Hz	50	50	50	50
Baseline Offset, mV	0	0	0	0
Backflush Time, s	11.0	6.5	8.0	N/A

A.5.1.3 Integrator settings and times events:

- Signal 1

Initial Setting		Value
Slope Sensitivity		2000,000
Peak Width		0.020
Area Reject		1.000
Height Reject		1.000
Shoulders		OFF
Advanced Baseline		OFF
Time	Event	Value
0.000	Integration	OFF
0.500	Integration	ON
1.350	Slope Sensitivity	1000,000

- Signal 2

Initial Setting		Value
Slope Sensitivity		10000,000
Peak Width		0.020
Area Reject		1.000
Height Reject		1.000
Shoulders		OFF
Advanced Baseline		OFF
Time	Event	Value
0.000	Integration	OFF
0.500	Baseline Now	
0.260	Integration	ON

- Signal 3

Initial Setting		Value
Slope Sensitivity		5000,000
Peak Width		0.040
Area Reject		1.000
Height Reject		1.000
Shoulders		OFF
Advanced Baseline		OFF
Time	Event	Value
0.000	Integration	OFF
0.480	Integration	ON
2.200	Slope Sensitivity	1000,000

- Signal 4

Initial Setting		Value
Slope Sensitivity		5000,000
Peak Width		0.040
Area Reject		1.000
Height Reject		1.000
Shoulders		OFF
Advanced Baseline		OFF
Time	Event	Value
0.000	Integration	OFF
0.420	Integration	ON
0.460	Integration	OFF
0.800	Integration	ON

A.5.2 Calibration Table:

Retention Time [min]	Sig	Lvl	Amount	Area	Amt/Area	Ref	Multiplier	Peak Name
0.000	2	1	1.00000	1.00000	1.00000e+000		1.00000	Peak32
0.347	2	1	2.99000	4.1296e+004	7.24041e-005		1.00000	CO2
0.409	2	1	2.00000	2.8415e+004	7.03854e-005		1.00000	C2H4
0.440	4	1	0.29900	1.2195e+004	2.45182e-005		1.00000	i-C4
0.449	2	1	3.99000	6.0647e+004	6.57906e-005		1.00000	C2H6
0.523	3	1	1.00000	1.0960e+004	9.12409e-005		1.00000	Propylene
0.548	2	1	1.00000	1.1746e+004	8.51354e-005		1.00000	C2H2
0.652	3	1	2.01000	1.9693e+004	1.02067e-004		1.00000	C3
0.665	1	1	12.10000	1.1501e+005	1.05208e-004		1.00000	Hydrogen
0.689	3	1	0.29900	3907.00000	7.65293e-005		1.00000	NC4
0.698	2	1	2.53000	3.2878e+004	7.69512e-005		1.00000	H2S
0.763	1	1	20.86000	1.9621e+004	1.06315e-003		1.00000	Oxygen
0.864	1	1	78.47200	6.2608e+004	1.25339e-003		1.00000	Nitrogen
0.872	2	1	5.02000	8.1948e+004	6.12584e-005		1.00000	COS
0.939	3	1	0.30000	3698.00000	8.11249e-005		1.00000	t-2 C4=
0.990	3	1	0.29900	3677.00000	8.13163e-005		1.00000	i-C4=
1.052	3	1	0.29900	3600.00000	8.30556e-005		1.00000	1-C4=
1.064	1	1	5.00000	9981.24000	5.00940e-004		1.00000	CH4
1.092	4	1	0.04990	2446.82000	2.03938e-005		1.00000	n-C6
1.126	3	1	0.29900	3603.00000	8.29864e-005		1.00000	c-2-C4=
1.218	2	1	0.96800	5.2089e+004	1.85836e-005		1.00000	1-2 prop=
1.289	1	1	1.02000	818.26000	1.24655e-003		1.00000	CO
1.399	3	1	0.10000	1326.91000	7.53631e-005		1.00000	i-C5
1.525	3	1	0.09980	1330.78900	7.49931e-005		1.00000	n-C5
1.684	3	1	0.30000	3000.50300	9.99832e-005		1.00000	1-3 butadiene
1.895	2	1	0.66800	1.2391e+004	5.39101e-005		1.00000	Water
2.064	2	1	0.98800	8573.95000	1.15233e-004		1.00000	MetyAcetylene
2.203	3	1	0.09970	1319.95000	7.55332e-005		1.00000	t-2-C5=
2.406	3	1	0.04850	623.18000	7.78266e-005		1.00000	2-meth-2-C4=
2.532	3	1	0.09990	1286.44000	7.76562e-005		1.00000	1-C5=
2.775	3	1	0.09500	1230.04000	7.72333e-005		1.00000	c-2-C5=
3.726	4	1	0.04990	2149.26200	2.32173e-005		1.00000	n-C8

A.5.3 RGA chromatograph example:

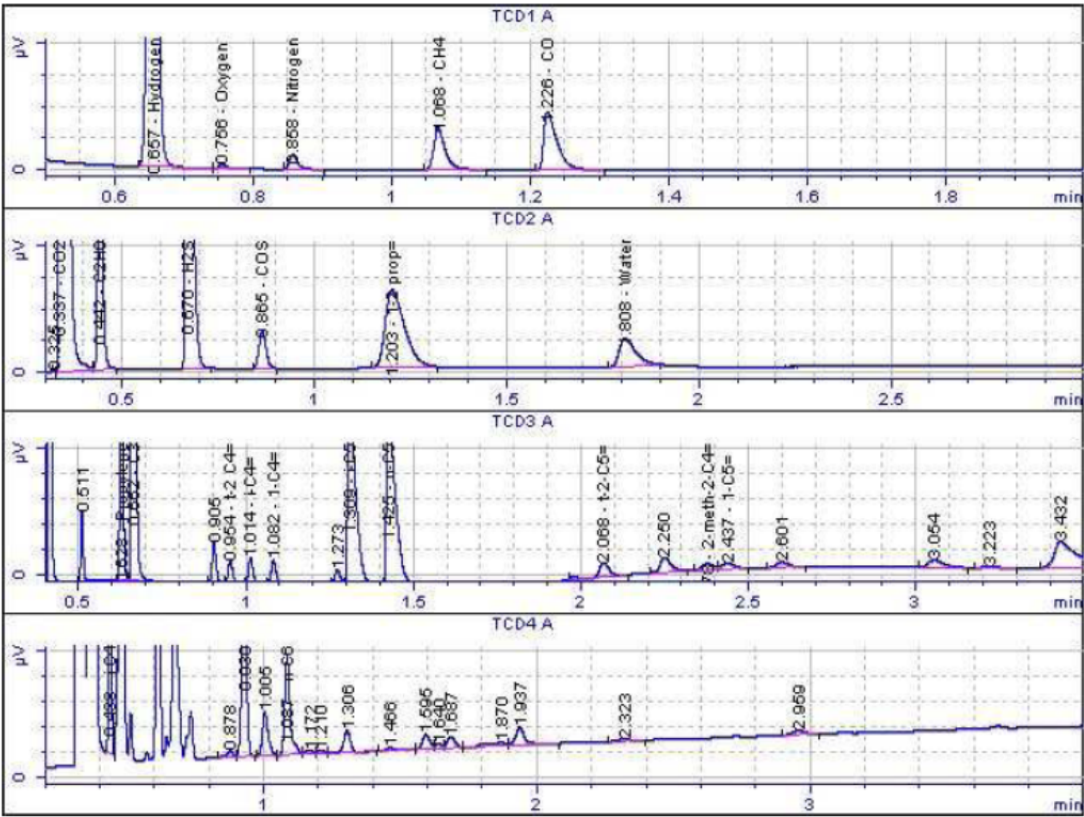


Figure A-5 RGA chromatograph for bitumen upgrading gas samples

A.6 IC

The working panel of this equipment was shown in Figure A-6.



Figure A-6 Dionex DX-500 ion exchanged chromatography equipment: (a) general structure; (b) core part: suppresser; (c) auto sampler; (d) sampler holder

IC calibration curves are shown in Figure A-7.

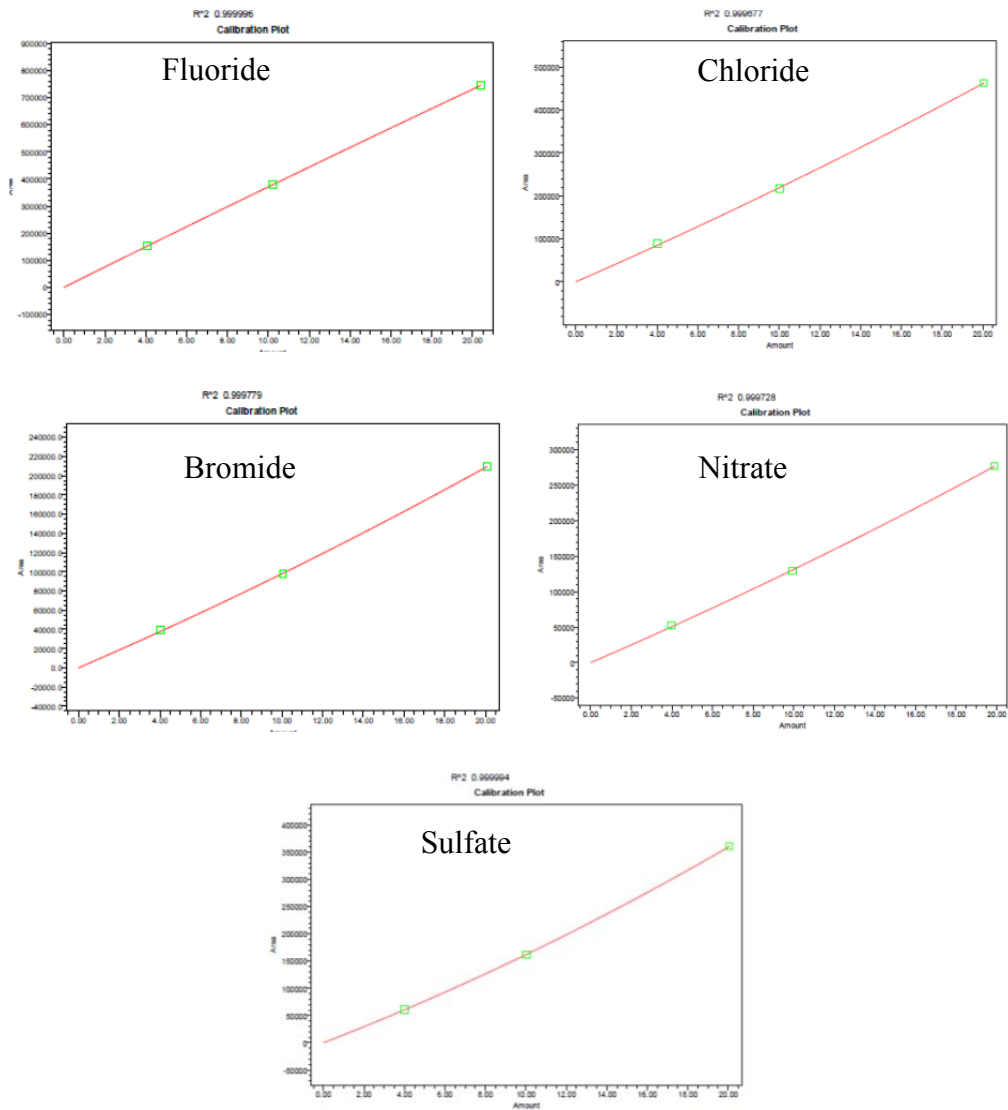


Figure A-7 Calibration curves for fluoride, chloride, bromide, nitrate and sulfate

Appendix B. Summary of Reaction Data

B.1 Upgrading of Cold Lake bitumen emulsion

B.1.1 Effect of temperature

(80g Cold Lake bitumen emulsion, 585psi CO, 15psi H₂S, 1408 ppmw Mo, 2 hours)

Table B-1 Cold Lake bitumen emulsion upgrading results at different reaction temperatures (product wt. yield%, asphaltene removal, S removal, WGSR conversion, max pressure, H₂ mole%)

	Feed	395°C	405°C	415°C
Naphtha	9%	11.17%	14.17%	12.21%
Kerosene	8%	13.64%	14.19%	16.37%
Distillate	12%	12.35%	12.00%	13.04%
Heavy Gas Oil	40%	35.56%	30.23%	28.85%
Pitch	30%	16.03%	13.72%	9.23%
HVOR		5.48%	4.80%	6.35%
Loss To Gas Phase		5.28%	10.65%	13.48%
Metal residue		0.33%	0.13%	0.23%
Coke		0.16%	0.10%	0.24%
Asphaltene removal %		63.8%	65.6%	66.0%
Total S removal %		43.91%	52.33%	48.36%
WGSR Conversion		80.37%	77.83%	88.12%
Max. Pressure /psi		3210	3491	3778
Yield of cracked gases		1.34%	1.73%	1.77%
H ₂ mole%		14.5%	17.4%	14.4%

B.1.2 Effect of reaction time

(405°C, 80g Cold Lake bitumen emulsion, 585psi CO, 15psi H₂S, 1408 ppmw Mo, 1-3 hours)

Table B-2 Cold Lake bitumen emulsion upgrading results at different reaction times (product wt. yield%, asphaltene removal, S removal, WGSR conversion, max pressure, H₂ mole%)

	Feed	1h	2h	3h
Naphtha	9%	8.69%	14.17%	20.24%
Kerosene	8%	10.10%	14.19%	21.61%
Distillate	12%	9.64%	12.00%	13.34%
Heavy Gas Oil	40%	29.28%	30.23%	20.62%
Pitch	30%	18.50%	13.72%	6.25%
HVOR		12.19%	4.80%	4.91%
Loss To Gas Phase		10.86%	10.65%	12.16%
Metal residue		0.55%	0.13%	0.24%
Coke		0.20%	0.10%	0.62%
Asphaltene removal %		48.7%	65.6%	77.9%
Total S removal %		41.89%	52.33%	51.97%
WGSR Conversion		76.13%	77.83%	73.94%
Max. Pressure /psi		3399	3491	3297
Yield of cracked gases		1.23%	1.73%	1.67%
H ₂ mole%		19.4%	17.4%	16.8%

B.1.3 Effect of reaction atmosphere

(405°C, 80g Cold Lake bitumen emulsion, 585psi feed gas, 15psi H₂S, 1408 ppmw Mo, 2 hours)

Table B-3 Cold Lake bitumen emulsion upgrading results at different reaction atmospheres (product wt. yield%, asphaltene removal, S removal, WGSR conversion, max pressure, H2 mole%)

	Feed	N2	H2	CO+H2	CO
Naphtha	9%	17.64%	11.31%	11.76%	14.17%
Kerosene	8%	17.39%	13.94%	13.47%	14.19%
Distillate	12%	12.17%	11.80%	11.35%	12.00%
Heavy Gas Oil	40%	28.58%	34.52%	32.88%	30.23%
Pitch	30%	5.84%	11.49%	14.10%	13.72%
HVOR		13.58%	6.90%	6.40%	4.80%
Loss To Gas Phase		3.45%	9.33%	9.72%	10.65%
Max. Pressure /psi		0.37%	0.13%	0.24%	0.13%
Coke		0.99%	0.57%	0.07%	0.10%
Asphaltene removal %		72.1%	64.0%	64.5%	65.6%
Total S removal %		23.31%	48.61%	64.46%	52.33%
WGSR Conversion		-	-	79.64%	77.83%
Max. Pressure /psi		3734	2937	3149	3491
Yield of cracked gases		3.24%	1.80%	1.04%	1.73%
H2 mole%		2.3%	75.2%	15.1%	17.4%

B.1.4 Effect of catalyst concentration

(405°C, 80g Cold Lake bitumen emulsion, 585psi CO, 15psi H₂S, 2 hours)

Table B-4 Cold Lake bitumen emulsion upgrading results at different catalyst concentrations (product wt. yield%, asphaltene removal, S removal, WGSR conversion, max pressure, H2 mole%)

	Feed	704 ppm Mo	1408 ppm Mo
Naphtha	9%	15.67%	14.17%
Kerosene	8%	12.75%	14.19%
Distillate	12%	10.48%	12.00%
Heavy Gas Oil	40%	28.12%	30.23%
Pitch	30%	16.97%	13.72%
HVOR		5.24%	4.80%
Loss To Gas Phase		10.41%	10.65%
Metal residue		0.18%	0.13%
Coke		0.18%	0.10%
Asphaltene removal %		53.1%	65.6%
Total S removal %		46.25%	52.33%
WGSR Conversion		83.32%	77.83%
Max. Pressure /psi		3602	3491
Yield of cracked gases		1.67%	1.73%
H2 mole%		18.2%	17.4%

B.1.5 Effect of Ni as a promoter

(405°C, 80g Cold Lake bitumen emulsion, 585psi CO, 15psi H₂S, 1408ppmw Mo, Ni:Mo=0.6, 2 hours)

Table B-5 Cold Lake bitumen emulsion upgrading results with and without Ni
(product wt. yield%, asphaltene removal, S removal, WGSR conversion, max pressure, H2
mole%)

wt.%	Feed	Mo	Ni-Mo
Naphtha	9%	14.17%	21.32%
Kerosene	8%	14.19%	17.51%
Distillate	12%	12.00%	14.32%
Heavy Gas Oil	40%	30.23%	32.65%
Pitch	30%	13.72%	7.99%
HVOR		4.80%	4.90%
Loss To Gas Phase		10.65%	0.84%
Metal residue		0.13%	0.35%
Coke		0.10%	0.11%
Asphaltene removal %		65.6%	60.4%
Total S removal %		52.33%	49.77%
WGSR Conversion		77.83%	78.51%
Max. Pressure /psi		3491	3052
Yield of cracked gases		1.73%	2.89%
H2 mole%		17.4%	11.6%

B.1.6 Asphaltenes composition (CHN and S contents)

Table B-6 Summary of CHN and S contents collected by CHN analyzer and XRF

Conditions	<i>Measured by CHN analyzer</i>			<i>Measured by XRF</i>
	N, Wt%	C, Wt%	H, Wt%	Sulfur, ppmw
Feed	0.906592	80.53671	7.576749	66212
415C	1.330172	78.04166	6.576892	44797
405C, 1400ppm MoS ₂ , 2h, CO (base case)	1.222298	90.23976	8.537944	47277
700 ppm MoS ₂	1.166616	79.02812	6.901203	48663
1h	1.013211	78.70975	7.592204	54184
395C	0.936984	78.90487	8.376335	51528
N ₂	2.000424	91.34105	6.658525	49032
Syngas	1.267837	78.5498	7.124147	42688
Ni-Mo	1.431201	78.52195	6.013236	46038
H ₂	1.188026	80.02533	6.97904	37218
3h	1.416909	81.16774	6.458681	43038

B.2 Upgrading of Athabasca bitumen

B.2.1 Significance of MoS₂ catalyst and *in situ* H₂

(415°C, 80g Athabasca bitumen, no OSPW, 585psi feed gas, 15psi H₂S, 0 or 1408ppmw Mo, 2 hours)

Table B-7 Athabasca bitumen upgrading results with and without MoS₂ catalyst and *in situ* H₂ (product wt. yield%, S removal, WGSR conversion, max pressure, H₂ mole%)

wt.%	Feed	Coking (N ₂)	No Catalyst 5mL H ₂ O	No Catalyst 10mL H ₂ O	MoS ₂ 5mL H ₂ O	MoS ₂ 10mL H ₂ O
Naphtha	0.70%	20.22%	15.57%	16.12%	15.80%	18.64%
Kerosene	3.58%	15.27%	16.26%	16.95%	17.08%	19.76%
Distillate	9.63%	9.40%	11.32%	12.71%	12.37%	13.76%
Heavy Gas Oil	31.64%	17.78%	24.30%	27.15%	28.80%	27.56%
Pitch	54.45%	3.88%	1.89%	2.19%	2.73%	7.19%
HVOR		14.69%	12.44%	8.84%	8.71%	6.05%
Loss To Gas Phase		12.58%	16.35%	14.37%	13.54%	6.36%
Metal residue		1.43%	0.39%	0.31%	0.37%	0.34%
Coke		4.75%	1.48%	1.35%	0.60%	0.33%
S Removal		27.59%	38.55%	34.80%	31.35%	29.76%
WGSR Conversion		100.00%	81.13%	71.47%	85.23%	74.88%
Max. Pressure /psi		2442	2246	2750	2349	2916
H ₂ mole%		5.8%	7.3%	9.9%	5.6%	7.6%

B.2.2 Effect of reaction time

(415°C, 80g Athabasca bitumen, 5mL OSPW, 585psi CO, 15psi H₂S, 1408ppmw Mo, 1-2 hours)

Table B-8 Athabasca bitumen upgrading results at different reaction time (product wt. yield%, S removal, WGS conversion, max pressure, H₂ mole%)

wt.%	Feed	1h	1.5h	2h
Naphtha	0.70%	13.17%	16.51%	15.80%
Kerosene	3.58%	14.46%	18.08%	17.08%
Distillate	9.63%	12.59%	13.66%	12.37%
Heavy Gas Oil	31.64%	33.39%	31.04%	28.80%
Pitch	54.45%	9.77%	7.96%	2.73%
HVOR		5.82%	5.11%	8.71%
Loss To Gas Phase		10.15%	6.96%	13.54%
Metal residue		0.50%	0.39%	0.37%
Coke		0.15%	0.28%	0.60%
S Removal		30.96%	25.58%	31.35%
WGS Conversion		71.47%	80.14%	85.23%
Max. Pressure /psi		2855	2325	2349
H ₂ mole%		11.7%	6.4%	5.6%

B.2.3 Effect of water and MoS₂ catalyst

(415°C, 80g Athabasca bitumen, 0 or 10mL OSPW, 585psi CO, 15psi H₂S, 0 or 1408ppmw Mo, 2 hours)

Table B-9 Athabasca bitumen upgrading results at different OSPW loadings with and without MoS₂ (product wt. yield%, S removal, WGSR conversion, max pressure, H₂ mole%)

wt.%	Feed	Coking (N ₂)	No MoS ₂ No H ₂ O	No MoS ₂ 5mL H ₂ O	No MoS ₂ 10mL H ₂ O	MoS ₂ No H ₂ O	MoS ₂ 5mL H ₂ O	MoS ₂ 10 mL H ₂ O
Naphtha	0.70%	20.22%	15.87%	15.57%	16.12%	16.53%	15.80%	18.64%
Kerosene	3.58%	15.27%	14.90%	16.26%	16.95%	14.80%	17.08%	19.76%
Distillate	9.63%	9.40%	10.23%	11.32%	12.71%	10.30%	12.37%	13.76%
Heavy Gas Oil	31.64%	17.78%	19.68%	24.30%	27.15%	23.50%	28.80%	27.56%
Pitch	54.45%	3.88%	2.07%	1.89%	2.19%	8.26%	2.73%	7.19%
HVOR		14.69%	15.78%	12.44%	8.84%	11.88%	8.71%	6.05%
Loss To Gas Phase		12.58%	18.64%	16.35%	14.37%	13.86%	13.54%	6.36%
Metal residue		1.43%	0.48%	0.39%	0.31%	0.36%	0.37%	0.34%
Coke		4.75%	2.34%	1.48%	1.35%	0.51%	0.60%	0.33%
S Removal		27.59%	36.25%	38.55%	34.80%	38.10%	31.35%	29.76%
WGSR Conversion		100.00%	65.88%	81.13%	71.47%	81.62%	85.23%	74.88%
Max. Pressure /psi		2442	1775	2246	2750	1866	2349	2916
H ₂ mole%		-	4.8%	7.3%	9.9%	5.5%	5.6%	7.6%

B.2.4 Effect of Ni

(415°C, 80g Athabasca bitumen, 5 or 10 mL OSPW, 585psi CO, 15psi H₂S, 1408ppmw Mo, Ni:Mo=0.6, 2 hours)

Table B-10 Athabasca bitumen upgrading results with and without Ni as promoter (product wt. yield%, S removal, WGSR conversion, max pressure, H₂ mole%)

wt.%	Feed	MoS ₂ 5mL H ₂ O	Ni/MoS ₂ 5mL H ₂ O	MoS ₂ 10mL H ₂ O	Ni/MoS ₂ 10mL H ₂ O
Naphtha	0.70%	15.80%	20.95%	18.64%	18.82%
Kerosene	3.58%	17.08%	16.93%	19.76%	20.39%
Distillate	9.63%	12.37%	12.00%	13.76%	14.98%
Heavy Gas Oil	31.64%	28.80%	23.72%	27.56%	29.41%
Pitch	54.45%	2.73%	8.46%	7.19%	5.09%
HVOR		8.71%	5.55%	6.05%	5.92%
Loss To Gas Phase		13.54%	10.46%	6.36%	4.62%
Metal residue		0.37%	0.56%	0.34%	0.37%
Coke		0.60%	1.37%	0.33%	0.40%
S Removal		31.35%	29.16%	29.76%	39.84%
WGSR Conversion		85.23%	86.42%	74.88%	75.68%
Max. Pressure		2349	2513	2916	2862
H ₂ mole%		5.6%	5.4%	7.6%	6.8%

B.2.5 Effect of reaction atmosphere by using Ni/MoS₂ catalyst

(415°C, 80g Athabasca bitumen, 5mL OSPW, 585psi feed gas, 15psi H₂S, 1408ppmw Mo, Ni:Mo=0.6, 2 hours)

Table B-11 Athabasca bitumen upgrading results under different reaction atmospheres by using Ni/MoS₂ catalyst (product wt. yield%, S removal, WGS conversion, max pressure, H₂ mole%)

wt.%	Feed	H ₂	Syngas	CO
Naphtha	0.70%	14.05%	17.33%	20.95%
Kerosene	3.58%	14.06%	16.47%	16.93%
Distillate	9.63%	9.55%	12.07%	12.00%
Heavy Gas Oil	31.64%	23.36%	25.28%	23.72%
Pitch	54.45%	3.60%	8.73%	8.46%
HVOR		29.73%	9.41%	5.55%
Loss To Gas Phase		3.35%	9.05%	10.46%
Metal residue		0.59%	0.51%	0.56%
Coke		1.70%	1.15%	1.37%
S Removal		29.05%	30.15%	29.16%
WGS Conversion		-	86.03%	86.42%
Max. Pressure /psi		2436	2513	2513
H ₂ mole%		26.2%	3.2%	5.4%

B.2.6 Effect of V

(415°C, 80g Athabasca bitumen, 10mL OSPW, 585psi CO, 15psi H₂S, 1408ppmw Mo, Ni:Mo=0.6, V:Mo=0.6, 2 hours)

Table B-12 Athabasca bitumen upgrading results with and without V for Ni/MoS₂ catalyst (product wt. yield%, S removal, WGSR conversion, max pressure, H₂ mole%)

wt.%	Feed	Ni/MoS ₂	V+Ni/MoS ₂
Naphtha	0.70%	18.82%	15.85%
Kerosene	3.58%	20.39%	15.56%
Distillate	9.63%	14.98%	10.73%
Heavy Gas Oil	31.64%	29.41%	18.53%
Pitch	54.45%	5.09%	5.42%
HVOR		5.92%	13.19%
Loss To Gas Phase		4.62%	19.06%
Metal residue		0.37%	0.55%
Coke		0.40%	1.11%
S Removal		39.84%	39.98%
WGSR Conversion		75.68%	74.15%
Max. Pressure		2862	2781
H ₂ mole%		6.8%	9.0%

B.2.7 Deactivation investigation by using “soft solids” instead of fresh catalysts

(415°C, 80g Athabasca bitumen, 5mL OSPW, 585psi CO, 15psi H₂S, 1408ppmw Mo, 2 hours)

Table B-13 Athabasca bitumen upgrading results by using fresh catalyst and “soft solid” (product wt. yield%, S removal, WGS conversion, max pressure, H₂ mole%)

wt.%	Feed	1st Run	2nd Run using "soft solids"
Naphtha	0.70%	15.80%	11.33%
Kerosene	3.58%	17.08%	11.41%
Distillate	9.63%	12.37%	8.69%
Heavy Gas Oil	31.64%	28.80%	19.37%
Pitch	54.45%	2.73%	4.31%
HVOR		8.71%	26.12%
Loss To Gas Phase		13.54%	12.33%
Metal residue		0.37%	1.61%
Coke		0.60%	4.82%
S Removal		31.35%	30.20%
WGS Conversion		85.23%	84.11%
Max. Pressure /psi		2349	2103
H ₂ mole%		5.6%	5.0%

B.3 Naphthenic acid removal

B.3.1 Simultaneous WGSR and 2-NA removal

(340°C, 80ml toluene, 10ml water, 15psi H₂S, 585psi CO, ~1641ppmw 2-NA in toluene, 673ppmw Mo, 2hours)

WGSR only

Table B-14 Gas analysis results obtained by RGA for “WGSR only” in the “simultaneous WGSR and 2-NA removal” discussion (system pressure, WGSR conversion, product partial pressures)

	Partial Pressure /psi					
Time /min	0	10	30	45	75	120
Pressure /psi	2421	2329	2245	2156	2055	2055
WGSR Conversion	27.46%	36.22%	45.13%	54.39%	58.18%	58.18%
P(H ₂)	503.78	626.33	768.44	801.08	837.61	763.27
P(CO)	1322.02	1093.30	812.09	622.39	519.45	373.14
P(CO ₂)	500.47	620.79	667.94	742.20	722.66	828.52
P(Water)	34.69	34.29	41.07	40.55	41.53	51.62
P(CH ₄)	0.00	0.11	0.74	1.05	1.47	1.71
P(C ₂ H ₄)	0.00	0.00	0.00	0.00	0.00	0.00
P(C ₂ H ₆)	0.00	0.00	0.00	0.13	0.19	1.01
P(H ₂ S)	35.82	39.34	34.96	35.09	31.20	34.06
P(COS)	8.36	6.04	3.55	2.51	1.90	1.67

NA+WGSR

Table B-15 Gas analysis results obtained by RGA for “NA+WGSR” in the “simultaneous WGSR and 2-NA removal” discussion (system pressure, WGSR conversion, product partial pressures)

	Partial Pressure /psi					
Time /min	0	10	30	45	75	120
Pressure /psi	2400	2287	2209	2129	2039	2039
WGSR Conversion	27.46%	34.70%	45.66%	58.15%	64.24%	64.24%
P(H2)	448.07	538.10	647.09	664.38	704.04	734.75
P(CO)	1404.25	1125.71	817.20	582.73	464.39	368.81
P(CO2)	392.96	598.21	686.57	809.80	834.16	815.66
P(Water)	52.37	32.80	31.10	40.88	35.43	40.61
P(CH4)	0.00	0.65	1.67	2.37	3.33	4.27
P(C2H4)	2.70	1.86	0.00	0.00	0.00	0.00
P(C2H6)	4.05	5.86	6.28	7.23	6.64	5.99
P(H2S)	66.97	73.44	79.17	87.05	70.78	60.32
P(COS)	16.79	12.32	8.98	6.69	4.09	2.92

B.3.2 Effect of reaction temperature under CO

(80ml toluene, 10ml water, 15psi H₂S, 585psi CO, ~1641ppmw 2-NA in toluene, 673ppmw Mo, 2hours)

300°C

Table B-16 Oil analysis results obtained by GC-FID for “300°C” in the “Effect of reaction temperature under CO” discussion (product mole %)

Time /min	Mole %				
	0	10	30	60	120
Decalin					
Benzoic acid	0.00%	0.00%	0.00%	0.00%	0.00%
Tetralin	0.00%	0.04%	0.15%	0.28%	0.49%
Naphthalene	0.00%	1.30%	2.74%	3.69%	3.98%
1,2,3,4-tetrahydro-2-methyl-Naphthalene	0.00%	0.00%	0.34%	1.18%	4.16%
1,2,3,4-tetrahydro-6-methyl-Naphthalene	0.00%	0.29%	1.04%	2.63%	7.26%
2-Methyl-Naphthalene	7.38%	41.96%	71.43%	86.80%	83.33%
DCH					
CHB					
BP					
2-Naphthoic acid	92.62%	56.41%	24.29%	5.42%	0.78%
TH-DBT					
DBT					

Table B-17 Gas analysis results obtained by RGA for “300°C” in the “Effect of reaction temperature under CO” discussion (system pressure, WGSR conversion, product partial pressures)

	Partial Pressure /psi				
Time /min	0	10	30	60	120
Pressure /psi	1898	2066	1936	1908	1736
WGSR Conversion	8.46%	11.21%	23.00%	32.89%	41.74%
P(H ₂)	181.94	296.85	392.18	498.91	554.75
P(CO)	1523.45	1533.98	1147.02	906.75	656.29
P(CO ₂)	140.88	193.63	342.63	444.38	470.24
P(Water)	23.70	14.90	15.13	14.93	15.06
P(CH ₄)	0.00	0.00	0.00	0.00	0.00
P(C ₂ H ₄)	1.68	2.38	4.22	3.31	1.70
P(C ₂ H ₆)	2.13	4.15	10.52	16.32	17.40
P(H ₂ S)	16.47	14.69	19.28	19.95	18.25
P(COS)	6.77	4.88	4.62	3.14	2.30

340°C

Table B-18 Oil analysis results obtained by GC-FID for “340°C” in the “Effect of reaction temperature under CO” discussion (product mole %)

Time /min	Mole %					
	0	10	30	45	75	120
Decalin						
Benzoic acid	0.00%	0.00%	0.00%	0.35%	0.34%	0.57%
Tetralin	0.16%	0.30%	0.53%	0.73%	1.10%	1.65%
Naphthalene	1.54%	2.76%	2.95%	2.87%	2.56%	2.05%
1,2,3,4-tetrahydro-2-methyl-Naphthalene	0.36%	1.85%	6.38%	10.30%	16.57%	22.66%
1,2,3,4-tetrahydro-6-methyl-Naphthalene	1.18%	4.70%	12.53%	19.01%	29.41%	40.07%
2-Methyl-Naphthalene	58.59%	83.47%	74.41%	63.67%	48.42%	33.00%
DCH						
CHB						
BP						
2-Naphthoic acid	38.17%	6.92%	3.21%	3.08%	1.59%	0.00%
TH-DBT						
DBT						

Table B-19 Gas analysis results obtained by RGA for “340°C” in the “Effect of reaction temperature under CO” discussion (system pressure, WGSR conversion, product partial pressures)

	Partial Pressure /psi					
Time /min	0	10	30	45	75	120
Pressure /psi	2400	2287	2209	2129	2039	2039
WGSR Conversion	21.86%	34.70%	45.66%	58.15%	64.24%	64.24%
P(H ₂)	448.07	538.10	647.09	664.38	704.04	734.75
P(CO)	1404.25	1125.71	817.20	582.73	464.39	368.81
P(CO ₂)	392.96	598.21	686.57	809.80	834.16	815.66
P(Water)	52.37	32.80	31.10	40.88	35.43	40.61
P(CH ₄)	0.00	0.65	1.67	2.37	3.33	4.27
P(C ₂ H ₄)	2.70	1.86	0.00	0.00	0.00	0.00
P(C ₂ H ₆)	4.05	5.86	6.28	7.23	6.64	5.99
P(H ₂ S)	66.97	73.44	79.17	87.05	70.78	60.32
P(COS)	16.79	12.32	8.98	6.69	4.09	2.92

415°C

Table B-20 Oil analysis results obtained by GC-FID for “415°C” in the “Effect of reaction temperature under CO” discussion (product mole %)

Time /min	Mole%					
	0	10	30	45	75	120
Decalin						
Benzoic acid	0.52%	0.36%	0.63%	0.84%	1.36%	1.97%
Tetralin	1.41%	1.76%	2.25%	2.38%	2.60%	2.71%
Naphthalene	8.26%	8.90%	8.59%	8.34%	8.55%	9.15%
1,2,3,4-tetrahydro-2-methyl-Naphthalene	4.55%	5.46%	6.72%	6.85%	7.18%	7.00%
1,2,3,4-tetrahydro-6-methyl-Naphthalene	11.01%	12.15%	14.46%	14.49%	15.07%	14.56%
2-Methyl-Naphthalene	66.01%	66.01%	65.38%	65.02%	65.23%	64.52%
DCH						
CHB						
BP						
2-Naphthoic acid	8.24%	5.36%	1.97%	2.08%	0.01%	0.09%
TH-DBT						
DBT						

Table B-21 Gas analysis results obtained by RGA for “415°C” in the “Effect of reaction temperature under CO” discussion (system pressure, WGSR conversion, product partial pressures)

	Partial Pressure /psi					
Time /min	0	10	30	45	75	120
Pressure /psi	3026	2849	2698	2540	2390	2390
WGSR Conversion	51.31%	58.03%	66.88%	71.60%	77.89%	77.89%
P(H ₂)	931.85	953.59	911.41	895.28	818.41	806.07
P(CO)	1004.52	815.43	605.17	478.68	340.46	268.39
P(CO ₂)	1058.74	1127.51	1222.17	1206.68	1199.65	1185.77
P(Water)	51.86	62.14	35.56	46.55	116.11	64.59
P(CH ₄)	3.31	4.95	7.15	8.48	9.00	11.05
P(C ₂ H ₄)	0.00	0.00	0.00	0.00	0.00	0.00
P(C ₂ H ₆)	10.51	10.15	10.27	10.46	8.56	8.98
P(H ₂ S)	47.76	49.00	54.70	49.95	46.29	43.94
P(COS)	4.45	3.23	2.58	1.93	1.52	1.20

B.3.3 Effect of gas feed

(300°C, 80ml toluene, 10ml water, 15psi H₂S, 585psi gas feed, ~1641ppmw 2-NA in toluene, 673ppmw Mo, 2hours)

CO

Table B-22 Oil analysis results obtained by GC-FID for “CO” in the “Effect of gas feed” discussion (product mole %)

Time /min	Mole %				
	0	10	30	60	120
Decalin					
Benzoic acid	0.00%	0.00%	0.00%	0.00%	0.00%
Tetralin	0.00%	0.04%	0.15%	0.28%	0.49%
Naphthalene	0.00%	1.30%	2.74%	3.69%	3.98%
1,2,3,4-tetrahydro-2-methyl-Naphthalene	0.00%	0.00%	0.34%	1.18%	4.16%
1,2,3,4-tetrahydro-6-methyl-Naphthalene	0.00%	0.29%	1.04%	2.63%	7.26%
2-Methyl-Naphthalene	7.38%	41.96%	71.43%	86.80%	83.33%
DCH					
CHB					
BP					
2-Naphthoic acid	92.62%	56.41%	24.29%	5.42%	0.78%
TH-DBT					
DBT					

Table B-23 Gas analysis results obtained by RGA for “CO” in the “Effect of gas feed” discussion (system pressure, WGSR conversion, product partial pressures)

	Partial Pressure /psi				
Time /min	0	10	30	60	120
Pressure /psi	1898	2066	1936	1908	1736
WGSR Conversion	8.46%	11.21%	23.00%	32.89%	41.74%
P(H ₂)	181.94	296.85	392.18	498.91	554.75
P(CO)	1523.45	1533.98	1147.02	906.75	656.29
P(CO ₂)	140.88	193.63	342.63	444.38	470.24
P(Water)	23.70	14.90	15.13	14.93	15.06
P(CH ₄)	0.00	0.00	0.00	0.00	0.00
P(C ₂ H ₄)	1.68	2.38	4.22	3.31	1.70
P(C ₂ H ₆)	2.13	4.15	10.52	16.32	17.40
P(H ₂ S)	16.47	14.69	19.28	19.95	18.25
P(COS)	6.77	4.88	4.62	3.14	2.30

H2

Table B-24 Oil analysis results obtained by GC-FID for “H2” in the “Effect of gas feed” discussion (product mole %)

Time /min	Mole %					
	0	10	30	45	75	120
Decalin						
Benzoic acid	0.00%	0.00%	0.00%	0.00%	0.00%	0.00%
Tetralin	0.00%	0.07%	0.09%	0.14%	0.14%	0.20%
Naphthalene	0.21%	0.88%	1.09%	1.30%	1.30%	1.43%
1,2,3,4-tetrahydro-2-methyl-Naphthalene	0.13%	0.24%	1.05%	3.36%	3.36%	6.66%
1,2,3,4-tetrahydro-6-methyl-Naphthalene	0.26%	0.63%	1.73%	4.47%	4.47%	8.36%
2-Methyl-Naphthalene	11.31%	40.82%	66.79%	78.25%	78.25%	83.35%
DCH						
CHB						
BP						
2-Naphthoic acid	88.08%	57.37%	29.26%	12.47%	12.47%	0.00%
TH-DBT						
DBT						

Table B-25 Gas analysis results obtained by RGA for “H2” in the “Effect of gas feed” discussion (system pressure, WGSR conversion, product partial pressures)

	Partial Pressure /psi					
Time /min	0	10	30	45	75	120
Pressure /psi	1794	1770	1739	1690	1633	1633
WGSR Conversion	0.00%	0.00%	0.00%	0.00%	0.00%	0.00%
P(H2)	1428.74	1649.20	1671.73	1584.55	1532.75	1477.59
P(CO)	80.54	26.80	9.63	3.86	1.91	1.06
P(CO2)	75.51	25.57	10.47	6.89	5.20	4.62
P(Water)	81.88	43.00	31.08	94.99	100.27	104.46
P(CH4)	0.00	0.00	0.00	0.00	0.00	0.00
P(C2H4)	0.00	1.28	1.26	1.36	1.51	1.36
P(C2H6)	0.73	2.12	2.90	4.29	5.70	6.41
P(H2S)	32.04	45.82	42.94	43.06	42.66	37.50
P(COS)	0.83	0.32	0.00	0.00	0.00	0.00

N2

Table B-26 Oil analysis results obtained by GC-FID for “N2” in the “Effect of gas feed” discussion (product mole %)

Time	Mole %				
	0min	10min	30min	60min	120min
Decalin					
Benzoic acid	16.67%	20.46%	21.91%	21.69%	20.31%
Tetralin	0.00%	0.00%	0.00%	0.00%	0.00%
Naphthalene	0.00%	0.30%	0.84%	1.58%	2.53%
1,2,3,4-tetrahydro-2-methyl-Naphthalene	0.00%	0.00%	0.00%	0.00%	0.00%
1,2,3,4-tetrahydro-6-methyl-Naphthalene	0.00%	0.00%	0.00%	0.00%	0.00%
2-Methyl-Naphthalene	0.52%	3.88%	14.57%	32.59%	57.14%
DCH					
CHB					
BP					
2-Naphthoic acid	82.81%	75.37%	62.67%	44.14%	20.02%
TH-DBT					
DBT					

Table B-27 Gas analysis results obtained by RGA for “N2” in the “Effect of gas feed” discussion (system pressure, WGSR conversion, product partial pressures)

	Partial Pressure /psi				
Time /min	0	10	30	60	120
Pressure /psi	1783	1904	1926	1849	1698
WGSR Conversion	100.00%	100.00%	100.00%	100.00%	100.00%
P(H2)	2.91	3.24	5.59	7.29	7.76
P(CO)	0.00	0.00	0.00	0.00	0.00
P(CO2)	2.03	1.21	1.16	1.06	1.14
P(Water)	25.58	18.43	10.35	18.80	13.07
P(CH4)	0.00	0.00	0.00	0.00	0.00
P(C2H4)	0.00	0.00	0.54	0.44	0.40
P(C2H6)	0.00	0.00	0.29	0.34	0.54
P(H2S)	37.67	36.00	41.44	32.18	36.40
P(COS)	0.00	0.00	0.00	0.00	0.00

B.3.4 Effect of catalysts

B.3.4.1 Comparison of MoS₂ and MoO₃ catalysts under CO

(300°C, 80ml toluene, 10ml water, 600psi total pressure, CO as gas feed, ~1641ppmw 2-NA in toluene, 337ppmw Mo, 2hours)

MoS₂

Table B-28 Oil analysis results obtained by GC-FID for “MoS₂” in the “Comparison of MoS₂ and MoO₃ catalysts under CO” discussion (product mole %)

Time	Mole%				
	0min	10min	30min	60min	120min
Decalin	0.71%	0.48%	0.33%	0.47%	1.69%
Benzoic acid	0.00%	0.00%	0.00%	0.00%	0.00%
Tetralin	0.00%	0.19%	0.55%	0.82%	1.28%
Naphthalene	0.15%	1.88%	4.37%	5.03%	5.18%
1,2,3,4-tetrahydro-2-methyl-Naphthalene	0.00%	0.00%	0.40%	1.24%	3.63%
1,2,3,4-tetrahydro-6-methyl-Naphthalene	0.00%	0.33%	1.51%	3.18%	6.80%
2-Methyl-Naphthalene	7.25%	35.79%	74.94%	84.01%	80.62%
DCH					
CHB					
BP					
2-Naphthoic acid	91.89%	61.32%	17.89%	5.24%	0.80%
TH-DBT					
DBT					

Table B-29 Gas analysis results obtained by RGA for “MoS₂” in the “Comparison of MoS₂ and MoO₃ catalysts under CO” discussion (system pressure, WGSR conversion, product partial pressures)

	Partial Pressure /psi				
Time /min	0	10	30	60	120
Pressure /psi	1948	1973	1902	1848	1709
WGSR Conversion	6.88%	12.31%	19.53%	27.94%	40.28%
P(H ₂)	157.85	269.61	389.87	516.93	559.17
P(CO)	1635.79	1457.89	1184.64	928.99	663.52
P(CO ₂)	120.90	204.68	287.43	360.19	447.47
P(Water)	12.75	13.46	11.65	16.00	13.53
P(CH ₄)	0.00	0.00	0.00	0.00	0.00
P(C ₂ H ₄)	0.00	0.00	0.00	0.00	0.00
P(C ₂ H ₆)	0.00	0.00	0.11	0.16	0.21
P(H ₂ S)	9.60	18.54	21.93	21.59	22.21
P(COS)	10.83	8.82	6.37	4.15	2.88

MoO₃

Table B-30 Oil analysis results obtained by GC-FID for “MoO₃” in the “Comparison of MoS₂ and MoO₃ catalysts under CO” discussion (product mole %)

	Mole%				
Time /min	0	10	30	60	120
Decalin	0.00%	0.00%	0.00%	0.00%	0.00%
Benzoic acid	0.00%	0.00%	0.00%	0.23%	0.27%
Tetralin	0.00%	0.00%	0.00%	0.00%	0.00%
Naphthalene	0.00%	0.43%	1.02%	1.90%	3.88%
1,2,3,4-tetrahydro-2-methyl-Naphthalene	0.00%	0.00%	0.00%	0.00%	0.00%
1,2,3,4-tetrahydro-6-methyl-Naphthalene	0.00%	0.00%	0.00%	0.00%	0.00%
2-Methyl-Naphthalene	0.24%	0.56%	1.50%	3.11%	6.65%
DCH					
CHB					
BP					
2-Naphthoic acid	99.76%	99.01%	97.48%	94.76%	89.21%
TH-DBT					
DBT					

Table B-31 Gas analysis results obtained by RGA for “MoO₃” in the “Comparison of MoS₂ and MoO₃ catalysts under CO” discussion (system pressure, WGSR conversion, product partial pressures)

	Partial Pressure /psi				
Time /min	0	10	30	60	120
Pressure /psi	1638	1649	1537	1484	1356
WGSR Conversion	1.67%	2.41%	4.01%	6.11%	8.99%
P(H ₂)	28.06	44.99	71.03	104.99	135.86
P(CO)	1576.32	1557.89	1400.49	1288.15	1104.52
P(CO ₂)	26.79	38.47	58.54	83.78	109.04
P(Water)	6.83	7.65	6.94	7.08	6.58
P(CH ₄)	0.00	0.00	0.00	0.00	0.00
P(C ₂ H ₄)	0.00	0.00	0.00	0.00	0.00
P(C ₂ H ₆)	0.00	0.00	0.00	0.00	0.00
P(H ₂ S)	0.00	0.00	0.00	0.00	0.00
P(COS)	0.00	0.00	0.00	0.00	0.00

No Catalyst

Table B-32 Oil analysis results obtained by GC-FID for “No Catalyst” in the “Comparison of MoS₂ and MoO₃ catalysts under CO” discussion (product mole %)

Time /min	Mole%					
	0	10	30	45	75	120
Decalin						
Benzoic acid	0.00%	0.00%	0.00%	0.00%	0.00%	0.00%
Tetralin	0.00%	0.00%	0.00%	0.00%	0.05%	0.09%
Naphthalene	0.15%	0.19%	0.42%	0.58%	1.04%	1.85%
1,2,3,4-tetrahydro-2-methyl-Naphthalene	0.00%	0.00%	0.00%	0.00%	0.00%	0.84%
1,2,3,4-tetrahydro-6-methyl-Naphthalene	0.10%	0.00%	0.00%	0.00%	0.00%	0.14%
2-Methyl-Naphthalene	1.02%	1.36%	3.22%	4.32%	8.57%	13.38%
DCH						
CHB						
BP						
2-Naphthoic acid	98.72%	98.45%	96.36%	95.10%	90.34%	83.70%
TH-DBT						
DBT						

Table B-33 Gas analysis results obtained by RGA for “No Catalyst” in the “Comparison of MoS₂ and MoO₃ catalysts under CO” discussion (system pressure, WGSR conversion, product partial pressures)

	Partial Pressure /psi					
Time /min	0	10	30	45	75	120
Pressure /psi	1955	1898	1842	1791	1719	1719
WGSR Conversion	1.74%	3.60%	7.12%	10.52%	14.50%	14.50%
P(H ₂)	52.51	87.42	152.10	199.26	240.70	293.00
P(CO)	1645.73	1729.46	1557.44	1411.26	1272.29	1090.38
P(CO ₂)	29.11	64.66	119.40	165.97	215.72	276.23
P(Water)	43.67	24.65	28.36	26.13	21.77	20.55
P(CH ₄)	0.00	0.00	0.00	0.00	0.00	0.00
P(C ₂ H ₄)	0.00	0.00	0.00	0.00	0.00	0.00
P(C ₂ H ₆)	0.00	0.00	0.00	0.00	0.00	0.00
P(H ₂ S)	24.49	30.26	25.99	26.65	29.18	30.08
P(COS)	11.48	18.55	14.71	12.74	11.34	8.77

B.3.4.2 Effect of MoS₂ loading under CO

(300°C, 80ml toluene, 10ml water, 15psi H₂S, 585psi CO, ~1641ppmw 2-NA in toluene, 0~673ppmw Mo, 2hours)

673 ppm

Table B-34 Oil analysis results obtained by GC-FID for “673 ppm” in the “Effect of MoS₂ loading under CO” discussion (product mole %)

Time /min	Mole%				
	0	10	30	60	120
Decalin					
Benzoic acid	0.00%	0.00%	0.00%	0.00%	0.00%
Tetralin	0.00%	0.04%	0.15%	0.28%	0.49%
Naphthalene	0.00%	1.30%	2.74%	3.69%	3.98%
1,2,3,4-tetrahydro-2-methyl-Naphthalene	0.00%	0.00%	0.34%	1.18%	4.16%
1,2,3,4-tetrahydro-6-methyl-Naphthalene	0.00%	0.29%	1.04%	2.63%	7.26%
2-Methyl-Naphthalene	7.38%	41.96%	71.43%	86.80%	83.33%
DCH					
CHB					
BP					
2-Naphthoic acid	92.62%	56.41%	24.29%	5.42%	0.78%
TH-DBT					
DBT					

Table B-35 Gas analysis results obtained by RGA for “673 ppm” in the “Effect of MoS₂ loading under CO” discussion (system pressure, WGSR conversion, product partial pressures)

	Partial Pressure /psi				
Time /min	0	10	30	60	120
Pressure /psi	1898	2066	1936	1908	1736
WGSR Conversion	8.46%	11.21%	23.00%	32.89%	41.74%
P(H ₂)	181.94	296.85	392.18	498.91	554.75
P(CO)	1523.45	1533.98	1147.02	906.75	656.29
P(CO ₂)	140.88	193.63	342.63	444.38	470.24
P(Water)	23.70	14.90	15.13	14.93	15.06
P(CH ₄)	0.00	0.00	0.00	0.00	0.00
P(C ₂ H ₄)	1.68	2.38	4.22	3.31	1.70
P(C ₂ H ₆)	2.13	4.15	10.52	16.32	17.40
P(H ₂ S)	16.47	14.69	19.28	19.95	18.25
P(COS)	6.77	4.88	4.62	3.14	2.30

337 ppm

Table B-36 Oil analysis results obtained by GC-FID for “337 ppm” in the “Effect of MoS₂ loading under CO” discussion (product mole %)

Time /min	Mole%				
	0	10	30	60	120
Decalin	0.71%	0.48%	0.33%	0.47%	1.69%
Benzoic acid	0.00%	0.00%	0.00%	0.00%	0.00%
Tetralin	0.00%	0.19%	0.55%	0.82%	1.28%
Naphthalene	0.15%	1.88%	4.37%	5.03%	5.18%
1,2,3,4-tetrahydro-2-methyl-Naphthalene	0.00%	0.00%	0.40%	1.24%	3.63%
1,2,3,4-tetrahydro-6-methyl-Naphthalene	0.00%	0.33%	1.51%	3.18%	6.80%
2-Methyl-Naphthalene	7.25%	35.79%	74.94%	84.01%	80.62%
DCH					
CHB					
BP					
2-Naphthoic acid	91.89%	61.32%	17.89%	5.24%	0.80%
TH-DBT					
DBT					

Table B-37 Gas analysis results obtained by RGA for “337 ppm” in the “Effect of MoS₂ loading under CO” discussion (system pressure, WGSR conversion, product partial pressures)

	Partial Pressure /psi				
Time /min	0	10	30	60	120
Pressure /psi	1948	1973	1902	1848	1709
WGSR Conversion	6.88%	12.31%	19.53%	27.94%	40.28%
P(H ₂)	157.85	269.61	389.87	516.93	559.17
P(CO)	1635.79	1457.89	1184.64	928.99	663.52
P(CO ₂)	120.90	204.68	287.43	360.19	447.47
P(Water)	12.75	13.46	11.65	16.00	13.53
P(CH ₄)	0.00	0.00	0.00	0.00	0.00
P(C ₂ H ₄)	0.00	0.00	0.00	0.00	0.00
P(C ₂ H ₆)	0.00	0.00	0.11	0.16	0.21
P(H ₂ S)	9.60	18.54	21.93	21.59	22.21
P(COS)	10.83	8.82	6.37	4.15	2.88

168 ppm

Table B-38 Oil analysis results obtained by GC-FID for “168 ppm” in the “Effect of MoS₂ loading under CO” discussion (product mole %)

Time /min	Mole%				
	0	10	30	60	120
Decalin	1.26%	0.84%	0.74%	0.68%	0.98%
Benzoic acid	0.00%	0.00%	0.00%	0.00%	0.00%
Tetralin	0.00%	0.00%	0.21%	0.47%	0.97%
Naphthalene	0.00%	1.20%	3.02%	5.72%	9.32%
1,2,3,4-tetrahydro-2-methyl-Naphthalene	0.00%	0.00%	0.00%	0.00%	0.48%
1,2,3,4-tetrahydro-6-methyl-Naphthalene	0.00%	0.00%	0.00%	0.49%	1.39%
2-Methyl-Naphthalene	2.74%	13.92%	28.44%	48.85%	71.55%
DCH					
CHB					
BP					
2-Naphthoic acid	96.00%	84.03%	67.59%	43.79%	15.31%
TH-DBT					
DBT					

Table B-39 Gas analysis results obtained by RGA for “168 ppm” in the “Effect of MoS₂ loading under CO” discussion (system pressure, WGSR conversion, product partial pressures)

	Partial Pressure /psi				
Time /min	0	10	30	60	120
Pressure /psi	1843	1898	1900	1848	1719
WGSR Conversion	4.53%	6.80%	11.64%	16.39%	23.25%
P(H ₂)	115.92	167.96	252.16	361.41	449.18
P(CO)	1614.96	1573.76	1419.54	1207.13	945.73
P(CO ₂)	76.67	114.83	187.08	236.59	286.45
P(Water)	12.90	12.08	9.21	15.08	13.41
P(CH ₄)	0.00	0.00	0.00	0.00	0.00
P(C ₂ H ₄)	0.00	0.00	0.33	0.44	0.46
P(C ₂ H ₆)	0.00	0.12	0.34	0.59	0.88
P(H ₂ S)	12.26	19.30	22.88	20.83	19.05
P(COS)	10.29	9.95	8.45	5.93	3.84

No Catalyst

Table B-40 Oil analysis results obtained by GC-FID for “No Catalyst” in the “Effect of MoS₂ loading under CO” discussion (product mole %)

Time /min	Mole%					
	0	10	30	45	75	120
Decalin						
Benzoic acid	0.00%	0.00%	0.00%	0.00%	0.00%	0.00%
Tetralin	0.00%	0.00%	0.00%	0.00%	0.05%	0.09%
Naphthalene	0.15%	0.19%	0.42%	0.58%	1.04%	1.85%
1,2,3,4-tetrahydro-2-methyl-Naphthalene	0.00%	0.00%	0.00%	0.00%	0.00%	0.84%
1,2,3,4-tetrahydro-6-methyl-Naphthalene	0.10%	0.00%	0.00%	0.00%	0.00%	0.14%
2-Methyl-Naphthalene	1.02%	1.36%	3.22%	4.32%	8.57%	13.38%
DCH						
CHB						
BP						
2-Naphthoic acid	98.72%	98.45%	96.36%	95.10%	90.34%	83.70%
TH-DBT						
DBT						

Table B-41 Gas analysis results obtained by RGA for “No Catalyst” in the “Effect of MoS₂ loading under CO” discussion (system pressure, WGSR conversion, product partial pressures)

	Partial Pressure /psi					
Time /min	0	10	30	45	75	120
Pressure /psi	1955	1898	1842	1791	1719	1719
WGSR Conversion	1.74%	3.60%	7.12%	10.52%	14.50%	14.50%
P(H ₂)	52.51	87.42	152.10	199.26	240.70	293.00
P(CO)	1645.73	1729.46	1557.44	1411.26	1272.29	1090.38
P(CO ₂)	29.11	64.66	119.40	165.97	215.72	276.23
P(Water)	43.67	24.65	28.36	26.13	21.77	20.55
P(CH ₄)	0.00	0.00	0.00	0.00	0.00	0.00
P(C ₂ H ₄)	0.00	0.00	0.00	0.00	0.00	0.00
P(C ₂ H ₆)	0.00	0.00	0.00	0.00	0.00	0.00
P(H ₂ S)	24.49	30.26	25.99	26.65	29.18	30.08
P(COS)	11.48	18.55	14.71	12.74	11.34	8.77

B.3.4.3 Comparison of MoS₂ and MoO₃ catalysts under H₂

(300°C, 80ml toluene, 10ml water, 600psi total pressure, H₂ as gas feed, ~1641ppmw 2-NA in toluene, 337ppmw Mo, 2hours)

MoS₂

Table B-42 Oil analysis results obtained by GC-FID for “MoS₂” in the “Comparison of MoS₂ and MoO₃ catalysts under H₂” discussion (product mole %)

Time /min	Mole%				
	0	10	30	60	120
Decalin	0.00%	0.00%	0.00%	0.00%	0.00%
Benzoic acid	0.00%	0.00%	0.00%	0.00%	0.00%
Tetralin	0.07%	0.24%	0.40%	0.51%	0.64%
Naphthalene	1.15%	1.92%	2.99%	2.99%	2.74%
1,2,3,4-tetrahydro-2-methyl-Naphthalene	0.00%	0.17%	0.68%	1.80%	3.71%
1,2,3,4-tetrahydro-6-methyl-Naphthalene	0.00%	0.45%	1.60%	3.36%	5.83%
2-Methyl-Naphthalene	9.79%	35.34%	75.74%	90.07%	87.07%
DCH					
CHB					
BP					
2-Naphthoic acid	88.99%	61.88%	18.58%	1.27%	0.00%
TH-DBT					
DBT					

MoO₃

Table B-43 Oil analysis results obtained by GC-FID for “MoO₃” in the “Comparison of MoS₂ and MoO₃ catalysts under H₂” discussion (product mole %)

Time /min	Mole%				
	0	10	30	60	120
Decalin	0.00%	0.00%	0.00%	0.00%	0.00%
Benzoic acid	0.00%	0.00%	0.00%	0.00%	0.00%
Tetralin	0.00%	0.00%	0.28%	0.39%	0.59%
Naphthalene	0.19%	0.94%	2.85%	4.15%	5.81%
1,2,3,4-tetrahydro-2-methyl-Naphthalene	0.00%	0.00%	0.16%	0.20%	0.37%
1,2,3,4-tetrahydro-6-methyl-Naphthalene	0.00%	0.28%	0.68%	0.87%	1.43%
2-Methyl-Naphthalene	1.08%	7.66%	23.56%	34.67%	47.39%
DCH					
CHB					
BP					
2-Naphthoic acid	98.72%	91.12%	72.46%	59.71%	44.42%
TH-DBT					
DBT					

No Catalyst

Table B-44 Oil analysis results obtained by GC-FID for “No Catalyst” in the “Comparison of MoS₂ and MoO₃ catalysts under H₂” discussion (product mole %)

Time /min	Mole%					
	0	10	30	45	60	120
Decalin						
Benzoic acid	0.00%	0.00%	0.00%	0.00%	0.00%	0.00%
Tetralin	0.00%	0.02%	0.07%	0.08%	0.17%	0.27%
Naphthalene	0.00%	0.50%	1.67%	1.89%	3.42%	5.03%
1,2,3,4-tetrahydro-2-methyl-Naphthalene	0.00%	0.00%	0.10%	0.11%	0.26%	0.49%
1,2,3,4-tetrahydro-6-methyl-Naphthalene	0.00%	0.00%	0.19%	0.22%	0.50%	0.95%
2-Methyl-Naphthalene	0.54%	3.08%	10.33%	12.99%	21.48%	35.46%
DCH						
CHB						
BP						
2-Naphthoic acid	99.46%	96.41%	87.64%	84.71%	74.17%	57.80%
TH-DBT						
DBT						

B.3.4.4 Effect of MoS₂ catalysts under N₂

(300°C, 80ml toluene, 10ml water, 15psi H₂S, 585psi N₂, ~1641ppmw 2-NA in toluene, 337ppmw Mo, 2hours)

MoS₂

Table B-45 Oil analysis results obtained by GC-FID for “MoS₂” in the “Effect of MoS₂ catalysts under N₂” discussion (product mole %)

Time /min	Mole%				
	0	10	30	60	120
Decalin					
Benzoic acid	16.67%	20.46%	21.91%	21.69%	20.31%
Tetralin	0.00%	0.00%	0.00%	0.00%	0.00%
Naphthalene	0.00%	0.30%	0.84%	1.58%	2.53%
1,2,3,4-tetrahydro-2-methyl-Naphthalene	0.00%	0.00%	0.00%	0.00%	0.00%
1,2,3,4-tetrahydro-6-methyl-Naphthalene	0.00%	0.00%	0.00%	0.00%	0.00%
2-Methyl-Naphthalene	0.52%	3.88%	14.57%	32.59%	57.14%
DCH					
CHB					
BP					
2-Naphthoic acid	82.81%	75.37%	62.67%	44.14%	20.02%
TH-DBT					
DBT					

No CatalystTable B-46 Oil analysis results obtained by GC-FID for “No Catalyst” in the “Effect of MoS₂ catalysts under N₂” discussion (product mole %)

Time /min	Mole%					
	0	10	30	45	75	120
Decalin						
Benzoic acid	0.00%	0.00%	0.00%	0.00%	0.00%	0.00%
Tetralin	0.13%	0.02%	0.00%	0.00%	0.00%	0.00%
Naphthalene	0.22%	0.15%	0.22%	0.26%	0.03%	0.53%
1,2,3,4-tetrahydro-2-methyl-Naphthalene	0.54%	0.24%	0.14%	0.12%	0.00%	0.00%
1,2,3,4-tetrahydro-6-methyl-Naphthalene	1.05%	0.45%	0.26%	0.26%	0.02%	0.13%
2-Methyl-Naphthalene	1.93%	1.13%	1.40%	1.56%	0.01%	2.88%
DCH						
CHB						
BP						
2-Naphthoic acid	96.14%	98.00%	97.99%	97.81%	99.94%	96.46%
TH-DBT						
DBT						

B.3.5 Effect of water on 2-NA removal

B.3.5.1 Effect of water on 2-NA under CO

(300°C, 80ml toluene, 10~20ml water, 15psi H₂S, 585psi CO, ~1641ppmw 2-NA in toluene, 673ppmw Mo, 2hours)

10mL H₂O

Table B-47 Oil analysis results obtained by GC-FID for “10mL H₂O” in the “Effect of water on 2-NA under CO” discussion (product mole %)

Time /min	Mole%				
	0	10	30	60	120
Decalin					
Benzoic acid	0.00%	0.00%	0.00%	0.00%	0.00%
Tetralin	0.00%	0.04%	0.15%	0.28%	0.49%
Naphthalene	0.00%	1.30%	2.74%	3.69%	3.98%
1,2,3,4-tetrahydro-2-methyl-Naphthalene	0.00%	0.00%	0.34%	1.18%	4.16%
1,2,3,4-tetrahydro-6-methyl-Naphthalene	0.00%	0.29%	1.04%	2.63%	7.26%
2-Methyl-Naphthalene	7.38%	41.96%	71.43%	86.80%	83.33%
DCH					
CHB					
BP					
2-Naphthoic acid	92.62%	56.41%	24.29%	5.42%	0.78%
TH-DBT					
DBT					

Table B-48 Gas analysis results obtained by RGA for “10mL H2O” in the “Effect of water on 2-NA under CO” discussion (system pressure, WGSR conversion, product partial pressures)

	Partial Pressure /psi				
Time /min	0	10	30	60	120
Pressure /psi	1898	2066	1936	1908	1736
WGSR Conversion	8.46%	11.21%	23.00%	32.89%	41.74%
P(H2)	181.94	296.85	392.18	498.91	554.75
P(CO)	1523.45	1533.98	1147.02	906.75	656.29
P(CO2)	140.88	193.63	342.63	444.38	470.24
P(Water)	23.70	14.90	15.13	14.93	15.06
P(CH4)	0.00	0.00	0.00	0.00	0.00
P(C2H4)	1.68	2.38	4.22	3.31	1.70
P(C2H6)	2.13	4.15	10.52	16.32	17.40
P(H2S)	16.47	14.69	19.28	19.95	18.25
P(COS)	6.77	4.88	4.62	3.14	2.30

15mL H2O

Table B-49 Oil analysis results obtained by GC-FID for “15mL H2O” in the “Effect of water on 2-NA under CO” discussion (product mole %)

Time /min	Mole%				
	0	10	30	60	120
Decalin					
Benzoic acid	0.00%	0.00%	0.00%	0.00%	0.00%
Tetralin	0.00%	0.08%	0.24%	0.44%	0.90%
Naphthalene	0.24%	1.55%	3.69%	4.89%	5.03%
1,2,3,4-tetrahydro-2-methyl-Naphthalene	0.00%	0.00%	0.54%	1.96%	7.19%
1,2,3,4-tetrahydro-6-methyl-Naphthalene	0.00%	0.31%	1.63%	4.32%	12.07%
2-Methyl-Naphthalene	6.29%	26.68%	60.57%	78.64%	74.25%
DCH					
CHB					
BP					
2-Naphthoic acid	93.47%	71.38%	33.33%	9.76%	0.56%
TH-DBT					
DBT					

Table B-50 Gas analysis results obtained by RGA for “15mL H₂O” in the “Effect of water on 2-NA under CO” discussion (system pressure, WGS conversion, product partial pressures)

	Partial Pressure /psi				
Time /min	0	10	30	60	120
Pressure /psi	2203	2262	2205	2169	2117
WGS Conversion	10.14%	18.28%	30.20%	41.17%	59.28%
P(H ₂)	294.14	450.11	666.50	949.49	1056.44
P(CO)	1675.74	1445.07	1045.30	696.98	418.20
P(CO ₂)	189.02	323.15	452.24	487.81	608.89
P(Water)	23.54	17.21	16.69	15.92	14.96
P(CH ₄)	0.00	0.00	0.00	0.00	0.43
P(C ₂ H ₄)	0.00	0.00	0.00	0.00	0.00
P(C ₂ H ₆)	0.00	0.23	0.41	0.47	0.56
P(H ₂ S)	14.90	20.58	20.27	16.24	16.68
P(COS)	5.66	5.17	3.18	1.51	0.84

20mL H2O

Table B-51 Oil analysis results obtained by GC-FID for “20mL H2O” in the “Effect of water on 2-NA under CO” discussion (product mole %)

Time /min	Mole%				
	0	10	30	60	120
Decalin					
Benzoic acid	0.00%	0.00%	0.00%	0.00%	0.00%
Tetralin	0.00%	0.00%	0.14%	0.42%	1.09%
Naphthalene	0.10%	0.99%	3.16%	6.39%	8.58%
1,2,3,4-tetrahydro-2-methyl-Naphthalene	0.00%	0.00%	0.19%	0.87%	4.03%
1,2,3,4-tetrahydro-6-methyl-Naphthalene	0.00%	0.00%	0.47%	1.93%	7.32%
2-Methyl-Naphthalene	2.57%	12.83%	35.17%	61.36%	74.87%
DCH					
CHB					
BP					
2-Naphthoic acid	97.34%	86.17%	60.85%	29.04%	4.10%
TH-DBT					
DBT					

Table B-52 Gas analysis results obtained by RGA for “20mL H2O” in the “Effect of water on 2-NA under CO” discussion (system pressure, WGS conversion, product partial pressures)

	Partial Pressure /psi				
Time /min	0	10	30	60	120
Pressure /psi	2369	2458	2375	2345	2300
WGS Conversion	17.94%	26.19%	41.23%	60.73%	82.02%
P(H2)	440.38	566.13	775.00	1125.95	1088.43
P(CO)	1525.25	1353.79	908.56	453.29	208.52
P(CO2)	333.53	480.35	637.43	700.94	951.55
P(Water)	39.29	22.03	20.83	35.52	22.16
P(CH4)	0.00	0.00	0.00	0.00	0.00
P(C2H4)	0.00	1.37	1.62	1.85	0.00
P(C2H6)	0.00	1.64	2.90	4.03	5.75
P(H2S)	23.57	27.19	25.15	21.00	23.00
P(COS)	5.57	4.73	2.88	1.32	0.58

B.3.5.2 Effect of water on 2-NA under N₂

(300°C, 80ml toluene, 10~20ml water, 15psi H₂S, 585psi N₂, ~1641ppmw 2-NA in toluene, 673ppmw Mo, 2hours)

10mL H₂O

Table B-53 Oil analysis results obtained by GC-FID for “10mL H₂O” in the “Effect of water on 2-NA under N₂” discussion (product mole %)

Time /min	Mole%				
	0	10	30	60	120
Decalin					
Benzoic acid	16.67%	20.46%	21.91%	21.69%	20.31%
Tetralin	0.00%	0.00%	0.00%	0.00%	0.00%
Naphthalene	0.00%	0.30%	0.84%	1.58%	2.53%
1,2,3,4-tetrahydro-2-methyl-Naphthalene	0.00%	0.00%	0.00%	0.00%	0.00%
1,2,3,4-tetrahydro-6-methyl-Naphthalene	0.00%	0.00%	0.00%	0.00%	0.00%
2-Methyl-Naphthalene	0.52%	3.88%	14.57%	32.59%	57.14%
DCH					
CHB					
BP					
2-Naphthoic acid	82.81%	75.37%	62.67%	44.14%	20.02%
TH-DBT					
DBT					

Table B-54 Gas analysis results obtained by RGA for “10mL H2O” in the “Effect of water on 2-NA under N₂” discussion (system pressure, WGSR conversion, product partial pressures)

	Partial Pressure /psi				
Time /min	0	10	30	60	120
Pressure /psi	1783	1904	1926	1849	1698
WGSR Conversion	100.00%	100.00%	100.00%	100.00%	100.00%
P(H ₂)	2.91	3.24	5.59	7.29	7.76
P(CO)	0.00	0.00	0.00	0.00	0.00
P(CO ₂)	2.03	1.21	1.16	1.06	1.14
P(Water)	25.58	18.43	10.35	18.80	13.07
P(CH ₄)	0.00	0.00	0.00	0.00	0.00
P(C ₂ H ₄)	0.00	0.00	0.54	0.44	0.40
P(C ₂ H ₆)	0.00	0.00	0.29	0.34	0.54
P(H ₂ S)	37.67	36.00	41.44	32.18	36.40
P(COS)	0.00	0.00	0.00	0.00	0.00

15mL H2OTable B-55 Oil analysis results obtained by GC-FID for “15mL H2O” in the “Effect of water on 2-NA under N₂” discussion (product mole %)

Time /min	Mole%				
	0	10	30	60	120
Decalin					
Benzoic acid	26.88%	33.05%	35.17%	36.48%	38.56%
Tetralin	0.00%	0.00%	0.00%	0.00%	0.00%
Naphthalene	0.00%	0.20%	0.42%	0.70%	1.17%
1,2,3,4-tetrahydro-2-methyl-Naphthalene	0.00%	0.00%	0.00%	0.00%	0.00%
1,2,3,4-tetrahydro-6-methyl-Naphthalene	0.00%	0.00%	0.00%	0.00%	0.00%
2-Methyl-Naphthalene	0.54%	1.29%	3.72%	8.17%	17.65%
DCH					
CHB					
BP					
2-Naphthoic acid	72.59%	65.45%	60.69%	54.65%	42.62%
TH-DBT					
DBT					

Table B-56 Gas analysis results obtained by RGA for “15mL H₂O” in the “Effect of water on 2-NA under N₂” discussion (system pressure, WGSR conversion, product partial pressures)

	Partial Pressure /psi				
Time /min	0	10	30	60	120
Pressure /psi	2156	2165	2064	1999	1936
WGSR Conversion	100.00%	100.00%	100.00%	100.00%	100.00%
P(H ₂)	0.59	1.93	3.40	4.31	5.04
P(CO)	0.00	0.00	0.00	0.00	0.00
P(CO ₂)	0.87	0.57	0.52	0.57	0.60
P(Water)	20.12	17.34	12.96	13.20	15.38
P(CH ₄)	0.00	0.00	0.00	0.00	0.00
P(C ₂ H ₄)	0.00	0.00	0.00	0.00	0.00
P(C ₂ H ₆)	0.00	0.00	0.00	0.00	0.00
P(H ₂ S)	41.29	41.30	39.93	43.77	39.58
P(COS)	0.00	0.00	0.00	0.00	0.00

20mL H2O

Table B-57 Oil analysis results obtained by GC-FID for “20mL H2O” in the “Effect of water on 2-NA under N₂” discussion (product mole %)

Time /min	Mole%				
	0	10	30	60	120
Decalin					
Benzoic acid	24.49%	29.71%	31.30%	32.64%	33.76%
Tetralin	0.00%	0.00%	0.00%	0.00%	0.00%
Naphthalene	0.00%	0.15%	0.34%	0.65%	1.21%
1,2,3,4-tetrahydro-2-methyl-Naphthalene	0.00%	0.00%	0.00%	0.00%	0.00%
1,2,3,4-tetrahydro-6-methyl-Naphthalene	0.00%	0.00%	0.00%	0.00%	0.00%
2-Methyl-Naphthalene	0.23%	0.54%	2.00%	4.49%	9.52%
DCH					
CHB					
BP					
2-Naphthoic acid	75.28%	69.60%	66.37%	62.23%	55.50%
TH-DBT					
DBT					

Table B-58 Gas analysis results obtained by RGA for “20mL H₂O” in the “Effect of water on 2-NA under N₂” discussion (system pressure, WGSR conversion, product partial pressures)

	Partial Pressure /psi				
Time /min	0	10	30	60	120
Pressure /psi	2290	2331	2219	2161	2090
WGSR Conversion	100.00%	100.00%	100.00%	100.00%	100.00%
P(H ₂)	0.00	1.88	3.26	4.92	6.05
P(CO)	0.00	0.00	0.00	0.00	0.00
P(CO ₂)	1.00	0.59	0.51	0.55	0.62
P(Water)	28.22	17.22	17.12	10.10	12.70
P(CH ₄)	0.00	0.00	0.00	0.00	0.00
P(C ₂ H ₄)	0.00	0.00	0.00	0.00	0.00
P(C ₂ H ₆)	0.00	0.00	0.00	0.00	0.00
P(H ₂ S)	34.94	41.30	35.52	37.84	34.80
P(COS)	0.00	0.00	0.00	0.00	0.00

B.3.6 Simultaneous 2-NA removal and HDS of DBT with *in situ* H₂

(300~340°C, 80ml toluene, 10ml water, 15psi H₂S, 585psi CO, ~1641ppmw 2-NA, ~5000ppmw DBT, 337ppmw Mo, 2~3hours)

NA@300°C

Table B-59 Oil analysis results obtained by GC-FID for “NA@300°C” in the “Simultaneous 2-NA removal and HDS of DBT with *in situ* H₂” discussion (product mole %)

Time /min	Mole%				
	0	10	30	60	120
Decalin	0.71%	0.48%	0.33%	0.47%	1.69%
Benzoic acid	0.00%	0.00%	0.00%	0.00%	0.00%
Tetralin	0.00%	0.19%	0.55%	0.82%	1.28%
Naphthalene	0.15%	1.88%	4.37%	5.03%	5.18%
1,2,3,4-tetrahydro-2-methyl-Naphthalene	0.00%	0.00%	0.40%	1.24%	3.63%
1,2,3,4-tetrahydro-6-methyl-Naphthalene	0.00%	0.33%	1.51%	3.18%	6.80%
2-Methyl-Naphthalene	7.25%	35.79%	74.94%	84.01%	80.62%
DCH					
CHB					
BP					
2-Naphthoic acid	91.89%	61.32%	17.89%	5.24%	0.80%
TH-DBT					
DBT					

Table B-60 Gas analysis results obtained by RGA for “NA@300°C” in the “Simultaneous 2-NA removal and HDS of DBT with in situ H2” discussion (system pressure, WGSR conversion, product partial pressures)

	Partial Pressure /psi				
Time /min	0	10	30	60	120
Pressure /psi	1948	1973	1902	1848	1709
WGSR Conversion	6.88%	12.31%	19.53%	27.94%	40.28%
P(H2)	157.85	269.61	389.87	516.93	559.17
P(CO)	1635.79	1457.89	1184.64	928.99	663.52
P(CO2)	120.90	204.68	287.43	360.19	447.47
P(Water)	12.75	13.46	11.65	16.00	13.53
P(CH4)	0.00	0.00	0.00	0.00	0.00
P(C2H4)	0.00	0.00	0.00	0.00	0.00
P(C2H6)	0.00	0.00	0.11	0.16	0.21
P(H2S)	9.60	18.54	21.93	21.59	22.21
P(COS)	10.83	8.82	6.37	4.15	2.88

DBT@300°CTable B-61 Oil analysis results obtained by GC-FID for “DBT@300°C” in the “Simultaneous 2-NA removal and HDS of DBT with in situ H₂” discussion (product mole %)

	Mole%				
Time /min	0	10	30	60	120
Decalin					
Benzoic acid					
Tetralin					
Naphthalene					
1,2,3,4-tetrahydro-2-methyl-Naphthalene					
1,2,3,4-tetrahydro-6-methyl-Naphthalene					
2-Methyl-Naphthalene					
DCH	0.00%	0.00%	0.00%	0.00%	0.00%
CHB	0.00%	0.00%	0.00%	0.00%	0.18%
BP	0.74%	0.75%	0.84%	1.04%	1.75%
2-Naphthoic acid					
TH-DBT	0.00%	0.09%	0.34%	0.78%	1.96%
DBT	99.26%	99.17%	98.83%	98.18%	96.11%

Table B-62 Gas analysis results obtained by RGA for “DBT@300°C” in the “Simultaneous 2-NA removal and HDS of DBT with in situ H₂” discussion (system pressure, WGSR conversion, product partial pressures)

	Partial Pressure /psi				
Time /min	0	10	30	60	120
Pressure /psi	1809	1926	1986	1938	1773
WGSR Conversion	7.39%	12.57%	20.19%	30.87%	40.56%
P(H ₂)	175.19	283.22	433.96	565.30	621.25
P(CO)	1478.24	1400.17	1204.50	921.52	630.14
P(CO ₂)	117.98	201.39	304.74	411.42	429.97
P(Water)	18.14	13.04	16.01	14.63	70.33
P(CH ₄)	0.00	0.00	0.00	0.00	0.00
P(C ₂ H ₄)	0.00	0.00	0.00	0.00	0.00
P(C ₂ H ₆)	0.00	0.00	0.14	0.38	0.00
P(H ₂ S)	13.68	21.75	21.95	21.56	18.73
P(COS)	5.77	6.43	4.69	3.20	2.57

NA+DBT@300°CTable B-63 Oil analysis results obtained by GC-FID for “NA+DBT@300°C” in the “Simultaneous 2-NA removal and HDS of DBT with in situ H₂” discussion (product mole %)

Time /min	Mole%				
	0	10	30	60	120
Decalin	0.28%	0.00%	0.00%	0.00%	0.00%
Benzoic acid	0.00%	0.00%	0.00%	0.00%	0.00%
Tetralin	0.00%	0.00%	0.32%	0.54%	0.75%
Naphthalene	0.00%	0.91%	2.21%	3.05%	3.28%
1,2,3,4-tetrahydro-2-methyl-Naphthalene	0.00%	0.00%	0.26%	0.87%	2.31%
1,2,3,4-tetrahydro-6-methyl-Naphthalene	0.00%	0.23%	1.17%	2.72%	4.84%
2-Methyl-Naphthalene	11.95%	35.94%	70.32%	88.44%	88.60%
DCH	0.00%	0.00%	0.00%	0.00%	0.04%
CHB	0.00%	0.00%	0.00%	0.00%	0.07%
BP	0.74%	0.74%	0.78%	0.90%	1.34%
2-Naphthoic acid	87.77%	62.92%	25.72%	4.37%	0.21%
TH-DBT	0.00%	0.06%	0.19%	0.50%	1.28%
DBT	99.26%	99.21%	99.04%	98.60%	97.27%

Table B-64 Gas analysis results obtained by RGA for “NA+DBT@300°C” in the “Simultaneous 2-NA removal and HDS of DBT with in situ H2” discussion (system pressure, WGSR conversion, product partial pressures)

	Partial Pressure /psi				
Time /min	0	10	30	60	120
Pressure /psi	1822	1908	1887	1804	1735
WGSR Conversion	6.23%	9.04%	14.90%	23.71%	35.66%
P(H2)	137.54	203.44	322.47	426.80	544.22
P(CO)	1536.60	1506.46	1291.56	1018.73	739.31
P(CO2)	102.13	149.79	226.16	316.61	409.84
P(Water)	12.40	13.67	14.75	11.52	14.47
P(CH4)	0.00	0.00	0.00	0.00	0.00
P(C2H4)	0.00	0.00	0.00	0.00	0.00
P(C2H6)	0.00	0.00	0.00	0.12	0.16
P(H2S)	23.69	25.22	24.90	25.20	23.89
P(COS)	9.63	9.43	7.16	5.01	3.10

NA@340°C

Table B-65 Oil analysis results obtained by GC-FID for “NA@340°C” in the “Simultaneous 2-NA removal and HDS of DBT with in situ H₂” discussion (product mole %)

Time /min	Mole%					
	0	10	30	60	120	180
Decalin	0.00%	0.00%	0.18%	0.26%	0.30%	0.00
Benzoic acid	0.00%	0.00%	0.00%	0.00%	0.00%	0
Tetralin	0.54%	1.49%	2.67%	4.42%	8.31%	0.115924
Naphthalene	6.79%	12.97%	13.89%	12.81%	9.87%	0.074869
1,2,3,4-tetrahydro-2-methyl-Naphthalene	0.00%	0.69%	2.36%	5.27%	11.19%	0.148306
1,2,3,4-tetrahydro-6-methyl-Naphthalene	0.67%	2.62%	6.15%	11.97%	23.84%	0.313997
2-Methyl-Naphthalene	56.73%	78.16%	74.32%	65.07%	46.48%	0.343688
DCH						
CHB						
BP						
2-Naphthoic acid	35.27%	4.07%	0.42%	0.19%	0.00%	0
TH-DBT						
DBT						

Table B-66 Gas analysis results obtained by RGA for “NA@340°C” in the “Simultaneous 2-NA removal and HDS of DBT with in situ H₂” discussion (system pressure, WGSR conversion, product partial pressures)

	Partial Pressure /psi					
Time /min	0	10	30	60	120	180
Pressure /psi	2383	2373	2270	2145	1973	1772
WGSR Conversion	12.79%	19.94%	29.74%	38.72%	44.86%	48.78%
P(H ₂)	370.83	485.47	640.48	740.24	782.04	739.15
P(CO)	1679.92	1464.23	1117.58	830.89	633.74	509.38
P(CO ₂)	246.42	364.70	473.06	525.06	515.59	485.04
P(Water)	51.48	18.01	5.63	16.47	16.96	16.87
P(CH ₄)	0.00	0.00	0.00	0.66	1.10	1.30
P(C ₂ H ₄)	0.00	0.00	0.00	0.00	0.00	0.00
P(C ₂ H ₆)	0.00	0.20	0.23	0.28	0.30	0.30
P(H ₂ S)	24.60	32.20	28.70	28.42	21.57	18.72
P(COS)	9.75	8.19	4.32	2.99	1.69	1.26

DBT@340°C

Table B-67 Oil analysis results obtained by GC-FID for “DBT@340°C” in the “Simultaneous 2-NA removal and HDS of DBT with in situ H₂” discussion (product mole %)

	Mole%					
Time /min	0	10	30	60	120	180
Decalin						
Benzoic acid						
Tetralin						
Naphthalene						
1,2,3,4-tetrahydro-2-methyl-Naphthalene						
1,2,3,4-tetrahydro-6-methyl-Naphthalene						
2-Methyl-Naphthalene						
DCH	0.00%	0.00%	0.00%	0.00%	0.13%	0.30%
CHB	0.06%	0.07%	0.36%	1.59%	6.06%	12.27%
BP	0.94%	1.55%	3.26%	6.50%	14.41%	24.32%
2-Naphthoic acid						
TH-DBT	0.35%	1.35%	3.25%	5.09%	6.05%	5.35%
DBT	98.65%	97.03%	93.13%	86.82%	73.35%	57.77%

Table B-68 Gas analysis results obtained by RGA for “DBT@340°C” in the “Simultaneous 2-NA removal and HDS of DBT with in situ H₂” discussion (system pressure, WGSR conversion, product partial pressures)

	Partial Pressure /psi					
Time /min	0	10	30	60	120	180
Pressure /psi	2304	2281	2166	2073	1973	1862
WGSR Conversion	16.76%	21.87%	28.56%	33.09%	43.21%	45.99%
P(H ₂)	436.92	519.05	608.49	665.97	697.10	720.33
P(CO)	1495.10	1325.13	1071.41	906.04	694.68	585.47
P(CO ₂)	301.10	370.86	428.40	448.12	528.53	498.54
P(Water)	26.54	22.28	18.79	19.31	16.13	27.13
P(CH ₄)	0.00	0.00	0.00	0.81	1.30	1.72
P(C ₂ H ₄)	0.00	0.00	0.00	0.00	0.00	0.00
P(C ₂ H ₆)	0.00	0.34	0.47	0.50	1.17	0.59
P(H ₂ S)	36.92	36.32	33.56	28.97	31.43	26.34
P(COS)	7.43	7.02	4.88	3.28	2.66	1.87

NA+DBT@340°C

Table B-69 Oil analysis results obtained by GC-FID for “NA+DBT@340°C” in the “Simultaneous 2-NA removal and HDS of DBT with in situ H₂” discussion (product mole %)

Time /min	Mole%					
	0	10	30	60	120	180
Decalin	0.00%	0.00%	0.21%	0.28%	0.35%	0.39%
Benzoic acid	0.00%	0.00%	0.00%	0.00%	0.00%	0.00%
Tetralin	0.44%	1.32%	2.21%	3.20%	5.82%	8.24%
Naphthalene	5.38%	10.53%	11.30%	11.04%	8.81%	6.67%
1,2,3,4-tetrahydro-2-methyl-Naphthalene	0.00%	0.80%	2.37%	4.40%	9.54%	13.67%
1,2,3,4-tetrahydro-6-methyl-Naphthalene	0.75%	2.94%	6.08%	9.92%	19.99%	27.74%
2-Methyl-Naphthalene	58.10%	80.03%	76.14%	70.38%	54.67%	42.65%
DCH	0.00%	0.04%	0.09%	0.12%	0.12%	0.30%
CHB	0.00%	0.00%	0.30%	1.10%	6.09%	13.05%
BP	0.84%	1.50%	3.09%	5.40%	13.80%	23.27%
2-Naphthoic acid	35.33%	4.38%	1.69%	0.77%	0.81%	0.65%
TH-DBT	0.22%	1.03%	2.48%	3.87%	5.35%	4.98%
DBT	98.94%	97.43%	94.04%	89.51%	74.64%	58.40%

Table B-70 Gas analysis results obtained by RGA for “NA+DBT@340°C” in the “Simultaneous 2-NA removal and HDS of DBT with in situ H₂” discussion (system pressure, WGSR conversion, product partial pressures)

	Partial Pressure /psi					
Time /min	0	10	30	60	120	180
Pressure /psi	2329	2311	2214	2167	2086	1992
WGSR Conversion	13.01%	18.84%	28.63%	36.45%	45.33%	52.69%
P(H ₂)	397.29	538.79	629.48	732.12	765.81	796.50
P(CO)	1633.44	1392.42	1092.86	878.78	691.86	541.97
P(CO ₂)	244.23	323.26	438.37	504.08	573.66	603.70
P(Water)	24.96	26.29	23.83	22.01	25.77	20.81
P(CH ₄)	0.00	0.00	0.00	0.59	1.12	1.44
P(C ₂ H ₄)	0.00	0.00	0.00	0.00	0.00	0.00
P(C ₂ H ₆)	0.00	0.30	0.41	0.46	0.55	0.82
P(H ₂ S)	21.46	24.13	25.06	25.84	25.10	25.13
P(COS)	7.62	5.82	3.99	3.11	2.13	1.63

B.3.7 Simultaneous 2-NA removal and HDA of naphthalene (NAPH) with *in situ* H₂

(300~320°C, 80ml toluene, 10ml water, 15psi H₂S, 585psi CO, ~1641ppmw 2-NA, ~5000ppmw NAPH, 337ppmw Mo, 2hours)

NA@300°C

Table B-71 Oil analysis results obtained by GC-FID for “NA@300°C” in the “Simultaneous 2-NA removal and HDA of NAPH with *in situ* H₂” discussion (product mole %)

Time /min	Mole%				
	0	10	30	60	120
Decalin	0.71%	0.48%	0.33%	0.47%	1.69%
Benzoic acid					
Tetralin	0.00%	0.19%	0.55%	0.82%	1.28%
Naphthalene	0.15%	1.88%	4.37%	5.03%	5.18%
1,2,3,4-tetrahydro-2-methyl-Naphthalene	0.00%	0.00%	0.40%	1.24%	3.63%
1,2,3,4-tetrahydro-6-methyl-Naphthalene	0.00%	0.33%	1.51%	3.18%	6.80%
2-Methyl-Naphthalene	7.25%	35.79%	74.94%	84.01%	80.62%
DCH					
CHB					
BP					
2-Naphthoic acid	91.89%	61.32%	17.89%	5.24%	0.80%
TH-DBT					
DBT					

Table B-72 Gas analysis results obtained by RGA for “NA@300°C” in the “Simultaneous 2-NA removal and HDA of NAPH with *in situ* H₂” discussion (system pressure, WGSR conversion, product partial pressures)

	Partial Pressure /psi				
Time /min	0	10	30	60	120
Pressure /psi	1948	1973	1902	1848	1709
WGSR Conversion	6.88%	12.31%	19.53%	27.94%	40.28%
P(H ₂)	157.85	269.61	389.87	516.93	559.17
P(CO)	1635.79	1457.89	1184.64	928.99	663.52
P(CO ₂)	120.90	204.68	287.43	360.19	447.47
P(Water)	12.75	13.46	11.65	16.00	13.53
P(CH ₄)	0.00	0.00	0.00	0.00	0.00
P(C ₂ H ₄)	0.00	0.00	0.00	0.00	0.00
P(C ₂ H ₆)	0.00	0.00	0.11	0.16	0.21
P(H ₂ S)	9.60	18.54	21.93	21.59	22.21
P(COS)	10.83	8.82	6.37	4.15	2.88

NAPH@300°CTable B-73 Oil analysis results obtained by GC-FID for “NAPH@300°C” in the “Simultaneous 2-NA removal and HDA of NAPH with *in situ* H₂” discussion (product mole %)

	Mole%				
Time /min	0	10	30	60	120
Decalin	0.00%	0.00%	0.00%	0.00%	0.03%
Benzoic acid					
Tetralin	0.00%	0.16%	0.66%	1.49%	4.68%
Naphthalene	100.00%	99.84%	99.34%	98.51%	95.29%
1,2,3,4-tetrahydro-2-methyl-Naphthalene					
1,2,3,4-tetrahydro-6-methyl-Naphthalene					
2-Methyl-Naphthalene					
DCH					
CHB					
BP					
2-Naphthoic acid					
TH-DBT					
DBT					

Table B-74 Gas analysis results obtained by RGA for “NAPH@300°C” in the “Simultaneous 2-NA removal and HDA of NAPH with *in situ* H₂” discussion (system pressure, WGSR conversion, product partial pressures)

	Partial Pressure /psi				
Time /min	0	10	30	60	120
Pressure /psi	1515	1609	1567	1485	1340
WGSR Conversion	7.95%	11.00%	18.48%	26.00%	35.64%
P(H ₂)	136.27	206.03	297.60	378.96	407.73
P(CO)	1223.06	1206.67	998.71	789.67	577.61
P(CO ₂)	105.56	149.10	226.38	277.52	319.89
P(Water)	13.80	10.08	9.50	8.19	7.69
P(CH ₄)	0.00	0.00	0.00	0.00	0.00
P(C ₂ H ₄)	0.00	0.27	0.44	0.54	0.55
P(C ₂ H ₆)	0.00	0.18	0.41	0.61	0.82
P(H ₂ S)	29.58	30.05	28.69	26.04	23.26
P(COS)	6.72	6.61	5.27	3.49	2.46

NA+NAPH@300°C

Table B-75 Oil analysis results obtained by GC-FID for “NA+NAPH@300°C” in the “Simultaneous 2-NA removal and HDA of NAPH with *in situ* H₂” discussion (product mole %)

Time /min	Mole%				
	0	10	30	60	120
Decalin	0.00%	0.00%	0.00%	0.00%	0.00%
Benzoic acid	0.00%	0.00%	0.00%	0.00%	0.00%
Tetralin	0.05%	0.21%	0.71%	1.77%	4.97%
Naphthalene	99.95%	99.79%	99.29%	98.23%	95.03%
1,2,3,4-tetrahydro-2-methyl-Naphthalene	0.00%	0.00%	0.24%	0.86%	2.55%
1,2,3,4-tetrahydro-6-methyl-Naphthalene	0.00%	0.00%	1.13%	3.02%	5.72%
2-Methyl-Naphthalene	7.45%	28.44%	70.70%	93.79%	91.73%
DCH					
CHB					
BP					
2-Naphthoic acid	92.55%	71.56%	27.93%	2.32%	0.00%
TH-DBT					
DBT					

Table B-76 Gas analysis results obtained by RGA for “NA+NAPH@300°C” in the “Simultaneous 2-NA removal and HDA of NAPH with *in situ* H₂” discussion (system pressure, WGSR conversion, product partial pressures)

	Partial Pressure /psi				
Time /min	0	10	30	60	120
Pressure /psi	1754	1824	1785	1689	1637
WGSR Conversion	6.08%	8.38%	14.21%	23.74%	33.62%
P(H ₂)	128.60	174.58	273.95	385.03	470.96
P(CO)	1476.56	1462.85	1254.77	961.21	746.46
P(CO ₂)	95.62	133.77	207.92	299.31	378.10
P(Water)	14.22	12.10	11.11	9.30	10.28
P(CH ₄)	0.00	0.00	0.00	0.00	0.00
P(C ₂ H ₄)	0.00	0.00	0.00	0.00	0.00
P(C ₂ H ₆)	0.00	0.00	0.00	0.11	0.40
P(H ₂ S)	27.76	29.11	29.29	29.40	27.39
P(COS)	11.24	11.59	7.96	4.64	3.41

NAPH@320°C

Table B-77 Oil analysis results obtained by GC-FID for “NAPH@320°C” in the “Simultaneous 2-NA removal and HDA of NAPH with *in situ* H₂” discussion (product mole %)

	Mole%				
Time /min	0	10	30	60	120
Decalin	0.06%	0.07%	0.00%	0.03%	0.08%
Benzoic acid					
Tetralin	0.24%	1.15%	4.45%	10.80%	22.88%
Naphthalene	99.70%	98.78%	95.55%	89.17%	77.04%
1,2,3,4-tetrahydro-2-methyl-Naphthalene					
1,2,3,4-tetrahydro-6-methyl-Naphthalene					
2-Methyl-Naphthalene					
DCH					
CHB					
BP					
2-Naphthoic acid					
TH-DBT					
DBT					

Table B-78 Gas analysis results obtained by RGA for “NAPH@320°C” in the “Simultaneous 2-NA removal and HDA of NAPH with *in situ* H₂” discussion (system pressure, WGSR conversion, product partial pressures)

	Partial Pressure /psi				
Time /min	0	10	30	60	120
Pressure /psi	2197	2218	2147	2089	2041
WGSR Conversion	12.34%	17.76%	24.78%	31.79%	33.65%
P(H ₂)	341.91	438.77	542.82	642.83	694.88
P(CO)	1582.79	1418.68	1167.42	953.43	866.07
P(CO ₂)	222.74	306.44	384.68	444.32	439.26
P(Water)	14.27	12.52	11.99	11.47	11.39
P(CH ₄)	0.00	0.00	0.00	0.00	0.00
P(C ₂ H ₄)	0.00	0.00	0.00	0.00	0.00
P(C ₂ H ₆)	0.00	0.00	0.00	0.10	0.11
P(H ₂ S)	27.53	34.06	34.49	32.80	26.18
P(COS)	7.77	7.53	5.61	4.05	3.12

NA+NAPH@320°C

Table B-79 Oil analysis results obtained by GC-FID for “NA+NAPH@320°C” in the “Simultaneous 2-NA removal and HDA of NAPH with *in situ* H₂” discussion (product mole %)

Time /min	Mole%				
	0	10	30	60	120
Decalin	0.00%	0.00%	0.00%	0.03%	0.07%
Benzoic acid					
Tetralin	0.18%	0.84%	3.26%	8.22%	20.96%
Naphthalene	99.82%	99.16%	96.74%	91.74%	78.97%
1,2,3,4-tetrahydro-2-methyl-Naphthalene	0.00%	0.23%	1.28%	3.37%	8.51%
1,2,3,4-tetrahydro-6-methyl-Naphthalene	0.00%	1.06%	3.77%	7.39%	16.41%
2-Methyl-Naphthalene	27.02%	65.76%	93.52%	89.24%	75.08%
DCH					
CHB					
BP					
2-Naphthoic acid	72.98%	32.95%	1.42%	0.00%	0.00%
TH-DBT					
DBT					

Table B-80 Gas analysis results obtained by RGA for “NA+NAPH@320°C” in the “Simultaneous 2-NA removal and HDA of NAPH with *in situ* H₂” discussion (system pressure, WGSR conversion, product partial pressures)

	Partial Pressure /psi				
Time /min	0	10	30	60	120
Pressure /psi	2144	2147	2076	1998	1906
WGSR Conversion	9.12%	14.84%	23.16%	32.67%	41.34%
P(H ₂)	267.62	378.84	536.36	627.75	708.01
P(CO)	1657.06	1462.03	1147.18	891.66	678.50
P(CO ₂)	166.32	254.84	345.82	432.56	478.20
P(Water)	12.59	12.30	10.75	11.46	10.74
P(CH ₄)	0.00	0.00	0.00	0.00	0.00
P(C ₂ H ₄)	0.00	0.00	0.00	0.00	0.00
P(C ₂ H ₆)	0.00	0.12	0.22	0.56	0.69
P(H ₂ S)	29.57	30.90	30.80	30.53	27.60
P(COS)	10.85	7.95	4.86	3.48	2.26

B.3.8 Effect of metal additives

(300°C, 80ml toluene, 10ml water, 15psi H₂S, 585psi CO, ~1641ppmw 2-NA in toluene, 673ppmw Mo, metal:Mo ratio=0.2, 2hours)

Mo

Table B-81 Oil analysis results obtained by GC-FID for “Mo” in the “Effect of metal additives” discussion (product mole %)

Time /min	Mole%				
	0	10	30	60	120
Decalin					
Benzoic acid	0.00%	0.00%	0.00%	0.00%	0.00%
Tetralin	0.00%	0.04%	0.15%	0.28%	0.49%
Naphthalene	0.00%	1.30%	2.74%	3.69%	3.98%
1,2,3,4-tetrahydro-2-methyl-Naphthalene	0.00%	0.00%	0.34%	1.18%	4.16%
1,2,3,4-tetrahydro-6-methyl-Naphthalene	0.00%	0.29%	1.04%	2.63%	7.26%
2-Methyl-Naphthalene	7.38%	41.96%	71.43%	86.80%	83.33%
DCH					
CHB					
BP					
2-Naphthoic acid	92.62%	56.41%	24.29%	5.42%	0.78%
TH-DBT					
DBT					

Table B-82 Gas analysis results obtained by for “Mo” in the “Effect of metal additives” discussion (system pressure, WGSR conversion, product partial pressures)

	Partial Pressure /psi				
Time /min	0	10	30	60	120
Pressure /psi	1898	2066	1936	1908	1736
WGSR Conversion	8.46%	11.21%	23.00%	32.89%	41.74%
P(H ₂)	181.94	296.85	392.18	498.91	554.75
P(CO)	1523.45	1533.98	1147.02	906.75	656.29
P(CO ₂)	140.88	193.63	342.63	444.38	470.24
P(Water)	23.70	14.90	15.13	14.93	15.06
P(CH ₄)	0.00	0.00	0.00	0.00	0.00
P(C ₂ H ₄)	1.68	2.38	4.22	3.31	1.70
P(C ₂ H ₆)	2.13	4.15	10.52	16.32	17.40
P(H ₂ S)	16.47	14.69	19.28	19.95	18.25
P(COS)	6.77	4.88	4.62	3.14	2.30

Co-Mo

Table B-83 Oil analysis results obtained by GC-FID for “Co-Mo” in the “Effect of metal additives” discussion (product mole %)

Time /min	Mole%				
	0	10	30	60	120
Decalin					
Benzoic acid	0.00%	0.00%	0.00%	0.00%	0.00%
Tetralin	0.00%	0.16%	0.55%	1.06%	1.51%
Naphthalene	0.41%	1.75%	4.56%	6.10%	6.16%
1,2,3,4-tetrahydro-2-methyl-Naphthalene	0.00%	0.18%	1.11%	3.76%	8.64%
1,2,3,4-tetrahydro-6-methyl-Naphthalene	0.18%	0.71%	3.73%	8.59%	15.55%
2-Methyl-Naphthalene	10.73%	34.37%	72.14%	78.91%	68.15%
DCH					
CHB					
BP					
2-Naphthoic acid	88.69%	62.83%	17.91%	1.58%	0.00%
TH-DBT					
DBT					

Table B-84 Gas analysis results obtained by for “Co-Mo” in the “Effect of metal additives” discussion (system pressure, WGSR conversion, product partial pressures)

	Partial Pressure /psi				
Time /min	0	10	30	60	120
Pressure /psi	1868	2033	1988	1940	1740
WGSR Conversion	9.21%	15.15%	27.94%	42.32%	53.70%
P(H ₂)	183.80	288.39	439.63	580.57	593.04
P(CO)	1475.77	1427.34	1073.87	755.81	507.91
P(CO ₂)	149.63	254.92	416.28	554.59	589.18
P(Water)	21.46	18.18	17.12	12.46	17.18
P(CH ₄)	0.00	0.00	0.00	0.00	0.00
P(C ₂ H ₄)	0.00	0.00	0.00	0.00	0.00
P(C ₂ H ₆)	0.00	0.00	0.00	0.00	0.00
P(H ₂ S)	25.27	32.28	33.62	32.60	29.88
P(COS)	12.07	11.88	7.48	3.96	2.81

Ni-Mo

Table B-85 Oil analysis results obtained by GC-FID for “Ni-Mo” in the “Effect of metal additives” discussion (product mole %)

Time /min	Mole%				
	0	10	30	60	120
Decalin					
Benzoic acid	0.00%	0.00%	0.00%	0.00%	0.00%
Tetralin	0.00%	0.12%	0.76%	1.39%	2.73%
Naphthalene	0.67%	2.10%	8.33%	9.67%	8.25%
1,2,3,4-tetrahydro-2-methyl-Naphthalene	0.00%	0.00%	1.09%	3.82%	12.02%
1,2,3,4-tetrahydro-6-methyl-Naphthalene	0.00%	0.27%	3.29%	8.23%	21.21%
2-Methyl-Naphthalene	8.39%	22.51%	73.64%	76.45%	55.79%
DCH					
CHB					
BP					
2-Naphthoic acid	90.94%	75.00%	12.89%	0.42%	0.00%
TH-DBT					
DBT					

Table B-86 Gas analysis results obtained by for “Ni-Mo” in the “Effect of metal additives” discussion (system pressure, WGSR conversion, product partial pressures)

	Partial Pressure /psi				
Time /min	0	10	30	60	120
Pressure /psi	1796	1948	1997	1967	1805
WGSR Conversion	14.79%	17.62%	34.78%	51.92%	70.29%
P(H ₂)	206.97	305.47	532.85	691.91	696.75
P(CO)	1302.11	1307.99	922.55	589.67	316.61
P(CO ₂)	226.00	279.74	491.93	636.75	748.99
P(Water)	16.91	16.62	15.07	17.87	13.22
P(CH ₄)	0.00	0.00	0.00	0.00	0.00
P(C ₂ H ₄)	0.00	0.00	0.00	0.00	0.00
P(C ₂ H ₆)	0.00	0.00	0.00	0.00	0.00
P(H ₂ S)	32.31	28.59	29.29	28.13	28.06
P(COS)	11.70	9.59	5.30	2.67	1.36

B.3.9 C7-BA removal

(300°C, 80ml toluene, 10ml water, 15psi H₂S, 585psi gas feed, 5224ppmw C7-BA in toluene, 377ppmw Mo, 2hours)

No catalyst under CO

Table B-87 Oil analysis results obtained by GC-FID for “No Catalyst under CO” in the “C7-BA removal” discussion (concentration)

Time /min	Concentration /ppmw				
	0	10	30	60	120
Decalin	0.00	0.00	0.00	0.00	0.00
Benzoic acid	0.00	0.00	0.00	0.00	0.00
Tetralin	0.00	0.00	0.00	0.00	0.00
Naphthalene	0.00	0.00	0.00	0.00	0.00
1,2,3,4-tetrahydro-2-methyl-Naphthalene	0.00	0.00	0.00	0.00	0.00
1,2,3,4-tetrahydro-6-methyl-Naphthalene	0.00	0.00	0.00	0.00	0.00
2-Methyl-Naphthalene	0.00	0.00	0.00	0.00	0.00
2-Naphthoic acid	0.00	0.00	0.00	0.00	0.00
DBT	0.00	0.00	0.00	0.00	0.00
C7-BA	5594.41	5482.63	5557.27	5327.78	5256.04

Table B-88 Gas analysis results obtained for “No Catalyst under CO” in the “C7-BA removal” discussion (system pressure, WGSR conversion, product partial pressures)

	Partial Pressure /psi				
Time /min	0	10	30	60	120
Pressure /psi	1765	1822	1800	1723	1617
WGSR Conversion	2.00%	2.98%	6.25%	8.34%	13.44%
P(H ₂)	57.71	79.24	137.23	214.76	252.73
P(CO)	1632.08	1647.69	1506.92	1347.66	1150.21
P(CO ₂)	33.34	50.52	100.39	122.61	178.51
P(Water)	11.78	12.76	26.27	13.70	10.05
P(CH ₄)	0.00	0.00	0.00	0.00	0.00
P(C ₂ H ₄)	0.00	0.00	0.00	0.00	0.00
P(C ₂ H ₆)	0.00	0.00	0.00	0.00	0.00
P(H ₂ S)	19.34	19.45	20.80	18.11	20.86
P(COS)	10.75	12.33	8.40	6.17	4.64

N2

Table B-89 Oil analysis results obtained by GC-FID for “N2” in the “C7-BA removal” discussion (concentration)

Time /min	Concentration /ppmw				
	0	10	30	60	120
Decalin	1.95	0.00	0.00	0.00	0.00
Benzoic acid	72.64	100.74	129.46	144.16	174.21
Tetralin	0.00	0.00	0.00	0.00	0.00
Naphthalene	0.00	0.00	0.00	0.00	0.00
1,2,3,4-tetrahydro-2-methyl-Naphthalene	0.00	0.00	0.00	0.00	0.00
1,2,3,4-tetrahydro-6-methyl-Naphthalene	0.00	0.00	0.00	0.00	0.00
2-Methyl-Naphthalene	0.00	0.00	0.00	0.00	0.00
2-Naphthoic acid	0.00	0.00	0.00	4.06	3.72
DBT	0.00	0.00	0.00	0.00	0.00
C7-BA	4918.47	5200.8 6	5026.5 7	4928.3 4	4821.9 8

Table B-90 Gas analysis results obtained for “N2” in the “C7-BA removal” discussion (system pressure, WGSR conversion, product partial pressures)

	Partial Pressure /psi				
Time /min	0	10	30	60	120
Pressure /psi	1659	1725	1732	1599	1420
WGSR Conversion	100.00%	100.00%	100.00%	100.00%	100.00%
P(H2)	1.36	2.44	4.08	4.74	5.94
P(CO)	0.00	0.00	0.00	0.00	0.00
P(CO2)	0.76	0.40	0.46	0.40	0.46
P(Water)	18.21	12.59	12.51	10.16	12.21
P(CH4)	0.00	0.00	0.00	0.00	0.00
P(C2H4)	0.00	0.00	0.00	0.09	0.17
P(C2H6)	0.00	0.00	0.00	0.00	0.00
P(H2S)	31.58	35.70	33.12	31.09	30.08
P(COS)	0.00	0.00	0.00	0.00	0.00

H2

Table B-91 Oil analysis results obtained by GC-FID for “H2” in the “C7-BA removal” discussion (concentration)

Time /min	Concentration /ppmw				
	0	10	30	60	120
Decalin	3.44	0.00	0.00	0.00	0.00
Benzoic acid	0.00	0.00	0.00	0.00	0.00
Tetralin	0.00	0.00	0.00	0.00	0.00
Naphthalene	0.00	0.00	0.00	0.00	0.00
1,2,3,4-tetrahydro-2-methyl-Naphthalene	0.00	0.00	0.00	0.00	0.00
1,2,3,4-tetrahydro-6-methyl-Naphthalene	0.00	0.00	0.00	0.00	0.00
2-Methyl-Naphthalene	0.00	0.00	0.00	0.00	0.00
2-Naphthoic acid	24.14	25.69	15.28	5.28	0.00
DBT	0.00	0.00	0.00	0.00	0.00
C7-BA	5126.54	4406.0 9	2681.2 6	853.76	75.58

Table B-92 Gas analysis results obtained for “H2” in the “C7-BA removal” discussion (system pressure, WGSR conversion, product partial pressures)

	Partial Pressure /psi				
Time /min	0	10	30	60	120
Pressure /psi	1690	1774	1744	1701	1636
WGSR Conversion	100.00%	100.00%	27.10%	30.83%	42.68%
P(H2)	1628.31	1716.56	1685.27	1649.54	1586.54
P(CO)	0.00	0.00	1.74	1.53	1.24
P(CO2)	1.56	0.79	0.65	0.68	0.92
P(Water)	22.63	18.85	20.89	16.09	16.20
P(CH4)	0.00	0.00	0.00	0.00	0.00
P(C2H4)	0.00	0.00	0.00	0.00	0.00
P(C2H6)	0.00	0.00	0.14	0.24	0.39
P(H2S)	37.50	37.80	35.31	32.92	30.71
P(COS)	0.00	0.00	0.00	0.00	0.00

CO

Table B-93 Oil analysis results obtained by GC-FID for “CO” in the “C7-BA removal” discussion (concentration)

Name	Concentration /ppmw				
	0	10	30	60	120
Decalin	9.66	3.03	2.27	0.00	0.00
Benzoic acid	0.00	0.00	0.00	0.00	0.00
Tetralin	0.00	0.00	0.00	0.00	0.00
Naphthalene	0.00	0.00	0.00	0.00	0.00
1,2,3,4-tetrahydro-2-methyl-Naphthalene	0.00	0.00	0.00	0.00	0.00
1,2,3,4-tetrahydro-6-methyl-Naphthalene	0.00	0.00	0.00	0.00	0.00
2-Methyl-Naphthalene	4.63	2.27	2.56	2.24	2.29
2-Naphthoic acid	18.54	21.33	16.40	7.62	0.00
DBT	0.00	0.00	0.00	0.00	0.00
C7-BA	4821.60	4633.7 0	3207.8 1	1158.06	207.57

Table B-94 Gas analysis results obtained for “CO” in the “C7-BA removal” discussion (system pressure, WGSR conversion, product partial pressures)

	Partial Pressure /psi				
Time /min	0	10	30	60	120
Pressure /psi	1828	1970	1953	1916	1887
WGSR Conversion	5.15%	7.81%	13.62%	22.34%	35.62%
P(H ₂)	120.32	201.26	318.42	435.96	625.78
P(CO)	1570.95	1580.41	1369.12	1110.79	781.60
P(CO ₂)	85.25	133.93	215.81	319.62	432.35
P(Water)	12.98	15.77	13.45	14.34	16.95
P(CH ₄)	0.00	0.00	0.00	0.00	0.00
P(C ₂ H ₄)	0.00	0.00	0.00	0.00	0.00
P(C ₂ H ₆)	0.00	0.00	0.11	0.23	0.39
P(H ₂ S)	26.77	27.51	27.57	28.85	26.42
P(COS)	11.73	11.12	8.52	6.21	3.50

Appendix C. Sampling Procedure When Using HC-276 Reactor

With all the valve numbers shown in Figure 2-2, the general operating procedure for liquid phase sampling with HC-276 reactor is summarized:

a. Pre-check

- i. Ensure tubes and valves are cleaned prior to sampling
- ii. Make sure all valves are closed;

b. Vacuum step

- i. Turn on vacuum pump connected with valve #7;
- ii. Open valves #7, #5, #2, #4 and #10 gradually;
- iii. Stay vacuum for 5min;
- iv. Close valves #7, #5, #2, #4 and #10;
- v. Turn off pump;

c. Flushing step

- i. Always ensure valve #2 is closed before opening valve #1;
- ii. Open valve #1 for 30 seconds, and then close valve #1;
- iii. Open valves #2, #4 and #10;
- iv. Open valve #9, and collect flushed liquid for mass balance measurement;
- v. Open valve #11 to ensure most flushed sample could be collected;
- vi. Close valves #11, #9, #10, #4 and #2;
- vii. Repeat at least one more time before sampling point;

d. Actual sampling step

- i. Always ensure valve #2 is closed before opening valve #1;
- ii. Open valve #1 for 30 seconds, and then close valve #1;
- iii. Open valves #2, #4 and #10;

- iv. Use a gas syringe to collect gas sample from the septum near valve #11;
- v. Open valve #11 to release pressure;
- vi. Open valve #9 to collect liquid sample;
- vii. Close valves #11, #9, #10, #4 and #2;

e. Tube and valve rinse

- i. After reactor is opened, open valves #14, #16 and #5;
- ii. Add organic solvents (first toluene, then ethanol for each time) through valve #14;
- iii. Open valves #2 and #1, and apply pressure through valve #14 by using an air pressure gun to rinse the sampling point tube within reactor with solvent;
- iv. After 3~4 times rinse with different solvent, use an air pressure gun alone to blow and evaporate the solvent residue;
- v. Close valves #1 and #2;
- vi. Open valves #4, #10 and #9;
- vii. Add organic solvents through valve #14;
- viii. Open valve #11, and Add organic solvents through valve #11;
- ix. Wait since gravity could help rinse the tubes towards valve #9;
- x. Apply air pressure gun to dry-off solvents
- xi. Repeat steps vi, vii, viii, ix, x and xi for 3~4 time with different solvents.

Appendix D. Sample Calculation

D.1 Bitumen upgrading

D.1.1 Mass balance

Take one test (Mar-26-2010) in Cold Lake bitumen emulsion upgrading as an example Condition was “405°C, 80g Cold Lake bitumen emulsion, 585psi CO, 15psi H₂S, 1408 ppmw Mo, 2 hours”.

Table D-1 Summary of materials in and out of the reaction system (405°C, 80g Cold Lake bitumen emulsion, 585psi CO, 15psi H₂S, 1408 ppmw Mo, 2 hours)

In	Feed stock (g)	80.47	Measured before reaction
	PMA solution (g)	2.5	Measured before reaction
	Gas in (g)	7.8122	Calculated shown in Eq. D-1
Out	H ₂ O (g)	11	Measured after reaction
	Light Oil out of Liner (LO)(g)	0.23	Measured after reaction
	Light Oil in Trapper (L) (g)	37.43	Measured after reaction
	Heavy Oil (H) (g)	19.92	Measured after reaction
	HVOR + Coke + Metal residue (g)	3.42	Measured after reaction
	Gas out (g)	9.4521	Calculated via ideal gas law, as shown in Eq. D-2

$$\begin{aligned}
 m(\text{gas in}) &= m(\text{H}_2\text{S}) + m(\text{CO}) = M(\text{H}_2\text{S}) * P(\text{H}_2\text{S}) * \frac{V(\text{gas})}{T * R} + M(\text{CO}) * P(\text{CO}) * \frac{V(\text{gas})}{T * R} \\
 &= \frac{34 \text{ g}}{\text{mol}} * 15 \text{ psi} * \frac{6.894745 \text{ kPa}}{1 \text{ psi}} * \frac{165.18 \frac{\text{mL}}{296.15\text{K}}}{8.314 \frac{\text{J}}{\text{mol}}} + \frac{28 \text{ g}}{\text{mol}} * 585 \text{ psi} \\
 &\quad * \frac{6.894745 \text{ kPa}}{1 \text{ psi}} * \frac{165.18 \frac{\text{mL}}{296.15\text{K}}}{8.314 \frac{\text{J}}{\text{mol}}} = 7.8122 \text{ g}
 \end{aligned}$$

(Eq. D-1)

Table D-2 Mole% of gas products obtained by RGA in Cold Lake bitumen emulsion upgrading (405°C, 80g Cold Lake bitumen emulsion, 585psi CO, 15psi H₂S, 1408 ppmw Mo, 2 hours)

Hydrogen	15.85%
Oxygen	0.00%
Nitrogen	0.00%
CH ₄	3.24%
CO	12.18%
CO ₂	57.03%
C ₂ H ₄	0.00%
C ₂ H ₆	1.94%
H ₂ S	7.58%
COS	0.15%
1-2 prop=	0.52%
Propylene	0.00%
C ₃	0.71%
NC ₄	0.00%
t-2 C ₄ =	0.04%
i-C ₄ =	0.03%
1-C ₄ =	0.02%
c-2-C ₅ =	0.14%
2-meth-2-C ₄ =	0.03%
i-C ₅ =	0.01%
i-C ₄ =	0.25%
n-C ₅	0.20%
n-C ₆	0.07%
n-C ₈	0.00%
Estimated molar mass for final gas products	32.6486

$$\begin{aligned}
 m(\text{gas out}) &= M(\text{gas out}) * P(\text{overnight}) * \frac{V(\text{gas})}{T(\text{overnight}) * R} \\
 &= \frac{32.5924 \text{ g}}{\text{mol}} * 627 \text{ psi} * \frac{6.894745 \text{ kPa}}{1 \text{ psi}} * \frac{165.18 \frac{\text{mL}}{296.15\text{K}}}{8.314 \frac{\text{J}}{\text{mol}}} + \frac{28 \text{ g}}{\text{mol}} * 585 \text{ psi} \\
 &* \frac{6.894745 \text{ kPa}}{1 \text{ psi}} * \frac{165.59 \frac{\text{mL}}{296.15\text{K}}}{8.314 \frac{\text{J}}{\text{mol}}} = 9.5680\text{g}
 \end{aligned}$$

(Eq. D-2)

Note: Pressure and temperature overnight were 627psi and 23°C. The working volume was 165.18 mL based on the amount of feedstock charged.

By summarizing the mass in and mass out as shown in Table D-1, mass balance was calculated following Eq. D-3 and shown in Table D-3.

$$\text{Mass balance}\% = \frac{\text{mass out}}{\text{mass in}} * 100\% = \frac{81.4521 \text{ g}}{90.7822 \text{ g}} * 100\% = 89.22\% \quad (\text{Eq. D-3})$$

Table D-3 Summary of mass in, mass out and mass balance (405°C, 80g Cold Lake bitumen emulsion, 585psi CO, 15psi H₂S, 1408 ppmw Mo, 2 hours)

Mass in (g)	90.7822
Mass out (g)	81.4521
Mass balance %	89.72%

Note: the mass balance shown here was a repeating data for condition “405°C, 80g Cold Lake bitumen emulsion, 585psi CO, 15psi H₂S, 1408 ppmw Mo, 2 hours”. The reported data shown in Chapter 3 was 90.7%, which was obtained from another experiment. Detailed reproducibility comparison will be shown in Appendix E.

D.1.2 Yield%

Table D-4 HVOR, coke and metal residue mass summary (405°C, 80g Cold Lake bitumen emulsion, 585psi CO, 15psi H₂S, 1408 ppmw Mo, 2 hours)

HVOR + Coke + Metal residue	HVOR (g)	3.2658	Measured after toluene rinse, as discussed in Section 2.3.1
	Coke + Metal residue (g)	0.1542	Calculated shown in Eq. D-4
	Coke % in "Coke + Metal residue"	44.16%	Obtained from TGA result
	Coke mass (g)	0.0681	Calculated shown in Eq. D-4
	Metal residue	0.0861	Calculated shown in Eq. D-6

$$m(\text{Coke} + \text{Metal residue}) = m(\text{HVOR} + \text{Coke} + \text{Metal residue}) - m(\text{HVOR}) = 3.4200 - 3.2658 = 0.1542 \text{ g} \quad (\text{Eq. D-4})$$

$$m(\text{Coke}) = m(\text{Coke} + \text{Metal residue}) * \text{coke \% in Coke} + \text{Metal residue} = 0.1542 \text{ g} * 44.16\% = 0.0681 \text{ g} \quad (\text{Eq. D-5})$$

$$m(\text{Metal residue}) = m(\text{Coke} + \text{Metal residue}) - m(\text{Coke}) = 0.1542 \text{ g} - 0.0681 \text{ g} = 0.0861 \text{ g} \quad (\text{Eq. D-6})$$

Based on all the mass for different products, yield could be calculated following Eq. 2-2, where the denominator should be “dry bitumen” mass as shown in Eq. D-6.

$$m(\text{dry bitumen}) = m(\text{emulsion}) - m(\text{water}) = 80.47 \text{ g} - 12.43 \text{ g} = 67.04 \text{ g} \quad (\text{Eq. D-6})$$

Note: 80g emulsion contained 12.20 g water, measured by distillation; so 80.47g emulsion would contain approximately 12.27g water.

As a result, yields were calculated by dividing the product mass with the dry bitumen mass as the denominator. Yield results were summarized in Table D-5.

Table D-5 Summary of product yield (405°C, 80g Cold Lake bitumen emulsion, 585psi CO, 15psi H₂S, 1408 ppmw Mo, 2 hours)

	Mass (g)	Yield %
Oil	57.58	84.43%
HVOR	3.2658	4.79%
Coke mass	0.0681	0.10%
Metal residue	0.0861	0.13%
Loss to gas		10.56%

It should be noted that the loss to gas was calculated following Eq. D-7.

$$\begin{aligned}
 \text{Yield (loss to gas)} &= \\
 100\% - \text{yield}(\text{oil}) - \text{yield}(\text{HVOR}) - \text{yield}(\text{coke}) - \text{yield}(\text{metal residue}) &= 1 - \\
 84.43\% - 4.79\% - 0.10\% - 0.13\% &= 10.56\% \qquad \qquad \qquad (\text{Eq. D-7})
 \end{aligned}$$

D.2 2-NA removal

D.2.1 Kinetic study

In Section 5.2.5, the kinetic analysis of 2-NA removal under CO atmosphere at 300°C was discussed. However, no numerical calculation or results were displayed. Furthermore, in the plots for different pathway's reaction rates, the cracking pathway slope was zero. This might bring confusion about the correctness and meaning for plotting cracking pathway. Here 2-NA removal under N₂ atmosphere at 415°C was chosen as an example, since it has low existing H₂ partial pressure to hydrogenate produced benzoic acid, which helped the understanding of kinetic analysis results. In order to clearly demonstrate the kinetic analysis procedure, some detailed calculation and results are shown in this section.

Table D-6 GC-FID results - mole% changes of different chemicals involved in 2-NA removal under N₂ atmosphere at 415°C (415°C, 80ml toluene, 10ml water, 15psi H₂S, 585psi N₂, ~1641ppmw 2-NA in toluene, no catalyst, 2hours)

Time /min	Mole %					
	0	10	30	45	75	120
Benzoic acid	1.96%	2.49%	3.10%	3.23%	3.15%	2.80%
Tetralin	0.00%	0.00%	0.00%	0.00%	0.07%	0.10%
Naphthalene	2.21%	5.57%	11.05%	13.25%	20.18%	23.85%
1,2,3,4-tetrahydro-2-methyl-Naphthalene	0.00%	0.00%	0.00%	0.00%	0.00%	0.00%
1,2,3,4-tetrahydro-6-methyl-Naphthalene	0.00%	0.00%	0.00%	0.00%	0.00%	0.00%
2-Methyl-Naphthalene	3.18%	6.63%	13.80%	17.05%	25.54%	31.78%
2-Naphthoic acid	92.65%	85.31%	72.05%	66.48%	51.07%	41.46%

Following the GC-FID results, mole% changes were plotted in Figure D-1. It was noticed that reaction was slower even at 415°C compared to the reaction shown in Figure 5-10, where *in situ* H₂ and catalyst were both used.

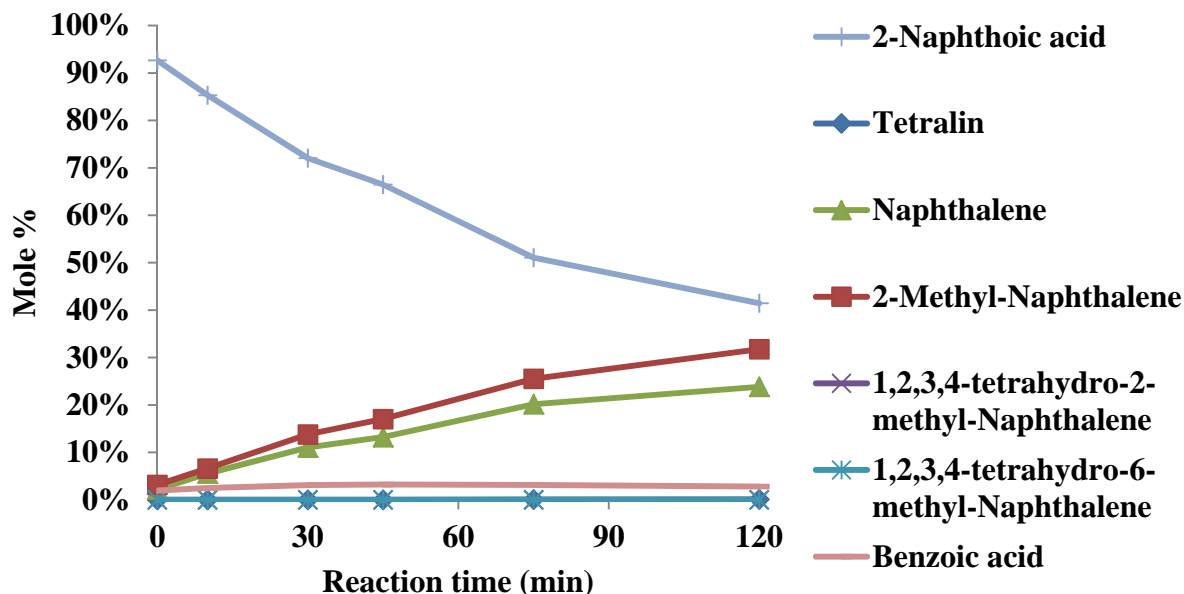


Figure D-1 Mole percentage changes during the 2-NA removal reaction (415°C, 80ml toluene, 10ml water, 15psi H₂S, 585psi N₂, ~1641ppmw 2-NA in toluene, no catalyst, 2hours)

Based on the mole% results in Table D-7, $\ln([NA]_0/[NA]_t)$ can be calculated following Eq. 5-3. For example at 0min, the $\ln([NA]_0/[NA]_t)$ is demonstrated below in Eq. D-8. By calculating all the numbers, Table D-7 was generated for kinetic plotting of 2-NA removal speed as a pseudo first order reaction.

$$\ln \frac{[2-NA]_0}{[2-NA]_t} = \ln(92.65\%) = 7.6302E - 02 \quad (\text{Eq. D-8})$$

Table D-7 $\ln([NA]_0/[NA]_t)$ changes with time in 2-NA removal under N₂ atmosphere at 415°C (415°C, 80ml toluene, 10ml water, 15psi H₂S, 585psi N₂, ~1641ppmw 2-NA in toluene, no catalyst, 2hours)

Time /sec	0	600	1800	2700	4500	7200	
$\ln([2-NA]_0/[2-NA]_t)$	7.6302E-02	1.5883E-01	3.2778E-01	4.0830E-01	6.7201E-01	8.8036E-01	Following Eq. 5-3

By assuming pseudo first order reaction for 2-NA removal and plot the $\ln([2-NA]_0/[2-NA]_t)$ with time by following Eq. 5-3, the total reaction rate k_{total} could be obtained as “1.3037E-04” from the slope of the plots shown in Figure D-2. It should be noticed that 120min point was abandoned due to high error, which was limited by the accuracy of pseudo first order calculation.

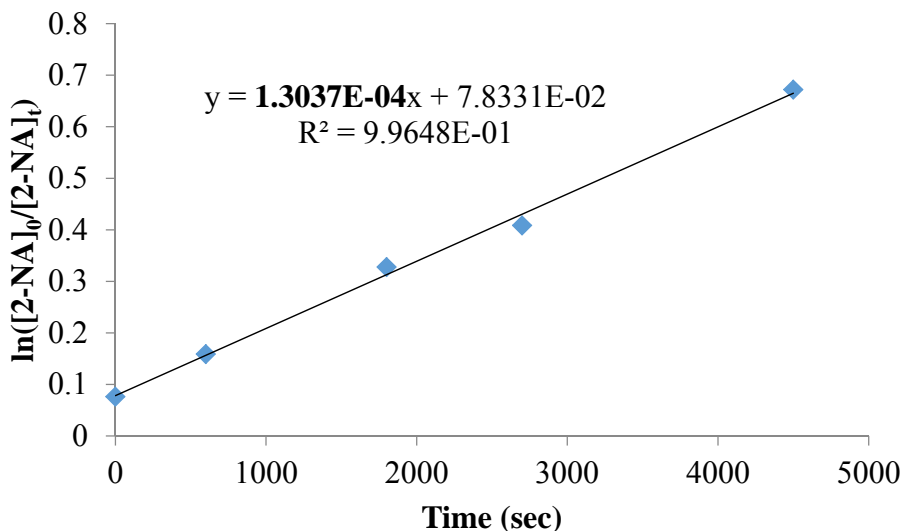


Figure D-2 Plot of $\ln([2-NA]_0/[2-NA]_t)$ values with time (415°C, 80ml toluene, 10ml water, 15psi H₂S, 585psi N₂, ~1641ppmw 2-NA in toluene, no catalyst, 2hours)

With the obtained total 2-NA removal rate, different pathway could be plotted with the numbers calculated from Eq. 5-6, 5-7 and 5-8 as shown in Table D-8. Take 10min for example, the plotting numbers were calculated in Eq. D-9, D-10, D-11 and D-12.

$$\exp(-k_{total} \cdot t) - 1 = \exp(-1.3037E - 04 \cdot 600) - 1 = -7.5241E - 2 \quad (\text{Eq. D-9})$$

$$\frac{[\text{decarboxylation product}] \cdot (-k_{total})}{[2-NA]_0} = [\text{Mole}\%(Tetralin) + \text{Mole}\%(Naphthalene)] \cdot (-k_{total}) =$$

$$(0.00\% + 5.57\%) * -1.3037E - 04 = 7.2553E - 6 \quad (\text{Eq. D-10})$$

$$\frac{[HDO \text{ product}] \cdot (-k_{total})}{[2-NA]_0} = [\text{Mole}\%(1,2,3,4 - tetrahydro - 6 - methyl - Naphthalene) +$$

$$\text{Mole}\%(1,2,3,4 - tetrahydro - 2 - methyl - Naphthalene) + \text{Mole}\%(2 - Methyl -$$

$$Naphthalene)] \cdot (-k_{total}) = (0.00\% + 0.00\% + 6.63\%) * -1.3037E - 04 = 8.6417E - 6$$

$$(\text{Eq. D-11})$$

$$\frac{[\text{cracking product}] \cdot (-k_{total})}{[2-NA]_0} = \text{Mole}\%(Benzoic \text{ acid}) \cdot (-k_{total}) = 2.49\% * -1.3037E - 04 =$$

$$3.2494E - 6 \quad (\text{Eq. D-12})$$

By repeating the calculation above, numbers for plotting different reaction pathways were generated as shown in Table D-8.

Table D-8 Numbers used to plotting different reaction pathways in 2-NA removal under N₂ atmosphere at 415°C (415°C, 80ml toluene, 10ml water, 15psi H₂S, 585psi N₂, ~1641ppmw 2-NA in toluene, no catalyst, 2hours)

Time /sec	0	600	1800	2700	4500	7200	
k_{total}	1.3E-04	1.3E-04	1.3E-04	1.3E-04	1.3E-04	1.3E-04	Obtained from the slope in above figure
$\{\exp[-k_{total}*t]-1\}$	0.0E+00	-7.5E-02	-2.1E-01	-3.0E-01	-4.4E-01	-6.1E-01	Obtained from total rate and time
$[DCB\ product]/[2-NA]_0*(-k_{total})$	-2.9E-06	-7.3E-06	-1.4E-05	-1.7E-05	-2.6E-05	-3.1E-05	Following Eq. 5-6
$[HDO\ product]/[2-NA]_0*(-k_{total})$	-4.1E-06	-8.6E-06	-1.8E-05	-2.2E-05	-3.3E-05	-4.1E-05	Following Eq. 5-5
$[CRC\ product]/[2-NA]_0*(-k_{total})$	-2.6E-06	-3.2E-06	-4.0E-06	-4.2E-06	-4.1E-06	-3.7E-06	Following Eq. 5-7

Notes:

- a) Decimal numbers in this table were controlled within one digit for fitting the page layout
- b) DCB – decarboxylation; HDO – hydrodeoxygenation; CRC – cracking

Figure D-3 was generated with the plot numbers shown in Table D-8. The slopes for 3 reactions were added with trend lines, which provided information on the corresponding pathways. For example, decarboxylation rate was 5.1609E-05; HDO rate was 6.5107E-05.

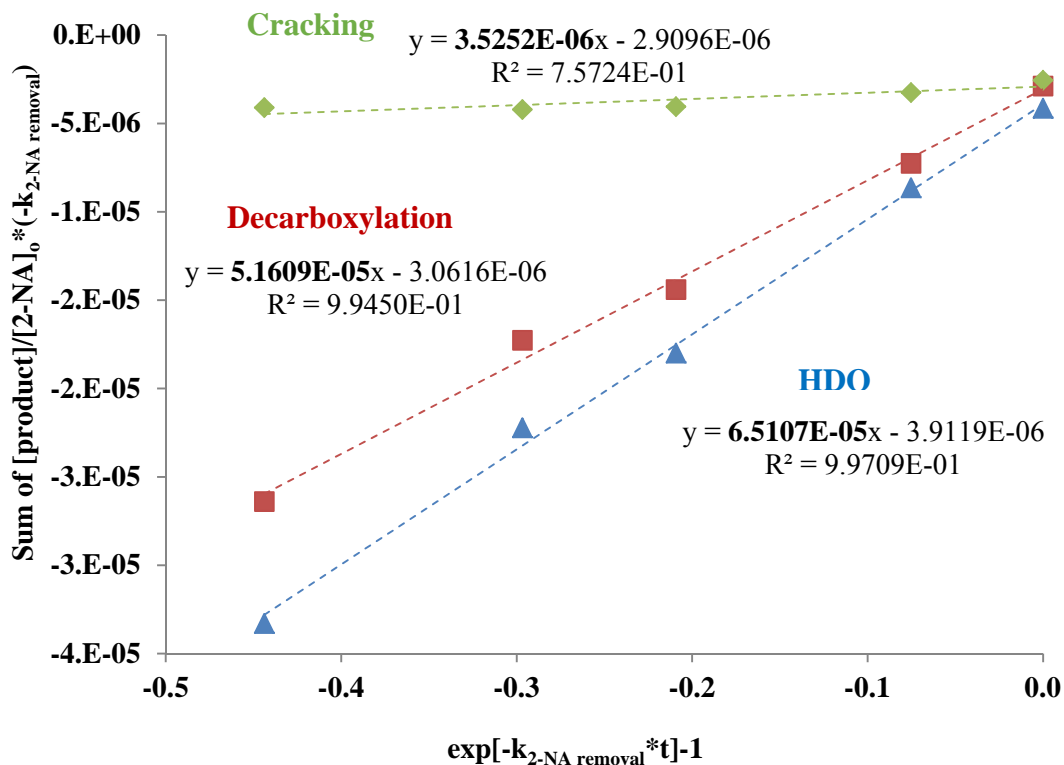


Figure D-3 Plot of sum of $[\text{product}]/[2\text{-NA}]_0 * (-k_{2\text{-NA removal}})$ values with time (415°C, 80ml toluene, 10ml water, 15psi H₂S, 585psi N₂, ~1641ppmw 2-NA in toluene, no catalyst, 2hours)

Not like Figure 5-12, cracking did have linear fitting instead of being zero. However, the fitting was not ideal, because not all cracking and consecutive products were captured for calculation. As discussed in Chapter 5, toluene, as the consecutive product for cracking pathway was the solvent. Hence toluene could not be measured in GC-FID. Due to the lack of toluene, the plot fitting in neither Figure 5-12 nor Figure D-3 could be used for estimating cracking pathway rate. As a result, cracking rate was calculated by substituting decarboxylation and HDO rates from the total 2-NA removal rates. Calculation example was shown in Eq. D-13 by following Eq. 5-8.

$$k_{\text{cracking}} = k_{\text{total}} - k_{\text{decarboxylation}} - k_{\text{HDO}} = (1.3037\text{E} - 04) - (5.1609\text{E} - 05) - (6.5107\text{E} - 05) = 1.3654\text{E} - 05 \quad (\text{Eq. D-13})$$

Table D-9 Kinetic results for different reaction pathways in 2-NA removal under N₂ atmosphere at 415°C (415°C, 80ml toluene, 10ml water, 15psi H₂S, 585psi N₂, ~1641ppmw 2-NA in toluene, no catalyst, 2hours)

k _{total}	1.3037E-04	k DCB	5.1609E-05	Obtained from above slope for DCB
		k HDO	6.5107E-05	Obtained from above slope for HDO
		k CRC	1.3654E-05	Following Eq. 5-8
		k CRC*	3.5252E-06	Obtained from above slope for CRC

D.2.2 Selectivity

Selectivity was calculated based on reaction rates. For example,

$$Selectivity_{Decarboxylation} = \frac{k_{Decarboxylation}}{k_{total}} \times 100\% = \frac{5.1609E-05}{1.3037E-04} \times 100\% = 39.6\% \quad (\text{Eq. D-14})$$

$$Selectivity_{HDO} = \frac{k_{HDO}}{k_{total}} \times 100\% = \frac{6.5107E-05}{1.3037E-04} \times 100\% = 49.9\% \quad (\text{Eq. D-15})$$

$$Selectivity_{Cracking} = \frac{k_{Cracking}}{k_{total}} \times 100\% = \frac{1.3654E-05}{1.3037E-04} \times 100\% = 10.5\% \quad (\text{Eq. D-16})$$

D.2.3 Oil and water yields

Vials were used in sampling during reaction. In order to obtain mass balance results, mass of vials used in sampling were measured before and after reaction, including flushing samples and leftover sample overnight. As shown in Table D-10, detailed mass records were listed. Then the oil and water yield can be calculated as:

$$\text{Oil Yield \%} = \frac{m(\text{oil solution})_f}{m(\text{oil solution})_0} \times 100\% = \frac{m(\text{oil})_{\text{sampling}} + m(\text{oil})_{\text{flushing}} + m(\text{oil})_{\text{overnight}}}{v(\text{toluene})_0 \cdot \rho(\text{toluene}) + m(2\text{-NA})} \times 100\% =$$

$$\frac{1.8492\text{g} + 2.1744\text{g} + 2.0907\text{g} + 1.8588\text{g} + 2.0182\text{g} + 1.8867\text{g} + 8.836\text{g} + 41.3722\text{g}}{80 \cdot 0.8669 + 0.1014\text{g}} \times 100\% = 89.39\%$$

(Eq. D-17)

$$\text{Water Yield \%} = \frac{m(\text{water})_f}{m(\text{water})_0 + \rho(\text{water}) \cdot V(\text{PMA solution})^*} \times 100\% = \frac{5.7008}{10\text{g} + 0\text{g}} \times 100\% = 57.1\%$$

(Eq. D-18)

Table D-10 Mass measurements in 2-NA removal under N₂ atmosphere at 415°C (415°C, 80ml toluene, 10ml water, 15psi H₂S, 585psi N₂, ~1641ppmw 2-NA in toluene, no catalyst, 2hours)

Sampling time /min	m(vial)/g	m(vial+sample)/g	m(sample)/g
0	5.2344	7.0836	1.8492
10	5.2218	7.3962	2.1744
30	5.2275	7.3182	2.0907
45	5.2548	7.1136	1.8588
75	5.242	7.2602	2.0182
120	5.2446	7.1313	1.8867
Flushing collection	14.6492	23.4852	8.836
Overnight oil phase	92.9931	134.365	41.3722
Overnight water phase	16.2798	21.9806	5.7008
Oil mass	62.0862	Oil yeild	89.52%
Water mass	5.7008	Water yield	57.01%
Mass balance	83.39%		

D.2.4 Mass balance

Summary of mass in and mass out is shown in Table D-11.

Table D-11 Mass in and mass out summary for in 2-NA removal under N₂ atmosphere at 415°C (415°C, 80ml toluene, 10ml water, 15psi H₂S, 585psi N₂, ~1641ppmw 2-NA in toluene, no catalyst, 2hours)

In			Out		
Toluene	80ml	69.3520g	Oil	62.0862g	
2-NA	0.1014g		Water	5.7008g	
H2O	10mL	10g	Gases	415psi@22°C in 210ml space	6.7830g
PMA	0g				
H2S	15psi	0.3009g			
N2	585psi	9.6649g			

Notes:

- Toluene density – 0.8669g/mL*
- Ideal gas law was used in gas mass estimation*
- Average mole mass for gas product was estimated based on the mole mass and mole fractions of the final gas product, as shown in Table D-12.*

$$\text{Mass balance \%} = \frac{m(\text{oil solution})_f + m(\text{water})_f + m(\text{PMA solution})_f + m(\text{gas feeds})_f}{m(\text{oil solution})_0 + m(\text{water})_0 + m(\text{PMA solution})_0 + m(\text{gas feeds})_0} \times 100\% =$$

$$\frac{62.0862g + 5.7008g + 0g + 6.7830g}{(69.3520g + 0.1014g) + 10g + 0g + (0.3009g + 9.6649g)} \times 100\% = 83.4\% \quad (\text{Eq. D-19})$$

Table D-12 Mole% of gas products obtained by RGA in 2-NA removal under N₂ atmosphere at 415°C (415°C, 80ml toluene, 10ml water, 15psi H₂S, 585psi N₂, ~1641ppmw 2-NA in toluene, no catalyst, 2hours)

H2	1.01406%
Oxygen	
Nitrogen	96.50713%
CH4	0.16202%
CO	0.11163%
CO2	0.24246%
C2H4	0.01185%
C2H6	0.03720%
C2H2	
H2S	0.84803%
COS	
prop=	
Water	1.06562%
Propylene	
C3	
NC4	
t-2-C4=	
i-C4=	
1-C4=	
c-2-C4=	
i-C5	
n-C5	
butadiene	
t-2-C5=	
2-meth-2-C4=	
1-C5=	
c-2-C5=	
i-C4	
n-C6	
Estimated molar mass for gas products	27.7008

D.2.5 Kinetics calculation with [H2] adjustment

Take Ni-Mo condition in Table 5-13 and Figure 5-30 for instance, the $\ln([2\text{-NA}]_t/[2\text{-NA}]_0)$ could be calculated following Eq. 5-16 based on raw numbers from Table B-85 and Table B-86.

For example, at 10min (600sec),

$$\ln \frac{[2\text{-NA}]_{600\text{sec}}}{[2\text{-NA}]_0} = \ln \text{Mole}\%(2 - \text{NA}) = \ln(75.00\%) = 0.09496496 \quad (\text{Eq. D-20})$$

Then the $\ln([2\text{-NA}]_0/[2\text{-NA}]_t)/[\text{H}_2]$ values were calculated following Eq. 5-17:

$$\frac{\ln \frac{[2\text{-NA}]_{600\text{sec}}}{[2\text{-NA}]_0}}{[\text{H}_2]} = \frac{0.09496496}{0.1152} = 0.82407952 \quad (\text{Eq. D-21})$$

Results were summarized in Table D-13, where the numbers were used for plotting Figure 5-28 (e) and (f).

Table D-13 Kinetic calculation example for [H2] adjustment (Ni-Mo in 2-NA removal: 300°C, 80ml toluene, 10ml water, 15psi H₂S, 585psi CO, ~1641ppmw 2-NA in toluene, 673ppmw Mo, Ni:Mo ratio=0.2, 2hours)

Time /sec	0	600	1800	3600	7200
$\ln([2\text{-NA}]_t/[2\text{-NA}]_0)$	0.09496496	0.287732	2.048827	5.462947	-
[H ₂]	0.1152	0.1568	0.2668	0.3518	0.3860
$\ln([2\text{-NA}]_0/[2\text{-NA}]_t)/[\text{H}_2]$	0.82407952	1.83489	7.678475	15.53033	-

Appendix E. Batch Reactor Experimental Reproducibility

Given the time and funding constraints in batch reactions, not all the results were repeated for statistical error analysis. However, certain reaction conditions were repeated to investigate the experimental reproducibility in the batch reactions for bitumen upgrading and 2-NA removal.

E.1 Experimental Reproducibility in Bitumen Upgrading

Three repeating experiments were carried out on March 20th, 23rd and 26th in 2010 respectively for the reaction condition “405°C, 80g Cold Lake bitumen emulsion, 585psi CO, 15psi H₂S, 1408 ppmw Mo, 2 hours”. The raw data is shown in Table E.1.

Table E.1 Raw data for the same condition tested on March 20th, 23rd and 26th in 2010 (405°C, 80g Cold Lake bitumen emulsion, 585psi CO, 15psi H₂S, 1408 ppmw Mo, 2 hours)

Yield	Mar-20-2010	Mar-23-2010	Mar-26-2010
Naphtha	13.95%	14.78%	14.17%
Kerosene	14.15%	14.24%	14.19%
Distillate	13.65%	11.69%	12.00%
Heavy Gas Oil	27.89%	28.67%	30.23%
Pitch	15.72%	13.70%	13.72%
HVOR	4.53%	3.80%	4.80%
Loss To Gas Phase	9.78%	12.90%	10.65%
Metal residue	0.20%	0.13%	0.13%
Coke	0.14%	0.10%	0.10%
Performance			
Asphaltene removal %	61.11%	70.0%	65.6%
Total S removal %	49.83%	52.87%	52.33%
WGSR Conversion	79%	82.04%	77.83%
Max. Pressure	3462	3561	3491
H ₂ mole%	18.65%	11.6%	17.4%

After processing and analyzing the results, the outcomes of these three experiments are listed in Table E.2 with standard deviation and errors.

Table E.2 Error analysis of the experiments on March 20th, 23rd and 26th in 2010 (405°C, 80g Cold Lake bitumen emulsion, 585psi CO, 15psi H₂S, 1408 ppmw Mo, 2 hours)

	Mar-20-2010	Mar-23-2010	Mar-26-2010	Standard Deviation	Error
Upgraded Oil Yield%	85	83	84	±0.9	1.1%
Pitch Conversion%	48	54	54	±3.2	6.1%
Max. Pressure (psi)	3462	3561	3491	±41.6	1.2%
WGSR Conversion%	79	82	78	±1.7	2.2%
H ₂ mole%	19	12	17	±3.1	19.5%
Asphaltene removal %	61	70	66	±3.6	5.5%
S Removal%	50	53	52	±1.3	2.6%
HVOR Yield%	4.5	3.8	4.8	±0.4	9.7%
Coke Yield%	0.1	0.1	0.1	±0.02	16.4%

It is noted that most of the results were repeated with relatively low error considering in a batch reaction. The errors in H₂ mole% and Coke yield were high, which could be attributed to the poor measurement or calibration of the corresponding characterization facilities (RGA and electronic balance).

In general, the batch reaction results repeated fairly well in bitumen upgrading experiments.

E.2 Experimental Reproducibility in 2-NA removal

Three repeating experiments were carried out for condition “300°C, 80ml toluene, 10ml water, 15psi H₂S, 585psi gas feed, ~1641ppmw 2-NA in toluene, 673ppmw Mo, 2hours”. The error analysis results are shown in Table E.3. Raw data for the experiments carried on Dec 11th 2011, Jan 11th 2012 and Jan 12th 2012 were shown in Table E.4, Table E.5 and Table E.6 respectively.

Table E.3 Error analysis of the experiments on Dec 11th 2011, Jan 11th 2012 and Jan 12th 2012 (300°C, 80ml toluene, 10ml water, 15psi H₂S, 585psi gas feed, ~1641ppmw 2-NA in toluene, 673ppmw Mo, 2hours)

	Dec-11-2011	Jan-11-2012	Jan-12-2012	Standard Deviation	Error	
NA Conversion % in Oil	99.7	99.2	99.3	± 0.2	0.2%	
NA Conversion % in H ₂ O	99.7	99.3	99.9	± 0.2	0.2%	
k _{NA Removal} (10 ⁻⁵ s ⁻¹)	85.2	78.2	113.3	± 15.2	16.4%	
k _{Decarboxylation} (10 ⁻⁵ s ⁻¹)	3.9	3.2	3.7	± 0.3	7.7%	
k _{HDO} (10 ⁻⁵ s ⁻¹)	74.1	68.4	87.3	± 7.9	10.3%	
k _{Cracking} (10 ⁻⁵ s ⁻¹)	7.2	6.6	22.4	± 7.3	60.6%	
Selectivity %	Decarboxylation	4.6	4.2	3.2	± 0.6	14.4%
	HDO	87.0	87.4	77.0	± 4.8	5.7%
	Cracking	8.4	8.4	19.7	± 5.3	43.7%
Product Distribution %	Decarboxylation	4.9	4.5	4.0	± 0.4	8.0%
	HDO	95.1	95.5	96.0	± 0.4	0.4%
	Cracking	0.0	0.0	0.0	± 0.0	-
WGSR Conversion %	51.6	41.7	59.7	± 7.3	14.4%	
k _{WGSR} (10 ⁻⁵ s ⁻¹)	15.8	14.8	18.4	± 1.5	9.3%	
H ₂ Partial Pressure (psi)	548	555	651	± 46.8	8.0%	
Max. Pressure (psi)	2053	2066	2010	± 23.9	1.2%	
Oil yield %	89.1	89.6	91.6	± 1.1	1.2%	
Water yield %	47.6	47.3	43.5	± 1.8	4.0%	
Mass balance %	83.5	84.1	83.7	± 0.2	0.3%	

It is noted that the error were relatively low except the reaction rate constant and selectivity for cracking pathway. The kinetic calculation procedure for cracking pathway was discussed in Section 5.2.5 and Appendix D.2, where the error of rate constant for cracking pathway could be a combination of the errors of rate constant estimation of total 2-NA removal, decarboxylation and HDO. Plus the experimental error, the error for cracking pathway kinetics should be the highest, which is consistent with the observation in Table E.3. This could be caused by the potential high systematic error existed in batch reaction and the poor cracking production measurement. However, it can be found that the results from the reactions carried out on Dec 11th 2011 and Jan 11th 2012 were very close, which were relatively far from the result collected on Jan 12th 2012.

Given the other relatively low errors observed in Table E.3, it can be concluded that the 2-NA experiments were quite repeatable.

Table E.4 Raw data for experiment carried out on Dec 11, 2011 (300°C, 80ml toluene, 10ml water, 15psi H₂S, 585psi gas feed, ~1641ppmw 2-NA in toluene, 673ppmw Mo, 2hours)

Dec-11-2011					
	Mole %				
Time /min	0	10	30	60	120
Benzoic acid	0.00%	0.00%	0.00%	0.00%	0.00%
Tetralin	0.00%	0.05%	0.17%	0.42%	0.50%
Naphthalene	0.00%	1.34%	2.85%	4.19%	4.35%
1,2,3,4-tetrahydro-2-methyl-Naphthalene	0.00%	0.00%	0.35%	1.53%	4.33%
1,2,3,4-tetrahydro-6-methyl-Naphthalene	0.00%	0.30%	1.09%	2.78%	7.78%
2-Methyl-Naphthalene	6.82%	42.91%	72.07%	86.84%	82.69%
2-Naphthoic acid	93.18%	55.40%	23.48%	4.23%	0.35%
	Gas Phase				
Time /min	0	10	30	60	120
Pressure /psi	1921	2053	1959	1885	1719
WGSR Conversion	8.37%	12.91%	24.43%	34.93%	41.93%
P(H ₂) /psi	175.20	310.64	415.58	511.62	548.42
P(CO) /psi	1554.33	1479.46	1132.58	861.30	648.68
P(CO ₂) /psi	141.95	219.30	366.12	462.38	468.29
P(Water) /psi	22.54	16.06	13.39	13.95	15.55
P(CH ₄) /psi	0.00	0.00	0.00	0.00	0.00
P(C ₂ H ₄) /psi	1.77	2.37	3.38	3.12	2.44
P(C ₂ H ₆) /psi	2.54	2.94	6.90	12.11	16.71
P(H ₂ S) /psi	15.22	16.24	17.36	17.61	16.77
P(COS) /psi	6.00	5.71	3.53	2.91	2.14

Table E.5 Raw data for experiment carried out on Dec 11, 2011 (300°C, 80ml toluene, 10ml water, 15psi H₂S, 585psi gas feed, ~1641ppmw 2-NA in toluene, 673ppmw Mo, 2hours)

Jan-11-2012					
	Mole%				
Time /min	0	10	30	60	120
Benzoic acid	0.00%	0.00%	0.00%	0.00%	0.00%
Tetralin	0.00%	0.04%	0.15%	0.28%	0.49%
Naphthalene	0.00%	1.30%	2.74%	3.69%	3.98%
1,2,3,4-tetrahydro-2-methyl-Naphthalene	0.00%	0.00%	0.34%	1.18%	4.16%
1,2,3,4-tetrahydro-6-methyl-Naphthalene	0.00%	0.29%	1.04%	2.63%	7.26%
2-Methyl-Naphthalene	7.38%	41.96%	71.43%	86.80%	83.33%
2-Naphthoic acid	92.62%	56.41%	24.29%	5.42%	0.78%
	Gas Phase				
Time /min	0	10	30	60	120
Pressure /psi	1898	2066	1936	1908	1736
WGSR Conversion	8.46%	11.21%	23.00%	32.89%	41.74%
P(H ₂) /psi	181.94	296.85	392.18	498.91	554.75
P(CO) /psi	1523.45	1533.98	1147.02	906.75	656.29
P(CO ₂) /psi	140.88	193.63	342.63	444.38	470.24
P(Water) /psi	23.70	14.90	15.13	14.93	15.06
P(CH ₄) /psi	0.00	0.00	0.00	0.00	0.00
P(C ₂ H ₄) /psi	1.68	2.38	4.22	3.31	1.70
P(C ₂ H ₆) /psi	2.13	4.15	10.52	16.32	17.40
P(H ₂ S) /psi	16.47	14.69	19.28	19.95	18.25
P(COS) /psi	6.77	4.88	4.62	3.14	2.30

Table E.6 Raw data for experiment carried out on Dec 11, 2011 (300°C, 80ml toluene, 10ml water, 15psi H₂S, 585psi gas feed, ~1641ppmw 2-NA in toluene, 673ppmw Mo, 2hours)

Jan-12-2012					
	Mole%				
Time /min	0	10	30	60	120
Benzoic acid	0.00%	0.00%	0.00%	0.00%	0.00%
Tetralin	0.08%	0.15%	0.32%	0.49%	0.74%
Naphthalene	0.55%	1.80%	3.02%	3.33%	3.22%
1,2,3,4-tetrahydro-2-methyl-Naphthalene	0.18%	0.29%	1.38%	3.92%	8.65%
1,2,3,4-tetrahydro-6-methyl-Naphthalene	0.40%	1.18%	4.21%	8.10%	15.04%
2-Methyl-Naphthalene	20.02%	53.85%	83.45%	82.74%	71.62%
2-Naphthoic acid	78.76%	42.74%	7.61%	1.43%	0.73%
	Gas Phase				
Time /min	0	10	30	60	120
Pressure /psi	1890	2010	1949	1895	1696
WGSR Conversion	8.86%	10.29%	26.53%	33.13%	51.61%
P(H ₂) /psi	199.09	323.38	491.12	670.72	650.61
P(CO) /psi	1503.55	1483.35	1039.78	796.10	488.29
P(CO ₂) /psi	146.13	170.07	375.49	394.42	520.70
P(Water) /psi	17.40	13.01	13.11	12.86	13.31
P(CH ₄) /psi	0.00	0.00	0.00	0.38	0.54
P(C ₂ H ₄) /psi	0.00	0.00	0.00	0.00	0.00
P(C ₂ H ₆) /psi	0.00	0.00	0.00	0.11	0.18
P(H ₂ S) /psi	15.78	14.87	24.53	17.95	20.56
P(COS) /psi	8.04	5.32	4.97	2.47	1.81